SCHOLARLY PUBLICATIONS

A CURRENT AWARENESS BULLETIN
OF RESEARCH OUTPUT

@DTU

(62nd Edition)

FEBRUARY, 2018

BY: CENTRAL LIBRARY

DELHI TECHNOLOGICAL UNIVERSITY
(FORMERLY *DELHI COLLEGE OF ENGINEERING)*
GOVT. OF N.C.T. OF DELHI
SHAHBAD DAULATPUR, MAIN BAWANA ROAD
DELHI 110042

PREFACE

This is the **Sixty Two** Issue of Current Awareness Bulletin started by Delhi Technological University, Central Library. The aim of the bulletin is to compile, preserve and disseminate information published by the faculty, students and alumni for mutual benefits. The bulletin also aims to propagate the intellectual contribution of Delhi Technological University (DTU) as a whole to the academia.

The bulletin contains information resources available in the internet in the form of articles, reports, presentations published in international journals, websites, etc. by the faculty and students of DTU. The publications of faculty and student which are not covered in this bulletin may be because of the reason that the full text either was not accessible or could not be searched by the search engine used by the library for this purpose.

The learned faculty and students are requested to provide their uncovered publications to the library either through email or in CD, etc. to make the bulletin more comprehensive.

This issue contains the information published during **February, 2018**. The arrangement of the contents is alphabetical. The full text of the article which is either subscribed by the university or available in the web is provided in this bulletin.

Central Library

CONTENTS

1. 16S metagenomic analysis and taxonomic distribution of enriched microbial consortia capable of simultaneous biodegradation of organochlorines by illumina platform, Saghee Madhu Raju and ***6.Rajkumar Bidlan***, Biotechnology, DTU

2. A Review on Medicinal Plants for Alzheimers Disease, ***6.Arpita Roy***, Biotech, DTU

3. A Robust Database Watermarking Algorithm using Bezier Cubic Curves, ***3.Manoj Kumar*** and ***3.Om Prakash Verma***, CSE, DTU

4. ANFIS Based Add-on Controller for Unbalance Voltage Compensation in Low Voltage Microgrid, Jaipal Saroha, ***3.Mukhtiar Singh*** and D. K. Jain, Electrical, DTU

5. Benzofuran Synthesis through Iodocyclization Reactions: Recent Advances, Saurabh Mehta, Chemistry, DTU

6. Big Data: A Driver of Innovation in the 21st Century, ***7.Mohini Yadav*** and ***3.Yasha Hasija***, Biotechnology, DTU

7. Characterization of the Sewage Sludge Samples Collected at Delhi, India, ***3.Rajeev Kumar Mishra***, ***6.Amit Krishan*** , ***8.Sandeep Kumar*** and G. L. Bajaj, ENVT, DTU

8. Comprehensive Analysis of Sub-20nm Black Phosphorus Based Junctionless-Recessed Channel MOSFET for Analog/RF Applications, ***6.Ajay Kumar***, ***3.M.M. Tripathi*** and ***3.Rishu Chaujar***, Electrical, DTU

9. Detection of Power Quality Event using Histogram of Oriented Gradients and Support Vector Machine, ***3.Rajiv Kapoor***, Rashmi Gupta, Le Hoang Son, Sudan Jha, Raghvendra Kumar, ECE, DTU

10. Effect of Various Culture Parameters on the Bio-surfactant Production from Bacterial Isolates, ***6.Arpita Roy***, Biotechnology, DTU

11. Employing X-ray absorption technique for better detector resolution and measurement of low cross-section events, ***6.Gaurav Sharma***, ***3.Nitin K. Puri***, Pravin Kumar and T. Nandi, Physics, DTU

12. Enhancing the processibility of high temperature polymerizing cardanol derived benzoxazines using eco-friendly curing accelerators, ***6.Pratibha Sharma***, ***3.Devendra Kumar*** and Prasun Kumar Roy, Chemistry and Polymer, DTU

13. Entropy-Based Adaptive Gamma Correction for Content Preserving Contrast Enhancement, ***3.Anil Singh Parihar***, Information Technology, DTU

14. Epitaxial Growth of GaN Nanostructure by PA-MBE for UV Detection Application, ***6.Lalit Goswami***, ***3.Rajeshwari Pandey*** and Govind Gupta, Electronics & Communication, DTU

15. Evidence and Positive Selection Test for Gene-loss Theory of Evolution, ***6.Prateek Sukumar***, ***6.Neha Kumari*** and ***3.Yasha Hasija***, Biotechnology, DTU

16. Exergy and sustainability investigation of waste heat recovery vapor compression refrigeration system with silver Nano fluid, Kapil Chopra and ***3.R.S Mishra,*** Mechanical, Production & Industrial, DTU

17. Fabrication & Mechanical Testing of AA6082/Si3N4 Composites, ***6.Ankit Tyagi***, ***6.Yashwant Koli*** and Deepak Sharma, Mechanical, DTU

18. Friction stir welding of aluminum alloy 6082-T6-t651 for improving tensile strength, hardness and wear rate properties, ***3.R.S. Mishra*** and Shaambhavi Ratnapriya, Mechanical, DTU

19. Globalization, ICT and Entrepreneurship: A Study of Women Engineers in India, ***3.Dr. Seema Singh***, Economics, DTU

20. Harmonic Reduction in Power Distribution Network using UPQC, ***3.J.N.Rai*** and ***3.Ram Bhagat***, Electrical, DTU

21. Identification and statistical analysis of performance parameters of it enabled supply chain management system, ***6.Sanjeev Kumar*** and ***3.R. S. Mishra***, Mechanical, Production & Industrial, DTU

22. Intelligent Automated Machine (IAM) for Dispensing Ready Fried Food (RFF), Nitin Agarwal , ***3.Dr. Kapil Sharma***, ***6.S. K. Agrawal*** and Dr. Prabhat Sharma, CSE, DTU

23. Laser-pulse shape effects on magnetic field generation in underdense plasmas, K Gopal, ***6.Md A Raja***, D N Gupta, K Avinash and ***3.S C Sharma,*** Physics, DTU

24. Mechanical Properties and Micrstructure of Al-5083 by TIG, Shailesh KumarSingha, Rasik Mohan Tiwaria, Anil kumara, Satyajeet Kumar, ***3.QasimMurtaza*** and Sanjeev Kumar, Mechanical, DTU

25. Object Tracking and Suspicious Activity Identification during Occlusion, Ravi Teja Yakkali, Raunaq Nayar and ***3.S. Indu,*** Electronics and Communication, DTU

26. Optimal Node Clustering and Scheduling in Wireless Sensor Networks, Palvinder Singh Mann and ***7.1.Satvir Singh,*** Electronics and Communication, DTU

27. PARAMETER ESTIMATION OF RC CIRCUITS USING EXTENDED KALMAN FILTER, ***6.Amit Kr Gautam*** and ***3.Sudipta Majumdar***, ECE, DTU

28. Performance improvement in integrated refrigeration system, ***3.R.S. Mishra***, Mechanical, DTU

29. Performance investigations of APSO tuned linear and nonlinear PIDcontrollers for a nonlinear dynamical system, ***3.Sudarshan K. Valluru*** and ***3.Madhusudan singh***, Electrical, DTU

30. Physical Insights on Negative Capacitance Transistors in Nonhysteresis and Hysteresis Regimes: MFMIS Versus MFIS Structures, ***8.1.Girish Pahwa***, Tapas Dutta, Member, Amit Agarwal, and Yogesh Singh Chauhan, ECE, DTU

31. Prediction of traffic noise descriptors using artificial neural network, ***3.Paras Kumar***, Mechanical, DTU

32. Reliability Issues of In2O5Sn Gate Electrode Recessed Channel MOSFET: Impact of Interface Trap Charges and Temperature ***6.Ajay Kumar***, ***3.M. M. Tripathi*** and ***3.Rishu Chaujar***, Electrical, DTU

33. Study of reflection losses in tuned and EBG power dividers at S, C, X and upper Ku bands, Suresh Angadi, ***6.Karteek Viswanadha***, R.Roopa Sree and Sowjanya Madaka, Electronics and Communication, DTU

34. Sustainability enhancement of corporate governance regime in India, ***6.Ruchi Kansil*** and ***6.Archana Singh,*** DSM, DTU

35. Thermodynamic model analysis of vapour compression refrigeration systems by using ecofriendly refrigerant (R1234yf) in primary circuit and R718 in the secondary circuit by mixing Nano particles (Al2O3) for improving thermal efficiencies, ***3.R.S. Mishra,*** Mechanical, DTU

36. Tuning the properties of segmented polyurea by regulating soft-segment length, ***6.Nahid Iqbal***, Manorama Tripathi, Surekha Parthasarathy, ***3.Devendra Kumar*** and Prasun Kumar Roy, Chemistry and Polymer, DTU

1. *Chancellor*

2. *Pro Vice Chancellor*	***2.1.*** *Ex Pro Vice Chancellor*
3. *Faculty*	***3.1.*** *Ex Faculty*
4. *Teaching-cum-Research Fellow*	***4.1.****Asst. Librarian*
5. *Alumni*	
6. *Research Scholar*	***6.1.*** *Ex Research Scholar*
7. *PG Scholar*	***7.1.*** *Ex PG Scholar*
8. *Undergraduate Student*	***8.1.*** *Ex Undergraduate Student*

SCIENTIFIC FEDERATION
ABODE FOR RESEARCHERS

Arpita Roy, SF J Herb Med, 2017, 1:1

SciFed Journal of Herbal Medicine

Review Article Open Access

A Review on Medicinal Plants for Alzheimers Disease

*Arpita Roy

*Department of Biotechnology,Delhi Technological University, New Delhi-110042, India

Abstract

Neurodegenerative diseases are commonly induced by irreversible destruction of central nervous system and neuronal networks which result in permanent functional impartment. There are several reported neurodegenerative disease, among them Alzheimer's disease is very common. There is no cure available for Alzheimer's disease, but symptomatic treatment may improve the memory and other related problems. Natural products such as herbs and medicinal plants have been used in the treatment of many memory disorders such as dementia, amnesia, as well as Alzheimer's disease since a long time. Medicinal plants have been utilized for treatment of various diseases and it shows potential roles in the management and cure of memory disorders. Most of herbs and plants have been chemically evaluated and their efficacy has also been proven in clinical trials. However, the underlying mechanisms of actions are still on the way. In this review role of different medicinal plants against Alzheimer's disease has been discussed.

Introduction

Neurodegenerative diseases are heterogeneous group of genetic disorders characterized by loss of neuronal structure, function and generally accompanied by neuronal loss. These diseases may result directly from degeneration of particular neuronal populations or indirectly from alterations in glial support cells. The particular topological pattern of brain involvement determines the specific clinical manifestations of each disease. Several of these diseases are characterized by an accumulation of abnormal or aggregated proteins or other biological materials either extracellular or within neurons. These accumulations take various forms and result in the neuritic plaques or neurofabrillary tangles in Alzheimer's disease, Lewy bodies in Parkinson's disease, glycogen and polyglucosan bodies in Lafora disease, or glycolipids and complex carbohydrates in the lysosomal storage diseases of the neurodegenerative diseases. Alzheimer's disease is considered to be responsible for 60% of all dementia in people aged 65 or older [1]. Alzheimer's disease (AD) is age related progressive neurodegenerative disorder caused due to aggregation of mis-folded proteins which accumulate fibrillary amyloid deposits in selective regions of central nervous system. Alzheimer's disease results in memory loss, unusual behaviour, personality changes, and loss of the ability to thinking. It starts with loss of short term memory, forgetting names and addresses, as this condition progresses, the change become more marked and even individuals forget the home way. Seventy percent of causes for Alzheimer's disease are genetic and twenty one percent is environmental. Most cases of Alzheimer's disease, approximately 95%, are the late-onset form, which develops after age of 60 [2]. At present, the most accepted

***Corresponding author:** Arpita Roy, Department of Biotechnology,Delhi Technological University, New Delhi-110042, India. E-mail: arpitaroy888@gmail.com

Received September 25, 2017; **Accepted** November 9, 2017; **Published** November 23, 2017

Citation: Arpita Roy (2017) A Review on Medicinal Plants for Alzheimers Disease. SF J Herb Med 1:1.

Copyright: © 2017 Arpita Roy. This is an open-access article distributed under the terms of the Creative Commons Attribution License, which permits unrestricted use, distribution, and reproduction in any medium, provided the original author and source are credited.

Alzheimer's disease treatment strategy is cholinesterase inhibitors that can inactivate the acetyl cholinesterase (AChE) enzyme in order to increase acetylcholine levels in the brain. Acetyl cholinesterase inhibitors include rivastigmine, tacrine, donepezil, and galantamine whereas methyl-D-aspartate receptor antagonist (memantine) has recently been prescribed. However, there is no cure for Alzheimer's disease, except to relieve symptoms of the disease [3]. The lifetime risk of Alzheimer's disease for those 65 years of age is estimated to be 10.5%. Although some risk factors have been implicated, expert consensus at the National Institutes of Health's State-of-the-Science Conference in 2010 indicates that firm conclusions cannot be drawn on modifiable risk factors for Alzheimer's disease. It appears to be a multi-factorial disease that consists of socio-demographic, genetic, environmental, and lifestyle risk factors. Studies on risk factors remain challenging due to long latency periods from risk factor to disease onset [4]. The present review deals with the information on medicinal plants used to cure the Alzheimer's disease.

Medicinal Plants against Alzheimer's Disease

Medicinal plants synthesize and conserve a variety of biochemical products, many of which are extractable and used as raw material for various scientific investigations. Many secondary metabolites from plant are commercially important and are used as pharmaceutical compounds. Over the past few years, the medicinal plants have regained a wide recognition due to a growing faith in herbal medicine in view of its lesser side effects compared to allopathic medicine and the necessity of meeting the requirements of medicine for an increasing human population. However, a continuous supply of the source material often becomes difficult due to the factors like environmental changes, cultural practices, diverse geographical distribution, labour cost, and selection of the superior plant stock and over exploitation by pharmaceutical industry [5]. Alzheimer's disease is the most common neurodegenerative diseases. Several studies have been reported that medicinal plants are used in the treatment of Alzheimer's disease. There are several medicinal plants recognized for the treatment of Alzheimer's disease which includes *Ginkgo biloba, Centella asiatica, Withania somnifera, Bacopa monnieri, Melissa officinalis, Salvia officinalis, Tinospora cordifolia, Hypericum perforatum* etc.

Bacopa Monnieri

Bacopa monnieri (Brahmi) is a bitter-tasting creeper plant found in damp and marshy areas and is commonly used in Ayurvedic medicine as a nervine tonic, diuretic, and cardiotonic and as a therapeutic agent against insomnia, asthma, epilepsy, and rheumatism. The principal constituents of Bacopa monnieri are saponins and triterpenoid bacosapo nins that include bacopasides III to V, bacosides A and B, and bacosaponins A,B ,C. other saponin glycosides include the jujubogenin bisdesmosides bacopasaponins D, E, and F. Other constituents include alkaloids, plant sterols, betulic acid, polyphenols, and sulfhydryl compounds that confer antioxidant activity [6]. Traditionally, *B. monnieri* was used to improve memory and cognitive function. *B.monnieri* extracts have been investigated extensively for their neuropharmacological effects and their nootropic actions [7]. In the hippocampus, *B. monnieri* enhances protein kinase activity that may contribute to its nootropic action [8]. *B. monnieri* also inhibited cholinergic degeneration and displayed a cognition-enhancing effect in a rat model of AD [9]. It has been reported that a standardized extract of *B. monnieri* reversed the cognitive deficits induced by intracerebroventricularly administered colchicines and ibotenic acid into the nucleus basalis magnocellularis [10]. In the same study, *B. monnieri* also reversed the (a) depletion of acetylcholine, (b) reduction in choline acetyltransferase activity, and (c) decrease in muscarinic cholinergic receptor binding in the frontal cortex and hippocampus [10]. *B. monnieri* extracts protected neurons from beta-amyloid-induced cell death by suppressing cellular acetylcholinesterase activity. In addition, *B. monnieri* extract-treated neurons expressed a lower level of reactive oxygen species, suggesting that *B. monnieri* restrained intracellular oxidative stress [11]. An enriched phytochemical composition of *B. monnieri* was evaluated for short-term safety and tolerance in healthy adult volunteers.

Centella Asiatica

Centella asiatica belongs to the Apiaceae family and commonly known as gotu kola. Asiaticoside derivatives, including asiatic acid and asiaticoside, were shown to reduce hydrogen peroxide-induced cell death, decrease free radical concentrations, and inhibit beta-amyloid cell death *in vitro*, suggesting a possible role for gotu kola in the treatment and prevention of Alzheimer's disease and beta-amyloid toxicity [12]. *Centella asiatica* extracts reversed the beta-amyloid pathology in the brains of mice and modulated the components of the oxidative

stress response [13]. It is one of the important rejuvenating herbs for nerve and brain cells and is believed to be capable of increasing intelligence, longevity, and memory [7].

Commiphora Whighitti

It belongs to the Burseraceae family. It shows potential role in memory improvement in scopolamine induced memory deficits [14]. Memory enhancing and anti-dementia activity of *Commiphora whighitti* has been reported due to its reduction in acetylcholinesterase contents in the hippocampus [15].

Curcuma Longa

Ii belongs to the Zingiberaceae family. It possesses anti-inflammatory activity which is also associated with reduced risk of Alzheimer's disease [16]. Curcumin reduces the deposition of plaque in the brain. It decreases oxidative stress and amyloid pathology [17]. In a study, low doses of *Curcumin* reduced Aβ level up to 40% in mice with Alzheimer's disease as compared to control drug . At lower dose curcumin caused 43% decrease in the plaque burden that these Aβ have on the brain of mice with Alzheimer's disease [17].

Ginkgo Biloba

Ginkgo biloba is the oldest tree on the earth, and it is native to China. *G. biloba* extract treat insufficiency of blood circulation problems, loss of consciousness, headaches, and depression in the elderly [18]. This extract is reported to contain about 24% flavonoids and 6% terpene lactones. There is reliable evidence that standardized ginkgo extract shows several molecular and cellular neuroprotective mechanisms, including the attenuation of apoptosis, the inhibition of membrane lipid peroxidation, anti-inflammatory effects and the direct inhibition of amyloid-b aggregation. There are extensive clinical investigations regarding its potential role in cognitive disorders [18]. Chronic treatment of *G. biloba* on learning and memory in mice showed that *G. biloba* improved acquisition, storage, and retrieval of a two-response sequence for food reward [19]. The antioxidant and free-radical scavenging properties of *G. biloba* extract are primarily attributed to the flavonoid fraction. *G. biloba* affects cognitive function in an animal model of Alzheimer's disease without altering the histopathological consequences of overexpression of β amyloid precursor protein [20]. *G. biloba* extract significantly inhibit the AChE activity in the brain. The inhibition of AChE activity can be correlated with improvement observed in scopolamine-induced deficits in passive avoidance by *G. biloba* extract. The decrease in AChE activity indicates an increase in the basal level of acetylcholine [21].

Glycyrrhiza Glabra

It belongs to Fabaceae family. It contains several bioactive compounds linalool oxide, terpinen, tetramethyl pyrazine, geraniol, benzoic acid, propionic acid, ethyl linolenate, butanediol, feuferaldehyde, methyl ethyl ketone, furfuryl formate, trimethylpyrazine, glycyrrhizin, tannin, and glycyrrhizic acid [22]. [23] Reported that in mice Glycyrrhiza glabra enhances memory. Three dose levels (75, 150, 300 mg/kg) of plant extracts were administered to mice in seven successive days and dose at 150 mg/kg was found effective in memory enhancement.

Lepidium Meyenii

It belongs to Brassicaceae family. It is known for its improving learning abilities and memory function [24]. It exhibited memory enhancing activity in Alzheimer's patients. It enhances memory by increasing the level of acetylcholine [25]. It improves experimental memory impairment induced by ovariectomy, due in part to its acetylcholinesterase inhibitory and antioxidant effects [26].

Magnolia Officinalis

It belongs to the family Magnoliaceae. It improves the scopolamine induced memory deficits (Lee *et al.*, 2009). It inhibits acetyl cholinesterase activity [27]. Magnolol and honokiol derived from *Magnolia officinalis*, have the ability to enhance the choline acetyltransferase effects and inhibit the acetylcholine cleavage and have also been shown to release acetylcholine from the hippocampus [28] Honokiol exhibits anti-inflammatory activity by reactive oxygen species synthesis inhibition [29]. As an anti-inflammatory and antioxidant agent, *Magnolia officinalis* plays an important role in the treatment of Alzheimer [30].

Tinospora Cordifolia

Tinospora cordifolia (Menispermaceae) possesses memory enhancing property on learning and memory in normal and memory deficits animals. *Tinospora cordifolia* mechanism of cognitive enhancement by immunostimulation and increasing the synthesis of acetylcholine, this supplementation of choline enhances the cognitive function [31]. *Tinospora cordifolia* is known

as learning and memory enhancer) in Ayurveda. The pure aqueous extract of the root of *Tinospora cordifolia* was found to enhance verbal learning and logical memory [32].

Withania Somnifera

Withania somnifera (Ashwagandha) is extensively used in Ayurveda as a nervine tonic (http://www.planetayurveda.com/ashwagandha_uses.htm), aphrodisiac, and 'adaptogen' and helps the body adapt to stress. *W. somnifera* is a member of the Solanaceae family, and the root is widely used. It is categorized as a rasayana and is believed to possess antioxidant activity, free radical scavenging activity, and an ability to support a healthy immune system [33]. Unlike other adaptogens, which tend to be stimulating, *W. somnifera* has a calming effect and thus may be particularly indicated in people with Alzheimer's disease [34]. A recent double-blind, randomized, placebo controlled study of the effects of *W. somnifera* on stress found that it reduced symptoms of stress and inability to concentrate and reversed forgetfulness in a dose-dependent manner, and 500 mg/day was more effective [35]. No additional adverse effects were found. *W. somnifera* contains steroidal compounds of great interest to researchers, such as the ergostane-type steroidal lactones, including withanolides A to Y, dehydro withanolide R, withasomniferin A, withasomidienone, withasomniferols A to C, withaferin A, and withanone. Other constituents include the phytosterols sitoindosides VII to X and beta-sitosterol as well as alkaloids (for example, ashwagandhine, cuscohygrine, tropine, pseudotropine, isopelletierine, and anaferine), a variety of amino acids (including tryptophan), and high amounts of iron [36]. A subset of these components (withanamides) has shown to scavenge free radicals generated during the initiation and progression of Alzheimer's disease. Neuronal cell death triggered by amyloid plaques was also blocked by withanamides [37]. Molecular modeling studies showed that withanamides A and C uniquely bind to active motif of beta-amyloid (Aβ 25-35) and prevent fibril formation [38]. Aqueous extracts of *W. somnifera* have been found to increase cholinergic activity, including increases in the acetylcholine content and cholineacetyl transferase activity in rats and this might partly explain the cognition-enhancing and memory-improving effects [39]. In addition to the reconstruction of pre- and post-synapses in the neurons, methanol extracts of *W. somnifera* reversed amyloid peptide-induced memory deficit in mice [40]. These in vivo effects of *W. somnifera* were maintained even after the discontinuance of the drug.

Conclusion

Interests in the use of different herbal products increase day by day. As several studies show that the uses of synthetic drugs have side effects, so there is a need of alternative source of drugs which have low or negligible side effects. Medicinal plants contain wide range of bioactive compounds which is an alternative of synthetic drug for the treatment of Alzheimer's disease. Medicinal plants can improve the quality of life of patients with AD and memory deficits. This review provides the information regarding the role of various medicinal plants against the Alzheimer's disease.

References

1. Francis PT, Plamer AM, Anape M, et al. (1999) The cholinergic hypothesis of Alzheimer's dieases:-A review of progress. J Neurol Neurosurg Psychiatry.

2. Herring A, Ambrée O, Tomm M, et al. (2009) Environmental enrichment enhances cellular Plasticity in transgenic mice with Alzheimer-like pathology. Exp Neurol 184-192.

3. Orhan I, Aslan M (2009) Appraisal of scopolamine-induced antiamnesic effect in mice and in Vitro antiacetylcholinesterase and antioxidant activities of some traditionally used Lamiaceae plants. J Ethnopharmaco 327-332.

4. Alistair B, Steve I (2009) Alzheimer's disease. Br Med J.

5. Joy PP, Thomas J, Mathew S, et al. (2001) Medicinal Plants. Tropical Horticulture 449-632.

6. Monograph (2004) *Withania somnifera*. Altern Med Rev 211-214.

7. Shinomol GK, Muralidharn, Bharat MM (2011) Exploring the role of 'Brahmi' (Bacopa monnieri And Centella asiatica) in brain function and therapy 33-49.

8. Singh HK, Dhawan BN (1982) Effect of Bacopa monniera Linn (Brahmi) extract on avoidance Responses in rat. JEthopharmacol 205-214.

9. Uabundit N, Wattanathorn J, Mucimapura S, et al. (2010) Cognitive enhancement and neuroprotective effects of *Bacopa monnieri* in Alzheimer's disease model. J Ethnopharmacol 26-31.

10. Bhattacharya SK, Bhattacharya A, Kumar A, et al. (2000)

Antioxidant activity of Bacopa monniera in rat frontal cortex, striatum and hippocampus. Phytother Res 174-179.

11. Limpeanchob N, Jaipan S, Rattana karuna S, et al. (2008) Neuroprotective effect of *Bacopamonnieri* on beta-amyloid-induced cell death in primary cortical culture. J Ethnopharmacol 112-117.

12. Dhanasekaran M, Holcomb LA, Hitt AR, et al. (2009) *Centella asiatica* extract selectively decreases amyloid beta levels in hippocampus of Alzheimer's disease animal model. Phytother Res 14-19.

13. Cervenka F, Jahodar L (2006) Plant metabolites as nootropics and cognitives. Ceska Slov Farm 219-229.

14. Gujran S, Singh SP, Pal R, et al. (2007) An extract of *Commiphora whighitti* with lipid lowering properties, has protective effects against streptozotocin induced memory deficits in mice. Pharmacol Biochem Behav 8: 797-805.

15. Lannert H, Hoyer S (1998) Intracerebroventricular administration of streptozotocin causes long-term diminutions in learning and memory abilities and in cerebral energy metabolism in adult rats. Behav Neurosci 112: 1199-1208.

16. Aggarwal B, Hari kumar K (2009) Potential therapeutic effects of *Curcumin*, the anti-inflammatory agent, against neurodegenerative, cardiovascular, pulmonary, metabolic, autoimmune and neoplastic diseases. Inter J Biochem Cell Biol 41: 40-59.

17. Mishra S, Palanivelu K (2008) The effect of *Curcumin* (turmeric) on Alzheimer's disease: An Overview. Ann Indian Acad Neuro l 11: 13-19.

18. Luo Y (2006) Alzheimer's disease, the nematode Caenorhabditis elegans, and *Ginkgo biloba* leaf extract. Life Sciences 2066-2072.

19. Winter E (1991) Effects of an extract of *Ginkgo biloba* on learning and memory in mice. Pharmacol Biochem Behav 109-114.

20. Stackman RW, Eckenstein F, Frei B, et al. (2003) Prevention of age-related spatial memory deficits In a transgenic mouse model of Alzheimer's disease by chronic *Ginkgo biloba* treatment. Exp Neurol 510-520.

21. Das A, Shanker G, Nath C, et al. (2002) A comparative study in rodents of standardized extracts of Bacopa monniera and Ginkgo biloba: anticholinesterase and cognitive enhancing activities. Pharmacol Biochem Behav 893-900.

22. Rekha S, Parvathi (2012) Evaluation of phytochemical constituents of the roots of Licorice, Indian ginseng, Indian madder and Indian Sarasaparilla. Biochemistry 3: 357-361.

23. Dhingra D, Parle M, Kulkarni S (2004) Memory enhancing activity of *Glycyrrhiza glabra* in mice. J Ethnopharmacol 91: 361-365.

24. Julio R, Dang H, Gong M, et al. (2007) Aqueous and hydroalcoholic extracts of black maca (*Lepidium meyenii*) improve scopolamine-induced memory impairment in mice. Food Chem Toxico 45: 1882-1890.

25. Wang R, Yan H, Tang X (2006) Progress in studies of huperzine A, a natural cholinesterase inhibitor from Chinese herbal medicine. Acta Pharmacol Sin 1: 1-26.

26. Rubio J, Qiong W, Liu X, et al. (2011) Aqueous extract of black maca (*Lepidium meyenii*) on memory impairment induced by ovariectomy in mice. Evid Based Complement Alternat Med 2: 1-5.

27. Jae L, Kyung L, Beom J, et al. (2009) Inhibitory effect of ethanol extract of *Magnolia officinalis* and 4-O-methylhonokiol on memory impairment and neuronal toxicity induced by beta-amyloid. Pharmacol Biochem Behav 95: 31-40.

28. Hou YC, Chao PD, Chen YT (2000) Honokiol and magnolol increased hippocampal acetylcholine release in freely moving rats. Am J Chin Med 28: 379-384.

29. Dikalov S, Losik T, Arbiser J (2008) Honokiol is a potent scavenger of superoxide and peroxyl radicals. Biochem Pharmacol 76: 589-596.

30. Liou KT, Shen YC, Chen CF, et al. (2003) The anti-inflammatory effect of honokiol on neutriprils: Mechanism in the inhibition of reactive oxygen species production. Eur J Pharmacol 47: 19-27.

31. Singh SS, Pandey SC, Srivastava S, et al. (2003) Chemistry and medicinal Properties of Tinospora cordifolia (Guduchi). Indian J Pharmacol 83-91.

32. Williamson, M.E. (2002) Major Herbs of Ayurveda. Churchill Livingston, London, UK.

33. Russo A, Izzo AA, Cardile V, et al. (2001) Indian medicinal plants as antiradicals and DNA cleavage Protectors. Phytomedicine 125-132.

34. Monograph (2004) *Bacopa monniera*. Altern Med Rev 79-85.

35. Auddy B, Hazra J, Mitra A, et al. (2008) A standardized Withania somnifera extract significantly reduces stress-related parameters in chronically stressed humans: a double-blind randomized, Placebocontrolled study. J Am Nutraceut Assn 50-56.

36. Matsuda H, Murakami T, Kishi A, et al. (2001) Structures of withanosides I, II, III, IV, V, VI, and VII, new withanolide glycosides, from the roots of Indian *Withania somnifera* DUNAL and inhibitory activity for tachyphylaxis to clonidine in isolated guinea-pig ileum. Bioorganic Med Chem Lett 1499-1507.

37. Jayaprakasam B, Padmanabhan K, Nair MG (2010) Withanamides in *Withania somnifera* fruit protects PC-12 cells from beta-amyloid responsible for Alzheimer's disease. Phytother Res 859-863.

38. Kumar S, Harris RJ, Seal CJ, et al. (2012) An aqueous extract of *Withania somnifera* root inhibits amyloid beta fibril formation in vitro. Phytother Res 113-117.

39. Schliebs R, Liebmann A, Bhattacharya SK (1997) Systemic administration of defined extracts from *Withania somnifera* (Indian Ginseng) and Shilajit differentially affects cholinergic but not glutamatergic and GABAergic markers in rat brain. Neurochem Int 181-190.

40. Kuboyama T, Tohda C, Komatsu K (2005) Neuritic regeneration and synaptic reconstruction induced by withanolide A. Br J Pharmacol 961-997.

Citation: Arpita Roy (2017) A Review on Medicinal Plants for Alzheimers Disease. SF J Herb Med 1:1.

International Journal of Pure and Applied Mathematics
Volume 117 No. 20 2017, 881-886
ISSN: 1311-8080 (printed version); ISSN: 1314-3395 (on-line version)
url: http://www.ijpam.eu
Special Issue

ijpam.eu

A Robust Database Watermarking Algorithm using Bezier Cubic Curves

Manoj Kumar
Delhi Technological University, Delhi, 110042, INDIA
mkumarg@dce.ac.in

Om Prakash Verma
Delhi Technological University, Delhi, 110042, INDIA
opverma@dce.ac.in

Abstract—The piracy of digital assets including databases is usually based on insertion of digital watermarks. In this paper we present a new robust database watermarking scheme for copyright protection of relational databases. A cubic Bezier curve is used as watermark A secret key based watermark embedding scheme is used to embed the watermark in relational database. Cubic curve parameters along with many other secret parameters and secret key makes this scheme very secure in comparison to other existing schemes. This scheme is resilient against wide variety of attacks such as database modifications, insertion of new records, deletion of existing records because these attacks do not destroy the watermark completely. Though extracted watermark sometimes contains too much noise but still cubic curve is visible and identifiable. Proposed scheme can use single or multiple attributes for embedding watermark.

Index Terms—Bezier cubic curves, curve control points, message digest, Message Authentication Code (MAC)

I. Introduction

Digital watermarking technology has been widely used as an effective method to achieve copyright protection, for the image, video, audio and other areas. The digital watermarking technology on relational databases has gradually increased, several relational databases watermarking algorithms have appeared, which provide necessary copyright protection for relational databases. Nowadays, sharing information online is an important activity for business and research. It also involves buying/selling of databases. Sharing of data related to sales, surveys, weather, stock markets, power consumption, consumer behavior, medical tests, scientific experiments, etc. is frequently required. Consequently ,there is a great need for providing security of databases to discourage illegal copying and distribution in today's internet-based application environment [1]. In this context, proof of ownership and tamper-proof-transportation of the databases are the most challenging issues these days[2]. However, the existing works do not fully consider how to utilize the human vision and other physiological characteristics to enhance the robustness of relational data watermarks. In this paper, the watermark used is a curve, an identifiable shape, comparing logos or small images which are usually not identifiable if distorted badly.

The remainder of this paper is organized as follows: section II describes some related work in database watermarking. Section III elaborated proposed work describing embedding and extraction process. Section IV analyzes experimental results. and finally, we conclude with a summary and discussions in section V.

II. Related Work

The groundbreaking study in this area was conducted by R. Agrawal and R. Sion in 2002 [3,4]. In 2003, X.M. Niu proposed that a meaningful string could be inserted into the relational database as the watermark [5]. Y. J. Li [6] raised a method of inserting watermark by changing the order of relational data index and keeping the physical location or data values unchanged to impair its use. While the index is additional information outside of relational data content, watermark information could be completely lost if the index of relational table is reestablished or deleted. Y. Zhang converted image information into watermark cloud droplets according to D.Y. Li's cloud model idea and then embedded it into relational data [7]. When being extracted, the cloud droplet should be compared with original copyright image. G. Gupta utilized difference expansion and Lowest-Effective-Bit on integers to achieve embedding and blind detection of the watermark. however, this method is restrictively used for integer data [8]. Many other watermark workers also make a lot of efforts to promote the development of database watermarking, [9,10,11,12] yet there are still many shortcomings in the said study. A novel approach for tamper detection, analysis and recovering original data back by adding a set of bits to the original data that acts as a watermark was proposed in [13]. The proposed system provides a strong validation and recovery scheme to maintain data security and integrity. Another scheme for embedding watermark information Reversible Watermarking uses the most irrelevant feature [14]. There is scope to apply this scheme to preserve data ownership of dataset which are used for supervised learning. Features importance depends on the relevance between the feature and the class feature in such datasets. Various attacks like insertion, deletion and modification are then performed to check the robustness of the watermark. The watermark robustness is too weak to resist various conventional database operations and

illegal watermark attacks, such as selection, addition, modification and so on. As a result, improving the robustness of database watermarking is a challenging and yet significant work.

II. Proposed Work

The proposed system makes use of a Cubic Bezier Curve according to the parameters provided and then hides the cubic curve in the database by using an embedding algorithm. Only floating point attributes are used to hide watermark information. Watermark information is hidden in the fractional part of the floating point attribute. Here we assume that the attribute used for hiding the watermark are such that small changes in some of their values are acceptable [3]. All floating point attributes are not used for watermarking. Proposed algorithm can be implemented using one, two or three attributes. Embedding algorithm utilizes a parameter γ and a secret key K which provides control for the hiding and recovery processes restricting extraction by those who do not possess the key or do not have access to it.γcontrols the embedding density by choosing one tuple out of α tuples in the database for hiding one point of the cubic curve. Bezier cubic curve is defined using four points P_0, P_1, P_2, and P_3. P_0 is the starting point for curve, and P_3 is the ending point of the curve. Line joining P_0 to P_1 defined the tangent on curve at point P_0, whereas line joining P_2 to P_3 defines tangent on curve at point P_3. Thus four points control the location and shape of the curve. Each point P_i is defined as (P_{ix}, P_{iy}). The algorithm makes use of security function Message Authentication Code (MAC). This is key base hashing algorithm H=MAC(P,K), which generates a MAC value for some input P based on a secret key *K*.

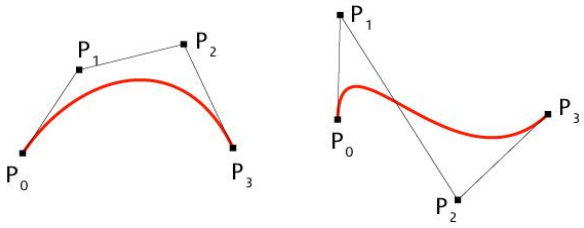


Fig. 1. Bezier Cubic Curve with four control points controlling shape of curve.

A. Embedding Process

Suppose that we are watermarking a database relation R whose scheme is R(P,A_0, . . . , A_{v-1}), where P is the primary key attribute.

Following are some parameters used in proposed algorithm:

- Secret key *K*, parameters γ, *i*, *j*, *k*, points P_0, P_1, P_2, and P_3 are known only to the owner of the database.
- All points P_0, P_1, P_2, and *P3* are normalized to have values between *0* and *1*.
- $0 \leq t \leq 1$and all computed *x(t)* and *y(t)* have values between *0* and *1*.

Table.1List of Parameters and symbols

η	Number of tuples in relation
ν	Number of attributes in relation
γ	Density control parameter
i, j	Attribute A_i for embedding *x(t)* value and A_j for embedding *y(t)* value.
K	A secret key
ω	Actual number of tuples marked
P_0, P_1, P_2, P_3	Four points controlling Cubic curve shape.
k	k-th byte of hash is used to derive parameter value t for the curve

```
1)  ω = 0;
2) for each tuple r ∈ R do
3)     compute hash H = MAC( r.P || K )
4)     if (H mod γ ) = 0) then // mark this tuple
5)          derive  t  from k-th byte of  H
6)          compute x(t) and y(t) from curve equation
7)          replace fractional part of r.A_i with x(t)
8)          replace fractional part of r.A_j with y(t)
9)          ω=ω + 1
10) return R
```

Fig.2. Watermark Insertion Algorithm: Embedding Process

- The curve which is to be hidden in the database is selected according to four parameters known as controlling points: $P_0(P_{0x},P_{0y})$, $P_1(P_{1x},P_{1y})$, $P_2(P_{2x},P_{2y})$, *and* $P_3(P_{3x},P_{3y})$.
- The embedding process includes hiding the coordinates of the points lying on the cubic curve in the selected tuples in the database.
- The tuple is selected based on the secret key and value of γ. For each tuple, the primary key of that tuple and secret key are concatenated and its hash is calculated. If the modulus γ of that hash value is zero then that tuple is selected to hide the curve points.
- *k-th* byte of the calculated hash value is normalized to a value between *0* and *1*. This normalized value is denoted by *'t'* and is used to calculate the coordinates of a point lying on the curve. The value of *'t'* is put into the equation of the cubic curve which gives the x and y co-ordinates of a point lying on the curve:

$$x(t) = (1-t)^3P_{0x} + 3t(1-t)^2P_{1x} + 3t^2(1-t)^3P_{2x} + t^3P_{3x}$$

$$y(t) = (1-t)^3P_{0y} + 3t(1-t)^2P_{1y} + 3t^2(1-t)^3P_{2y} + t^3P_{3y}$$

Two attributes of the selected tuple- A_i and A_j are used to hide the x and y coordinates calculated above by replacing the decimal part of A_i and A_j with the x and y coordinates respectively.

B. Extraction Process

- Four curve parameters: P_0, P_1, P_2 and P_3, which have been used to select the curve during the embedding process, are required to extract the hidden curve from the database.
- The tuple is selected based on the secret key and value of γ. For each tuple, the primary key of that tuple and secret key are concatenated and its hash is

calculated. If the modulus γ of that hash value is zero then that tuple has the hidden curve points.

- $i^{th}$and j^{th} attribute of the selected tuple- A_i and A_j are used to extract the hidden x and y coordinates from the decimal part of A_i and A_j respectively.
- The eleventh byte of the calculated hash value is normalized to a value between *0* and *1*. This normalized value is denoted by *'t'*and is used to calculate the coordinates of a point lying on the curve. The value of *'t'* is used in the equation of the cubic curve to compute x and y coordinates of a point lying on the curve:

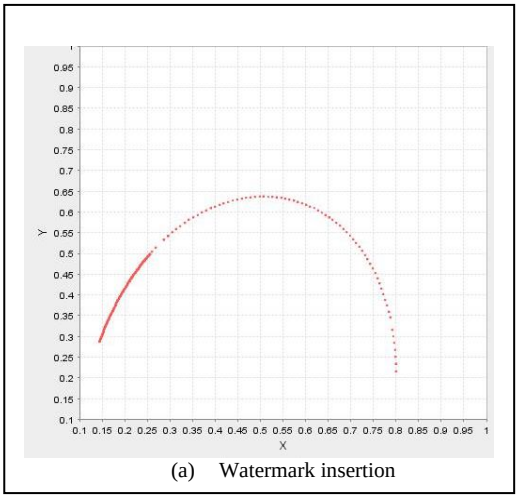
$$x(t) = (1-t)^3 P_{0x} + 3t(1-t)^2 P_{1x} + 3t^2(1-t)^3 P_{2x} + t^3 P_{3x}$$

$$y(t) = (1-t)^3 P_{0y} + 3t(1-t)^2 P_{1y} + 3t^2(1-t)^3 P_{2y} + t^3 P_{3y}$$

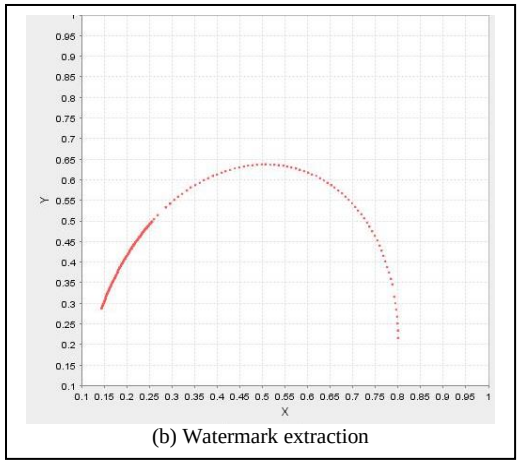
- Then the calculated curve points are compared with the extracted curve points. If they are same then this curve point is a match.

III. Results

The proposed watermarking scheme was applied on a database containing 10,000 records. A two-dimensional cubic curve was used for watermarking. For two-dimensional cubic curves, only two attributes were selected for inserting watermark in each tuple. Control points for cubic curve was used are $P_0(0.1,0.1)$, $P_1(0.2,0.8)$, $P_2(0.8,0.8)$, and $P_3(0.8,0.2)$.



(a) Watermark insertion



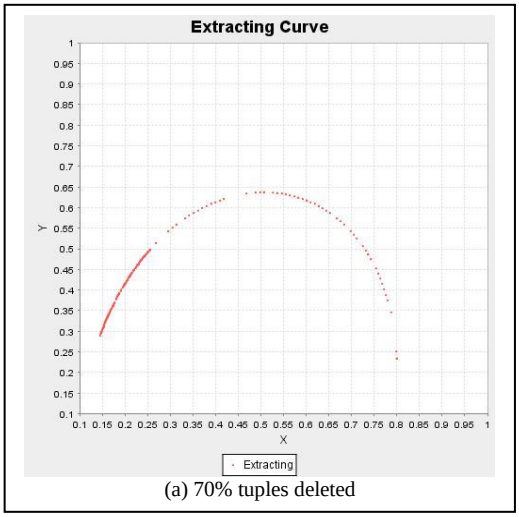
(b) Watermark extraction

Density control parameter γused here is *10* means only 10% tuples are selected for watermarking. Watermark extracted was exactly similar to watermark inserted.

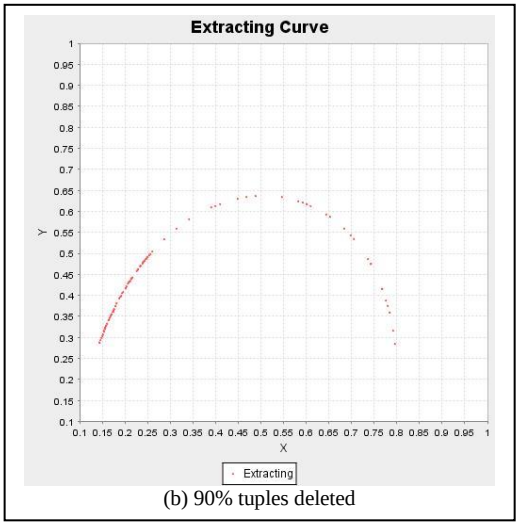
Attacks on watermarked database: Experimental setup is used to observe the effect of various types of database modification operations on watermark identification. Various type of operations which modify database contents are DELETE, UPDATE, and INSERT.

A. Deletion Attacks:

Effect of deleting some of the tuples from a database will not affect identification of extracted watermark. As we have inserted watermarks in only 10% of total tuples, deleting some of the tuples from database will only delete a very small number of those tuples having watermarking information. Deleting those tuples containing watermarking information will only eliminate some points on extracted cubic curve. Even if 90 percent of the points on the cubic curve are removed, the shape of the curve is still recognizable.



(a) 70% tuples deleted

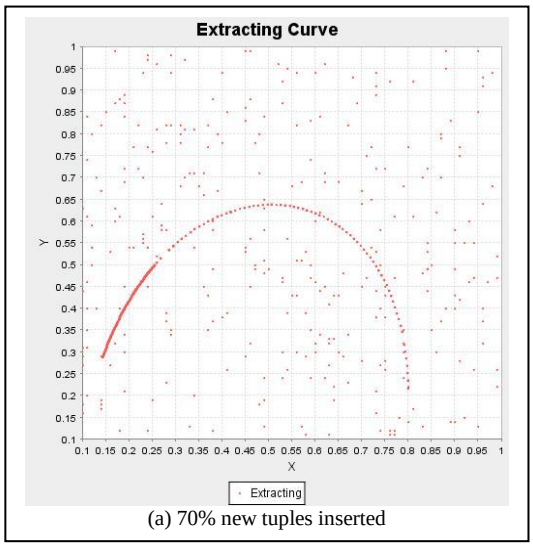


(b) 90% tuples deleted

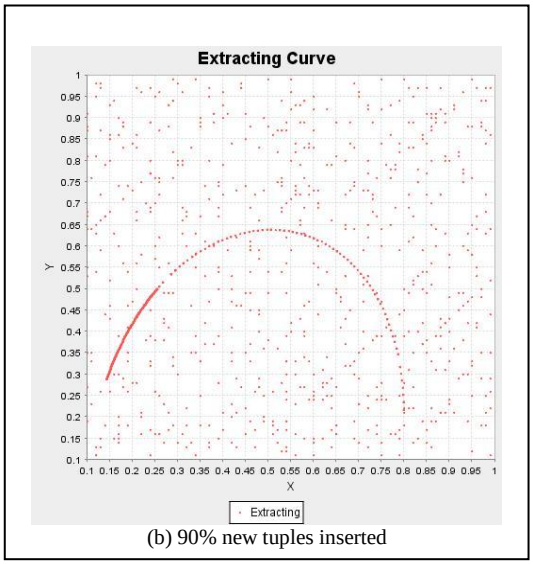
Fig.4. Watermark extraction results after deletion attacks

A. Insertion Attacks

Watermarking scheme is robust against insertion attack according to the algorithm. New records inserted actually do not have any watermark hidden in attributes. Watermark extraction process to extract watermark information from these tuples will extract invalid watermark which looks like noise in extracted pattern. The level of noise will increase as we increase the percentage of newly inserted tuples. But original tuples which contain watermark are not disturbed and all watermark information we have embedded earlier are extracted. Therefore, extracted watermark will contain all the watermark information along with some noise representing invalid watermarks detected in newly inserted tuples.



(a) 70% new tuples inserted

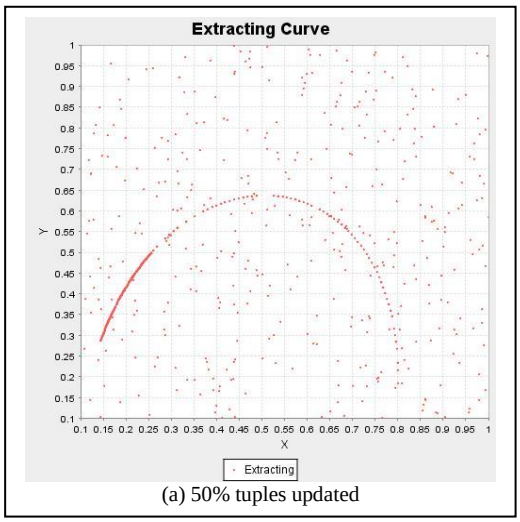


(b) 90% new tuples inserted

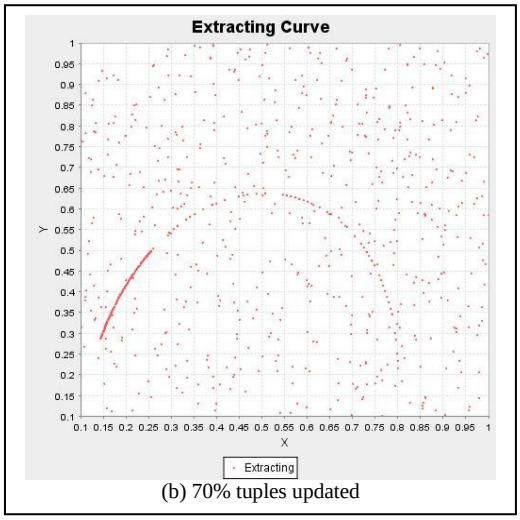
Fig. 5.Watermark extraction results after insertion attacks

C. Update Attacks:

Updating a tuple where a watermark is embedded will create a noise during the extraction process. As we have used small percentage of tuples for watermarking, chances of updating an attribute of a tuple which is watermarked are very low. So only a few tuples having watermarks will be updated and their watermark will not match during the extraction process. Thus, very few noise marks will be created when a fraction of tuples are updated. In extracted watermark, the shape of the curve can be recognized easily.



(a) 50% tuples updated



(b) 70% tuples updated

Fig. 6. Watermark extraction results after updation attack

Comparing the results with image-based algorithm for watermarking relational databases [9], it is observed that in image based algorithm 70-80 percent updation attack destroyes the embedded image beyond recognition. Where as in proposed method curve can be recognized even after updation of 90 percent of the tuples. We can easily distinguish between valid curve points and noise in extracted curve image. Similar results were observed in

case deletion attack. When 80 percent tuples are deleted from image based watermarked database, extracted watermark image is too much distorted. In proposed method, curve is still recognizable as deletion of tupples only reduces density of points on curve.

IV Conclusion

We presented a new approach using Bezier curves and discussed the insertion and extraction watermarking algorithms in details. Usually, other database watermarking algorithms alter properties of tuples. Later during the extraction phase, we count a number of tuples having matching property. Exact matching of the watermark is achieved if 100 percent watermarked information is extracted. It means that we are able to extract the correct watermark from all tuples where watermarks have been inserted earlier. If due to some alteration in the database, we are unable to extract complete watermark information, then a threshold is usually set on the percentage of matching watermarked tuples. Due to this, if the database is altered beyond the acceptable limits, we are unable to prove the existence of the watermark in the database. In the proposed scheme, extracted watermark is identifiable even if a small fraction of the watermark is extracted. Our goal has been to ensure that our watermarking approach is robust for Watermarking Relational Databases. Our approach has been discussed analytically in terms of robustness, however, the quantitative evaluation is to be done. In fact, evaluating watermarks for Relational Database is a challenge and requires further consideration. However, the persistency of the watermark after both malicious and benign updates, as a sub-problem, might be evaluated by acquiring access to a log of user queries on a particular database over a reasonably long period of time. Then run the log on the watermarked database and observed whether the watermark detection algorithm confirms the presence of the watermark in the database.

References

[1] R. Chamlawi, A. Khan, I. Usman, Authentication, and recovery of images using multiple watermarks, Computers & Electrical Engineering 36 (2010), 578–584.

[2] R. Sion, M. Atallah, and S. Prabhakar, Rights Protection for Relational Data, IEEE Transactions on Knowledge and Data Engineering, vol. 16, no.12, (2004), pp. 1509-1525.

[3] R. Agrawal and J. Kiernan, Watermarking Relational Databases, Proc. VLDB'02, (2002), pp. 155-166.

[4] R. Sion, M. Atallah, and S. Prabhakar, On Watermarking Numeric Sets, Proc. IWDW, (2002), pp. 12-15.

[5] X. Niu, et al., Watermarking Relational Databases for Ownership Protection, Chinese Journal of Electronics (in Chinese), vol. 31, no. 12A, (2003), pp. 2050-2053.

[6] Y. J. Li, V. Swarup and S. Jajodia, Fingerprinting Relational Databases: Schemes and Specialties, IEEE Transactions on Dependable Secure Computing, vol. 2, no. 1, (2005), pp. 34-45.

[7] Y. Zhang, X. M. Niu and D. N. Zhao, A Method of Protecting Relational Databases Copyright with Cloud Watermark, Proc. World Academy of Science, Engineering and Technology, vol. 3, (2005), pp. 68-72.

[8] G. Gupta and J. Pieprzyk, Reversible and Blind Database Watermarking Using Difference Expansion, International Journal of Digital Crime and Forensics, vol. 1, no. 2, (2009), pp. 42-54.

[9] Zhongyan Hu,Zaihui Cao, Jianhua Sun, An image-based algorithm for watermarking relational databases, In Proc of IEEE International Conference on Measuring Technology and Mechatronics Automation, 2009.

[10] Franco-Contreras J, Coatrieux G, Cuppens-Boulahia N, Cuppens F, Roux C. Robust lossless watermarking of relational databases based on circular histogram modulation. IEEE T. Inf. Foren. Sec. 2014; 9(3): 397–410.

[11] Deshpande A. and Gadge J., New Watermarking Technique for Relational Databases, IEEE International Conference on Emerging Trends in Engineering and Technology, Nagpur, 2009, PP 664-669.

[12] Shehab M., Bretino E., and Ghofoor A., Watermarking Relational Databases using Optimization Based Techniques, IEEE transactions on Knowledge and Data Engineering, 2008, vol 20, no 1, PP 116-129.

[13] Unnikrishnan K., Pramod K.V., Dynamic Prediction Based Watermarking for Temporal Relational Databases, International Conference on Data Science and Engineering (ICDSE)-2016.

[14] Madhuri V. Gaikwad, Roma A. Kudale, Robust Reversible Watermarking For Relational Database, IEEE International WIE Conference on Electrical and Computer Engineering (WIECON-ECE) 19-21 December 2016, AISSMS, Pune, India.

This article has been accepted for publication in a future issue of this journal, but has not been fully edited. Content may change prior to final publication. Citation information: DOI 10.1109/TII.2018.2803748, IEEE Transactions on Industrial Informatics
Manuscript No. TII-17-2578.R1

ANFIS Based Add-on Controller for Unbalance Voltage Compensation in Low Voltage Microgrid

Jaipal Saroha[1], *Member, IEEE*, Mukhtiar Singh[2], *Member, IEEE* and D. K. Jain[3], Sr., *Member, IEEE*

***Abstract*— This paper presents an adaptive add-on controller for the unbalance voltage compensation in low voltage microgrid (LVMG) constituting multiple voltage source converters (VSC) based distributed generation. Since, the VSC based LVMG is almost inertia-less system and any kind of load variations have very significant impact on voltage profile, which is highly undesirable. Presence of unbalance load at point of common coupling (PCC) further exaggerates the problem. In order to mitigate the negative effect of unbalance load, an ANFIS based add on control loop has been added in to the conventional VSC control. Here, the add-on controller sets the reference current gains equivalent to voltage unbalance factor. These reference current gains obtained from add-on controller are added to the output of voltage control loop to set the modified reference current for inner current control loop. The extensive simulation results with experimental validation have been provided to validate the proposed control algorithm.**

***Index Terms*— Droop control, micro-grid, VSI, ANFIS control, Voltage unbalance.**

I. Introduction

In the recent time, the concept of microgrid is gaining lot of popularity worldwide due to their ability of working independently in islanding mode. The microgrid also allows the optimal utilization of available renewable energy sources (RES) in a coordinated way in order to feed remotely placed isolated locations where grid is not readily available. Thus, the microgrid is expected to work both in grid tied mode and off grid (islanded) mode. In grid tied mode, the grid voltage sets the reference for DG interfacing VSC's and chances of internal conflict among different VSC's are very rare. However, in islanded mode of operation, the different VSC's are needed to be controlled in such a way that the load demand must be shared by all interconnected VSC's in proportion to their individual rating [1]-[4]. Therefore, the VSC's in microgrid may either be controlled in centralised manner with dedicated communication channel between them or they may be controlled individually with droop control which may require low bandwidth communication channel or no communication channel at all [5]- [7]. The later one is more preferable; as it is easily implementable with enhanced security and reliability. The traditional droop control method have some issues related to the inaccuracy in determining the power to be shared by individual DG and deviation in voltage at PCC due to fluctuation as well as unbalance in load demand [8]-[11].

The manuscript received on Nov. 01, 2017, revised on Dec. 22, 2017 and finally got accepted for publication on Jan. 14, 2018.

[1] Department of Instrumentation, Kurukshetra University, Kurukshetra 136119, Haryana, India (sarohajp@yahoo.com).

[2] Department of Electrical Engineering, Delhi Technological University, Delhi 110042, India (smukhtiar_79@yahoo.co.in).

[3] Department of Electronics and Communication Engineering, Deenbandhu Chhotu Ram University of Science and Technology, Murthal 131039, Haryana, India (jaindk66@gmail.com).

To mitigate the aforementioned disadvantages of conventional droop control, several control algorithms have been proposed by researchers all over the world. As a primary control measure, virtual impedance and negative-sequence impedance methods have been proposed to share the unbalance load demand by various DG's [12]-[13]. In such kinds of methods, a measurement unit is required to transmit the negative-sequence component of unbalanced load to all interconnected DG's. Moreover, any mismatch in actual impedance of feeder due to connected transformer, filtering inductor or capacitor and cable connection may result in inaccurate power sharing among DG's. Therefore, within a control loop the virtual impedance adjusts the equivalent inverter impedance to have proper power sharing among DG's [14]-[15]. In [16] the positive, negative and zero sequence components of the VSC current and the Voltage at PCC have been controlled separately. However, setting the control limits for all the three sequence current components is very cumbersome task. A hierarchical control based centralised secondary control approach has been presented in [7], and [17]. However, such control scheme requires dedicated communication channel and also eliminates the major advantages of plug & play capability of microgrid.

In proposed work, a novel ANFIS based add-on controller has been proposed to compensate the ill effect of dynamically varying unbalance load. The capability of adaptive neuro fuzzy inference systems (ANFIS) are well known as it has both the capabilities of handling the uncertainties like fuzzy system and learning from processes like neural system [18]-[21]. Therefore, the difficulty in settling the control limit under dynamic conditions is adaptively handled by ANFIS controller. In proposed approach, the unbalance voltage factor is determined by extracting -ve sequence voltage component. This -ve sequence voltage component is fed to ANFIS controller, which in turns yields the equivalent unbalance current component. The equivalent unbalance current component is added to the output of outer voltage control loops in order to have modified reference current for the inner current control loops.

II. System Description

The main purpose of microgrid is to serve the local load connected at distributed level even in the absence of main grid. Thus, the microgrid must have its own generation, transmission and distribution network confined to a much smaller geographical area in comparison to main grid. A typical

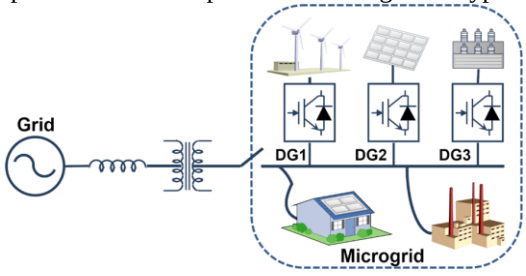


Fig. 1 Microgrid

1551-3203 (c) 2018 IEEE. Personal use is permitted, but republication/redistribution requires IEEE permission. See http://www.ieee.org/publications_standards/publications/rights/index.html for more information.

This article has been accepted for publication in a future issue of this journal, but has not been fully edited. Content may change prior to final publication. Citation information: DOI 10.1109/TII.2018.2803748, IEEE Transactions on Industrial Informatics

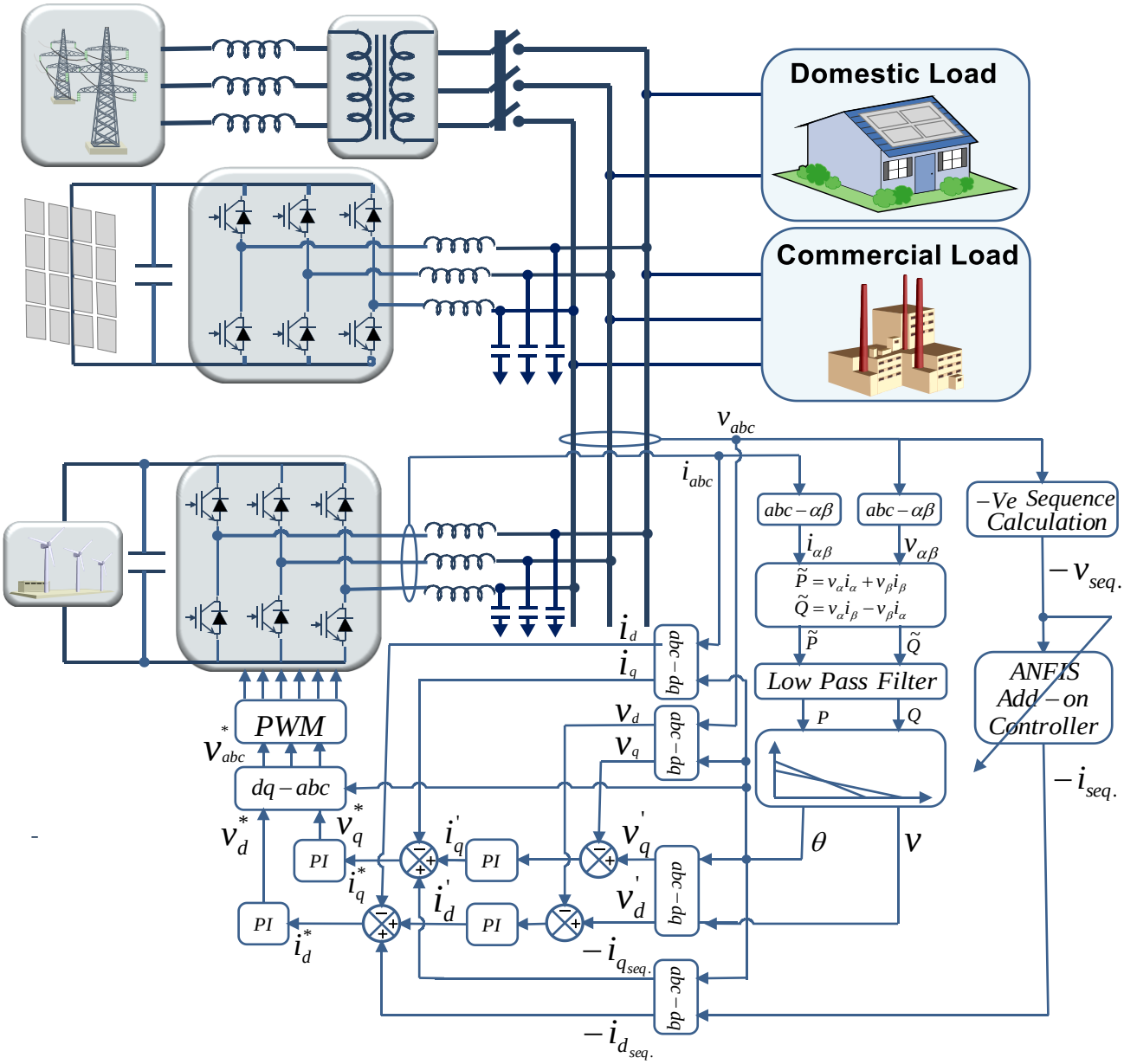


Fig. 2 Microgrid Control Description

microgrid may have several DG's operating in parallel and interfaced by power electronics based VSC's forming an AC network. A simpler form of microgrid is shown in Fig. 1. The microgrid mainly comprises RES based generation like solar photovoltaic system, wind turbine, and small back up in the form of battery energy storage system. The load may be three phases as well as single phase which may have both balanced and unbalanced profile.

Since, the microgrid is almost inertia-less system and any kind of variation in load conditions have negative impact on voltage pattern. Thus, any kind of unbalance load may lead to unbalance in supply voltage profile. Therefore, the VSC's connected in parallel are required to be controlled in such a way that they supply unbalance current in compliance of load demand without affecting the desired sinusoidal and balanced voltage profile. This enables all the parallel connected DG's to share the load demand in proportion to their rating just like a conventional droop control without having any significant circulating current among themselves.

III. Control Design

The detailed description of the overall system with proposed control approach is shown in Fig. 2. The three-phase system with floating neutral have been considered for the proposed microgrid. Since, the microgrid is a small system with unbalance load, the supply voltage at PCC is never easy to be maintained as a perfect set of three-phase balanced voltages. Therefore, the supply voltage is bound to have all the three sequence components (+ve seq., -ve seq., and Zero seq.). Due to the absence of neutral wire, the zero sequence compo nent has not been considered. However, for voltage unbalance compensation purpose, the -ve sequence voltage has been extracted. The -ve sequence component is further minimised using ANFIS based add-on controller.

1551-3203 (c) 2018 IEEE. Personal use is permitted, but republication/redistribution requires IEEE permission. See http://www.ieee.org/publications_standards/publications/rights/index.html for more information.

This article has been accepted for publication in a future issue of this journal, but has not been fully edited. Content may change prior to final publication. Citation information: DOI 10.1109/TII.2018.2803748, IEEE Transactions on Industrial Informatics
Manuscript No. TII-17-2578.R1

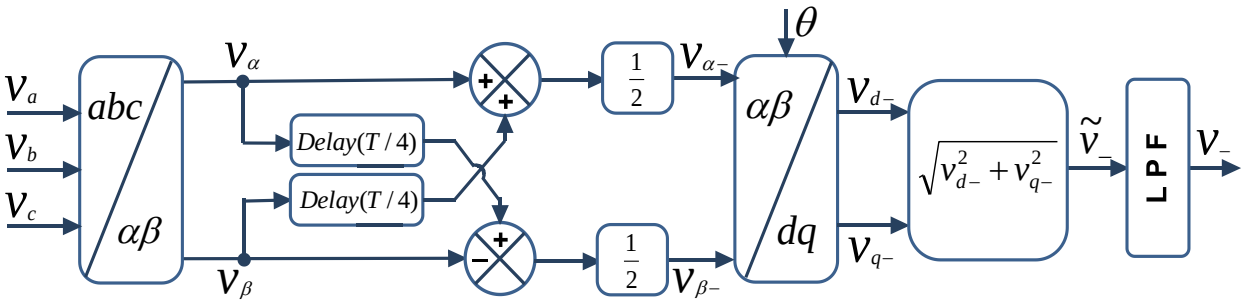


Fig. 3 -Ve Sequence Voltage Extraction

A. -Ve sequence Voltage Extraction

The unbalance phenomenon in power system network is one of the complex things to explain. The symmetrical components method is one of the most commonly used tool to determine the type of asymmetry or distortion in system voltages. The only issue with symmetrical component method is that it uses phasors as input instead of time domain signals and some transformation is required in order to extract desired sequence component out of the rotating space vector. Several transformations have been developed to express the unbalance voltages mathematically. Clarke's and Park's transformations are most commonly used for voltage regulation as well as control implementation. However, under unbalance conditions the -ve sequence component introduces 2nd order harmonics in the transformed set of voltages. Therefore, the Clarke's and Park's transformations need to be redefined in order to extract the -ve sequence component for voltage regulation purpose.

The voltage equations of three-phase system without neutral wire may be written in terms of +ve and -ve sequence components as given below:

$$v_a = v_p \cdot \cos(\omega t) + v_n \cdot \cos(-\omega t) \quad (1)$$

$$v_b = v_p \cdot \cos(\omega t - \tfrac{2\pi}{3}) + v_n \cdot \cos(-\omega t + \tfrac{2\pi}{3}) \quad (2)$$

$$v_c = v_p \cdot \cos(\omega t + \tfrac{2\pi}{3}) + v_n \cdot \cos(-\omega t - \tfrac{2\pi}{3}) \quad (3)$$

On applying Clarke's transformation, the *abc-αβ* equations may be written as

$$v_\alpha = v_p \cdot \cos(\omega t) + v_n \cdot \cos(\omega t) = v_{\alpha+} + v_{\alpha-} \quad (4)$$

$$v_\beta = v_p \cdot \sin(\omega t) - v_n \cdot \sin(\omega t) = v_{\beta+} + v_{\beta-} \quad (5)$$

Where $v_{\alpha+}$ and $v_{\beta+}$ are +ve sequence components and $v_{\alpha-}$ and $v_{\beta-}$ are -ve sequence components.

On assuming that the symmetrical components remain constant for at least a quarter of cycle, the equations (4) and (5) may be written as

$$v_{\alpha+}(t) = \frac{1}{2}\left(v_\alpha(t) - v_\beta\left(t - \frac{T}{4}\right)\right) \quad (6)$$

$$v_{\beta+}(t) = \frac{1}{2}\left(v_\alpha\left(t - \frac{T}{4}\right) + v_\beta(t)\right) \quad (7)$$

$$v_{\alpha-}(t) = \frac{1}{2}\left(v_\alpha(t) + v_\beta\left(t - \frac{T}{4}\right)\right) \quad (8)$$

$$v_{\beta-}(t) = \frac{1}{2}\left(v_\alpha\left(t - \frac{T}{4}\right) - v_\beta(t)\right) \quad (9)$$

These -v sequence components as derived in equation (8) and (9) are further transformed into rotating reference frame (Park's transformation) in order to extract the -ve sequence equivalent component as shown in Fig. 3.

B. Design of ANFIS Based Add-on Controller

The main aim of proposed controller is to maintain -ve sequence voltage to zero so that balanced set of three-phase voltages could be obtained at PCC while feeding an unbalance load. Under the unbalance dynamic load conditions, the -ve sequence voltage may have lot of fluctuations and it is very tedious task to set the optimal gains of conventional *PI* controller regulating the voltage unbalance. Therefore, an ANFIS based add on controller is designed which adaptively sets its structural gains according to the operating conditions.

Takagi-Kang-Sugeno fuzzy model based ANFIS controller having 1:3:3:3:1 architecture with single input and single output has been used. The proposed ANFIS architecture has been adopted from our previous publication [22]. Therefore, the proposed ANFIS controller have five layers, where the first layer is known as fuzzification layer and in this layer the -ve sequence voltage is fuzzified with the help of three membership functions. Here, trapezoidal and triangular functions are used where the coefficients of the equations representing

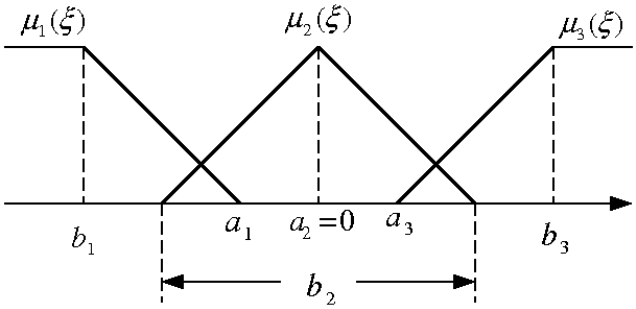


Fig. 4. Fuzzy Membership Functions.

1551-3203 (c) 2018 IEEE. Personal use is permitted, but republication/redistribution requires IEEE permission. See http://www.ieee.org/publications_standards/publications/rights/index.html for more information.

This article has been accepted for publication in a future issue of this journal, but has not been fully edited. Content may change prior to final publication. Citation information: DOI 10.1109/TII.2018.2803748, IEEE Transactions on Industrial Informatics
Manuscript No. TII-17-2578.R1

these functions are continuously updated with change in input. The trapezoidal functions as shown in Fig. 4 can expressed mathematically as under:

$$\mu_{A_1}(\xi)=\begin{cases}1 & \xi \le b_1\\ \dfrac{\xi-a_1}{b_1-a_1} & b_1 \langle \xi \langle\ a_1\\ 0 & \xi \ge a_1\end{cases} \tag{10}$$

$$\mu_{A_2}(\xi)=\begin{cases}1-\dfrac{\xi-a_2}{0.5b_2} & |\xi-a_2| \le 0.5b_2\\ 0 & |\xi-a_2| \ge 0.5b_2\end{cases} \tag{11}$$

$$\mu_{A_3}(\xi)=\begin{cases}0 & \xi \le a_3\\ \dfrac{\xi-a_3}{b_3-a_3} & a_3 \langle \xi \langle\ b_3\\ 1 & \xi \ge b_3\end{cases} \tag{12}$$

where the value of parameters $\{a_i, b_i\}$ changes with the change in error and accordingly generates the linguistic value of each membership function. Parameters in this layer are referred as *premise parameters* or *precondition parameters*. The

The second layer known as multiplication layer pass overs the signals to third layer as there is only one input at each node. In third layer, the signals are normalized. The fourth layer is also known as consequent layer, where all the parameters are again updated as per the variations. The fifth layer is simply an output layer where all the signals coming from various nodes of fourth layer are summed up. The complete diagram of ANFIS architecture is shown in Fig. 5.

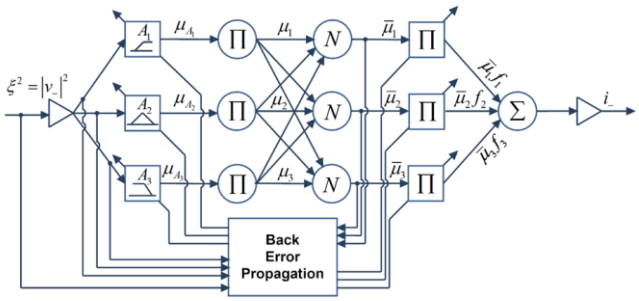


Fig. 5 ANFIS Architecture

C. Training of ANFIS Architecture

The -ve sequence voltage component itself has been taken as error and accordingly ANFIS is tuned to minimize this error. Here, the gradient descent method is used where the weights are updated by propagating the error from output layer to input layer. This process of updating the weights is commonly known as backpropagation, where the weights are tuned in two stages: pre-condition tuning (First layer) and consequent tuning (Fourth layer). The square of -ve sequence voltage component is taken as objective function.

$$\xi^2 = (0 - v_-)^2 = |v_-|^2 \tag{13}$$

(a). Precondition parameter tuning: Here, it is pertinent to mention that the Precondition parameters are tuned to update the fuzzy membership functions. The change in precondition parameter and error function are co-related as

$$\Delta a_{A_i} = -\eta \frac{\partial \xi^2}{\partial a_{A_i}} \qquad i = 1,2,3. \tag{14}$$

Where η is the learning rate. The updated value of the consequent parameter is written as

$$a_{A_i}(n+1) = a_{A_i}(n) + \Delta a_{A_i} \qquad i = 1,2,3. \tag{15}$$

or

$$a_{A_i}(n+1) = a_{A_i}(n) - \eta \frac{\partial \xi^2}{\partial a_{A_i}} \qquad i = 1,2,3. \tag{16}$$

Here the partial derivative term in equation (16) may be found by the differentiation chain rule as follows:

$$\frac{\partial \xi^2}{\partial a_{A_1}} = \frac{\partial \xi^2}{\partial V_-} \cdot \frac{\partial V_-}{\partial i_-} \cdot \frac{\partial i_-}{\partial \bar{\mu}_1} \cdot \frac{\partial \bar{\mu}_1}{\partial \mu_{A_1}} \cdot \frac{\partial \mu_{A_1}}{\partial a_{A_1}} \tag{17}$$

where

$$\frac{\partial \xi^2}{\partial V_-} = -2(0 - V_-) = -2\xi\ ; \tag{17.a}$$

$$\frac{\partial V_-}{\partial i_-} = J \tag{17.b}$$

$$i_- = \bar{\mu}_1 . f_1 + \bar{\mu}_2 . f_2 + \bar{\mu}_3 . f_3 \Rightarrow \frac{\partial i_-}{\partial \bar{\mu}_1} = f_1\ ; \tag{17.c}$$

$$\bar{\mu}_1 = \frac{\mu_{A_1}}{\mu_{A_1} + \mu_{A_2} + \mu_{A_3}} \Rightarrow \frac{\partial \bar{\mu}_1}{\partial \mu_{A_1}} = \frac{(\bar{\mu}_2 + \bar{\mu}_3)}{\mu_{A_1} + \mu_{A_2} + \mu_{A_3}}\ ; \tag{17.d}$$

$$\mu_{A_1} = \frac{\xi - a_{A_1}}{b_{A_1} - a_{A_1}} \Rightarrow \frac{\partial \mu_{A_1}}{\partial a_{A_1}} = \frac{\mu_{A_1} - 1}{b_{A_1} - a_{A_1}}\ ; \tag{17.e}$$

Here J is Jacobean matrix, which is taken as constant being single input single output system and its effect is incorporated in learning rate itself. On computing all the terms of equation (17) and putting in equation (16), we can find the updated value of parameter a_{A1} as follows:

$$a_{A_1}(n+1) = a_{A_1}(n) + 2 \cdot \eta \cdot \xi(n) \cdot f_1(n) \cdot \frac{\bar{\mu}_2(n) + \bar{\mu}_3(n)}{\mu_{A_1}(n) + \mu_{A_2}(n) + \mu_{A_3}(n)} \cdot \frac{\mu_{A_1}(n) - 1}{b_{A_1}(n) - a_{A_1}(n)} \tag{18}$$

Similarly

$$b_{A_1}(n+1) = b_{A_1}(n) - 2 \cdot \eta \cdot \xi(n) \cdot f_1(n) \cdot \frac{\bar{\mu}_2(n) + \bar{\mu}_3(n)}{\mu_{A_1}(n) + \mu_{A_2}(n) + \mu_{A_3}(n)} \cdot \frac{\mu_{A_1}(n)}{b_{A_1}(n) - a_{A_1}(n)} \tag{19}$$

In the same way, the precondition parameters for the rest of fuzzy membership functions are derived as follows:

$$b_{A_2}(n+1) = b_{A_2}(n) + 2 \cdot \eta \cdot \xi(n) \cdot f_2(n) \cdot \frac{\bar{\mu}_1(n) + \bar{\mu}_3(n)}{\mu_{A_1}(n) + \mu_{A_2}(n) + \mu_{A_3}(n)} \cdot \frac{1 - \mu_{A_2}(n)}{b_{A_2}(n)} \tag{20}$$

$$a_{A_3}(n+1) = a_{A_3}(n) + 2 \cdot \eta \cdot \xi(n) \cdot f_3(n) \cdot \frac{\bar{\mu}_1(n) + \bar{\mu}_2(n)}{\mu_{A_1}(n) + \mu_{A_2}(n) + \mu_{A_3}(n)} \cdot \frac{\mu_{A_3}(n) - 1}{b_{A_3}(n) - a_{A_3}(n)} \tag{21}$$

1551-3203 (c) 2018 IEEE. Personal use is permitted, but republication/redistribution requires IEEE permission. See http://www.ieee.org/publications_standards/publications/rights/index.html for more information.

This article has been accepted for publication in a future issue of this journal, but has not been fully edited. Content may change prior to final publication. Citation information: DOI 10.1109/TII.2018.2803748, IEEE Transactions on Industrial Informatics

$$b_{A_3}(n+1) = b_{A_3}(n) - 2\cdot\eta\cdot\xi(n)\cdot f_3(n)\cdot\frac{\bar{\mu}_1(n)+\bar{\mu}_1(n)}{\mu_{A_1}(n)+\mu_{A_2}(n)+\mu_{A_3}(n)}\cdot\frac{\mu_{A_3}(n)}{b_{A_3}(n)-a_{A_3}(n)} \quad (22)$$

(b). Consequent Parameter Tuning: For tuning the consequent parameters in *Layer 4*, the following updated laws are used:

$$a_{0_i}(n+1) = a_{0_i}(n) - \eta_c\cdot\frac{\partial\xi^2}{\partial a_{0_i}} \qquad i=1,2,3. \quad (23)$$

$$a_{1_i}(n+1) = a_{1_i}(n) - \eta_c\cdot\frac{\partial\xi^2}{\partial a_{1_i}} \qquad i=1,2,3. \quad (24)$$

where η_c is the learning rate for consequent parameters. The derivative terms in equations (23)-(24), may also be determined by the chain rule as follows:

$$\frac{\partial\xi^2}{\partial a_{0_i}} = \frac{\partial\xi^2}{\partial V_-}\cdot\frac{\partial V_-}{\partial i_-}\cdot\frac{\partial i_-}{\partial f_i}\cdot\frac{\partial f_i}{\partial a_{0_i}} \qquad i=1,2,3. \quad (25)$$

$$\frac{\partial\xi^2}{\partial a_{1_i}} = \frac{\partial\xi^2}{\partial V_-}\cdot\frac{\partial V_-}{\partial i_-}\cdot\frac{\partial i_-}{\partial f_i}\cdot\frac{\partial f_i}{\partial a_{1_i}} \qquad i=1,2,3. \quad (26)$$

Here the first two terms on R.H.S. of equations (25)-(26) are already known and the last two terms can be derived as:

$$\frac{\partial i_-}{\partial f_i} = \frac{\mu_i}{\mu_{A_1}+\mu_{A_2}+\mu_{A_3}} \qquad i=1,2,3. \quad (27)$$

$$\frac{\partial f_i}{\partial a_{0_i}} = 1 \qquad i=1,2,3. \quad (28)$$

$$\frac{\partial f_i}{\partial a_{1_i}} = \xi \qquad i=1,2,3. \quad (29)$$

On substituting the terms derived in equations (27)-(29) in to the equations (25)-(26), the updated value of consequent parameters can be derived as follows:

$$a_{0_i}(n+1) = a_{0_i}(n) + 2\cdot\eta_c\cdot\xi\cdot\frac{\mu_i}{\mu_{A_1}+\mu_{A_2}+\mu_{A_3}} \qquad i=1,2,3. \quad (30)$$

$$a_{1_i}(n+1) = a_{1_i}(n) + 2\cdot\eta_c\cdot\xi\cdot\frac{\mu_i}{\mu_{A_1}+\mu_{A_2}+\mu_{A_3}}\cdot\xi \qquad i=1,2,3. \quad (31)$$

IV. Result Analysis and Discussion

The proposed system with its control description is modelled and simulated in MATLAB. The simulation results are shown in Fig. 6, where the traces of voltages, current, % voltage unbalance factor(%VUF) and the control timing of add-on controller are shown. Here, it can be observed that the voltage is perfectly balanced initially due to presence of balanced load and % voltage unbalance is almost zero. However, at 0.2 sec., when one of the load phase is switched off (Unbalanced load), the voltages becomes unbalanced and the % voltage unbalance factor jumps to more than 6%. At 0.3 sec., proposed ANFIS based add-on controller is introduced in the system.

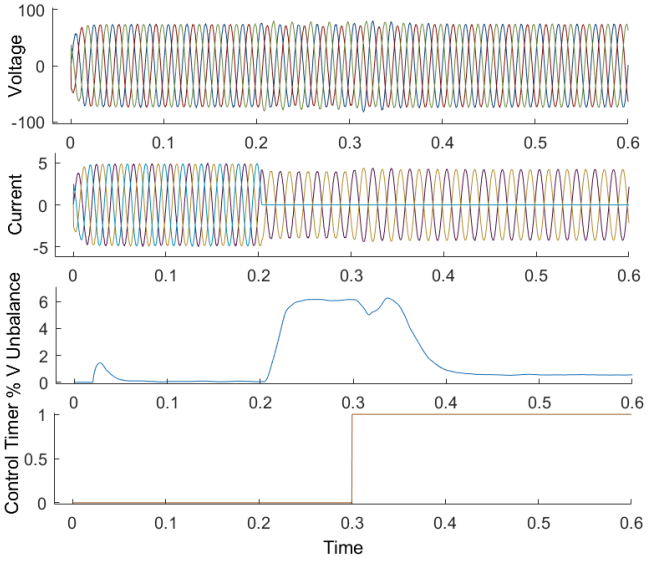


Fig. 6 Simulation Results

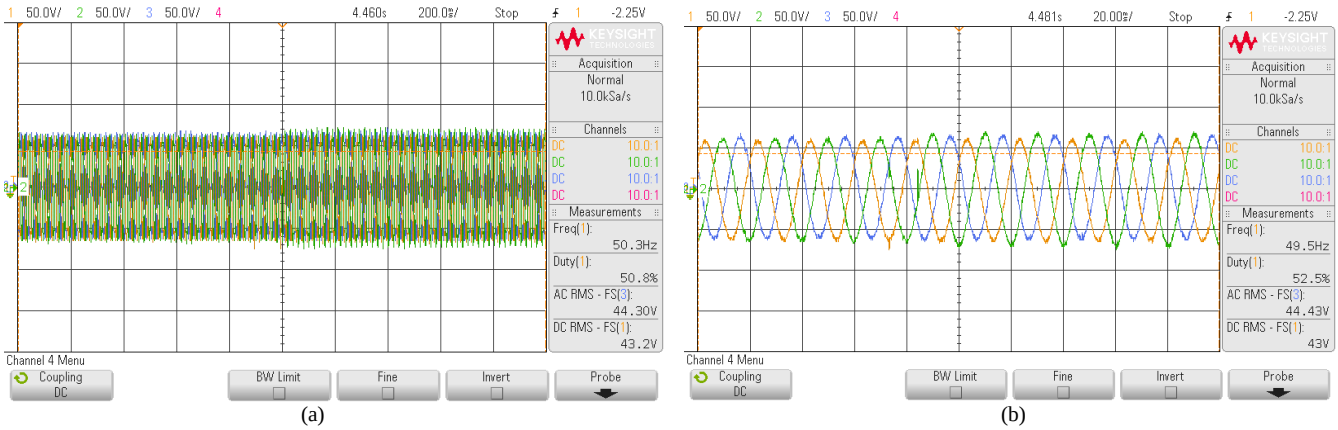
Here, it can be noticed that just after the introduction of add-on controller, the voltages become balanced and the % voltage unbalance factor also falls to almost zero value despite of unbalance load. Thus, the proposed system is successfully able to handle the unbalance load without having any significant impact on voltage profile. Finally, the simulation results are presented in Fig. 6 have been verified on small scale hardware prototype, where a microgrid is realized with two 3-ph, 2-level inverters with output LC-filter. Two separate battery sources have been used to feed both the inverters separately. Here, the batteries may be charged externally through regular supply or via any RES like solar or wind using DC/DC or AC/DC converters. Here, the out power from individual inverter may be changed by changing their respective droop coefficients as per the state of charge (SOC) of their batteries. This approach also allows the control of individual inverter independently in a microgrid having multiple VSC's. The proposed control algorithm is fully implemented in discrete time domain using FPGA (Xilinx zynq-7000 SOC, Zedboard) platform. All computations are performed in fixed point numbers. The fixed-point number based computation may have a lot of design complexities, but still, it is preferable over floating point numbers as they can be easily implemented with limited hardware resources.

The experimental results are shown in Fig. 7 to Fig. 9. Here, the main purpose of this particular experimental study is to see the impact of current unbalance on load terminal voltage. Therefore, the load terminal voltage and current waveforms have been captured during dynamic load conditions. In Fig. 7, the voltage waveforms are shown to indicate the effect of load transition from balanced to unbalanced conditions. Here, the Fig. 7 (a) shows the actual voltages and Fig. 7(b) shows its zoomed in version, where it can be visualised that the voltage waveforms become unbalanced as soon as the load is changed from balanced to unbalance load. The corresponding current waveforms from balanced to unbalanced loading are shown in Fig. 8, where, the Fig. 8 (a) shows the actual load current profile, while the Fig. 8(b) shows its zoomed in version. Here, it can be observed that one of the phase current is suddenly dropped to zero value which indicates the highly unbalanced conditions. In Fig. 9, the voltage waveforms with and without proposed ANFIS based add-on controller are shown. Here, in Fig. 9 (a), the voltages without

1551-3203 (c) 2018 IEEE. Personal use is permitted, but republication/redistribution requires IEEE permission. See http://www.ieee.org/publications_standards/publications/rights/index.html for more information.

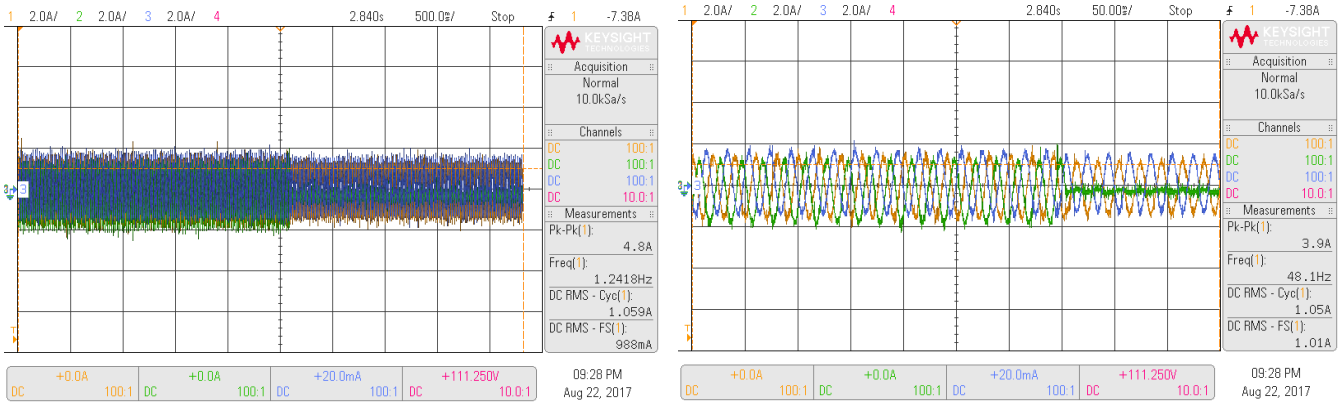
This article has been accepted for publication in a future issue of this journal, but has not been fully edited. Content may change prior to final publication. Citation information: DOI 10.1109/TII.2018.2803748, IEEE Transactions on Industrial Informatics

add-on controller are shown, where the unbalance load effect is clearly reflected on voltage waveforms. The Fig. 9 (b) shows the voltage waveforms with add-on controller, where, the unbalance load has almost negligible effect on voltage profile. As per standard practice, the voltage unbalance should not be allowed to go beyond 5%. With the conventional controller the %VUF are found to be more than 6%. However, with the proposed add-on ANFIS controller, this factor has been brought down from 6% to 2% under highly unbalanced loading conditions.



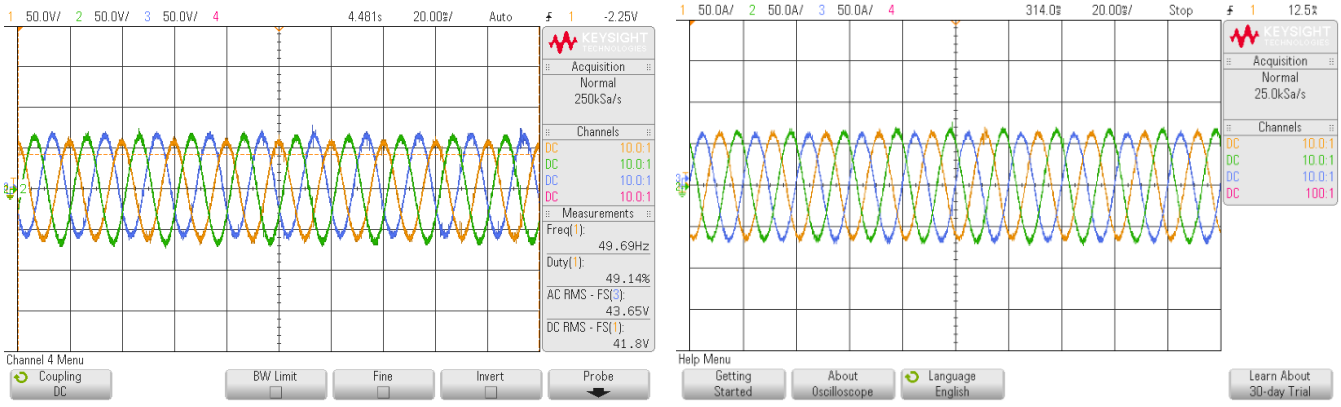
(a) (b)

Fig. 7 Voltage Waveforms [(a) Actual, (b) Zoomed in]



(a) (b)

Fig. 8 Current Waveforms [(a) Actual, (b) Zoomed in]



(a) Without Add-on Controller (b) With Add-on Controller

Fig. 9 Voltage Waveforms

V. Conclusion

In this manuscript, an ANFIS based add-on controller has been modelled, simulated and successfully implemented on laboratory based scaled hardware prototype. Here, it has been demonstrated that individual VSC can be controlled in a microgrid in such a way that the load disturbances have very negligible impact on voltage profile. The extreme load unbalance conditions have been considered for this particular study, where a phase is suddenly switched off to make it 3-phase balance load to unbalance 2-phase load. However, such abrupt behaviour of load has no impact on voltage waveform. The simulation results supported by experimental results have been presented and thoroughly discussed to validate the impact of proposed control algorithm.

1551-3203 (c) 2018 IEEE. Personal use is permitted, but republication/redistribution requires IEEE permission. See http://www.ieee.org/publications_standards/publications/rights/index.html for more information.

This article has been accepted for publication in a future issue of this journal, but has not been fully edited. Content may change prior to final publication. Citation information: DOI 10.1109/TII.2018.2803748, IEEE Transactions on Industrial Informatics

Appendix

TABLE I
SYSTEM PARAMETERS

Parameters	**INV-I**
DC –voltages	168 V
PWM frequency	5khz
Filter Inductance and ESR	2.2mH,0.1 Ω
Filter capacitance	25uF,1 Ohm
Nominal Frequency	50 Hz
Nominal AC voltage*	54 V, (*230 V in simulation)
Transmission line Inductance and Resistance	R = 0.1 Ω L=3.0 mH
Droop coefficient frequency (m_f)	0.1-1.0Hz/Kw
Droop coefficient voltage (m_f)	2V/KVar

VI. REFERENCES

[1]. J. Rocabert, A. Luna, F. Blaabjerg, and P. Rodrguez, "Control of Power Converters in AC Microgrids," *IEEE Transactions on Power Electronics*, vol. 27, pp. 4734-4749, Nov. 2012.

[2]. Y. W. Li, D. M. Vilathgamuwa, and P. C. Loh, "A Grid-Interfacing Power Quality Compensator for Three-Phase Three-Wire Microgrid Applications," *IEEE Transactions on Power Electronics*, vol. 21, pp. 1021-1031, Jul. 2006.

[3]. C. Marnay, H. Asano, S. Papathanassiou, and G. Strbac, "Policymaking of Microgrids, Economic and regulatory issue of microgrid implementation," *IEEE Power \& Energy magazine*, May 2008.

[4]. B. Sorensen, *Renewable Energy*, 4th ed. Acadmic Press, Elsevier, 2011.

[5]. Trivedi, D. K. Jain, and M. Singh, "A modified droop control method for parallel operation of VSItextquotesingles in microgrid," in *2013 IEEE Innovative Smart Grid Technologies-Asia (ISGT Asia)*, Nov. 2013.

[6]. Trivedi and M. Singh, "Repetitive Controller for VSIs in Droop Based AC-Microgrid," *IEEE Transactions on Power Electronics*, pp. 1-1, 2016.

[7]. M. Savaghebi, A. Jalilian, J. C. Vasquez, and J. M. Guerrero, "Secondary Control Scheme for Voltage Unbalance Compensation in an Islanded Droop-Controlled Microgrid," *IEEE Trans. Smart Grid*, vol. 3, pp. 797-807, Jun. 2012.

[8]. M. Savaghebi, A. Jalilian, J. C. Vasquez, and J. M. Guerrero, "Autonomous Voltage Unbalance Compensation in an Islanded Droop-Controlled Microgrid," *IEEE Trans. Ind. Electron.*, vol. 60, pp. 1390-1402, Apr. 2013.

[9]. Y. T. X. L. Y. D. Q. Liu and X. He, "Voltage unbalance and harmonics compensation for islanded microgrid inverters," *IET Power Electronics*, vol. 7, pp. 1055-1063, May 2014.

[10]. D. De and V. Ramanarayanan, "Decentralized Parallel Operation of Inverters Sharing Unbalanced and Nonlinear Loads," *IEEE Transactions on Power Electronics*, vol. 25, pp. 3015-3025, Dec. 2010.

[11]. Pillay P. and Manyage M., "Definitions of Voltage Unbalance," *IEEE Power Engineering Review*, vol. 22, pp. 50-51, May 2001.

[12]. Hamzeh, M., Karimi, H., Mokhtari, H., "Harmonic and negative-sequence current control in an islanded multi-bus MV microgrid," *IEEE Trans. Smart Grid*, vol. 5(1), pp. 167–176, 2014.

[13]. Hamzeh, M., Karimi, H., Mokhtari, H., "A new control strategy for a multibus MV microgrid under unbalanced conditions," *IEEE Trans. Power Syst*., vol. 27, no. 4 , pp. 2225–2232, 2012.

[14]. Cheng, P.T., Chen, C.A., Lee, T.L., et al., "A cooperative imbalance compensation method for distributed generation interface converters," *IEEE Trans. Ind. Appl*, vol. 45, no. 2, pp. 805–815, 2009.

[15]. He, J., Li, Y.W., Blaabjerg, F., "An enhanced islanding microgrid reactive power, imbalance wer, and harmonic power sharing scheme," *IEEE Trans. Power Electron*., vol. 30, no. 6, pp. 3389–3401, 2015.

[16]. N. R. Merritt, C. Chakraborty, and P. Bajpai, " New Voltage Control Strategies for VSC-Based DG Units in an Unbalanced Microgrid," *IEEE Trans. Ind. Electron.*, vol. 8, no. 3, pp. 1127-1139, Jul. 2017.

[17]. F. Guo, C. Wen, J. Chen, J. Mao and Y. D. Song, " Distributed cooperative secondary control for voltage unbalance compensation in an islanded microgrid," *IEEE Transactions on Industrial Informatics*, vol. 11, no. 5, pp. 1078-1088, Oct., 2015.

[18]. Hui Li, K. L. Shi, P. G.McLaren, "Neural-Network-Based Sensorless Maximum Wind Energy Capture With Compensated Power Coefficient," *IEEE Trans. Ind. Appl.*, vol. 41, no. 6, pp. 1548-1556, Nov. 2005

[19]. M. Singh, and A. Chandra, "ANFIS Based Speed & Position Sensorless Control of Grid Connected, PMSG coupled Wind Turbine with 3P4W Non-Linear Unbalance Load Compensation ," *IEEE Trans. Power Electron.*,vol. 26, no.1, pp. 165-175, Jan. 2011.

[20]. J. Shing and R. Jang, "ANFIS: Adaptive-Network-Based Fuzzy Inference System," *IEEE Trans. On Systems, Man, and Cybernetics*, vol. 23, no. 3, pp. 665-685, May 1993.

[21]. P. Garcia, C.A. Garcia, L.M. Fernandez, F. Llorens and F. Jurado, "ANFIS-based Control of a Grid-connected Hybrid System Integrating Renewable Energies, Hydrogen and Batteries," *IEEE Trans. Ind. Informatics*, vol.10,no.2, pp.1107-1117, May 2014.

[22]. M. Singh, and A. Chandra, "Real Time Implementation of ANFIS Control for Renewable Interfacing Inverter in 3P4W Distribution Network," *IEEE Trans. Industrial Electron*, vol. 60, no.1, pp. 121-128, Jan. 2013.



Jaipal Saroha received his B. Tech. and M. Tech. degrees from Deenbandhu Chhotu Ram University of Science and Technology, Sonipat, India in 1999, and National Institute of Technology (Erstwhile REC Kurukshetra), Kurukshetra, India, in 2001, respectively.

He is presently working as Assistant Professor in Kurukshetra University, Haryana, India and pursuing for his Ph.D degree from Deenbandhu Chhotu Ram University of Science and Technology, Sonipat, India.



Mukhtiar Singh (M'11) received the B.Tech. and M.Tech. degrees in electrical engineering from National Institute of Technology (Erstwhile REC Kurukshetra), Kurukshetra, India, in 1999 and 2001, respectively, and the Ph.D. degree from Ecole de Technologie Superieure, University of Quebec, Montreal, QC, Canada. He is presently working as full Professor in the Department of Electrical Engineering, Delhi Technological University (DTU), New Delhi, India.

Dr. Singh is recipient of the IEEE student scholarship for one of the best paper in 34th IEEE Conference on Industrial Electronics, IECON-2008, held at Orlando, FL, USA. He is also the winner of Researchers Merit Scholarship of the University of Quebec, Montreal, Canada for the three years consecutively, 2008, 2009, and 2010.



Dr. D. K. Jain is with Department of Electrical Engineering, Deenbandhu Chhoturam University of Science and Technology, Murthal, Haryana, India

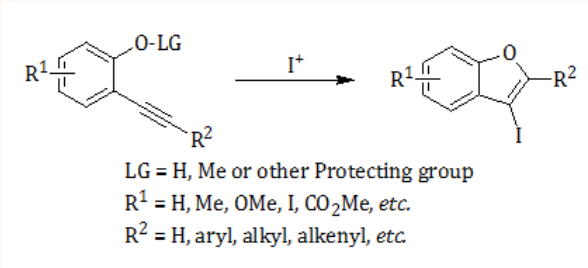
He received the B.Sc., M.Tech. and Ph.D. in electrical engineering from Regional Engineering College, Kurukshetra, Haryana, India, in 1987, 1993 and 2001, respectively. He is currently a Professor with the Deparment of Electrical Engineering at Deenbandhu Chhoturam University of Science and Technology, Murthal, Haryana, India. His research interests include power system protection, electric power quality, electric drives, and renewable energy systems.

1551-3203 (c) 2018 IEEE. Personal use is permitted, but republication/redistribution requires IEEE permission. See http://www.ieee.org/publications_standards/publications/rights/index.html for more information.

Benzofuran Synthesis through Iodocyclization Reactions: Recent Advances

Abstract

Recent advancements (2014-17) in the benzofuran synthesis through iodocyclization have been summarized. The successful use of various iodinating agents, bases, additives etc. make iodocyclization a versatile and efficient methodology. The methodology has been applied for the synthesis of more complex benzofuran derivatives, and may open interesting avenues in the area of heterocyclic chemistry.



Keywords: Annulations; Alkyne; Benzofuran; Iodocyclization; Heterocycle

Mini Review

Volume 1 Issue 7 - 2017

Saurabh Mehta*

Department of Applied Chemistry, Delhi Technological University, India

***Corresponding author:** Saurabh Mehta, Department of Applied Chemistry, Delhi Technological University, Bawana Road, Delhi, 110042 India, Tel: +91 8800665868; Email: saurabh.mehta@dtu.ac.in; saurabh.dtu@gmail.com

Received: December 17, 2017 | **Published:** December 29, 2017

Introduction

Benzo[*b*]furan is a privileged heterocyclic scaffold. Several compounds containing this scaffold have interesting biological activities, such as anti-cancer, anti-viral, anti-inflammatory, etc. [1] Few derivatives are even used as commercial drugs, such as Amiodarone [2], or investigational drugs, such as Bufuralol, [3] etc. (Figure 1).

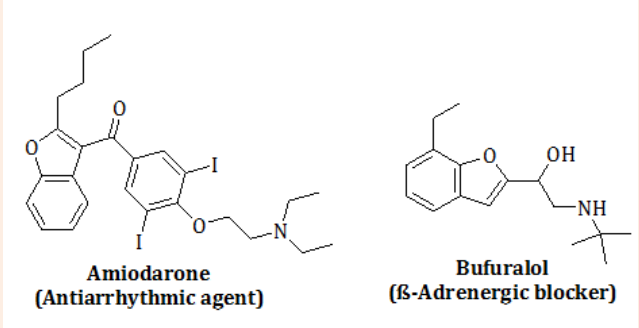


Figure 1: Examples of Benzo[*b*]furan scaffold containing drugs.

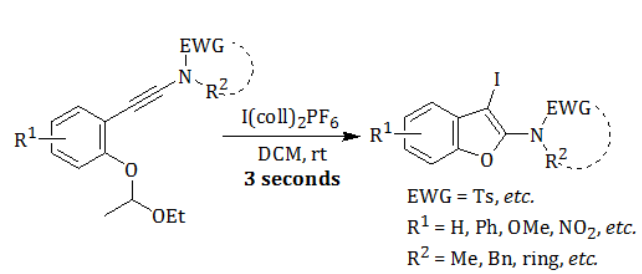
Over the years many synthetic routes have been reported for the preparation of benzofurans [1,4,5]. Iodocyclization of functionalized alkynes is one of the most important and efficient synthetic methodologies for the synthesis of important heterocyclic compounds, including benzofurans [6,7]. Due to our continuous interest in the synthesis and biological evaluation of important heterocycles, [8-10] we became interested in Benzofuran synthesis. Here the recent advances (2014-17) in this powerful strategy for making benzofurans are reported.

Discussion

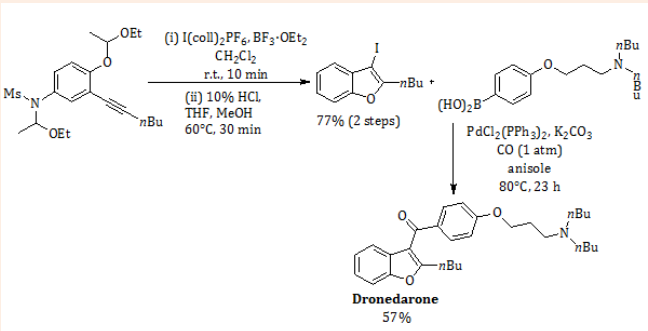
Okitsu et al. [11] recently reported a versatile synthesis of benzo[*b*]furans through iodocyclization of the ethoxyethyl ether-substituted alkynes (Scheme 1) [11]. The reactions get completed within three seconds at room temperature and the corresponding benzofuran derivatives were obtained in high yields (84%–100%) under mild conditions. The authors demonstrated that the choice of bis(2,4,6-collidine)iodonium hexafluorophosphate [$I(coll)_2PF_6$] as the iodinating agent was necessary for the success of the reaction. Also, the ethoxyethyl ether group acted as a protecting group as well as a good leaving group.

The authors used a similar and previously reported methodology [12] for the synthesis (Scheme 2) of an antiarrhythmic agent Dronedarone (marketed as Multaq® from Sanofi-Aventis) [13].

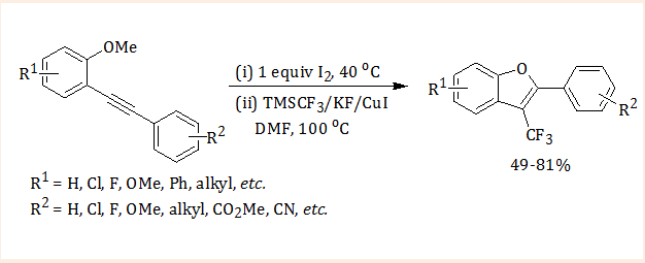
Wang et al. [14] developed a novel and straightforward way for the preparation of 3-trifluoromethylbenzofurans [14]. The methodology involves a two-step, one-pot tandem iodocyclization and trifluoromethylation reaction and affords the 3-trifluoromethylbenzofurans in moderate to excellent yields (Scheme 3).



Scheme 1

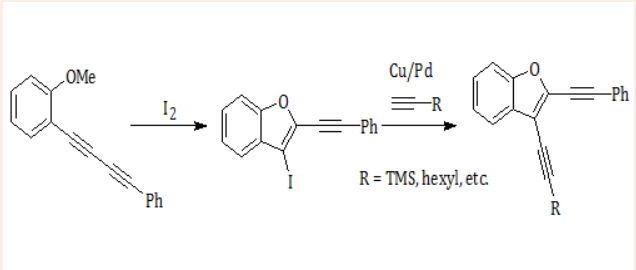


Scheme 2



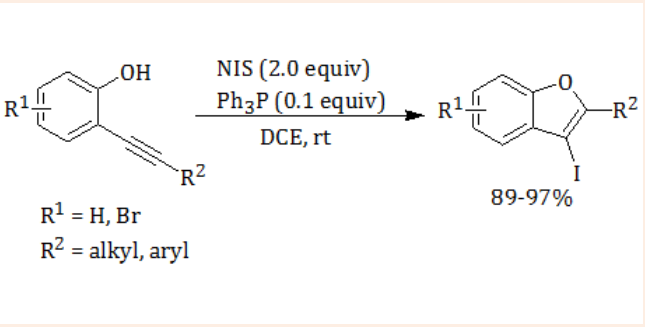
Scheme 3

Danilkina et al. [15] reported an efficient strategy for the synthesis of asymmetrically substituted enediynes fused to benzofuran, and other important heterocycles (Scheme 4) [15]. The authors also demonstrated the extension of the methodology for the synthesis of fused macrocycles of indole derivatives.



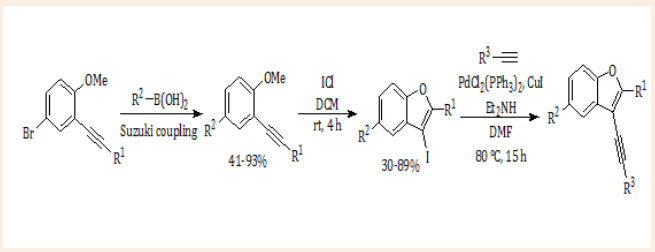
Scheme 4

Li et al. [16] demonstrated that a variety of 3-iodobenzo[*b*]furan derivatives can be conveniently prepared from the corresponding 2-alkynylphenols through Ph_3P-catalyzed iodocyclization in the presence of N-iodosuccinimide (NIS) [16]. This protocol provides a quick access to and 3-iodobenzo[*b*]furans in good to excellent yields under mild conditions (Scheme 5).



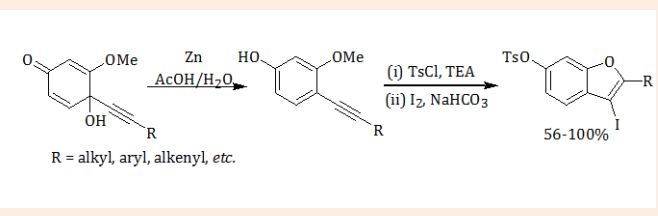
Scheme 5

Using the iodocyclization methodology (Scheme 6) [17,18]. He et al. [19] designed and synthesized a 45-compound library of multi-substituted benzofurans, and using a high-throughput, cell-based HCV luciferase reporter assay studied its anti-hepatitis C virus (HCV) activity [19]. The optimization of the scaffold resulted in the identification of several potent inhibitors (EC_{50} < 100 nM) of HCV with low cytotoxicity (CC_{50} >25 μM), and good selectivity (selectivity index = CC_{50}/EC_{50}, > 371-fold).



Scheme 6

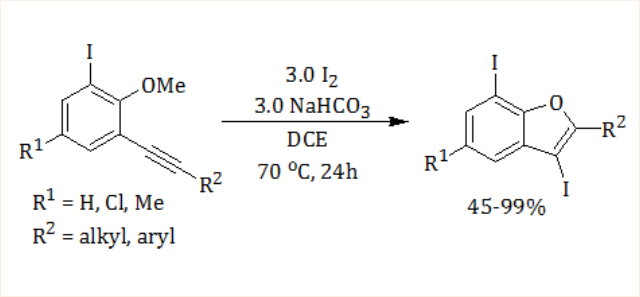
Jung et al. [20] recently reported an efficient synthetic approach to polysubstituted benzofurans where 2-methoxyquinone was used as a benzofuran backbone. The starting quinols were reduced to the phenols, the -OH group was protected and these substrates were further subjected to iodocyclization conditions affording the corresponding benzofurans (Scheme 7) [20].



Scheme 7

Raminelli et al. [21] recently reported an interesting methodology for synthesizing diiodo-functionalized benzo[*b*]

furans [21]. The reaction involves the iodocyclization of alkynylated 2-iodoanisoles using I_2 in the presence of sodium bicarbonate as base (Scheme 8). The resulting products containing two C-I bonds offer opportunities for further diversification of this important scaffold.



Scheme 8

Conclusion

Thus, the iodocyclization strategy presents an efficient approach for the synthesis of diverse benzo [*b*] furan derivatives. The choice of reagents, fast and high yielding reactions combined with the functional group tolerance make it a strategy of choice for many heterocyclic chemists. Further advances in this area of research are expected.

Acknowledgement

The author thanks Delhi Technological University for the resources provided for the completion of this work.

Conflict of Interest

There is no conflict of interest.

References

1. Khanam H, Shamsuzzaman (2015) Bioactive Benzofuran Derivatives: A Review. Eur J Med Chem 97: 483-504.
2. Siddoway LA (2003) Amiodarone: Guidelines for Use and Monitoring. Am Fam Physician 68(11): 2189-2196.
3. Narimatsu S, Takemi C, Kuramoto S, Tsuzuki D, Hichiya H, et al. (2003) Stereoselectivity in the Oxidation of Bufuralol, a Chiral Substrate, by Human Cytochrome P450s. Chirality 15(4): 333-339.
4. Abu-Hashem AA, Hussein HAR, Aly AS, Gouda MA (2014) Synthesis of Benzofuran Derivatives via Different Methods. Synth Commun 44(16): 2285-2312.
5. Wu XF, Li Y (2017) Transition Metal-Catalyzed Benzofuran Synthesis. Elsevier, Amsterdam, Netherlands, pp. 1-71.
6. Godoi B, Schumacher RF, Zeni G (2011) Synthesis of Heterocycles via Electrophilic Cyclization of Alkynes Containing Heteroatom. Chem Rev 111(4): 2937-2980.
7. Gabriele B, Mancuso R, Larock RC (2014) Recent Advances in the Synthesis of Iodoheterocycles via Iodocyclization of Functionalized Alkynes. Curr Org Chem 18(3): 341-358.
8. Mehta S, Waldo JP, Larock RC (2009) Competition Studies in Alkyne Electrophilic Cyclization Reactions. J Org Chem 74(3): 1141-1147.
9. Mehta S, Waldo JP, Neuenswander B, Lushington GH, Larock RC (2013) Solution-Phase Parallel Synthesis of a Multisubstituted Cyclic Imidate Library. ACS Comb Sci 15(5): 247-254.
10. Huang Q, Rui EY, Cobbs M, Dinh DM, Gukasyan HJ, et al. (2015) Design, Synthesis, and Evaluation of NO-Donor Containing Carbonic Anhydrase Inhibitors to Lower Intraocular Pressure. J Med Chem 58(6): 2821-2833.
11. Okitsu T, Nakata K, Nishigaki K, Michioka N, Karatani M, et. al. (2014) Iodocyclization of Ethoxyethyl Ethers to Ynamides: An Immediate Construction to Benzo[*b*]furans. J Org Chem 79(12): 5914-5920.
12. Okitsu T, Nakazawa D, Taniguchi R, Wada A (2008) Iodocyclization of Ethoxyethyl Ethers to Alkynes: A Broadly Applicable Synthesis of 3-Iodobenzo[*b*]furans. Org Lett 10(21): 4967-4970.
13. Okitsu T, Ogasahara M, Wada A (2016) Convergent Synthesis of Dronedarone, an Antiarrhythmic Agent. Chem Pharm Bull (Tokyo) 64(8): 1149-1153.
14. Wang WY, Hu BL, Deng CL, Zhang XG (2014) One-Pot Synthesis of 3-Trifluoromethylbenzofurans via Tandem Iodocyclization and Trifluoromethylation of 2-Alkynylanisoles. Tet Lett 55(8): 1501-1503.
15. Danilkina NA, Kulyashova AE, Khlebnikov AF, Bräse S, Balova IA (2014) Electrophilic Cyclization of Aryldiacetylenes in the Synthesis of Functionalized Enediynes Fused to a Heterocyclic Core. J Org Chem 79(19): 9018-9045.
16. Li YL, Li J, Yu SN, Wang JB, Yu YM, et al. (2015) A Concise Approach for the Synthesis of 3-Iodoindoles and 3-Iodobenzo[*b*]furans via Ph_3P-Catalyzed Iodocyclization. Tetrahedron 71(43): 8271-8277.
17. Yue D, Yao T, Larock RC (2005) Synthesis of 2,3-Disubstituted Benzo[*b*] furans by the Palladium-Catalyzed Coupling of O-Iodoanisoles and Terminal Alkynes, Followed by Electrophilic Cyclization. J Org Chem 70(25): 10292-10296.
18. Cho CH, Neuenswander B, Lushington GH, Larock RC (2008) Parallel Synthesis of a Multi-Substituted Benzo[***b***]furan Library. J Comb Chem 10(6): 941-947.
19. He S, Jain P, Lin B, Ferrer M, Hu Z, et al. (2015) High-Throughput Screening, Discovery, and Optimization to Develop a Benzofuran Class of Hepatitis C Virus Inhibitors. ACS Comb Sci 17(10): 641-652.
20. Jung Y, Kim I (2016) Chemoselective Reduction of Quinols as an Alternative to Sonogashira Coupling: Synthesis of Polysubstituted Benzofurans. Org Biomol Chem 14(44): 10454-10472.
21. Frota C, Rossini AFC, Casagrande GA, Pizzutia L, Raminelli C (2017) Synthesis of Diiodo-Functionalized Benzo[*b*]furans via Electrophilic Iodocyclization. J Braz Chem Soc 28(10): 2038-2044.

MAT JOURNALS

Journal of Environmental Engineering and Studies
Volume 3 Issue 1

Characterization of the Sewage Sludge Samples Collected at Delhi, India

Rajeev Kumar Mishra[1], Amit Krishan[2, 3*], Sandeep Kumar[4]
[1]Assistant Professor, [2]Research Scholar, [4]UG Student
Department of Environmental Engineering, Delhi Technological University,
Shahbad Daulatpur, Main Bawana Road, Delhi-110042, India.
[3]Assistant Professor,
Department of Civil Engineering, G. L. Bajaj Institute of Technology & Management,
Greater Noida - 201306, G. B. Nagar, Uttar Pradesh, India
[*]Corresponding Author E-mail: krishan001amit@gmail.com

Abstract

This manuscript deals with the characterization of different sewage sludge samples. The physiochemical parameters such as pH, organic carbon, organic matter, Total Kjeldahl Nitrogen (TKN), C/N ratio, phosphate, potassium, calcium as well as sodium were evaluated for four different sewage sludge samples obtained in various parts of Delhi, India. The analysis report shows that the sewage sludge has an average value of pH equals to 6.78±0.28. The study revealed that the concentration of organic matter and organic carbon varied from 45.09 % to 49.41% and 77.73 % to 85.18 % respectively. The C/N ratio of the sewage sludge was high which ranged from 6.6 to 23.0 with a mean of 15.9. It was observed that the Total Kjeldahl Nitrogen (TKN) content ranged from 19.6 to 74.02 mg/g, whereas phosphate was found from 2.34 to 9.68 mg/g. The range of potassium concentrations was observed from 5.70 to 11.59 mg/g which shows that sewage sludge is a rich source of nutrients. The concentrations of calcium and sodium varied from 3.53 to 8.57 mg/g and 3.74 to 4.66 mg/g respectively. It can be concluded from the study that sewage sludge is useful in sustainable agricultural as it works as a soil conditioner and biological organic fertilizer. It can be useful in stimulating biological action, rejuvenating soil health as well as in improving the status of an organic matter and the humus content of the soil.

Keywords: *sewage sludge, characteristic, organic matter, nutrient, fertilizer*

INTRODUCTION

Urbanization and industrialization increase water consumption which results in a remarkable growth in the volume of municipal wastewater generation worldwide and therefore the sewage sludge production increased rapidly (Zorpas et al., 2011). It is estimated that Indian cities and towns together generate approximately 19127 tons of sludge per day (Bhatt et al., 2015). The municipal wastewater contains all the organic and inorganic substances that enter in human metabolisms, such as food, beverages, pharmaceuticals, household chemicals and the substances discharged from trade and industry to the sewer system (Bright et al., 2003). Moreover, stormwater runoff from roads, other paved area and its contact materials also contribute to this composition (Usman et al., 2012). As a result, the constituent of the municipal wastewater discharged into the sewer system is a mirror of our modern civilization.

Sewage sludge is an unwanted but inevitable by-product of wastewater treatment process (Jia-yid et al., 2006). It is the residue generated by physical, chemical and biological processes during the primary, secondary and tertiary treatment of municipal wastewater. The sources of solids in a treatment plant vary

Page 1-7 © MAT Journals 2018. All Rights Reserved

according to the type of plant and its method of operation (Theodoratos et al., 2000). To manage wastewater treatment plants effectively and efficiently, it is necessary to extract waste sludge, in order to prevent their accumulation into the system. A number of methods have been proposed to dispose of both liquid and dried sludge. The land application technique is found to be efficient and effective and is considered as one of the methods. Sludge may be useful to agricultural land, forest and can be applied to disturbed land or dedicated disposal sites (Murphy et al., 2000; Bhogal et al., 2003; Scancar et al., 2000; Alvarez et al., 2003; During et al., 2003; Walker et al., 2003). Sewage sludge may improve many soil properties, such as organic matter, nutrients and pH thus the agricultural land application appears to be a reasonable use of it (Lopz-Mosquera et al., 2000; Sastre et al., 2001). Sewage sludge can improve aggregate stability, bulk density, water retention, movement and porosity of soil and increases the crop production as an effective fertilizer (Wang et al., 2008). It also helps to maintain the organic pool and reduce the use of mineral fertilizers, a limited resource or produced under large energy consumption (Jensen et al., 2005). Although raw sewage sludge contains valuable nutrients such as nitrogen, phosphorus, organic matter, and essential trace elements. It also contains various toxins, especially heavy metals, which can cause harm to a soil-plant system and further pose a serious risk to human health (Turkdogan et al., 2003; Wang et al., 2003). By regulating and controlling the use of sewage sludge unacceptable environmental effects, excessive fertilization and contaminants accumulation can be avoided. The attention of environmental authorities, the public and scientists have been attracted by advantages and disadvantages of land application of sewage sludge (Ahumada et al., 2004) therefore it is considered as an important biological resource for sustainable agriculture.

The aim of this study was to identify the nutrient content in sewage sludge of four sewage treatment plants in Delhi (India) and the feasibility of sludge to be used as fertilizer. The finding of the study may be helpful for the proper application of sewage sludge in agriculture soils.

MATERIALS AND METHODS

Sewage Sludge: Four sewage sludge samples were taken from four sewage treatment plants (STP) located in the Delhi, India. Sewage Sludge 1 (SS – 1) was collected from Rithala STP with a treatment capacity of 40 MGD (Millions of Gallons per Day) mostly residential wastewater. Sewage Sludge 2 (SS – 2) was obtained from Keshopur, opposite to Keshopur Mandi, West Delhi. The Keshopur STP has been divided into 3 phases in which Phase III bear 40 MGD capacity, Phase II bear 20 MGD capacity and Phase I bear 12 MGD capacity which is not in operation from past 8 years. Sewage Sludge 3 (SS – 3) was collected from Rohini sector 25 STP which has a capacity of 15 MGD treating mostly industrial wastewater. Sewage Sludge 4 (SS – 4) was collected from Nilothi STP with a capacity of 20 MGD.

Chemical Analysis: A sufficient amount of the composite sewage sludge samples were taken, air-dried and then ground to pass a 1 mm sieve for chemical analysis of nutrient levels. Sewage sludge was analyzed for pH, organic carbon, organic matter, Total Kjeldahl Nitrogen (TKN), C/N ratio, phosphate, potassium, calcium and sodium. For the determination of those parameters were used several methods which have been describing elsewhere (APHA, 2005).

Page 1-7 © MAT Journals 2018. All Rights Reserved

RESULTS AND DISCUSSION

The pH, organic carbon, organic matter, Total Kjeldahl Nitrogen (TKN), C/N ratio, phosphate, potassium, calcium and sodium were analyzed for each sewage sludge sample. The result is presented in Table 1.

pH values of sewage sludge samples

The analysis report (Figure 1) shows that the sewage sludge samples have an average value of pH equals to 6.78 with a standard deviation of 0.28. This value is approximately in the acidic range of pH with an exception of sewage sludge 3 (SS – 3). In general, the sewage sludge is acidic in nature but the sludge of Rohini sector 25 STP (SS – 3) was found slightly alkaline in nature (pH=7.1) because it is treating mostly industrial wastewater. This result can be explained by the fact that a large fraction of organic nitrogen present in sewage sludge may get decomposed into amino acids which ionized and produced hydrogen ion and results in acidity (El-Nahhal et al., 2014). However, this value of pH indicates that the sludge acidity is not so severe and it is in the acceptable range in terms of agricultural use (Sial et al., 2006). The pH value of sludge is important because the solubility of heavy metals in sewage sludge is pH-dependent. The solubility of heavy metals in sewage sludge gets enhanced in acidic media which make them dynamically toxic. Thus, the alkaline pH range may be associated with low risk and the acidic pH range may be associated with high risk (El-Nahhal et al., 2014).

Organic carbon and C/N ratio of sewage sludge

The concentration of organic matter was found 83.15 %, 85.18 %, 80.46 % and 77.73 % in sample SS – 1, 2, 3 and 4 respectively (Figure 2). Turkdogan et al. (2003) also studied the presence of organic matter in sewage sludge. 48.23 %, 49.41%, 46.67 % and 45.09 % of organic carbon was found in sample SS – 1, 2, 3 and 4 respectively as shown in figure 2. The highest concentration of organic carbon and organic matter was found in sewage sludge 2 (SS – 2). The variation in organic carbon and the organic matter seemed to be independent of sludge type. The similar study was reported by Malamis et al. (2014) and Azzouz et al. (2017). An increase in organic matter reduces the bulk density, increases aggregate stability, increases water holding a capacity of soils and promotes greater water infiltration (Wang et al., 2008). Organic matter also influences nutrient storage and turnover, soil biota and diversity as well as vulnerability to erosion. The high fraction of organic matters in sludge is responsible for the high values of water drip penetration time (WDPT) which enhance water repellency and water runoff (El-Nahhal et al., 2014).

The C/N ratio of the sewage sludge samples was found high with ranged from 6.6 to 23.0 with a mean of 15.9 (Figure 3). It means that there is the inadequate mobilization of nitrogen by incorporation into cell mass, which makes the amount of nitrogen accessible at a later period when it is required by most for plants during development phase (Bhatt et al., 2015).

Nutritional value of sewage sludge

After the analysis of sewage sludge samples, it was observed that the Total Kjeldahl Nitrogen (TKN) content ranged from 19.6 to 74.02 mg/g, whereas phosphate was from 2.34 to 9.68 mg/g. raw sewage sludge contains valuable nutrients such as nitrogen and phosphorus according to Turkdogan et al. (2003) and Pazos et al. (2010) found elements with high agricultural value (P and K). The range of potassium concentrations was from 5.70 to 11.59 mg/g which shows that sewage sludge is a rich source of nutrients. Zorpas et al. (2001) investigated that the concentration of potassium in the dry base from Komotinis STP (Greece, mainly

Page 1-7 © MAT Journals 2018. All Rights Reserved

municipal waste) was 2.36 mg/g. The nutritional values are presented in Figure 4. Sewage sludge is applied to improve the physicochemical and biological properties of soils, which in turn facilitates the better growth of plants (Kumar et al., 2004). The high cation exchange capacities of the sludge samples along with nitrogen content demonstrate a positive result for application of sludge for agricultural purposes on the grounds that such association of nitrogen with cation exchange capacity implies the slow release of nutrients. What's more increment in cation exchange capacity brings about reduced the mobility of inhibitory and potentially toxic heavy metals. With respect to agricultural uses the sewage sludge samples, therefore, carry a low risk of potential heavy metal toxicity (Mtshali et al., 2014).

Macronutrients value of sewage sludge

The concentrations of calcium and sodium varied from 3.53 to 8.57 mg/g and 3.74 to 4.66 mg/g respectively (Figure 5). Zorpas et al. (2001) were found 14.50 mg/g Ca and 1.16 mg/g Na in the dry base from Komotinis STP (Greece, mainly municipal waste) and Pazos et al. (2010) studied the presence of calcium which has high agricultural value. These macronutrients are beneficial for plant growth and the amount of the sewage sludge are of considerable value as a fertilizer replacement.

CONCLUSION

On the basis of physiochemical analysis of sewage sludge samples collected from four sewage treatment plant within Delhi. It can be concluded that sewage sludge is very important biological organic fertilizer and soil conditioner for sustainable agriculture. It adds both macro and micronutrients and improves status of organic matter in the soil. It can be useful in stimulating biological action, rejuvenating soil health by improving the status of an organic matter. Sewage sludge also increases the humus content of the soil. A higher level of soil organic matter can sequester carbon and mitigate greenhouse gas emissions.

The concentration of organic matter, macro and micronutrients were found less in sewage sludge 4 (SS – 4) in compare to other sewage sludge samples because disc filters are used instead of conventional gravity sand filters for tertiary treatment at Nilothi STP and sludge treatment system uses digesters equipped with gas mixing system to optimize production of biogas.

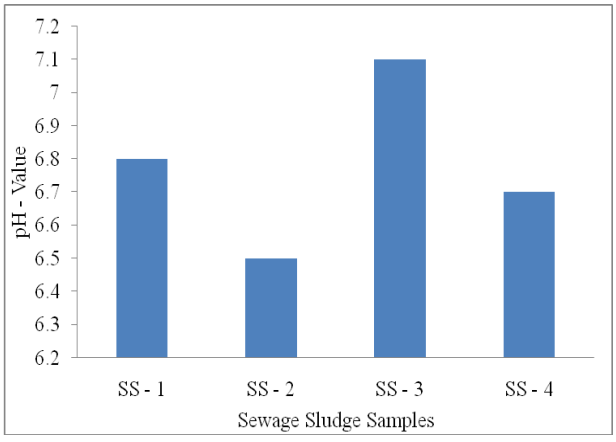


Fig 1. *pH value of different sewage sludge samples*

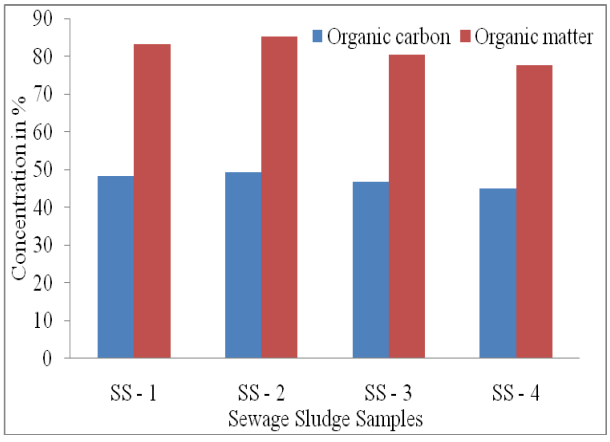


Fig 2. *Concentration of organic carbon & organic matter in different sewage sludge samples*

Page 1-7 © MAT Journals 2018. All Rights Reserved

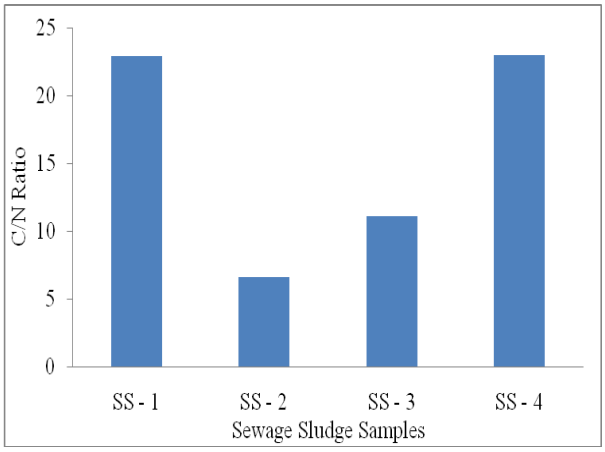


Fig 3. *C/N ratio of different sewage sludge samples*

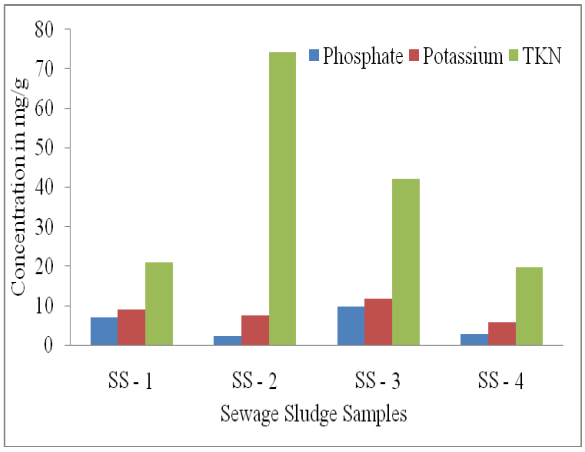


Fig 4. *Concentration of Nutritional values in different sewage sludge samples*

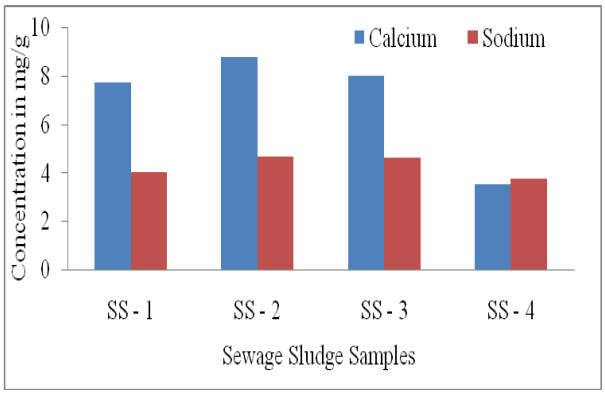


Fig 5. *Concentration of calcium & sodium in different sewage sludge samples*

Table 1. *Composition of sewage sludge samples*

	SS - 1	**SS - 2**	**SS – 3**	**SS - 4**
pH	6.8	6.5	7.1	6.7
Phosphate (mg/g)	7.03	2.34	9.68	2.71
Potassium (mg/g)	9.04	7.58	11.59	5.70
Total Kjeldahl nitrogen (mg/g)	21.00	74.20	42.00	19.60
Organic carbon (%)	48.23	49.41	46.67	45.09
Organic matter (%)	83.15	85.18	80.46	77.73
C/N ratio	22.90	06.60	11.10	23.00
Calcium (mg/g)	7.72	8.77	7.98	8.53
Sodium (mg/g)	4.03	4.66	4.61	3.74

REFERENCES

1. Ahumada, I., P. Escudero, M.A. Carrasco, G. Castillo, L. Ascar and E. Fuentes. 2004. Use of sequential extraction to assess the influence of sewage sludge amendment on metal mobility in Chilean soils. J. Environ. Monitor., 6: 327–334.
2. Alvarez, E., M.L.F. Marcos and C. Vaamonde. 2003. Heavy metals in the dump of an abandoned mine in Galicia (NW Spain) and in the spontaneously oncoming vegetation. Sci. Total Environ., 3(13): 185-197.
3. APHA, Standard Methods for the Examination of Water and Wastewater, 21st Ed. 2005. American Public Health Association, Washington, DC.
4. Azzouz, A.A.H., N.A. Naas and K.M. Darwish. 2017. Physicochemical

Page 1-7 © MAT Journals 2018. All Rights Reserved

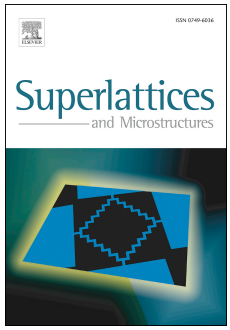
Characterization of the Sewage Sludge from Guarchia Wastewater Treatment Plant in Benghazi-Libya Evaluation of the Organic Composition. MOJ Biorg Org Chem 1(2): 1-19.
5. Bhatt, P., N. Mathur, A. Singh and P. Bhatnagar. 2015. Recycled Sewage Sludge: A Step to Sustainable Agriculture. Int. J. Chem. Sci., 13(4): 1611-1620.
6. Bhogal, A., F.A. Nicholson and B.J. Chambers. 2003. Effects of past sewage sludge additions on heavy metal availability in light textured soils: implications for crop yields and metal uptakes. Environ. Pollut., 121: 413-423.
7. Bright, D.A. and N. Healey. 2003. Contaminant risks from biosolids land application: Contemporary organic contaminant levels in digested sewage sludge from five treatment plants in Greater Vancouver, British Columbia. Environmental Pollution, 126: 39–49.
8. During, R.A., T. Hob and S. Gath. 2003. Sorption and bioavailability of heavy metals in long-term differently tilled soils amended with organic wastes. Sci. Total Environ., 313: 227-234.
9. El-Nahhal, I.Y., H. Al-Najar and Y. El-Nahhal. 2014. Physicochemical Properties of Sewage Sludge from Gaza. International Journal of Geosciences, 5: 586-594.
10. Jensen, J. and S.E. Jepsen. 2005. The production, use and quality of sewage sludge in Denmark. Waste Management, 25: 239–247.
11. Jia-yid, D., C. Lin, Z. Jim-fb and M. Naz. 2006. Characteristics of sewage sludge and distribution of heavy metal in plants with amendment of sewage sludge. Journal of Environmental Sciences, 18(6): 1094-1100.
12. Kumar, V. and A.K. Chopra. 2014. Accumulation and Translocation of Metals in Soil and Different Parts of French Bean (Phaseolus vulgaris L.) Amended with Sewage Sludge. Bull. Environ. Contam. Toxicol., 92(1): 103-108.
13. Lopz-Mosquera, M.E., C. Moiron and E. Caral. 2000. Use of dairy-industry sludge as fertilizer for grasslands in northwest Spain: heavy metal level in the soil and plant. Resour. Conserv. Recycl., 30: 95–109.
14. Malamis, S., E. Katsou, S. Di Fabio, D. Bolzonella and F. Fatone. 2014. Biological Nutrients Removal from the Supernatant Originating from the Anaerobic Digestion of the Organic Fraction of Municipal Solid Waste. Critical Reviews in Biotechnology, 34(3): 244-257.
15. Mtshali, J.S., A.T. Tiruneh and A.O. Fadiran. 2014. Characterization of Sewage Sludge Generated from Wastewater Treatment Plants in Swaziland in Relation to Agricultural Uses. Res. Environ., 4(4): 190-199.
16. Murphy, A.P., M. Coudert and J. Barker. 2000. Plants as biomarkers for monitoring heavy contaminants on landfill sites using sequential extraction and inductively coupled plasma atomic emission spectrophotometry (ICP-AES). J. Environ. Monitor, 2: 621-627.
17. Pazos, M., G.M. Kirkelundb and L.M. Ottosenb. 2010. Electrodialytic treatment for metal removal from sewage sludge ash from fluidized bed combustion. Journal of Hazardous Materials 176: 1073–1078.
18. Sastre, L., M.A. Vicente and M.C. Lobo. 2001. Behaviour of cadmium and nickel in a soil amended with sewage sludge. Land Degrad. Dev., 12: 27–33.
19. Scancar, J., R. Milacic and M. Strazar. 2000. Total metal concentrations and partitioning of Cd, Cr, Cu, Fe, Ni and Zn in sewage sludge. Sci. Total Environ., 250: 9-19.
20. Sial, R. A., M.F. Chaudhary, S.T. Abbas, M.I. Latif and A.G. Khan.

Page 1-7 © MAT Journals 2018. All Rights Reserved

2006. Quality of Effluents from Hattar Industrial Estate. Journal of Zhejiang University Science B, 7: 974-980.
21. Theodoratos, P., A. Moirou, A. Xenidis and I. Paspaliaris. 2000. The use of municipal sewage sludge for the stabilization of soil contaminated by mining activities. Journal of Hazardous Materials, B77: 177–191.
22. Turkdogan, M.K., F. Kilcel, K. Kara, I. Tuncer and I. Uygai, 2003. Heavy metals in soil, vegetables and fruits in the endemic upper gastrointestinal cancer region of Turkey. Environ. Toxicol. Pharm., 13: 175–179.
23. Usman, K., S. Khan, S. Ghulam, M.U. Khan, N. Khan, M.A. Khan and S.K. Khalil. 2012. Sewage Sludge: An Important Biological Resource for Sustainable Agriculture and Its Environmental Implications. American Journal of Plant Sciences, 3: 1708-1721.
24. Walker, D.J., R. Clemente and A. Roig. 2003. The effects of soil amendments on heavy metal bioavailability in two contaminated Mediterranean soils. Environ. Pollut., 122: 303-312.
25. Wang, Q. R., Y.S. Cui, X.M. Liu, Y.T. Dong and P. Christe. 2003. Soil contamination and plant uptake of heavy metals at polluted sites in China. J. Environ. Sci. Health A—Toxic/Hazard. Subst. Environ. Eng., 38: 823–838.
26. Wang, X., T. Chen, Y. Ge and Y. Jia. 2008. Studies on land application of sewage sludge and its limiting factors. Journal of Hazardous Materials, 160: 554–558.
27. Zorpas, A.A., M. Loizidou, V.J. Ingklezakis and A. Papadopoulos. 2001. Improvement of the composts production from municipal solid waste and sewage sludge from several STPs in Greece with natural minerals. Technical Report. National Technical University of Athens – National Institute of Geological and Mineral Research . Greece.
28. Zorpas, A.A., C. Coumi, M. Drtil and I. Voukalli. 2011. Municipal sewage sludge characteristics and waste water treatment plant effectiveness under warm climate conditions. Desalination and Water Treatment, 36: 319–333.

Page 1-7 © MAT Journals 2018. All Rights Reserved

Accepted Manuscript



Comprehensive analysis of sub-20nm Black Phosphorus based Junctionless-Recessed Channel MOSFET for Analog/RF applications

Ajay Kumar, M.M. Tripathi, Rishu Chaujar

PII: S0749-6036(18)30064-8

DOI: 10.1016/j.spmi.2018.02.018

Reference: YSPMI 5510

To appear in: *Superlattices and Microstructures*

Please cite this article as: Ajay Kumar, M.M. Tripathi, Rishu Chaujar, Comprehensive analysis of sub-20nm Black Phosphorus based Junctionless-Recessed Channel MOSFET for Analog/RF applications, *Superlattices and Microstructures* (2018), doi: 10.1016/j.spmi.2018.02.018

This is a PDF file of an unedited manuscript that has been accepted for publication. As a service to our customers we are providing this early version of the manuscript. The manuscript will undergo copyediting, typesetting, and review of the resulting proof before it is published in its final form. Please note that during the production process errors may be discovered which could affect the content, and all legal disclaimers that apply to the journal pertain.

ACCEPTED MANUSCRIPT

Highlights

- ✓ Comprehensive analog and RF performance BP-JL-RC MOSFET has been explored at 45nm technology node (Gate length=20nm).
- ✓ BP-JL-RC-MOSFET leads to higher I_D (0.3mA), excellent switching ratio (10^{11}) and improvement in sub-threshold slope (SS) (67mV/dec).
- ✓ f_T (3.88 times) and f_{MAX} (~8 times) enhances significantly in BP-JL-RC-MOSFET as compared to CRC.
- ✓ RF FOMs f_T, f_{MAX}, stern stability factor, various power gains have been investigated.
- ✓ Further, parasitic capacitances at THz frequency range have been evaluated.
- ✓ BP-JL-RC-MOSFET acts as a potential candidate for low power analog and RF applications.

ACCEPTED MANUSCRIPT

ACCEPTED MANUSCRIPT

Comprehensive Analysis of Sub-20nm Black Phosphorus Based Junctionless-Recessed Channel MOSFET for Analog/RF Applications

Ajay Kumar[1], M.M. Tripathi[1] and Rishu Chaujar[2*]
[1]Electrical Engineering Department, [2]Engineering Physics Department,
Delhi Technological University, Delhi India
ajaykumar@dtu.ac.in, mmtripathi@dce.ac.in, and chaujar.rishu@dtu.ac.in*

Abstract- In this work, a comprehensive analog and RF performance of a novel Black Phosphorus-Junctionless-Recessed Channel (BP-JL-RC) MOSFET has been explored at 45nm technology node (Gate length=20nm). The integration of black phosphorus with junctionless recessed channel MOSFET, leads to higher drain current of about 0.3mA and excellent switching ratio (of the order of 10^{11}) due to reduced off-current which leads to improvement in sub-threshold slope (SS) (67mV/dec). Further, RF performance metrics have also been studied with an aim to analyze high-frequency performance. The following FOMs have been evaluated: cut-off frequency (f_T), maximum oscillator frequency (f_{MAX}), stern stability factor, various power gains and parasitic capacitances at THz frequency range. Thus, in addition to the high packing density offered by RC MOSFET, the proposed design finds numerous application at THz frequency making it a promising candidate at wafer scale integration level.

Keywords- Analog, CRC-MOSFET, frequency, gain, parasitic capacitance, RF, BP-JL-RC-MOSFET.

1. Introduction

Continuous scaling of MOSFET in sub-20nm gate length develops opportunities for high speed and low power applications. Several THz cut-off frequencies can be achieved in highly scaled MOSFETs, making CMOS technology appropriate for RF application [1-4]. In sub-20nm gate length, source/drain capacitances called parasitic capacitances increases and hence, gate control over the channel reduces [5]. Short channel effects (SCEs) also arises due to the scaling down of device dimensions which is not suitable for analog and RF applications [6]. The problems associated with SCEs are threshold voltage roll-off [7], hot carrier effects (HCEs) [8], drain induced barrier lowering (DIBL) [9, 10], punch through and gate tunneling current [11]. These effects can be eliminated (reduced) by changing the gate material as well as doping profile of the MOSFET. To reduce these effects and for high-performance transistor application, a new class of material called black phosphorus is used in a recessed structure [12]. Black phosphorus is one of the promising material due to very high mobility (~1000 $cm^2V^{-1}s^{-1}$ at room temperature) and a layered structure which can be realized at sub-1nm thick channel [13]. From bulk (0.3 eV) to single layer (1.0-1.5 eV), black phosphorus has tunable band gap [14-16]. Due to these properties, black phosphorus is the most suitable 2D material in comparison to graphene and transition metal dichalcogenides while graphene has high mobility but band gap is zero [17], and transition metal dichalcogenides have low mobility (~10-250 $cm^2V^{-1}s^{-1}$) but large band gap (1-2 eV) [18-20]. Black phosphorus is frequently used in MOSFET for high-performance transistor applications [21, 22], but SCEs [23] are the main disadvantages of conventional MOSFET at sub-20 nm gate length. To enhance the performance of the recessed channel MOSFET, black phosphorus is used as a 2D gate material, and the doping profile of source, drain, and channel is uniform to make it as a junctionless transistor. The physics and basic properties of the junctionless transistor are introduced by JP Colinge [24], and it is observed that the sub-threshold swing, DIBL and switching ratio is improved due to the junctionless phenomenon.

For high-performance analog and RF applications, we have combined two techniques, namely recessed gate technique and junctionless technique in this work. In the recessed gate, few layers of black phosphorus are amalgamated as black phosphorus is a most attractive 2D material and the symmetric doping is done to eliminate the junction from the device. BP-JL-RC-MOSFET is a novel device in which the electrical characteristics of a transistor are enhanced due to the tremendous value of switching ratio (due to the lower value of I_{OFF}). Such a high I_{ON} and low I_{OFF} makes black phosphorus a promising material for digital electronics applications [17]. BP JL-RC MOSFET is a highly scaled device, and the gate length is 20 nm which increases the packing density of the integrated circuits (ICs).

2. Device Design and its parameters

Fig. 1 shows the simulated 20 nm device structure of BP JL-RC MOSFET. All the design parameters are given in Table-I, and the biasings are applied at room temperature (T=300 K).

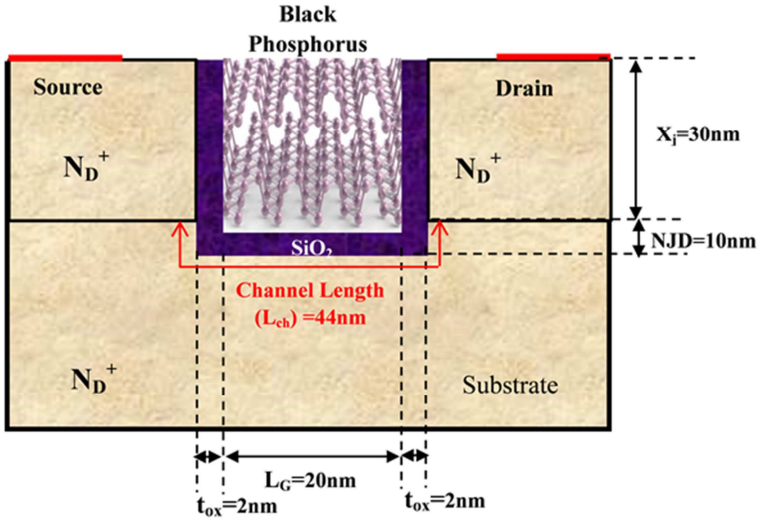


Fig. 1. Schematic structure of BP-JL-RC-MOSFET.

Table-I: Design parameters of BP-JL-RC-MOSFET and CRC-MOSFET

Device Parameters	BP-JL-RC-MOSFET	CRC-MOSFET
Gate Length (L_g)	20 nm	20 nm
Channel Length (L_{ch})	44 nm	44 nm
Source and the Drain region Length	30 nm	30 nm
Width of the Device (W)	200 nm	200 nm
Groove Depth	38 nm	38 nm
Negative Junction Depth (NJD)	10 nm	10 nm
Substrate Doping	$5x10^{16}$ cm^{-3} (N_D^+)	$1x10^{17}$ cm^{-3} (N_A)
Source/Drain Doping (N_D^+)	$5x10^{16}$ cm^{-3} (N_D^+)	$1x10^{19}$ cm^{-3} (N_D^+)
Physical Oxide Thickness (t_{ox})	2 nm	2 nm
Metal work function (Φ)	5.16 eV	4.4 eV
Gate to source voltage (V_{gs})	1.5 V	1.5 V
Drain to source voltage (V_{ds})	0.2 V	0.2 V

3. Simulation methodology and calibration

ATLAS is a powerful simulation tool which is used for the extraction of reliability results and all Figure of Merits (FOM) [25]. Various simulation models have been used such as Lombardi CVT model to consider all the mobilities such as scattering mechanism which is caused by the parallel and perpendicular field applied on the device. For carrier generation-recombination, we have used Shockley-Read-Hall (SRH) Recombination. Fermi-Dirac statistics is used in case of very highly doped material. To consider the information about the low energy (temperature) of the carriers, we have used Energy Balance Transport (EBT) model [25]. Further, to obtain the numerical solutions, two numerical techniques such as Gummel and Newton have been considered [25] to obtain better convergence.

The calibration of Physical Model parameters of the simulated device with the experimental data by Joerg Appenzeller et al. in 2002 [26] is shown in Fig. 2. To validate the simulation results, the statistics have been drawn-out [26] for 36 nm groove MOSFET and then plotted as evident in Fig. 2. It is detected from Fig. 2 that simulated results almost matched with the experimental data in sub-40 nm groove MOSFET, thus validating the simulation models.

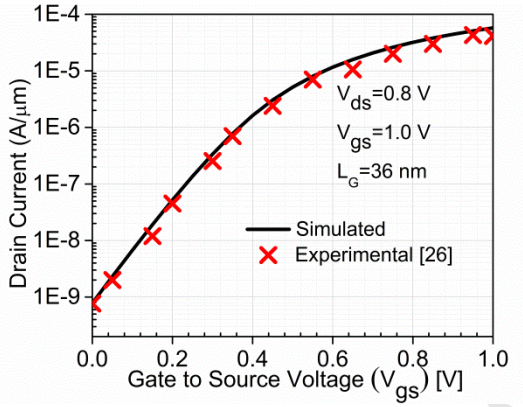


Fig. 2. Experimental and simulation of I_{ds}-V_{gs} characteristics of 36 nm gate length recessed channel MOSFET.

4. Fabrication Feasibility of BP-JL-RC-MOSFET

The fabrication feasibility of BP-JL-RC-MOSFET is shown in Fig. 3. Moreover, the groove MOSFET has been fabricated by different researchers such as Joerg Appenzeller et al., in 2002 [26], fabricated 36nm groove gate and M. Xiao-Hua et al., in 2006 [27], fabricated 140 nm groove gate MOSFET. First of all, a p-type silicon substrate wafer is taken and then n-well region is created by a diffusion process. The active region is then identified and Drive-In diffusion and gate oxidation process is carried out.

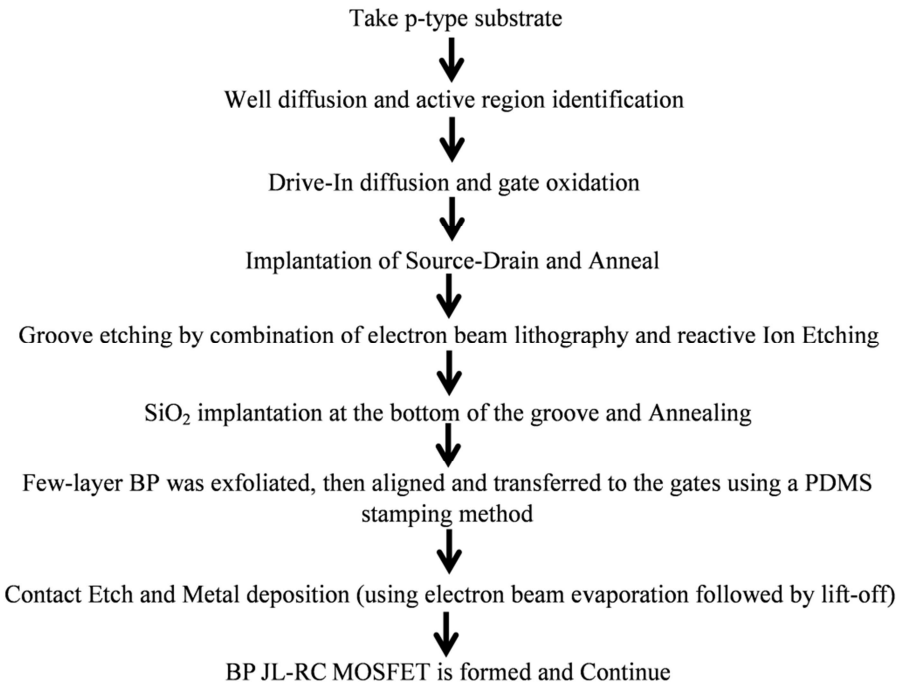


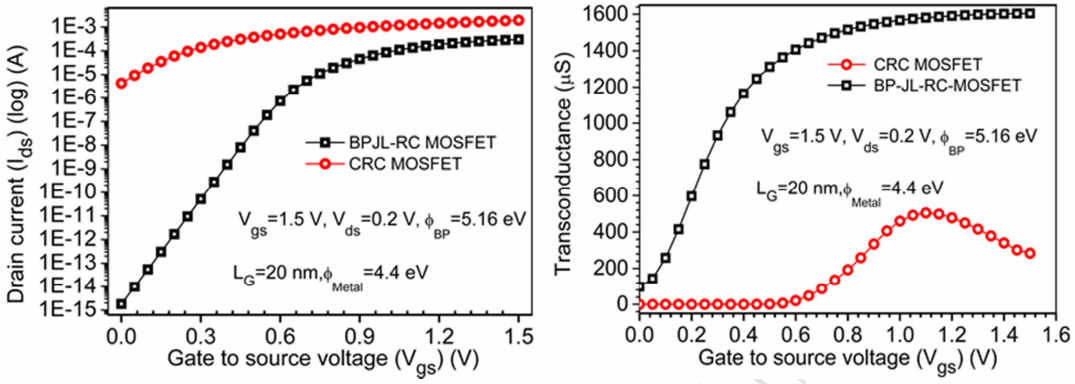
Fig. 3. Fabrication flowchart of BP-JL-RC-MOSFET.

Source-drain implantation and anneal process are done before groove etching by a combination of electron beam lithography and reactive ion etching; and then SiO_2 implant at the bottom of the groove is done. In the groove region, black phosphorus is exfoliated, then aligned and transferred to the gate using a PDMS (polydimethylsiloxane) stamping method (PDMS stamps are pieces of polydimethylsiloxane, a silicone, that have usually been patterned against a master to form a relief pattern used in soft lithography) [21]. PMMA (Poly (methyl methacrylate)) was immediately spin-coated (acting as a temporary passivation layer) to minimize the

black phosphorus degradation. At last, contact etches and metal deposition (using electron beam evaporation followed by lift-off) process is done. Thus, the BP-JL-RC-MOSFET can be fabricated using the above device design schemes, in which the benefits of the transparent gate engineering scheme have been combined with groove gate for accomplishing improved characteristics.

5. Results and Discussions

5.1. Analysis of analog performance:



4(a) 4(b)

Fig. 4.(a): Transfer characteristics and (b): Transconductance; of CRC-MOSFET and BP-JL-RC-MOSFET.

.

In order to investigate the impact of the Junctionless phenomenon in which black phosphorus is used as gate material on drain current, CRC and BP-JL-RC-MOSFET were simulated using ATLAS 3D device simulator [25]. Fig. 4(a-b) reflects the transfer characteristics and transconductance profile respectively, for BP-JL-RC and CRC devices. Drain current improves in the proposed device as shown in Fig. 4(a) and due to the improvement in drain current, Fig. 4(b) reflects the enhanced transconductance in BP-JL-RC-MOSFET as compared to CRC-MOSFET. It is clearly observed that large difference in off-currents (10^{-6} A and 10^{-11} A) is observed while on-currents ($1.89x10^{-3}$ A and $3x10^{-4}$ A) are nearly equal between CRC and BP-JL-RC devices due to which the switching ratio of the proposed device is much higher than conventional one as shown in Fig. 5. Reduction in off-current is observed due to the presence of Junctionless phenomenon as well as amalgamation of black phosphorus in the groove (recessed) gate of BP-JL-RC-MOSFET. Black phosphorus improves the gate controllability and hence, shrinks HCEs and SCEs in BP-JL-RC-MOSFET. The switching capability and gate controllability in BP-JL-RC-MOSFET are achieved at a very low drain bias (0.2V), and gate biasing is ramped from 0 to 1.5V due to which BP-JL-RC device emerged as an ultra-low power device for analog applications. Fig. 5 also reflects the reduced sub-threshold slope in BP-JL-RC-MOSFET (67.2 mV/dec) as compared to the conventional device (151 mV/dec). The low sub-threshold slope is also responsible for higher switching performance of the device.

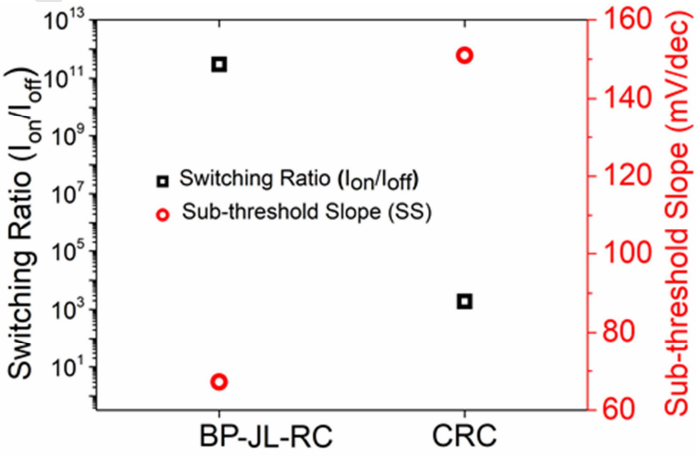
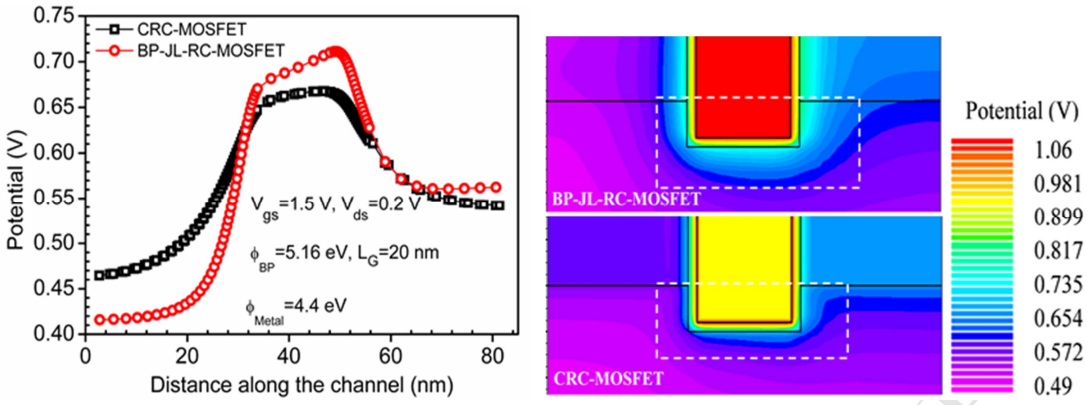


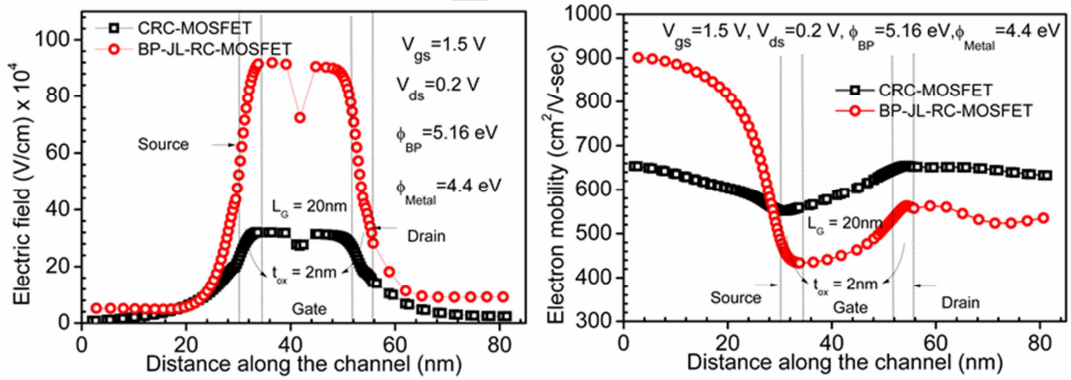
Fig. 5. Switching ratio and sub-threshold slope of BP-JL-RC-MOSFET and CRC-MOSFET.



6(a) 6(b)

Fig. 6. (a) Potential, with respect to the distance along the channel for CRC and BP-JL-RC-MOSFET. (b) Contour plot CRC and BP-JL-RC-MOSFET.

Fig. 6(a) and 6(b) shows the potential and contour plot along the channel for CRC and BP-JL-RC-MOSFET, and it is observed that the potential is higher in the channel region for BP-JL-RC-MOSFET as compared to the conventional device due to the incorporation of black phosphorus on to the recessed gate. Proposed device reflects the lowering of barrier potential at source side which indicates a reduction in DIBL and more pronounced in conventional MOSFET mainly due to the absence of junction in the BP-JL-RC-MOSFET. To evaluate analog parameters in BP-JL-RC-MOSFET and CRC-MOSFET, electric field and electron mobility are two important parameters. It is evident from Fig. 7(a) that, the channel electric field is enhanced by three-times in BP-JL-RC-MOSFET (9×10^5 V/cm) as compared to CRC-MOSFET (3×10^5 V/cm). Enhancement in channel electric field is due to the higher electron mobility of black phosphorus (shown in Fig. 7(b)) as well as junctionless profile of the BP-JL-RC-MOSFET in which electrons feel negligible resistance to reach from drain to source and hence, mobility of the charge carriers (present in channel region) is more at the source side as compared to drain side as shown in Fig. 7(b). Higher electron mobility is also one of the reason due to which the switching ratio is very high in BP-JL-RC-MOSFET (shown in Fig. 5).

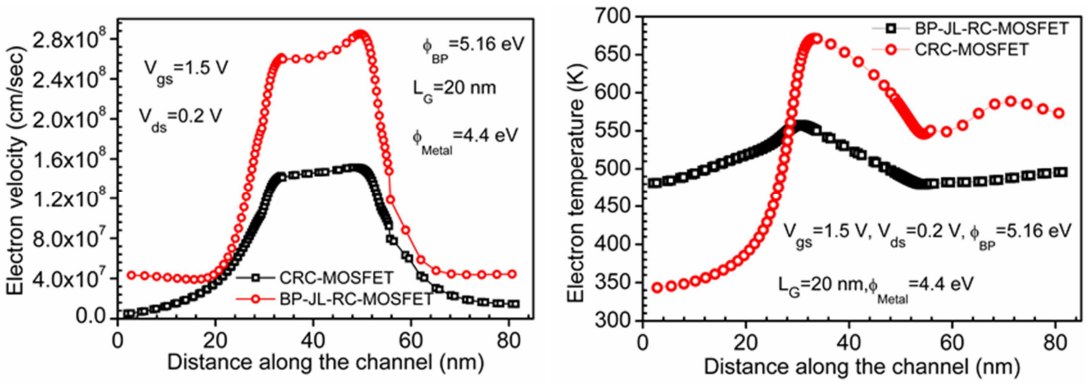


7(a) 7(b)

Fig. 7. (a) Electric field and (b) Electron mobility; with respect to the distance along the channel for CRC and BP-JL-RC-MOSFET.

Further, electron velocity and electron temperature have been evaluated for both the devices and it is found that electron velocity (shown in Fig. 8(a)) has enhanced significantly for BP-JL-RC-MOSFET as compared to the conventional device due to the enhancement in electric field as the electric field has a direct impact on the electron velocity. Due to the higher electron velocity, which is doubled in BP-JL-RC-MOSFET as compared to CRC-MOSFET, switching ratio is also high thus; BP-JL-RC device is a suitable candidate for higher switching applications. Fig. 8(b) reflects the variation of electron temperature for BP-JL-RC-MOSFET and CRC-MOSFET along the channel, and it is evident that electron temperature is varied from source to drain. First, the electron temperature of BP-JL-RC is high (470K) as compared to CRC (350K) at the source side but reduces in the channel region for BP-JL-RC (550K) as compared to CRC (680K) and it is very low (less varying) throughout the channel for BP-JL-RC-MOSFET. The electron temperature should be as low as possible for eliminating (minimizing) the leakage currents such as hot electron injected gate current and impact ionization

substrate current for building it suitable for switching and ultra-low power applications. Low electron temperature is observed for BP-JL-RC due to Junctionless phenomenon and higher electron mobility of the device as well as gate material (black phosphorus) used in the recessed region.



8(a) 8(b)

Fig. 8. (a) Electron temperature and (b) Electron velocity; with respect to the distance along the channel for CRC and BP-JL-RC-MOSFET.

5.2. Analysis of RF performance

Moreover, power gains are significant in the designing of RF amplifiers, but for the designing of low-noise amplifiers (LNA), stability is one of the primary standards. For the designing of an amplifier for very high frequency, oscillation should be avoided. Stability of an amplifier, also evaluated as Stern stability factor (*K*), ia found to have a value of *K* usually greater than one at high frequency and less than one at low frequency [28, 29]. By using equation (1) [30, 31], K can be defined as-

$$K = \frac{1+|\Delta|^2-|S_{11}|^2-|S_{22}|^2}{2.|S_{12.}\cdot S_{21}|} \quad (1)$$

where S_{11} and S_{22} represent the reflection coefficients and S_{12} and S_{21} are transmission coefficients, and s-matrix Δ is defined as

$$\Delta = S_{11}\times S_{22} - S_{12}\times S_{21} \quad \ldots\ldots\ldots\ldots\ldots (2)$$

K has been evaluated for both the devices as shown in Fig. 9. At high frequency, *K* is greater than one for the conventional device, and at very low frequencies, it is less than one while for the proposed device, it is ~1 (slightly > 1 at a higher frequency and < 1 at low frequency) which is suitable for designing of RF amplifiers as shown in Fig. 9.

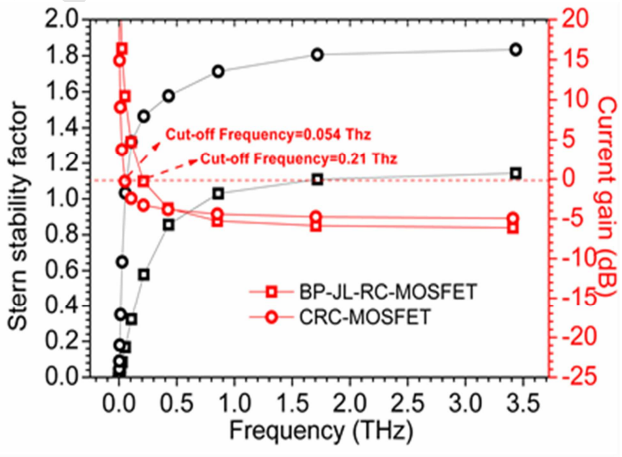


Fig. 9. Stern stability factor and Current gain (to find cut-off frequency) for CRC and BP-JL-RC-MOSFET.

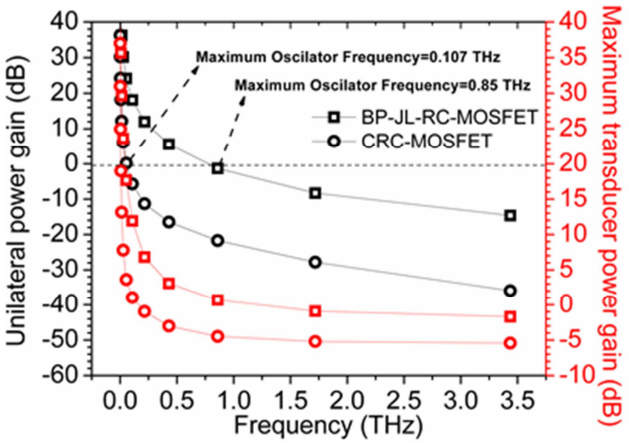


Fig. 10. Unilateral power gain (to find maximum oscillator frequency) and Maximum transducer power gain for CRC and BP-JL-RC-MOSFET.

For RF applications, cut-off frequency, f_T [32] is considered when comparing transistors. f_T is a measurement of speed and swing for high-speed digital applications, and it is defined as given in equation (3) [33-35]:

$$f_T = \frac{g_m}{2\pi\left(C_{gs} + C_{gd}\right)} \qquad \ldots\ldots\ldots\ldots\ldots\ldots (3)$$

where transconductance is denoted by g_m and parasitic capacitances are denoted by C_{gd} and C_{gs}. f_T is evaluated when the current gain is unity [36]. Results show that f_T improves 3.88 times in BP-JL-RC-MOSFET as compared to CRC-MOSFET which is reflected in Fig. 9 due to enhanced ON current and transconductance (shown in Fig. 4(a) and (b)). Further, the analysis of maximum oscillator frequency (f_{MAX}) is more important for high switching and high speed of CMOS device. f_{MAX} should be as high as possible, and it is defined as given in equation (4) [36, 37]:

$$f_{MAX} = \frac{f_T}{\sqrt{4R_g\left(g_{ds} + 2\pi f_T C_{gd}\right)}} \qquad \ldots\ldots\ldots\ldots\ldots\ldots (4)$$

Sometimes f_{MAX} is also evaluated when the unilateral power gain is unity [32]. Fig. 10 reflects ~8 times higher f_{MAX} in BP-JL-RC-MOSFET due to the enhancement in carrier mobility (shown in Fig. 7(b)) which reduces gate resistance and hence improves f_{MAX}, as f_{MAX} is directly proportional to transconductance and inversely related to gate resistance [32]. A higher value of f_T and f_{MAX} show the ability of BP-JL-RC-MOSFET for RF applications.

Moreover, the device comparison of BP-JL-RC and CRC-MOSFET have been performed in terms of other RF metrics such as Gma (maximum available power gain) and Gms (maximum stable power gain). Fig. 11 shows the improved maximum theoretical power gain in BP-JL-RC-MOSFET as compared to the conventional device as required for high-frequency applications. In a two-port network, Gma is defined by the ratio of maximum power available at load to the maximum power available at the source, and it is given as in equation 5. For high frequency (THz) applications, Gma and Gms should be large for the device and thus; BP-JL-RC device shows a significant enhancement due to the useful electrical property of black phosphorus.

$$G_{ma} = \frac{P_{load,\max}}{P_{source,\max}} \qquad \ldots\ldots\ldots\ldots\ldots\ldots (5)$$

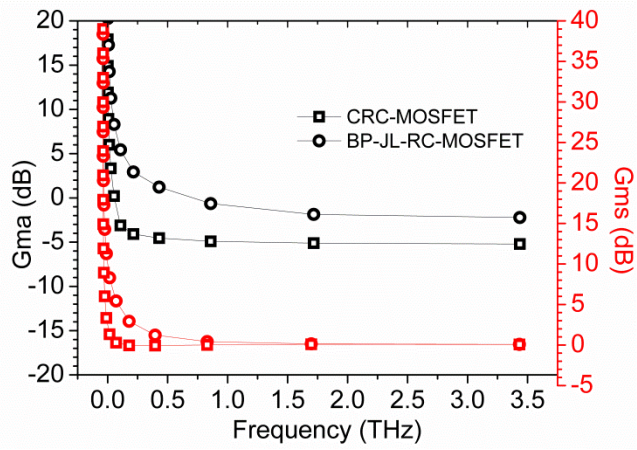
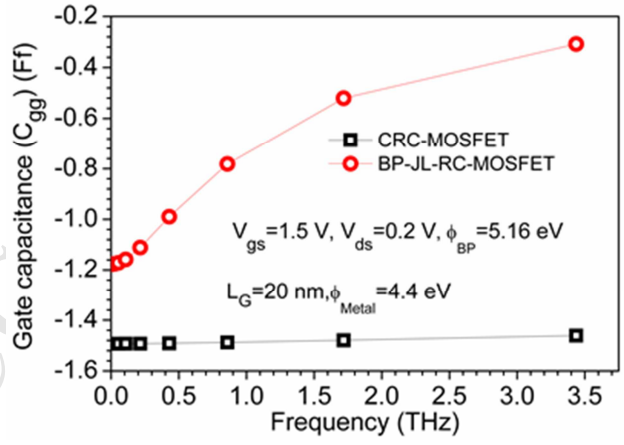
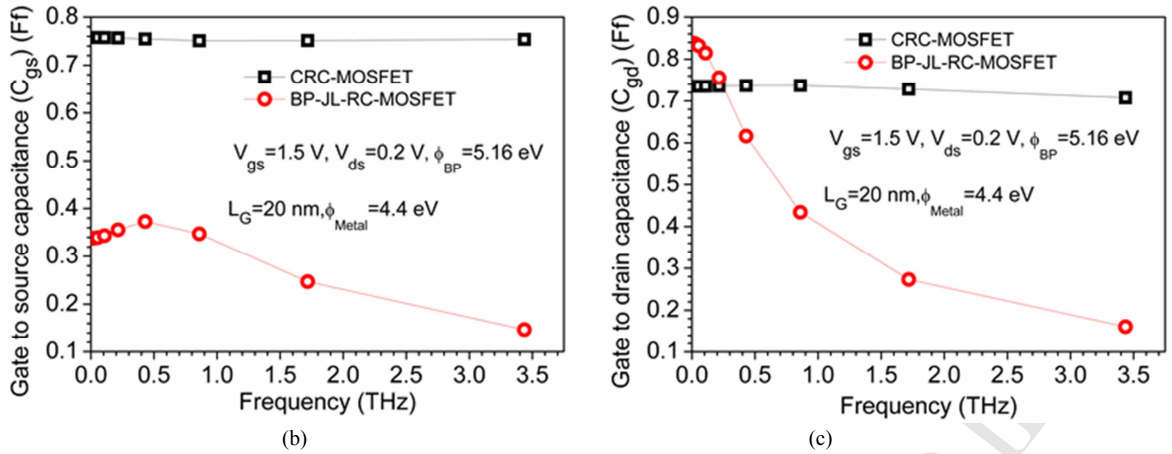


Fig. 11. Gma (Maximum Available Power Gain) and Gms (Maximum Stable Power Gain) for CRC and BP-JL-RC-MOSFET.

Further, the parasitic capacitances have been evaluated as for the high performance of the device; parasitic capacitances should be as small as possible due to the dependency of speed of a transistor on parasitic capacitances [38, 39], which causes a delay in logic-cell. Rise and fall times of a digital device may increase at the input and output side due to the parasitic capacitances as we know that, the maximum speed of a digital switching circuit mainly affects the rise time and fall time [40]. Thus, for RF applications, the investigation of parasitic capacitances is necessary. Many RF amplifiers may have low gain, and sometimes oscillation occurs in the amplifier due to these parasitic losses (parasitic capacitances). In this section, parasitic capacitances have been evaluated in terms of gate capacitance (C_{gg}), the gate to source capacitance (C_{gs}) and gate to drain capacitance (C_{gd}) shown in Fig. 12(a), (b) and (c) respectively for BP-JL-RC and CRC-MOSFET. Results show that BP-JL-RC-MOSFET exhibits very small C_{gg}, C_{gs} and C_{gd} as compared to CRC-MOSFET when frequency increases from few Hz to THz range due to the high carrier mobility across the channel (shown in Fig .7(b)) and junctionless phenomenon in BP-JL-RC-MOSFET.



(a)



(b) (c)

Fig. 12. (a): C_{gg}, (b) C_{gs} and (c) C_{gd} for CRC and BP-JL-RC-MOSFET.

Table II: Summary of Analog and RF FOMs

Device / Parameters	BP-JL-RC-MOSFET	CRC-MOSFET
g_m (μS)	1600	500
I_{on}/ I_{off}	3×10^{11}	1.9×10^{3}
Subthreshold slope (mV/dec)	67.2	151
Electric field (V/cm)	9×10^{5}	3×10^{5}
Electron mobility ($cm^2V^{-1}s^{-1}$)	900	650
Electron temperature (K)	550	680
f_T (THz)	0.21	0.0536
f_{MAX} (THz)	0.85	0.107
C_{gs} (ff)	0.15	0.75
C_{gd} (ff)	0.15	0.7
C_{gg} (ff)	0.3	1.5

Conclusion

This analysis examines the effectiveness of black phosphorus, a new class of material as a gate metal and a junctionless technology on to the RC MOSFET. This study is done in terms of analog and RF FOMs at room temperature (300K). Results so obtained reveals that black phosphorus significantly enhances the ON-current, whereas junctionless scheme reduces OFF-current remarkably which thus improves the switching ratio and thus, the analog performance of RC MOSFET at a low bias voltage. Moreover, it is observed that parasitic capacitances which hamper the device performance at high frequency are greatly reduced in BP-JL-RC-MOSFET in comparison to the conventional counterpart. Also, f_T (3.88 times) and f_{MAX} (~8 times) is enhanced significantly, which makes BP-JL-RC-MOSFET a potential candidate for low power analog and RF applications.

Acknowledgement

The authors are thankful to University Grants Commission (UGC), Electrical Engineering Department, Microelectronics Research Lab, and Delhi Technological to carry out this work.

ACCEPTED MANUSCRIPT

References

[1] M. Saito, M. Ono, R. Fujimoto, H. Tanimoto, N. Ito, T. Yoshitomi, T. Ohguro, H.S. Momose, H. Iwai, 0.15-μm RF CMOS technology compatible with logic CMOS for low-voltage operation, Electron Devices, IEEE Transactions on 45(3) (1998) 737-742.

[2] L.E. Larson, Silicon technology tradeoffs for radio-frequency/mixed-signal" systems-on-a-chip", Electron Devices, IEEE Transactions on 50(3) (2003) 683-699.

[3] V. Kilchytska, A. Nève, L. Vancaillie, D. Levacq, S. Adriaensen, H. Van Meer, K. De Meyer, C. Raynaud, M. Dehan, J.-P. Raskin, Influence of device engineering on the analog and RF performances of SOI MOSFETs, Electron Devices, IEEE Transactions on 50(3) (2003) 577-588.

[4] J.-Y. Yang, K. Benaissa, D. Crenshaw, B. Williams, S. Sridhar, J. Ai, G. Boselli, S. Zhao, S.-P. Tang, N. Mahalingam, 0.1 μm RFCMOS on high resistivity substrates for system on chip (SOC) applications, IEDm: international electron devices meeting, 2002, pp. 667-670.

[5] R. Murali, J.D. Meindl, Modeling the effect of source/drain junction depth on bulk-MOSFET scaling, Solid-state electronics 51(6) (2007) 823-827.

[6] Q.B. Chen, Compact modeling of multi-gate MOSFETs for RF designs, 2013 IEEE International Wireless Symposium (IWS), 2013.

[7] Z.-H. Liu, C. Hu, J.-H. Huang, T.-Y. Chan, M.-C. Jeng, P.K. Ko, Y.C. Cheng, Threshold voltage model for deep-submicrometer MOSFETs, IEEE Transactions on electron devices 40(1) (1993) 86-95.

[8] E. Takeda, C.Y.-W. Yang, A. Miura-Hamada, Hot-carrier effects in MOS devices, Academic Press1995.

[9] C.V. Mouli, SOI device with reduced drain induced barrier lowering, Google Patents, 2009.

[10] A. Kumar, N. Gupta, R. Chaujar, Analysis of novel transparent gate recessed channel (TGRC) MOSFET for improved analog behaviour, Microsystem Technologies 22(11) (2016) 2665-2671.

[11] J.-i. Nishizawa, T. Ohmi, Short channel MOSFET with buried anti-punch through region, Google Patents, 1995.

[12] R. Chaujar, R. Kaur, M. Saxena, M. Gupta, R. Gupta, TCAD assessment of gate electrode workfunction engineered recessed channel (GEWE-RC) MOSFET and its multilayered gate architecture—part I: hot-carrier-reliability evaluation, Electron Devices, IEEE Transactions on 55(10) (2008) 2602-2613.

[13] K.-T. Lam, Z. Dong, J. Guo, Performance limits projection of black phosphorous field-effect transistors, IEEE Electron Device Letters 35(9) (2014) 963-965.

[14] H. Liu, A.T. Neal, Z. Zhu, Z. Luo, X. Xu, D. Tománek, D.Y. Peide, Phosphorene: an unexplored 2D semiconductor with a high hole mobility, (2014).

[15] A. Castellanos-Gomez, L. Vicarelli, E. Prada, J.O. Island, K. Narasimha-Acharya, S.I. Blanter, D.J. Groenendijk, M. Buscema, G.A. Steele, J. Alvarez, Isolation and characterization of few-layer black phosphorus, 2D Materials 1(2) (2014) 025001.

[16] S. Das, W. Zhang, M. Demarteau, A. Hoffmann, M. Dubey, A. Roelofs, Tunable transport gap in phosphorene, Nano letters 14(10) (2014) 5733-5739.

[17] F. Schwierz, Graphene transistors, Nature nanotechnology 5(7) (2010) 487-496.

[18] C. Gong, H. Zhang, W. Wang, L. Colombo, R.M. Wallace, K. Cho, Band alignment of two-dimensional transition metal dichalcogenides: Application in tunnel field effect transistors, Applied Physics Letters 103(5) (2013) 053513.

[19] H. Fang, S. Chuang, T.C. Chang, K. Takei, T. Takahashi, A. Javey, High-performance single layered WSe2 p-FETs with chemically doped contacts, Nano letters 12(7) (2012) 3788-3792.

[20] N.R. Pradhan, D. Rhodes, S. Feng, Y. Xin, S. Memaran, B.-H. Moon, H. Terrones, M. Terrones, L. Balicas, Field-effect transistors based on few-layered α-MoTe2, ACS nano 8(6) (2014) 5911-5920.

[21] M.C. Robbins, S.J. Koester, Black Phosphorus p-and n-MOSFETs With Electrostatically Doped Contacts, IEEE Electron Device Letters 38(2) (2017) 285-288.

[22] N. Haratipour, S.J. Koester, Ambipolar black phosphorus MOSFETs with record n-channel transconductance, IEEE Electron Device Letters 37(1) (2016) 103-106.

[23] F. D'Agostino, D. Quercia, Short-channel effects in MOSFETs, Introduction to VLSI design (EECS 467) (2000).

[24] J. Colinge, C. Lee, N.D. Akhavan, R. Yan, I. Ferain, P. Razavi, A. Kranti, R. Yu, Junctionless transistors: physics and properties, Semiconductor-On-Insulator Materials for Nanoelectronics Applications, Springer2011, pp. 187-200.

[25] I. SILVACO, ATLAS User's Manual, Santa Clara, CA, Ver 5 (2011).

[26] J. Appenzeller, R. Martel, P. Avouris, J. Knoch, J. Scholvin, J.A. del Alamo, P. Rice, P. Solomon, Sub-40 nm SOI V-groove n-MOSFETs, IEEE Electron Device Letters 23(2) (2002) 100-102.

[27] M. Xiao-Hua, H. Yue, S. Bao-Gang, G. Hai-Xia, R. Hong-Xia, Z. Jin-Cheng, Z. Jin-Feng, Z. Xiao-Ju, Z. Wei-Dong, Fabrication and characterization of groove-gate MOSFETs based on a self-aligned CMOS process, Chinese Physics 15(1) (2006) 195.

[28] S.K. Pati, K. Koley, A. Dutta, N. Mohankumar, C.K. Sarkar, Study of body and oxide thickness variation on analog and RF performance of underlap DG-MOSFETs, Microelectronics Reliability 54(6-7) (2014) 1137-1142.

ACCEPTED MANUSCRIPT

[29] E. Dastjerdy, R. Ghayour, H. Sarvari, Simulation and analysis of the frequency performance of a new silicon nanowire MOSFET structure, Physica E: Low-dimensional Systems and Nanostructures 45 (2012) 66-71.

[30] A. Kumar, N. Gupta, R. Chaujar, Power gain assessment of ITO based Transparent Gate Recessed Channel (TGRC) MOSFET for RF/wireless applications, Superlattices and Microstructures 91 (2016) 290-301.

[31] N. Gupta, A. Kumar, R. Chaujar, Impact of device parameter variation on RF performance of gate electrode workfunction engineered (GEWE)-silicon nanowire (SiNW) MOSFET, Journal of Computational Electronics 14(3) (2015) 798-810.

[32] A. Sarkar, R. Jana, The influence of gate underlap on analog and RF performance of III–V heterostructure double gate MOSFET, Superlattices and Microstructures 73 (2014) 256-267.

[33] A. Kumar, N. Gupta, R. Chaujar, TCAD RF performance investigation of Transparent Gate Recessed Channel MOSFET, Microelectronics Journal 49 (2016) 36-42.

[34] A. Kumar, M. Tripathi, R. Chaujar, Reliability Issues of In2O5Sn Gate Electrode Recessed Channel MOSFET: Impact of Interface Trap Charges and Temperature IEEE Transactions on electron devices 99(3) (2018) 1-7.

[35] A. Kumar, Effect of trench depth and gate length shrinking assessment on the analog and linearity performance of TGRC-MOSFET, Superlattices and Microstructures 109 (2017) 626-640.

[36] B. Nae, A. Lazaro, B. Iniguez, High frequency and noise model of gate-all-around MOSFETs, Electron Devices, 2009. CDE 2009. Spanish Conference on, IEEE, 2009, pp. 112-115.

[37] N. Gupta, R. Chaujar, Investigation of temperature variations on analog/RF and linearity performance of stacked gate GEWE-SiNW MOSFET for improved device reliability, Microelectronics Reliability 64 (2016) 235-241.

[38] N.R. Mohapatra, M.P. Desai, S.G. Narendra, V.R. Rao, Modeling of parasitic capacitances in deep submicrometer conventional and high-K dielectric MOS transistors, IEEE Transactions on Electron devices 50(4) (2003) 959-966.

[39] A. Kumar, M. Tripathi, R. Chaujar, Investigation of parasitic capacitances of In2O5Sn gate electrode recessed channel MOSFET for ULSI switching applications, Microsystem Technologies 23(12) (2017) 5867-5874.

[40] P. Malik, R.S. Gupta, R. Chaujar, M. Gupta, AC analysis of nanoscale GME-TRC MOSFET for microwave and RF applications, Microelectronics Reliability 52(1) (2012) 151-158.

ACCEPTED MANUSCRIPT

Measurement 120 (2018) 52–75

Contents lists available at ScienceDirect

Measurement

journal homepage: www.elsevier.com/locate/measurement

Detection of Power Quality Event using Histogram of Oriented Gradients and Support Vector Machine

Rajiv Kapoor[a], Rashmi Gupta[b], Le Hoang Son[c,d,*], Sudan Jha[e], Raghvendra Kumar[f,g]

[a] ECE Department, Delhi Technological University, India
[b] ECE Department, AIACT&R, GGSIPU, Delhi, India
[c] Division of Data Science, Ton Duc Thang University, Ho Chi Minh City, Viet Nam
[d] Faculty of Information Technology, Ton Duc Thang University, Ho Chi Minh City, Viet Nam
[e] School of Computer Engineering, Kalinga Institute of Industrial Technology, Odisha, India
[f] Computer Science and Engineering Department, LNCT College, MP, India
[g] VNU University of Science, Vietnam National University, Hanoi, Viet Nam

ARTICLE INFO

Keywords:
Power quality (PQ)
Event detection
Histogram of oriented gradients (HOG)
Support vector machine (SVM)

ABSTRACT

This paper proposes a new method to distinguish power quality events based on the Histogram of Oriented Gradients (HOG) and Support Vector Machine (SVM). We examine energy quality events such as sag, interruptions, swell, harmonic, transient, notch and flicker. The proposed method calculates numerous power quality disturbances such as flickering with harmonics, intrusion with harmonics, and sagging with harmonics. It has less processing time than the previous methods due to multiple events occurring at same time. Numerical experiments performed on a real database of power quality disturbances show that there is less calculation in the proposal in comparison with the wavelet change, S-transform and Hilbert change. Recognition with the assistance of HOG gives better and precise outcome in time area with faster reaction.

1. Introduction

Detection and monitoring power quality is a vital issue for recognizing causes and characteristics in power quality events due to increasing in non-linear electrical loads in industries, commercial as well as domestic applications [17,18]. Distorted voltage waveform mainly depends on current drawn by non-linear loads, switching activities, etc. [14]. Distortion in voltage waveform causes odd behavior in control devices such as programmable logic controllers, electric drives, or in industries due to equipment breakdown in production line [19]. This problem is eradicated by recording and analysis of power quality events and statistical information. Accurate detection is necessary and useful for electrical engineers in solving issues related to power quality events. With the approach of signals preparing specialists in control quality applications, it is necessary to build up methods of discovery of power quality events for recording and investigation [20].

Power quality (PQ) event is the sudden disrupting impact that appears in power frameworks [21]. Presence of more than one kind of events is a multiple power quality event such as interruption with harmonics, sag with impulse, etc. It happens because of ground faults, lightning strikes, capacitor switching, switching of substantial and non-linear loads [21]. Numerous PQ events are created in control framework due to concurrent operations of these events. Programmed occasion disturbance acknowledgment is basic in sparing season of electric designers identifying, arranging and taking care of issues between consumers and utilities event analysis [22].

Various methods have been used for detection of power quality events such as Fourier transforms (FT), Short-time Fourier transform (STFT), Wavelet transform [1], EMD-HT [3], and Detection of Power-Quality Events Using Discrete Gabor Transform [4]. Power quality disturbances have also been classified using non-linear dimension reduction technique [5] which depends on the idea of nearby non-straight connection and non-direct fuzzy capacity to extricate elements. Statically matched wavelet methods have been used in light of the attributes of the PQ event utilizing the idea of partial Brownian movement. They are contrasted with Daubechies wavelet that demonstrates pre-

* Corresponding author at: Division of Data Science, Ton Duc Thang University, Ho Chi Minh City, Viet Nam. Tel.: +84 904 171 284.
E-mail addresses: rajivkapoor@dce.ac.in (R. Kapoor), rashmig71@yahoo.com (R. Gupta), lehoangson@tdt.edu.vn (L.H. Son), jhasudan@hotmail.com (S. Jha), raghvendraagrawal7@gmail.com (R. Kumar).

https://doi.org/10.1016/j.measurement.2018.02.008
Received 19 September 2017; Received in revised form 1 February 2018; Accepted 6 February 2018
Available online 07 February 2018
0263-2241/ © 2018 Elsevier Ltd. All rights reserved.

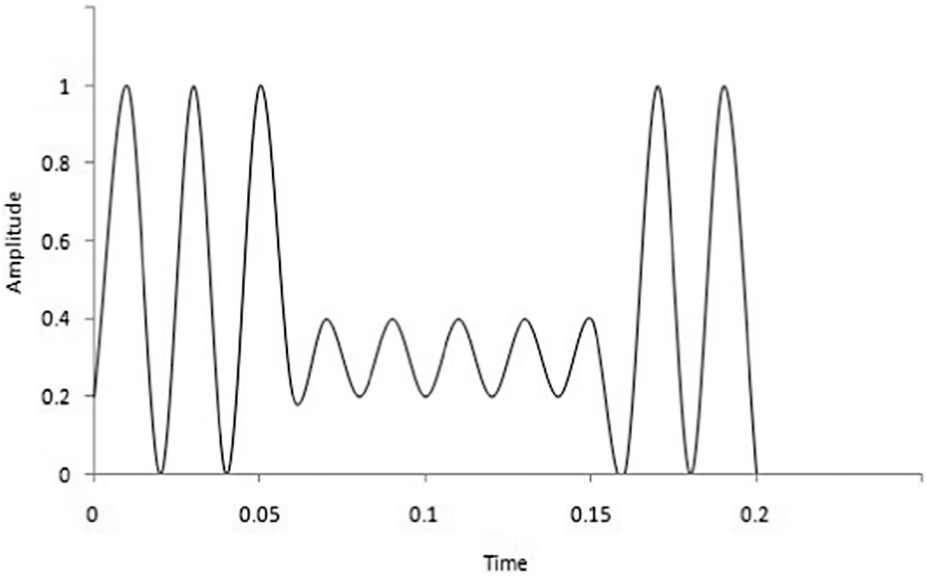


Fig. 1. Voltage sag.

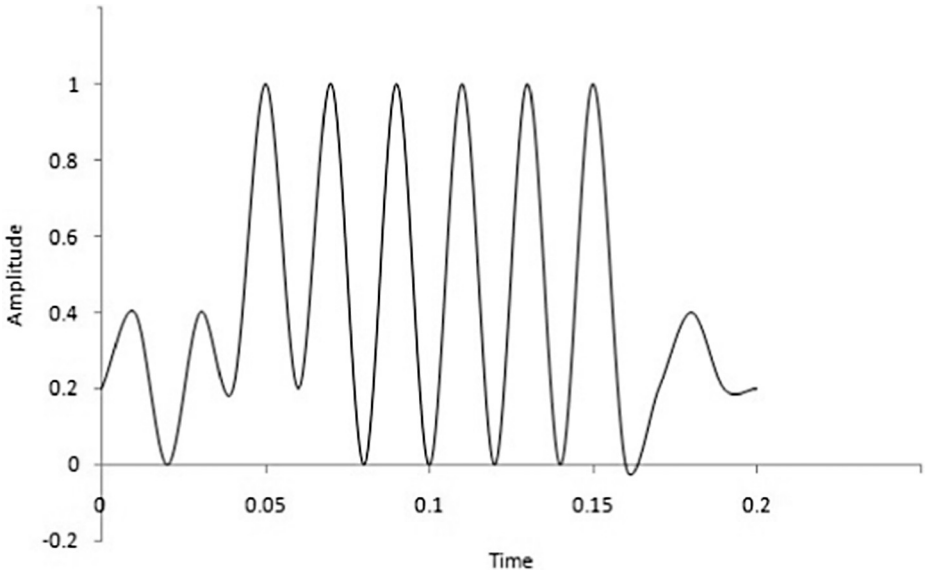


Fig. 2. Voltage swell.

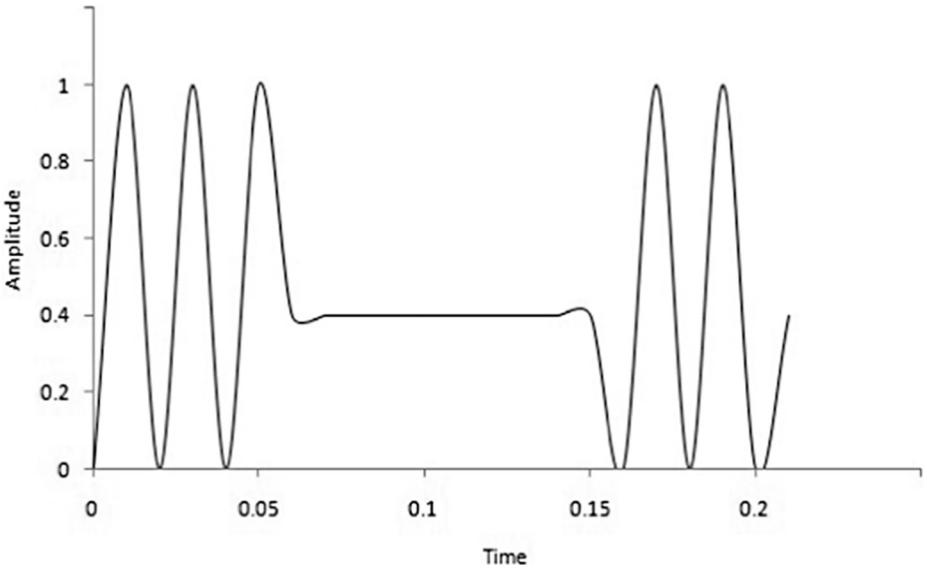


Fig. 3. Voltage interruption.

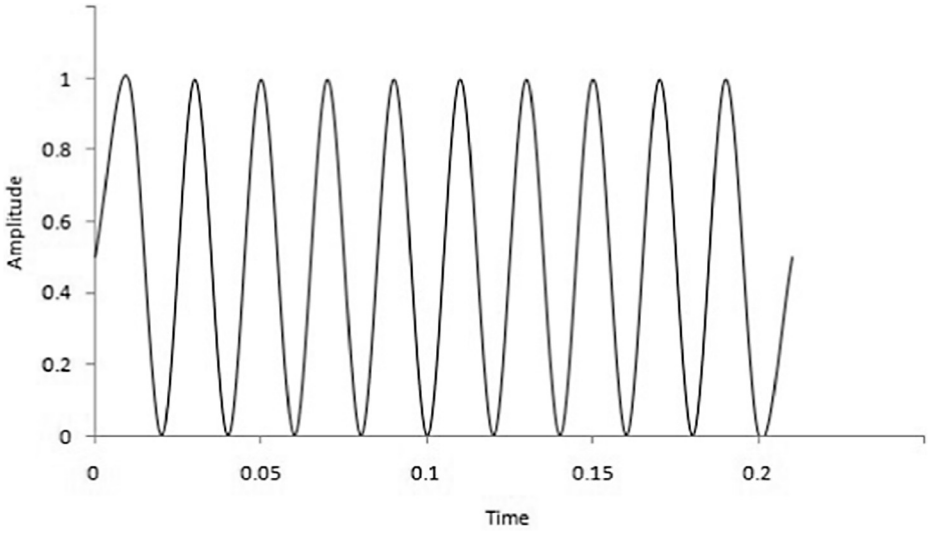


Fig. 4. Impulsive transient.

Table 1
Impulsive transients categories.

Impulsive transient	Spectral content	Typical duration
Nanosecond	5 ns rise	< 50 ns
Microsecond	1 μs rise	50 ns–1 ms
Millisecond	0.1 ms rise	> 1 ms

Table 2
Oscillatory transients classification.

Oscillatory transient	Spectral content	Typical duration	Typical voltage magnitude
Low frequency	< 5kHz	0.3–50 ms	0–4 pu
Medium frequency	5–500 kHz	20 μs	0–8 pu
High frequency	0.5–5 MHz	5 μs	0–4 pu

dominance in recognition of PQ events. Multi-wavelet transform [6] was used as an alternative mean to wavelet transform as it gives more accurate results and less numbers of samples compared to the wavelet transform. Real time discovery of power quality is vital to discovery of power quality unsettling influence [7]. More comprehensive studies on power quality event classification can be found in [8], and its applications can be found in [23–27].

Till now, we have observed that some techniques are good for detecting time domain behavior and some are good for frequency behavior. As the accuracy of detection increases complexity like in the case

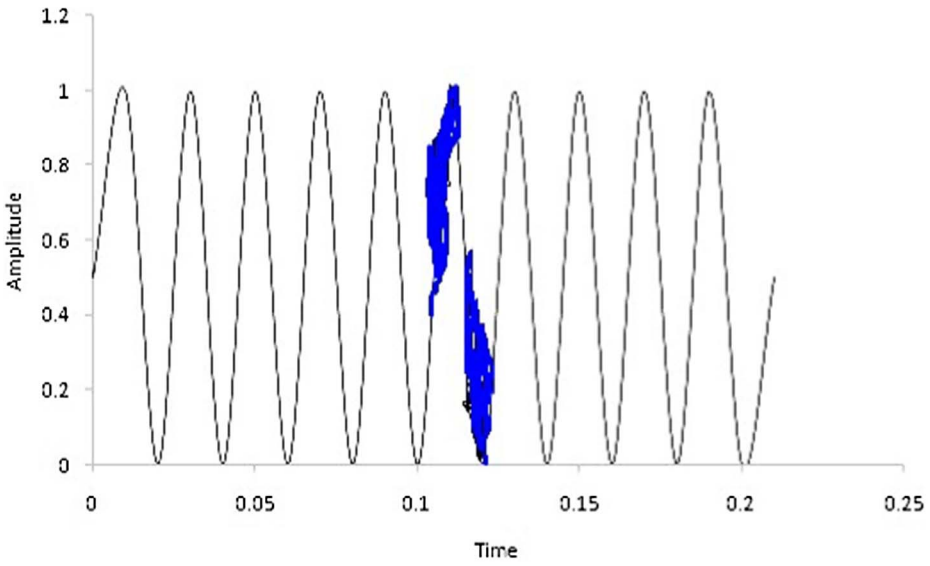


Fig. 5. Oscillatory transients.

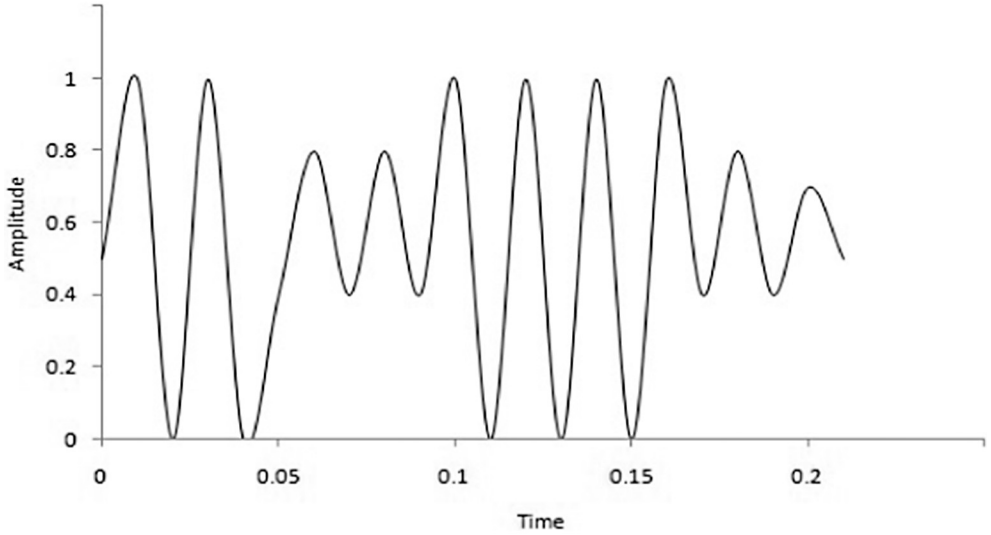


Fig. 6. Voltage flicker.

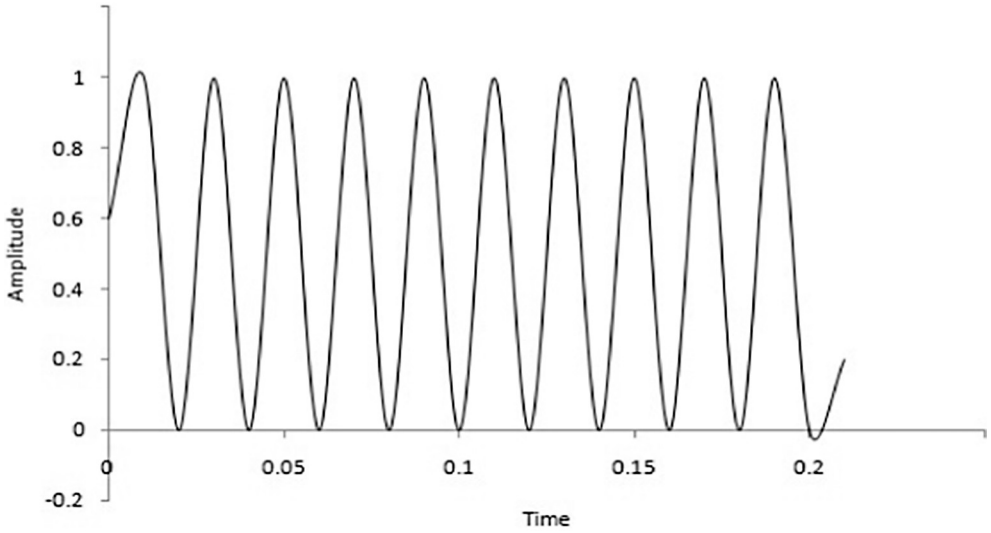


Fig. 7. Harmonics.

of wavelet transform and S-transform, it is indeed necessary to find new techniques that can detect event quickly and help the classifier to classify the event. After successful detection of disturbance, the next step is to classify the disturbance correctly so that it can be rectified by taking suitable actions. Regarding this, many techniques have been used in the past namely the support vector machine (SVM) [1,2,4], Neural Network, and fuzzy logic (FL) [9–11]. Accuracy of the classifier depends on features used in the training step. Many features like Standard Deviation, Energy, Maximum value and Total harmonic distortion have been frequently used.

In this paper, we propose a new method to distinguish power quality events based on the Histogram of oriented gradients (HOG) and Support Vector Machine (SVM). HOG can easily detect events in the signal with fast rate, good accuracy and few computations so that it can be efficiently implemented as compared to various time frequency analysis techniques [16]. The analysis of energy quality events such as sag, interruptions, swell, harmonic, transient, notch and flicker is examined in the new method. It calculates on numerous power quality disturbances, for example flickering with harmonics, intrusion with harmonics, sagging with harmonics and so forth. Therein, HOG is used to detect variations in the power signal and SVM classifier is used for classification of various events. The new method is experimentally validated.

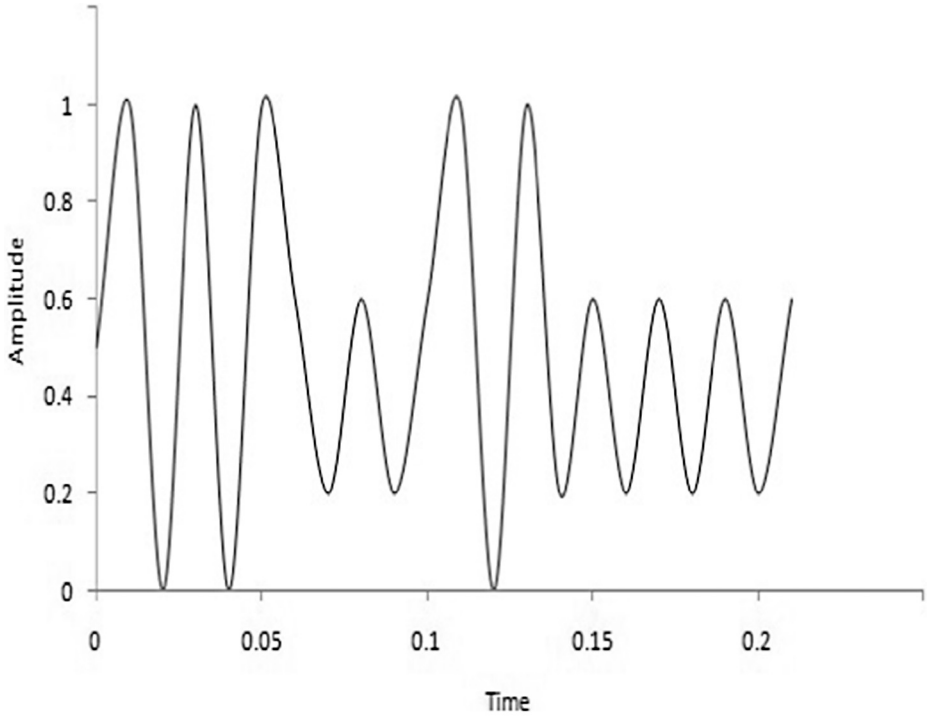


Fig. 8. Harmonics with flicker.

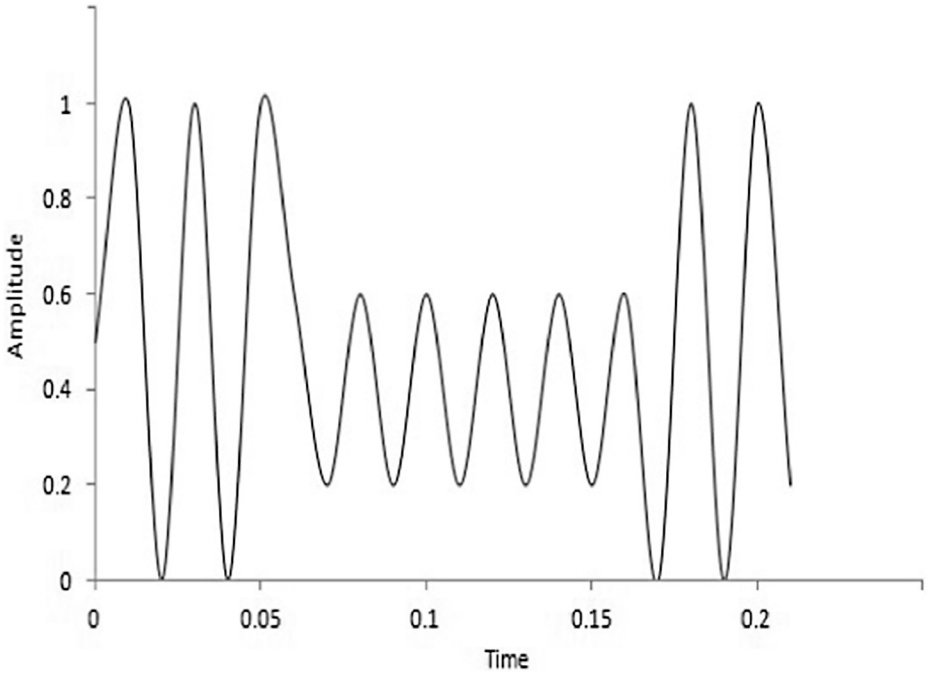


Fig. 9. Harmonics with sag.

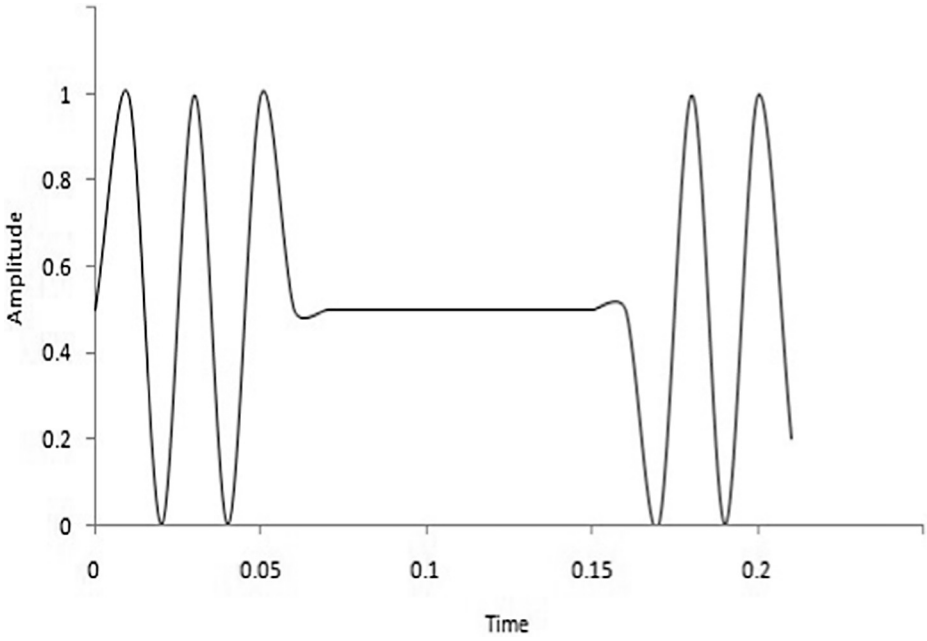


Fig. 10. Harmonics with interruption.

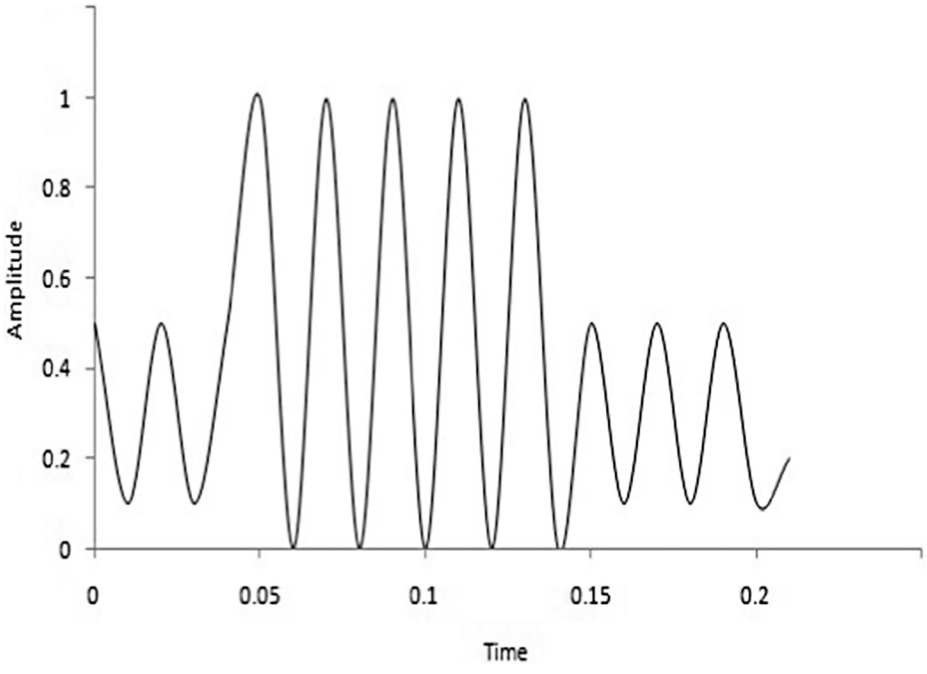


Fig. 11. Harmonics with swell.

The rest of the paper is organized as follows. Section 2 introduces the HOG method. Section 3 takes an overview of power quality events. Section 4 demonstrates the new algorithm for power quality event detection. Section 5 presents the power quality event classification using the SVM method. Section 6 shows the experimental results. Finally, Section 7 concludes the paper and delineates further studies.

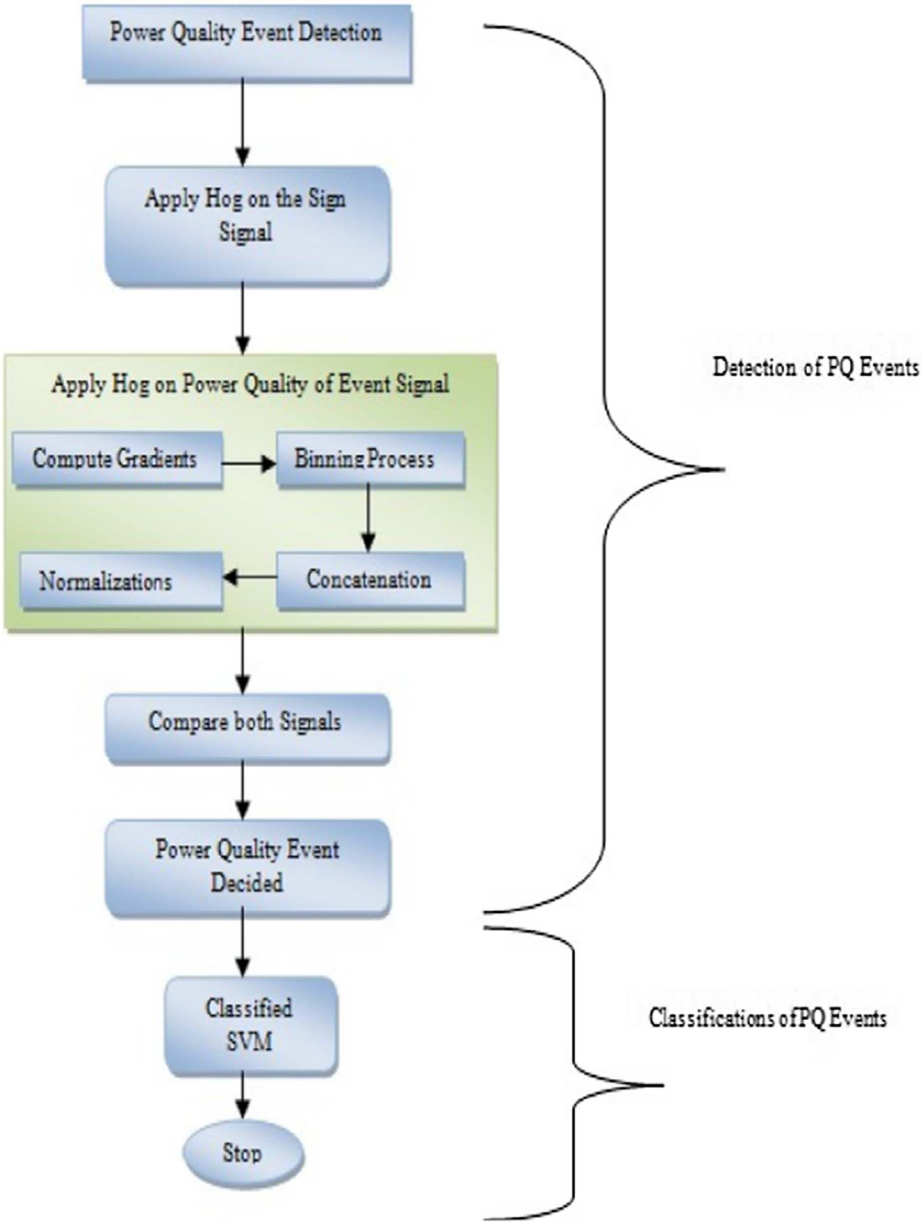


Fig. 12. Recognition of PQ event.

2. Histogram of oriented gradients

Histogram of oriented gradient (HOG) was firstly used to detect the pedestrians. It is implemented in four steps [15,17]. First step is preprocessing the data, second is calculating gradient, third is orientation and fourth is normalization. Four steps are defined as follows:

2.1. Preprocessing

Preprocessing is initially used to reduce noises. The reduction is compulsory; otherwise it gives false output of gradient vectors. Preprocessing is mainly done with the help of filters by convolving the signal with the filter. Multiplication of image with the filter can also be called as a kernel or mask. The multiplication or convolving the signal is simply sliding the filter over an image [19]. To reduce noises, various filters are used such as Gaussian filters, etc.

2.2. Gradient computation

In order to get accurate shape and appearance gradient, gradient

Table 3
List of power quality events.

PQ disturbance	Model	Parameter
Sine	$f(t) = A\sin(\omega t)$	Frequency = 50 Hz A = 1
Sag	$f(t) = A(1-a(u(t-t_1)-u(t-t_2)))\sin(\omega t)$	$0.1 \leqslant a \leqslant 0.9$; $T \leqslant t_2 - t_1 \leqslant 9T$
Swell	$f(t) = A(1 + a(u(t-t_1)\text{-}u(t\text{-}t_2)))\sin(\omega t)$	$0.1 \leqslant a \leqslant 0.8$; $T \leqslant t_2 - t_1 \leqslant 9T$
Interruption	$f(t) = A(1-a(t\sin(\omega t)$	$0.1 \leqslant a \leqslant 0.9$; $T \leqslant t_2 - t_1 \leqslant 9T$
Flicker	$f(t) = A(1 + \alpha_f \sin(\beta_f \omega t))\sin(\omega t)$	$\alpha_f = 0.1-0.2$; $\beta_f = 5-10Hz$
Harmonic	$f(t) = A(\alpha_1 \cdot \sin(\omega t) + \alpha_3 \sin(3\omega t) + \alpha_5 \cdot \sin(5\omega t) + \alpha_7 \cdot \sin(7\omega t))$	$0.05 \leqslant \alpha_3 \leqslant 0.15$; $0.05 \leqslant \alpha_5 \leqslant 0.15$ $0.05 \leqslant \alpha_7 \leqslant 0.15$; $\sum \alpha_i^2 = 1$
Transient	$f(t) = A\sin(\omega t) + \alpha_{OSC} \cdot \exp(-(\frac{t-t_1}{T_{OSC}})) \cdot \sin\omega_{nosc}(t-t_1))$	$T_{osc} = 0.008-0.04$ s $\omega_{nosc} = 100-400$ Hz
Swell with Harmonic	$f(t) = A(1 + \alpha(u(t-t_1)-u(t-t_2))) \cdot \alpha_1 \sin(\omega t) + \alpha_3 \cdot \sin(3\omega t) + \alpha_5 \cdot \sin(5\omega t) + \alpha_7 \cdot \sin(7\omega t))$	$0.1 \leqslant \alpha \leqslant 0.8$; $T \leqslant t_2 - t_1 \leqslant 9T$ $0.05 \leqslant \alpha_i \leqslant 0.15$; $\sum \alpha_i^2 = 1$
Sag with harmonics	$f(t) = A(1-a(u(t-t_1)-u(t-t_2))) * A(\alpha_1 \cdot \sin(\omega t) + \alpha_3 \sin(3\omega t) + \alpha_5 \cdot \sin(5\omega t) + \alpha_7 \cdot \sin(7\omega t))$	$0.1 \leqslant a \leqslant 0.9$; $T \leqslant t_2 - t_1 \leqslant 9T$ $0.05 \leqslant \alpha_3 \leqslant 0.15$ $0.05 \leqslant \alpha_5 \leqslant 0.15$; $0.05 \leqslant \alpha_7 \leqslant 0.15$ $\sum \alpha_i^2 = 1$
Flicker with harmonics	$f(t) = A(1 + \alpha_f \sin(\beta_f \omega t))\sin(\omega t) * A(\alpha_1 \cdot \sin(\omega t) + \alpha_3 \sin(3\omega t) + \alpha_5 \cdot \sin(5\omega t) + \alpha_7 \cdot \sin(7\omega t))$	$\alpha_f = 0.1-0.2$; $\beta_f = 5-10$ Hz $0.05 \leqslant \alpha_3 \leqslant 0.15$; $0.05 \leqslant \alpha_5 \leqslant 0.15$ $0.05 \leqslant \alpha_7 \leqslant 0.15$; $\sum \alpha_i^2 = 1$
Interruption with harmonics	$f(t) = A(1-a(t\sin(\omega t) * A(\alpha_1 \cdot \sin(\omega t) + \alpha_3 \sin(3\omega t) + \alpha_5 \cdot \sin(5\omega t) + \alpha_7 \cdot \sin(7\omega t))$	$0.1 \leqslant a \leqslant 0.9$; $T \leqslant t_2 - t_1 \leqslant 9T$ $0.05 \leqslant \alpha_3 \leqslant 0.15$; $0.05 \leqslant \alpha_5 \leqslant 0.15$ $0.05 \leqslant \alpha_7 \leqslant 0.15$; $\sum \alpha_i^2 = 1$
Spikes	$f(t) = \sin(\omega t) + sign(\sin(\omega t)) * \sum k * (u(t-(t_1 + 0.02n)) - (u(t-(t_2 - 0.02n)))$	$0.1 \leqslant k \leqslant 0.4, 0 \leqslant t_1$ $t_2 \leqslant 0.5T, 0.01T \leqslant t_2 - t_1 \leqslant 0.05T$

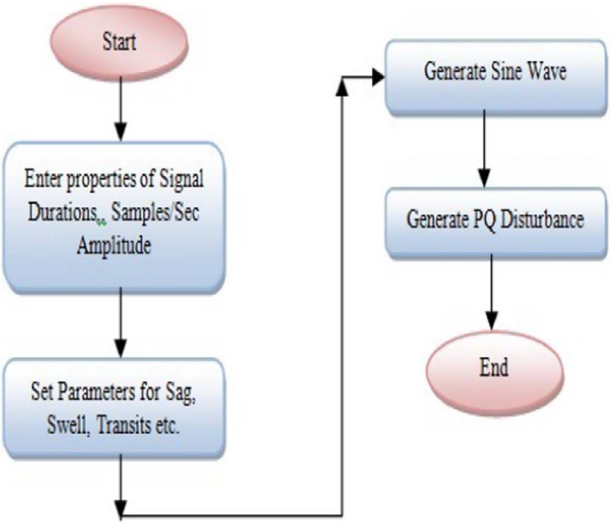


Fig. 13. Flow chart for PQ signal disturbance.



Fig. 14. Operating procedures of classifiers.

computation is used in feature extraction of an image. This function is based on calculating the derivatives of each function $\partial f/\partial x$ and $\partial f/\partial y$ at each pixel coordinate. To find the edge detection of the image, magnitude is calculated as below.

$$(Magnitude)^2 = [Gx^2 + Gy^2] \tag{1}$$

After calculating gradient, direction can be calculated:

$$\tan^{-1}\varnothing \text{ where } \varnothing = \frac{Gy}{Gx} \tag{2}$$

where $\varnothing$ represents the resultant angle whereas Gy and Gx are the component along x and y directions.

2.3. Binning orientation

In HOG analysis, weighted magnitude and binning orientation play a key role. In each pixel, gradient of magnitude and orientation is calculated. Each pixel has a weighted magnitude represented in histogram channels (*bins*). The magnitudes are concatenated into bins. The region over this accumulation is said to be cells. The bins contain angles from 0 to 180° or 0 to 360°. Choice of good orientation produces better detection of patterns. The performance can be increased by adding the number of bins. For calculating the weight of each pixel, gradient is used. Then, all pixels are concatenated to form the histogram.

2.4. Normalization

Generally, there are variations in the image such as illumination, background and foreground contrast and brightness. They vary the

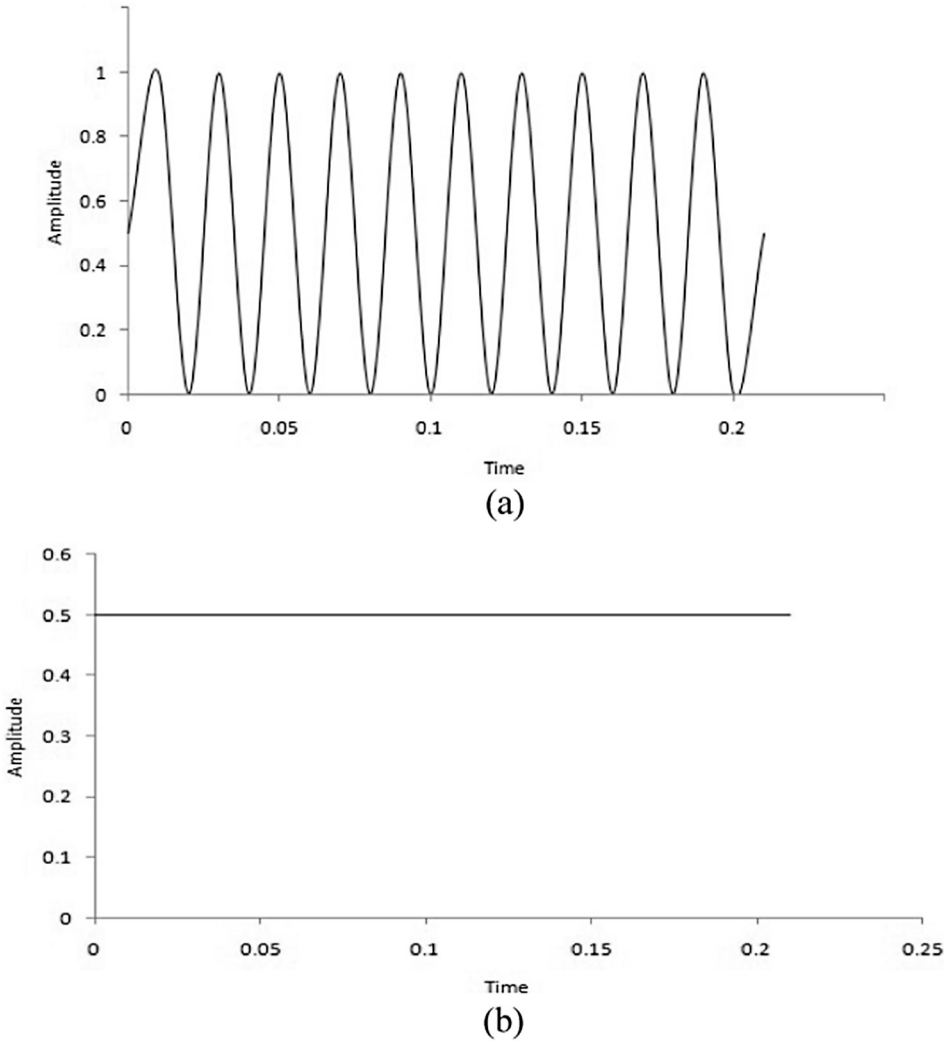


Fig. 15. (a) Sine wave and (b) HOG without any disturbance.

gradient strength over a wide range. Without applying normalization, result is not that much accurate. There are various methods to perform normalization.

$$l2{-}norm{:}\ v \rightarrow v/\sqrt{v_2^2 + \varepsilon^2}$$
$$l1{-}norm{:}\ v \rightarrow v/(v_1 + \in)$$
$$l1{-}sqrt{:}\ v \rightarrow v/(v_1 + \in) \quad (3)$$

By using Eq. (3), normalization is performed where $\boldsymbol{v}$ is the vector corresponding to the histogram of the block after combining $\in$, which is a small constant. After calculating the above equation, we get the normalized featured vector of HOG.

3. Power quality event

This section summarizes some types of power quality events namely sag, swell, and interruption, flickered [2–3].

3.1. Voltage Sag

Voltage sag demonstrated in Fig. 1 can be characterized as the decline in the nominal *rms* voltage between 0.1 p.u. and 0.9 p.u. The time length of voltage sag can fluctuate from 0.5 cycles to 1 min. Sag happens for the most part because of presence of Single Line to Ground (SLG) faults, starting of heavy motors and heavy current drawn activities. Voltage sag might likewise be characterized as the small-time decline of the voltage level. On the other hand, if decline in the voltage exists for over 1-moment, we utilize under voltage. Voltage sag can be separated into three wide classes based on the duration. These classes are instantaneous, momentary and temporary sag.

3.2. Voltage swell

Voltage swell as indicated in Fig. 2 can be characterized as the increment in the nominal *rms* voltage between 1.1 p.u. and 1.8 p.u. The

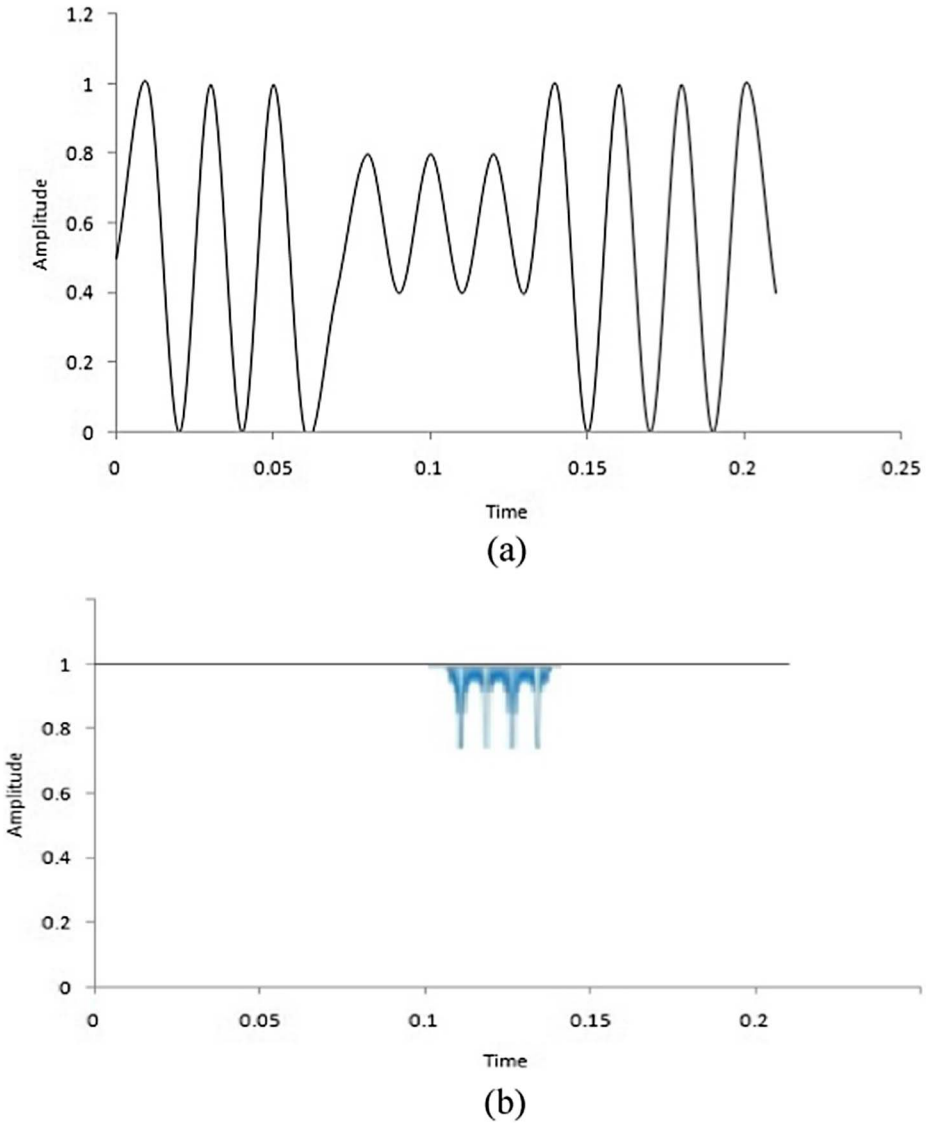


Fig. 16. (a) Sag and (b) HOG of disturbance.

event recurrence of voltage swell is low when contrasted with event of voltage sag. The time length of voltage swell can differ from 0.5 cycles to 1 min, which is same if there should be an occurrence of voltage sag. The component that may come about voltage swell incorporates light system loading, incorrect tap setting of the transformer and so on. Setting fast acting tap changers in the electrical system can be utilized to mitigate voltage swell. The severe effects of voltage swell event include overheating of devices and high iron loss in maximum machines applications.

3.3. Interruption

Voltage Interruption is can be characterized as the decline in *rms* voltage such that resultant is not greater than 0.1 p.u. For the most part, voltage interruption happens after the event of voltage sag. It happens as an aftereffect of loose connection, major faults and reclosing of electrical switch. Reclosing of electrical switch activity results in transient phenomenon took after by interruption can likewise be watched. The voltage interruption results in inconvenience trip and false operation of the overall system. As shown in Fig. 3, voltage interruption shows that there are almost zero voltages and no more power supply is available for the system.

3.4. Impulsive transient

Impulsive transient happens in unsettling disturbance that is experienced by the electrical clients. The immediate change in size of voltage magnitude for impulsive transient is unidirectional having

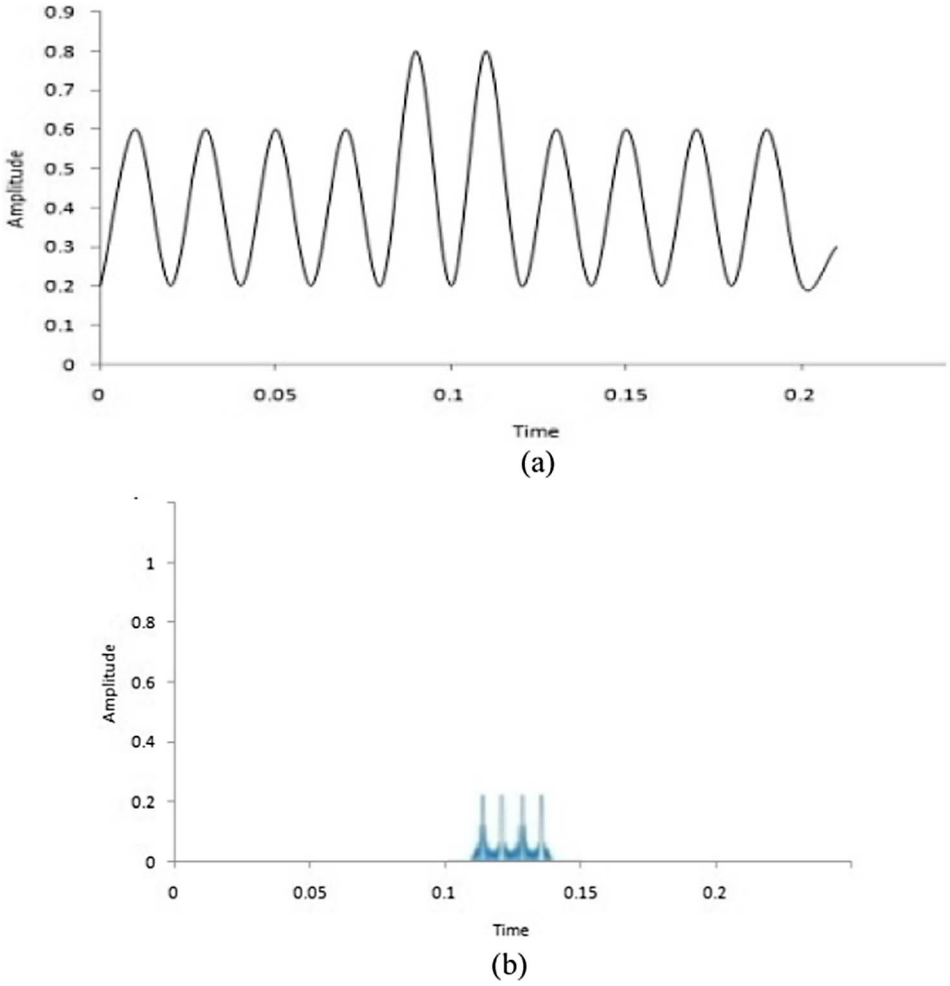


Fig. 17. (a) Swell and (b) HOG of disturbance.

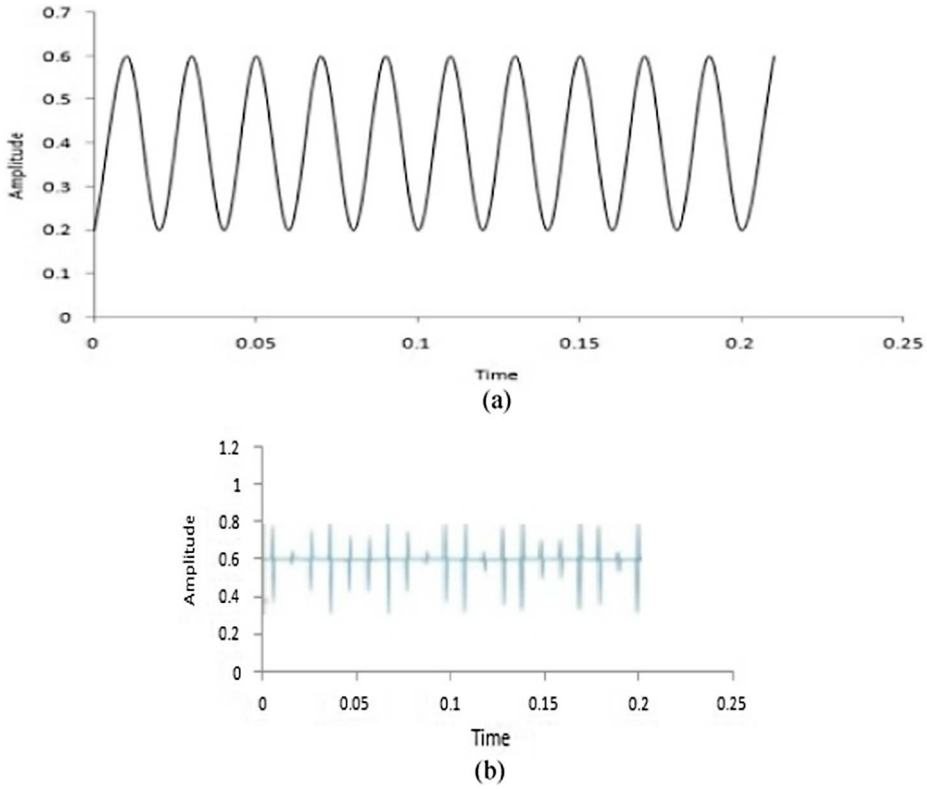


Fig. 18. (a) Flicker and (b) HOG of disturbance.

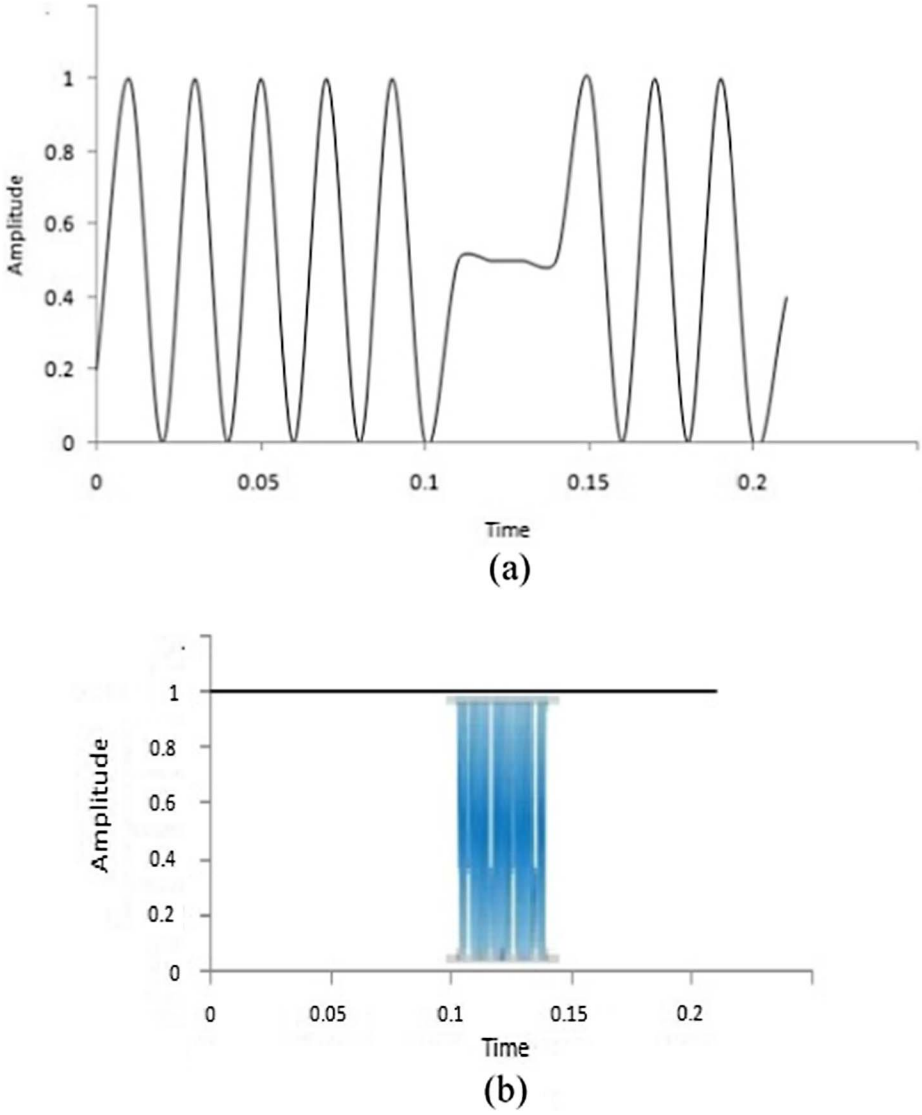


Fig. 19. (a) Interruption & (b) HOG of disturbance.

positive extremity. This event is recognized by its short rise and fall times as indicated in Fig. 4. Impulsive transients are further subdivided into three classes as given in Table 1. The most widely recognized reason that produces impulsive transient is lightning strike.

3.5. Oscillatory transient

Oscillatory transient occasion is another kind of PQ phenomenon that happens from the previous ones. The transient is sudden change in magnitude of voltage. The ordinary time length of this unsettling influence is between 5 μs and 50 ms. The maximum magnitude in arise of an occurrence of transient may reach up to 2.0 p.u. In the majority of average cases, most extreme size of oscillatory transient is between 1.2 and 1.5 p.u. demonstrated in Fig. 5. The sudden changes in the magnitude of the event oscillatory transients can be positive or negative in extremity. Oscillatory transient is subdivided into three classes as given in Table 2. These were based on selected frequency ranges, which correspond to common types of power system oscillatory transient phenomena. The frequency of the oscillation gives a trace to the origin of the disturbance. The transient might be generated as a result of capacitor switching, load switching and reclosing of circuit breaker.

3.6. Voltage flicker

Voltage flicker or flickering can be characterized as cyclic variations in magnitude of voltage with amplitude below 10% of the nominal

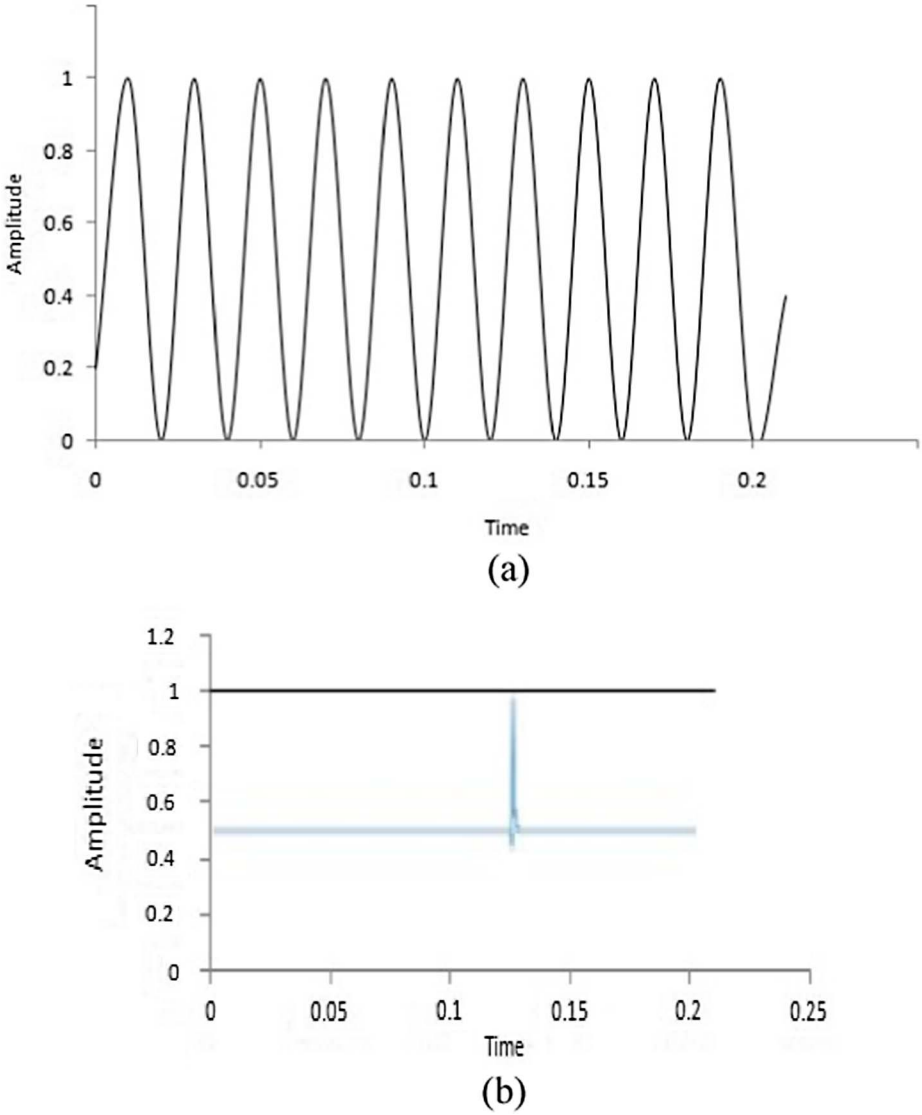


Fig. 20. (a) Impulsive transient & (b) HOG of disturbance.

value (Fig. 6). Electrical devices are not harmed by voltage variances, but rather these fluctuations may bring about adjustment in brightening intensity of light devices. Voltage flicker may result in unpleasant visual sensation, which becomes the source of complaints from utility customers. The disturbance level and unpleasant visual sensation depends on the type of lamp and characteristics (amplitude, frequency and duration) of the flickering.

3.7. Harmonics

Harmonics are created in an electric power framework as the result of nearness of non-linear loads. Consonant voltages and current in the power matrix framework are one of the successive explanations behind power quality issues. Harmonics in framework causes over warming of gadgets and conductors, false activating in factor speed drives, and torque varieties in engines. Diminishment or finish departure of harmonics is regarded as appealing. Most essential instances of gadgets as non-straight loads will join standard office equipment's, for instance, PCs and printers, Fluorescent lighting, battery chargers and many others. Harmonics are portrayed as sinusoidal voltages or currents having frequencies that are entire number results of essential recurrence at which the power framework is planned to work. Fig. 7 depicts Harmonics consolidating with basic voltage or current conveying a non-sinusoidal shape, along these lines, a waveform bending power quality issue. The non-sinusoidal shape relates to the entirety of various sine waves with various sizes and stage points, having frequencies that are results of the framework recurrence.

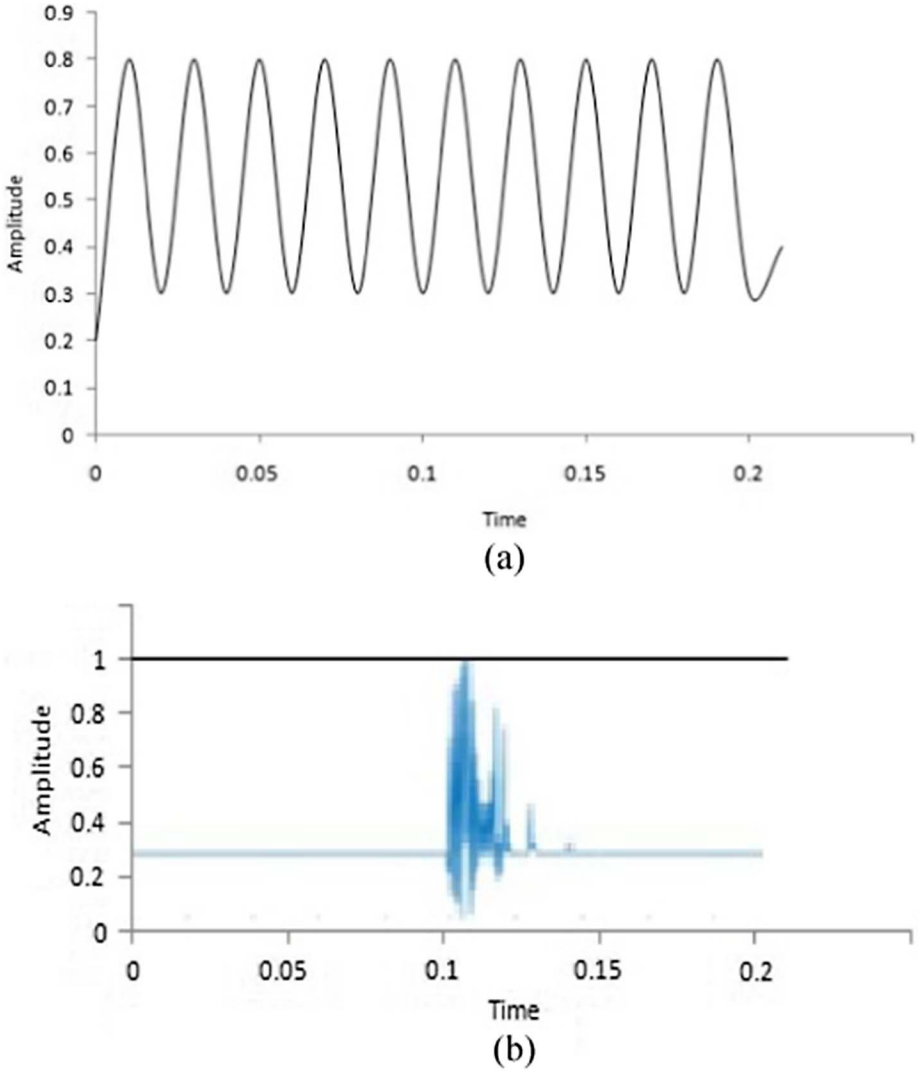


Fig. 21. (a) Oscilatory transient & (b) HOG of disturbance.

3.8. Other PQ disturbances

Other PQ disturbances are called multistage events. Multistage events occur due to experience of the more than one kind of events. In the meantime, many other types of disturbances can also occur due to various combinations of above events.

1. Harmonics with Flicker shown in Fig. 8.
2. Harmonics with Sag shown in Fig. 9.
3. Harmonics with Interruption shown in Fig. 10.
4. Harmonics with Swell shown in Fig. 11.

4. A new algorithm for power quality event detection

Fig. 12 shows the new algorithm for detection of power quality events. The algorithm consists of two parts: detection and classification. Detection is done with the help of HOG and classification is done with the help of SVM.

The proposed method for power quality event detection has four parts: preprocessing, gradient computation, binning orientation and normalization. Preprocessing is done for incoming events to reduce noises with the help of various filters. After preprocessing, gradient is computed for each pixel similarly to find gradient orientation. Binning process and normalization are then used. Synthetic information of PQ event has advantage in assessing the limit of classifier [1–3,12–13]. The availability of continuous power quality event data is compelled as it obliges long observation time with unsteadiness in the event of power quality event. Along these, mathematical models of power quality event are used for redirection. Particular power quality event is produced using addition of mathematical model of single stage control quality

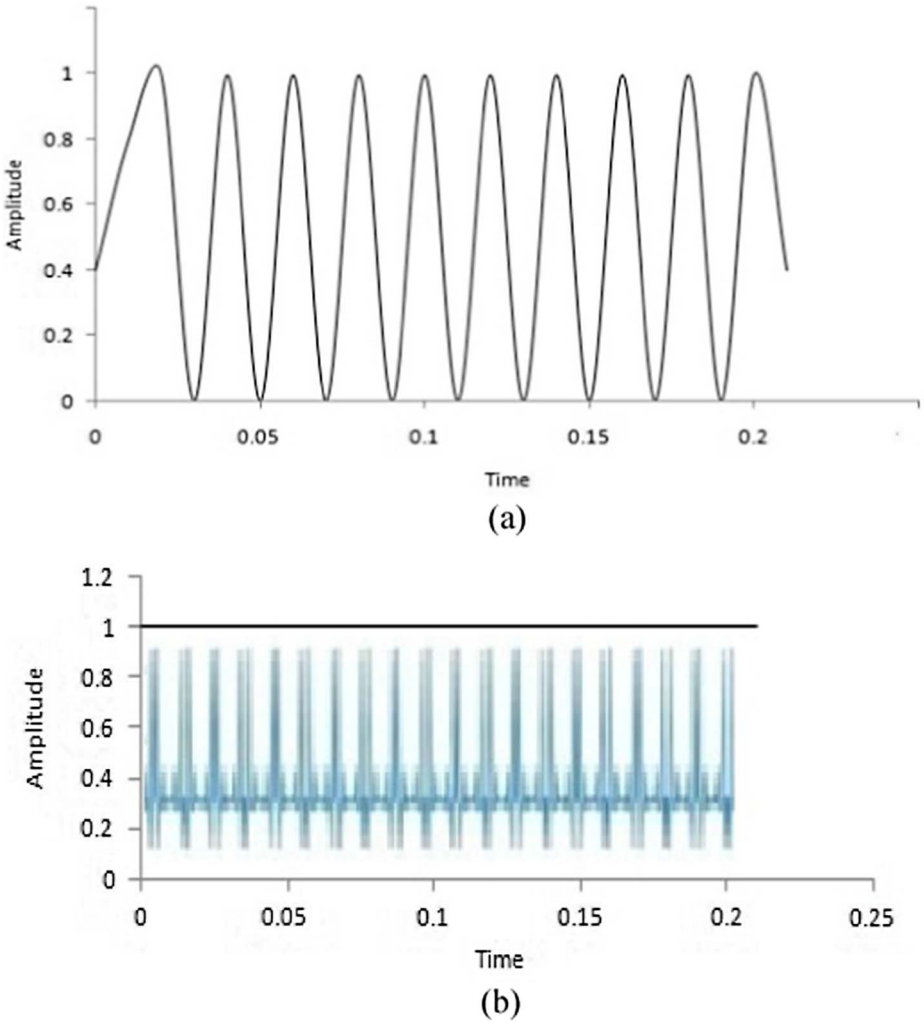


Fig. 22. (a) Harmonics & (b) HOG of disturbance.

occasion.

Diverse power quality disturbances same as Sag, Swell, Interruption, Harmonics with Sag and Harmonics with Swell are generated with different magnitudes as in Table 3. Fig. 13 shows the flow chart for PQ signal disturbance generation.

5. Power quality event classification using Support Vector Machine

Classifier plays an important role in pattern recognition. The objective of classifier utilized is to characterize events on the premise of few qualities. Numerous classifiers have been utilized for power quality event classification like ANN, SVM, Fuzzy Logic [2,11]. Keeping in mind the end goal to get great results of decision boundary, the most suitable way is to minimize the error level for reducing Mean squared error.

Support Vector Machine (SVM) is an algorithm with numerous favorable circumstances in classification. Firstly, it gives precise classification with state vectors which is not influenced by noises. Also, the utilization of kernels helps SVM to take care of nonlinear issues without making a feature space with explicit high dimension. Thirdly, SVM has capacity to be connected for both double and multiclass characterization. State vector machine classifier is utilized generally as a part of power quality event detection task. The main procedures of SVM classifier are shown in Fig. 14. It minimizes the edge of linear hyperplane and tries to discover best separation between examples. However, the major drawback of this strategy is that it is a binary classifier which can order just two classes at one time.

6. Results and discussions

6.1. Detection of PQ events

The simulation is produced in MATLAB. The disturbance signals given in Table 3 demonstrate the signal generation models and their controlled parameters. The below figures show disturbance signals

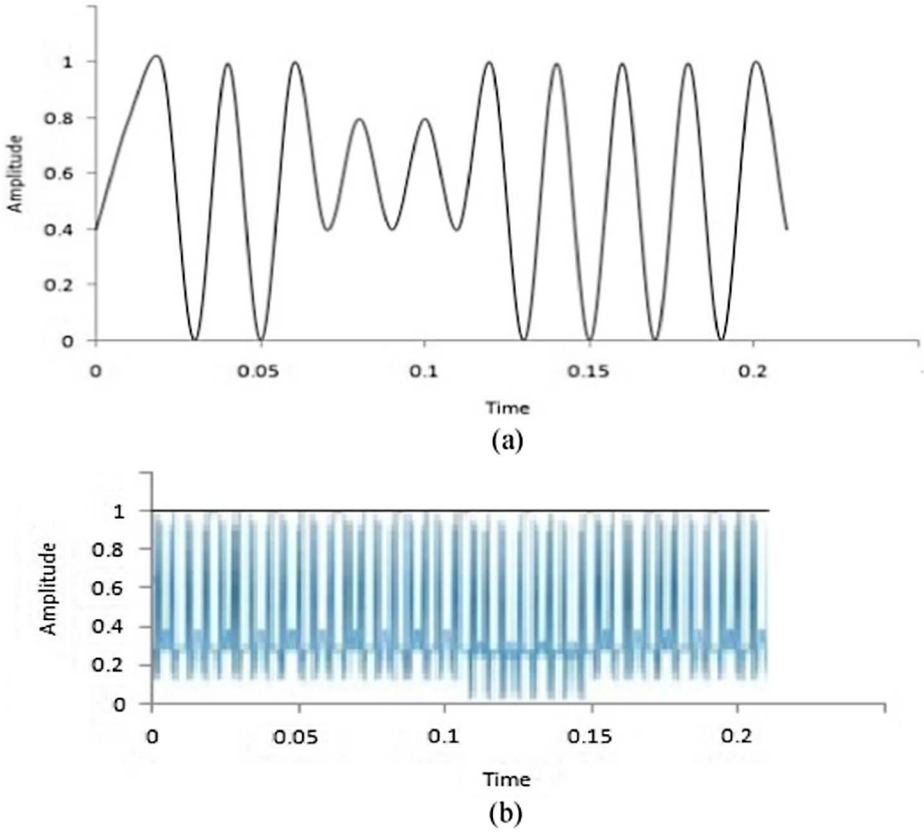


Fig. 23. Harmonics with (a) Sag & (b) HOG of disturbances.

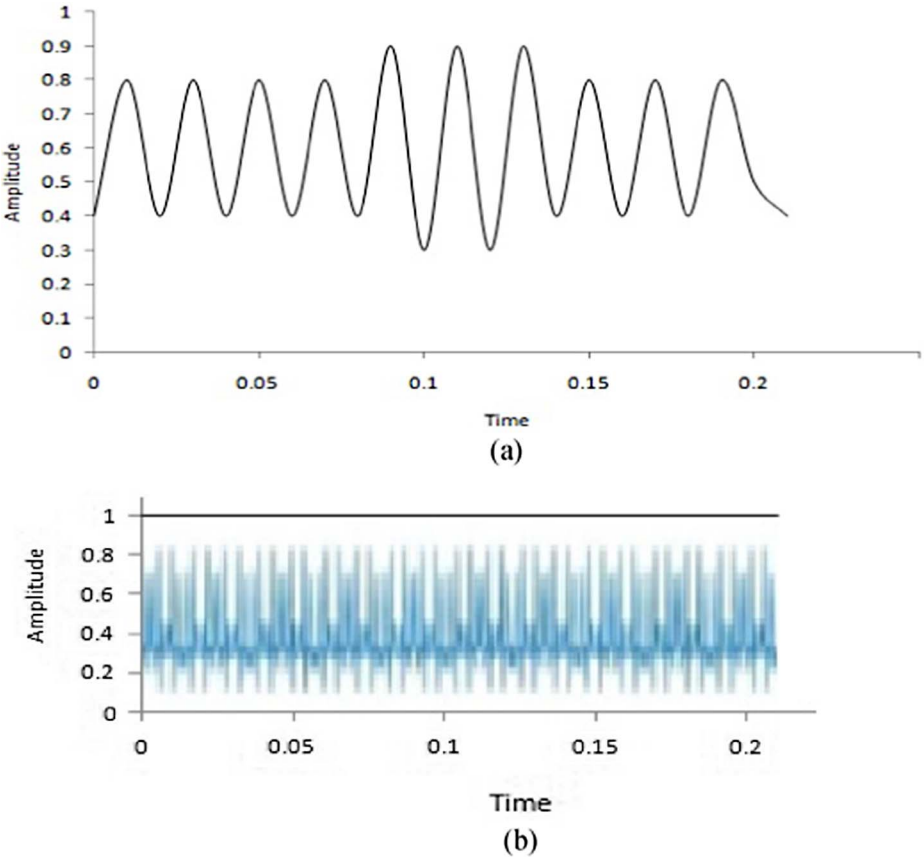


Fig. 24. Harmonics with (a) swell & (b) HOG.

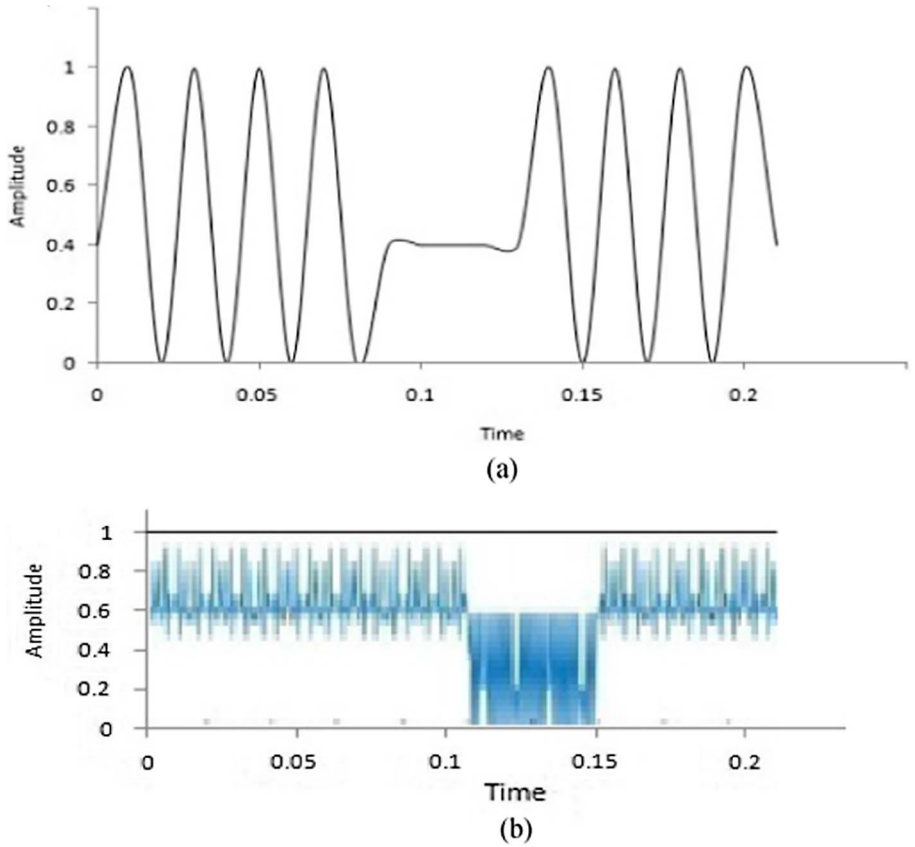


Fig. 25. Harmonic with (a) interruption and (b) HOG.

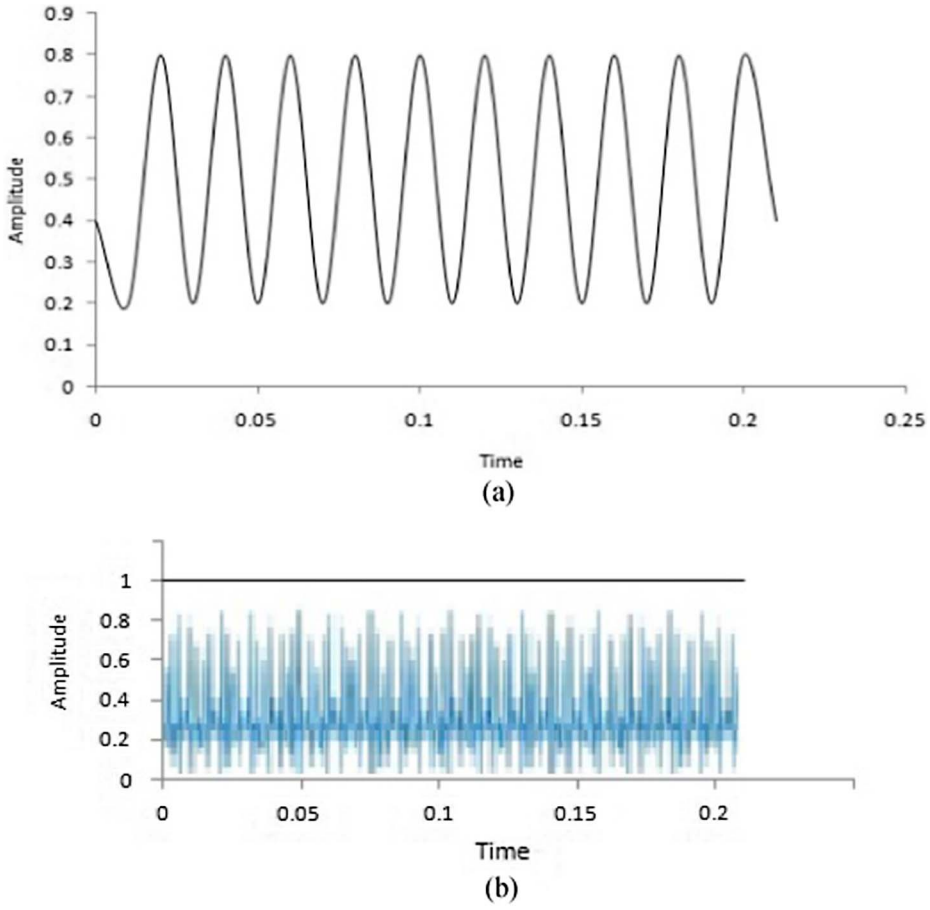


Fig. 26. Harmonics with (a) flicker and (b) HOG.

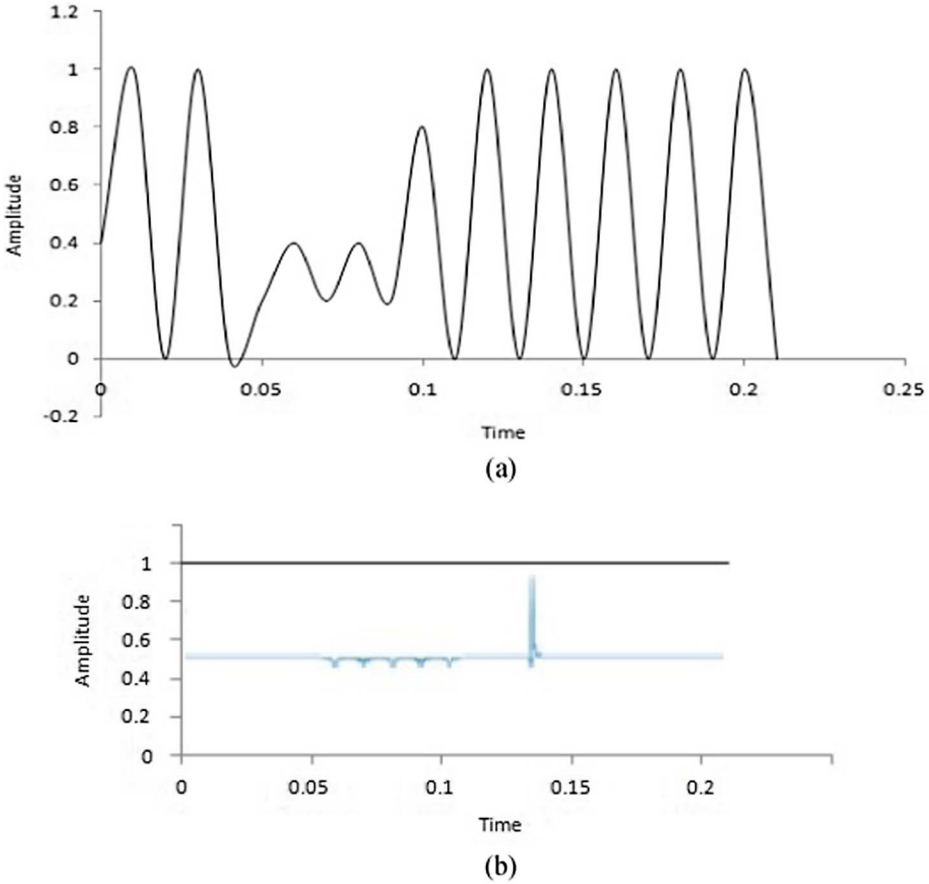


Fig. 27. Sag with (a) impulsive transient & (b) HOG.

generated and their respective HOG after subtracting the HOG of sine wave. Therefore, the HOG shown in all figures corresponds to the HOG of disturbance. Any adjustments in the pattern of signals can be recognized. To the extent identification and limitation concerned, the HOG is satisfactory to identify and confine any disturbance in the signals. As found in Fig. 15 for an immaculate signal, the outcome is zero.

Any adjustments in the signal can be distinguished and limited in time because of changes in the HOG. This gives accurate result as shown from Figs. 16–28. There are various events and detection with the HOG gives exact result in less computation. In Table 4, data for ST and EMD-HT are taken from [1,13] respectively. In EMD-HT dataset, eight events have been used. We can detect not only single events but multiple events i.e. two or more than two events occurring simultaneously in previous studies either single events or two events occurring at a time has been taken. With this technique, this is the unique feature so that more than three events can be detected simultaneously (see Table 5).

Figs. 16–22 show successful detection of single events and sine wave in Fig. 15. Figs. 23–27 show the detection of two events. Fig. 28 shows the detection of three events in input signals.

6.2. Classification of PQ events

The gigantic number of PQ events happens in distribution frameworks. There is a necessity for a technique that can be utilized for quick and precise recognition of PQ events. The fundamental preferred standpoint of the proposed strategy is low execution time and noteworthy precision. When the disturbance is detected, it becomes essential to classify which type of events is present. For this, we use the value of Entropy and Standard Deviation obtained from the HOG of disturbance in first part and for the SVM classifier (Fig. 29).

Before testing, the classifier needs to be trained with sample values. SVM classifier is a binary classifier applied to each node given in Table 4. For training of SVM classifier with different samples, we have used the samples of Sag, Swell, Interruption, etc. Figs. 30–38 show the classification data at each node of Fig. 29. From Figs. 30–38, it is clear that events can be classified easily but in some cases, it is difficult to classify where data from two events overlap as in Figs. 32, 33, 36 and 37. 10 events have been classified but this technique can be further extended to any number of events as HOG can efficiently detect the multiple events and all possible combinations.

6.3. Comparative analysis

The purpose of this section is to theoretically justify our results with those of the relevant works. From Table 6, it is clear that HOG can be effectively used for detection of single as well as multiple power quality

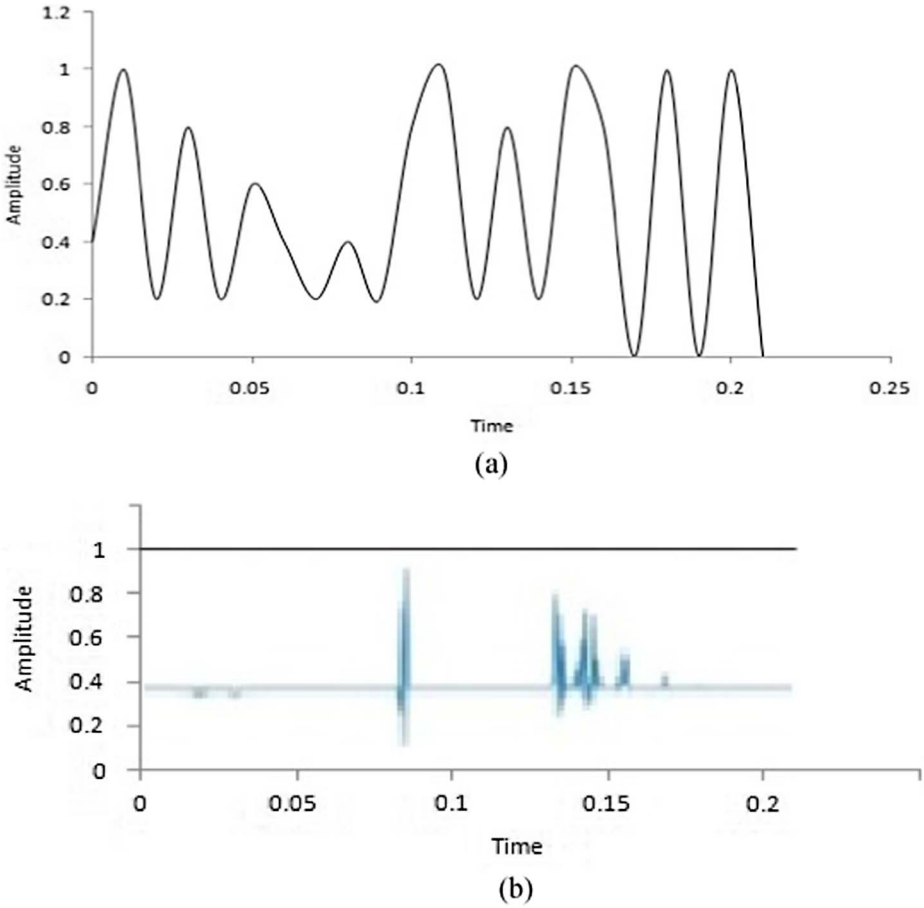


Fig. 28. Sag with impulse transient with (a) oscilatory transient & (b) HOG.

Table 4
Comparision of ST [17], EMD-HT [3] and the proposed method.

Event	ST	EMD-HT	Proposed method
Sag	NO	NO	YES
Swell	NO	NO	YES
Flicker	YES	YES	YES
Interruption	YES	YES	YES
Harmonics	YES	YES	YES
Harmonics with sag	YES	YES	YES
Harmonics with swell	YES	YES	YES
Oscillatory transients	YES	YES	YES
Impulsive transients	YES	YES	YES
Notches	YES	YES	YES
Sag + Swell + Interuption	NO	NO	YES
Sag + Impulse + Oscilatory	NO	NO	YES
3 or more events simultaneously	NO	NO	YES

events. Our model is applicable to multiple events occurring at same time; hence feature selection is not an issue. SVM is used for detection and classification of some events with more than 1000 training values for each event being used to train.

The comparative analysis in Table 6 showed that our approach

Table 5
Represents the events at various nodes in Fig. 29.

Node	Events
1	All events
2	Sine + Sag + Swell + Flicker + Interruption
3	Harmonics + Harmonics with Sag + Harmonics with Swell + Harmonics with Flicker + Harmonics with Interruption
4	Swell + Flicker
5	Sag + Sine + Interruption
6	Harmonics + Harmonics with Swell + Harmonics with Flicker
7	Harmonics with Sag + Harmonics with Interruption
8	Swell
9	Flicker
10	Sine
11	Sag + Interruption
12	Harmonics with Swell + Harmonics with Flicker
13	Harmonics
14	Harmonics with Sag
15	Harmonics with Interruption
16	Sag
17	Flicker
18	Harmonics with Swell
19	Harmonics with Flicker

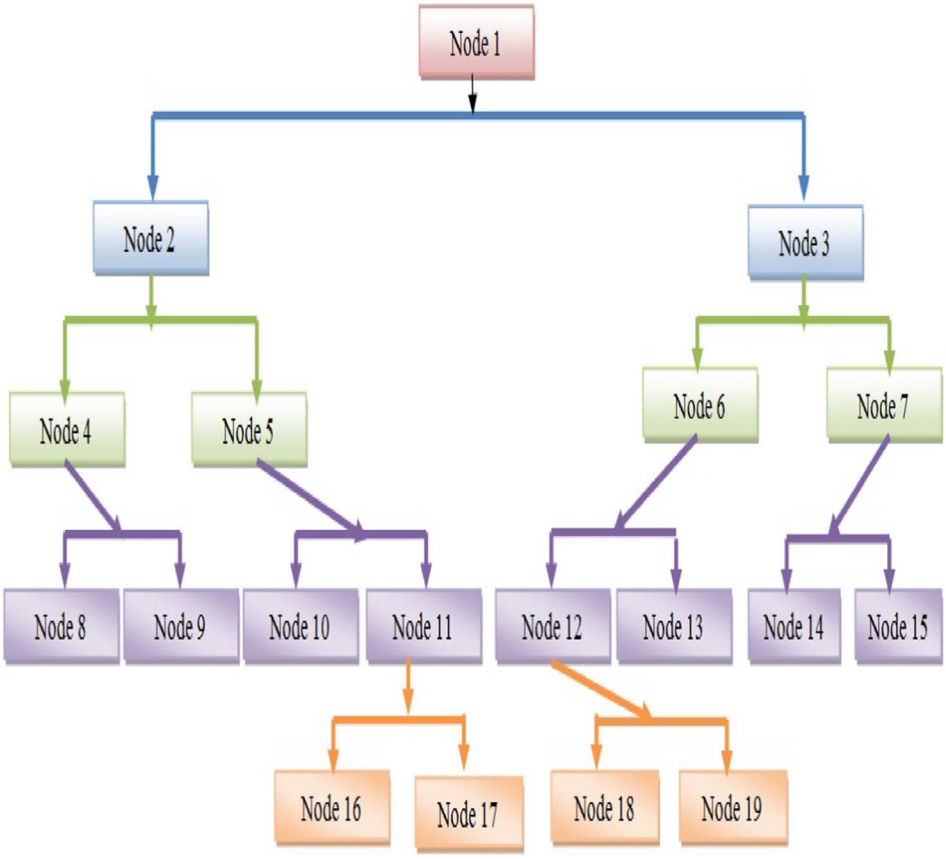


Fig. 29. Flowchart showing the process of classification using SVM.

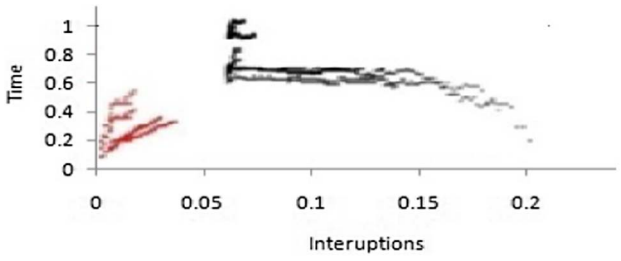


Fig. 30. Events at node 1.

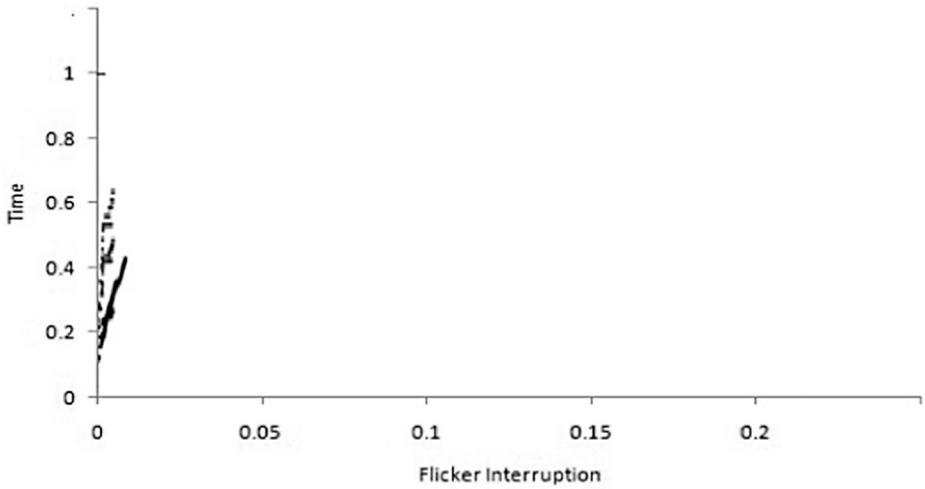


Fig. 31. Events at node 2.

clearly identifies power quality events with the help of HOG and SVM. We have also performed the classification, which has not been performed so far. This clearly indicates the efficiency of our approach.

7. Conclusions

In this paper, we have proposed a new method combining HOG and SVM for power quality events detection. It is clear that HOG can be effectively used for detection of single as well as multiple power quality events. It is more effective than other techniques because of less processing time since this technique can be applied to multiple events occurring at same time. After detection, classification using SVM has

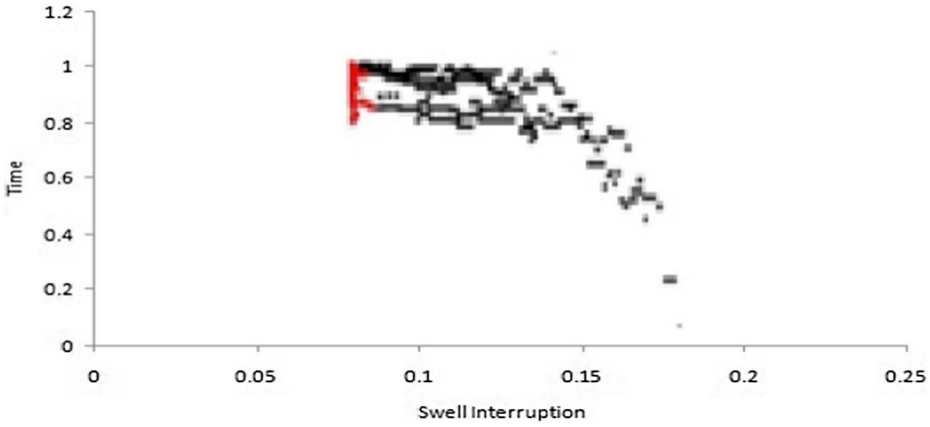


Fig. 32. Events at node 3.

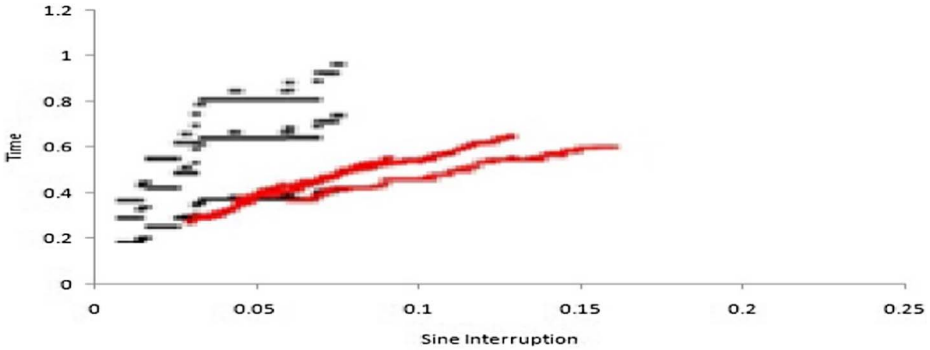


Fig. 33. Events at node 4.

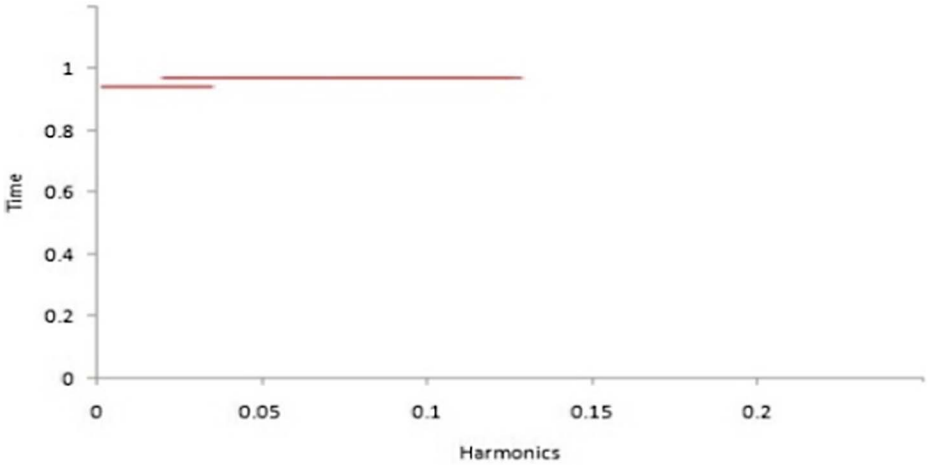


Fig. 34. Events at node 5.

been performed on 1000 training values for each event. The experimental results have shown that SVM can classify events more effectively than the other methods. All the events have been generated synthetically as per IEEE standards so the results obtained are highly reliable.

Future studies would extend the proposed algorithm with more

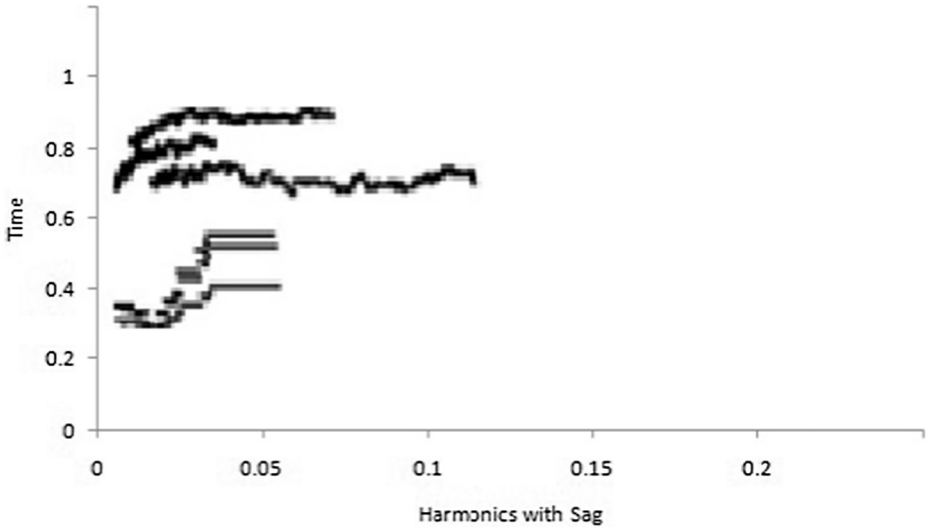


Fig. 35. Events at node 6.

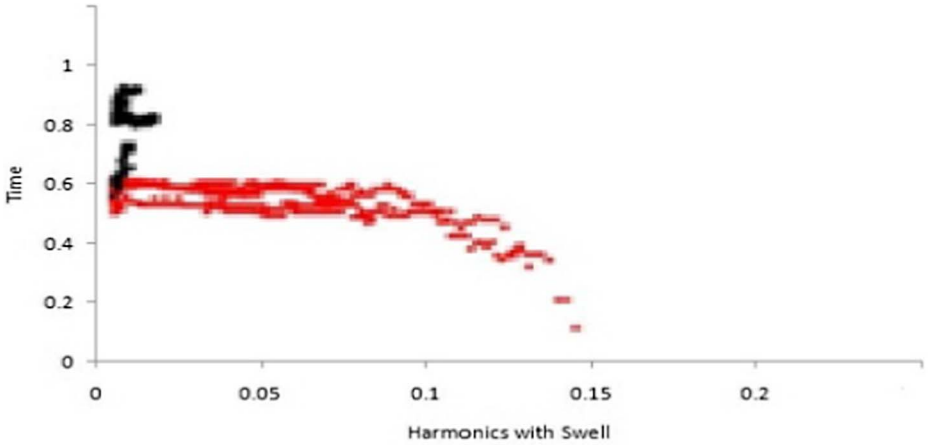


Fig. 36. Events at node 7.

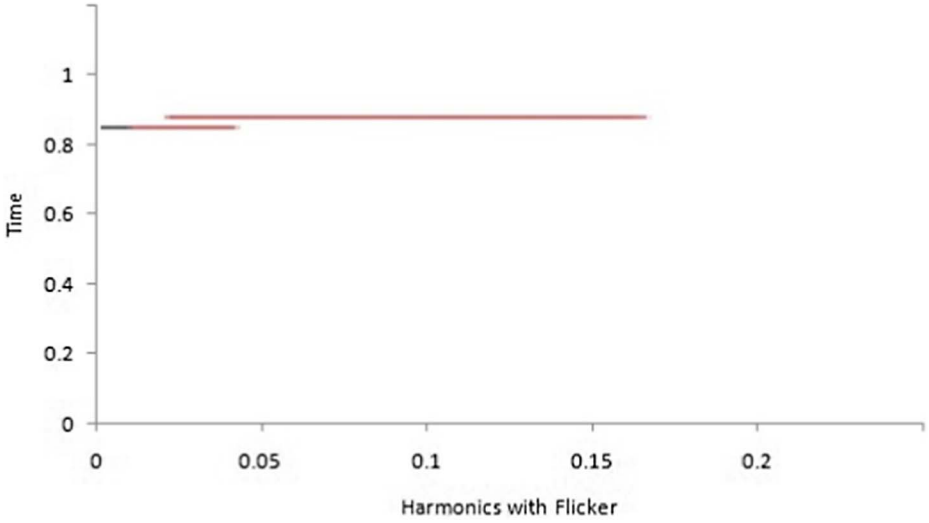


Fig. 37. Events at node 11.

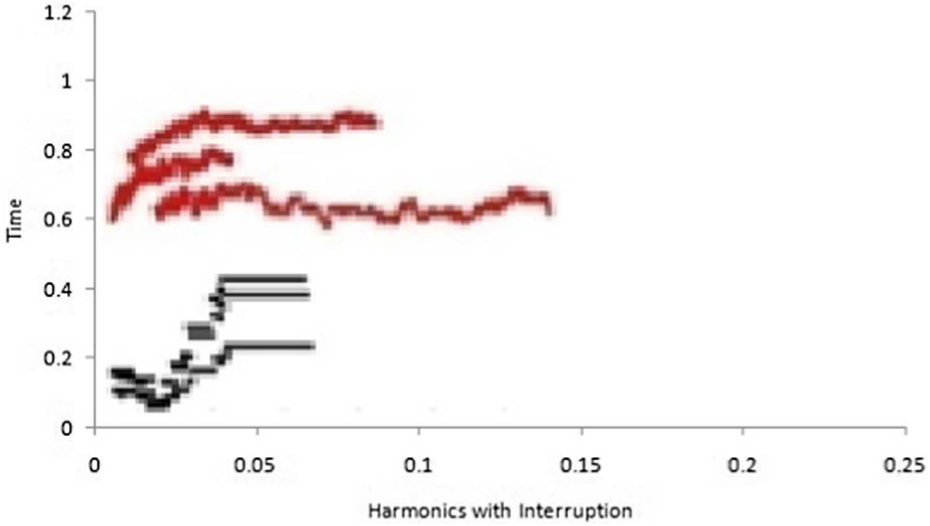


Fig. 38. Events at node 12.

Table 6
Theoretical comparison with the relevant studies.

S/ No.	Authors	Authors findings	Our findings
1.	Mahela et al. [15]	The S-transform based decision tree initialized Fuzzy C-means (FCM) clustering technique was proposed for recognition of PQ disturbances. Sum absolute values curve was introduced to increase efficiency of the algorithm. Validation of results was carried out with 100 data sets of each PQ disturbance with and without noise in real time.	Power quality events have been detected with the help of HOG and SVM. HOG is significantly used for detection of single as well as multiple power quality events. More effective due to less processing time.
2.	Cambron et al. [16]	Power curve and control charts have been validated with simulated data. The detection of 1% annual ramp shift in approximately 230 days. It does not provide neither the source of failure nor the moment of behavior change.	Extensive simulations have been done to carry out detection. After detection, classification has been performed using SVM with more than 1000 training values. All events have been generated synthetically as per IEEE standards so the results obtained are highly reliable. Our method is more effective than this one.
3.	Khadse et al. [19]	Use Artificial Neural Network but the proposed real time power quality monitoring scheme only gives voltage sag. Mathematical model of conjugate gradient back-propagation method was realized using basic blocks only. The voltage signals of sag and swell are acquired in real time using data acquisition system from the single phase 230 V hardware setup	Our approach uses Histogram and SVM with no voltage sag. Power gradient quality is significantly better than this research. Sinusoidal signals as shown in Fig. 15 clearly indicate that there is no as such voltage swell is required because HOG is used for detection of single as well as multiple power quality events. Voltage is not constraint because our model can be applied to multiple events
4.	Khokhar et al. [20]	Optimal feature selection and classification were done to identify sources of the disturbances. The best suitable features and spread constant have been selected based on the highest classification accuracy obtained by the proposed PNN-ABC classification system. It was used for identifying the single and multiple PQDs as compared to traditional classification systems. It does not focus on various aspects like inter-harmonics disturbances	No feature selection. Gradient has been considered using Histogram and SVM. We have generalized and there are no disturbances. No noise. SVM was used for detection and classification using SVM and training data of some events
5.	Velazquez et al. [22]	Smart sensor network was proposed to monitor an electrical installation. The developed system is able to detect power quality events and correlate them. Three case study (residential, industrial, and hospital facilities) were presented. It is able to calculate real-time indexes and big-data logging	Absolute mathematical model and detection method were used. Power system was detected using gradient. This paper is not case based. We have given the result with high occurrences and better power density with improved sinusoidal function

reliable results and fast processing time. Here, reliability indicates parameters namely disturbances, transmission impairments, noises, cross over interferences. Speed up the computational time of the method is also our next target.

References

[1] D. Saxena, K.S. Verma, Wavelet transform based power quality events classification using artificial neural network and SVM, Int. J. Eng. Sci. Technol. 4 (1) (2012) 87–96.
[2] J. Li, M.V. Chilukuri, Power supply quality analysis using S-transform and SVM classifier, J. Power Energy Eng. 2 (04) (2014) 438.
[3] B. Biswal, M. Biswal, S. Mishra, R. Jalaja, Automatic classification of power quality events using balanced neural tree, IEEE Trans. Ind. Electron. 61 (1) (2014) 521–530.
[4] S. Naderian, A. Salemnia, Detection and classification of power-quality events using discrete Gabor transform and Support Vector Machine, in: Power Electronics, Drives Systems &Technologies Conference (PEDSTC), 2015 6th, IEEE, 2015, pp. 544–54.
[5] R. Kapoor, R. Gupta, Classification of power quality disturbances using non-linear dimension reduction, Electr. Eng. (Archiv fur Elektrotechnik) (2013) 1–10.
[6] R. Kapoor, M.K. Saini, Multiwavelet transform based classification of PQ events, Int. Trans. Electr. Energy Syst. 22 (4) (2012) 518–532.
[7] M.K. Saini, R. Kapoor, Detection and tracking of power system disturbances using modified potential function, Int. J. Electr. Power Energy Syst. (in press), 2012 (Elsevier).
[8] M.K. Saini, R. Kapoor, Classification of power quality events–a review, Int. J. Electr. Power Energy Syst. 43 (1) (2012) 11–19.
[9] L. K. Behera, M. Nayak, Pattern recognition of power quality events using Fuzzy neural network based rule generation, in: Advances in Engineering, Science and Management (ICAESM), 2012 International Conference on, IEEE, 2012, pp. 73–78.
[10] M.K. Saini, R. Kapoor, B.B. Sharma, PQ event classification using fuzzy classifier, in: Advanced Materials Research, vol. 403, Trans Tech Publications, 2012, pp. 3854–3858.
[11] R. Kapoor, M.K. Saini, Hybrid demodulation concept and harmonic analysis for single/multiple power quality events detection and classification, Int. J. Electr. Power Energy Syst. 33 (10) (2011) 1608–1622.
[12] M.J. Afroni, D. Sutanto, D. Stirling, Analysis of nonstationary power-quality waveforms using iterative Hilbert Huang transform and SAX algorithm, IEEE Trans.

Power Deliv. 28 (4) (2013) 2134–2144.
[13] R. Kumar, B. Singh, D.T. Shahani, A. Chandra, K. Al-Haddad, Recognition of power-quality disturbances using S-transform-based ANN classifier and rule-based decision tree, IEEE Trans. Ind. Appl. 51 (2) (2015) 1249–1258.
[14] B. Sen, M. Goswami, S. Mazumdar, B.K. Sikdar, Towards modular design of reliable quantum-dot cellular automata logic circuit using multiplexers, Comput. Electr. Eng. 45 (2015) 42–54.
[15] O.P. Mahela, A.G. Shaik, Power quality recognition in distribution system with solar energy penetration using S-transform and Fuzzy C-means clustering, Renew. Energy 106 (2017) 37–51.
[16] P. Cambron, R. Lepvrier, C. Masson, A. Tahan, F. Pelletier, Power curve monitoring using weighted moving average control charts, Renew. Energy 94 (2016) 126–135.
[17] S.A. Deokar, L.M. Waghmare, Integrated DWT–FFT approach for detection and classification of power quality disturbances, Int. J. Electr. Power Energy Syst. 61 (2014) 594–605.
[18] A.S. Yilmaz, A. Subasi, M. Bayrak, V.M. Karsli, E. Ercelebi, Application of lifting based wavelet transforms to characterize power quality events, Energy Convers. Manage. 48 (1) (2007) 112–123.
[19] C.B. Khadse, M.A. Chaudhari, V.B. Borghate, Conjugate gradient back-propagation based artificial neural network for real time power quality assessment, Int. J. Electr. Power Energy Syst. 82 (2016) 197–206.
[20] S. Khokhar, A.A.M. Zin, A.P. Memon, A.S. Mokhtar, A new optimal feature selection algorithm for classification of power quality disturbances using discrete wavelet transform and probabilistic neural network, Measurement 95 (2017) 246–259.
[21] M. Hajian, A.A. Foroud, A new hybrid pattern recognition scheme for automatic discrimination of power quality disturbances, Measurement 51 (2014) 265–280.
[22] L. Morales-Velazquez, R. de Jesus Romero-Troncoso, G. Herrera-Ruiz, D. Morinigo-Sotelo, R.A. Osornio-Rios, Smart sensor network for power quality monitoring in electrical installations, Measurement 103 (2017) 133–142.
[23] L.H. Son, A novel kernel fuzzy clustering algorithm for geo-demographic analysis, Inf. Sci. 317(C) (2015) 202–223.
[24] H.V. Long, N.T.K. Son, N.T.M. Ha, The existence and uniqueness of fuzzy solutions for hyperbolic partial differential equations, Fuzzy Optim. Decis. Making 13 (4) (2014) 435–462.
[25] T.M. Tuan, T.T. Ngan, L.H. Son, A novel semi-supervised fuzzy clustering method based on interactive fuzzy satisficing for dental x-ray image segmentation, Appl. Intelli. 45 (2) (2016) 402–428.
[26] L.H. Son, Generalized picture distance measure and applications to picture fuzzy clustering, Appl. Soft Comput. 46(C) (2016) 284–295.
[27] T. Le, B. Vo, S.W. Baik, Efficient algorithms for mining top-rank-k erasable patterns using pruning strategies and the subsume concept, Eng. Appl. Artif. Intell. 68 (2018) 1–9.

ResearchGate

See discussions, stats, and author profiles for this publication at: https://www.researchgate.net/publication/322740052

Effect of Various Culture Parameters on the Bio-surfactant Production from Bacterial Isolates

Article · January 2017

DOI: 10.4172/2157-7463.1000350

CITATIONS
0

READS
10

1 author:



Arpita Roy
Delhi Technological University
32 PUBLICATIONS **9** CITATIONS

SEE PROFILE

Some of the authors of this publication are also working on these related projects:



Micropropagation of Plumbago zeylanica and production of plumbagin View project



Micropropagation of Centella asiatica View project

All content following this page was uploaded by Arpita Roy on 01 February 2018.

The user has requested enhancement of the downloaded file.

Journal of Petroleum & Environmental Biotechnology

ISSN: 2157-7463

Roy, J Pet Environ Biotechnol 2017, 8:6
DOI: 10.4172/2157-7463.1000350

Research Article Open Access

Effect of Various Culture Parameters on the Bio-surfactant Production from Bacterial Isolates

Arpita Roy*

Department of Biotechnology, Delhi Technological University, New Delhi, India

Abstract

Biosurfactants are those compounds which contains both hydrophilic and hydrophobic moieties i.e., amphiphilic in nature. They have advantages over the chemical surfactant such as low toxicity, eco-friendly, etc. They possess wide range of industrial applications such as bioremediation, food processing, oil industries and health care. Various microorganisms have the ability to produce the potential biosurfactant. In the present study, microbial culture which showed highest biosurfactant activity i.e., SA3 based on the oil displacement activity and emulsion layer was selected for various culture parameters optimization. Sodium nitrate as a nitrogen source and dextrose as a carbon gives the highest biomass and biosurfactant production. Further 2% of dextrose and 2% of inoculum size provides the highest biomass and biosurfactant production. Growth kinetics and biosurfactant kinetics study reveals that the maximum biomass was produced after 96 h and maximum production of biosurfactant was after 72 h of incubation period. Overall, the results indicated the potential use of SA3 isolate in bioremediation processes.

Keywords: Biosurfactant; Carbon source; Nitrogen source; Inoculum size; Growth kinetics

Introduction

Consumption of petroleum is increasing rapidly in the industry due to this large amount of hydrocarbons are discharged into the environment, either deliberately or accidentally. In addition to this many small spills occur during the oil transport, recovery and refining [1]. Hydrocarbon contaminated soil causes severe damage to the local system as these pollutants accumulated in animals and plant tissue which lead to death [2]. Now-a-days there is an increased demand for innovative and environmentally friendly techniques to deals with these problems. A wide range of microbes has reported showing potential biosurfactant activity; these microbes have the ability to break down the organic compounds which they used as energy sources. Utilization of bio-compounds has emerged as a promising method to enhance and improve the effectiveness of bioremediation processes [3]. Biosurfactants are amphiphilic compounds which have the ability to reduce surface and interfacial tension of the surface. Biosurfactant can have several structures i.e., glycolipids, polysaccharide–lipid composite, phospholipid, mycolic acid, lipopeptide, lipoprotein, or the microbial cell surface itself [4]. Due to unique properties and a vast array of application, identification of new biosurfactant producing microbes are in great demand. Biosurfactants have various advantages they can be used as dispersing agents, moistening agents, emulsifiers, pharmaceuticals and cosmetics, mining, petroleum, beverages, and foods, etc [5]. In spite of these advantages, the low yield of biosurfactant is a major problem influencing its commercialization. The type and quantity of biosurfactants produced also depends on various factors like nitrogen and carbon source, temperature, aeration and trace elements also affect their production [6]. By considering the importance of biosurfactants and their potential role in biodegradation of hydrocarbons the present study was conducted to optimize the various culture parameters for the production of biosurfactant as well as the growth of the isolated culture.

Material and Methods

Sample collection and isolation

10 g of petroleum contaminated soil sample was collected and placed into sterile zip lock bag and stored at 4°C immediately after they bought to the laboratory. Microbial cultures were isolated using Minimal salt medium (MSM). MSM contain (for 1L) 0.9 g of Na_2HPO_4, 0.7 g of K_2HPO_4, 2.0 g of $NaNO_3$, 0.4 g $MgSO_4 \cdot 7H_2O$, 0.1 g of $CaCl_2$, 20 g of glucose and 2 g/l of Trace salt ($FeSO_4$ and $MnSO_4$). pH of the medium was adjusted to 7.2 by using 1N NaOH and autoclaved at 121°C and 15 psi pressure for 20 minutes. Bacteria were isolated and stored at 4°C for further use. From the ten bacterial cultures isolates the best biosurfactant producing isolate was chosen for optimization of various culture parameters i.e., SA3.

Effect of different nitrogen source on the production of biosurfactant

The choice of nitrogen source affects the biosurfactant production. In order to obtain higher biosurfactant activity, it is necessary to have proper combination of macro-nutrients in media. MSM containing six different nitrogen sources i.e., sodium nitrate, yeast extract, beef extract, peptone, ammonium chloride and ammonium sulphate were used for biosurfactant production and biomass production. All the cultures were incubated at 37°C for 72 h.

Effect of different carbon source on the biosurfactant production

Five different carbon sources i.e., dextrose, galactose, sucrose, fructose and xylose were used for biosurfactant production. In shake-flask experiments, MSM containing different carbon source were tested to observe the effect on biomass and biosurfactant production. All the cultures were incubated at 37°C for 72 h.

***Corresponding author:** Arpita Roy, Department of Biotechnology, Delhi Technological University, New Delhi-110042, India, Tel: (+98)-71-32424127; E-mail: arbt2014@gmail.com

Received October 12, 2017; **Accepted** December 15, 2017; **Published** December 22, 2017

Citation: Roy A (2017) Effect of Various Culture Parameters on the Bio-surfactant Production from Bacterial Isolates. J Pet Environ Biotechnol 8: 350. doi: 10.4172/2157-7463.1000350

Copyright: © 2017 Roy A. This is an open-access article distributed under the terms of the Creative Commons Attribution License, which permits unrestricted use, distribution, and reproduction in any medium, provided the original author and source are credited.

Effect of different carbon concentration on the biosurfactant production

The biosurfactant production was found to be dependent on the composition of the medium. In shake-flask experiments, three different percentage of carbon source i.e., dextrose (1%, 2% and 5%) were used in MSM medium to observe the effect on biomass and biosurfactant production. All the cultures were incubated at 37°C for 72 h.

Effect of different size of inoculum on the biosurfactant production

MSM medium containing three different concentration of inoculum size (1%, 2% and 3%) were used in medium for the biomass and biosurfactant production. All the cultures were incubated at 37°C for 72 h and wet biomass was recorded.

Screening methods for biosurfactant activity

All the samples were tested for their biosurfactant production by using two methods.

Oil spreading assay: Oil spreading assay was developed by Morikawa [7]. 50 ml of distilled water was added to the petri plate and the 20 µl of diesel was added in to this petri plate to form a thin layer of oil. After this 10 µl of culture supernatant was placed gently on the centre of the oil layer. Displacement of oil layer by formatting a clear zone indicates the biosurfactant presence. Formation of oil displacement was visualized under visible light and measured after 30 seconds, this correlates to the biosurfactant activity of isolates.

Emulsification assay: Emulsification assay was developed by Cooper and Goldenberg [8]. 2 ml of diesel was taken in a test tube in which 1 ml of culture supernatant was added and vortexed for 2 minutes for homogenous mixing. Emulsification activity was observed after 24 h and calculated by using the formula:

$$E_{24} = h_{emulsion}/h_{total} \times 100$$

Biosurfactant production and bacterial growth kinetics

Production and growth kinetics study was conducted for the 168 h. The study was done in 250 ml flask using 25 ml of mineral salt media containing 2% dextrose as carbon source, sodium nitrate as a nitrogen source and 2% inoculum size. The cultures were incubated in orbital shaker at 37°C temperature for 168 h and readings were taken at regular interval of 24 h.

Results and Discussion

This study revealed the effect of various culture parameters on biosurfactant production. Previously isolation of a new biosurfactant producing microbes was carried out in samples collected from petroleum contaminated soil. Ten morphologically distinct microbial colonies were screened for their potential activity. Out of these ten isolated bacteria, SA3 was chosen which has shown maximum oil displacement activity and emulsifying activity for further studies. Oil displacement method are indicative of surface wetting activity and emulsion assay is one of the criteria to support the selection of potential biosurfactant producers [5]. More than one screening method should be used for the primary screening to identify the potential biosurfactant producers [9].

Different culture parameters like nitrogen source, carbon source, the concentration of carbon source, initial inoculum size of the bacterial culture, etc effects the production of biosurfactant. The role of different nitrogen sources on biosurfactant production was observed (Table 1) and found that maximum production of biosurfactant was observed in the MSM medium containing sodium nitrate followed by MSM medium containing ammonium sulphate. This result was in agreement with Abdel-Mawgoud [10] who reported that most elevated production of biosurfactant utilizing ammonium nitrate and sodium nitrate as nitrogen sources. Wu [11] reported that nitrogen sources play a vital role in the production of biosurfactant. It was reported that Urea and $NaNO_3$ were most efficient nitrogen source for bacterial isolates [5]. Ghribi and Ellouze-Chaabouni [12] reported the role of urea as a nitrogen source in biosurfactant production. Makkar and Cameotra [13] reported that some *Bacillus* isolates were not able to utilize the ammonium sulfate for biosurfactant or biomass production; however, they were able to utilize ammonium nitrate, sodium nitrate, or potassium nitrate.

Effect of various carbon sources in the biosurfactant production was also done (Table 2). It was observed that the medium containing dextrose as a carbon source was only able to produce biosurfactant activity while in another carbon source like galactose, sucrose, fructose, and xylose there was no production but the growth was present. The concentration of dextrose was also an important parameter for biosurfactant production (Table 3) and it was found out of 1%, 2% and 5%, 2% of dextrose-containing medium gives maximum production and biomass of a 190.373 mg (Wet weight). Cunha [14] reported the use of gasoline as a carbon source for the production of biosurfactant. Zhang [11] reported the ability of *P. aeruginosa* for the biosurfactant

Nitrogen source	24 hours		48 hours		72 hours		Wet weight After 72 hours (mg)
	OD (cm)	EL (cm)	OD (cm)	EL (cm)	OD (cm)	EL (cm)	
$NaNO_3$	0.0	0.0	1.1	18.7%	3.5	35%	208.14
Yeast extract	0.0	0.0	0.3	5.0%	1.0	11.7%	111.21
Beef extract	0.0	0.0	0.5	11.7%	0.4	17.6%	78.52
Peptone	0.0	0.0	0.6	11.7%	1.5	17.6%	219.97
$(NH4)_2SO_4$	0.0	0.0	1.2	18.7%	3.3	29%	293.72
NH_4Cl	0.0	0.0	0.9	17.6%	3.0	23%	280.95
OD: Oil Displacement, EL: Emulsion Layer							

Table 1: Effect of various nitrogen source on the biosurfactant production.

Carbon source	24 hours		48 hours		72 hours		Wet weight After 72 hours (mg)
	OD (cm)	EL (cm)	OD (cm)	EL (cm)	OD (cm)	EL (cm)	
Dextrose	0.0	0.0	1.5	16.6%	4.0	38%	108.60
Galactose	0.0	0.0	0.0	0.0	0.0	0.0	84.69
Fructose	0.0	0.0	0.0	0.0	0.0	0.0	22.24
Sucrose	0.0	0.0	0.0	0.0	0.0	0.0	161.99
Xylose	0.0	0.0	0.0	0.0	0.0	0.0	89.86
OD: Oil Displacement, EL: Emulsion Layer							

Table 2: Effect of various carbon sources on the biosurfactant production.

Concentration of dextrose	24 hours		48 hours		72 hours		Wet weight After 72 hours (mg)
	OD (cm)	EL (cm)	OD (cm)	EL (cm)	OD (cm)	EL (cm)	
1%	0.0	0.0	3.0	38.2%	2.7	20%	200.687
2%	0.0	0.0	1.1	18.7%	3.633	38%	190.373
5%	0.0	0.0	0.0	0.0	0.767	10%	158.737
OD: Oil Displacement, EL: Emulsion Layer							

Table 3: Effect of different carbon concentration on the production of biosurfactant.

production in 30 g/L glycerol. Fleurackers [15] demonstrated the use of waste frying oils for biosurfactants production in *Candida bombicola* ATCC 22214.

Then the influence of the different size of inoculum on the biosurfactant production was studied (Table 4), and it was observed that biosurfactant was best produced at 2% of inoculum. Biosurfactant production kinetics showed that the maximum amount of biosurfactant produced after 72 h (Table 5 and Figure 1) i.e., oil displacement of 4.2 cm and maximum growth of bacterial culture was at 96 h i.e., OD-1.596 (Table 5 and Figure 2).

Size of inoculum	24 hours		48 hours		72 hours		Wet weight After 72 hours (mg)
	OD (cm)	EL (cm)	OD (cm)	EL (cm)	OD (cm)	EL (cm)	
1%	0.0	0.0	0.6	18.7%	3.5	28%	183.06
2%	0.0	0.0	1.1	18.7%	3.6	38%	190.373
3%	0.0	0.0	1.0	35.2%	3.5	26%	197.733
OD: Oil Displacement, EL: Emulsion Layer							

Table 4: Effect of different size of Inoculum on the production of biosurfactant.

Time (in hours)	Production Kinetics (Oil displacement activity (in cm)	Growth Kinetics (OD)
0	0	0
24	0	0.329
48	1.5	1.364
72	4.0	1.468
96	3.8	1.596
120	3.0	1.570
144	2.4	1.557
168	1.5	1.412

Table 5: Biosurfactant production and bacterial growth kinetics.

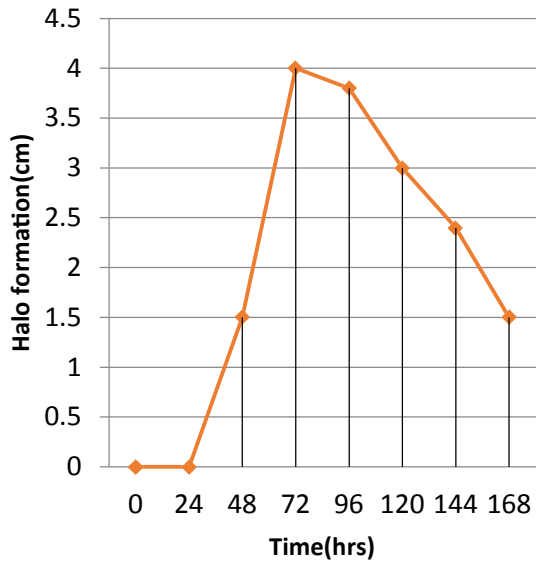


Figure 1: Production kinetics curve.

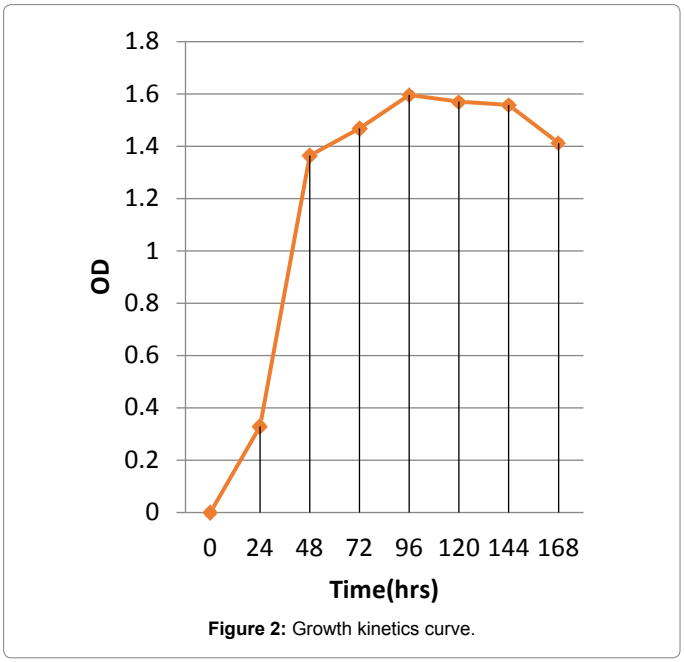


Figure 2: Growth kinetics curve.

Conclusion

The present study concludes that the culture parameters play vital role in the biosurfactant production as well as the biomass amount. It was observed that sodium nitrate, 2% dextrose and 2% inoculum size provides the best condition for the growth of the isolated bacterial culture and also the biosurfactant production. The culture is potential for production of biosurfactant and can be utilized further for larger production.

Conflict of Interest

The authors declare that there are no conflicts of interest.

References

1. Bolliger C (2000) Bioremediation of a heating oil-contaminated aquifer-quantification of processes by chemical, biological and s isotope analyses.
2. Alvarez PJJ, Vogal TM (1991) Substrate interactions of benzene, toluene and oara-xylene during microbial deyredation by pure cultures and mixed culture quifer slurries. Applied and Environmental Microbiology 57: 2931-2985.
3. Ayed BH, Jemil N, Maalej H, Bayoudh A, Hmidet N, et al. (2015) Enhancement of solubilization and biodegradation of diesel oil by biosurfactant from *Bacillus amyloliquefaciens* AN6. Int Biodeter Biodegr 99: 8-14.
4. Ma Y, Oliveira RS, Freitas H, Zhang C (2016) Biochemical and molecular mechanisms of plant-microbe-metal interactions: Relevance for phytoremediation. Front Plant Sci 7: 918.
5. Elazzazy AM, Abdelmoneim TS, Almaghrabi OA (2015) Isolation and characterization of biosurfactant production under extreme environmental conditions by alkali-halo-thermophilic bacteria from Saudi Arabia. Saudi Journal of Biological Sciences. 22: 466-475.
6. Santos DKF, Rufino RD, Luna JM, Santos VA, Sarubbo LA (2016) Biosurfactants: Multifunctional Biomolecules of the 21st Century. Taubert A (ed.) Int J Mol Sci 17: 401.
7. Morikawa M, Hirata Y, Imanaka T (2000) A study on the structure-function relationship of lipopeptide biosurfactants. Biochim Biophys Acta 1488: 211-218.
8. Cooper D, Goldenberg B (1987) Surface-active agents from 2 *Bacillus* species. Appl Environ Microbiol. 53: 224-229.
9. Satpute SK, Bhawsar BD, Dhakephalkar, Chopade BA (2008) Assessment of different screening methods for selecting biosurfactant producing marine bacteria. Indian J Mar Sci 37: 243-250.

10. Abdel-Mawgoud AM, Aboulwafa MM, Hassouna NAH (2008) Optimization of surfactin production by Bacillus substilis BS5. Appl Biochem Biotechnol. 150: 305-325.

11. Zhang G, Wu Y, Qian X, Meng Q (2005) Biodegradation of crude oil by Pseudomonas aeruginosa in the presence of rhamnolipids. J. Zhejiang Univ Sci B 6: 725-730.

12. Ghribi D, Ellouze-Chaabouni S (2011) Enhancement of *Bacillus subtilis* lipopeptide biosurfactants production through optimization of medium composition and adequate control of aeration. Biotechnol Res Int 1: 2.

13. Makkar RS, Cameotra SS (1997) Biosurfactant production by a thermophilic *Bacillus subtilis* strain. J Ind Microbiol Biotechnol 18: 37-42.

14. Cunha CD, Do Rosário M, Rosado AS, Leite SGF (2004) *Serratia* sp. Svgg16: A promising biosurfactant producer isolated from tropical soil during growth with ethanol-blended gasoline. Process Biochem. 39: 2277-2282.

15. Fleurackers SJJ (2006) On the use of waste frying oil in the synthesis of sophorolipids. Eur J Lipid Sci Technol 108: 1-5.

View publication stats

Nuclear Inst, and Methods in Physics Research B 419 (2018) 14–18

Contents lists available at ScienceDirect

Nuclear Inst. and Methods in Physics Research B

journal homepage: www.elsevier.com/locate/nimb

Employing X-ray absorption technique for better detector resolution and measurement of low cross-section events

Gaurav Sharma[a], Nitin K. Puri[a], Pravin Kumar[b], T. Nandi[b,*]

[a] Delhi Technological University, Bawana Road, Delhi 110042, India
[b] Inter University Accelerator Centre, Aruna Asaf Ali Marg, New Delhi 110067, India

ARTICLE INFO

Keywords:
X-ray absorption technique
Beam-foil spectroscopy
One-electron-one-photon transitions
Two-electron-one-photon transition
Low cross section processes
Lifetime measurements

ABSTRACT

The versatility of X-ray absorption technique is experimentally employed for enhancing the detector resolution and to rejuvenate the low probable transitions obscured in the pile-up region, during a beam-foil spectroscopy experiment. The multiple aluminum absorber layers (10 μm each) are used to suppress the pile-up contribution drastically and to restore a weak transition which is about 1.38×10^4 times weaker than a one-electron-one-photon transitions viz. K_α and K_α^h. The weak line is possibly originating from a two-electron-one-photon transition in He-like Ti. Further, the transitions, which were obscured in the spectra due to high intensity ratio, are revived by dissimilar line intensity attenuation using this technique. The measured lifetimes of K_α line with and without intensity attenuation match well within error bar. The present technique finds potential implications in understanding the structure of multiple-core-vacant ions and other low cross section processes in ion-solid collisions.

1. Introduction

The formation of two K-shell vacancies either in the target atoms or the projectile ions is often seen in the energetic heavy ion-solid collisions [1]. These two vacancies are mostly filled sequentially by emitting a $K_{\alpha h}$ or $K_{\beta h}$ (hypersatelite) line and another K_α or K_β line [2]. However, there is a small probability that the two vacancies can be filled simultaneously by two electrons resulting in an emission of a single photon of nearly twice the energy of K_α or K_β [2–5] line. Therefore, the signature of the two-electron-one-photon (TEOP) transitions ($K_{\alpha\alpha}$, $K_{\alpha\beta}$) is mostly buried in the spectral region affected by the pile-up phenomenon. Several pile-up rejection techniques such as pulse shape discrimination [6], pile-up rejection circuits, reduction of the counting rates [7–9], and use of selective filters [10–14] are well known. The relative yield for $K_{\alpha\alpha}/K_\alpha$ is of the order of 10^{-4} in Ar atom [15]. This ratio improves for the lighter atoms and deteriorates further for the heavier atoms [3]. Therefore, the detection of such processes requires sufficiently high **count** rate of TEOP transitions, which can be enhanced by increasing the number of incident ions. However, this will further increase the one-electron-one-photon (OEOP) transition count rate leading to more pile-up events in the spectrum. As a solution, the techniques capable of handling high counting rates and elimination of pile-up simultaneously, can only be used for such experiments. Nevertheless, the commonly used electronic techniques [7–9] cannot completely reject the pile-up contributions. Rate of pile-up rejection depends on $n^2\tau$, where n is the true counting rate and τ is the system dead time, which has certain limiting value. Thus, an elegant method of solving the problem requires limited event rate in the detector even though count rate is high in the experiment. The absorption technique abruptly decreases the count rate of intense X-ray transitions (which is main cause of the pile-up) on low energy side, but barely attenuates the low intensity transitions lying on the high energy side. Hence, it increases the effective count rate for the low intensity processes by decreasing the pile-up contributions to an extreme limit.

The maximum resolution of any detector is characterized by least overlapping of the peaks. This overlapping can be minimized by either, (i) increasing the spectral separation between the peaks or (ii) improving the spectral width of the transition. This overlapping depends on the intensities of the adjacent peaks and minimum for the identical intensities. Therefore, it is possible that the two transitions existing within the resolution of the detector may not be experimentally resolved. The high resolution spectroscopy method [17] help resolving them, but it requires absorber with specific K or L absorption edge. Note that such transitions can be resolved in a delayed spectrum [16] if the lifetimes of the excited levels corresponding to the different lines differ significantly. In this paper, we have used the absorption technique to validate our earlier theoretical studies (i) to improve the resolution for closely separated transitions having different intensities and (ii) to

* Corresponding author.
E-mail address: nandi@iuac.res.in (T. Nandi).

https://doi.org/10.1016/j.nimb.2018.01.021
Received 13 November 2017; Received in revised form 26 December 2017; Accepted 23 January 2018
0168-583X/ © 2018 Published by Elsevier B.V.

detect a low cross section TEOP process in the pile-up affected spectrum of a beam-foil spectroscopy (BFS) experiment [18].

2. Experiment

The present experiment was done at IUAC, New Delhi, India using the 15UD Pelletron accelerator. An ion beam of 110 MeV Ti^{8+} is allowed to pass through the carbon target of thickness 80 μg/cm^2 to create various excited states in the highly charged projectile ions. The thickness of the target was measured using the energy loss of alpha particle in the carbon target. The energy of the Ti beam was chosen to overcome the Coulomb barrier so that the X-ray of the projectile-like ions can also be produced along with the other different lines including the TEOP transition. The self-supported carbon foils prepared using the electron gun evaporation technique were further annealed at 900 K in the N_2 environment to obtain better uniformity and mechanical stability. The carbon target on an aluminum holder was mounted on a lifetime measurement assembly having translational measurement accuracy better than 1 μm, which is equivalent to a delay of 0.047 ps. The target can be moved to and fro up to a 50 mm distance along the beam axis from the detector window. Two low energy germanium X-ray detectors were placed outside the vacuum chamber at an angle of ± 90° to the beam direction. The X-ray produced at the beam-foil interaction region were collected through a 6 μm thick mylar window. The absorption of X-ray in the mylar has been taken into consideration in the calculations. A Faraday cage was used to normalize the X-ray spectra during the lifetime measurements. An electron suppressor ring at a potential of −1 kV was used before the Faraday cage to avoid the charge collection due to stray electrons for better normalization. Thin multiple layers of aluminum absorbers of 10 μm each were used in front of the X-ray detectors to attenuate the intensity accordingly. The thickness of the aluminum layers were confirmed by weighing and the energy loss method. During the experiment, the pressure of about 10^{-7} torr was maintained in the vacuum chamber. The schematic of the experimental set up used is shown in Fig. 1.

3. Results and discussions

Fig. 2 shows the X-ray spectra with different numbers of aluminum absorbers. Multiple layers of 10.0 ± 0.2 μm thick aluminum filters are used to modify the X-ray intensities. A broad peak with a hump at the pulse pile-up region is seen when absorber is not used. With increasing the number of the absorber foils, the broad peak and the peak at the pile-up region get resolved with reasonable intensities. We have also measured the intensity decay as a function of the distance upstream the beam direction.

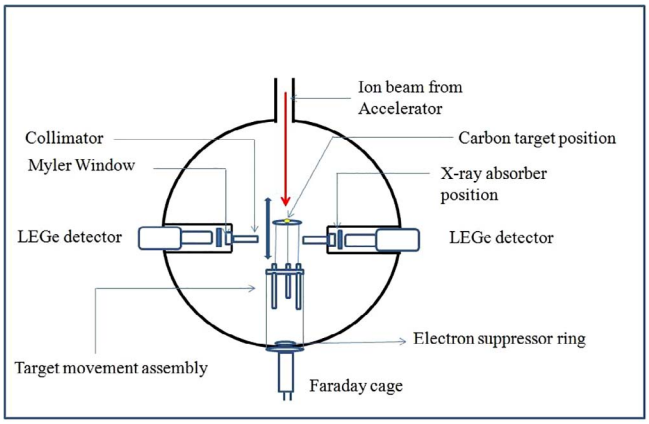


Fig. 1. The schematic of the experimental set up. The target movement assembly was used for measuring the atomic lifetimes by changing the target position with respect to the detector window.

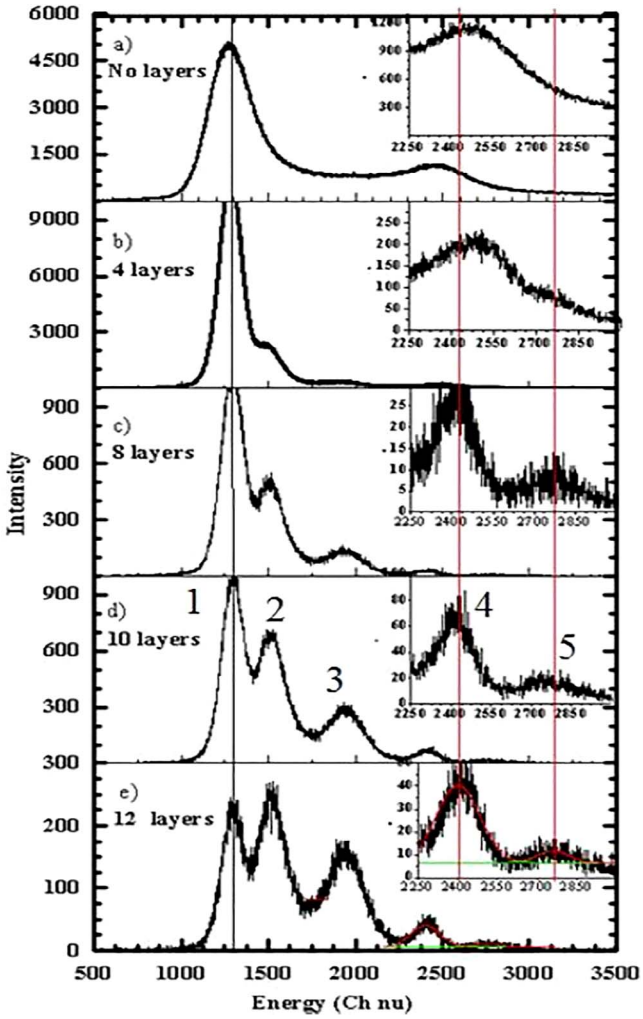


Fig. 2. The X-ray spectra with the different numbers of absorbers: Figures (a)–(e) represent the spectra taken with different numbers of Al absorber foils. The measured spectra show improved resolution with increasing total thickness of absorber foils. Peaks marked with 1, 2, 3 and 4 represent Kα, Kβ, REC and TEOP transitions of He-like Ti at 4.73 keV, 5.5 keV, 7.36 keV, 9.34 keV, respectively. The transition marked as 5 at 10.72 keV belongs also to TEOP category.

The intensities, centroid and full width at half maximum (FWHM) of the peaks are consistent with different numbers of the aluminum layers realizing that the fundamental properties have not been modified by introducing the absorbers. It is important to note that all the peaks lie within the energy range of 4–11 keV and the efficiency of the detector remains constant in this range [19]. Still we have accounted for the efficiency of the detector as well as the absorption in the air and mylar of the exit port for X-ray window. The Beer-Lambert equation for X-ray absorption is used to evaluate the original intensity in the absence of absorber. The attenuation coefficient (μ) values for the calculations are taken from National institute of standard and technology [20] and the thickness of absorber (t) is measured using the weighing method; μ and t are utilized for further calculations. The intensity correction for ten absorber layers is shown in Table 1.

As seen from Table 1, the most intense peak in Fig. 2(a) is suppressed by introducing ten layers thick Al absorber. Also, the gradual elimination of the pile-up effect is seen in Fig. 2(c)–(e). These spectra represent the real transitions taking place in the ion-solid collisions with attenuated intensities. The first two peaks observed can be assigned to K_α and K_β from He-like Ti projectile ions. Whereas the third peak is mainly due to radiative electron capture (REC), but little admixture from H-like Co ions is possible. The Hartree-Fock calculations

Table 1
The attenuation corrected X-ray intensities: The intensities of the measured peaks with ten layers of Al absorbers (100 ± 2 μm) are corrected to have the actual intensities and corresponding measurement uncertainty is given in 3rd column. The figures in the 7th column show the relative intensities after eliminating the pile-up effects; indicating that a 10^{-4} times weaker transition can also be detected.

Channel number (Energy in keV)	Attenuated Int.	% error	Trans. % (Al)	Total trans. %	Corrected Int.	Corrected Int. Ratio
1293.7 (4.73)	1.52E + 05	1.28	0.20	0.02	7.53E + 08	1.00E + 00
1508.7 (5.5)	1.49E + 05	0.82	1.72	0.37	3.98E + 07	5.29E − 02
2023.7 (7.36)	9.09E + 04	0.38	17.15	4.06	2.23E + 06	2.97E − 03
2482.5 (9.34)	1.20E + 04	0.21	38.44	11.51	1.04E + 05	1.38E − 04

are used to assign the transitions with the help of Cowan code [21]. The spectrum from the projectile and the projectile-like ions in a beam-foil experiment are only obtained due to the fact that the beam energy is above the Coulomb barrier. The Co ions might be originating via proton evaporation from the compound nucleus. The signature of such spectra is reported elsewhere [22].

3.1. Two-electron-one-photon (TEOP) transition

Another aspect of studying this technique is to detect very low intensity transitions obscured in the pile-up region or in the background. For instance, the TEOP process has ~4 to 5 order lower cross section than the corresponding (K_α or K_β) [3]. The pile-up [7] occurring due to high count rate creates a false peak at a position of twice energy and also induces the tailing effect in the original Gaussian peak. The energy of the TEOP event lies within the pile-up region and makes the detection difficult. As mentioned earlier the electronic techniques are not suitable for complete pile-up rejection [7] even if they equally reduce the original count of TEOP process present in the pile-up region. Another way of rejecting the pile-up is via decreasing the number of incident ions, but that too decrease the TEOP count and increases the collection time for their detection. Whereas while using an absorber of desired thickness, it drastically reduces the counts of the low energy (high count) photons which are main cause of the pile-up in the spectrum but affects the high energy photons (low count TEOP) counts gently. This is because of the differential absorption (E^{-3} dependence of absorption) of X-ray, which is high of low energy and low for high energy photons as shown in Table 1. The energy of $2s2p - 1s^2$ and $2p^2 - 1s^2$ transition is nearly same in reference of detector used. The transition $2p^2 - 1s^2$ does not satisfy the Heisenberg selection rules [23,24], $\Delta l_1 = \pm 2$ or 0 and $\Delta l_2 = \pm 1$ for transition of TEOP, therefore, the transition is assigned to $2s2p - 1s^2$. The energy of the TEOP transitions $2s2p - 1s^2$ is 9.64 keV [20] whereas, the measured value is 9.34 keV. The theoretical values are assigned using the Hartree–Fock calculations for the COWAN configuration interaction code [25]. The branching ratio of the TEOP to OEOP transitions is found to be 10^{-4}. Thus, an attenuation factor of $> 10^4$, in the pile-up region, is required, which matches with the used attenuator thickness. The measured branching ratio of the TEOP and OEOP transition is 1.38E − 04 and is given in Table 1.

The hump-like structure in the Fig. 2(a) is a result of the contributions from both the pile-up due of intense peaks present at lower energies and the presence of two atomic transitions in the pile-up region. The last peak of the spectra at high energy side is probably originated from the TEOP transition [2–5]. Interestingly, the pile-up channel number (~2588ch) corresponding the first peak (~1294ch) falls in between last two peaks (peak 4 and 5) appearing at the channel numbers 2483 and 2748. Further, these peaks are not coinciding with the pile-up constituting of first and second lines (~2803ch). Thus, it reveals that the hump like structure observed in Fig. 2(a) is due to the pile-up contribution of the sole peak at the lower energies and the two peaks measured in the pile-up region are genuine. Although these two atomic transitions are tiny compared to the intense ones as can be seen in Table 1, but the uncertainty in intensity measurement is very small (< 2%). The theoretical value of the attenuation constant does not specify the uncertainty and hence the corresponding error is ignored in the uncertainty calculation. The uncertainty in the thickness of the absorber foils and the statistical variations are the main sources of the error. The background noise during data acquisition has been filtered out. Therefore, the energy of the spectral lines and the branching ratio of the TEOP to OEOP transitions are measured within 1% error.

3.2. Resolution improvement and intensity ratio

Theoretically, a detector can efficiently resolve two peaks if they are separated by the sum of half width at half maxima. Even when this condition is met by a detector, an experimental limitation, where one of the peaks to be resolved is much stronger than the other, can still be encountered to deteriorate the resolution. In this case, the low intensity peaks tend to be veiled in the broad base of the intense peak as shown in the simulated spectra (Fig. 3(a–c) iii) and consequently they cannot be resolved. Interestingly, this problem can be circumvented by decreasing the relative intensity ratios substantially. A few such cases are represented in Fig. 3. Fig. 3 explains the complete scenario to have better resolution of spectra shown in Fig. 2(c–e). For resolving such peaks, the technique of the X-ray absorption works well provided (a) the intense peak lies at the lower energies and (b) they are theoretically resolvable by the detector.

This technique is solely dependent on the Beer-Lambert law of the absorption of the X-ray intensities. The absorption coefficient varies as E^{-3}, where E is the energy of incident photons. This dependence of absorption on E gives us an excellent tool to play with intensity ratios. The intensity ratio of the peaks can be made comparable by selecting the appropriate absorber and its thickness. This approach is used in the present experiment and three peaks at lower energies have clearly been resolved in the spectra shown in Fig. 2(c)–(e).

3.3. X-ray spectrum simulations

Using the intensities and the centroid energies given in Table 1, we have simulated the spectrum shown in Fig. 2(a) in two different conditions i.e. with and without pile-up as demonstrated in Fig. 4(a) and 4(b), respectively. Fig. 4(a) resembles well with the measured spectrum shown in Fig. 2(a). Certain background level along with the pile-up contribution has been taken into consideration in simulating the data. The initial structure of Fig. 2(a) and Fig. 4(b) is quite similar, whereas the hump like structure due to the pile-up in Fig. 2(a) is completely missing in Fig. 4(b). In place of it, two peaks, which were totally submerged in the noise level as shown in Fig. 2(a), are clearly visible in inset of Fig. 4(b).

3.4. Lifetime measurement

Having resolved the peaks using the present technique, the lifetime measurement method [26] have been used for the first peak shown in Fig. 2 under two different conditions, (a) with 10 layers of aluminum absorber and (b) without any absorber. Note that during the delay method [16] only the metastable levels survive and thus without any absorber the lifetime measurements succeeds well. Hence, for the first case, the lifetime is measured to be 67 ± 8 ps, whereas for the second

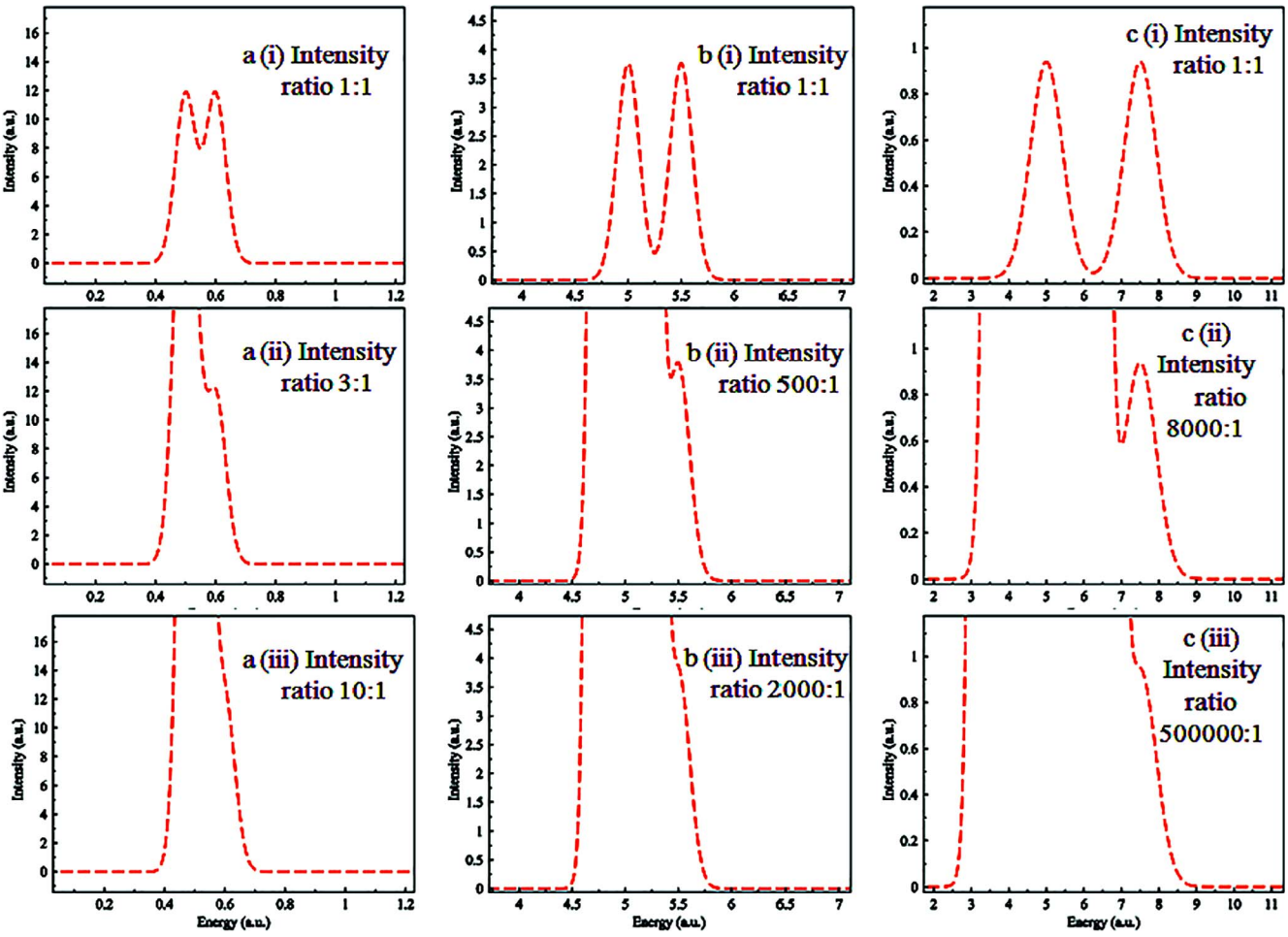


Fig. 3. A comparison of simulated peak resolution with different intensity ratios and line separations; figures (a–c)-i show two completely resolved peaks, (a–c)-ii display only hump like signature of the weaker peak, and (a–c)-iii show a broad peak due to merging of low intensity peak with nearby high intensity peak which strongly depends on the initial peak intensities.

case, the lifetime turns out to be 62 ± 7 ps [18], which is thus well within the uncertainty. The energy of the first peak in delayed spectrum matches with the He-like Ti 1s2s $^3S_1 - 1s^2\ ^1S_0$ (M1 line) & 1s2p $^3P_2 - 1s^2\ ^1S_0$ (M2 line) and Li-like Ti 1s2s2p $^4P_2 - 1s^2\ ^1S_0$ (M2 line). However, the lifetime of the upper levels of these lines are larger than the measured value in the present experiment. We know the surface wake field may quench the lifetime values due to Stark mixing and Stark mixing may take place only for 1s2s $^3S_1$ level due to the presence of the close lying 1s2p $^3P_1$ level. Hence, the measured lifetime can be attributed to He-like 1s2s $^3S_1$ level.

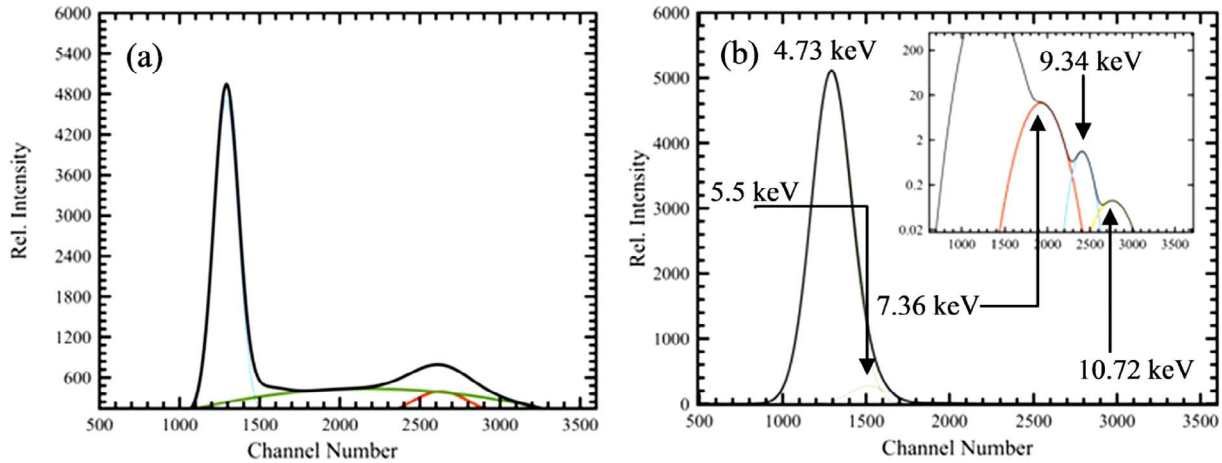


Fig. 4. The simulated X-ray spectrum: (a) In addition to the intensity of the X-ray energy peaks given in the Table 1, the pile-up contribution (red in color) of the first peak (blue in color) and certain back ground level (green in color) are taken into consideration to simulate the measured spectra as shown in Fig. 2 (a) & (b) The spectrum is simulated by using the actual X-ray peak intensities (as given in Table 1) without pile-up. Two atomic transitions are clearly visible in the inset of Fig. 4(b), which were totally submerged in the pulse pile-up region of Fig. 4(a). (For interpretation of the references to colour in this figure legend, the reader is referred to the web version of this article.)

4. Conclusion

We employed the X-ray absorption technique to improve a spectrum in which peaks are theoretically resolvable by the detector but obscured in the pulse pile-up region and neighborhood of intense peaks. The use of absorber foils increases the effective counting rate of the detector for the weak transitions present at higher energy in accordance to Beer-Lambert law (the intensity attenuation coefficient varies as E^{-3}). We have measured $2s2p - 1s^2$ TEOP transition at 9.34 keV in He-like Ti using this pile-up rejection method, which is 10^4 times weaker than the most intense transition. For very close lying satellite lines, which cannot be resolved with this method, any high resolution techniques such as Doppler tuned spectroscopy [17] can be used. Whatsoever, the present technique is most suited to investigate the physics of the TEOP transition as well as the properties of the highly charged ions produced by the nuclear reactions in the form of the projectile-like, the target-like ions, or both [27,28].

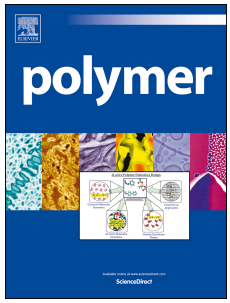
Acknowledgements

The authors are thankful to Mr. Sarvesh Sharma and Mr. Udai Singh for their kind help during the experiment and Mr. Basu Kumar for providing the carbon targets. Gaurav Sharma acknowledges UGC, India for providing the financial support of his research work. T. Nandi acknowledges DST, India for funding the project No SP/S2/LOP-0006/2011.

References

[1] S. Andriamonje, H.J. Andra, A. Simionovici, Z. Phys. D 21 (1991) S349.
[2] C. Stoller, W. Wolfli, G. Bonani, M. Stockli, M. Suter, Phys. Rev. A 15 (1977) 990.
[3] J. Auerhammer, H. Genz, A. Kumar, A. Richter, Phys. Rev. A 38 (1988) 688.
[4] J.A. Tanis, J.M. Feagin, W.W. Jacobs, S.M. Shafroth, Phys. Rev. Lett. 38 (1977) 868.
[5] T. Aberg, K.A. Jamison, P. Richard, Phys. Rev. Lett. 37 (1976) 63.
[6] K.A. Sjiland, P. Kristiansson, Nucl. Instr. Meth. B 94 (1994) 333.
[7] Glenn F. Knoll, Ch-17, Linear and Logic Pulse Functioning, (2009).
[8] R. Rolle, Nucl. Instr. Meth. 114 (1973) 121.
[9] S.L. Blatt, J. Mahieux, D. Kohler, Nucl. Instr. Meth. 60 (1967) 221.
[10] S.A.E. Johansson, J.L. Campbell, K.G. Malmqvist, Particle Induced X-Ray Emission Spectrometry (PIXE), Wiley & Sons, 1995, p. 51.
[11] C.P. Swann, S.J. Fleming, Nucl. Instr. Meth. B 49 (1990) 65.
[12] R. Van Grieken and A. Markowicz, Handbook of X-Ray Spectrometry 2, 618,729, 2001.
[13] J.L. Campbell, W.J. Teesdale, N.M. Halden, Can. Mineral. 33 (1995) 279.
[14] J. S. Greenberg, P. Vincent, in: D. Allan Bromley (Ed.), Treatise on Heavy Ion Science, High-Energy Atomic Phys, 5 Springer, 1985, p. 178.
[15] T.K. Mukherjee, P.K. Mukherjee, Z. Phys. D 42 (1997) 29.
[16] T. Nandi, P. Marketos, P. Joshi, R.P. Singh, C.P. Safvan, P. Verma, A. Mandal, A. Roy, R.K. Bhowmik, Phys. Rev. A 66 (2002) 52510.
[17] R.K. Karn, C.N. Mishra, N. Ahmad, S.K. Saini, C.P. Safvan, T. Nandi, Rev. Sci. Instrum. 85 (2014) 66110.
[18] G. Sharma, N.K. Puri, T. Nandi, Nucl. Instr. Meth. B 408 (2017) 289.
[19] B.P. Mohanty, P. Balouria, M.L. Garg, T.K. Nandi, V.K. Mittal, I.M. Govil, Nucl. Instr. Meth. A 584 (2008) 186.
[20] NIST Atomic Spectra Database, Http://www.nist.gov/pml/data/asd.cfm (n.d.).
[21] J. Hata, I.P. Grant, J. Phys. B: At. Mol. Phys. 16 (1983) 507.
[22] H.J. Karwowski, S.E. Vigdor, W.W. Jacobs, S. Kailas, P.P. Singh, F. Soga, T.G. Throwe, T.E. Ward, D.L. Wark, J. Wiggins, Phys. Rev. C 25 (1982) 1355.
[23] B. Hodge, Phys. Rev. A 16 (1977).
[24] S. Goudsmit, L. Gropper, Phys. Rev. 1121 (1931) 225.
[25] R.D. Cowan, The Theory of Atomic Structure and Spectra (Berkeley, CA: University of California Press) and Cowan Code Package for Windows by A. Kramida, Available from http://das101.isan.troitsl.ru/COWAN (1982).
[26] G. Sharma, N.K. Puri, T. Nandi, Nucl. Instr. Meth. B 408 (2017) 178.
[27] A.P. Mishra, T. Nandi, B.N. Jagatap, J. Quant. Spectrosc. Radiat. Transfer 118 (2013) 70.
[28] T. Nandi, J. Phys. B: At. Mol. Opt. Phys. 42 (2009) 125201.

Accepted Manuscript



Enhancing the processibility of high temperature polymerizing cardanol derived benzoxazines using eco-friendly curing accelerators

Pratibha Sharma, Devendra Kumar, Prasun Kumar Roy

PII: S0032-3861(18)30112-5

DOI: 10.1016/j.polymer.2018.01.084

Reference: JPOL 20344

To appear in: *Polymer*

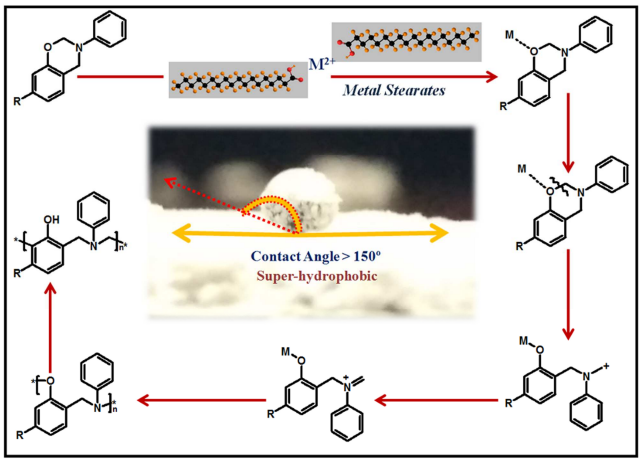
Received Date: 7 December 2017

Revised Date: 22 January 2018

Accepted Date: 30 January 2018

Please cite this article as: Sharma P, Kumar D, Roy PK, Enhancing the processibility of high temperature polymerizing cardanol derived benzoxazines using eco-friendly curing accelerators, *Polymer* (2018), doi: 10.1016/j.polymer.2018.01.084.

This is a PDF file of an unedited manuscript that has been accepted for publication. As a service to our customers we are providing this early version of the manuscript. The manuscript will undergo copyediting, typesetting, and review of the resulting proof before it is published in its final form. Please note that during the production process errors may be discovered which could affect the content, and all legal disclaimers that apply to the journal pertain.



ACCEPTED MANUSCRIPT

ACCEPTED MANUSCRIPT

Enhancing the processibility of high temperature polymerizing cardanol derived benzoxazines using eco-friendly curing accelerators

Pratibha Sharma[a, b], Devendra Kumar[b], Prasun Kumar Roy[a*]

a. Centre for Fire, Explosive and Environment Safety, DRDO, Timarpur, Delhi 110054, India.

b. Department of Applied Chemistry and Polymer Technology, Delhi Technological University, Delhi 110042, India.

Corresponding author. Tel.:+911123907191; Fax:+911123819547.

* E-mail addresses:pk_roy2000@yahoo.com (Prasun Kumar Roy)

ACCEPTED MANUSCRIPT

ACCEPTED MANUSCRIPT

Abstract

The advent of bio-based benzoxazine in the field of polybenzoxazines is a major breakthrough towards their sustainable development. Cardanol derived benzoxazine offers solvent less synthesis and processing benefits over the petro based resin, however these mandate high curing temperatures. The polymerization temperature can be alleviated through structural modifications or physical blending with curing accelerators; the latter approach being preferred in view of its economic viability. Most of the curing accelerators are moisture sensitive, which adversely affect the end performance of the polymer. In this paper, the potential of eco-friendly stearates based on transition metals as curing accelerators for the polymerization of cardanol based benzoxazine resin has been demonstrated. Metal stearates were formulated with bio-based monomer which leads to significant lowering of the curing profiles, the extent of which was proportional to the amount of accelerator. The hydrophobicity associated with the long alkyl chain in stearate bestows it hydrolytic stability, which allows its use under ambient conditions without special caution. Zinc(II) stearate exhibit highest activity towards acceleration and its inclusion does not alter the viscosity of the formulation offering a processing advantage. Kinetic parameters associated with polymerization of the resin were established using Kissinger Akahira Sunose method.

Keywords*: Accelerator, cardanol, toxicity, polymerization, viscosity, stearate*

ACCEPTED MANUSCRIPT

1. Introduction

Polybenzoxazines is a new class of phenolic-like thermosetting resins based on the ring opening polymerisation of the benzoxazine monomer, which exhibit extremely interesting properties, notably negligible volume shrinkage during curing[1], low water absorption[2] and thermal stability[3, 4]. In addition, molecular designing flexibility through the astute choice of the amine and phenolic components bestow an extremely interesting feature to these materials in terms of tunablity, thereby opening up new vistas of application[5-9].

Biobasedbenzoxazine monomers appear to be proficient in satisfying the increasing demands of polymer industry. However, a major drawback associated with bio-based benzoxazine resin is its high curing temperature[10, 11], which restricts its usage for widespread applications[12, 13]. It is extremely desirable to develop sustainable benzoxazine formulations with low curing temperatures. Temperature associated with the curing process can be alleviated through structural modifications [14-16] or addition of curing accelerators[11, 17-19]; the latter methodology being preferred in view of its economic viability. In this context, accelerators for curing of petro-based as well as bio-based benzoxazines are commercially available with Huntsman (DT300 and DT310), however the chemical composition is not available in public domain.

Several accelerators, based on organic acids[10, 20] and Lewis acids[21, 22]have been reported for accelerating polymerization, but their presence in the resin reportedly affect the chemical resistance of the polymer and deteriorate the physical properties of the resulting cross-linked product[17]. Organic bases such as amines[23], and imidazoles[24]have also been explored, and the effectiveness of acid-base combination has also been studied[25]. Sudo et.al[11] studied the efficiency of acetylacetonato complexes of 4^{th} period transition metals as catalysts, and reported that the complexes of manganese, iron, cobalt and zinc exhibited the

highest activity. Due to high surface area and acidic sites, metal organic frameworks (MOFs) based on zinc have also been explored as curing accelerators[26]. The studies indicate that Lewis acidic Zn_4O nodes of atomic precision, which are available throughout the surface of the framework, are responsible for the decrease in the curing temperature.

Inopportunely, metal complexes are relatively intolerant towards moisture ,which deteriorate the mechanical performance of the material. Acetylacetonato complexes with hexafluoroacetylacetonate ligand (F_6-acac)are relatively more efficient accelerators, in view of their enhanced Lewis acidity of the metal center due to the presence of strong electron-withdrawing group[11]. In addition, the replacement of acetylacetonate with the hexafluoroacetylacetonate also improved the moisture tolerance of the accelerator. However, fluorinated compounds are toxic which imposes operability issues and are relatively expensive. This motivated us to consider the possibility of tailoring the chemical environment around the metal centre and explore the potential of stearates based on transition metals, which proves to be efficient, ecofriendly and economically viable, in the context of curing of bio-based benzoxazine monomer.

Metal stearates,coordination complexes of long chain fatty acids with transition metals, are of greatest commercial importance. The organic ligand, i.e. stearic acid is derived from saponification of the triglycerides obtained from natural sources (cocoa butter and shea butter)[27]. Among the many interesting properties of metallic stearates, the most important are water repellence[28], gelling capacity, and stabilizing effect[29]. The LD_{50}values of zinc compounds are high (186 to 623 mg zinc/kg/day) which is indicative of its low toxicity[30].Most of the metal stearates, undergo solid to liquid transition ca ~150°C; conditions under which cardanol based benzoxazine curing is negligible[8]. In addition, metal stearates do not undergo

thermal degradation during processing of the resin, rendering them excellent candidature as curing accelerators.

The present work deals with the preparation of a series of transition metal stearates and to explore their potentialas curing accelerators for cardanol-aniline benzoxazine, a value added, industrially significant high performance material.

2. Experimental

2.1 Materials

Cardanol (ρ =0.927-0.935 g/cm^3; Iodine value 250; Acid Value Max 5; Hydroxyl Value 180-190) was obtained from Satya Cashew Chemicals Pvt. Ltd. (India). The HPLC chromatogram of cardanol is presented in the supplementary section (Figure S1)[14]. Aniline, paraformaldehyde was purchased from CDH chemicals. Cardanol-aniline benzoxazine was synthesized as reported previously[13, 14, 26] and is used as resin for the screening of curing accelerators. Manganous chloride, ferric chloride, cobaltous chloride, nickel sulphate, cuprous chloride, zinc sulphate, and stearic acid were purchased from CDH were used as received. Zinc acetate anhydrous ('AR', E.Merck), was used without further purification.Double distilled water was used throughout the course of this work.

2.2 Characterization methods

Fourier Transform Infrared (FT-IR) spectra of samples were recorded using a Thermo scientific FT-IR (NICOLET 8700) analyzer with an attenuated total reflectance (ATR) crystal accessory. The angle of incidence of the germanium ATR crystal used was characteristically 45° and the spectra was recorded in the wavelength range 4000-500 cm^{-1},with a resolution of 4 cm^{-1}.Thermal behavior was investigated using Perkin Elmer Diamond STG-DTA under N_2 atmosphere (flow rate = 50 ml min^{-1}) in the temperature range 50-700 °C. A heating rate of 10 °C/min and sample mass of 5.0 ± 0.5 mg was used for each experiment. Calorimetric studies

were performed on a Differential Scanning Calorimeter (TA instruments Q 20). For dynamic DSC scans, the sample (5 ± 2 mg) was sealed in aluminum pans using T_{zero} press, and heated from 30 to 300 °C at three different rates 5, 7 and 10°C /min. N_2 was purged at rate of 50 ml/min to minimize oxidation of the sample during the curing process. Prior to the experiments, the instrument was calibrated for temperature and enthalpy using standard Indium and Zinc. Thermal equilibrium was regained within 1 min of sample insertion, and the exothermic reaction was considered to be complete when the recorder signal leveled off to the baseline. The total area under the exothermic curve was determined to quantify the heat of curing.

Anton Paar Rheometer MCR-102 was used to study the rheological behavior of the resin. Temperature-sweep experiment was performed by applying oscillatory mode in three intervals: 30-150°C at 5°C min^{-1}, 150-250°C at 3°C min^{-1} followed by isothermal at 250°C for 1h. A constant strain of 0.5% and constant angular frequency of 10 rad/s was maintained during each interval (parallel plate size of diameter 8 mm and gap thickness was maintained at 1.00mm)

2.3 Synthesis of metal stearates

Transition metal stearates were synthesized using double decomposition technique of sodium stearate with metal salt as per the procedure reported in the literature[31]. Sodium stearate was prepared by the reaction of stearic acid with stoichiometric amount of sodium hydroxide. Subsequently, the temperature was increased to 75°C, and the desired aqueous metal salt solution was added dropwise till complete precipitation of the metal stearates was observed. The metal stearates formed were filtered, washed repeatedly with hot water and finally dried under vacuum at 60°C.

2.4 Polymerisation of cardanol based benzoxazine (C-a) using metal stearates.

To an accurately weighed amount of the cardanol-derived benzoxazine (C-a),varying amount of metal stearates (1-10 %w/w) were added and stirred at room temperature; conditions

under which no polymerization was perceptible. The details of the formulations prepared along with their sample designations have been mentioned in supplementary section (Table S1). Neat benzoxazine has been referred to as C-a and the compositions containing metal stearates have been referred to as MStXC-a where X indicates the mass percent of metal stearate present in the sample. For e.g. C-a containing 10% w/w zinc(II) stearate has been designated as ZnSt10C-a. A control set of curing studies were also performed on benzoxazine resin containing stearic acid and zinc acetate anhydrous. Sample was placed in a DSC aluminium pan and heated at a uniform rate of 10°C/min, while measuring the heat flow associated with polymerization. The corresponding DSC profiles of formulations were used to quantify characteristic curing parameters.

3. Results and Discussions

The potential of stearates based on transition metals as curing accelerator for benzoxazine resins has been explored. Non-isothermal calorimetric studies were performed to study the curing behavior of benzoxazine in the presence of stearates.

3.1 Transition metal stearates

Metallic stearates were synthesized by double decomposition process involving formation of sodium stearate followed by the replacement of the sodium cation with transition metal to form an insoluble metal stearate (Scheme 1).



Scheme 1: Double decomposition method for metal stearate preparation

FT-IR spectra of all the stearates exhibited absorbance at 1545 cm^{-1}; attributable to asymmetric vibration stretching of the carboxylic group coordinated to the metal ion (Figure 1 (i)).Three intense bands in the 1300–1600 cm^{-1} region were also observed. The 1545 cm^{-1} band

is assigned to the carboxylate antisymmetric stretch and 1465 cm^{-1} to the CH_2 bending. The 1399 cm^{-1} band may be assigned to the C_xH_{2x} bending and/or the carboxylate symmetric stretch, both of which should be observed in the infrared spectrum.DSC traces presented in Figure 1(ii),reveal that all the stearates undergo melting prior to the onset of the polymerization of the benzoxazine monomer (~242°C). This is expected to result in homogeneous blending of the stearate with the monomer, thereby enhancing their candidature as accelerators. Thermo gravimetric analysis (Figure1(iii)) revealed that all metal stearates are thermally stable within the processing window of the benzoxazine monomer ca~ 250°C.

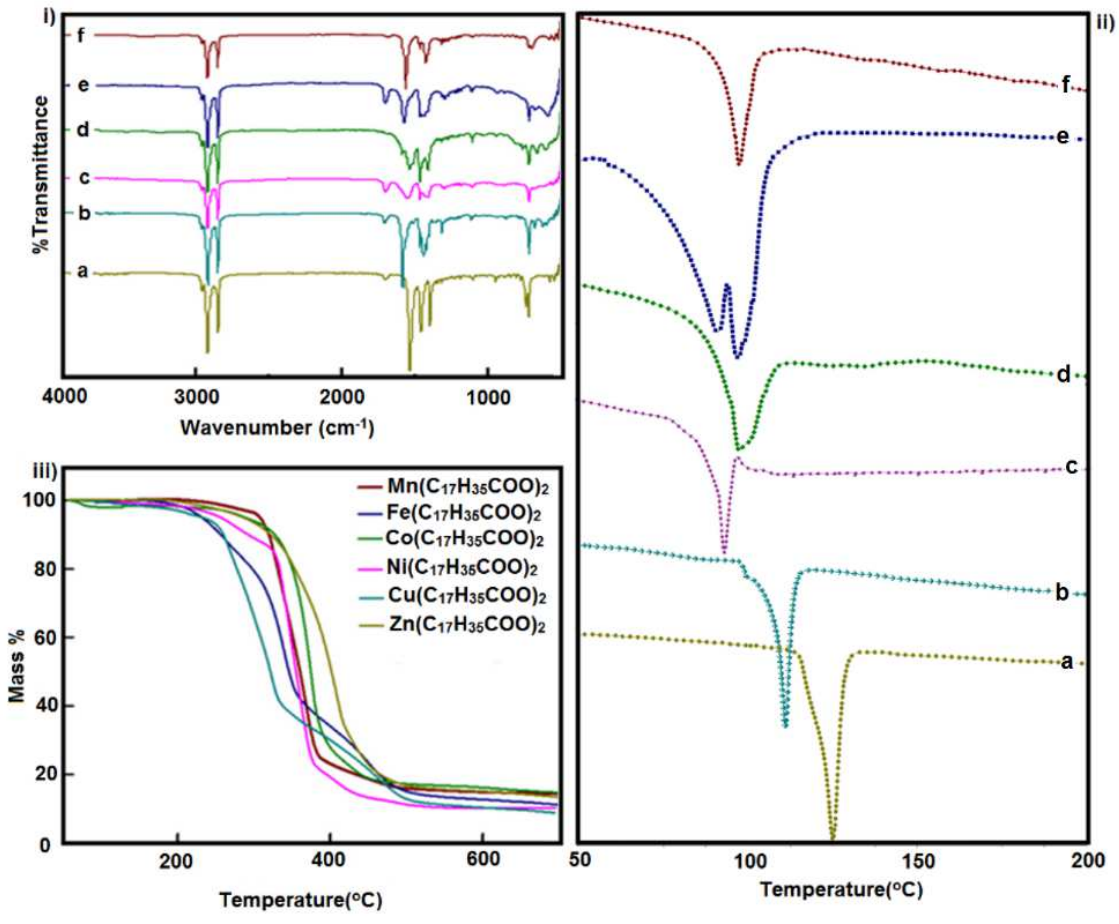


Figure 1: Characterization of metal stearates i) FT-IR ii) DSC and iii) TGA traces of a) zinc(II) b) copper(II)c) nickel(II) d) cobalt(II) e) iron(II) f) manganous(II)stearate

All the metal stearates were found to be insoluble in water and soluble in THF, DMF, xylene and toluene. The contact angle of zinc(II) stearate powder has been reported to be 154.6 ± 1.5°[28], which is a direct evidence of its super hydrophobic surface. The same was confirmed from the mobile water drops over surface of zinc(II) stearate powder as can be seen in digital images presented in supplementary section (Figure S2). In this context, it is imperative to mention that zinc stearate find extensive use as a lubricant additive which improves filler dispersion in hydrophobic plastic media[32].The hydrolytic stability of the metal stearates is an extremely interesting feature, which bestow them ideal candidature as curing accelerator for benzoxazine curing. Characteristic thermal properties like non-volatile content (%) and ash content (%) of metal stearates were determined as per the standard procedure (supplementary section) and the results are tabulated in supplementary section (Table S2). All metal stearates exhibited a nonvolatile content >95% and ash content of 12–15%. The ash content has been reported to be dependent on the oxidation state of the central metal[31].As per theoretical calculations, the metal content corresponding to all the stearates should be 6.25±0.21%. However, this figure is not in concordance with the char content obtained during TGA, which can be attributed to the conversion of the metal to its oxide form during the thermal decomposition process.

The acidic co-reactants were completely consumed during the formation of metal stearate, which was confirmed from the negligible free fatty acid content, as determined using established procedure presented in supplementary section.

3.2 Screening of accelerators based on DSC analysis of polymerization of cardanol benzoxazine monomer

Benzoxazine monomers undergo thermally accelerated cationic ring opening polymerization and results in thermally stable polymer. The presence of curing accelerators in

the formulation is expected to shift the curing profile towards lower temperatures and alter the kinetics of the oxazine ring opening stage through several reported mechanisms[25, 33-37]. Non-isothermal calorimetric studies were performed to assess the potential of metal stearates towards acceleration in polymerization of benzoxazine resins. The results of the DSC analyses in terms of characteristic curing temperatures and enthalpy are summarized in Table 1[38].

Table 1: Effect on introduction of accelerators on characteristic curing temperatures (β=10°C/min)

Sample designation	**T_o (°C)**	**T_{peak}(°C)**	**% Reduction**		**Enthalpy of polymerization (J/g)**
			T_o	**T_{peak}**	
C-a	242	263	-	-	63
St10C-a	223	244	7.8	7.2	88
MnSt10C-a	187	226	22.7	14.0	97
FeSt10C-a	206	225	14.8	14.4	94
CoSt10C-a	183	213	24.3	19.0	97
NiSt10C-a	205	236	15.2	10.2	97
CuSt10C-a	212	234	12.3	11.0	73
ZnSt1C-a	226	247	6.6	6.0	79
ZnSt5C-a	193	222	20.2	15.5	82
ZnSt10C-a	169	202	30.1	23.1	92
ZnAc10C-a	218	222	9.9	15.5	68

The presence of metal stearates based on manganese(II), iron(II), cobalt(II)and zinc(II)in the formulation led to a remarkable decrease in the curing parameters, with copper(II) and nickel(II)stearate being relatively less effective. Cobalt(II) complexes have been reported to

exhibit high levels of toxicity and pose adverse effect on the environment[39].In view of these concerns, zinc(II) stearate, was selected as the most suitable accelerator and representative curing profiles of formulations containing varying amounts of zinc stearate are presented in Figure 2.The enthalpy of polymerization associated with the prepared formulations is listed in Table 1. An increased enthalpy of polymerization was observed in formulations containing curing accelerators. A similar increase in the enthalpy of polymerization has been reported earlier[18]. The increase in the heat of polymerization can be attributed to the destabilization of the oxazine moiety due to interaction with the Lewis acidic accelerators. This interaction results in a strained benzoxazine molecule with relatively higher potential energy, which leads to a larger potential energy difference between the reactant and product.

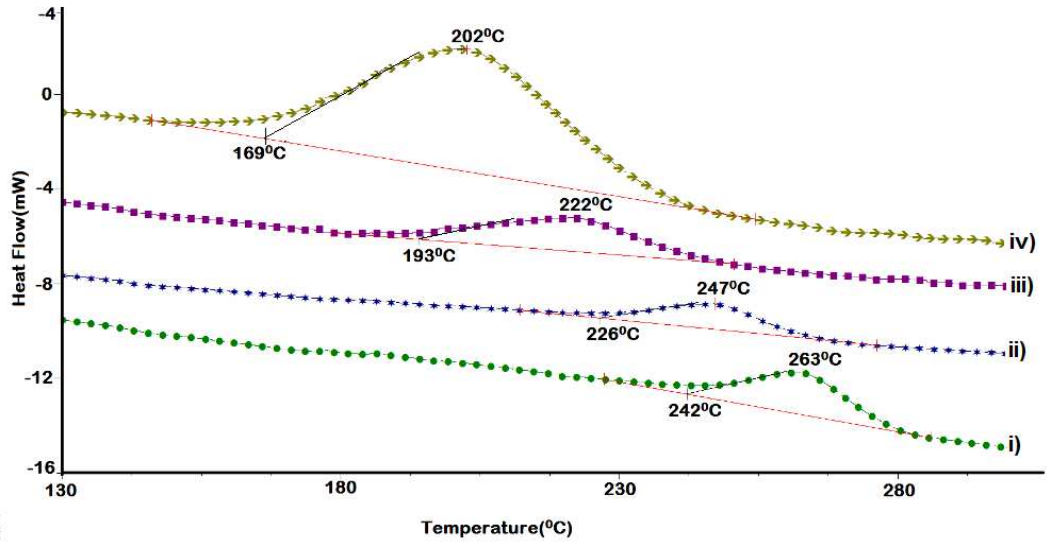


Figure 2: DSC profile i) C-a, ii) ZnSt1C-a, iii) ZnSt5C-a and iv) ZnSt10C-a

It has already been mentioned that the ring opening polymerization of cardanol based benzoxazine initiates at 242°C with a peak at 263°C (Figure 2(i)).It can be seen from the figure that the curing profile shifts towards lower temperature in the presence of zinc(II) stearate, the extent of which was found to be proportional to its amount in the formulation. Inclusion of

zinc(II) stearate (10%w/w) in the formulation was found to decrease the curing temperature of neat benzoxazine from ~263°C to ~202°C (23% decrease) (Figure 2(ii)-(iv)). Acetylacetonate complexes have been previously reported to decrease the curing temperature of BA-a (bisphenol-aniline benzoxazine) by 23%[11]. Commercially available accelerators DT310 and DT300 (Huntsman), post addition in BA-a have been reported to decrease the curing temperature by 16.8 and 7.2 % respectively.

Extensive characterization studies on zinc(II) stearate[40] confirm the presence of acidic Zn_4O nodes, which are coordinatively linked to four carboxylate moieties with a Zn-O distance of 0.195 nm.(Figure 3). It is the presence of these Lewis acidic Zn_4O nodes, which is responsible for accelerating activity of zinc(II) stearate[26]. As the temperature is increased, a solid–liquid phase transition occurs in zinc(II) stearate at ~130°C, however the coordination structure reportedly remains unaffected[40].

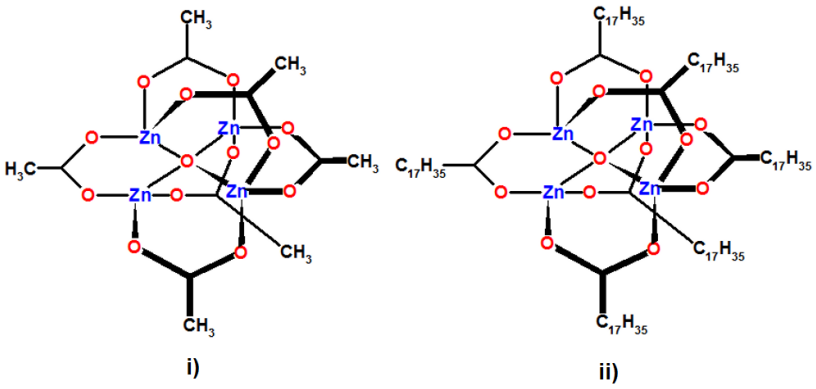


Figure 3: Chemical Structures of i) anhydrous zinc(II) acetate and ii) zinc(II) stearate

To understand the importance of the chemical environment around the central zinc species, curing studies were also performed in the presence of zinc(II) acetate anhydrous, which also has been reported to possess Zn_4O nodes[40], and the results are included in Table 1. It can be speculated that the synergistic combination of acidic Zn_4O nodes and the uniform dispersion

due to the hydrophobic stearate chains (Figure 4(i)) result in the observed acceleration of the curing reaction.

The proposed mechanism of zinc(II) stearate accelerated polymerization of benzoxazine is presented in Figure 4(ii). The Zn_4O nodes available in zinc(II) stearate interact with the oxygen to form a cyclic oxonium cationic species, which is followed by an electronic rearrangement leading to the formation of a resonance stabilized iminium cation. Subsequently, benzoxazine monomer adds to the cationic imine moiety, forming another electron deficient cyclic oxonium species. Repetitive electrophilic substitutions result in a polymeric network with thermally unstable aryl ether structure, which undergoes rearrangement resulting in a polymer with phenolic structure.

ACCEPTED MANUSCRIPT

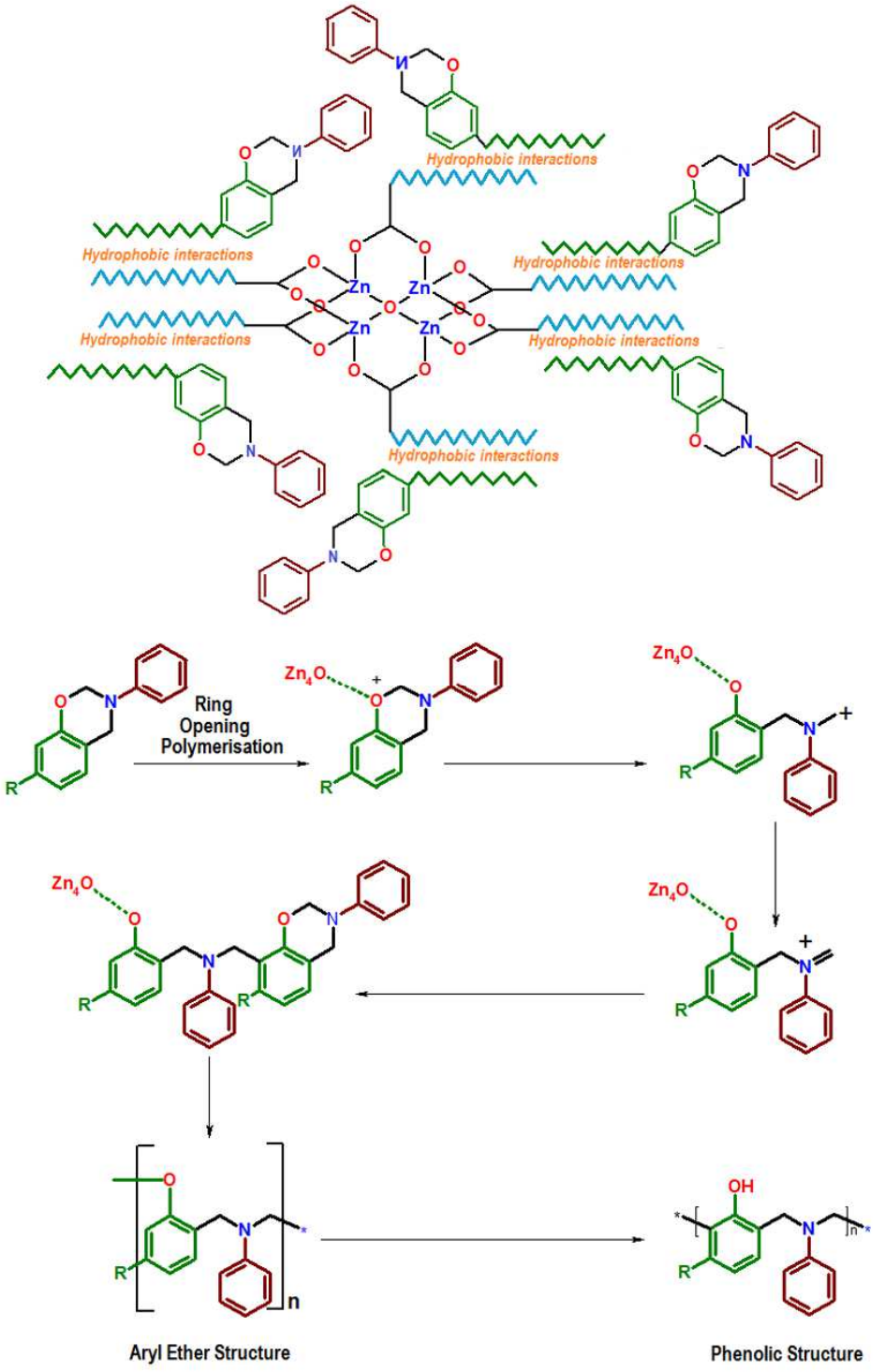


Figure 4: i) Hydrophobic interactions present within zinc(II) stearate and C-a resulting in uniform dispersion of accelerator in the resin. ii) Proposed mechanism for ring opening polymerization of C-a in the presence of zinc(II) stearate as curing accelerator.

To gain an insight into this aspect, the rheological behavior of the resin post- introduction of zinc(II) stearate has been investigated by temperature sweep experiments. The variation of complex viscosity and loss-storage modulus with respect to temperature is presented in Figure 5. It can be seen that at room temperature, viscosity of the formulation (ZnSt10C-a) is higher than that of the neat resin (C-a). However, increasing the temperature to 130°C leads to a precipitous drop in the viscosity of the formulation, which is accompanied by a concomitant decrease in storage and loss modulus, a phenomenon that can be attributed to the melting of zinc(II) stearate. Our studies indicate that the introduction of accelerator does not lead to any increase in the viscosity of the formulation. The ring-opening of oxazine moieties leads to the formation of open Mannich bases, possessing hydrogen bonding interactions, however till ~220°C, the viscosity buildup is practically negligible[41]. Subsequently, polymerisation is initiated where the linear chains associate with each other leading to a sudden increase in viscosity. The phenolic hydroxyl groups generated, act as polymerization catalysts which leads to gelation at ~220°C, observed as a crossover of loss and storage modulus[41, 42] (Figure 5(ii)), while the same is achieved at ~257°C (for the neat resin) as shown in the Figure 5(i), which further confirms the accelerating activity of zinc(II) stearate. Further increase in temperature leads to an increase in the viscosity as well as the moduli, which finally levels off.

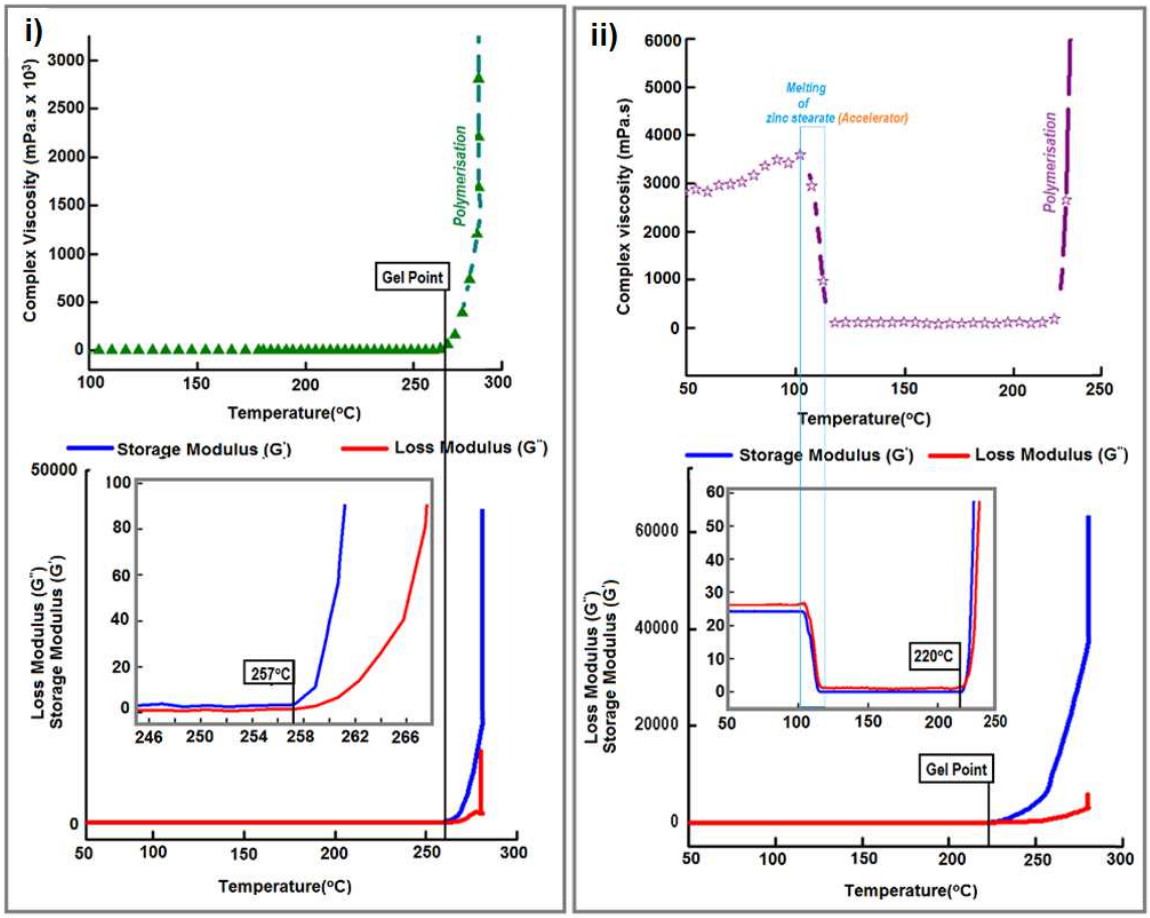


Figure 5: Rheological behavior of i) C-a and ii) ZnSt10C-a during polymerization.

3.3 Kinetics of metal stearate accelerated polymerization

DSC traces of a representative formulation (ZnSt10C-a) at various heating rates viz. 5, 7 and 10°C/min are presented in Figure 6. Increasing the heating rate (β) leads to systematic shift in the trace towards higher temperatures, which can be attributed to the reduced time available with the reactants at higher heating rates. The curing of cardanol based benzoxazine resin is typically a multi-step process, which exhibits complex reaction kinetics[43-45]. The process is accompanied with a dramatic change in the physical state of the reaction medium. At the early stages, the reaction medium is a liquid composing primarily of monomers. With the progress of the reaction, the molecular weight and viscosity of the polymer formed increases, which in turn

results in a decrease in the molecular mobility. The sudden decrease in the mobility however occurs with the cross-linking of polymer chains, where the chains lose their ability to move past one another, and the medium turns to a solid that can be either rubbery or glassy, depending upon the T_g of the cured resin. Characteristic parameters associated with the curing of the resin i.e. ΔH_{cure}, T_{onset} and T_{peak} are summarized in Table 2.

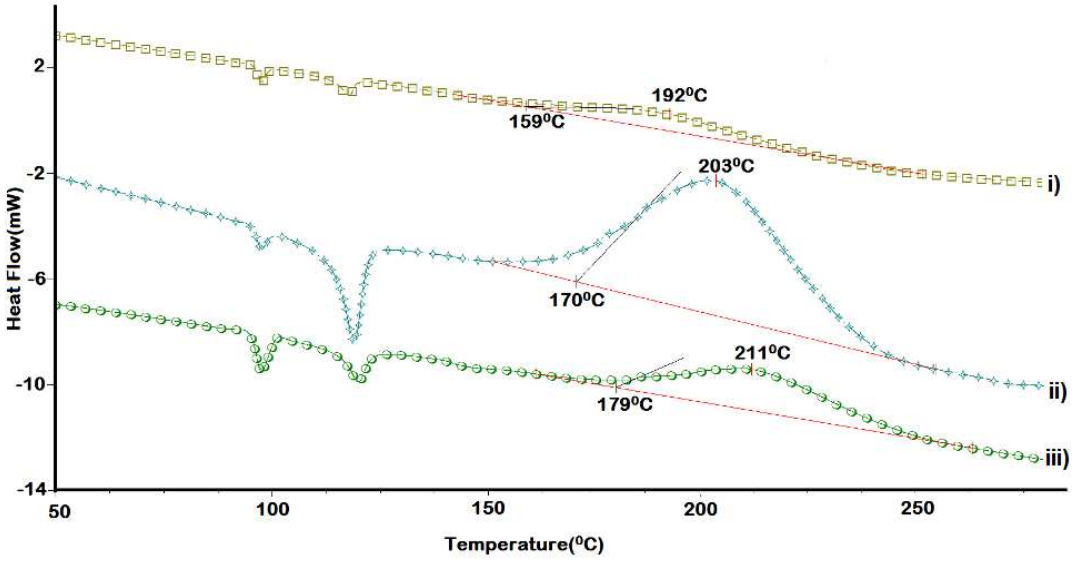


Figure 6: Effect of heating rate(β) on the curing profile of ZnSt10C-a i) 5, ii) 10 and iii) 15 °C/min.

The extent of conversion, α at any particular temperature (T_α) was calculated as the ratio of the areas under the exothermic DSC peak and expressed as:

$$\alpha = \frac{\Delta H_{T_\alpha}}{\Delta H_{cure}} \text{.....(1)}$$

where ΔH_{T_α} is the heat of reaction of partially cured samples (till temperature T_α) and ΔH_{cure} is the total heat of curing. The increase in the degree of conversion with temperature for ZnSt10C-a at different heating rates is presented in Figure 7(i).

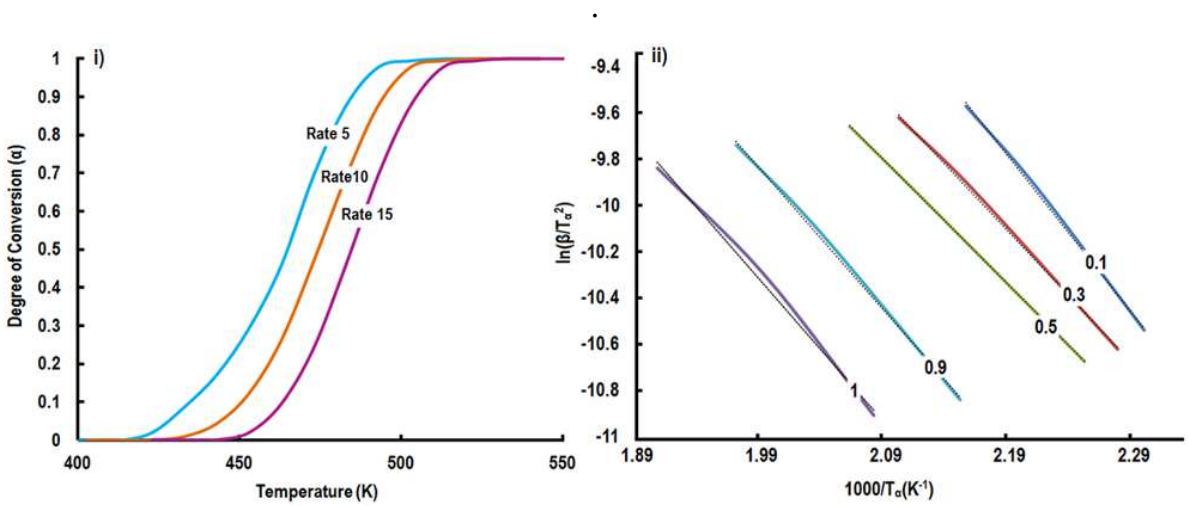


Figure 7: i) Effect of temperature on the degree of conversion of cardanol based benzoxazine in the presence and absence of zinc(II) stearate (β = 5, 10 and 15 °C/min) ii) Iso-conversion plots associated with various degree of conversions (α).

It can be seen that in the presence of zinc(II) stearate, complete curing is attained at ~203°C while the same for a neat monomer is achieved at 280°C[26], clearly demonstrating the effectiveness of zinc(II) stearate as an curing accelerator for benzoxazine.

Table 2: Characteristic curing parameters of C-a (neat benzoxazine)and ZnSt10C-a

Sample	β(°C/min)	T_{onset}(°C)	T_{peak}(°C)	Activation energy (kJ/mol)
C-a	5	224	246	98
	10	236	255	
	15	241	263	
ZnSt10C-a	5	159	192	51
	10	170	203	
	15	179	211	

In view of its simplicity, Kissinger–Akahira–Sunose equation[46] was applied for determination of activation energies (E_α) from the plot of $ln\left(\frac{\beta_i}{T_{\alpha,i}^2}\right)$ against $1/T_\alpha$.

$$ln\left(\frac{\beta_i}{T_{\alpha,i}^2}\right) = \text{Constant} - \frac{E_\alpha}{RT_{\alpha,i}} \quad \text{.....(2)}$$

Where, β is the heating rate, T_α is the temperature associated with a particular conversion (α) at the corresponding heating rate, E_α is the activation energy at that α and R is the gas constant. The linear plots at few representative conversions for ZnSt10C-a are presented in the Figure 7(ii), which were used to arrive at the activation energy. The variation in $E_\alpha$with degree of conversion for ZnSt10C-a is presented in supplementary section (Figure S3) and the average value is reported in Table 2. The presence of zinc(II) stearate led to a substantial decrease in the activation energy from 98 kJ/mol for neat resin to 51 kJ/mol (ZnSt10C-a).

3.4 Thermal properties of polybenzoxazines

Thermogravimetric analysis was performed on the cured resins, to investigate the effect of introducing zinc(II) stearate on the thermal stability of cardanol based polybenzoxazine. The TG and DTG traces of poly(C-a) and poly(ZnSt10C-a) are presented in Figure 8. The thermal decomposition of cardanol based benzoxazines is a multi-step process occurring through the degradation of the phenolic linkages and of the Mannich bridges in the polybenzoxazine[47, 48]. The double bond α-carbon of the cardanol undergoes scission at ~200°C[49] and the methylene linkages in the cured polymer have been reported to undergo cleavage at 440-500°C[50].

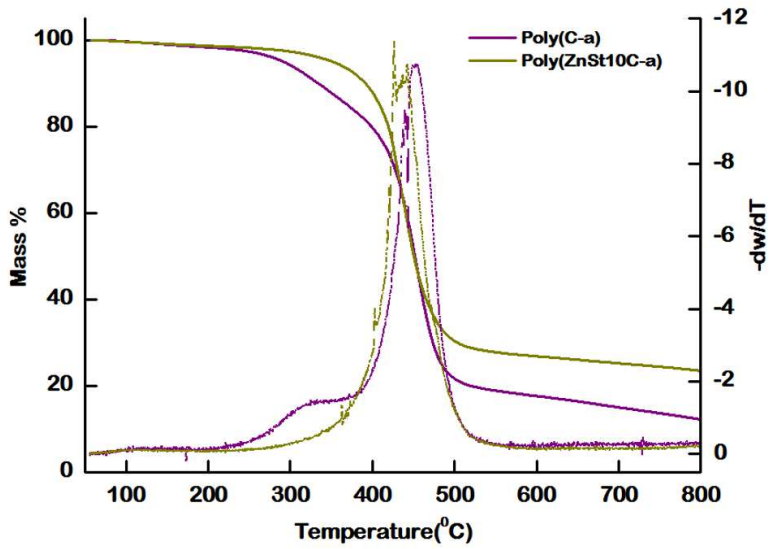


Figure 8: TG-DTG traces of Poly(C-a) and Poly(ZnSt10C-a)

Decomposition temperatures associated with characteristic mass loss at 5%, 10% and char content (at 600°C) are presented in Table 3. An appreciable increase in the $T_{5\%}$ and $T_{10\%}$ values is evident from the traces, and the increase in the char content can be attributed to the presence of zinc oxide formed during the thermal degradation of the cured formulation. Polybenzoxazines have been reported to exhibit excellent fire, smoke and toxicity (FST) properties, which can be preliminarily adjudged through Limiting oxygen index (LOI) studies. The same refers to the minimum amount of oxygen (%) in an oxygen-nitrogen mixture that is just sufficient to maintain combustion (post-ignition) of the material[51]. A significant correlation between the char residue (CR) and LOI has been reported, LOI=17.5+0.4×CR[52]. The LOI for poly(C-a) was calculated to be 24, which is considered to be suitable for application of these polymers in areas necessitating flame retardance[14]. The same was found to increase substantially to 28 upon addition of 10 %w/w zinc stearate indicating superior flame retardancy of the developed formulation.

Table 3: Characteristic thermo-oxidative degradation parameters

Sample Designation	$T_{5\%}$ (°C)	$T_{10\%}$(°C)	Char content at 600 °C (%)	LOI
Poly (C-a)	292	331	18	24
Poly(ZnSt10C-a)	351	390	27	28

4. Conclusions

The accelerating ability of zinc(II) stearate on the ring opening polymerization of a representative bio-based cardanol based benzoxazine(C-a) has been systematically studied. Addition of zinc(II) stearate(10%w/w) in the resin, was found to decrease the curing temperature of neat benzoxazine from ~263°C to ~202°C (23% decrease). This exceptional accelerating ability has been attributed to the presence of acidic Zn_4O nodes in addition to the long alkyl chain of stearate, which helps in the dispersion of the accelerator in the resin. KAS method was used to determine the activation energy of polymerization, which was found to decrease from 98 kJ/mol (neat resin) to 51 kJ/mol for formulation containing zinc(II) stearate (10%w/w). The cured resins obtained in the presence of zinc(II) stearate exhibited relatively high thermal stability ($T_{5\%}$ = 351°C) as compared to the neat polymer ($T_{5\%}$ = 292°C). Our studies clearly highlight the enormous scope of metal stearates as eco-friendly accelerators for polymerization of bio-based benzoxazine resins, which requires high temperatures for curing. In view of the flexibility in designing and controlling the architecture of these hybrid structures, sustainable benzoxazine systems with low curing temperatures and improved performance can be formulated in the future.

Supplementary Information

HPLC chromatogram of cardanol (Figure S1), Details of formulations and sample designation (Table S1), Digital images of mobile water drop over super hydrophobic surface of zinc(II)

stearate(Figure S2), Non-volatile content determination, Ash content determination, Free fatty acid content determination, Physiochemical characterization of the metal stearates (Table S2), Variation of Activation energy with degree of conversion for C-a and ZnSt10C-a (Figure S3)

Acknowledgements

The authors gratefully acknowledge Director, CFEES for providing logistic support to perform this work.

ACCEPTED MANUSCRIPT

References

[1] H. Ishida, H.Y. Low, A Study on the Volumetric Expansion of Benzoxazine-Based Phenolic Resin, Macromolecules 30(4) (1997) 1099-1106.

[2] H. Ishida, D.J. Allen, Physical and mechanical characterization of near-zero shrinkage polybenzoxazines, Journal of Polymer Science Part B: Polymer Physics 34(6) (1996) 1019-1030.

[3] S.B. Shen, H. Ishida, Development and characterization of high-performance polybenzoxazine composites, Polymer Composites 17(5) (1996) 710-719.

[4] N.N. Ghosh, B. Kiskan, Y. Yagci, Polybenzoxazines—New high performance thermosetting resins: Synthesis and properties, Progress in Polymer Science 32(11) (2007) 1344-1391.

[5] Y. Yagci, B. Kiskan, N.N. Ghosh, Recent advancement on polybenzoxazine—a newly developed high performance thermoset, Journal of Polymer Science Part A: Polymer Chemistry 47(21) (2009) 5565-5576.

[6] P. Thirukumaran, A. Shakila Parveen, M. Sarojadevi, Synthesis and Copolymerization of Fully Biobased Benzoxazines from Renewable Resources, ACS Sustainable Chemistry & Engineering 2(12) (2014) 2790-2801.

[7] O.S. Taskin, B. Kiskan, A. Aksu, N. Balkis, J. Weber, Y. Yagci, Polybenzoxazine: A Powerful Tool for Removal of Mercury Salts from Water, Chemistry-A European Journal 20(35) (2014) 10953-10958.

[8] E. Calo, A. Maffezzoli, G. Mele, F. Martina, S.E. Mazzetto, A. Tarzia, C. Stifani, Synthesis of a novel cardanol-based benzoxazine monomer and environmentally sustainable production of polymers and bio-composites, Green Chemistry 9(7) (2007) 754-759.

[9] P. Sharma, B. Lochab, D. Kumar, P.K. Roy, Sustainable Bis-benzoxazines from Cardanol and PET-Derived Terephthalamides, ACS Sustainable Chemistry & Engineering 4(3) (2015) 1085-1093.

[10] H. Ishida, Y. Rodriguez, Catalyzing the curing reaction of a new benzoxazine-based phenolic resin, Journal of Applied Polymer Science 58(10) (1995) 1751-1760.

[11] A. Sudo, S. Hirayama, T. Endo, Highly efficient catalysts-acetylacetonato complexes of transition metals in the 4th period for ring-opening polymerization of 1,3-benzoxazine, Journal of Polymer Science Part A: Polymer Chemistry 48(2) (2010) 479-484.

[12] P. Sharma, B. Lochab, D. Kumar, P.K. Roy, Interfacial encapsulation of bio-based benzoxazines in epoxy shells for temperature triggered healing, Journal of Applied Polymer Science 132(47) (2015) DOI: 10.1002/app.42832.

[13] P. Sharma, S. Shukla, B. Lochab, D. Kumar, P. Kumar Roy, Microencapsulated cardanol derived benzoxazines for self-healing applications, Materials Letters 133 (2014) 266-268.

[14] S. Shukla, A. Mahata, B. Pathak, B. Lochab, Cardanol Benzoxazines - Interplay of Oxazine Functionality (Mono to Tetra) and Properties, RSC Advances 5(95) (2015) 78071-78080.

[15] P. Sharma, D. Kumar, P.K. Roy, Poly(benzoxazine–co–urea): A Solventless Approach Towards The Introduction of Alternating Urea Linkages In Polybenzoxazine, ChemistrySelect 2(19) (2017) 5372-5377.

[16] P. Sharma, D. Kumar, P.K. Roy, Microwave-Assisted Sustainable Synthesis of Telechelic Poly(ethylene glycol)s with Benzoxazine End Groups, ChemistrySelect 1(21) (2016) 6941-6947.

[17] A. Sudo, T. Endo, A. Taden, R. Schoenfeld, T. Huver, Benzoxazine-containing formulations polymerizable/curable at low temperature, US20100144964 A1 (2010).

[18] L. Zhang, J. Mao, S. Wang, Y. Yang, Y. Chen, H. Lu, Meta-phenylenediamine formaldehyde oligomer: A new accelerator for benzoxazine resin, Reactive and Functional Polymers 121(Supplement C) (2017) 51-57.

[19] W. Chow, S. Grishchuk, T. Burkhart, J. Karger-Kocsis, Gelling and curing behaviors of benzoxazine/epoxy formulations containing 4, 4'-thiodiphenol accelerator, Thermochimica acta 543 (2012) 172-177.

[20] A.A. Gallo, Method for preparing polybenzoxazine, US 6376080 B1 (2002).

[21] Y.X. Wang, H. Ishida, Cationic ring-opening polymerization of benzoxazines, Polymer 40(16) (1999) 4563-4570.

[22] H. Ishida, Cationic ring-opening polymerization of benzoxazines, US6225440 B1 (2001).

[23] J. Sun, W. Wei, Y. Xu, J. Qu, X. Liu, T. Endo, A curing system of benzoxazine with amine: reactivity, reaction mechanism and material properties, RSC Advances 5(25) (2015) 19048-19057.

[24] B.A. A. Rucigaj, M. Krajnc, U. Sebenik, Curing of bisphenol A-aniline based benzoxazine using phenolic, amino and mercapto accelerators, Express Polymer Letters 9(7) (2015) 647-657.

[25] A. Sudo, R. Kudoh, H. Nakayama, K. Arima, T. Endo, Selective Formation of Poly(N,O-acetal) by Polymerization of 1,3-Benzoxazine and Its Main Chain Rearrangement, Macromolecules 41(23) (2008) 9030-9034.

[26] P. Sharma, M. Srivastava, B. Lochab, D. Kumar, A. Ramanan, P.K. Roy, Metal-Organic Frameworks as curing accelerators for benzoxazines, ChemistrySelect 1(13) (2016) 3924-3932.

[27] D. Undurraga, A. Markovits, S. Erazo, Cocoa butter equivalent through enzymic interesterification of palm oil midfraction, Process Biochemistry 36(10) (2001) 933-939.

[28] Z. Wang, Q. Li, Z. She, F. Chen, L. Li, X. Zhang, P. Zhang, Facile and fast fabrication of superhydrophobic surface on magnesium alloy, Applied Surface Science 271 (2013) 182-192.

[29] H. ısmet Gökçel, D. Balköse, U. Köktürk, Effects of mixed metal stearates on thermal stability of rigid PVC, European Polymer Journal 35(8) (1999) 1501-1508.

[30] L.M.Z. Wengong, Research on the new heat stabilizer of calcium soap and zinc soap with high efficiency and less toxicity [J], POLYVINGYI CHLORIDE 1 (2000) 010.

[31] P.K. Roy, P. Surekha, R. Raman, C. Rajagopal, Investigating the role of metal oxidation state on the degradation behaviour of LDPE, Polymer Degradation and Stability 94(7) (2009) 1033-1039.

[32] E. Richard, C. Anandan, S.T. Aruna, Fabrication of Superhydrophobic Zinc Stearate Hierarchical Surfaces from Different Precursors, Materials and Manufacturing Processes 31(9) (2016) 1171-1176.

[33] J. Dunkers, H. Ishida, Reaction of benzoxazine-based phenolic resins with strong and weak carboxylic acids and phenols as catalysts, Journal of Polymer Science Part A: Polymer Chemistry 37(13) (1999) 1913-1921.

[34] P. Chutayothin, H. Ishida, Cationic Ring-Opening Polymerization of 1,3-Benzoxazines: Mechanistic Study Using Model Compounds, Macromolecules 43(10) (2010) 4562-4572.

[35] C. Liu, D. Shen, R.M. Sebastián, J. Marquet, R. Schönfeld, Mechanistic Studies on Ring-Opening Polymerization of Benzoxazines: A Mechanistically Based Catalyst Design, Macromolecules 44(12) (2011) 4616-4622.

[36] G. Riess, J.M. Schwob, G. Guth, M. Roche, B. Laude, Ring Opening Polymerization of Benzoxazines — A New Route to Phenolic Resins, in: B.M. Culbertson, J.E. McGrath (Eds.), Advances in Polymer Synthesis, Springer US, Boston, MA, 1985, pp. 27-49.

[37] Y.-X. Wang, H. Ishida, Synthesis and Properties of New Thermoplastic Polymers from Substituted 3,4-Dihydro-2H-1,3-benzoxazines, Macromolecules 33(8) (2000) 2839-2847.

[38] P.K. Roy, P. Sharma, D. Kumar, Process for preparation of polybenzoxazines, Indian Patent 201711005289 (2017).

[39] D. Lison, Human Toxicity of Cobalt-Containing Dust and Experimental Studies on the Mechanism of Interstitial Lung Disease (Hard Metal Disease), Critical Reviews in Toxicology 26(6) (1996) 585-616.

[40] T. Ishioka, K. Maeda, I. Watanabe, S. Kawauchi, M. Harada, Infrared and XAFS study on structure and transition behavior of zinc stearate, Spectrochimica acta. Part A, Molecular and biomolecular spectroscopy 56A(9) (2000) 1731-1737.

[41] R. Huang, S.O. Carson, J. Silva, T. Agag, H. Ishida, J.M. Maia, Interplay between rheological and structural evolution of benzoxazine resins during polymerization, Polymer 54(7) (2013) 1880-1886.

[42] P.J. Halley, M.E. Mackay, Chemorheology of thermosets—an overview, Polymer Engineering & Science 36(5) (1996) 593-609.

[43] H. Ishida, Y. Rodriguez, Curing kinetics of a new benzoxazine-based phenolic resin by differential scanning calorimetry, Polymer 36(16) (1995) 3151-3158.

[44] C. Jubsilp, S. Damrongsakkul, T. Takeichi, S. Rimdusit, Curing kinetics of arylamine-based polyfunctional benzoxazine resins by dynamic differential scanning calorimetry, Thermochimica acta 447(2) (2006) 131-140.

[45] C. Jubsilp, K. Punson, T. Takeichi, S. Rimdusit, Curing kinetics of benzoxazine–epoxy copolymer investigated by non-isothermal differential scanning calorimetry, Polymer Degradation and Stability 95(6) (2010) 918-924.

[46] P. Budrugeac, E. Segal, Applicability of the Kissinger equation in thermal analysis, Journal of Thermal Analysis and Calorimetry 88(3) (2007) 703-707.

[47] H. Yee Low, H. Ishida, Structural effects of phenols on the thermal and thermo-oxidative degradation of polybenzoxazines, Polymer 40(15) (1999) 4365-4376.

[48] S.-i. Kuroda, K. Terauchi, K. Nogami, I. Mita, Degradation of aromatic polymers—I. Rates of crosslinking and chain scission during thermal degradation of several soluble aromatic polymers, European Polymer Journal 25(1) (1989) 1-7.

[49] S. Manjula, C.K.S. Pillai, V.G. Kumar, Thermal characterization of cardanol-formaldehyde resins and cardanol-formaldehyde/poly(methyl methacrylate) semi-interpenetrating polymer networks, Thermochimica acta 159 (1990) 255-266.

[50] D. O'Connor, F.D. Blum, Thermal stability of substituted phenol-formaldehyde resins, Journal of Applied Polymer Science 33(6) (1987) 1933-1941.

[51] C.A. Wilkie, A.B. Morgan, Fire retardancy of polymeric materials, CRC press2009.

[52] D.W. van Krevelen, Some basic aspects of flame resistance of polymeric materials, Polymer 16(8) (1975) 615-620.

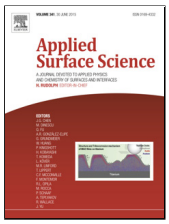
ACCEPTED MANUSCRIPT

ACCEPTED MANUSCRIPT

1. Transition metal stearates were explored as curing accelerators for cardanol-aniline benzoxazine resin.
2. Inclusion of zinc stearate led to a remarkable reduction in the polymerisation temperature of the bio-based resin.
3. The rheological behavior of the resin was not adversely affected due to the inclusion of zinc stearate.
4. Curing kinetics of the polymerisation of benzoxazine resin was studied and activation energy was calculated using KAS method.
5. Polymer with improved thermal stability was obtained using zinc stearate as curing accelerator.

ACCEPTED MANUSCRIPT

Accepted Manuscript



Title: Epitaxial Growth of GaN Nanostructure by PA-MBE for UV Detection Application

Authors: Lalit Goswami, Rajeshwari Pandey, Govind Gupta

PII: S0169-4332(18)30311-8
DOI: https://doi.org/10.1016/j.apsusc.2018.01.287
Reference: APSUSC 38426

To appear in: *APSUSC*

Received date: 29-9-2017
Revised date: 17-1-2018
Accepted date: 30-1-2018

Please cite this article as: Lalit Goswami, Rajeshwari Pandey, Govind Gupta, Epitaxial Growth of GaN Nanostructure by PA-MBE for UV Detection Application, Applied Surface Science https://doi.org/10.1016/j.apsusc.2018.01.287

This is a PDF file of an unedited manuscript that has been accepted for publication. As a service to our customers we are providing this early version of the manuscript. The manuscript will undergo copyediting, typesetting, and review of the resulting proof before it is published in its final form. Please note that during the production process errors may be discovered which could affect the content, and all legal disclaimers that apply to the journal pertain.

ACCEPTED MANUSCRIPT

Epitaxial Growth of GaN Nanostructure by PA-MBE for UV Detection Application

Lalit Goswami[1,2], Rajeshwari Pandey[1,*] and Govind Gupta[2,†,*]

[1]*Department of Electronics & Communication Engineering, Delhi Technological University, New Delhi-110042.*
[2]*Advanced Materials & Devices, CSIR-National Physical Laboratory, Dr. K.S. Krishnan Marg, New Delhi- 110012, India.*
[†]*Academy of Scientific &Innovative Research, CSIR-NPL Campus, Dr. K. S. Krishnan Road, New Delhi- 110012, India.*
[*]Corresponding Author: govind@nplindia.org; Telephone: +91-1145608403; rpandey@dce.ac.in

Highlights

- Epitaxial growth of Gallium-Nanostructures (GaN-NS) by PA-MBE.
- Fabrication of Ultraviolet Photodetector with Au-GaN-NS.
- Bias dependent enhancement in photo-responsivity.

Abstract

We report the growth of lower aspect ratio, nano-island shaped, lower stress and strain facilitated gallium nitride nanostructures (GaN-NS) on Si (111) substrate via plasma assisted molecular beam epitaxy (PA-MBE) and fabrication of GaN-NS based UV photo-detection device even with NS's tiny dimensionality. GaN-NS were grown on Si (111) substrate with an inhomogeneous layer of Si_3N_4 which act as anti-surfactant to Ga atoms and also offer localized compressive strain. The developed strain can be relaxed by the growth of inhomogeneously oriented GaN NS. The three dimension (3D) growth of GaN-NS in real time was observed by in-situ RHEED technique which displays transformation from streaky to spotty pattern. A micro-Raman technique has been employed to elaborate NS's crystallinity and lower stress value which is found be in good agreement with related lower strain as evaluated by HR-XRD spectra. A sharp near band edge emission at 363.2 nm is observed by room temperature photoluminescence measurement which signifies the presence of GaN. Metal semiconductor metal Au-GaN-NS/Si(111) device was fabricated to specifically analysed its ability to detect harmful ultraviolet radiations (325nm) with GaN islands of just 26nm height and 50nm width. The performance of the fabricated device was analysed at fixed optical power of 13mW with varying bias voltages (0.4-3V).

Keywords: Gallium Nitride, Nanostructures, PA-MBE, Ultraviolet Photodetector.

1. Introduction

Gallium nitrides (GaN) semiconductor (SC) exhibits significant advantages for next generation optoelectronic devices due its promising material properties [1]. The GaN material is chemically and mechanically stable and having wide-direct bandgap, high thermal conductivity, high mobility as well as high thermal stability. [2-4] The comprehensive outcome realized as GaN

ACCEPTED MANUSCRIPT

material is an excellent choice for efficient and durable device fabrication.[5-7] As compared to 2D (two dimension) thin films, bulk 3D (Three dimensional) GaN-nanostructure (NS) established their dominance by offering plentiful advantages such as significantly reduced dislocations, excellent opto-electrical & thermal properties [8], quantum confinement effect, non-linear optical effect [9-11], high surface to volume ratios (SVRs) and reduce dimension of effective conductive channel. Due to numerous advantages offered by GaN-NS, have attracted much attention in the domain of optoelectronics and high power–high frequency applications [12-14]. Recently, the constructive effect of GaN-NS has been noticed specifically in ultraviolet (UV) photodetectors (PDs) in terms of higher responsivity as well as higher photoconductivity gain. [15-16] Beside this, the tapering active area due to nanoscale dimensionality offered by NS, provide shorten transit time [17]. Therefore, the NS are found to be promising candidates to increase the gain and sensitivity of the device by high photons absorption as an implication of high SVR and high electrical transport capability [18-20].

III-Nitride NS are more often grown on Si (111) as compared to other available substrates like Si (100), SiC, and sapphire by self- assembly process using PA-MBE [21-23]. The epitaxial growth of GaN layer on Si substrate (GaN/Si) having large mismatch lattice constant of 17%. This large lattice mismatch and difference in thermal expansion coefficient induced large substantial elastic strains at the heterointerface. Unlike 2D thin film, the self assemble 3D GaN NSs accommodates this lattice mismatch with substrate and grow fully relaxed and free of extended defect (threading dislocations or basal plan stacking faults).[24,25] Therefore, III-nitride NSs proved themselves potential candidates to develop highly efficient optoelectronic device ranging from ultraviolet-visible to infrared region. Till now, a series of studies were reported on synthesis of high quality GaN-NSs directly on Si by various growth techniques such as, metal-organic chemical vapor deposition (MOCVD) [26], hydride vapor phase epitaxy (HVPE) [27], chemical vapor deposition (CVD)[28] and molecular beam epitaxy (MBE) [29]. In recent years, the growth of GaN-NS via PA-MBE (plasma assisted molecular beam epitaxy) have been realized in detail by various groups under well-established nitrogen rich conditions (III/V ratio <1).[30-32] The previous reports demonstrates the fabrication of numerous NS based devices such as the conventional PDs in conjunction with various nanostructured materials, confirmed plenty of exciting functionalities, such as gas detection,[33,34] rewritable features,[35,36] and as well as optical logic gates,[37] etc. In this experiment, we have grown GaN-NS on Si(111) substrate via

ACCEPTED MANUSCRIPT

PA-MBE under nitrogen rich condition. Subsequently, the quality of as-grown GaN-NS/ Si heterojunction is investigated in terms of its morphological, structural, optical and opto-electrical properties. The opto-electrical property reveals that, the fabricated structure confirmed its application as UV PD. This is the first study of its own kind where, we have grown catalyst free self assemble, non-homogenously distributed, nano island shaped GaN-NS on Si (111) substrate. These low aspect ratio GaN nano-islands, unlike high aspect ratio conventional NS such as: nanorods, nanocolumn, nanoribbon, nanoflower etc, have been grown with very low material requirement which not only made the device fabrication more economical but also reduce the sample fabrication time. The aspect ratio of grown GaN-NS is evaluated by cross section view of FESEM and AFM image evaluated histogram. These tiny dimensional, catalyst free GaN-NS based nano-islands with ultra-thin films directly grown on Si substrate (without buffer layer) with very low stress (as analyzed by Micro-raman) and corresponding lower strain (as analyzed by HR-XRD technique), having UV detection capability even at lower voltages added novelty to this work.

2. Experiment

GaN-NSs were grown on Si (111) substrate using PAMBE system (Riber Compact 21) equipped with a RF- plasma source and Knudsen cell which provides active nitrogen species and gallium metal respectively. The substrate was chemically pre-cleaned by ultrasonification with acetone followed by chemical cleaning in solution of Di-H_2O:HF and blown dry with N_2 gas. Standard thermal cleaning process was adopted to clean Si substrate [16] and reconstructed pattern of Si (111) 7×7 was observed at temperature of 830°C. Prior to growth of GaN-NS, a very thin non-continuous, anti-surfactant Si_3N_4 layer (as shown in Fig.1a) was introduced which guided the vertical growth of GaN-NSs. Si_3N_4 layer was formed by nitridation of reconstructed Si (111) 7x7 surface at 880°C using 400W plasma power (N_2 flow of 1.5sccm). After that a self catalyzed wet layer of Gallium (Ga) was deposited for 10 sec at low temperature of 700°C (as shown in Fig.1(b-c)) to proceed the nucleation process of NS. After the nucleation process of Ga droplets, N_2 ion active species start converting Ga droplets into GaN as shown in Fig. 1(d). Further, these GaN droplets follow the Stranski–Krastanov (SK) growth mode under the influence of offered substrate temperatures, applied N_2 and Ga-flux. Accordingly high density GaN-NS have been grown (as shown in Fig.1(e)) at substrate temperature of 770°C in presence of N_2 plasma (1.5

ACCEPTED MANUSCRIPT

sccm) and Ga beam equivalent (BEP) of 6.5×10^{-7} torr for 120min . The real time monitoring of grown structural (GaN-NS/Si (111)) has been performed by reflection high electron diffraction (RHEED) under in-situ using STAIB electron gun (12keV) to realize 3D growth (shown in Fig.2). An infrared optical pyrometer has been deployed for real time monitoring of growth temperature (with error value of ±5°C) calibrated with thermocouple. The morphological, optical and structural analysis of grown GaN-NSs were characterized by AFM (Multimode-V Veeco), FESEM (ZEISS AURIGA), photoluminescence spectroscopy (Edinburg, FLS-980) and High Resolution X-Ray diffraction (HRXRD) (PAN-Analytic), Micro-Raman Spectroscopy respectively. The micro Raman measurement has been performed at room temperature using a triple Raman spectrometer under backscattering mode where an argon ion laser was used as excitation source. The operating wavelength range is set to 514nm with applied power of 50 mW. Beside this, for data collection, a charge coupled device system has been used with an accuracy value of $0.5cm^{-1}$. Moreover, the room temperature (RT) photoresponse measurement (Cascade Microtech EPS150TRIAX with shield enclosure EPS-ACC-SE750) was utilized to investigate the potential of the grown structure application in the area of ultraviolet (UV) photodetection devices specifically at low voltages ≤3V.

3. Results & Discussion

3.1 RHEED

The real time monitoring of growth has been performed with the help of in-situ RHEED technique throughout the growth process. Initially, Si (111) substrate displays streaky pattern as shown in fig. 2(a), indicating the Si surface before the thermal cleaning process. Prior to the growth, the Si (111) substrate was flash heated at 830°C which allow 7×7 reconstruction of Si surface as shown in Fig.2(b). The reconstructed Si (111) 7x7 surface is used as a template to grow Si_3N_4 layer which was formed by nitridation process. The formation of Si3N4 is observed by "(8/3×8/3)" surface reconstruction (fainted RHEED pattern as shown in fig. 2(c)) due to inadequate surface arrangement of nitrogen adatoms [38]. During the nitridation process, the Si substrates not only provide active nucleation sites but also high temperature nitridation which allow the penetration of nitrogen atoms, resulting a non-homogeneous Si_3N_4 layer. The formed Si_3N_4 layer generate localized compressive strains due to longer Si-N bond as compared to the substrate Si-Si bond has been fully relaxed in terms of extended defects free GaN-NS [39,40].

ACCEPTED MANUSCRIPT

The growth of GaN nanostructures (under nitrogen rich condition) can be visualized by spotty RHEED patterns (Fig. 2(d)). This transformation from streaky to spotty pattern displays real time growth execution process of GaN-NS on Si surface. The high temperature sustainability due to bond energies variation of Si-N (4.5eV) and Ga-N (2.2eV) [41-43] in conjunction with anti-surfactant behaviour of Si_3N_4 layer allow the growth of GaN-NS specifically in the lateral direction [44]. The Ga atoms having high mobility on sidewall facets due to which they find their suitability to sit only vertically i.e., at the top of the droplet or island.

3.2 Structural, Morphological and Optical Properties

The structural properties of as-grown GaN-NS were analysed via HRXRD measurements. Fig.3(a) shows the 2θ-ω scan of the grown GaN film with 2θ peak positioned at 34.5° displaying the wurtzite single crystalline growth along [0001] direction.[45] The peaks located at ~ 28.5 and ~ 58.5 degrees corresponds to plan of diffraction of Si(111) and Si(222) planes respectively.[46] The peak positions in the 2θ−ω scan of GaN along (0002) was used to estimate the lattice constant (c) by using Bragg's law equations as follows [47]

$$d_{hkl} = \frac{\lambda}{2\sin(\theta_{hkl} + \Delta\theta)}$$

where d is lattice spacing, (hkl) are the Miller indices of the diffraction planes, λ stand for the wavelength of X-ray source i.e., 0.154 nm (for Cu Kα radiation), θ_{hkl} is the measured angle of reflection from the (hkl) plane, and Δθ is HRXRD instrumental zero error and

$$d_{hkl} = \frac{1}{\sqrt{\frac{4(h^2+hk+k^2)}{3a^2} + \left(\frac{l}{c}\right)^2}}$$

for hexagonal geometry, where a and c are the lattice parameters of the grown GaN-NS. Consequently, the strain has been calculated by using the following equation [47]

$$\varepsilon = \frac{c - c_0}{c_0}$$

where c is the lattice constant of the grown GaN film and c_o is the lattice constant of strain-free GaN (given a_o = 0.3188 nm and c_o = 0.5185 nm).[1] The evaluated value of strain in as grown GaN nanostructures is found to be 0.17%. Beside this, in order to understand the crystalline quality and dislocation density in the grown structure, HR-XRD omega scan along (0002) plan

ACCEPTED MANUSCRIPT

diffraction has been performed, where the large FWHM value of 3.8° attributes the screw dislocation density value i.e., $1.8\times10^{11}cm^{-2}$. The possible reason of such large FWHM value and corresponding dislocation density might be due to very low thickness of the film i.e., 26nm (nano-island height).

Raman-scattering is an important technique to investigate the crystallinity of materials and also provide the information of developed defects in the grown structure in terms of raman peak shift (red or blue shift) guided stress values. Fig.3(b) shows the Raman spectra of GaN-NS grown on Si (111) substrates. The Raman spectra shows, E2-high mode of grown GaN nanostructure located at $567.77cm^{-1}$. It has been observed that, as compared to standard frequency value of E2(high) phonon mode of bulk GaN ($568cm^{-1}$) [48] the E2(high) peak of grown GaN-NS was shifted to lower wave-numbers (red-shift) of about $0.23cm^{-1}$. The red-shift in the position of E2 (high) indicated that the GaN-NS suffered from tensile stress.[49,50] As studied by Aggarwal et al., the stress levels of the GaN epilayer and the Raman shift are related by [47]

$$\Delta w = 4.3\sigma_{xx}$$

The biaxial stress (σ_{xx}) can be calculated from the variation in wave number (Δw) of E2 (high) mode. The tensile stress is estimated to be 0.053GPa for the GaN grown on Si (111) substrates. The Raman spectra indicated that the grown GaN/Si (111) exhibited the very low stress value as compared to a high aspect ratio 3D GaN-NSs and 2D thin films as shown in table 1. This lower stress value result is in good agreement with calculated lower strain by HR-XRD analysis. The calculated lower stress value corresponds to lower strain as a consequence of reduced defects in grown GaN-NS. Another observed band marked with an asterisk at $620cm^{-1}$ and $670cm^{-1}$ related to Si substrate as it is already observed in pure Si materials earlier.[56]

Table 1. State of art of bixial stress of GaN/Si(111) reported by various groups.

Sample	Bixial Stress 'σ_{xx}'(GPa)	Reference
Doped GaN/Si(111)	2.32	Velazquez et al.(51)
Doped GaN/ Si (111)	1.09	Zhao et al. (52)
GaN/3c-SiC/Si(111)	0.65	Gao et al. (53)
GaN-NS/n-Si(111)	0.28	Saron et al. (54)
GaN-NS/Si(111)	0.06	Seo et al. (55)
GaN-NS/Si(111)	0.053	This Work

ACCEPTED MANUSCRIPT

The morphological studies of the grown NS were performed via AFM and FESEM measurements as represented in Fig. 4(a-c). It was found that high-density, asymmetric and vertically oriented GaN-NS were successfully grown over Si (111) substrate. The histogram (shown in inset Fig.4 elucidates the distribution density of grown GaN-NS in terms of their variation in NS size with respect to their quantity (in counts) distributed on the substrate. The histogram states the average size of grown NS is 50 ± 5nm with a distribution density of $2x10^{10}$ cm^{-2} yielding an average surface roughness of 5.80nm. The grown GaN-NSs are nano-island in shape having average height of ~26nm concluded from cross sectional view of FESEM at different positions as shown in Fig. 4(c). The average width and height of island is 50nm and 26nm respectively. The calculated aspect ratio (width/height) of as grown island shaped GaN-NS is 1.92. These low dimensional islands with high distribution density and increased effective surface area (optical Area) offered by NS is an essential merit to increase its light absorption ability which can be utilized for photodetector and semiconducting optoelectronic device applications. Inset in Fig. 4(b) shows EDX spectrum measured from the as-grown GaN-NSs provide evidence of N_2, Ga and Si in as-grown GaN-NS with respect to their corresponding weight, atomic percentage of (10.19%, 19.58%), (9.77%, 3.77%) and (80.04%, 76.66%) respectively.

Fig.5 shows RT-photoluminescence spectra of the grown GaN NS displaying a band edge emission of GaN at 363.2 nm which is closely related to the bulk GaN (3.4eV) PL emission.[48] Inset view shows the de-convoluted PL spectra in range of 350 to 420 nm. It was observed that besides the near band emission (NBE), an additional peak at 380 nm was also recorded. This additional peak at 380nm was attributed to the donor acceptor pair (DAP) generated by un-intentional doping caused by diffusion of Si in GaN.[57] High intensity of PL NBE peak shows high level of radiative recombination though the absence of yellow band emission (YBE) indicates significantly reduced dumping zone of valuable electrons and holes offered by defects and impurities at interfaces. Such PL spectra indicate the high crystal quality of grown GaN NSs [58]. However, the grown GaN NS with high aspect ratio will result in more photons absorption sites to generate higher number of electron-hole pairs (EHP). The high densities of photo-excited electrons sites which contribute to emit high intensity photoluminescence of electron hole plasma as compared to continuous single crystalline GaN thin films.

ACCEPTED MANUSCRIPT

3.3 Photo-Response

The as-grown GaN-NS/Si(111) structure is converted into the metal-semiconductor-metal (MSM) based UV-PD device with the help of two metal (Au) contacts from top of the GaN-NS. The schematic diagram and optical image of the fabricated device is shown in Fig.6(a) and inset of Fig. 6(b) respectively. In order to investigate the performance of fabricated UV-PD device, photoresponse experiments were performed to explore the device efficiency and its saturation limit. The performance of fabricated UV PD (Au-GaN-NS/Si) is explored by illuminating the active area of device with UV-laser of 325nm at fixed optical power of 13mW. Fig. 6(b) shows the time co-related photo-response of fabricated device where time vs. photocurrent spectra is plotted with varying bias from 0.4V to 3V. The performance parameter, responsivity (R) of the device can be defined as [59]

$$\boldsymbol{R = \frac{I_{ph}}{P_{inc} \times (A_o)}}$$

where Iph is the photocurrent, P_{inc} power density of optical power and Ao stands for effective optical area of the device. On applying bias of 400mV, the change in the photocurrent is found to be 7.2 µA and the corresponding calculated responsivity is 2.2mA/W. On further increasing the bias voltage to 600mV, 800mV & 1V, the Iph value is 11.8 µA, 15.3 µA and 17.5 µA and their respective calculated R value is 3.79 mA/W, 4.8 mA/W and 5.7 mA/W. The observation reveals that, there is a linear dependency of I_{ph} and R with applied bias. On further increasing the applied bias from 2V to 3V, a significant enhancement in the I_{ph} value from 27.5 µA to 43.5 µA is witnessed which leads to very high R value from 8.66 mA/W to 13.48 mA/W. This increasing photo-responsivity elucidate that, the grown GaN-NS/Si(111) structure capable enough and can be used for harmful UV-radiation detection applications.

4. Conclusion

Self-assembled GaN-NSs have been grown on Si (111) substrate with an intermediate inhomogeneous layer of Si_3N_4. The localized compressive strains fields due to bond length variation between Si-Si and Si-N, are relaxed by inhomogeneously oriented, low aspect ratio (1.92) GaN-NS of distribution density $2\times10^{10}cm^{-2}$ and average surface roughness of 5.80 nm. These tiny dimensional nano-island shaped lower stress and strain facilitated GaN-NS of just 26nm height and 50nm diameter showing its potential to detect the UV rays in MSM structure

ACCEPTED MANUSCRIPT

format (i.e., Au/GaN/Au) having a responsivity value of 5.7mA/W even at lower voltage of 1V. The study demonstrates that the NS with lower stress-strain, without any buffer layer, low aspect ratio and compatibility with Si-technology can open a new era of more economical futuristic nano-optoelectronic devices. RT-PL measurements revealed a near band edge emission at 363.2 nm along with the presence of donor acceptor pairs. Though defects states associated with yellow band were absent in the grown NS. The application of grown GaN-NS/Si(111) structure in UV-detection is also visualized in terms of GaN-NS MSM-UV-PD, where UV-laser source (13mW, 325nm) is illuminated on active area of the device where an increasing trend of photo-responsivity w.r.t applied bias has been observed. The potential of the grown device was motivating for the further in-depth investigation and explore its future prospective.

Acknowledgments:

The authors gratefully acknowledge Dr. D.K Aswal, Director, CSIR-NPL, New Delhi, for his everlasting encouragement and support. The work is supported by CSIR-network projects (PSC-0109 and NWP-55). We would also like to thanks to Dr. K.K Maurya, Mr. Sandeep Singh, Dr. Nidhi Singh, Ms. Mandeep Kaur, Shweta Sharma and Dr. S. Hausale for performing HR-XRD, AFM, FESEM, Micro-raman and Photoresponse experiments.

References

[1] L. Liu, J. H Edgar, Substrates for gallium nitride epitaxy, Materials Science and Engineering R37 (2002) 61-127.
[2] N. Fu, E. Li, Z. Cui, D. Ma, W. Wang, Y. Zhang, S. Song, J. Lin, The electronic properties of phosphorus-doped GaN nanowires from first-principle calculations. J. Alloys Compd. 596 (2014) 92–97.
[3] B. Xu, D. Yang, F. Wang, J. Liang, and S. Ma, Synthesis of large-scale GaN nanobelts by chemical vapor deposition. Appl. Phys. Lett. 89 (2006) 074106.
[4] Y. Q. Wang, R. Z. Wang, Y. J. Li, Y. F. Zhang, M. K. Zhu, B. B. Wang and H. Yan, From powder to nanowire: a simple and environmentally friendly strategy for optical and electrical GaN nanowire films, Cryst Eng Comm 15 (2013) 1626–1634.
[5] S. J. Pearton, B. S. Kang, S. Kim, F. Ren, B. P. Gila, C. R. Abernathy, J. Lin and S. N. G. Chu, GaN-based diodes and transistors for chemical, gas, biological and pressure sensing, J. Phys.: Condens. Matter, vol. 16 (2004) R961-994.
[6] M. Neuberger, T. Zimmermann, P. Benkart, M. Kunze, I. Daumiller, A. Dadgar, A. Krost, E. Kohn, GaN based piezo sensors, Device Research Conference, 45-46 (2004).
[7] B. S. Kang, J. Kim, S. Jang, F. Ren, J. W. Johnson, R. J. Therrien, P. Rajagopal, J. C. Roberts, E. L. Piner, K. J. Linthicum, S. N. G. Chu, K. Baik, B. P. Gila, C. R. Abernathy, and S. J. Pearton, Capacitance pressure sensor based on GaN high electron-mobility transistor-on-Si membrane, Appl. Phys. Lett. vol. 86 (2005) 253502.
[8] J. Y. Huang, H. Zheng, S. X. Mao, Q. Li, and G. T. Wang, In Situ Nanomechanics of GaN Nanowires, Nano Lett. 11 (2011), 1618–1622.
[9] G. Konstantatos, E. H. Sargent, Nanostructured Materials for Photon Detection, Nat. Nanotechnol. 5 (2010) 391.
[10] A. Thiaville, J. Milta, Small Is Beautiful, Science, 284 (1999) 5422 1939-1940,
[11] C. Soci, A. Zhang, X. Y. Bao, H. Kim, Y. Lo, D. Wang, Nanowire photodetectors, J. Nanosci.Nanotechnol. 10 (2010) 1430.
[12] S. N. Mohammad, A. Salvador, H. Morkoc, Proceedings of the IEEE 83 (1996) 1420–1422.
[13] L. Shen, S. Heikman, B. Moran, R. Coffie, N. Q. Zhang, D. Buttari, I. P. Smorchkova, S. Keller, S. P. DenBaars, U. K. Mishra, IEEE Electron Device Letters 22(2001) 457–459.
[14] A. Dadgar, M. Poschenriender, J. Blasing, O. Contreras, F. Bertram, T. Riemann, A. Rieher, M. Kunze, I. Daumiller, A. Krtschil, A. Diez, A. Kaluza, A. Modlich, M. Kamp, J. Christen, F. A. Ponce, E. Kohn, A. Krost, Journal of Crystal Growth 248 (2003) 556–562.
[15] L. Li, P. C. Wu, X. S. Fang, T. Y. Zhai, L. Dai, M. Y. Liao, Y. Koide, H. Q. Wang, Y. Bando, D. Golberg, Single-Crystalline CdS Nanobelts for Excellent Field-Emitters and Ultrahigh Quantum-Efficiency Photodetectors, Adv. Mater. 22 (2010) 3161.

ACCEPTED MANUSCRIPT

[16] N. Aggarwal, S. Krishna, A. Sharma, L. Goswami, D. Kumar, S. Husale, G. Gupta, Highly Responsive Self-driven UV Photodetector using GaN Nanoflowers, Adv. Electron. Mater. 3 (2017) 1700036.
[17] S. Liu, J. F. Ye, Y. Cao, Q. Shen, Z. F. Liu, L. M. Qi, X. F. Guo, Tunable hybrid photodetectors with superhigh responsivity, Small, 4 (2009) 2371.
[18] T. Y. Wei , C. T. Huang , B. J. Hansen , Y. F. Lin , L. J. Chen , S. Y. Lu ,Z. L. Wang , Large enhancement in photon detection sensitivity via Schottky-gated CdS nanowire nanosensors, Appl. Phys. Lett., 96 (2010) 013508.
[19] T. Y. Zhai , L. Li , Y. Ma , M. Y. Liao , X. Wang , X. S.Fang , J. N. Yao ,Y. Bando , D. Golberg , One-dimensional inorganic nanostructures: synthesis, field-emission and photodetection, Chem. Soc. Rev. 40 (2011) 2986 .
[20] K. M. Deng, L. Li, CdS Nanoscale Photodetectors, Adv Mater, 26 (2014) 2619-2635.
[21] M. Yoshizawa, A. Kikuchi, M. Mori, N. Fujita, and K. Kishino, Growth of Self-Organized GaN Nanostructures on Al_2O_3(0001) by RF-Radical Source Molecular Beam Epitaxy, Jpn. J. Appl. Phys. (1997) 36 L459.
[22] M. A. Sánchez-García, E. Calleja, E. Monroy, F. J. Sánchez, F. Calle, E. Muñoz, and R. Beresford, The effect of the III/V ratio and substrate temperature on the morphology and properties of GaN- and AlN-layers grown by molecular beam epitaxy on Si(111), J. Cryst. Growth 183 (1998) 23.
[23] L. Cerrutti, J. Ristic, S. Fernández-Garrido, E. Calleja, A. Trampert, K. H. Ploog, S. Lazic, and J. M. Calleja, Wurtzite GaN nanocolumns grown on Si(001) by molecular beam epitaxy, Appl. Phys. Lett. 88 (2006) 213114.
[24] A. Trampert, J. Ristic, U. Jahn, E. Calleja, and K. H. Ploog, TEM study of (Ga,Al)N nanocolumns and embedded GaN nanodiscs, Inst. Phys. Conf. Ser. 180 (2003) 167.
[25] S. A. Kukushkin, A. V. Osipov, V. N. Bessolov, B. K. Medvedev, V. K. Nevolin and K. A. Tcarik, Substrates for epitaxy of gallium nitride: new materials and techniques, Rev. Adv. Mater. Sci. 17 (2008), 1-32.
[26] S. Haffouz, V. Kirilyuk, P. R. Hageman, L. Macht, J. L. Weyher, P. K. Larsen, Improvement of the optical properties of metalorganic chemical vapor deposition grown on GaN on sapphire by an in situ SiN treatment. Appl Phys Lett 79 (2001) 2390–2392.
[27] T. Paskova, V. Darakchieva, E. Valcheva, P. P. Paskov, I. G Ivanov, B. Monemar, T. Bottcher, C. Roder, D. Hommel, Hydride vapor-phase epitaxial GaN thick films for quasi substrate applications. J Electron Matter 33 (2004) 389–394.
[28] F. K. Yam, L. L Low, S. A. Oh, Z. Hassan, Gallium nitride: an overview of structural defects. In Optoelectronic Materials and Technique. Edited by P. Predeep, Malaysia: InTech publication, (2011) 99–137.
[29] R. Calarco, R. J. Meijers, R. K. Debnath, T. Stoica, E. Sutter, H. Lu, Nucleation and growth of GaN nanowires on Si (111) performed by molecular beam epitaxy. Nano Lett 7 (2007) 2248–2251.
[30] M. A. Sánchez-García, E. Calleja, E. Monroy, F. J. Sánchez, F. Calle, E. Muñoz, and R. Beresford, The effect of the III/V ratio and substrate temperature on the morphology and properties of GaN- and AlN-layers grown by molecular beam epitaxy on Si(111)
J. Cryst. Growth 183 (1998) 23.
[31] R. Calarco, R. J. Meijers, R. K. Debnath, T. Stoica, E. Sutter, and H. Lüth, Nucleation and growth of GaN nanowires on Si(111) performed by molecular beam epitaxy, Nano Lett. 7 (2007) 2248.
(32) C. T. Foxon, S. V. Novikov, J. L. Hall, R. P. Campion, D. Cherns, I. Griffiths, and S. Khongphetsak, A complementary geometric model for the growth of GaN nanocolumns prepared by plasma-assisted molecular beam epitaxy, J. Cryst. Growth 311 (2009) 3423.
[33] N. Gogurla , A. K. Sinha , S. Santra , S. Manna , S. K. Ray , Multifunctional Au-ZnO plasmonic nanostructures for enhanced UV photodetector and room temperature NO sensing devices, Sci. Rep. 4 (2014) 6483.
[34] Z. Yang , L. Guo , B. Zu , Y. Guo , T. Xu , X. C. Dou, CdS/ZnO Core/ShellNanowire-Built Films for Enhanced Photodetecting and Optoelectronic Gas-SensingApplication, Adv. Opt. Mater. 2 (2014) 738.
[35] P. Irvin , Y. J. Ma , D. F. Bogorin , C. Cen , C. W. Bark , C. M. Folkman , C. B. Eom , J. Levy , Rewritable nanoscale oxide photodetector, Nat. Photonics 4 (2010) 849.
[36] K. Roy , M. Padmanabhan , S. Goswami , T. P. Sai , G. Ramalingam , S. Raghavan , A. Ghosh , Graphene-MoS_2 hybrid structures for multifunctional photoresponsive memory devices. , Nat. Nanotechnol. 8 (2013) 826 .
[37] Y. Q. Bie , Z. M. Liao , H. Z. Zhang , G. R. Li , Y. Ye, Y. B. Zhou , J. Xu , Z. X. Qin , L. Dai , D. P. Yu, Self-Powered, Ultrafast, Visible Blind UV Detection and Optical Logical Operation based on ZnO/GaN Nanoscale pn Junctions, Adv. Mater. , 23 (2011) 649 .
[38] Nobuhiko Yamabe, Yuka Yamamoto, and Tadashi Ohachi, Epitaxial growth of β-Si3N4 by the nitridation of Si with adsorbed N atoms for interface reaction epitaxy of double buffer AlN(0001)/ β-Si_3N_4/Si(111), Phys. Status Solidi C 8(5) (2011) 1552–1555.
[39] R. Calarco and M. Marso, GaN and InN nanowires grown by MBE: A comparison, Appl. Phys. A 87 (2007) 499.
[40] A. Urbancyzk, F. W. M. Van Otten, and R. Notzel, Self-aligned epitaxial metal-semiconductor hybrid nanostructures for plasmonics, Appl. Phys. Lett. 98 (2011) 243110.
[41] T. Stoica, E. Sutter, R. J. Meijers, R. K. Debnath, R. Calarco, H. Luth, D. Grützmacher, Interface and Wetting Layer Effect on the Catalyst-Free Nucleation and Growth of GaN Nanowires, Small 4 (2008) 751.
[42] H. D. Batha, E. D. Whitney, Kinetics and mechanism of the thermal decomposition of silicon nitride, J. Am. Ceram. Soc. 56 (1973) 365.
[43] R. Groh, G. Gerey, L. Bartha, Pankove, On the thermal decomposition of GaN in vacuum, J. Phys. Status Solidi A 26 (1974) 353.
[44] T. Markurt, L. Lymperakis, J. Neugebauer, P. Drechsel, P. Stauss, T. Schulz, T. Remmele, V. Grillo, E. Rotunno, M. Albrecht, Blocking Growth by an Electrically Active Subsurface Layer: The Effect of Si as an Antisurfactant in the Growth of GaN, Phys. Rev. Lett. 110 (2013) 036103.
[45] M. Forsberg, A. Serban, I. Poenaru, C. L Hsiao, M. Junaid, J. Birch and G. Pozina, Stacking fault related luminescence in GaN nanorods. Nanotechnology 26 (2015) 355203 (9).
[46] W. Wang, H. Wang, W. Yang, Y. Zhu & G. Li, A new approach to epitaxially grow high-quality GaN films on Si substrates: the combination of MBE and PLD, Scientific Reports 6 (2016) 24448.
[47] N. Aggarwal, S. Krishna, L. Goswami, M. Mishra, G. Gupta, K. K. Maurya, S. Singh, N. Dilawar, and M. Kaur, Extenuation of Stress and Defects in GaN Films Grown on a Metal−Organic Chemical Vapor Deposition-GaN/c-Sapphire Substrate by Plasma-Assisted Molecular Beam Epitaxy, Cryst. Growth Des. 15 (2015), 2144−2150.
[48] A. Denis, G. Goglio, and G. Demazeau, Gallium nitride bulk crystal growth process: a review, Mater. Sci. Eng. R50 (2006) 167-194.
[49] K. Jeganathan, R. Debnath, R. Meijers, T. Stoica, R. Calarco, D. Grutzmacher, and H. Luth, Raman scattering of phonon-plasmon coupled modes in self-assembled GaN nanowires, J. Appl. Phys. 105(2009), 123707.
[50] L. Zhang, K. Cheng, S. Degroote, M. Leys, M. Germain, and G. Borghs, Strain effects in GaN epilayers grown on different substrates by metal organic vapor phase epitaxy, J. Appl. Phys. 108(2010), 073522.

ACCEPTED MANUSCRIPT

[51] R. Velazquez, A. Aldalbahi, M. Rivera, and P. Feng, Fabrications and application of single crystalline GaN for high-performance deep UV photodetectors, AIP ADVANCES 6 (2016), 085117.
[52] D. G. Zhao, S. J. Xu, M. H. Xie, and S. Y. Tong, Stress and its effect on optical properties of GaN epilayers grown on Si(111), 6H-SiC(0001), and c-plane sapphire, Appl. Phys. Lett., 83(2003), 4.
[53] X. Gao, J. Li, G. Sun, N. Zhang, L. Wang, W. Zhao, Y. Zeng, Molecular beam epitaxial growth of GaN on 3c-SiC/Si(111) substrates using a thick AlN buffer layer, 13th International conference on Semiconducting and Insulating materials (SIMC-XIII),2004 (IEEE), doi: 10.1109/SIM.2005.1511383.
[54] K. M. A. Saron, M. R. Hashim, N. Naderi and Nageh K. Allam, Enhanced light sensing characteristics of nanostructured gallium nitride/silicon heterojunctions: Interface matters, J. Appl. Phys. 114(2013), 134510.
[55] H. W. Seo, Q. Y. Chen, and M. N. Iliev, Epitaxial GaN nanorods free from strain and luminescent defects, Appl. Phys. Lett. 88 (2006), 153124.
[56] W. J. Salcedo, F. J. R. Fernandez, and J. C. Rubimc, Influence of laser excitation on Raman and photoluminescence spectra and FTIR study of porous silicon layers, Brazilian Journal of Physics 29(4), (1999) 751.
[57] K. W. Liu, S. J. Young, S. J. Chang, T. H. Hsueh, H. Hung, S. X. Chen, Y. Z. Chen, Growth of gallium nitride on silicon by molecular beam epitaxy incorporating a chromium nitride interlayer, Journal of Alloys and Compounds 511 (2012) 1–4.
[58] Y. Inoue, T. Hoshino, S. Takeda, K. Ishino, A. Ishida, H. Fujiyasu, H. Kominami, H. Mimura, and Y. Nakanishi and S. Sakakibara, Strong luminescence from dislocation-free GaN nanopillars, Appl. Phys. Lett., 85 (2004) 12.
[59] S. Krishna, A. Sharma, N. Aggarwal, S. Husale, G. Gupta, Ultrafast photoresponse and enhanced photoresponsivity of Indium Nitride based broad band photodetector, Solar Energy Materials and Solar Cells 172 (2017) 376–383.

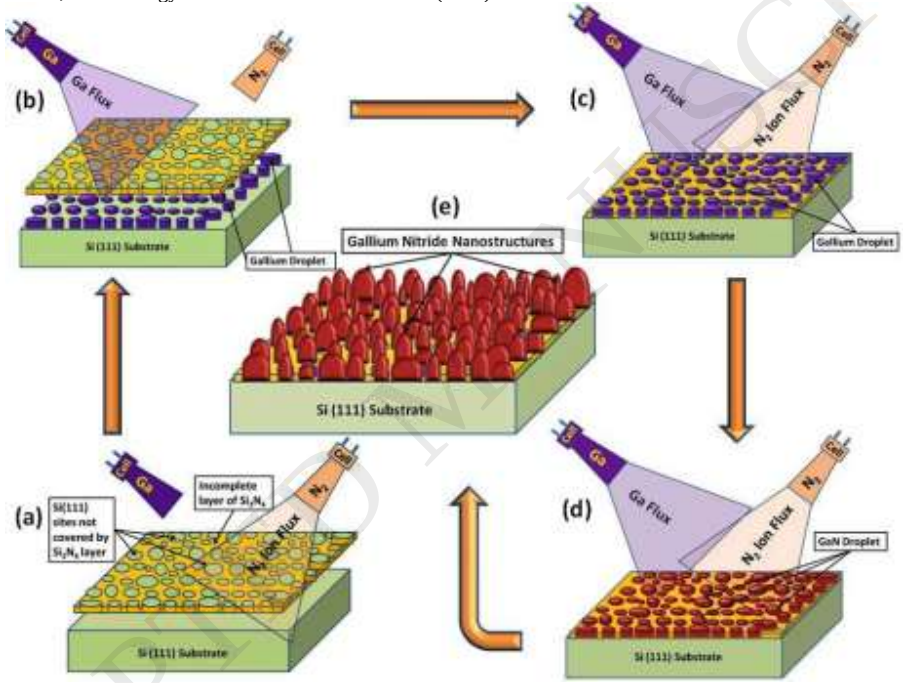


Fig.1 Schematic diagram of growth process of GaN-NS on Si(111) substrate

ACCEPTED MANUSCRIPT

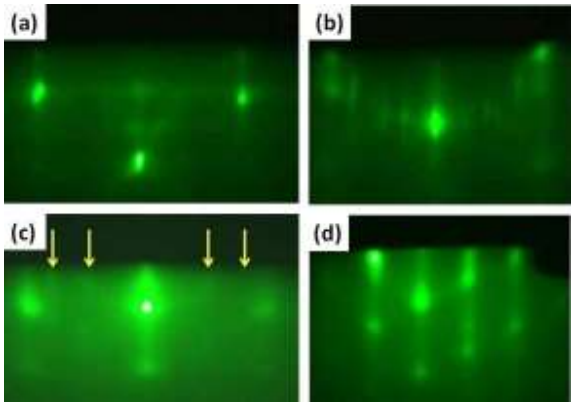


Fig2.(a) RHEED reflections image of the Si(111) substrate before thermal cleaning; (b) Si(111)-7×7 surface reconstruction after annealing at 830°C; (c) arrow marks shows Si_3N_4- 8/3×8/3 surface reconstruction in-continuation after nitridation of Si(111)- 7×7 at 880°C; (d) Reflection of GaN 3D nanostructure's spotty pattern after ramp down the temperature at 770°C for 120 min.

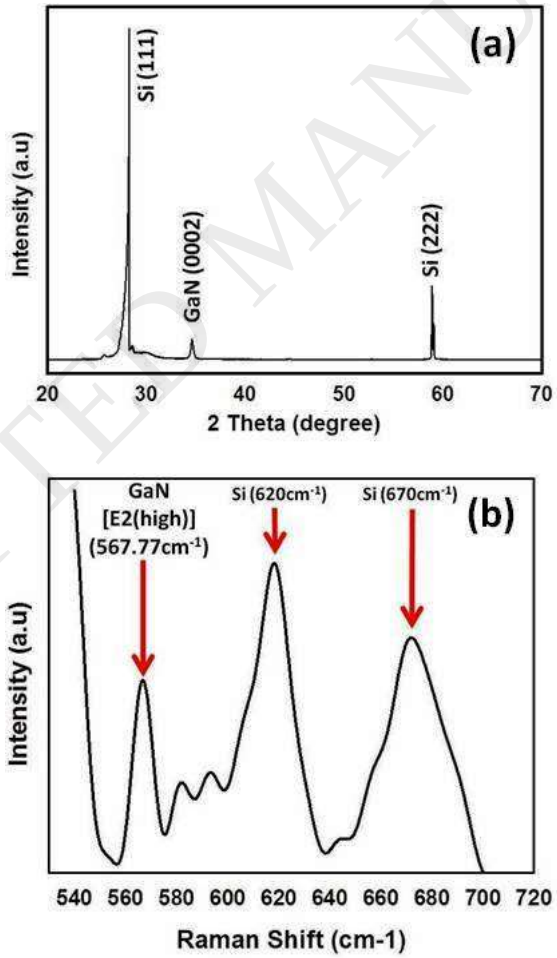


Fig.3(a) HR-XRD 2θ-ω scan of GaN-NS grown on Si substrate,(b) Micro-Raman Spectra of GaN-NS/Si(111).

ACCEPTED MANUSCRIPT

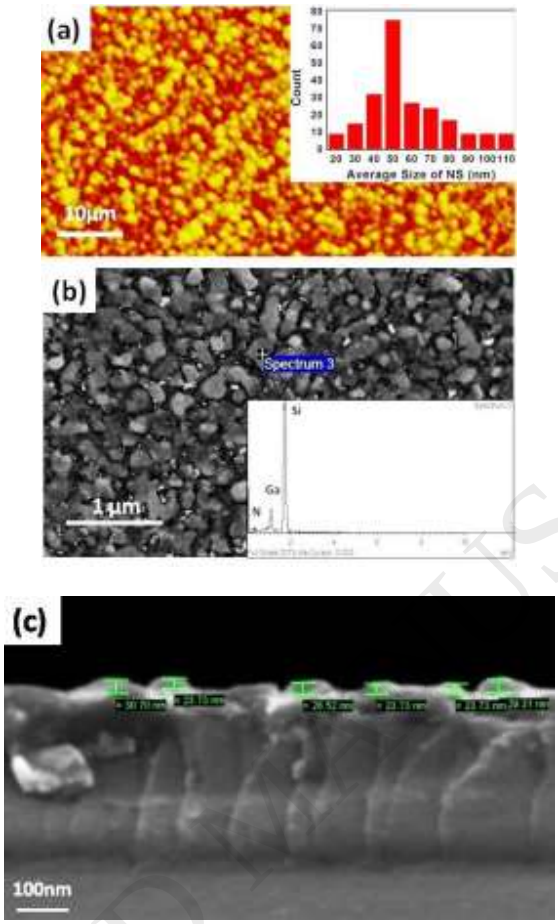


Fig.4(a) AFM image of GaN-NS; inset shows the average size distribution histogram of as-grown GaN-NS; (b) FESEM image of high denisty GaN-NS; inset shows EDX of GaN-NS; (c) Cross sectional FESEM image of tiny dimensional island shaped GaN-NS.

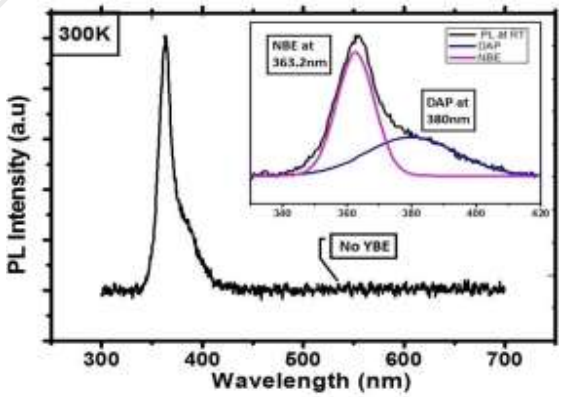


Fig.5 RT-PL spectra of grown GaN-NS.

ACCEPTED MANUSCRIPT

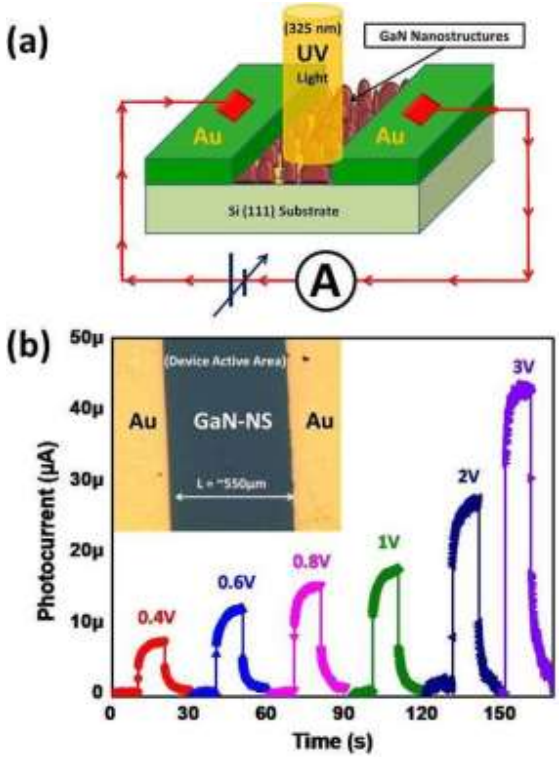


Fig.6(a) Schematic of fabricated MSM UV PD, (b) Increasing trend of photocurrent w.r.t to applied bias, inset shows optical image of fabricated UV PD.

ACCEPTED MANUSCRIPT

International Journal of Research in Engineering and Innovation (IJREI)
journal home page: http://www.ijrei.com
ISSN (Online): 2456-6934



Exergy and sustainability investigation of waste heat recovery vapor compression refrigeration system with silver Nano fluid

Kapil Chopra[1], R.S Mishra[2]

[1]*Assistant Professor, Mechanical Engineering Department, Shri Mata Vaishno Devi University, Katra (J&K) India*
[2]*Professor, Department of Mechanical, Production & Industrial Engineering, Delhi Technological University, Delhi, India*

Abstract

In this paper influence of cooling base fluid mass flow rate (500-2000 kg.h^{-1}) with water and silver Nano fluid as cooling base fluid on performance parameters were experimentally evaluated. It was observed that cooling effectiveness, sustainability index, heating capacity, exergy efficiency increases while condensing & evaporation pressures and exergy destruction in components of refrigerant circuit decreases with increasing mass flow rate of cooling base fluid. Cooling effectiveness, exergy efficiency, sustainability index, heating capacity of the considered system improved in the range of 11.71-18.25%, 1.9-4.56% ,0.3-0.7% and 26-80% respectively by using 0.05 vol% silver Nano fluid compared to water as cooling based fluid for considerable range of cooling base fluid flow rate. Improvement was recorded using 0.05 vol% silver Nano fluid compared to water for considerable range of cooling base fluid mass flow rate as exergy destruction decreases in the range of 29-30.18%, 65.77-69.61%, 14.31-15.33%, 17-22% in compressor, condenser, evaporator and expansion valve respectively. © 2018 ijrei.com. All rights reserved
Keywords: Waste heat, Exergy, Sustainability, Global warming, Energy-Exergy Analysis, Nano Technology

1. Introduction

The increasing demand of energy leads to global warming and environmental imbalance in the society. In order to satisfy the needs, utilization of energy available at the systems should be in best way. The primary function of system based on vapour compression refrigeration technology is to reject heat at higher temperature and absorb at lower temperature. Heat rejected by condenser generally not utilized for constructive applications instead of this heat is wasted either to the surrounding or to the water circulating from cooling tower. Like milk plant, vapour compression refrigeration system is used for cooling of milk for the purpose of preserving the same for long time and heat rejected by condenser is wasted to water circulating from cooling tower. In same plant large amount heat is also required for heating of milk to kill bacteria. This much amount of heat is taken either from burning of diesel or other non-renewable resources.

It is very important to increase coefficient of performance, exergy efficiency, and sustainability index on the other hand reduction of exergy destruction in the components of vapour compression refrigeration system. Along with above mentioned parameters, it is also important to utilization of energy available at vapour compression refrigeration system. In view of above factors experimental test rig was fabricated which is used for both cooling and heating of water. Cooling is done by evaporator and utilizes the waste heat from condenser is for heating of water. Silver Nano fluid with 0.01% and 0.05% volume concentration ratio used as cooling base fluid for enhancing of heating. The purpose of using of Nano fluid to improve the performance parameters like effectiveness, exergy efficiency, sustainability index and decrease the irreversibility in components of VCR.

The leakage test of developed test rig was done by filling of nitrogen gas. After successful completion of leakage test, test rig has been evacuated by using of vacuum pump. The vacuum was held for 30 hr and after that the correct amount of R22 was charged in refrigerant circuit. After completion of leakage testing and charging of refrigerant, cooling base fluid

Corresponding author: R.S. Mishra
Email Id: hod.mechanical.rsm@dtu.ac.in

pump, cooling secondary fluid pump, chilled water pump and chilled secondary fluid pump was switched on. Chilled water mass flow rate (300 kg/hr) remain constant for considered number of experiments. Thermostat attached with heating coil used to maintain constant inlet temperature (T_7 =26 ºC) of chilled secondary fluid and thermostat of same configuration attached with cooling coil for constant inlet condition (T_{11} =22 ºC) of cooling secondary fluid. Then compressor of refrigerant circuit was switched on. Before collection of experimental data, system was allowed to run until the steady state condition was reached. Experimental data were recorded six times during one hour. Experiments were done with water followed by 0.01 and 0.05 vol% silver Nano fluid as cooling base fluid with same above described procedure. It should be noted that any fluid to be heated or cooled can be used as cooling or chilled secondary fluid. In the present study water is used in both cooling and secondary fluid circuit. The above discussed experimentation was done under constant (T_a=25 ºC) surrounding condition.

2. Literature Review

Elcock [1] found that TiO_2 nanoparticles can be used as additives to enhance the solubility of the mineral oil with the hydro fluorocarbon (HFC) refrigerant. Author also reported that refrigeration systems using a mixture of HFC134a and mineral oil with TiO_2 nanoparticles appear to give better performance by returning more lubricant oil to the compressor. Hindawi [2] carried out an experimental study on boiling heat transfer characteristics of R22 refrigerant with Al_2O_3 nanoparticles and found that the nanoparticles enhanced the refrigerant heat transfer characteristics by reducing bubble sizes. Eastman et al.[3] investigated the pool boiling heat transfer characteristics of R11 refrigerant with TiO_2 nanoparticles and showed that the heat transfer enhancement reached by 20% at a particle loading of 0.01 g/L. Liu et al.[4] investigated the effects of carbon nanotubes (CNTs) on the nucleate boiling heat transfer of R123 and HFC134a refrigerants. Authors reported that CNTs increase the nucleate boiling heat transfer coefficients for these refrigerants. Jiang et al.[5] experimental results showed that the thermal conductivity of carbon nanotubes (CNT) Nano refrigerants are much higher than those of CNT–water Nano fluids or spherical nanoparticle–R113 Nano refrigerants. Authors reported that the smaller the diameter of CNT larger the thermal conductivity enhancement of CNT Nano refrigerant. Hwang et al.[6] suggested that thermal conductivity enhancement of Nano fluids is greatly influenced by thermal conductivity of nanoparticles and base fluid. For instance, thermal conductivity of water based Nano fluid with multiwall carbon nanotubes has noticeably higher thermal conductivity compared to SiO_2 nanoparticles in the same base fluid. Yoo et al. [7] argued that surface to volume ratio of nanoparticles is a dominant factor. Surface to volume ratio is increased with smaller sizes of nanoparticles. Choi et al.[8] reported that 150% thermal conductivity enhancement was observed in poly (a-olefin) oil by addition of multiwall carbon nanotubes (MWCNT) at 1% volume fraction. Yang.[9] reported, a 200% thermal conductivity enhancement for poly (a-olefin) oil containing 0.35% (v/v) MWCNT. It is important to note that this thermal conductivity enhancement was accompanied by a three order of magnitude increase in viscosity. Eastman et al.[10] observed 40% thermal conductivity enhancement for ethylene glycol with 0.3% (v/v) copper nanoparticles (10 nm diameter), although the authors also added that about 1% (v/v) thioglycolic acid helpful for dispersion of nanoparticles in base fluid. The addition of this dispersant yielded a greater thermal conductivity than the same concentration of nanoparticles in the ethylene glycol without the dispersant.

Author also reported that refrigeration systems using a mixture of HFC134a and mineral oil with TiO_2 nanoparticles appear to give better performance by returning more lubricant oil to the compressor. Hindawi [2] carried out an experimental study on boiling heat transfer characteristics of R22 refrigerant with Al_2O_3 nanoparticles and found that the nanoparticles enhanced the refrigerant heat transfer characteristics by reducing bubble sizes. Eastman et al.[3] investigated the pool boiling heat transfer characteristics of R11 refrigerant with TiO_2 nanoparticles and showed that the heat transfer enhancement reached by 20% at a particle loading of 0.01 g/L. Liu et al.[4] investigated the effects of carbon nanotubes (CNTs) on the nucleate boiling heat transfer of R123 and HFC134a refrigerants. Authors reported that CNTs increase the nucleate boiling heat transfer coefficients for these refrigerants. Jiang et al.[5] experimental results showed that the thermal conductivity of carbon nanotubes (CNT) Nano refrigerants are much higher than those of CNT–water Nano fluids or spherical nanoparticle–R113 Nano refrigerants. Authors reported that the smaller the diameter of CNT larger the thermal conductivity enhancement of CNT Nano refrigerant. Hwang et al.[6] suggested that thermal conductivity enhancement of Nano fluids is greatly influenced by thermal conductivity of nanoparticles and base fluid. For instance, thermal conductivity of water based Nano fluid with multiwall carbon nanotubes has noticeably higher thermal conductivity compared to SiO_2 nanoparticles in the same base fluid. Yoo et al. [7] argued that surface to volume ratio of nanoparticles is a dominant factor. Surface to volume ratio is increased with smaller sizes of nanoparticles. Choi et al.[8] reported that 150% thermal conductivity enhancement was observed in poly (a-olefin) oil by addition of multiwall carbon nanotubes (MWCNT) at 1% volume fraction. Yang.[9] reported, a 200% thermal conductivity enhancement for poly (a-olefin) oil containing 0.35% (v/v) MWCNT. It is important to note that this thermal conductivity enhancement was accompanied by a three order of magnitude increase in viscosity. Eastman et al.[10] observed 40% thermal conductivity enhancement for ethylene glycol with 0.3% (v/v) copper nanoparticles (10 nm diameter), although the authors also added that about 1% (v/v) thioglycolic acid helpful for dispersion of nanoparticles in base fluid. The addition of this dispersant yielded a greater thermal conductivity than the same concentration of

nanoparticles in the ethylene glycol without the dispersant. Kang et al.[11] reported , a 75% thermal conductivity enhancement for ethylene glycol with 1.2% (v/v) diamond nanoparticles between 30 and 50 nm diameter. Despite of these remarkable results, some researchers also measured the thermal conductivity of Nano fluids and found no anomalous results. Lee et al.[12] revealed that optimum combination of pH level and surfactant leads to 10.7% thermal conductivity enhancement of 0.1% Cu/H2O Nano fluid. They also concluded that during Nano fluid preparation stage thermal conductivity of Nano fluid is affected by pH level and addition of surfactant. Jiang et al.[13] added that thermal conductivity of Nano fluids also depend on the nanoparticles size and temperature. Wu et al.[14] observed that the pool boiling heat transfer was enhanced at low TiO_2 nanoparticles concentration in R11 but deteriorated under high nanoparticles concentration. Trisaksri and Wongwises [15] investigated TiO_2 in HCFC 141b in a cylindrical copper tube and found that the nucleate pool boiling heat transfer deteriorated with increasing nanoparticle concentrations especially at higher heat fluxes. Hao et al.[16] investigated flow boiling inside a smooth tube at different nanoparticles concentration, mass fluxes, heat fluxes, and inlet vapor qualities in order to analyze the influence of nanoparticles on the heat transfer characteristics of refrigerant-based Nano fluid. Authors observed that the heat transfer coefficient of refrigerant-based Nano fluid in flow boiling is larger than that of pure refrigerant and the maximum enhancement is about 29.7% when observed with a mass fraction of 0–0.5 wt%. Hao et al. [17] studied experimentally the nucleate pool boiling heat transfer characteristics of refrigerant/oil mixture with diamond nanoparticles. The results indicate that the nucleate pool boiling heat transfer coefficient of R113/VG68 oil mixture with diamond nanoparticles is larger than that of R113/oil mixture by 63.4%.Enhancement in same factor increases with the increase of nanoparticles concentration in the nanoparticles/oil suspension and decreases with the increase of lubricating oil concentration. Wang et al. [18] carried out an experimental study of boiling heat transfer characteristics of R22 with Al_2O_3 nanoparticles and found that nanoparticles enhanced the refrigerant heat transfer characteristics by reduction of bubble sizes that moved quickly near the heat transfer surface. Li et al. [19] investigated the pool boiling heat transfer characteristics of R-11 with TiO_2 nanoparticles and showed that the heat transfer enhancement reached by 20% at a particle loading of 0.01 g/L. Peng et al. investigated the influence of CuO nanoparticles on the heat transfer characteristics of R-113 refrigerant-based Nano fluids and presented a correlation for prediction of heat transfer performance of refrigerant based Nano fluids. Authors reported that the heat transfer coefficient of refrigerant-based Nano fluids is higher than that of pure refrigerant, and the maximum enhancement of heat transfer coefficient found to be about 29.7%. Kumar and Elansezhian [21] experimentally investigated the effect of varying concentration of ZnO nanoparticles on various performance parameters like COP, suction temperature, input power and pressure ratio with 152a as working fluid in vapour compression refrigeration system. They found that 0.5% v ZnO nanoparticles with R152a gives maximum COP of 3.56 and 21% reduction in power input. Pressure ratio decreases with increase in ZnO concentration. Mahbubul et al.[22] measured thermo physical properties, pressure drop and heat transfer performance of Al_2O_3 nanoparticles and R-134a mixture. Thermal conductivity of Al_2O_3/R-134a Nano refrigerant increased with temperature and augmentation of particle concentration. It was also observed that pumping power, viscosity, pressure drop, and heat transfer coefficients of the Nano refrigerants show significant increment with the increase of volume fractions. The frictional pressure drop also shows rapid increment with 3 vol. % particle fraction.

3. Description of experimental test rig and Instrumentation

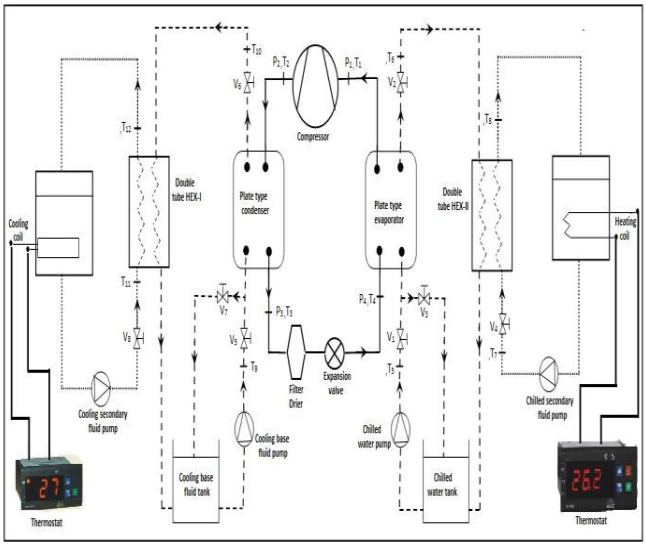


Figure 1: experimental test rig comprising of refrigerant

As shown in Fig.1. experimental test rig comprising of refrigerant, chilled water, chilled secondary fluid, cooling base fluid and cooling secondary fluid circuits. Refrigerant circuit used R22 as working fluid consists of single cylinder hermetically sealed reciprocating compressor, plate type condenser, thermal expansion valve, plate type evaporator and accessories like filter, drier, power meter used for measurement of electricity consumed by compressor and sight glass. Due to high heat transfer coefficient and compact design, plate type heat exchangers.

4. Preparation of Nano fluid

In literature one-step and two-step commonly used for preparation Eastman et al.[10] developed one-step procedure for preparation of Nano fluid. In this method problem of agglomeration was reduced by great extent and preparation and dispersion of solid nanoparticles in base fluid

concurrently occurred. This method leads to uniform and stable distribution of nanoparticles in the base fluid. In order to produce Nano fluids in large scale one step procedure is not economical. Zhu et al. developed another method for preparation of Nano fluids called two-step method. In this process nanoparticles directly dispersed in base fluid.

In this paper, two-step method is adopted for preparation of silver nanoparticles and water mixture. Silver nanoparticles of spherical morphology with average particle size 50 nm size and bulk density 0.312 g/cm^3. The TEM image, UV spectrophotometer analysis and raman analysis of silver nanoparticles presented in Fig.2-3 respectively. 0.01 and 0.05% volume concentration ratio silver nanoparticles were measured by digital balance and mixed with water. Probe type ultrasonicator as shown in Fig.4 was used for stable and uniform distribution of nanoparticles in base fluid for 30 min. As shown in Fig 5 shows before ultra-sonication of silver nanoparticles in water. No settlement of nanoparticles and water mixture were observed after 2, 4,6,8,10 and 6 h respectively. As a result 0.01 and 0.05% volume solution has selected for solubility test

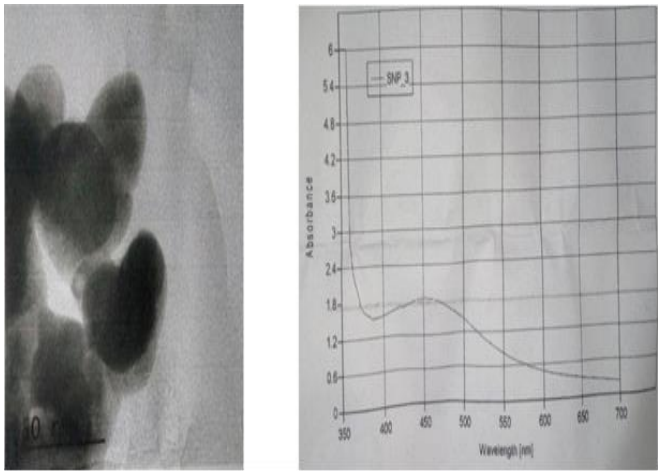


Figure 2: TEM image of silver nanoparticles

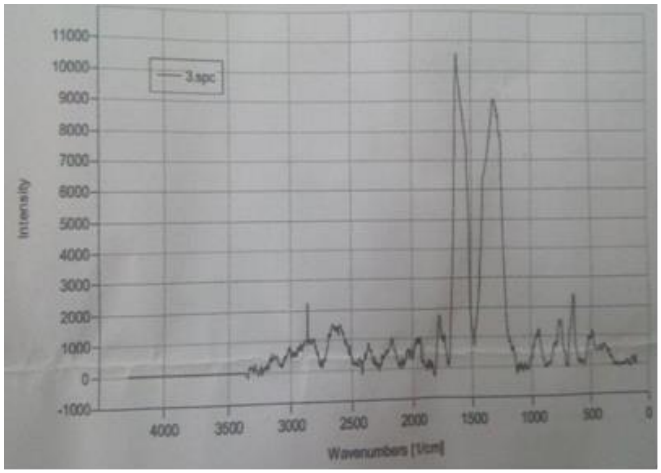


Figure 3: Raman analysis of silver nanoparticles



Figure 4: Probe type sonicator and Digital balance



Figure 5: Solubility test

5. Result and Discussion

Fig.6 and Fig.7 presents the effect of variation of mass flow rate of cooling base fluid on working pressures of refrigerant circuit.. It was observed that with increase of mass flow rate of cooling base fluid, operating pressures decreases due to enhancement of heat exchange between refrigerant and cooling base fluid. Both of these figures also revealed that variation of mass flow rate give a more prominent effect on condensing pressure rather than evaporating pressure. Deviation of evaporation and condensation pressures with various working parameters were studied with water, 0.01 and 0.05 vol. % silver Nano fluid as cooling base fluid. As shown in Fig. 6, water and 0.05 vol. % silver Nano fluid give maximum & minimum condensation pressure respectively. Pertaining to evaporation pressure, Fig.7 reveals that water gives highest while 0.05 vol. % silver Nano fluids gives lowest evaporating pressure. The average values of condensation pressure for water, 0.01 and 0.05 vol. % silver Nano fluid as cooling base fluids are 1417.06, 1393.57 and 1230.73 KPa while their evaporation pressures are 196.13, 192.26 and 169.16 KPa respectively over wide range of

cooling base fluid mass flow rate (Fig 6 & 7).Mean condensation pressure of water and 0.01 vol. % silver Nano fluid are greater than 0.005 vol% silver Nano fluid by 15.13% and 13.23% respectively. On the other hand average evaporation pressure of water and 0.001 vol. % silver Nano fluids are higher than 0.001 vol. % silver Nano fluid by 15.94% and 13.65% respectively.

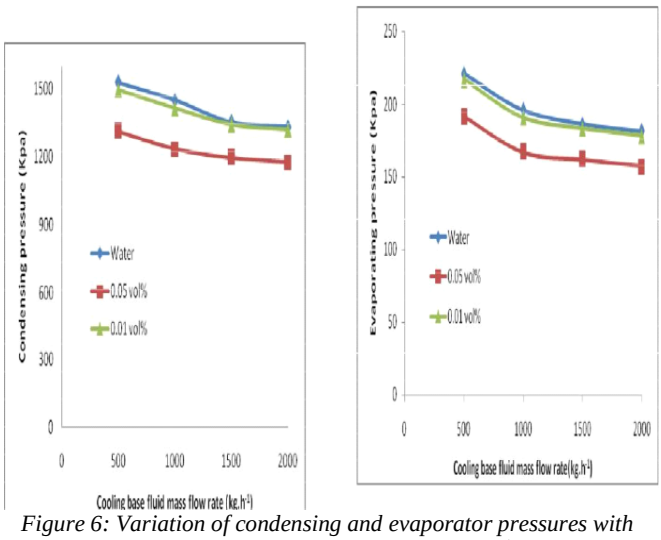


Figure 6: Variation of condensing and evaporator pressures with cooling base fluid mass flow rate (kg.h^{-1})

Variation of cooling effectiveness verses mass flow rate of cooling base fluid is shown in Fig.8. It is evident that higher mass flow rate of cooling base fluid responsible for lower compressor work due to decreasing of compressor to evaporator ratio and increases cooling & heating effectiveness. Increases cooling & heating capacity and decrement in compressor work increases the cooling and heating effectiveness of the system. Average cooling effectiveness of system using 0.05 vol. % silver Nano fluid as cooling base fluid is higher than that of water by 14.98% as cooling base fluid over considered range of mass flow rate of cooling base fluid (fig.8). and Fig.9 show the impact of mass flow rate of cooling base fluid on exergy efficiency and exergy destruction ratio respectively. Since exergy efficiency is the ratio of useful output in term of cooling capacity to the input energy given to the system.

We know that the input energy given in term of compressor work gets lower down with increase of mass flow rate of cooling base fluid. Like compressor work numerator of exergy efficiency also follow the same trend. Combined effect of both discussed terms increase the exergy efficiency.

The behavior of trends is due to fact that exergy destruction ration and exergy efficiency are inversely proportional to each other. Behavior of Sustainability index with change of mass flow rate of cooling base fluid was also analyzed. The sustainability index is the function of exergy efficiency. Sustainability index determines the impact on environmental or surrounding conditions. Lower sustainability index of the system put adverse effect on the environmental conditions.

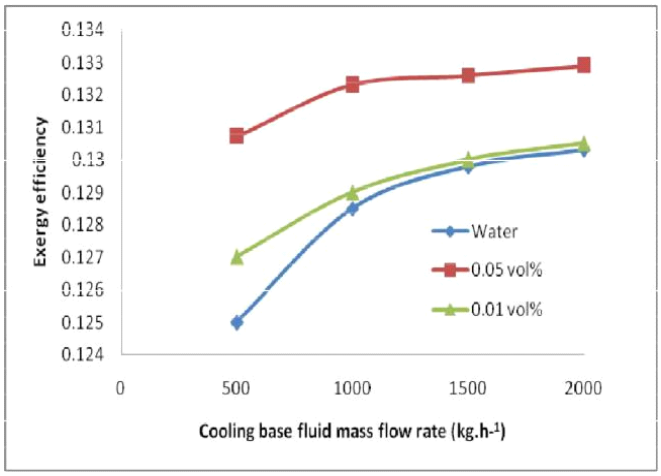


Figure 7: Variation of Exergy efficiency with cooling base fluid mass flow rate (kg.h^{-1})

The Average value of sustainability index of the system using water, 0.01 vol% and 0.05 vol% Nano fluid as cooling base fluid are 1.147, 1.148., and 1.152 respectively. Base fluid. Average specific heat of 0.05 and 0.01 vol% Nano fluid is higher than water; also temperature rise of 0.05 vol% of Nano fluid is much higher than water and 0.01 vol% Nano fluid over entire range of cooling base fluid mass flow rate. This increase in heat transfer termed as heating capacity of condenser, maximum 80% heat capacity higher when 0.05 vol% Base fluid. Average specific heat of 0.05 and 0.01 vol% Nano fluid is higher than water; also temperature rise of 0.05 vol% of Nano fluid is much higher than water and 0.01 vol% Nano fluid over entire range of cooling base fluid mass flow rate. This increase in heat transfer termed as heating capacity of condenser, maximum 80% heat capacity higher when 0.05 vol%. the performance with nano fluid are shown in Fig-7-9 respectively.

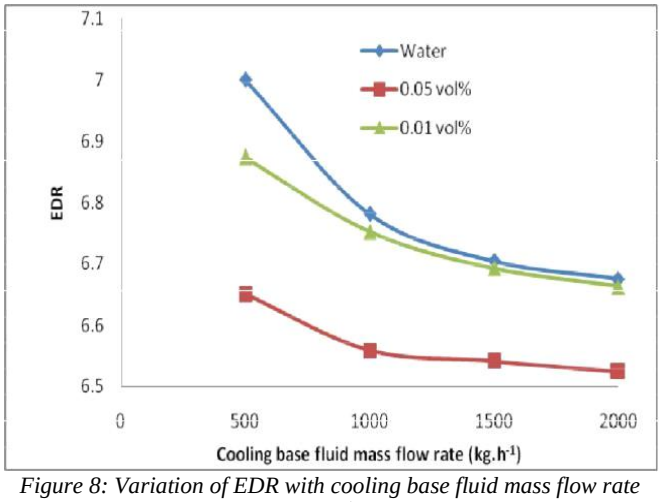


Figure 8: Variation of EDR with cooling base fluid mass flow rate (kg.h^{-1})

The heating capacity is the product of mass flow rate, specific heat and temperature rise of cooling base fluid. By keeping constant mass flow rate of water and discussed percentage of Nano fluid remaining Nano fluids is used instead of water at 2000 Kg/h cooling base fluid mass flow rate. two factors i.e specific heat and temperature difference of cooling base fluid responsible for increase of heat transfer between refrigerant through condenser and cooling two factors i.e specific heat and temperature difference of cooling base fluid responsible for increase of heat transfer between refrigerant through condenser and cooling

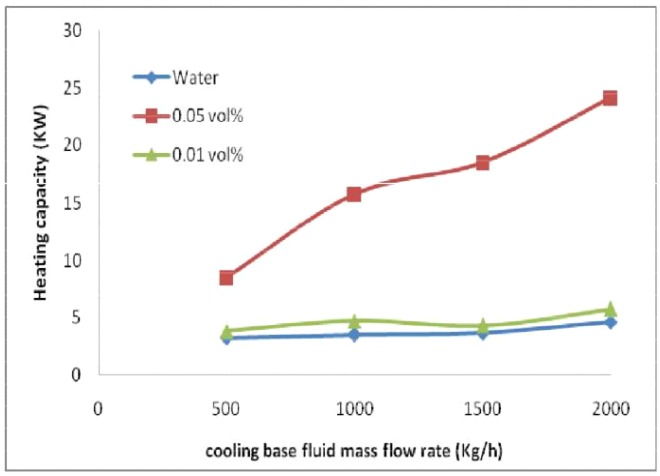


Figure 9: Variation of heating capacity with cooling base fluid mass flow rate ($kg.h^{-1}$)

Table-1(a) : exergy destruction in compressor, condenser, expansion valve & evaporator

Cooling base mass flow rate of water	$\dot{E}_{1-2}$	$\dot{E}_{2-3}$	$\dot{E}_{3-4}$	$\dot{E}_{4-1}$
($Kg.h^{-1}$)	(W)	(W)	(W)	(W)
500	918.2	206.2	23.83	99.13
1000	869.6	185.9	22.47	98.44
1500	867.5	169.1	22.28	96.00
2000	837.4	161.4	21.41	95.85

Table-1(b) : exergy destruction in compressor, condenser, expansion valve & evaporator

Cooling base mass flow rate of water 0.01 vol% nano	$\dot{E}_{1-2}$	$\dot{E}_{2-3}$	$\dot{E}_{3-4}$	$\dot{E}_{4-1}$
($Kg.h^{-1}$)	(W)	(W)	(W)	(W)
500	856.3	173.4	22.81	97.82
1000	814.4	155.5	21.62	96.73
1500	807.4	142.6	21.52	94.62
2000	781.8	136.19	0.85	94.22

Table-1(c) : exergy destruction in compressor, condenser, expansion valve & evaporator

Cooling base mass flow rate of water 0.05 vol% nano	$\dot{E}_{1-2}$	$\dot{E}_{2-3}$	$\dot{E}_{3-4}$	$\dot{E}_{4-1}$
($Kg.h^{-1}$)	(W)	(W)	(W)	(W)
500	708.9	123.4	19.50	86.72
1000	677.8	109.6	18.61	85.35
1500	666.6	101.9	18.61	83.77
2000	648.1	97.36	18.20	83.16

Table-1 illustrate the variation of exergy destruction in compressor, condenser, expansion valve & evaporator with variation in mass flow rate of cooling base fluid. Exergy destruction in component is due to depletion of input energy in particular component. It also gives idea about best and worst component of the system. It was observed that expansion valve and compressor are the best and worst component of the system respectively for entire range of mass flow rate of cooling base fluid. It is clear from Table.1 that average exergy destruction over wide range of mass flow rate of cooling base fluid in compressor, condenser, expansion valve and evaporator is lowest by 29.92, 67.16, 20.11 and 14.8% respectively when 0.05 vol. % silver nanofluid compared to water used as cooling base fluid. Mean exergy destruction in compressor, condenser, capillary tube & evaporator ***is*** 873.18, 180.65, 22.50 and 97.36 W respectively which is highest in case of water used as secondary fluid through evaporator. 7.13, 18.88,3.68 and 1.57 % reduction of exergy destruction in compressor, condenser, expansion valve & evaporator respectively by using of 0.01 vol. silver Nano fluid used as cooling base fluid compared to water.

6. Conclusion

In this paper, various performance parameters of waste heat recovery vapor compression refrigeration system with water, 0.01 and 0.05vol. % silver Nano fluid as cooling base fluid through condenser were experimentally evaluated and compared over considered range of working states.
Based on the experimental investigation, following results are discussed:

(i) Maximum evaporation and condensation pressure produces with when water is used as cooling base fluid. While 0.05 vol. % silver Nano fluid as cooling base fluid generate minimum evaporation and condensation pressure.
(ii) Maximum cooling effectiveness was monitored when 0.05 vol. % silver Nano fluid compared to water used as cooling base fluid. However lesser effect was observed in cooling effectiveness of the system by using 0.05 vol. % silver Nano fluid in comparison with water as cooling base fluid.
(iii) Minimum exergy destruction and exergy ratio produces in components of the system with 0.05 vol. % silver Nano fluid as cooling base fluid.
(iv) Highest sustainability index, heating capacity and exergy efficiency is observed with 0.05 vol. % silver Nano fluid as cooling base fluid.
(v) Insignificant effect on performance parameters was observed with 0.01 vol. % silver Nano fluid as cooling base fluid.

References

[1] Elcock D. Potential, Impacts of nanotechnology on energy transmission applications and needs, Environmental Science Division, Argonne National Laboratory (2007).

[2] Hindawi, Special issue on heat transfer in nanofluids (2009)

[3] Eastman JA, Choi US, Thompson LJ and Lee S, Enhanced thermal conductivity through the development of nanofluids, Mater Res Soc Symp Proc, 457 (1996) 3–11.

[4] Liu MS, Lin MCC, Huang IT and Wang CC, Enhancement of thermal conductivity with CuO for Nanofluids, Chemical Engineering and Technology 29(1) (2006) 72–77.

[5] Jiang W, Ding G and Peng H, Measurement and model on thermal conductivities of carbon nanotube nanorefrigerants, International Journal of Thermal Sciences 48 (2009) 1108–1115

[6] Hwang YJ, Ahn YC, Shin HS, Lee CG, Kim GT and Park HS, Investigation on characteristics of thermal conductivity enhancement of nanofluids, Current Applied Physics 6(6) (2006) 1068–1071.

[7] DH, Hong KS and Yang HS, Study of thermal conductivity of nanofluids for the application of heat transfer fluids, Thermochimica Acta 2007;455(1–2):66–69.

[8] Choi SUS, Zhang ZG, Yu W, Lockwood FE and Grulke EA. , Anomalous thermal conductivity enhancement in nanotube suspensions, Applied Physics Letters 79(14) (2001) 2252–2254.

[9] Yang Y. Carbon nanofluids for lubricant application. University of Kentucky (2006).

[10] Eastman JA, Choi SUS, Li S, Yu W, and Thompson LJ, Anomalously increased effective thermal conductivities of ethylene glycol-based nanofluids containing copper nanoparticles. Applied Physics Letters 78(6) (2001) 718–720.

[11] Kang H.U, Kim S.H and Oh J.M., Estimation of thermal conductivity of nanofluid using experimental effective particle, Experimental Heat Transfer 19(3) (2006) 181–191.

[12] Lee J.H, Hwang K.S, Jang S.P, Lee B.H, Kim J.H and Choi SUS, Effective viscosities and thermal conductivities of aqueous nanofluids containing low volume concentrations of Al2O3 nanoparticles. International Journal of Heat and Mass Transfer 51 (2008) 2651–2656.

[13] Jiang W, Ding G and Peng H., Measurement and model on thermal conductivities of

[14] carbon nanotube nanorefrigerants. International Journal of Thermal Sciences 48 (2009) 1108–1115.

[15] Wu X.M, Li P, Li H and Wang W.C, Investigation of pool boiling heat transfer of R11 with TiO_2 nano-particles. Journal of Engineering Thermophysics 29(1) (2008) 124–126.

[16] Trisaksri V and Wongwises S, Nucleate pool boiling heat transfer of TiO_2–R141b nanofluids, International Journal of Heat and Mass Transfer 52 (2009) 1582–1588.

[17] Hao P, Guoliang D, Weiting J, Haitao H and Yifeng G, Heat transfer characteristics of refrigerant-based nanofluid flow boiling inside a horizontal smooth tube. International Journal of Refrigeration 32 (2009) 1259–1270.

[18] Hao P, Guoliang D, Haitao H, Weiting J, awei Z and Kaijiang W. Nucleate pool boiling heat transfer characteristics of refrigerant/oil mixture with diamond nanoparticles. International Journal of refrigeration 33 (2010) 347–358.

[19] Wang K.J, Ding G.L and Jiang WT, Nano-scale thermal transporting and its use in engineering, Proceedings of the 4th symposium on refrigeration and air condition (2006) 66–75.

[20] Li P, Wu XM and Li H, Pool boiling heat transfer experiments of refrigerants with nanoparticles TiO_2, Proceedings of the 12th symposium on engineering thermo physics, (2006) 325–333.

[21] Peng H, Ding G, Jiang W, Hu H and Gao Y, Heat transfer characteristics of refrigerant-based nanofluid flow boiling inside a horizontal smooth tube. International Journal of Refrigeration 32 (2009):1259– 1270.

[22] D.Sendil Kumar and R. Elansezhian, ZnO nanorefrigerant in R152a refrigeration system for energy conservation and green environment, J Front Mech Engg (2014) 1-6.

[23] I.M. Mahbubul,S.A. Fadhilah, R. Saidur, K.Y. Leong and M.A. Amalina, Thermophysical properties and heat transfer performance of Al_2O_3/R-134a Nano refrigerants, International Journal of Heat and Mass Transfer 57 (2013) 100–108.

ResearchGate

See discussions, stats, and author profiles for this publication at: https://www.researchgate.net/publication/322888242

Fabrication & Mechanical Testing of AA6082/Si3N4 Composites

Article · February 2018

CITATIONS
0

READS
6

3 authors, including:



Ankit Tyagi
Delhi Technological University
3 PUBLICATIONS **0** CITATIONS

SEE PROFILE

Some of the authors of this publication are also working on these related projects:



Fabrication & Mechanical Testing of AA6082/Si3N4 Composites View project



Studies on AA6082-Si 3 N 4 & AA7075-Si 3 N 4 Composites View project

All content following this page was uploaded by Ankit Tyagi on 02 February 2018.

The user has requested enhancement of the downloaded file.

© 2018 IJSRST | Volume 4 | Issue 2 | Print ISSN: 2395-6011 | Online ISSN: 2395-602X
Themed Section: Science and Technology

Fabrication & Mechanical Testing of AA6082/Si3N4 Composites

Ankit Tyagi*[1], Yashwant Koli[1], Deepak Sharma[2]
*[1]Department of Mechanical Engineering, Delhi Technological University, Delhi, India
[2]bWorld College of Technology & Management, Farukh nagar, Gurgaon, Haryana, India

ABSTRACT

AA6082 based aluminum lattice composites (AMC) were effectively created by including silicon nitride (Si3N4) particulates as fortifications utilizing mix throwing process. A definitive rigidity (UTS) was likewise tried. Three syntheses of AMC were outlined by changing the weight level of silicon nitride particles between 4 to 12%. UTS results was observed to be expanded with expanding weight level of silicon nitride.

Keywords: AMC, AA6082, Si3N4, UTS.

I. INTRODUCTION

Metal matrix composites (MMCs) exceptionally aluminum lattice composites (AMC) are getting prominent step by step because of their various applications, for example, aviation, airplanes, car parts, electronic parts, turbine edges, golf clubs etc.[9]. MMCs are notable for their gigantic properties like wear protection, high particular modulus, high quality, solidness, damping limit and so on [9]. The region of use of MMCs is expanding persistently because of their high quality to weight proportion [1]. MMCs are constituted essentially of two stages to be specific framework stage and support stage [5]. Lattice stage comprises of some sort of base metal or compound, for example, aluminum, magnesium, copper, titanium and so forth [2]. Support stage comprises of strengthening particles, for example, Al2O3, SiC, TiO2, BN, B4C, Si3N4 and so forth [3,4]. Fortifications are acquainted in metal lattice with acquire wanted customized properties [5] or to upgrade microstructural conduct.

Concentrates on aluminum amalgams/SiC composite demonstrate that a definitive rigidity and hardness increments with increment in wt. % of SiC [1,2,6,8]. Pardeep Sharma et al. [4] explored that the hardness and dry sliding wear protection of AA6082/Si3N4 composites increment with expanding level of fortification. C. S. Ramesh et al. [12] uncovered that the wear protection of AA6061/Ni/P/Si3N4 composite used to increment with increment in weight level of Si3N4. It is because of the expansion in hardness of composite w.r.t. weight level of fortification. M. N. Wahab [11] and B. Ashok Kumar [15] considered the conduct of aluminum/AlN composites and announced increment in hardness and extreme elasticity with increment in weight level of fortification.

MMCs can be manufactured utilizing different methods, for example, strong stage creation forms (powder metallurgy, dissemination holding and so forth.), fluid stage manufacture forms (blend throwing, crush throwing and so on.), semi-strong creation forms (shower and rheo throwing, Compo throwing and so on.) [16]. Out of the above said forms the mix throwing is the most generally utilized process in light of its straightforwardness, adaptability and minimal effort [10,14]. It is specified that the powder metallurgy causes break harm to support and are costly as strengthened particles required in this procedure is in powder shape. Press throwing cause serious harm to fortification and direct costly with less or little porosity is seen in MMCs [10]. Mix throwing makes less harm support, adaptable, efficient and not limited to shape and size, but rather porosity with non-uniform circulation of fortification is seen in

MMCs [2,4,5,8,10]. Stir– Squeeze throwing makes less or no harm support and no or little porosity with uniform dissemination of fortification in MMCs [7].

In spite of the fact that there is a lot of writing accessible with respect to creation of composite materials, in any case; a not very many research ponders have been accounted for on manufacture and portrayal of silicon nitride fortified AA6082 aluminum amalgam grid composites. Along these lines, AA6082 aluminum combination is picked as framework because of its great mechanical and tribological properties [4]. Si3N4 is taken as the fortification. The arranged AMC is created utilizing blend throwing process. UTS test is done to describe the created AMC.

II. EXPERIMENTAL SETUP

AA6082 was used as matrix for AMC production; the chemical composition of which is given in table 1. The silicon nitride particles were added in the matrix as reinforcement. The specifications of Si_3N_4 are given in table 2. The proposed aluminium matrix composites were fabricated using Stir casting technique. In order to produce MMCs using stir casting; various parameters are to be kept in consideration such as stirrer type, stirring time, pouring temperature, mould type, preheat of reinforcement and preheat of mould.

The proposed AMC are casted in three different compositions as mentioned below:

- ✓ AA6082/ Si_3N_4/ 4_p (4% Si_3N_4 particles by weight and remaining AA6082 alloy)
- ✓ AA6082/ Si_3N_4/ 8_p (8% Si_3N_4 particles by weight and remaining AA6082 alloy)
- ✓ AA6082/ Si_3N_4/ 12_p (12% Si_3N_4 particles by weight and remaining AA6082 alloy)

The three structure of AMC comprises of 4 %, 8 % and 12 % silicon nitride (Si3N4) particles by weight and remaining AA6082 aluminum combination. The little bits of AA6082 aluminum composite are taken in the graphite cauldron and warmed in the electric suppress heater between the temperature scopes of 800oC to 900oC. The heater is furnished with persistent supply of argon gas so as to keep the soften from air sullying. After the composite is softened down the fortification i.e. silicon nitride (Si3N4) particulates are added to the soften gradually. The fortification is preheated to a temperature of 500oC out of an electric heater. The soften is consistently blended utilizing a mechanical stirrer amid expansion of fortification. The stirrer is pivoted at various rates running between 300 to 500rpm. The mixing time of 10 minutes is given to liquid AMC so the fortification particles are consistently appropriated in the liquefy. Following 10 minutes of blending, the pot is removed from heater and liquid AMC is threw as cuboids of measurement 115 x 55 x 75 mm. The shape is preheated at 500oC preceding throwing. The threw AMC squares are then additionally cut into thin AMC plates of measurement 100 x 50 x 6 mm.

III. RESULTS AND DISCUSSION

The variety of extreme elasticity (UTS) w.r.t. wt. %age of Si3N4 is appeared in fig.1. The pliable test outcomes demonstrate that the UTS of as threw AA6082 Al composite 144.4MPa, which uncovers that AA6082 is a medium quality amalgam. The UTS of AA6082/Si3N4/4p comes out to be 166.24MPa, which demonstrates an augmentation of 15.76 % as contrast with the UTS of as threw AA6082 combination tests. The UTS of AA6082/Si3N4/8p observed to 175.64MPa, which is ascribed by an expansion of 22.86 % as contrast with the UTS of as threw AA6082 Al combination tests. The UTS of AA6082/Si3N4/12p is come out to be 185.4MPa, which demonstrates the 30.06 % expansion as contrast with the UTS of as threw AA6082 Al composite examples.

The malleable test outcomes obviously uncover that a definitive elasticity increments with expansion of Si3N4 particles in AA6082 amalgam lattice. This is in

likeness of the outcomes said somewhere else that the expansion of strengthening particles brings about an increment in the UTS of the AMC [2,15]. It is likewise settled that the UTS increments with expanding weight level of Si3N4 in the AMC [6,15]. This expansion in UTS is credited because of good holding of included Si3N4 particles with AA6082 Al composite. This may likewise be closed to be the consequence of expanded separation thickness around the Si3N4 particles amid the AMC cementing and lessened grain measure [15,17].

IV. CONCLUSION

The AA6082/Si3N4 AMC were fabricated successfully using stir casting technique. The produced AMC were found to be free of defects like porosity, blow holes, pin holes etc. The tensile tests reveal that the ultimate tensile strength increases as the weight percentage of reinforcement in the AMC is increased. Further it is concluded that the AMC having 12% Si3N4 shows an increment of 30.06% (185.4 MPa) in UTS as compared to the as casted AA6082 alloy (144.4 MPa).

There is a further scope of research to study the characteristics of AMC with higher concentrations of silicon nitride. Density tests of the fabricated AMC are to be done in forth coming studies.

Table 1. Chemical composition of AA6082 alloy

Element	Al	Sl	Mg	Mn	Fe	Cu	Cr	Zn	Ti	Vn
(wt%)	97.5	0.91	0.59	0.51	0.24	0.08	<0.038	0.098	<0.018	0.01

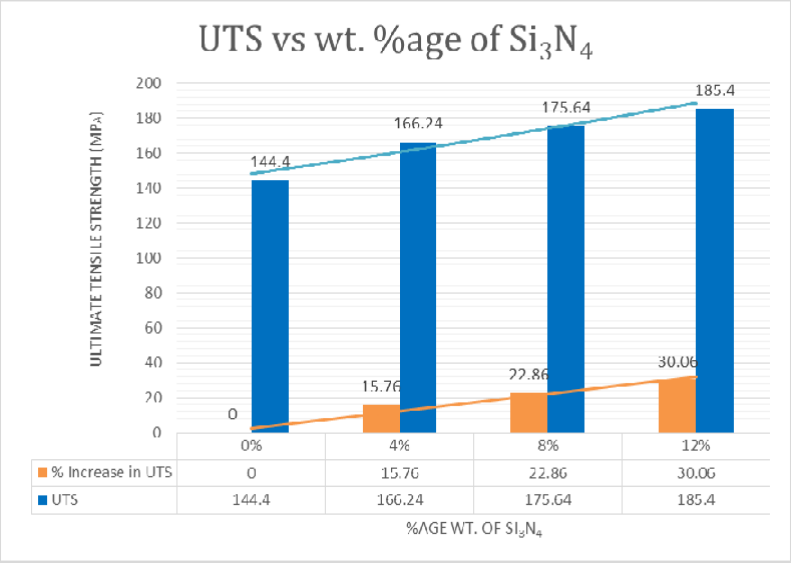


Figure 1. Variation of ultimate tensile strength w.r.t. weight percentage of Si_3N_4

V. REFERENCES

[1]. Ajit Kumar Senapati, R. I. Ganguly, R.R. Dash, P. C. Mishra, B. C. Routra, " production, characterization and analysis of mechanical properties of newly developed novel aluminium-silicon alloy based metal matrix composited", Procedia Materials Science 5 (2014) 472-481.

[2]. Pradyumna Phutane, Vijay Kumar S. Jatti, Ravi Sekhar, T. P. Singh, "Synthesis and characterization of SiC reinforced HE-30 Al

alloy particulate MMCs", International Journal of Engineering and Technology (IJET) Vol. 5 No. 3 jun-jul 2013 ISSN: 0975-4024.

[3]. Kenneth kanayoAlanema, Michael Oluwatosin, Adebimpe A. Awe, "Microstructure, mechanical and fracture properties of groundnut shell ash and silicon carbide dispersion strengthened aluminium matrix composites", Journal of King Saud University- Engineering Sciences (2016).

[4]. Pardeep Sharma, Dinesh Khanduja,Satpal Sharma, "Parametic study of dry sliding wear of aluminium metal matrix composites by response surface methodology", Materials Today: Proceeding 2 (2015) 2687-2697.

[5]. Manoj Singla, D Deepak Dwivedi, Lakhvir Singh, Vikas Chawla, "Development of Aluminium Based Silicon Carbide Particulate Metal Matrix Composite", Journal of Minerals & Materials Characterization & Engineering, Vol. 8, No.6, 2009, pp. 455-467.

[6]. K. L. Meena, Dr. A. Manna, Dr. S. S. Banwait, Dr. Jaswanti, "An Analysis of Mechanical Properties of the Developed Al-SiC-MMC's", American Journal of Mechanical Engineering, 2013, Vol. 1, No. 1, pp. 14-19.

[7]. K. N. P. Prasad, M. Ramachandra, " Effect of squeeze pressure on hardness and wear resistance of aluminium flyash composite manufactures by stir-squeeze casting", International Journal of Engineering Inventions, e-ISSN:2278-7461, p-ISSN 2319-6491, Volume 3 Issue 4 (November 2013) PP: 01-08.

[8]. Mohammad M. Ranjbaran, "Experimental Investigation of Fracture Toughness in Al 356-SiC Aluminium Matrix Composite" American Journal of Scientific and Industrial Research, 2010.

[9]. Sijo MT, KR Jayadevan, "Analysis of stir cast aluminium silicon carbide metal matrix composite: A comprehensive review", Procedia Technology 24 (2016) 379-385.

[10]. J. Hashim, L Looney, M S J Hashmi, "Metal Matrix Composites: Production by the Stir Casting Method", Journal of Material Processing and Technology, Vol. 92, 1999, pp. 1-7.

[11]. M. N. Wahab, A. R. Daud, M. J. Ghazali, "Preparation and characterization of stir cast-aluminium nitride reinforced aluminium metal matrix composites", International Journal of Mechanical and Materials Engineering (IJMME), Vol. 4 (2009), No. 2, 115-117.

[12]. C.S. Ramesh, R. Keshavamurthy, B.H. Channabasappa, S. Pramod, "Friction and wear behaviour of Ni-P coated Si3N4 reinforced Al6061 composites", Tribology International. 43(2010) 623–634.

[13]. H. Arik, "Effect of mechanical alloying process on mechanical properties of α-Si3N4 reinforced aluminium-based composite materials", Materials and Design. 29 (2008) 1856–1861.

[14]. Y. H. Seo, C. G. Kang, "Effects of Hot Extrusion Through a Curved Die on the Mechanical Properties of Al-SiC Composites Fabricated by Melt-Stirring", Composites Science and Technology, Vol.59, 1999, pp. 643-654.

[15]. B. Ashok, N. Murugan, "Metallurgical and mechanical characterization of stir cast AA6061-T6-AlNp composite", Materials and Design 40 (2012) 52-58.

[16]. S. Naher, D Brabazon, L Looney, "Development and Assessment of a New Quick Quench Stir Caster Design for the Production of Metal Matrix Composites", Journal of Material Processing Technology, Vol. 166, 2004, pp. 430-439.

[17]. Dinaharan I, Murugan N, Parameswaran S., " Influence of in situ formed ZrB2 particles on microstructure and mechanical properties of AA6061 metal matrix composites", Mater Sci Eng A, 528, 2011, pp. 5733–40.

View publication stats

International Journal of Research in Engineering and Innovation (IJREI)
journal home page: http://www.ijrei.com
ISSN (Online): 2456-6934



Friction stir welding of aluminum alloy 6082-T6-t651 for improving tensile strength, hardness and wear rate properties

R.S. Mishra[1], Shaambhavi Ratnapriya[2]

[1] *Department of Mechanical Engineering, Delhi Technological University, Delhi, India*
[2] *P.G. Scholar, IIM Indore*

Abstract

Regression analysis is a powerful tool used for determining the relationship between dependent and one or more independent parameters. In this paper, Friction Stir Welding (FSW) was carried out on 6082-T6-T651 aluminum alloy with the aim of deriving the regression equation for the dependent variables of Tensile strength, Hardness and Wear rate with respect to the independent variables of tool speed, tool feed and tool tilt angle using Taguchi analysis in Minitab 17 software. Plots for means and S-N ratios were also obtained for the above mentioned parameters of Tensile strength, Hardness and Wear. © 2017 ijrei.com. All rights reserved
Key words: Friction Stir Welding, Regression analysis, Taguchi analysis, Tensile strength, Hardness, Wear rate.

1. Introduction

Friction Stir Welding (FSW) i.e. the solid state technique of joining metals has gained wide popularity in the automotive, marine and air-craft industries primarily owning to its highly positive eco-friendly energy coefficient. The mechanism of FSW is also quite simple wherein it employs a non-consumable rotating tool comprising of a pin and a shoulder. The pin is plunged to the requisite depth inside the work-piece and local heat and plastic deformation produced help to weld the given two pieces together.

A thorough analysis and comparison of FSW with the traditional electric arc welding process highlighted the following advantages of FSW:

- No toxic fumes/ gases released
- Less residual wastes generated
- No shielding gases or extra pipelines required for gas transportation as these are eliminated in FSP/FSW
- Less post-welding/ processing treatments thus reducing cost and energy requirements considerably
- Clean technology

Invented in 1991 by "The Welding Institute UK", this technique has now come a long way forward and has evolved into the famous processing technique Friction Stir Processing (FSP). FSP is used primarily as a microstructural refinement technique which it achieves by the mechanism of dynamic recrystallization as studied by Mishra et al [1]. It also helps in improving wear rates and hardness of the sample [2-3].

In this paper, FSW was carried out on 6082- T6- T651 aluminum alloy. This alloy is considered one of the best for machining operations and is widely employed in highly stressed applications like making bridges, truss, frame-works, etc. Thereafter a regression analysis was performed on the tensile strength, hardness and wear rate data to study their dependence on experimental parameters tool feed, tool speed and tool tilt angle.

Work- pieces of dimension 200X40X7 mm were used and H13 tool steel was employed as the tool material. The cylindrical pin had dimensions of 4X5mm. while the tool shoulder had a diameter of 20 mm [4].

The major objectives of this paper were as follows:

- Derive regression equation for tensile strength of the specimen in the welded region
- Derive regression equation for hardness of the specimen in the welded region
- Derive regression equation for wear rate of the specimen in the welded specimen

All the above equations were derived using Taguchi Analysis in Minitab 17 software.

Welding parameter such as tool rotation, transverse speed and axial force have a significant effect on the amount of heat generated and strength of FSW joints. Microstructure

Corresponding author: R.S. Mishra
Email Id: hod.mechanical.rsm@dtu.ac.in

evaluation of FSW joints clearly shows the formation of new fine grains and refinement of reinforcement particles in the weld zone with different amount of heat input by controlling the welding parameter [5-7]

2. Experimental Procedure

6082- T6- T651 aluminum alloy work- pieces of dimensions 200X40X7 mm. in sets of two were clamped in the FSW machine as shown below and a total of nine readings were taken.



Figure 1: FSW machine

The feed in this machine could be adjusted in the +/- X direction. The tool speed could be adjusted using a digital switches provided behind the machine. The machine was hydraulically operated.
H 13 tool steel was used for conducting the experiment. The tool speed, tool feed and tool tilt angle parameters were varied as follows.

Table-1: Experimental Data

Tool Feed	Tool Speed	Tool Tilt Angle
60	500	0.0
60	700	2.5
60	900	5.0
80	500	2.5
80	700	5.0
80	900	0.0
100	500	5.0
100	700	0.0
100	900	2.5

Thereafter, tensile test, Vicker's hardness test and Wear rate tests were performed. The tensile test was performed on a 50 KN H50kS Universal testing machine shown below [4].



Figure 2: UTM machine

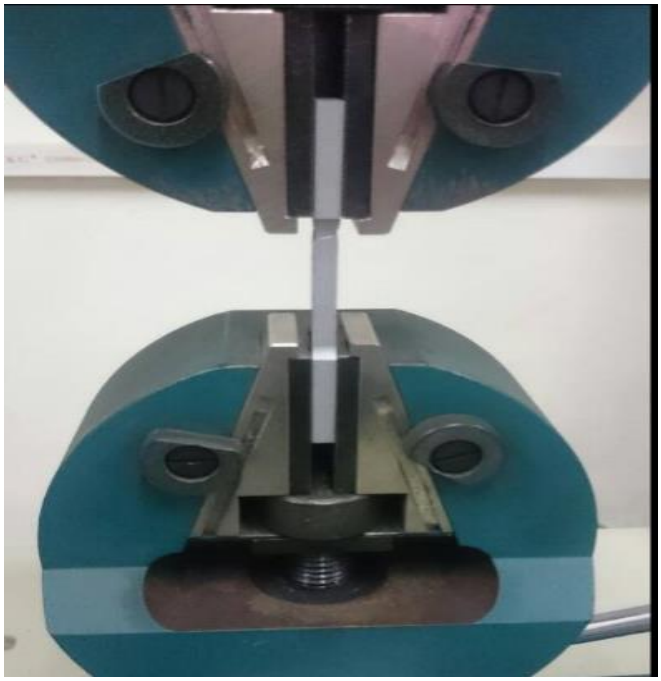


Figure 3: Clamped specimen in a UTM

The tensile test specimens were cut according to the following dimensions [4].

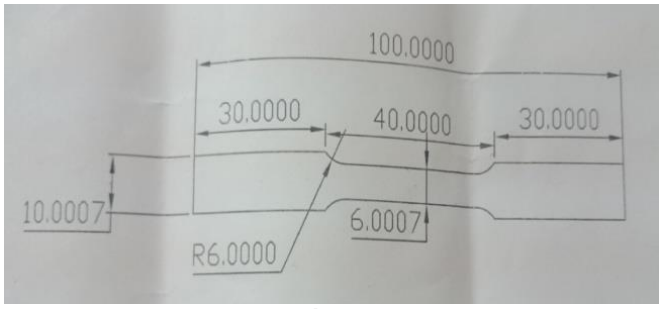


Figure 4: Tensile testing specimen

Hardness testing was carried out using Vickers hardness testing procedure. The results were obtained in the units HV 0.2 using testing method- ASTM E348.

Wear tests were carried out using Pin on disc (as shown) testing apparatus. A pin of diameter 10mm and length 32 mm was employed as the top wearing surface. The bottom wearing surface comprised of a disc of diameter 165 mm. and material EN31. A normal load of 5 Kg. (49.033 N) was applied.

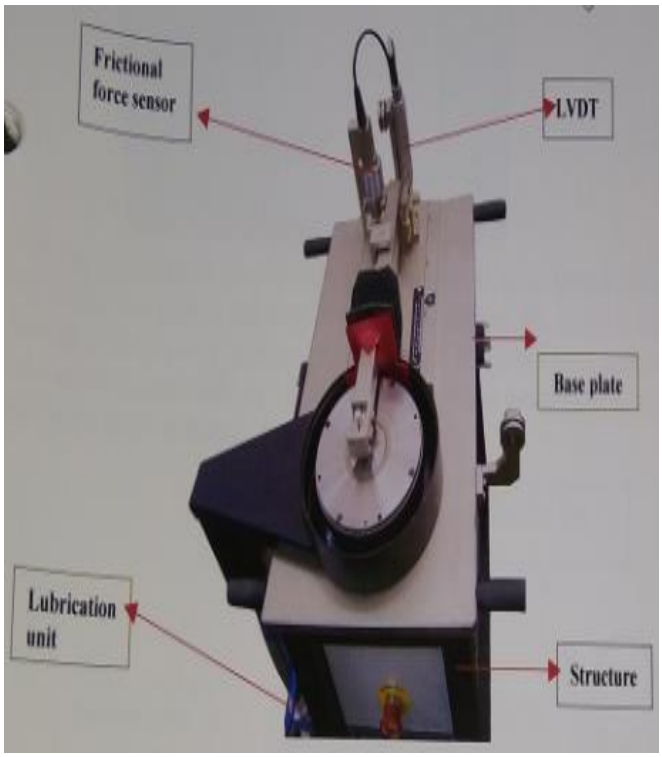


Figure 5: Pin on Disc wear apparatus

3. Result and Discussions

3.1 Tensile, Hardness and Wear rate analysis results

All the data was analyzed taking three steps of the concerned variables of tool feed (60mm/ min., 80 mm/min., and 100 mm/ min.); tool speed (500 rpm, 700 rpm, 900 rpm) and tool tilt angle (0º, 2.5º, 5º). The results of the tensile test were obtained as follows.

Table-2: Tensile Test Result Data

Feed	Speed	Tool tilt	Tensile strength
60	500	0	4540
60	700	2.5	6170
60	900	5	6280
80	500	0	4950
80	700	2.5	3560
80	900	5	6650
100	500	0	5600
100	700	2.5	6690
100	900	5	7280

Similarly, the results for hardness were

Table-3: Hardness Test Result Data

Feed	Speed	Tool tilt	Hardness
60	500	0	79
60	700	2.5	77
60	900	5	77
80	500	0	78
80	700	2.5	77
80	900	5	77
100	500	0	76
100	700	2.5	76
100	900	5	75

The wear rate data were calculated by taking into account the initial weight of the specimen and the final weight of the specimen using the following formulas:

Wear amount= Weight Loss= Initial Weight – Final Weight

Wear Rate= $\frac{Weight\ Loss}{Test\ Duration}$

Table-4: Wear Rate Test Result Data

Wear-rate(*10^{-5})	Weight Loss	Test Duration
2.1017	0.0215	1023
1.8107	0.0197	1088
1.6073	0.0185	1151
2.0154	0.0209	1037
1.8650	0.0199	1067
1.5004	0.0176	1173
2.1786	0.0222	1019
1.747	0.0192	1099
1.8904	0.0200	1058

Table-5: Tensile Test Result Data

Feed	Speed	Tool tilt	Tensile strength
60	500	0.0	4540
60	700	2.5	6170
60	900	5.0	6280
80	500	2.5	4950
80	700	5.0	3560
80	900	0.0	6650
100	500	5.0	5600
100	700	0.0	6690
100	900	2.5	7280

The above given tables (2-5) represent the table values formulated for Taguchi analysis performed in MINITAB 17 software.

3.2 Taguchi Analysis using MINITAB 17

Taguchi methods were developed to improve the quality of goods manufactured. In the MINITAB 17 software under Stat column DOE was selected followed by Create Taguchi Design to formulate an orthogonal array of size L9 (3 ^3) which designated the factors involved as levels as shown in the following tables 6-7.

Table- 6: Level for Tensile and Hardness Test

A	B	C
1	1	1
1	2	2
1	3	3
2	1	2
2	2	3
2	3	1
3	1	3
3	2	1
3	3	2

Table- 7: Factor Level Information

Factor	Type	Levels	Values
A	Fixed	3	1, 2, 3
B	Fixed	3	1, 2, 3
C	Fixed	3	1, 2, 3

Plot for Means shows the variation of means between different groups. The graphical means plots have been shown below for values of hardness, tensile strength and wear rate analysis.

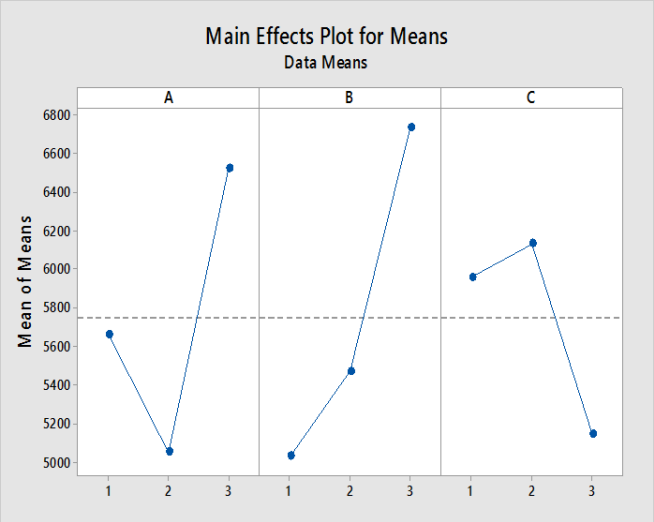


Figure 6. Plot for Means for Tensile strength

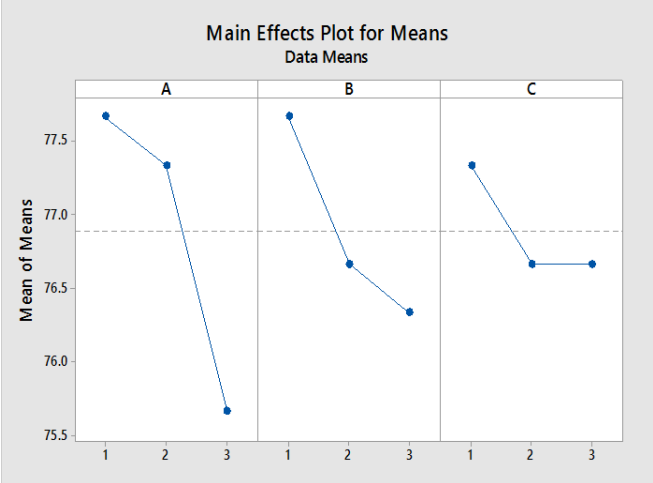


Figure 7. Plot for Means for Hardness values

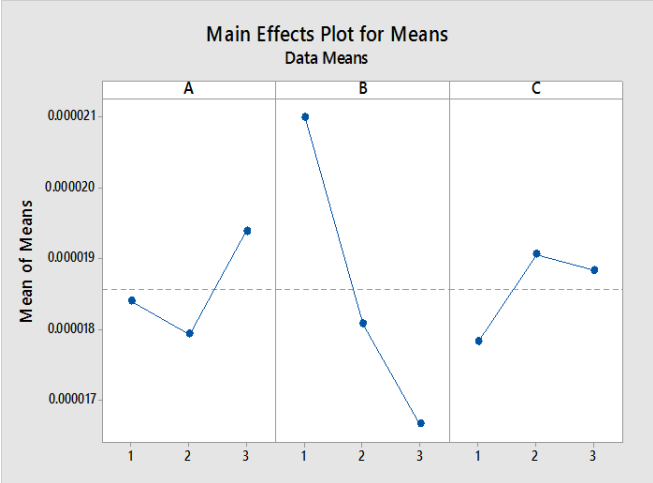


Figure 8: Plot for Means for Wear rate values

Similarly the S/N plots i.e. the signal to noise ratio plots were obtained as follows

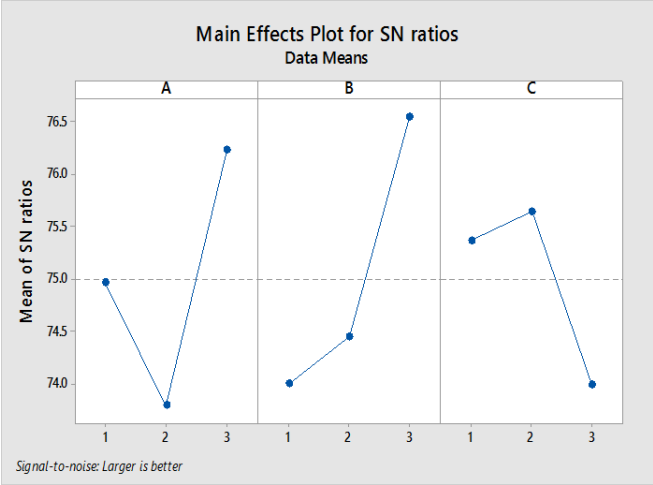


Figure 9: S/N ratio plot for Tensile strength

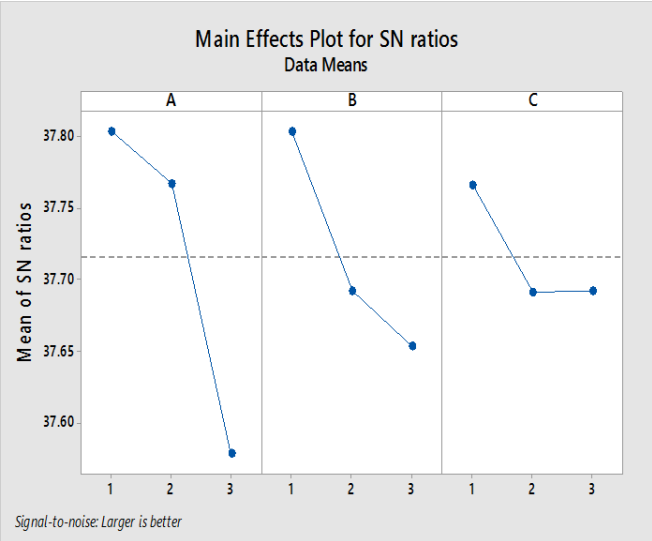


Figure 10: S/N ratio plot for Hardness

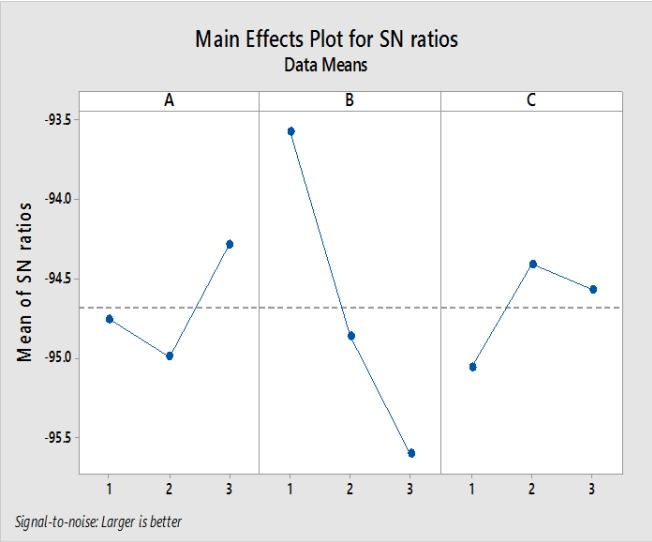


Figure 11: S/N ratio plot for Wear rate

The above graphs were obtained on the scale of Larger is Better.

3.3 Variance Analysis

Variance analysis for Tensile, Hardness and Wear analysis respectively values were obtained as given below

Table 8: Analysis of Variance for Tensile strength

Source	DF	Adj SS	Adj MS	F-Value	P-Value
Feed	2	3272600	1636300	1.85	0.351
Speed	2	4705267	2352633	2.66	0.274
Tilt	2	1665067	832533	0.94	0.515
Error	2	1771467	885733		
Total	8	11414400			

Table 9: Analysis of Variance for Hardness:

Source	DF	Adj SS	Adj MS	F-Value	P-Value
Feed	2	2.889	1.111	13	0.071
Speed	2	6.89	3.44	31	0.031
Tilt	2	0.889	0.44	4	0.2
Error	2	0.22	0.11		
Total	8	10.889			

Table 10: Analysis of Variance for Wear rates

Source	DF	Adj SS	Adj MS	F-Value	P-Value
A	2	0	0	0.77	0.566
B	2	0	0	6.79	0.128
C	2	0	0	0.6	0.627
Error	2	0	0		
Total	8	0			

4. Conclusions

Taguchi analysis conducted using the software MINITAB 17 gave the following equations were developed for tensile strength, hardness and wear rate of aluminum alloy (6082- T6-T651) using regression analysis. These equations clearly show their dependence on the parameters of tool feed, tool speed and tool tilt angle.

Regression Equation for Tensile strength

Tensile strength = 5747-83 Feed _1- 693 Feed_2 + 777 Feed_3 -717 Speed _2 +990 Speed_3 + 213 Tilt _1 + 387 Tilt_2- 600 Tilt _3.

Regression Equation for Hardness

Hardness= 76.889 + 0.778 Speed_1- 0,222 Speed_ 2- 0.556 Speed_3 + 0.778 Feed_1 + 0.444 Feed_2- 1.222 Feed _3 + 0.444 Tilt _1- 0.222 Tilt _2- 0.222 Tilt_3

Regression Equation for Wear rate

Wear Rate= 0.000019 - 0.000000 A_1 - 0.000001 A_2
+ 0.000001 A_3 + 0.000002 B_1 - 0.000000 B_2
- 0.000002 B_3 - 0.000001 C_1 + 0.000000 C_2
+ 0.000000 C_3

References

[1] V. Jegannathan Arulmoni, Ranganath M.S., R.S.Mishra: "Effect of process parameters on friction stir processed Copper and Enhancement of the mechanical properties of the composite material: A Review on Green Process Technology", International Journal Of Sustainable Science & Engineering, Vol.2(4), (2014), pp. 1-10

[2] V. Jegannathan Arulmoni, Ranganath M.S., R.S.Mishra, Experimental Investigations on Friction Stir Processed Copper and Enhancement of Mechanical Properties of the composite Material, International Journal of Advance research and innovation, Vol. 2(3), (2014), pp. 557-563

[3] A.G. Rao, B.R.K. Rao, V.P. Deshmukh, A.K. Shah, B.P. Kashyap(2009)- Microstructural refinement of a cast hypereutectic Al-

[4] 30Si alloy by friction stir processing, Vol.-Materials Letters, pp. 2628-2630
[5] R.S.Mishra, Z.Y. Ma, I. Charit (2002), Friction stir processing: a novel technique for fabrication of surface composite International journal of Material Science and engineering, Vol-A341,, pp.307-310.
[6] Husain Mehdi, R.S. Mishra, Mechanical properties and microstructure studies in Friction Stir Welding (FSW) joints of dissimilar alloy- A Review, Journal of Achievements in Materials and Manufacturing Engineering 77/1 (2016) 31-40.
[7] Husain Mehdi, R.S. Mishra, Influences of Process Parameter and Microstructural Studies in Friction Stir Weldingof Different Alloys: A Review, International Journal of Advanced Production and Industrial Engineering, IJAPIE-SI-MM 509 (2017) 55–62.
[8] Husain Mehdi, R.S. Mishra, Mechanical and microstructure characterization of friction stir welding for dissimilar alloy- A Review, International Journal of Research in Engineering and Innovation, vol-1, Issue-5 (2017), 57-67.
[9] Mehdi Zohoor, M.K. BesharatiGivi, PSalami (2012) Effect of processing parameters on fabrication of Al-Mg/Cu composites via friction stir processing , International journal of Materials and design, Vol-39, pp.358-365.
[10] H.J.Liu, X.L. Feng(2012): Effect of post-processing heat treatment on microstructure and micro hardness of water-submerged friction stir processed 2219-T6 Aluminium alloy, International journal of Materials and design, Vol-47, pp.101-105
[11] A.Orozco-Caballer, C.M. Cepeda-Jimenez, P. Hidalgo-Manrique, P.Rey, D. Gesto, D. Verdera, O.A. Ruano, F. Carreno(2013): Lowering the temperature for high strain rate super plasticity in an AL-Mg-Zn-Cu alloy via cooled friction stir processing, Materials Chemistry and Physics, Vol.-142 pp. 182-185
[12] Adem Kurt, Ilyas Uygur, Eren Cete(2013)- Surface modification of aluminium by friction stir processing, Jounal of Materials Processing Technology, Vol.- 211, pp.313-317
[13] T. Dieguez, A. Burgueno, H. Svoboda (2012)- Superplasticity of a Friction Stir Processed 7075-T651 aluminum alloy Vol.- Procedia Materials Science, pp. 110-117
[14] B. Zahmatkesh, M.H. Enayati, F. Karimzadeh (2010)- Tribological and microstructural evaluation of friction stir processed Al2024 alloy, Vol.- Materials and Design 31, pp. 4891-4896.

Globalization, ICT and Entrepreneurship: A Study of Women Engineers in India

Dr. Seema Singh
Associate Professor of Economics
Delhi Technological University
Delhi- 110 042, India

Abstract: Purpose - The purpose of this paper is to discuss impact of globalization and advent of Information and Communication Technology (ICT) on the growth of entrepreneurship among women engineers in India. Engineering is otherwise considered a male bastion. Design/methodology/approach – This study utilises an extensive review of extant literature on impact of globalization and advent of ICT on women engineers and emerging trends of entrepreneurship among them. The paper also discusses measures taken by other stakeholders as Universities, Government and Associations as NASSCOM and SIDBI to help women engineers to initiate entrepreneurship. The literature, propositions and discussion are intended to provide a bridge between entrepreneurship and women engineers. Findings/ Implication – Suggest a framework of all the stakeholders for development of entrepreneurship among women engineers. Research limitations – The paper is based on review of literature and primary information through case study of ten women engineer entrepreneur and analysis of a small sample of final year women engineering student and engineers who have passed out within three years. The paper lacks rigorous statistical analysis. Originality/value – Women Entrepreneurship has largely discussed for poverty alleviation, enhancing family income, women empowerment etc. but hardly discussed regarding innovation entrepreneurs among empowered women especially in context of India. The paper fills the gap.

Key word- Globalization, Information and Communication Technology (ICT), Entrepreneurship, Women Engineers

JEL Classification: F 66; I 23; J 24; Q 38; P 46

1. Introduction

The capitalist framework of production recognizes the role of entrepreneur[1] and considers it, a very crucial among the four factors of production. It assesses the gap (opportunity), brings other three factor of production i.e. land, labour and capital together and takes the risk. Various theories of entrepreneurship consider different perspectives on entrepreneurial behaviour and activities[2]. For example, economic perspectives consider entrepreneurs to be those who drives technological change or exploit new technological breakthroughs or commercialize commercial breakthrough to create new combinations, products, distribution systems or new market (Schumpeter, 1947; Holmes and Schmitz, 1990; Braunerh et.al. 2010) , McClelland's (1961) work focused on psychological traits that were identified in samples of young men as risk taking, achievement, locus of control while Kirzner (1985) identifies entrepreneurs as those who are able to utilize information in a way that allows them to discover opportunities that others may not. From the sociology perspective, Aldrich (1999) defines the nascent entrepreneur as one who initiates new activities intended to culminate in a viable business start-up (Aldrich, 1999, p. 77). More recently, Shane (2003, p. 4) defines the entrepreneur as an individual who

discovers, evaluates, and exploits opportunities to introduce new goods and services, ways of organizing, markets, processes, and raw materials through organizing efforts that previously did not exist. In these discussions, an implicit assumption is that the individual entrepreneur is "generic" and rather does not differ except when contrasted to non-entrepreneurs. However, the theories have been developed on samples of men. Therefore, there are chances that they have not fully capture women's entrepreneurial traits and behaviour (Hurley, 1991). As Joanne Martin (2000) asserts, organizational theories are seldom gender neutral. Therefore, the gender neutral theories may not fully explain or capture the full essence of entrepreneurial behaviour[2] in the background of patriarchal societies. There is growing appreciation that the conditions which support women's ability to start and grow ventures may be different from those that help men, and therefore, there is a need to examine factors that impact women's enterprise development (OECD, 2004; Bosma and Levie, 2010). The same logic may be applicable for factor driven, efficiency driven and innovative driven entrepreneurship for women also. Again, engineering is considered as a male bastion not only in India but in the other part of the globe too. However, women participation has experienced a threefold increase in India during the period of post-globalisation (Singh, Seema 2013). At the same time, the advent of Information and Communication Technology (ICT) has drastically changed the way we work and work is performed. It has provided a virtual platform to interact, negotiate and exchange things without being there physically present. In this background, the paper discusses, the status of entrepreneurship among women engineers under the era of globalisation and ICT. The second and third section of the paper discusses the International and Indian experience of the status of women entrepreneurship respectively. Globalisation, Information Technology and Expansion of Engineering Education in India have been discussed in the fourth section. The fifth section deals with the case studies regarding successful women engineer entrepreneur. It has been supplemented by a quantitative study of fifty final women engineering students and women engineers who have graduated during less than three years, and the next section makes inferences from the fifth section. Various initiatives which have been taken by the Government, Associations, universities and venture capitalists to help and assist women engineer entrepreneur have been discussed in the seventh section. The eighth section provides a framework of Quadruple Helix Programme for Development of Women Engineer Entrepreneurs where all stakeholders as the university through various programmes, association, the government and venture capitalists will provide required assistance in a coordinated way to women engineer for developing entrepreneurship among them. The last section concludes the discussion.

2. Status of Women Entrepreneurship – International Experience

Entrepreneurship is dominated by men. In many societies around the world, there are expectations from the women will be at home to take care of families, and therefore, the burden of child care falls squarely on their

shoulders. Entrepreneurship is in and of itself a male mentality and experience, which means that researchers and society in general are more likely to associate entrepreneurial actions with men (Bruni, Gherardi, & Poggio, 2004). In the broad sense, women are less likely than men to engage in entrepreneurship, but when they do, they are more likely to do so out of necessity. Women are nearly one-third more likely to start businesses out of necessity than men. And this is also a fact that over half of the entrepreneurs in India along with Chile have stated that they have innovative products or services (Kelly et.al. 2015). According to the Female Entrepreneurship Index (FEI), the US stands at the top of that ranking. The U.S. is often cited as a model to emulate; women-owned firms accounted for only 28% of all businesses. In the U.K. in 2004, a meagre 15% or so of enterprises were female-owned (Carter and Marlow, 2006). Exceptions include the study by Bruni (2004), which shows that while the percentage of female-owned firms is relatively high for micro-enterprises in Latin America (although lower than 50%, except in Honduras), it never reaches 20% for larger businesses. According to the figures in the 2014 Global Entrepreneurship Monitor report, the same is true for many other developing countries (Kelley, 2015). The gender diversity in the top management is recognized as a potential driver of firm performance (Oakley, 2000; Krishnan et al., 2005; Smith et al., 2006). However, an emerging body of comparative international entrepreneurship research on female entrepreneurs suggests that many environmental factors must be considered to increase female entrepreneurship (Terjesen, Hessels, and Li, 2014; e.g., Verheul, van Stel, and Thurik, 2006). For example, family-related institutions such as greater provision of childcare services and family leave are associated with higher levels of female entrepreneurship (Elam, 2008; Terjesen and Elam, 2012) as women tend to start ventures at a later age (ages 35-40) than men, and must manage work-family conflicts (Shelton, 2006). Furthermore, educational training can help women to build confidence in their business skills and ability to identify entrepreneurial opportunities (OECD, 2004). Levels of female entrepreneurship are also influenced by differences across countries regarding women's freedom to work and travel due to the traditional family and religious norms (Terjesen and Elam, 2012). Other important institutions which impact female entrepreneurship include equal legal rights, access to education, networks, technology, capital, social norms, values, and expectations. Furthermore, the overall business environment regarding laws, regulations, and business stability will affect businesses' ability to thrive and grow.

3. Status of Women Entrepreneurs – Indian Experience

India is one of the fastest emerging economies, and the importance of entrepreneurship is realized across the gamut. However, Workforce Participation Rate (WPR) for women has declined in recent times despite three decades of relatively rapid GDP growth. The WPR in India have historically been significantly lower than the corresponding male rates and are among the lower rates to be observed even in the developing world. It implies that there is a real tendency at work that has to be understood and explained. The 2015 Gender GEDI Female Entrepreneurship Index ranks India a dismal 70 out of the 77 countries included with a score of 25.3 per cent.

This index measures a country's potential to encourage and fuel the development and growth of female entrepreneurship. India also received the lowest score regarding the economic Labour Force Parity on an institutional level. Women's role in reproduction and care work overpower their role in the economic production. If Push Factor as if they are required to support the family financially, they start the work but by and large, they are confined to small business and tiny cottage industries. Factors which influence for entrepreneurship can be grouped into two i.e. push factors and pull factors. As for sense towards independent decision-making, if an activity is taken up as a challenge etc. are Pull Factor. Out of Push and Pull Factors, Push Factors are seen as more prominent in the case of women entry into the business, or say, entrepreneurship is traced out as an extension of their kitchen activities mainly to 3 Ps viz, pickles, powder, and papad. Women engaged in business activities due to family compulsion, and the responsibility is thrust upon them. At present, almost 10% of the entrepreneurs are women. Their number in the four southern states and Maharashtra account for over 50% of all women-led units in India. With growing awareness about business and spread of education among women over the period, women have started shifting from 3 Ps to 3 modern E's, viz. Engineering, Electronics and Energy. It encourages women to have an independent occupation and stands on their own.

4. Globalisation, Information Technology and Expansion of Engineering Education in India

In the era of Globalization and Information and Communication Technology (ICT), the market has become very competitive. Firms are continuously upgrading their technology to enhance the quality of their product and productivity of resources. Any change in technology requires a different skill set. After globalization, many Transnational and Multinational companies are coming to India to get the advantage of cost effective English speaking engineering manpower (Singh 2005). Besides other, it has led to exponential growth in engineering education. At present, there are almost 3500 engineering institutions with 1.67 million seats. Traditionally participation of women in engineering education was minuscule not only in India but even in the developed countries and has and grown over the years. But though it has reached its plateau in the developed countries as US, UK, Australia and ranging from 15 to 20 %, women in growing numbers are joining the profession in India in the era of globalization. In 1990-91, women participation was a meager 7.6 per cent in Engineering and Technology which rose to almost 28 per cent in 2010-11. Credit may be given to those State Governments and engineering colleges which have reserved seats for women candidates by various criteria (Singh Seema 2005; Singh Seema, 2014, Singh Seema and Fenton' 2015).

5. **Case Studies of Successful Women Engineer Entrepreneur**

In this section, first of all, ten case studies have been discussed of women engineer entrepreneur[3]

Case 1: Ms. Sangeeta Wiz

Ms. Sangeeta Wij graduated in civil engineering from famous Delhi College of Engineering. Post-college, she worked in a couple of private firms as a Structural Design Engineer before joining RITES, a Government of India enterprise providing engineering, consultancy, and project management services in 1984 as an Assistant Manager Designs. Meanwhile, she also completed her M.Tech. Part-Time from an IIT. In 1995, she accepted a Project Coordinator's assignment with USAID. However, this role had little to offer her as a civil/ structural engineer, and Wij quit USAID to start her consultancy firm on Structural and Civil Engineering. She is perhaps the first woman structural engineering consultant in India. Initial days of entrepreneurship were tough, looking for projects, executing the designs/drawings on time and also realising the payments from clients, which according to her was the trickiest of the part.

Her proprietorship firm gradually built a good reputation and was able to attract medium-sized government and private sector projects. Nevertheless, intending to increase its employee strength and improve the office infrastructure, Wij got into a partnership in 2007 and acted as the Managing Director of the new venture, which took over her firm. However, they can not manage scale and the new venture made losses for consecutive years and as a result, the partners decided to split. Wij gave up her stake amidst disillusionment but decided to move on in life. The former DCEite is now with Prime SD Engineering Consultants Ltd, as a Managing Director of their new consulting firm, handling turnkey consulting and PMC assignments for prestigious in-house and external projects.

Case 2: Prof. Goldi Gabrani

After 21 years in academics, she joined her husband's entrepreneurial venture viz. Tecpro group in the year 2007, wherein Tecpro group grew ten times from Rs. 300 crores to about Rs. 3000 crores what it is today. The group today has about 2000 employees. Earlier she was a Whole Time Director of the group's flagship company, Tecpro Systems Limited and is currently a Whole Time Director of Hydro Power Corporation Limited. Hydro is focusing on four segments of electrical projects with high growth potential namely Transmission and Distribution lines, Substations, Railway Overhead Electrification and Electrical Balance of Plant (eBoP).

She is working towards a cohesive approach of taking her group to achieve greater heights along with benefitting the society. Her passion for education and learning still continues to dominate her life in every sphere.

She has been actively contributing towards the development of a Training and Research Center through a partnership between Industry and Academia. As part of one of her pioneering efforts, the group has recently tied up with IGNOU and Haryana Government to offer One Year Diploma in Power Transmission and Distribution. She is also contributing in designing an integrated curriculum for national level skill development programmes in the Power sector.

Further, she has incorporated a trust by the name of Divine Asian Education Trust, which is developing a sprawling campus of around 30 acres and diversifying the group into world- class education and research. She has dedicated her past life to quality education and hopes to continue doing that for the rest of her life, through such initiatives.

Case 3: Upasana Taku

She is a graduate from NIT Jalandhar and masters in management science and engineering from Stanford University. She started a career in payments and financial services which spanned a period of over eleven years. She is the Director and CEO at Zaakpay.com and apart from her job, Upasna, co-founded MobiKwik with Bipin Singh in 2009. Mobikwik has recently raised $25 Mn in its Series B round of funding from Tree Line Asia and others. The company is now planning to raise another $100 Mn.

Caes 4: Suruchi Wagh

A 2007 computer engineering graduate from College of Engineering Pune and Co-founder of Jombay.com. It is a talent measurement and analytics platform which helps companies to measure human behavior to identify required talent to have better human resource. After completing her Master's in Science and Engineering Management in 2008 from University of Southern California, she joined Tata Consultancy Services.

Caes 5: Ms. **Sangeeta Nagrath**

After graduating from college, she worked with Stallion Shox Ltd for a year, which was followed by a two-year stint with the IDM (earlier IBM). After that, she started an entrepreneurial venture along with a part of a couple of mechanical engineering manufacturing companies. She is a Founder Partner at Tekniktrad International since June 1990, a Director at N.V. Comp. Pvt. Ltd. from March 2004 and a Partner at M.V. Engineering Industries since March 2005. Nagrath also developed and sold a few software solutions over the years. In 2005, she became a part of a start-up company 'HR Bridges', a niche Human Resource Consulting firm involved in organized recruitment and other HR services in India. "The birth of my daughter was the turning point in my life when I chose to quit a full-time job and take a break. This only motivated me, to start a few ventures of my own.

Case 6: Ms. Purukalpa Sankar

In 2013 she did B.Tech. in Chemical & Bio-molecular Engineering from Nanyang Technological University. Co-founder of Social Crop, a mission-driven data company. She dreams to power the Indian Army and manage disaster some day with better data.

Case 7: Ms. Aditi **Avasthi**

She is the Founder and CEO of Embibe, a Mumbai-based ed-tech startup that was backed by Kalaari Capital and LightBox Ventures. The venture combines technology and data sciences and helps students prepare better for difficult competitive exams. Earlier this year, Embibe acquired 100Marks, a Morpheus Gang company started in April 2012 to help students crack the IIT-JEE, one of the most rigorous entrance tests globally.

Case 8: Ms. Neeru Sharma

Neeru Sharma co-founded Infibeam.com with Vishal Mehta, Vijayakumar Subramanian and Sachin Oswal in 2007. Being an engineer with an MBA degree from Carnegie Melon University, Neeru had worked with Amazon, the US in the Department of corporate development and media retail. She played an important role in $850 Mn Zappos acquisition before founding Infibeam.

The self-funded startup was initially funded by Vishal Mehta with a sum of INR 10-15 Cr. The firm has executed two acquisitions so far – picsquare.com, a personalised photo printing website in 2008 and Odigma, a digital marketing company for $5 Mn in 2014.

The startup had filed the draft red herring prospectus (DRHP) with SEBI for a public issue of its equity on June 30th, this year. It became the first e-commerce company in the country to be listed with capital markets regulator Securities and Exchange Board of India (SEBI), giving its approval to the company to raise $69 Mn.

Case 9: Ms. Surabhi Dewara

After working as an engineer at Freescale semiconductors and as a promoter at Catalog Educational Services, Surabhi, decided to implement the idea of exploring the education sector and providing a better quality of education. A holistic approach towards career counseling was missing in the country, and this is what inspired

her to start Meracareerguide.com in 2009. An undisclosed amount has been invested by Vishal Gondal and Ronnie Screwvala in the venture.

Case 10: Ms. Anu Sridharan

She is the founder of NextDrop, a company which allows Indian residents in the urban areas to track the availability of piped water through SMS. Anu has Bachelors in Civil Engineering and a Masters in Civil Systems Engineering from the University of California, Berkeley. Her Master's research focused on the optimization of piped networked systems in developing economies to her credit. Anu has also been selected to the Forbes "30 Social Entrepreneurs Under 30″ list.

These ten case studies is supplemented by a quantitative study of a small sample of fifty women engineers and final year students[4]. No one from the sample has thought of being an entrepreneur. The reasons given by them are as follows. Some of them gave more than one reason also. I have grouped those reasons on the basis of their nature.

6. Inference from the case studies and responses of young engineer/ engineering student given in Table 1 at the Annexure I

Getting pen-sketch of female engineer entrepreneurs is not difficult in the era of internet and 'Make in India' initiative of the Government of India. However, the idea is to find out some common traits of women engineer entrepreneur which may be beneficial for the stake holders of engineering education in enhancing the quality of services they are providing. They are as follows:

a. It is their intrapreneurship in the wage employment which ultimately led to the entrepreneurial venture.
b. Senior engineers could not manage the dual responsibility of the corporate sector and home.
c. The engineering graduates are not ready to start a business activity.
d. Raising capital is difficult.
e. The absence of a group.
f. Absence of guidance/ advice/ mentorship
g. It is difficult to get venture capital.

According to data compiled by Your Story, startups had raised USD 1.7 billion in first quarter 2015 alone. The number of deals in the second quarter of 2015 has increased by 50 per cent from the previous quarter. However, when we look at businesses with women at the helm — start ups founded and run solely by women, the number

is small, and when we talk about the ones who have received funding, it does not even cross single digits(Saha, 2016). There are various reasons for this which can be pointed out:

- Investors tend to make safe bets and pedigree universities are always helpful. If there are two equivalent companies, with one team having a pedigree, they are more likely to get funded.
- Founders from these universities tend to have good networks, which help in the early stages in allowing these entrepreneurs make deeper inroads.
- Since these entrepreneurs have more exposure, many times, companies coming from pedigree universities are more mature and are likely to succeed (Mehta, 2015). The perception about women entrepreneur is that they may not be serious; their priority may change after marriage (Singh Rajiv, 2016).

In nutshell, as discussed by Kassicieh, S.K. (2010), good quality telecommunication infrastructure has led to growth of so many technology start ups in India too. Opportunities before a women engineer entrepreneur under Globalisation and Information & Communication Technology (ICT) in India is very large. Area needs to be selected as par knack and interest. Then, they need to research the product/ service and assess the market. They need to prepare the plane judiciously. Manage required fund. Once they start, they need to do proper networking and consult with professional.

7. Initiatives Assist Women Engineers to become Opportunity Entrepreneurship[5]

Apart from different schemes initiated by the Government, SIDBI and several Banks for women entrepreneur which is listed at Annexure II, following are various already launched programmes and various initiatives from various stake holders:

7.1 Saha Fund

It is looking to invest in women led companies across different sectors. Added to this, the fund is keen on companies that use technology to scale . Saha Fund has a 'Mentors Circle' that consists of industry stalwarts to help, mentor and guide the women entrepreneurs. Even if they don't invest in the portfolio company but, they create equity to the companies. There are several stereotypes that need to change and that change is possible when there's gender parity in entrepreneurship and management rules (Kashyap, 2015).

7.2 National Entrepreneurship Network (NEN)

It is a flagship initiative of Wadhwani Foundation since 2003. Co-founded by IIT Bombay, IIM Ahmedabad, BITS Pilani, SP Jain Institute of Management & Research and Institute of Bio-informatics and Applied Biotechnology, Bangalore. Since inception, NEN hass resulted in 2000 new startsup with 12000 = direct and 50000+ indirect jobs and is now tracking 1500+ new companies each year. NEN has built a strong network with 600 colleges 1000+ mentor and 3200 faculty in India (Wadhwani Foundation, 2016).

7.3 NASSCOM INITIATIVE

It has started a, 'Girl in Technology' Programme for women engineers under its 10,000 startups programme for technology start ups. Since its inception NASSCOM has conducted various programme in Bengaluru, Chennai

and Delhi (NASSCOM, 2016.a). NASSCOM and the Karnataka government have partnered to set up a 50,000 square feet Start-up Warehouse Next Gen-cum-Hack-cellerator in Bengaluru, one of the first few in the world. The Start-up Warehouse – which reaffirms Bengaluru's status as the country's Start-up capital – will act as a large integrated platform housing and hosting companies for a six month incubation term. Once fully finished, the facility will have capacity to hold over 100 start-ups (with 1-12 employees each), on a 24x7 basis – (NASSCOM, 2016.b)

7.4 Initiatives taken at University Level

The academic world has progressively shown interest in developing entrepreneurship. Though there are some institutions exclusively to develop entrepreneurship but in rest of the universities also, the seminar, conferences and conclave are organized. Courses on developing entrepreneurial skills are being integrated in the engineering B.Tech. curricula. Recently DTU has announced to give Entrepreneurship break to its students for working on their entrepreneurial ventures. Alumini groups are helping and mentoring college/ unniversity students.

7.5 Association for Women Entrepreneurs

As par Table 2 of Annexure I, there are several association and societies which are exclusively for women entrepreneurs. They have been developed or established by various state Governments and business associations. Some NGOs as Women in Science and Engineering (WISE-India) is also organizing lectures and is mentoring woman engineering college students who wish to pursue entrepreneurship.

7.6 UN Women Entrepreneurship Day

It is observed on November 19 th' November which has been started by Wendy Diamond. Several programmes are organised to observe and discuss the work of women entrepreneurs. 144 nations overall recognized the first WED in 2014, which included the presentation of the Women's Entrepreneurship Day Pioneer Awards also. The organization behind WED also has an ambassadorship & fellowship program (WED, 2016).

8. Quadruple Helix Programme for Development of Women Engineer Entrepreneurs

All the important stakeholders as Government, University, Business/ Women Associations and Financing Companies/ Venture Capitalists need to come together to work in a coordinated way as a Quadruple Helix fashion to assist Women Engineer Entrepreneurs . As par the case study, all young women engineers entrepreneurs are foreign education many of them have B.Tech. as well as MBA degree. It means the B.Tech, curricula need to revamp itself and incorporate the courses of financial management, skills to become global workforce, knowledge of taxing system, legal system etc.

9. Conclusion and Recommendation

At present, Women Entrepreneur in India is almost 10% of the total and maximum of them are also working at the lower rung of the business cycle. At the same time, we have large reservoir of women engineers who are capable to run innovative entrepreneurships. All the important stakeholders as Government, University, Business/ Women Associations and Financing Companies/ Venture Capitalists are aware of the situation and are already launched many programmes. However, they need to in a a Quadruple Helix fashion to assist Women Engineer Entrepreneurs. As par the case study, all young women engineers entrepreneurs are foreign education many of them have B.Tech. as well as MBA degree. It means the B.Tech, curricula need to revamp itself and incorporate the courses of financial management, skills to become global workforce, knowledge of taxing system, legal system etc.

Notes:

1. The origin of the basic word Entrepreneurship is from a French word Entrepreneurship, where it cradled and originally meant to designate an organizer of certain musical or other entertainments. The Oxford English Dictionary (of 1897) defines the term Entrepreneur in similar way as the director or a manager of a public musical institution, one who gets-up entertainment arranged , especially musical performance. Initially in the early 16th century, it was applied to those who were engaged in military expeditions. In 17th century, it was extended to cover civil engineering activities such as construction and fortification.

   According to Government of India, “A women enterprise is an enterprise owned and controlled by a woman and having a minimum financial interest of 51 per cent of the capital and giving at least 51 per cent of employment generated in the women”. Last ten years Indian economy made it evident that the structure of ownership in the industrial sector, in agriculture, in the trade and commerce sectors has changed. Many women entered the world of business, of trade commerce and they have become successful entrepreneurs in various business activities.
2. The discussion on Psychological and Sociological traits have been largely taken from Bruin et. al. 2006.
3. The case studies have been collected through the Website (Team Inc42 (2015), Linden and face book and personal interview with some of them.
4. This is part of a larger study which is in progress. Here I am discussing some salient points of the study.
5. Global Entrepreneurship Monitor has divided entrepreneurship into three. They are Factor Driven Entrepreneurship, Efficiency Driven Entrepreneurship, and Innovation Driven entrepreneurship. Engineers may work in Innovation-Driven Enterprises (Kelley et.al., 2015)

Reference

1. Aldrich, H. (1999), "Organizations Evolving" Thousand Oaks, CA: Sage Publications.
2. Braunerh, P. Acs, Z.J. Audretsch, D.B. & Carloson B. (2010), "The Missing Link: The Knowledge Filter and Entrepreneurship in Endogenous Growth, Small Business Economics", 34(02), pp. 105-125.
3. Bruin Anne de, Candida G. Brush and Friederike Welter (2006) Special Issue towards the Introduction to Building Cumulative Knowledge on Women's Entrepreneurship: Theory and Practice, pp. 585 – 593 retrieved from https://www.researchgate.net/publication/228044987 on 26/4/2016.
4. Bosma, N.S. and Levies J(2010) Global Entrepreneurship Monitor 2009, Executive Report.
5. Bruni, A., Gherardi, S., & Poggio, B. (2004). Entrepreneur-mentality, gender and the study of women entrepreneurs. *Journal of Organizational Change Management*, *17*(3), 256–269.
6. Carter, S. and S. Marlow (2006). Female Entrepreneurship, in Carter, N.M., C. Henry, B.Ó Cinnéide, and K. Johnston (Eds), Female Entrepreneurship: Implications for Education, Training, and Policy, Abingdon: Routledge, p. 206-215.
7. James G. Henry and K. Satyanarayana (2015) Women Entrepreneurship in India- Problems and Prospects, International Journal of Academic Research, ISSN: 2348-7666 Vol.2, Issue-2(8), April-June pp.
8. Holmes T.J. and Schmitz, J.A. Jr. (1990), "A Theory of Entrepreneurship and its applications to the study of Business Transfers", Journal of Political Economy, 98(02), PP 265 – 294.
9. Hueley, A. (1991), "Incorporating Feminist Theories into Sociological Theories of Entrepreneurship", Paper presented at the Annual Meetings of the Academy of Management, Miami FL, August.
10. Kashyap Sindhu (2015), "For by and of Women Entrepreneurs – SAHA is India's First Women Venture Capital Fund", Retrieved from http://yourstory.com/2015/09/women-entrepreneurs-saha-india-venture-capital-fund/ on 12/5/2016.
11. Kassicieh SK (2010), "The Knowledge Economy and Entrepreneurial Activities in Technology-based Economic Development" The Journal of The Knowledge Economy, 01(01), pp. 24-47.
12. Kelley Donna, Slovica Singer and Mike Herrington (2015), "Global Entrepreneurship Monitor", 2015/16 Global Report, The Global Entrepreneurship, and Development Institute, Washington.
13. Kirzner I. (1985), "Discovery and the Capitalist Process" Chicago University of Chicago Press.
14. Krishnan, H.A., and D. Park (2005), " A Few Good Women—on Top Management Teams", Journal of Business Research 58(12), pp. 1712-1720.
15. McClelland, D. (1961), "The Achieving Society", New York: The Free Press.
16. Mehta Jubin (2015), "60%b of the Series A Companies in India have Founders from IIT/ IIM, and All of them are Male" Retrieved from http://yourstory.com/2015/07/funded-founders-india/ on 2/5/2016

17. NASSCOM (2016.a), Retrieved from http://www.nasscom.in/nasscom%E2%80%99s-10000-startup-program-expands-its-partnership-black-box-connect-launches-female-founders-e on 25/3/2016

18. NASSCOM (2016.b) Retrieved from http://www.nasscom.in/nasscomkarnataka-government-launch-startup-warehouse-nextgen-edition?fg=880017 on 25/3/2016

19. Oakley, J.G. (2000), "Gender-Based Barriers to Senior Management Positions: Understanding the Scarcity of Female CEOs", Journal of Business Ethics, 27(4), pp. 321-334.

20. OECD (2004), "Women Entrepreneurship Issues and Policies," Turkey Conference, Istanbul.

21. Saha (2016), "Creating a Women Specific Venture Capital" retrieve from http://www.stratos-invest.in/for-by-and-of-women-entrepreneurs-saha-is-indias-first-womens-venture-capital-fund/ on 15/5/2016

22. Shane (2003), "A General Theory of Entrepreneurship", Cheltenham UK Edward Elgar.

23. Singh Seema and Er. Susan Lee Fenton (2014), ""Women Engineers: A Comparative Study between India and Australia" International Journal of Advancements in Research & Technology, 0 3(07), July-2014, pp. 108-122. Retrieved from http://www.ijoart.org/research-paper-publishing_july-2014.shtml on 15/5/2016

24. ---------- (2013), "Women Engineers in India"(2013) in Dr Ravi Prakash Yadav (eds.) Women Workers in Informal Sector, Aavishkar Publishers, distributers, Jaipur, pp. 115-125.

25. ----------(2005), "MNCs Effect on Employment of Engineers" The Indian Journal of Technical Education, 28(2), pp. 38-44.

26. Singh Rajiv (2016), "How Gritty Women Entrepreneurs are Fighting prejudice in Startup Funding Ecosystem" retrieved on http://tech.economictimes.indiatimes.com/news/startups/how-gritty-women-entrepreneurs-are-fighting-prejudice-in-startup-funding-ecosystem/51285635 on 12/5/2016

27. Schumpeter. J.A. (1947), "The creative response in Economic History," Journal of Economics, Vol 77. P.149-15

28. Shelton, L. M. (2006), "Female entrepreneurs, work–family conflict, and venture performance: New insights into the work–family interface", Journal of Small Business Management, 44(2) pp. 285-297.

29. Smith, N., V. Smith, and M. Verner (2006), "Do women in Top Management Affect Firm Performance? A Panel Study of 2,500 Danish Firms", International Journal of Productivity and Performance Management, 55(7), pp.: 569-593.

30. Team Inc42 (2015), "Inspiring Stories of Some Amazing Women Entrepreneurs of the Indian Startup Ecosystem" https://inc42.com/entrepreneurship/indian-women-entrepreneurs/ retrived on 10/5/2016

31. Terjesen, S., and A. Elam (2012). 'Women entrepreneurship: A force for growth', International Trade Forum Magazine. United Nations International Trade Centre.

32. Terjesen, S., J. Hessels, and D. Li. (2014).'Comparative international entrepreneurship research: A review and research agenda,' Journal of Management. Forthcoming.

33. Terjesen Siri and Ainsley Lloyd (2015), "The Female Entrepreneurship Index (FEI)" Global Entrepreneurship Development Institute, Washington DC.

34. Verheul, I., A. van Stel and R. Thurik (2006). 'Explaining female and male entrepreneurship at the country level,' Entrepreneurship and Regional Development, 18(2): 151-83.

35. Venugopal V. (2016), "Investigating Women's Intension for Entrepreneurial Growth", International Journal of Gender and Entrepreneurship, 08(01), pp. 2-27.

36. WED (2016), "Women's Entrepreneurship Day" Retrieved from http://womenseday.org/ on 15/5/2016.

37. William Anuj (2013), "Engineering Institution DCE Speaks" http://indianfusion.aglasem.com/36024/dce-delhi-college-of-engineering-alumni/ retrieved on 10/5/2016

38. Wadhwani Foundation, (2003), National Entrepreneurship Network (NEN), Retrieved from https://wadhwani-foundation.org/initiatives/nen-india/?gclid=Cj0KEQjwoM63BRDK_bf4_MeV3ZEBEiQAuQWqkQAlJYyqSlQoZqLdbzfHrfOe5KZiS9eAwZWoOD9LojUaAvRt8P8HAQ on 15/5/2016.

Annexure 1

Table1: Reasons for Not Opting for Entrepreneurship

A. Knowledge Aspect	
1.	They are not ready to face the challenge.
2.	After four-five years of working in the organisation, they may think.
3.	Absence of guidance/ advice/ mentorship
4.	They are trying for MBA from US university or preparing for CAT
B. Risk Aspect	
1.	There is a financial risk. They may incur loss
2.	There is no fixed frame work for getting the financial return.
3.	They may not be able to fulfill their other obligation.
4.	They are getting wage employment easily then

	why to think of entrepreneurship.
C. Financial Aspect	
1.	Difficulty in getting capital
D. Social Aspect	
1.	Pressure from Parents/ Self decision to get married.
2.	Delhi is not a safe city
3.	No group and cannot start alone

Source: Compiled by Author

Table 2: Association for Women Entrepreneurs

SN	Name	Web site
1.	The Marketing Organisation of Women Enterprises (MOOWES)	
2.	Federation of Indian Women Entrepreneurs (FIWE)	http://www.fiwe.org/
3.	Consortium of Women Entrepreneurs (CWEI)	http://www.cwei.org/
4.	Association of Women Entrepreneurs of Karnataka (AWAKE)	http://awakeindia.org.in/
5.	Self-Employed Women's Association (SEWA)	http://www.sewa.org/
6.	Women Entrepreneurs Promotion Association (WEPA)	
7.	Bihar Mahila Udyog SanghBihar Mahila Udyog Sangh	http://www.biharmahilaudyogsangh.com/
8	Mahakaushal Association of Woman Entrepreneurs (MAWE)	http://www.maweindia.com/
9	SAARC Chamber Women Entrepreneurship Council	http://www.scwec.com/index.htm
10	TiE Stree Shakti (TSS)	http://www.tiestreeshakti.org/
11	Women Empowerment Corporation	http://www.wecindia.org

Source: Compiled by the Author from the respective Websites

Annexure II

SCHEMES FOR PROMOTION AND DEVELOPMENT OF WOMEN ENTREPRENEURS

In order to promote progressively women enterprises in the MSE sector, various schemes have been formulated by Ministry and Banks to develop women enterprises in India:

1. Trade related entrepreneurship assistance and development scheme for women (TREAD): With the objective of encouraging women in starting their own ventures, government launched a Scheme, namely, (TREAD) Trade Related Entrepreneurship Assistance and Development during the 11th Plan. The scheme envisaged economic empowerment of 297 women through the development of their entrepreneurial skills in non-farm activities. There are three major parts of the scheme; Govt. of India has grant up to 30% of the total project cost to the Non-Government Organizations (NGOs) for promoting entrepreneurship among women. The remaining 70% of the total project cost is financed by the lending agency as loan for undertaking activities as envisaged in the project. Up to Rs.1 lakh per program can be granted by govt. of India to training institutions / NGOs for providing training to the women entrepreneurs. 2. Micro & Small Enterprises Cluster Development Programme (MSE-CDP): a) Existing Clusters: Cluster is described as a group of enterprises, normally 20 or more producing same/similar products/services. The Cluster Development Programme being implemented envisages diagnostic study of identified clusters of traditional skill-based MSEs to identify suitable technologies and their providers and to facilitate adoption of available technology meeting the specific needs of the end users. The Cluster Development goals at improved competitiveness, technology improvement, adoption of best manufacturing practices, marketing of products, employment generation etc. The scheme provides support for capacity building, common facilities, marketing etc. the delivery, absorption and diffusion of the identified technology from its producers to the recipient user/cluster of small enterprises. b) Physical infrastructure: This Ministry implemented the IID Scheme to provide developed sites with infrastructural facilities like exhibition/display centers, telecommunications, drainage and pollution control facilities power distribution network, roads, water, raw materials, common service facilities storage and marketing outlets, and technological back-up services, etc. This scheme has been subsumed in the MS-ME-Cluster Development Programme. All the features of IID Scheme have been retained. To create physical infrastructure for women enterprises central grant of 40% of the project cost subject to a maximum of Rs.2 crore is available. The Ministry of MSME is trying to enhance the quantum of grant to 80% in a project of Rs.10 crore. 3. Credit guarantee fund scheme: In May, 2000 The Government had introduced the Credit Guarantee Fund Scheme for Small Industries with the objective of providing credit to SSI units, particularly small units, for loans up to Rs. 25 lakh with no collateral/ third party guarantees. The Scheme is being operated by the Credit Guarantee Fund Trust for Small Industries (CGTSI) set up jointly by the Government of India and SIDBI. In the case of women enterprises, the guarantee cover is up to

80% of the credit subject to maximum guarantee limit of Rs. 20 lakh. The member lending institutions (MLI) availing of guarantee from the Trust have to pay a one-time guarantee fee of 1.5% of the credit facility (comprising term loan and / or working capital) allowed by the lending institution to the borrower and annual service fee of 0.75% per annum on the amount of credit facility extended by the MLI, which is covered under the scheme. 298 4. Help for Entrepreneurial and Managerial Development: MSME DIs regularly conducts EDPs/MDPs for existing and potential entrepreneurs and charge fee for such courses. To encourage more entrepreneurs from among the SC/ST, women and physically challenged groups, it is proposed that such beneficiaries will not be charged any fees but, instead paid a stipend of Rs.500/- per capita per month. 20% of courses conducted by these Institutions shall be exclusively for women

5. Scheme for Women Entrepreneurs to Encourage Small & Micro Manufacturing Units DC (MSME) has formulated a scheme for women entrepreneurs to support Small & Micro manufacturing units owned by women in their efforts at developing overseas markets, to enhance participation of representatives of small/micro manufacturing enterprises under SIDO stall at International Trade Fairs/Exhibitions, to enhance export from such units. Under this scheme participation of women entrepreneurs in 25 international exhibitions is envisaged during the 11th Plan. For the year 2007-08 a good number of outstanding women entrepreneur associations have been requested to sponsor their members for participation in 5 international exhibitions scheduled during the months of Jan.-March, 2008, With a view to give confidence to women entrepreneurs for participating in the International Exhibitions.

6. Dena Bank to support India's women entrepreneur. Dena Bank will help Government of India's initiative to promote women entrepreneurs for self-employment ventures in any kind of non-farm activity.

ResearchGate

See discussions, stats, and author profiles for this publication at: https://www.researchgate.net/publication/323218874

International journal of advanced production and industrial engineering Harmonic Reduction in Power Distribution Netw....

Article · February 2018

CITATIONS
0

READS
4

2 authors:



Dr. Jitendra Nath Rai
Delhi Technological University, Government ...
46 PUBLICATIONS **47** CITATIONS
SEE PROFILE



Ram Bhagat
Delhi Technological University
4 PUBLICATIONS **1** CITATION
SEE PROFILE

Some of the authors of this publication are also working on these related projects:



STUDY OF INTELLIGENT CONTROLLERS AND COPARISION View project

All content following this page was uploaded by Dr. Jitendra Nath Rai on 16 February 2018.

The user has requested enhancement of the downloaded file.

Available online at www.ijapie.org

INTERNATIONAL JOURNAL OF ADVANCED PRODUCTION AND INDUSTRIAL ENGINEERING

IJAPIE-2017-07-319, Vol 2 (3), 82-88

IJAPIE
Connecting Science & Technology withManagement.
A Journal for all Products &Processes.

Harmonic Reduction in Power Distribution Network using UPQC

J.N.Rai*, Ram Bhagat
(Department of Electrical Engineering, Delhi Technological University, Delhi, India)
**Email: jnrai.phd@gmail.com*

Abstract : Unified Power Quality Conditioner (UPQC) is a versatile custom power device. It consists of two VSCs connected back-to-back to compensate for both distorted Point at Common Coupling (PCC) voltage and supply current imperfections. UPQC is designed to prevent the harmonics injected by the non-linear load from entering the source terminal. Regulation of voltage at the point of common coupling is carried out by series connected converter. SRF based current control method is used for current compensation by the shunt device. Hysteresis voltage control technique is used for shunt compensation by the series device which simultaneously acts as shunt and series active power filters. Maintaining a constant value for dc link voltage is essential for UPQC to perform normally which is carried out by shunt connected VSC. MATLAB based simulation is carried out to demonstrate the effectiveness of the proposed control scheme.

Keywords : UPQC, Non-Liner RL Load, Harmonics, synchronous reference frame (SRF), Hysteresis Voltage, Control Point at Common Coupling (PCC).

I. INTRODUCTION

Use of non–linear and time varying loads has led to distortion of voltage and current waveforms and increased reactive power demand in AC mains. Distortion due to harmonics is known to be the source of several problems, such as increased power losses, excess heating in rotating machinery, flicker and audible noise, significant interference with communication circuits, and incorrect operation of sensitive loads[1].Power electronics based equipment which includes adjustable–speed motor drives, DC motor drives, electronic power supplies, electronic ballasts, battery chargers are responsible for the rise in power quality related problems. Power quality is affected by harmonic distortion, temporary interruptions, voltage sag, voltage swell, under voltages, voltage spikes and noise [2]. Non-linear loads appear to be prime sources of harmonic distortion in a power distribution system. As the harmonic currents pass through the line impedance of the system, harmonic voltages appear, causing distortion at the coupling point. Harmonics have a number of undesirable effects on the distribution system. There are two basic categories: short term and long term. Short–term effects are usually the most noticeable and are related to excessive voltage distortion. Long–term effects often go undetected and are usually related to increased resistive losses or voltage stress [3]. In addition, harmonic currents produced by nonlinear loads can interact adversely with a wide range of power system equipment, most notably capacitors, transformers and motors, causing additional losses, overheating and overloading. As the presence of harmonics in distribution system is harmful, there is a need to define a framework to suppress it. To mitigate these identified power quality problems efforts are going on in the field of filters. Present day power quality renders these efforts futile. New technology known as custom power devices(CPD) has been developed for such distribution systems. These devices are applicable to distribution systems for enhancing the reliability and quality of the power supply. CPDs include DSTATCOM, DVR[6] and UPQC.

The Unified Power Quality Conditioner (UPQC) (figure 1) is one of the versatile custom power device, which can compensate both current and voltage related problems, simultaneously. The series Active Power Filter (APF) compensates voltage-based distortions, while the shunt APF cancels current-based distortions such as harmonics, reactive power and negative sequence current etc.

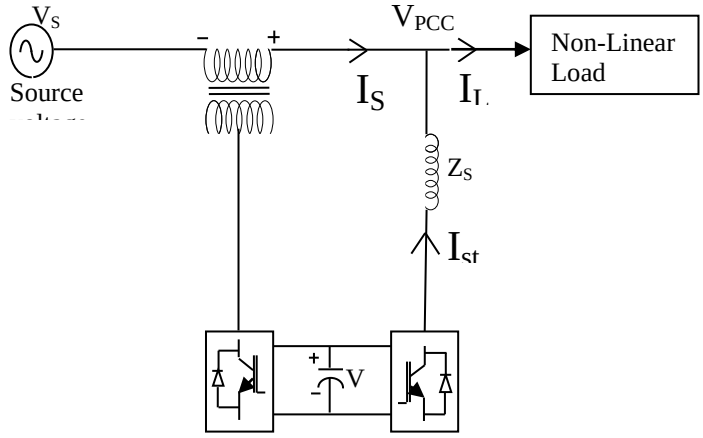


Fig.1. UPQC Block Diagram

The investigator has gone through a number of literatures in this regard. Some of them are:(a) the indirect current control approach, in terms of its simplicity and effectiveness, for the operation of a series APF[4].(b)Simulation of instantaneous

active and reactive theory based shunt active filter with MATLAB/ Simulink, a better solution for reduction of the harmonics[5].(c)A series active harmonic compensator which compensates the harmonic contents present in load voltage at PCC[7].

In this paper UPQC is designed to remove the harmonic injected by the non-linear load from entering into the source terminal. Regulation of voltage at the point of common is carried out by series connected converter. SRF based current control method is used for current compensation by the shunt device and Hysteresis voltage control technique is used for series device which simultaneously act as shunt and series active power filters.

II. SYSTEM DESCRIPTION

The system under consideration is shown in Fig.2.The UPQC is connected before the load to protect a sensitive load from any voltage based distortions and simultaneously making the source currents sinusoidal. The UPQC is realized by using two voltage source inverters (VSIs) connected back to back with a common DC link Voltage. One VSI is acting as a shunt APF, while the other as series APF. The series APF[8] is connected between the source and the load with the help of three single phase injection transformer. Injection transformer is used to inject voltage in the line by the series APF. While, shunt APF is connected at point of common coupling (PCC). Each APF is realized by using six Insulated Gate Bipolar Transistors (IGBT) switches[10]. The load under consideration is a non-linear load. A three-phase diode bridge rectifier with a RL load is considered as a non-linear load. The values of the circuit parameters and load under consideration are given in Appendix.

III. CONTROL SCHEME

The series active filters control has been carried out by means of following compensation strategy-

Control strategy which measures the load voltage to make that the APF generates a voltage with that same harmonic content and the opposite sign [9].

$$V_{ch} = K_v \cdot V_{lh} \qquad (1)$$

The measurement of the load voltage harmonic generally depends on the instrumentation sensibility k_v. The voltage supplied by the APF is expressed as follows:

$$V_{ch} = K_v \cdot V_{lh} \qquad (2)$$

From equation 2, the voltage in the point of common coupling is, for a specific harmonic :

$$V_{cch} = V_{lh}\left(1 - K_v\right) \qquad (3)$$

REFERENCE SIGNAL GENERATION

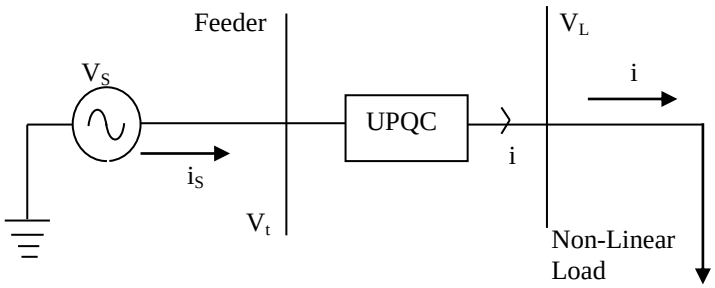


Fig.2 System Under Consideration

The Reference signal generation is done by using UTT theory[11]. The equations showing the generation of the reference signals are given below-

A. Series Active filter

The extraction of three-phase voltage reference signal for series APF is based on Unit Vector Template Generation, achieved with the help of PLL. These Unit Vector Templates are multiplied with the desirable peak amplitude (V_{tmn}) of load voltage to obtained reference load voltages denoted by V_{lar}, V_{lbr} and V_{lcr} for phase a, b and c respectively and are given by-

$$V'_{lar} = V_{tmn} \cdot u_a \qquad (4)$$

$$V'_{lbr} = V_{tmn} \cdot u_b \qquad (5)$$

$$V'_{lcr} = V_{tmn} \cdot u_c \qquad (6)$$

where u_a, u_b and u_c are unit vector templates which are in phase with supply voltage and are given by-

$$u_a = sin(\omega t) \qquad (7)$$

$$u_b = sin(\omega t + 120) \qquad (8)$$

$$u_c = sin(\omega t - 120) \qquad (9)$$

B. Shunt Active Filter

Unit vector template generation theory is again used here. These Unit Vector Templates are multiplied with the desirable peak amplitude I_{tmn} to obtain the reference currents denoted by I_{lar}, I_{lbr} and I_{lcr} for phase a, b and c respectively and are given by-

$$I'_{lar} = I_{tmn} \cdot i_a \qquad (10)$$

$$I'_{lbr} = I_{tmn} \cdot i_b \qquad (11)$$

$$I'_{lcr} = I_{tmn} \cdot i_c \qquad (12)$$

Where i_a, i_b and i_c are unit vector templates which are in phase with supply current and are given by-

$$i_a = sin(\omega t) \qquad (13)$$

$$i_b = sin(\omega t + 120) \qquad (14)$$

$$i_c = sin(\omega t - 120) \qquad (15)$$

HYSTERSIS CURRENT CONTROL METHOD

In this method, the actual current continually tracks the command current within a hysteresis-band. Pre-set upper and lower tolerance limits are compared to the extracted error signal. As long as the error is within the tolerance band, no switching action takes place. Switching occurs whenever the error leaves the tolerance band. The hysteresis current control is the fastest method with minimum hardware and software. In this article the hysteresis current control method is used, because of its simplicity of implementation and robustness. This strategy provides satisfactory control of current without requiring extensive knowledge of control system model or its parameters.

SIMULATION WITHOUT UPQC: The simulation waveforms are given as figure 3 for load voltage and current source ,figure 4 shows THD in source current and whereas figure 5 shows THD in load voltage without UPQC

The simulation Circuits and waveforms are given below

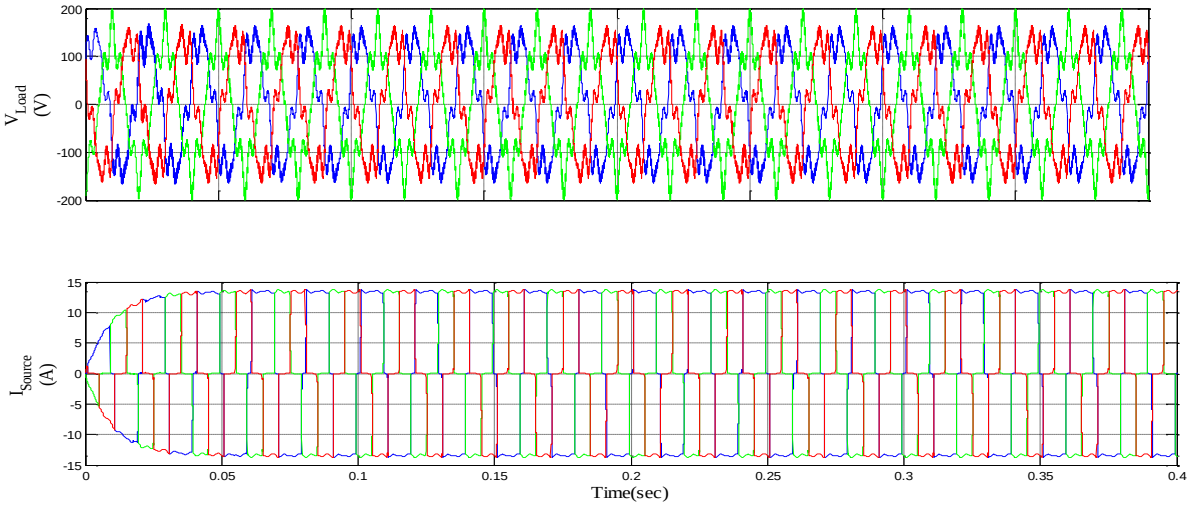


Fig.3. Load Voltage and Source Current without UPQC

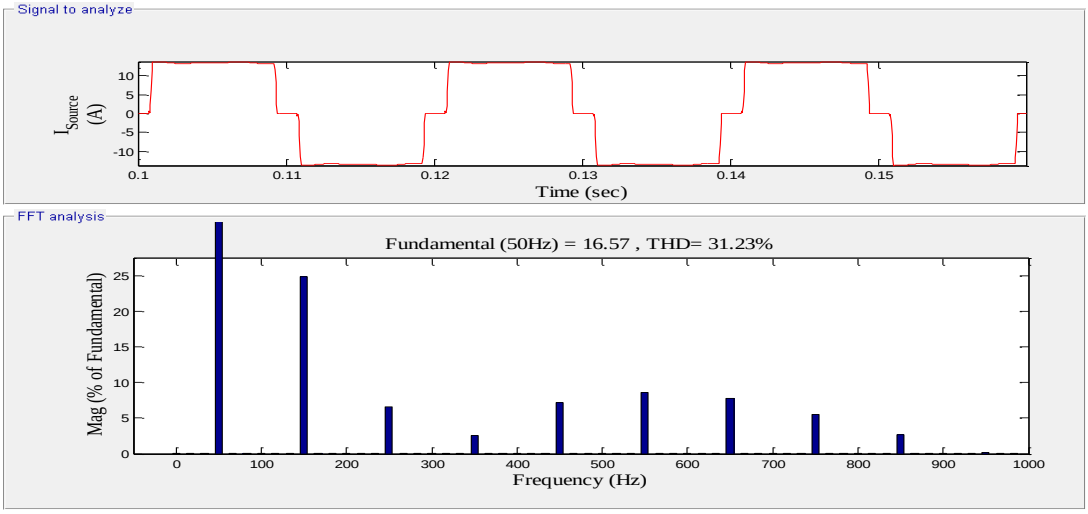


Fig.4. THD in source current without UPQC.

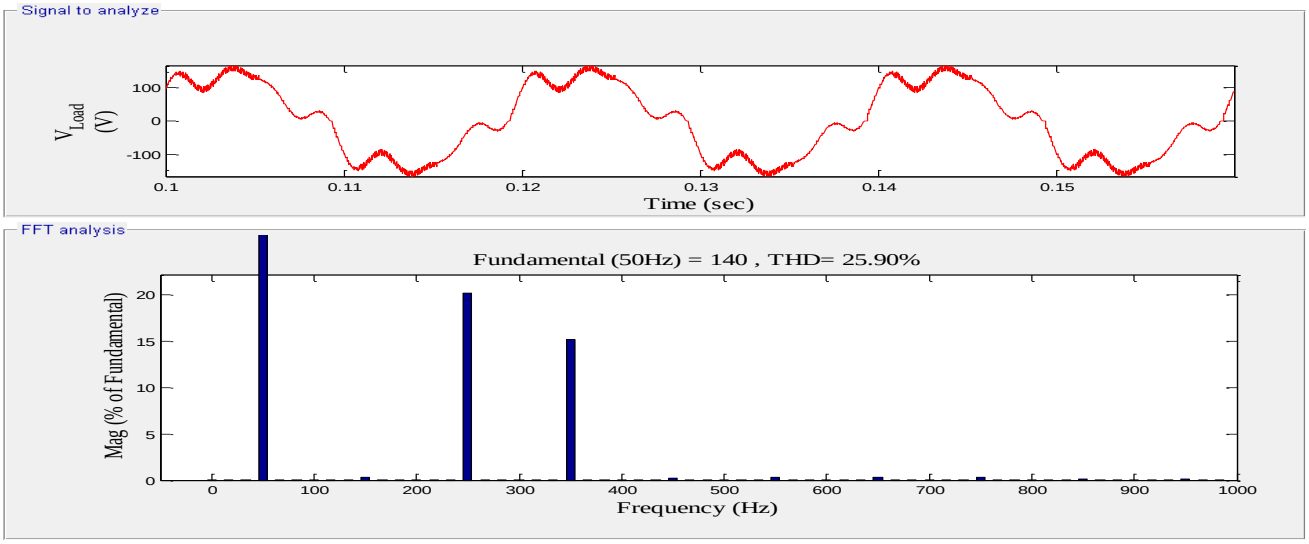


Fig.5. THD in Load Voltage without UPQC

IV. SIMULATION RESULTS AND DISCUSSION

The objectives of work carried out can be summarized as follows:

1. Reduction in the harmonics in the voltage at PCC.
2. Reduction in the harmonics in the source current.

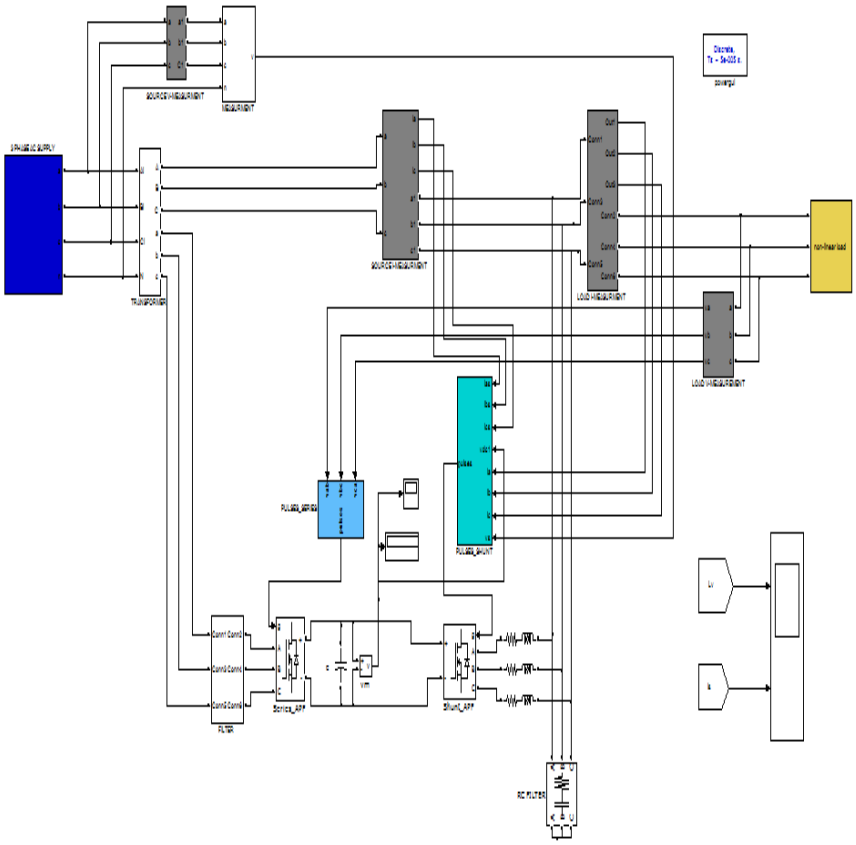


Fig 6 : Simulation model of circuit with rectifier fed RL Load using UPQC.

SIMULATION WITH UPQC

Simulation model of circuit using unified power quality conditioner is given figure 6 below along with their corresponding waveforms of voltage at PCC and source current shown in figure 7. In the present study, hysteresis band gap controllers and Unit Vector Template Technique(UTT) generation theory are used for both series and shunt active power filters. To show the clear operation of UPQC, both Series active power filter and shunt active power filter are put in operation at t = 0.1s so that the distorted current and voltage waveform can be shown in a single diagram along with compensated voltage and current waveforms. To show the improvement in power quality improvement in distribution network as shown in table .The response of UPQC for THD in load voltage and THD in source voltage shown in figure 8 & 9.

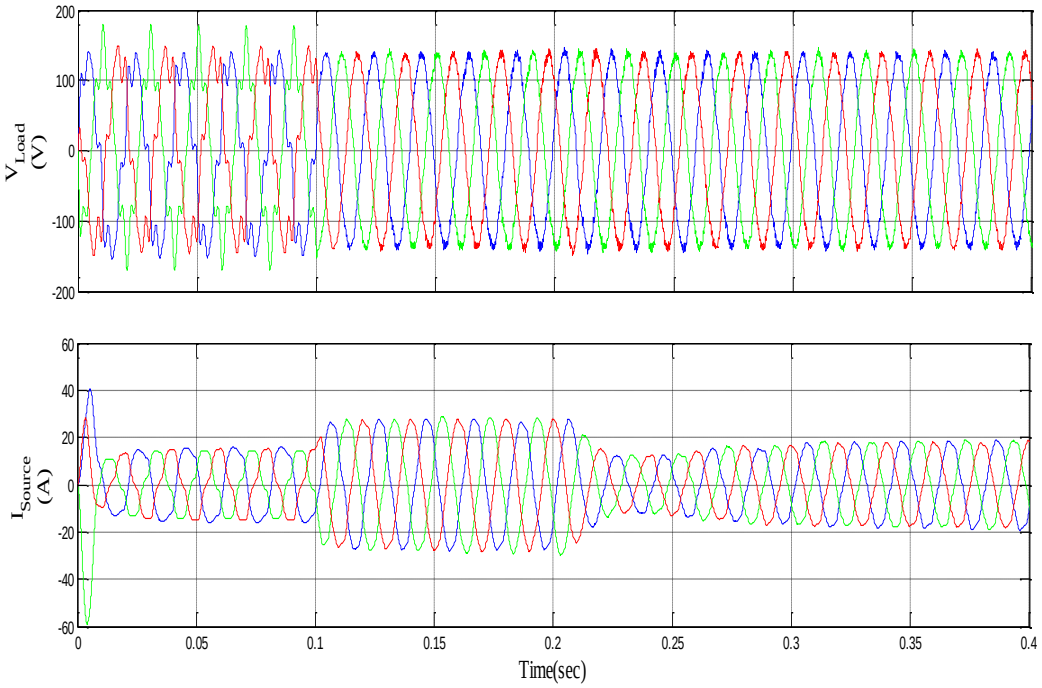


Fig.7. Load Voltage and Source Current with UPQC

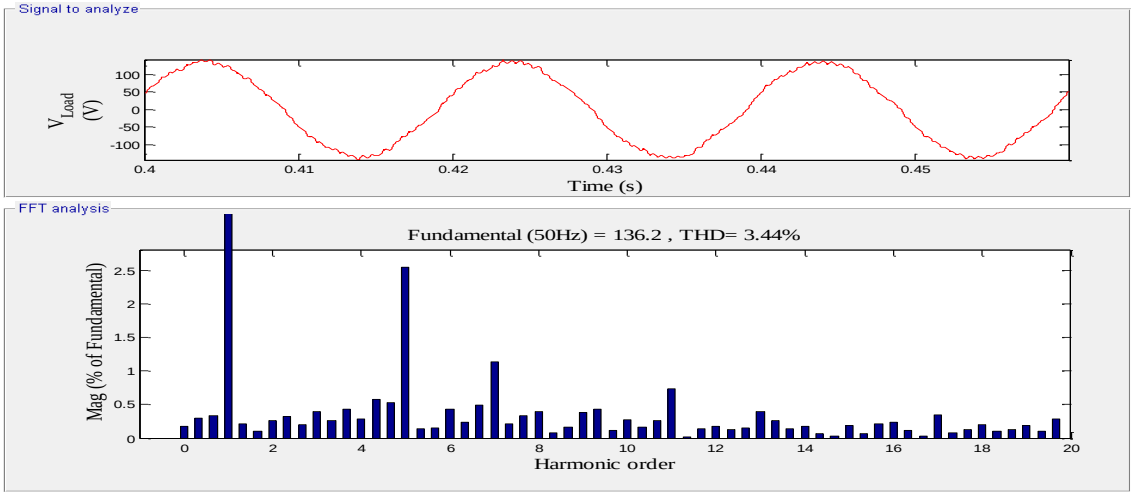


Fig.8. THD in Load Voltage using UPQC.

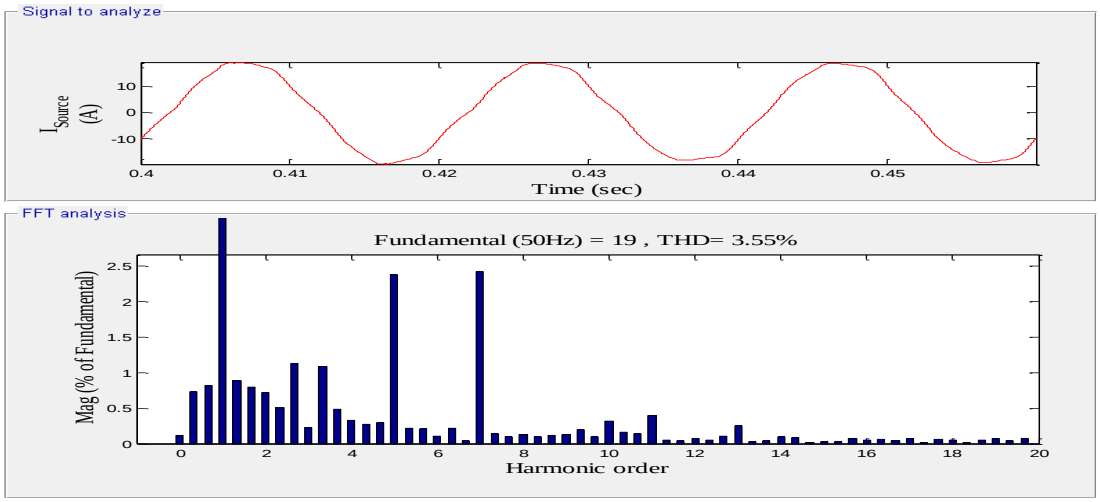


Fig.9. THD in Source Voltage using UPQC.

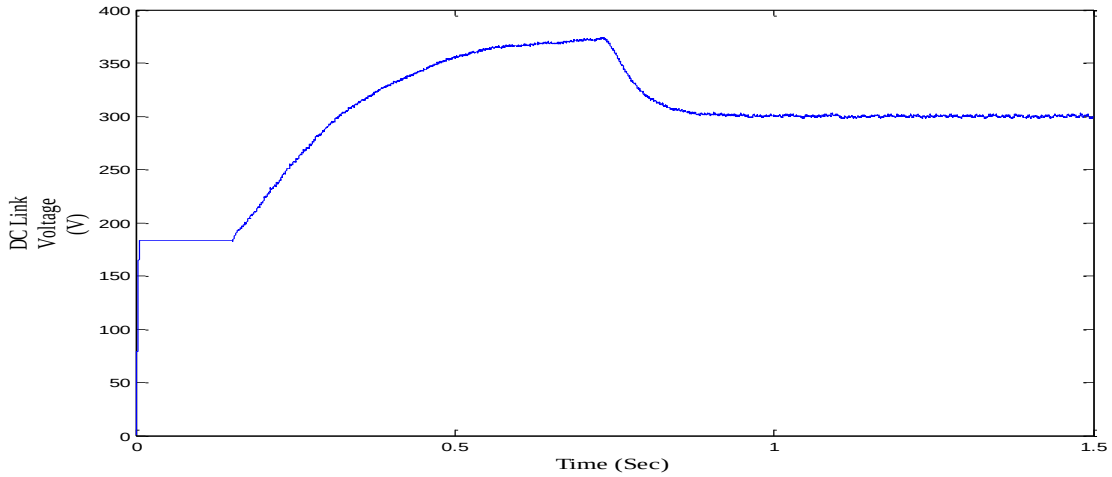


Fig 10 : DC Link Voltage

V. Result & Discussion

The THD in voltage and current is calculated using Fast Fourier Transform and is given by:

$$THD = \frac{\sqrt{\sum_{n}^{\infty} V_n^2}}{V_1} \qquad (1)$$

Where V_n denotes the magnitude of the n harmonic voltage and V_1 is the magnitude of the fundamental voltage. Similar expressions can also be written for current harmonics. The response of DC link voltage corresponding to time shown in figure 10.

Table 1: Simulation Results

Sr No	Without UPQC	With UPQC
1	THD in source current 31.23 %	THD in source current 3.55 %
2	THD in voltage at PCC 25.90 %	THD in voltage at PCC 3.44 %

From Table -1 it can be elucidated that the use of UPQC has considerably reduced the THD in source current from more than 30% to only about 3.55% which is well within the IEEE tolerance limits of 5.0%. The THD in voltage waveform has also reduced from about 25% to about 3.44% which also is within the IEEE tolerance limits.

Thus, the overall quality of the power has considerably improved by employing UPQC.

VI. CONCLUSIONS

The UPQC has become the most important technique for improvement of power in electrical power distribution systems. In this paper, a model for 3-phase UPQC for non-linear loads connected at PCC is simulated using MATLAB/ Simulink for the reduction of harmonics in voltage at PCC. The simulation studies demonstrate the Performance of UPQC

The performance of UPQC is verified with simulation results. From the results, it is clear that the harmonics have reduced by

nearly 7-8 times .The THD in voltage at PCC without using UPQC was about 25.90%.The THD in voltage at PCC reduced to about 3.55% after using the UPQC.THD in source current reduced to about 3.44% from more than

30%.Harmonics levels are maintained below IEEE-519 standards.

APPENDIX

The system parameters are used as follows:
Source voltage: 110(ph-ph), 50Hz
Transformer: 1000VA, 240/24, 50Hz
Filter: R=16Ω, 200μF
Load: a three-phase diode bridge
rectifier with R=20Ω and L=100mH on DC side.

REFERENCES

[1] Srinivas Bhaskar Karanki, Nagesh Geddada, Mahesh K. Mishra and B. Kalyan Kumar,"Modified Three-Phase Four-Wire UPQC Topology with Reduced DC-Link Voltage Rating," *IEEE Trans. Industrial Electronics*, vol.60, no.9, Sept.2012.
[2] B.Singh and V.Verma, "A New Control Scheme of Series Active Filter for Varying Rectifier Loads," *IEEE Conf. Power Electron.* , vol.1, pp. 612-620, 1997.
[3] Metin Kesler and Engin Ozdemir, "Synchronous-Reference-Frame-Based Control Method for UPQC Under Unbalanced and Distorted Load Conditions*," IEEE Trans. Industrial Electronics*,vol.58, no.9, Sept.2011.
[4] Norman Mariun, AhsanulAlam, SenamMehmod and HashimHisram, "Review of control strategy for power quality conditioner", *In Proc. National Power & Energy Conference (PECon)*, pp. 109-115, Malaysia. Nov 2004.
[5] Naresh K. Kummari, Asheesh K. Singh, "Comparative Evaluation of DSTATCOM Control Algorithms for Load Compensation," *IEEE Conf. Industrial Harmonics and Quality of Power*, pp. 299-306, 2012.
[6] Yash Pal and A. Swaroop, "Performance of UPQC for power quality improvement," *IEEE PEDES. Joint Internatinal conf.* , pp.1-7, 2010.
[7] L. H. Tey, andP. L. So, "System Harmonics Compensation using PWM Voltage Source Inverter-Based Active Filters", *In Proc. IEEE Power Tech Conference* vol.1, Portugal ,Sept. 2001.
[8] Vinod Khadkikar, "Enhancing Electric Power Quality Using UPQC: A Comprehensive Overview," *IEEE Trans. Power Electron.*, vol. 27, pp.2284-2297, 2012.
[9] Enio R. Ribeiro and Ivo Barbi, "Harmonic Voltage Reduction Using a Series Active Filter Under Different Load Conditions", *IEEE Trans. Power Electronics*, Vol. 21, No. 5, Sept. 2006.
[10] P. Salmeron and S. P. Litran, "Improvement of the Electric Power Quality Using Series Active and Shunt Passive Filters", *IEEE Trans. Power Delivery*, Vol. 25, No. 2, April 2010.
[11] S.P. Litan, P. Salmeron, R.S.Herrera, J.R. Vazquez, "Control of Series Active Filter by state feedback," *Comision IEE Proc.Electr.Power Appl.*, vol, 151,no.3, pp. 276-282, May 2004.



J.N Rai, received the Ph.D degree in Electrical Engineering in 2016 from Jamia Millia Islamia (Central University). His research interest are in Power generation, Power system modeling , Power system Operation & Control and Advanced Modeling and Control Techniques applied to Power Plant. He is currently working as a Professor in Department of Electrical Engineering, Delhi Technological University (formerly Delhi College of Engineering), India.



Ram Bhagat, received the B.TechM.E. degree in Electrical Engineering in 1997and 2004 respectively. His research interest are in Analog Signal Processing, Control System and Automation. He is currently working as an Assistant Professor in Delhi Technological University (formerly Delhi College of Engineering), India.

View publication stats

International Journal of Research in Engineering and Innovation (IJREI)
journal home page: http://www.ijrei.com
ISSN (Online): 2456-6934



Identification and statistical analysis of performance parameters of it enabled supply chain management system

Sanjeev Kumar[1], R. S. Mishra[2]

[1]*Phd Scholar, Department of Mechanical, Production & Industrial Engineering, Delhi Technological University, Delhi*
[2]*Professor, Department of Mechanical, Production & Industrial Engineering, Delhi Technological University, Delhi*

Abstract

The increasing use and application of information technology in supply chain management can be attributed to the performance improvements and value creation in organizations. There has been a considerable evolution of scientific investigations over the past few years. From a comprehensive and updated literature review, it has been observed that use of IT systems have a great impact on performance of the organization. The application of electronic data interchange, enterprise resource planning systems, such as SAP and Oracle has been extended to supply chain partnership, enabling supply chain partners to plan and synchronize their processes. Effective performance measurement is key area for successful implementation of strategy. Individual firms must choose the performance measures that reflect the unique operations of their business. The performance parameters of strategic, tactical, and operational level were identified. To perform statistical analysis, principal component extraction method of factor analysis with varimax rotation was applied using SPSS software. © 2018 ijrei.com. All rights reserved

Key words: Natural convection solar hot water systems, Pressurized and non-pressurized solar water heating systems

1. Introduction

Any business is composed of three main activity namely input, processing and output. If we consider the manufacturing sector, the processing activity is performed the firm itself, the input to the firm are man machine and material and further the output is the product of the company. According to Sukati et. al. (2012), supply chain is the set of nodes or activities through which values are added and connects the enterprise's suppliers as well as its customer. As the size of the organization or business increases the number of the intermediate units or sub units also surges and the supply chain network become large and complex and this complex network is very difficult to manage or coordinate. But with the advent of the electronic information system or technology and computer it is become quite easy to handle or coordinate such complex network. Marinagi et al. (2014); Subramanian and Gunasekaran (2015) told that techniques of information technology and methods can help companies to become efficient, increase their productivity and thereby respond rapidly to customer needs. The implementation of information technology in businesses should be incorporated in active areas. Barros et al. (2015) proposed a model depicting the evaluation of the influences of the adoption of Information are Cost reduction, Operational efficiency and process improvement, Quality, reliability, and accuracy of information, Integration and collaboration. Premkumar G. P. (2000); Shaik M. N. and Abdul K. W. (2013) explained that the adoption of inter organizational information systems (IOS) for supply chain management has been proposed to enable external integration which include Electronic Data Interchange (EDI) networks, extranets, customer oriented strategic systems, electronic commerce (e-commerce) and electronic markets. Rylkova Z. and Bernatik W. (2013) emphasized that to obtain objectives or ensure continuous improvement, the performance of the processes must be measured

2. Literature Review

Sukati et al. (2012) told that a supply chain may be described as the set of values adding activities connecting the suppliers and its customers of the enterprise. Marinagi (2014) defines supply chain that a supply chain is a system that contains of dealers, producers, warehouses, distributors and retailers who

Corresponding author: R.S. Mishra
Email Id: hod.mechanical.rsm@dtu.ac.in

coordinate their strategies and actions in order to translate raw resources to finished goods to deliver to the ultimate user. Gunasekaran A. and Ngai E. W. T. (2004) explored in their research that effective supply chain management is important to build and sustain competitive advantage in product and services of the firms. Barua et al. (2004); Rai A., Patnayakuni R. and Seth N. (2006); Huo et al. (2015) told that although information technology can potentially boost supply chain management, many firms fail to realize this potential due to the lack of supply chain coordination over information technology, or since their dealing associates may not have the capability to align with them.. Marinagi et al., (2011) and Torabizadeh et al. (2012), told that alignment of information systems with supply chain management strategies and explained how they affect on supply chain and performance of the organization. Jeyaraj A. and Seth B. (2010) and Subramanian and Gunasekaran (2015) demonstrate that the information technology of a supply chain refer to handling information flows in modern, global supply chains. Bayraktar et al. (2009) told that due to intensifying competition in global markets, today's most of the companies have been increasingly integrating supply chain management with information systems practices. In their research they found that there is a moderating impact with regard to the relationship between information systems practices and operational performance. Singh A. and Teng J. T. C. (2016) suggested that where Inter-organizational system empowered B2B e-commerce arrangements were found to reduce transactional costs.
Gunasekaran et al. (2001) explained the supply chain performance as its overall productivity and effectiveness. Beamon (1999) recommends three aspects for measuring supply chain performance, namely, assets measurement, productivity measurement, and flexibility. Singh et al. (2016), define supply chain performance for tractability, incorporation, and customer responsiveness**.** According to Kumar et al. (2015), performance measurement can be defined as the process of quantifying the effectiveness of various procedures being followed by the business.

2.1 Identification of performance parameters

Frohlich (2002); Rai A., Patnayakuni R. and Seth N. (2006), explained that for effective measurement of performance and improvement, goals of measurement must represent organizational goals and metrics selected should show an equal approach between financial and non-financial measures that can be related to strategic, tactical and operational levels of decision making and control. By the extensive literature review twenty seven parameters are chosen, as shown in Table-1.

2.2 Research Methodology

Research methodology in this work includes, development of questionnaire, data collection, and statistical analysis of the collected data with reference to the identified performance parameter.

2.3 Questionnaire Development

A questionnaire is developed on five point likert scale, in which '1' is taken for the least importance and '5' for the most importance. This questionnaire consists of three segments. In the first segment, the detail of industry was asked from field experts in which they are working. The second segment includes the twenty seven performance parameters of strategic, tactical and operational level in combined form. The third segment or the last segment of the questionnaire includes details of the profile of the field expert. This questionnaire is uploaded on the google in the form of google form for data collection. The respondents for questionnaire were the field experts, working in different industries in Delhi NCR mostly in automobile sector; however some field experts are from other industries. The Questionnaire is sent to two hundred seventeen number of the field experts, working in different organization located near about National Capital Region Delhi for their response. The mode of communication of the questionnaire was mainly email; however the responses were received on the google form. Total sixty responses were received. Hence the response rate is 27.64%

2.4 Statistical Analysis

The reliability test of collected data is done using SPSS software. The value of Cronbach's alpha (α) for the collected data comes as 0.932. According to Liu et al. (2013); Kumar et al (2015) and Nunnally (1978) the value of Cronbach's α, should exceeds the minimum requirements of 0.5 for an exploratory study. Hence on the basis of the Cronbach's α reliability test, our data may be utilized for further exploratory study.

3. Result and Discussion

The result of the reliability test shows that the collected data is fit for the exploratory study. To perform the factor analysis, principal component extraction method was applied with spss software support.

Table 1: Performance parameters

S. N	Parameter	References	Remarks
1	Proper responsiveness to urgent orders	Bhagwat R. and Sharma M. K.(2007); Rossiter J. R. (2009); Joshi S. (2013); Qrunfleh S. and Tarafdar M. (2014); Huo B. et al. (2015).	Urgent orders are taken on priority as compared to the existing orders, and organization equipped with IT has to deal with this situation properly.
2	Forecast ease for market demand	Bhagwat R. and Sharma M. K.(2007); Tracht K. et al. (2013); Colin M. et al. (2015); Kumar R. et. al. (2015).	IT enabled supply chain helps for market demand forecasting i.e. to know about the near future sale or consumption.
3	Productivity improvement	Marinagi C. et al. (2014); Barros A. P. D. et al. (2015).	It means the number of item of required quality produced or amount of service given in a specified time.
4	Proper visualization of customer needs	Marinagi C. et al. (2014); Qrunfleh S. and Tarafdar M. (2014); Barros A. P. D. et al. (2015); Huo B. et al. (2015); Kumar R. et al. (2015).	IT enabled supply chain helps in understanding that what the customer wants.
5	Total lead time reduction	Tracht K. et al. (2013); Azfar K. R. W. et al. (2014); Colin M. et al. (2015).	It means the time elapsed between the moment customer places an order and get the delivery. IT enabled supply chain helps in reduction of total lead time
6	Total Inventory cost reduction	Tracht K. et al. (2013); Azfar K. R. W. et al. (2014); Qrunfleh S. and Tarafdar M. (2014); Kumar R. et al. (2015).	Less number of items for less time are stored in IT enabled supply chain.
7	Increase the level of Customer satisfaction	Tracht K. et al. (2013); Barros A. P. D. et al. (2015).	
8	Improve the relationships with suppliers and customer relation	Tracht K. et al. (2013); Marinagi C. et al. (2014); Barros A. P. D. et al. (2015).	In IT enabled supply chain it is very easy make fast and clear communication with supplier and customer hence improved relationship.
9	Proper visibility among the supply chain stages	Azfar K. R. W. et al. (2014); Qrunfleh S. and Tarafdar M. (2014).	IT enabled supply chain has proper visibility among its stages
10	Helps in enhancing the cooperation among the existing stages	Rylkova Z. and Bernatik W. (2014); Marinagi C. et al. (2014); Subramanian N. and Gunasekaran A. (2015).	Information Technology enhances the cooperation among the existing stages of supply chain
11	Helps in Maintaining the stability in the competitive market place	Marinagi C. et al. (2014); Subramanian N. and Gunasekaran A. (2015).	IT enabled sc helps to understand the strategy of the competitor and the decision are taken accordingly, which helps in Maintaining the stability in the competitive market place.
12	Easiness in Decision making	Luthra S. and Haleem A. (2015); Colin M. et al. (2015); Singh A. and Teng J. T.C. (2016).	As the required information for making a decision is received fast and correct, the manager feels easiness in Decision making.
13	Reduction in coordination cost	Marinagi C. et al. (2014); Colin M. et al. (2015); Singh A. and Teng J. T.C. (2016).	There is no need to go everywhere physically and the communication may be made easily and fast in IT enabled supply chain, which reduces coordination cost
14	Information processing capability	Marinagi C. et al. (2014); Colin M. et al. (2015); Singh A. and Teng J. T.C., (2016),	IT enabled supply chain enhances information processing capability
15	partnership structure enhancement	Marinagi C. et al. (2015); Barros A. P. D. et al. (2015); Singh A. and Teng J. T.C. (2016).	Due the transparency ease, clarity and proper visibility in the business, IT enabled supply chain enhances the structure of partnership
16	Helps in automation of exchange procedures	Singh A. and Teng J. T.C. (2016).	Automation means the no interfere of human for the activity and the IT enabled supply chain makes the automation of exchange procedures.
17	Reduction in uncertainty	Koh S.C.L. and Saad S. M. (2006); Bayraktar E. et al. (2009); Singh A. and Teng J. T.C. (2016).	Use of the Information Technology reduces uncertainty in any business activity.
18	Reduction of non-value added activities	Qrunfleh S. and Tarafdar M. (2014); Azfar K. R. W. et al. (2014).	IT enabled supply chain, non-value added activities are reduced
19	Improve the Reengineering capability	Denolf J. M. et al. (2015); Barros A. P. D. et al. (2015).	Use of the Information Technology, due to its vast application in the business sphere, its reengineering capability is improved.

20	Improve the Capability to integrate different business activities	Bayraktar E. et al. (2009); Marinagi C. et al. (2014); Barros A. P. D. et al. (2015); Colin M. et al. (2015).	Any business includes various smaller or sub activities and for a effective business all the sub activities are to be joined in proper manner.
21	Reduce the customer order path	Gunasekaran A. et al. (2004); Denolf J. M. et al. (2015).	Use of the Information Technology, reduces the customer order path i.e. the channels or the steps which have to approach by the customer to place an order.
22	Reduce the Purchase order cycle time	Gunasekaran A. et al. (2004); Colin M. et al. (2015); Kumar R. et. al. (2015).	Use of the Information Technology, reduces the Purchase order cycle time i.e. the time elapsed to place a purchase order; hence the IT enabled supply chain.
23	Flexibility capability Enhancement	Gunasekaran A. et al. (2004); Azfar K. R. W. et al. (2014).	Flexibility means to fulfill the varying demand of the customer without the major change in the existing setup of the organization.
24	Helps in Quality improvement	Gunasekaran A. et al. (2004); Qrunfleh S. and Tarafdar M. (2014).	IT enabled supply chain helps in Quality improvement
25	Improvement in the Effectiveness of scheduling techniques	Gunasekaran A. et. al. (2004); Tracht K. et al. (2013),	Scheduling means that the clock and calendar time fixed to do an activity and use of the Information Technology in scheduling techniques i.e. JIT, MRP and MIS etc improves the effectiveness of scheduling techniques
26	Reduction in customer query time	Gunasekaran A. et al. (2004); Qrunfleh S. and Tarafdar M. (2014); Kumar R. et al. (2015).	When a customer seeks the information about the product or service, the time elapsed for it is reduced by use of the Information Technology.
27	Helps the Top Management in taking Initiative for an activity	Luthra S. and Haleem A. (2015); Denolf J. M. et al. (2015); Kumar R. et. al. (2015).	IT enabled supply chain helps the Top Management in taking Initiative for an activity

Table 2: Total Variance Explained

	Initial Eigenvalues			Extraction Sums of Squared Loadings			Rotation Sums of Squared Loadings		
Component	Total	% of Variance	Cumulative %	Total	% of Variance	Cumulative %	Total	% of Variance	Cumulative %
1	10.250	37.962	37.962	10.250	37.962	37.962	3.764	13.941	13.941
2	2.275	8.425	46.388	2.275	8.425	46.388	3.423	12.676	26.617
3	1.854	6.865	53.253	1.854	6.865	53.253	3.227	11.952	38.569
4	1.634	6.053	59.306	1.634	6.053	59.306	3.036	11.244	49.813
5	1.422	5.265	64.571	1.422	5.265	64.571	2.399	8.884	58.697
6	1.369	5.071	69.643	1.369	5.071	69.643	2.378	8.806	67.503
7	1.113	4.121	73.764	1.113	4.121	73.764	1.691	6.261	73.764
8	0.976	3.615	77.380						
9	0.788	2.919	80.298						
10	0.675	2.501	82.800						
11	0.673	2.492	85.292						
12	0.543	2.013	87.305						
13	0.500	1.852	89.157						
14	0.421	1.559	90.716						
15	0.370	1.372	92.088						
16	0.342	1.268	93.355						
17	0.289	1.070	94.426						
18	0.265	0.983	95.409						
19	0.260	0.961	96.370						
20	0.221	0.820	97.190						
21	0.210	0.776	97.966						
22	0.161	0.596	98.562						
23	0.134	0.496	99.058						
24	0.096	0.357	99.415						
25	0.079	0.291	99.706						
26	0.047	0.173	99.879						
27	0.033	0.121	100.000						
Extraction Method: Principal Component Analysis.									

Table 3: Case Processing Summary

		N	%
Cases	Valid	56	93.3
	Excluded[a]	4	6.7
	Total	60	100.0
a. List wise deletion based on all variables in the procedure.			

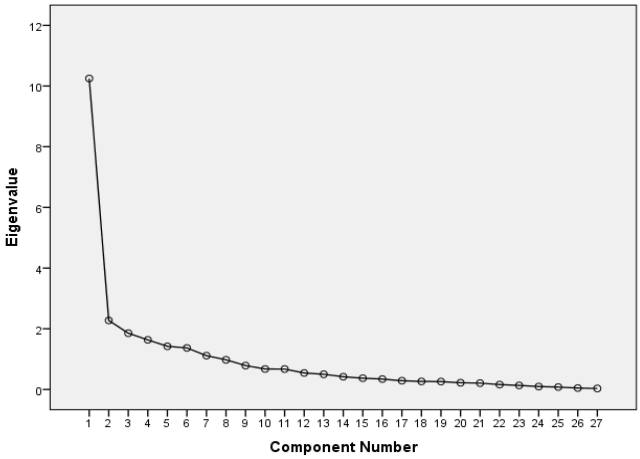


Figure 1: Variation of eigen value and component number

In the fig. 1 the scree plot is drawn, showing eigen values of the all of the twenty seven parameters. In this plot, the components are taken on the horizontal axis and the eigen value of the parameters are given on the vertical axis. It may be seen from the scree plot that there are seven parameters those have the eigen value more than 1.

The eigen value, extraction sum of square loading and rotation sum of square loading of the components are calculated in terms of the total, percentage variable and percentage cumulative using principal component analysis of extraction method. The component matrix is given in table 5, showing the factor loading of the components and on the basis of the factor loading, seven components have been extracted.

Table 4 Reliability Statistics

Cronbach's Alpha	N of Items
.932	27

Table 5: Component Matrix

	Component						
	1	2	3	4	5	6	7
VAR00022	0.784						
VAR00011	0.776						
VAR00026	0.775						
VAR00012	0.768						
VAR00020	0.751						
VAR00008	0.744						
VAR00003	0.674		-0.534				
VAR00019	0.670				-0.552		
VAR00024	0.654						
VAR00005	0.651						
VAR00021	0.624						
VAR00027	0.620						
VAR00014	0.604	0.509					
VAR00017	0.597						0.469
VAR00013	0.590						
VAR00007	0.589		-0.535				
VAR00015	0.567		0.465				
VAR00018	0.566	-0.475					
VAR00002	0.560						
VAR00004	0.549		-0.449				
VAR00016	0.545		0.418				
VAR00006	0.540				0.484		
VAR00009	0.537	-0.515					
VAR00025	0.496	0.565					
VAR00023		0.563	0.406				
VAR00001				0.771			
VAR00010	0.540					0.550	
Extraction Method: Principal Component Analysis.							
a. 7 components extracted.							

Table 6: Rotated Component Matrix

	Component						
	1	2	3	4	5	6	7
VAR00013	0.728				0.436		
VAR00005	0.707	0.440					
VAR00019	0.690					0.445	
VAR00020	0.575		0.491				
VAR00022	0.569						
VAR00012	0.510			0.419			
VAR00004		0.775					
VAR00003		0.749					
VAR00007		0.744					
VAR00026		0.544			0.419		
VAR00016			0.668			0.431	
VAR00027			0.660				
VAR00021	0.567		0.608				
VAR00006		0.441	0.579				
VAR00015			0.504	0.415			
VAR00010				0.814			
VAR00009				0.785			
VAR00011				0.627			
VAR00008		0.462		0.487			
VAR00024							
VAR00025					0.746		
VAR00023					0.743		
VAR00014	0.446				0.560		
VAR00018						0.784	
VAR00017						0.743	
VAR00001							0.795
VAR00002			0.533				0.541
Extraction Method: Principal Component Analysis. Rotation Method: Varimax with Kaiser Normalization.[a]							
a. Rotation converged in 27 iterations.							

Table-7: Component Transformation Matrix

Component	1	2	3	4	5	6	7
1	0.508	0.445	0.445	0.414	0.259	0.313	0.095
2	0.230	-0.113	0.062	-0.396	0.722	-0.445	0.234
3	-0.178	-0.770	0.441	0.208	0.203	0.311	0.002
4	-0.368	0.115	-0.139	0.139	0.031	0.153	0.888
5	-0.654	0.361	0.507	0.100	0.126	-0.347	-0.199
6	-0.070	-0.083	-0.501	0.720	0.354	-0.246	-0.180
7	-0.298	0.216	-0.276	-0.284	0.478	0.634	-0.277
Extraction Method: Principal Component Analysis. Rotation Method: Varimax with Kaiser Normalization.							

In the rotated component matrix, it is shown that which factor contributes a component significantly. Factor loading above 0.6 is taken as the significant loading. The factors having loading less than 0.6 will be eliminated from the further study. Also, using the rotated component matrix, the remaining factors are grouped into the seven components based upon the factor loading. For example, factors 13, 5, 19, 20, 22, 12, 21 and 14 have loading 0.728, 0.707, 0.690, 0.575, 0.569, 0.510, .567 and 0.446 respectively, for component 1. So, the factors 20, 22, 12, 21 and 14 may be considered as eliminated and the factors 13, 14 and 19 will be considered as the part of the component 1 for the further study. Similarly, component 2 comprises of factors 4, 3 and 7, component 3 comprises factors 16, 27 and 21, component 4 comprises of factors 10, 9 and 11, component 5 comprises of factors 25 and 23, component 6 comprises of 18 and 17 and component 7 comprises of factors 1. The retained factors are given in table 8.

Table 8: Retained Factor

S. No.	Parameter Number and Name
1	(5) Total lead time reduction
	(13) Reduction in coordination cost
	(19) Improve the Reengineering capability
2	(4) Proper visualization of customer needs
	(3) Productivity improvement
	(7) Increase the level of Customer satisfaction
3	(16) Helps in automation of exchange procedures
	(27) Helps the Top Management in taking Initiative for an activity
	(21) Reduce the customer order path
4	(10) Helps in enhancing the cooperation among the existing stages
	(9) Proper visibility among the supply chain stages
	(11) Helps in Maintaining the stability in the competitive market place
5	(25) Improvement in the Effectiveness of scheduling techniques
	(23) Flexibility capability Enhancement
6	(18) Reduction of non-value added activities
	(17) Reduction in uncertainty
7	(1) Proper responsiveness to urgent orders

4. Result and Discussion

(i) Twenty Seven Performance Parameters as per the table 1 were identified based on the literature review and the discussion held with the field experts of the supply chain.
(ii) Reliability test is performed, in which the value of Cronbach's alpha (α) for the data collected of these twenty seven parameters was calculated 0.932 and the data is found fit for an exploratory study.
(iii) Communalities initial and after extraction of all the parameters are calculated. Total variance, the eigen value, extraction sum of square loading and rotation sum of square loading of the components are calculated in terms of the total, percentage variable and percentage cumulative using principal component analysis of extraction method.
(iv) The Scree plot for the components is given in the figure 1, which shows that there are seven components having Eigen values greater than 1.Scree plot is drawn, which shows there are seven components having eigen value greater than 1.
(v) Based the statistical analysis the parameters having poor loading extracted from further study and remaining are grouped into seven components as per the table 2.

In the rotated component matrix, it is shown that which factor contributes a component significantly. Factor loading above 0.6 is taken as the significant loading. The factors having loading less than 0.6 will be eliminated from the further study. Also, using the rotated component matrix, the remaining factors are grouped into the seven components based upon the factor loading. For example, factors 13, 5, 19, 20, 22, 12, 21 and 14 have loading 0.728, 0.707, 0.690, 0.575, 0.569, 0.510, .567 and 0.446 respectively, for component 1. So, the factors 20, 22, 12, 21 and 14 may be considered as eliminated and the factors 13, 14 and 19 will be considered as the part of the component 1 for the further study. Similarly, component 2 comprises of factors 4, 3 and 7, component 3 comprises factors 16, 27 and 21, component 4 comprises of factors 10, 9 and 11, component 5 comprises of factors 25 and 23, component 6 comprises of 18 and 17 and component 7 comprises of factors 1. The retained factors are given in table 8.

5. Conclusion

For the performance evaluation of the IT enabled supply chain, twenty seven performance parameters were identified based on the literature review and the discussion held with the field experts of the supply chain. Reliability test is performed, in which the value of Cronbach's alpha (α) for the data collected of these twenty seven parameters was calculated 0.932 and the data is found fit for an exploratory study. Communalities initial and after extraction of all the parameters are calculated. Total variance, the eigen value, extraction sum of square loading and rotation sum of square loading of the components are calculated in terms of the total, percentage variable and percentage cumulative using principal component analysis of extraction method. Based the statistical analysis the parameters having poor loading extracted from further study and remaining are grouped into seven components.

References

[1] Azfar K. R. W., Khan N. and Gabriel H.F., (2014), "Performance Measurement: A Conceptual Framework for Supply Chain Practices", Procedia - Social and Behavioral Sciences 150.
[2] Barros A. P. D., Ishikiriyama C. S., Rafael C. P. and Carlos F. S. G., (2015), "Processes and benefits of the application of information technology in supply chain management: an analysis of the literature," Procedia - Social and Behavioral Sciences 175.
[3] Barua A., Konana P., Whinston A.B. and Yin F. (2004), "An empirical investigation of eneabled business value," MIS Quarterly, 28, 585-620.
[4] Bayraktar E., Demirbag M., Koh S.C.L and Zaim E.T.H., (2009), "A causal analysis of the impact of information systems and supply chain management practices on operational performance: Evidence from manufacturing S M Esin Turkey", International Journal Production Economics, 122.

[5] Beamon B.M. (1999), Measuring supply chain performance, International Journal of Operation and Production Management, 19 (3), 275–292.
[6] Bhagwat R. and Sharma M. K., (2007), "Performance measurement of supply chain management: A balanced scorecard approach", Computers & Industrial Engineering, 53, 43–62.
[7] Colin M., Galindo R. and Hernandez O., (2015), "Information and Communication Technology as a Key Strategy for Efficient Supply Chain Management in Manufacturing SMEs" Procedia Computer Science 55.
[8] Denolf J. M., Trienekens M. J. H., Vorst W.J.V. and Omt S.W.F. , (2015), "Towards a framework of critical success factors for implementing supply chain information systems", Computers in Industry 68.
[9] Frohlich M. T. (2002) "e-Integration in the Supply Chain: Barriers and Performance", Decision Sciences, 33, (4), 537–556.
[10] Gunasekaran A. and Ngai E.W.T. (2004), "Information systems in supply chain integration and management" European Journal of Operational Research 159, 269–295.
[11] Gunasekaran A., C. Patel and Ronald E. M. G., (2004), "A framework for supply chain performance measurement", International Journal Production Economics, 87, 333-347.
[12] Huo B., Zhang C. and Zhao X., (2015), "The effect of IT and relationship commitment on supply chain coordination: A contingency and configuration approach", Information & Management, 52.
[13] Ince H. et al. (2013) "The Impact of ERP Systems and Supply Chain Management Practices on Firm Performance: Case of Turkish Companies" Procedia - Social and Behavioral Sciences, 99, 1124 – 1133.
[14] Jean R. B., Rudolf R. Sinkovics, and Daekwan Kim, (2008) "Information technology and organizational performance within international business to business relationships: A review and an integrated conceptual framework", International Marketing Review, 25 (5), 563 – 583.
[15] Jeyaraj A. and Seth B. (2010), "Implementation of Information Systems Infrastructures for supply chain visibility", Proceedings of the Southern Association for Information Systems Conference, Atlanta, GA, USA, March 26-27.
[16] Kumar R., Singh R. K. and Shankar R. (2015), "Critical success factors for implementation of supply chain management in Indian small and medium enterprises and their impact on performance", IIMB Management Review, 27, 92-104.
[17] Liu H. et al. (2013), "The impact of IT capabilities on firm performance: The mediating roles of absorptive capacity and supply chain agility", Decision Support Systems, 54, 1452–1462.
[18] Luthra S. and Haleem A. (2015), "Hurdles in implementing sustainable supply chain management: An analysis of Indian automobile sector" Procedia - Social and Behavioral Sciences, 189, 175 – 183.
[19] Marinagi C., Trivellas P. and Reklitis P. (2015), "Information Quality and Supply Chain Performance: The Mediating Role of Information Sharing", Procedia - Social and Behavioral Sciences 175.
[20] Marinagi C., Trivellas P. and Sakas D. P. (2014), "The impact of Information Technology on the development of Supply Chain Competitive Advantage", Science Direct Procedia - Social and Behavioral Sciences, 147, 586-591.
[21] Marinagi C. and Akrivos C. K. (2011), "Strategic Alignment of ERP, CRM and e-business: A value creation", In Advances on Integrated Information Conference Proceedings, 347-350.
[22] Premkumar G.P. (2000), "Inter organization systems and supply chain management: an information processing perspective", Information Systems Management, 17 (3), 1–14.
[23] Qrunfleh S. and Tarafdar M. (2014), "Supply chain information systems strategy: Impacts on supply chain Performance and firm performance", International Journal Production Economics, 147.
[24] Rai A., Patnayakuni R. and Seth N. (2006), "Firm Performance Impacts of Digitally Enabled Supply Chain Integration Capabilities" MIS Quarterly, 30 (2), 225-246.
[25] Rylkova Z. and Bernatik W. (2014), "Performance measurement and management in Czech enterprises", Procedia - Social and Behavioral Sciences, 110.
[26] Shaik M. N. and Abdul K. W. (2013), "Inter organizational Information Systems Adoption in Supply Chains: A Context Specific Framework", International Journal of Information Systems and Supply Chain Management, 6(1), 24–40.
[27] Singh A. and Teng J.T.C. (2016), "Enhancing supply chain outcomes through Information Technology and Trust", Computers in Human Behavior 54.
[28] Subramanian N., Gunasekaran A. (2015), "Cleaner supply-chain management practices for twenty-first-century organizational competitiveness: Practice-performance framework and research propositions", International Journal Production Economics, 164.
[29] Sukati I., Hamida A. B., Baharuna R. and Yusoffa R. M. (2012), "The Study of Supply Chain Management Strategy and Practices on Supply Chain Performance", Procedia - Social and Behavioral Sciences 40.
[30] Tan K.C., Kannan V., and Handheld R. B. (1998), "Supply chain management: supplier performance and firm performance", International Journal of Purchasing and Materials Management, 34(3), 2–9.
[31] Thomas D. J. and Griffin P. M. (1996), "Coordinated Supply Chain Management", European Journal of Operational Research, 94, 1–15.
[32] Torabizadeh M., Khatami R. M. and Noshadi A. (2012), "Effect of Information System Strategies on Supply Chain Strategies and Supply Chain Performance", World Academy of Science, Engineering and Technology, 61, 940-945.
[33] Tracht K., Niestegge A. and Schuh P. (2013), "Demand planning based on performance measurement systems in closed loop supply chains", Procedia CIRP, 12.
[34] Tyagi M., Kumar P. and Kumar D. (2014), "Selecting alternatives for improvement in IT enabled supply chain performance", International Journal Procurement Management, 7 (2), 168–182.
[35] Uysal F. (2012), "An integrated model for sustainable performance measurement in supply chain", Procedia - Social and Behavioral Sciences, 62, 689 – 694.

© 2018 IJSRSET | Volume 4 | Issue 1 | Print ISSN: 2395-1990 | Online ISSN : 2394-4099
Themed Section : Engineering and Technology

Intelligent Automated Machine (IAM) for Dispensing Ready Fried Food (RFF)

Nitin Agarwal[1] , Dr. Kapil Sharma[2], S. K. Agrawal[2] , Dr. Prabhat Sharma[3]
[1]Electronics and Communication Department Indian Institute of Technology (IITR) Roorkee, Uttarakhand , India
[2]Department of Computer Engineering Delhi Technological University, Delhi, India
[3]Visvesvaraya National Institute of Technology, Nagpur, Maharashtra, India

ABSTRACT

The present research paper generally relates to a fully automated machine for preparing food products, and particularly to a fully automatic machine for preparation and dispensing of fried foods such as chowmein or the like called as fried fast food chowmein (F3C). The FAM includes an instruction box through which the order can be placed; a plurality of openings for feeding food constituents into the machine. Further, FAM-F3C contains set of choppers for chopping various food ingredients; a boiling structure for boiling the desired constituent; a frying chamber with stirrers; an e- nose sensor to control the heat transfer to the frying box, at least two balancing devices; and a dispensing mechanism to dispense the ordered food and a rotary platform to hold the empty and filled plates with the dispensed food. The machine can quickly and automatically prepare fried fast foods (chowmein) and thus can realize an unmanned shop for such foods.

Keywords: Intelligent Automated Machine (IAM), Ready Fried Food (RFF)

I. INTRODUCTION

Day to day increasing automation in every area also giving promising automation in the area of dispensing fried fast food machines and processing food in more automated and intelligent manner. Several prior arts exist pertinent to the field of the present research and the literature discloses automatic preparation and dispensing of noodles. The device maintains the taste of packaged noodles and expedites the sales and preparation processes for user convenience by using electricity to cook the noodles and automating the noodle preparation and sales processes. The art does not disclose any method for chopping of ingredients, and stirring and frying of the ingredients. Literature describes a machine for automatic preparing of Chowmein [1-7].

Although the machine facilitates an automatic frying process, yet it does not indicate of either automatic dispensing or fully automatic preparation of food. Literature Art discloses an automatic conveyor structure for preparing and dispensing of fried fast foods. However, this Literature fails to achieve automatic boiling or chopping of ingredients. Moreover, the order of dropping the ingredients into the frying box cannot be altered and the ingredients get fried separately in their respective containers. This conveyor-based structure requires a large number of burners and containers which leads to an additional cost and size of the machine. Various software techniques are also proposed for vending machines and software developed for vending machines can go through various testing phases to provide robust vending machine [7-14].

The present research paper relates to a fully automated machine for preparation and dispensing of cooked food, more particularly to a fully automated machine for preparation and dispensing of fried fast food.

II. OBJECT OF INTELLIGENT AUTOMATED MACHINE (IAM) FOR DISPENSING READY FRIED FOOD (RFF)

A fully automated intelligent automated machine (IAM) for dispensing ready fried food (RFF)for preparation and dispensing of fried fast food for fully automatic preparation and dispensing of cooked foods includes a main frame to house various intelligent automated machine (IAM) for dispensing ready fried food (RFF)components and a first upper section consisting of food ingredient specific FAM-F3C sections, each FAM-F3C section with an opening at its upper surface to feed desired food ingredients into the machine. A fully automated intelligent automated machine (IAM) for dispensing ready fried food (RFF)for preparation and dispensing of fried fast food further includes at least one chopping means included in at least one of the FAM-F3C sections and at least one boiling structure integrated with at least one of the FAM-F3C sections. A second middle section to carry out mixing and frying of the food ingredients, the section including : at least one balancing structure , a frying chamber, an electric heating means, and an electronic nose for controlling the frying process; a third lower section to dispense the prepared food into a container and to thereafter convey the container outside the machine, a rotary platform to hold multiple take away containers; a plurality of motors to supply mechanical energy to one or more intelligent automated machine (IAM) for dispensing ready fried food (RFF)components; a user interface panel, positioned on outer wall of the main frame, includes: a display screen, an instruction box and a payment structure ; plurality of sub-supervisors to activate one or more intelligent automated machine (IAM) for dispensing ready fried food (RFF)components; and a master supervisor m communication with the plurality of sub- supervisors.

III. DETAILS OF INTELLIGENT AUTOMATED MACHINE (IAM) FOR DISPENSING READY FRIED FOOD (RFF)

The intelligent automated machine (IAM) for dispensing ready fried food (RFF)of fully automated intelligent automated machine (IAM) for dispensing ready fried food (RFF), further the chopping means are specific to the food ingredients. The intelligent automated machine (IAM) for dispensing ready fried food (RFF)of fully automated intelligent automated machine (IAM) for dispensing ready fried food (RFF), further the quantity of food ingredients is controlled optionally in a time-based or a mass-based manner.

The intelligent automated machine (IAM) for dispensing ready fried food (RFF)of fully automated intelligent automated machine (IAM) for dispensing ready fried food (RFF), further the frying chamber consists of a plurality of stirring devices. The intelligent automated machine (IAM) for dispensing ready fried food (RFF)of fully automated intelligent automated machine (IAM) for dispensing ready fried food (RFF), further the electronic nose detects and recognizes odours, flavors and smoke present in the middle section of the machine. The intelligent automated machine (IAM) for dispensing ready fried food (RFF)of fully automated intelligent automated machine (IAM) for dispensing ready fried food (RFF), further the electric heating means includes a plurality of electric heating plates. The intelligent automated machine (IAM) for dispensing ready fried food (RFF)of fully automated intelligent automated machine (IAM) for dispensing ready fried food (RFF)further includes a conveyor structure to convey the food filled container outside. The intelligent automated machine (IAM) for dispensing ready fried food (RFF)of fully automated intelligent automated machine (IAM) for dispensing ready fried food (RFF), further the rotary platform can hold variable sized take away containers. The intelligent automated

machine (IAM) for dispensing ready fried food (RFF)of fully automated intelligent automated machine (IAM) for dispensing ready fried food (RFF), further the intelligent automated machine (IAM) for dispensing ready fried food (RFF)can be instructed through the instruction box to vary the amount, degree of frying and quantity of ingredients according to the taste of the user. The intelligent automated machine (IAM) for dispensing ready fried food (RFF)of fully automated intelligent automated machine (IAM) for dispensing ready fried food (RFF), further the payment structure is optionally coin-based, card-based or user-identification-based. The intelligent automated machine (IAM) for dispensing ready fried food (RFF)of fully automated intelligent automated machine (IAM) for dispensing ready fried food (RFF), further an alert structure is conjugated to give an alert for refilling of food ingredients into the FAM-F3C sections.

In view of the foregoing, the main objective of the present research paper is to provide a fully automated machine for preparation and dispensing of cooked food, incorporating an e- nose sensor for controlled heating of the frying pan. Another objective of the present research paper is to provide a fully automated machine which integrates the mechanisms for chopping, boiling and frying of food constituents to accomplish the preparation of cooked food. Yet another objective of the present research paper is a fully automatic machine for preparation and dispensing of cooked food that can dispense a desired quantity upon acceptance of coin or a card or by authentication of the user.

Accordingly the research paper provides a fully automated machine for preparation and dispensing of cooked food, which integrates the mechanisms for chopping, boiling and frying of food constituents to accomplish the preparation of cooked food. The intelligent automated machine (IAM) for dispensing ready fried food (RFF)includes various sub-sections as shown in figure 1 and discussed like:

- ✓ an instruction box through which the order can be placed
- ✓ a plurality of openings for feeding food constituents into the machine
- ✓ set of choppers for chopping various food ingredients
- ✓ a boiling structure for boiling the desired constituent
- ✓ a frying chamber with stirrers
- ✓ a frying pan
- ✓ a sensing structure attached with the frying chamber
- ✓ at least two balancing devices and
- ✓ a dispensing mechanism to dispense the ordered food in the output area

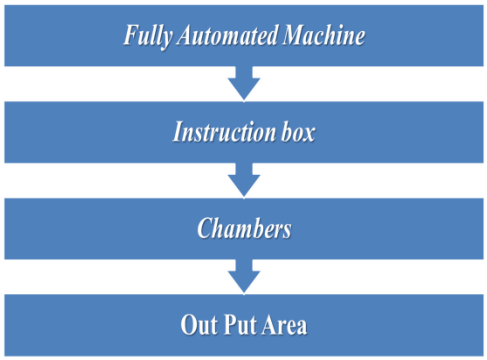


Figure 1. Basic sub-structure s of Intelligent Automated Machine (IAM) for Dispensing Ready Fried Food (RFF)

The intelligent automated machine (IAM) for dispensing ready fried food (RFF)can be divided into three major sections as shown in figure 2 and discussed below:

- ✓ a first upper section for feeding raw ingredients into the machine
- ✓ a second middle section for carrying out the frying process and
- ✓ a third lower section for dispensing the prepared cooked food item

The upper section includes various FAM-F3C sections having food ingredient specific functionalities. Some of these FAM-F3C sections include choppers and at least one of the FAM-F3C sections includes a boiling structure while other

FAM-F3C sections do not have either of choppers or boiling structure . All the above-mentioned FAM-F3C sections can also serve the purpose of storing their specific ingredients. The raw food ingredients are manually fed in to their respective FAM-F3C sections through openings to these FAM-F3C sections, where these ingredients can be chopped or boiled or simply stored.

The second section of the intelligent automated machine (IAM) for dispensing ready fried food (RFF)has a balancing structure and a frying chamber integrated with stirrers, electric heaters and an e-nose sensing structure . Certain ingredients from the upper section are first weighed by the balancing structure , and are thereafter dropped in to the frying chamber. While certain other ingredients from the upper section are directly dropped into the frying chamber. There are two types of mechanisms to drop the ingredients one is through time setting (TS) and another is through mass setting (MS). The stirrers of the frying chamber are characterized with oscillatory and rotary movements which help in homogeneous mixing and frying of the dropped ingredients.

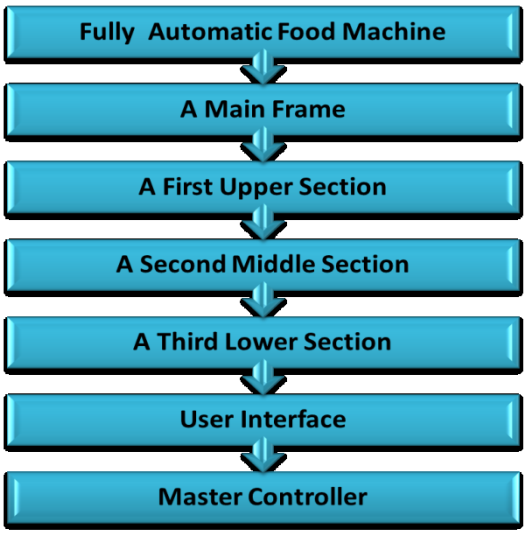


Figure 2. Major Sections of intelligent automated machine (IAM) for dispensing ready fried food (RFF)

The heat transfer to the frying chamber can be controlled by an electronic nose (e-nose) sensor. The e-nose sensor can check the status of the fried food and based on that the amount of heat transfer can be controlled for the frying chamber. The e-nose has the capability to sense the gas or odor and give the electrical output signal based on the sensed gas. The e-nose also assures adequateness and accuracy of ingredients in food preparation process. This is done by checking weather odour and flavor of the food is consistent with that of ordered food. The prepared cooked food from the second section is dropped on to the balancing structure of third section and thereafter dispensed out of the intelligent automated machine (IAM) for dispensing ready fried food (RFF)through a conveyor in a take away container.

The take away container can be placed on a rotary platform so that if chowmein is to be prepared for multiple plates, these plates are placed on the rotary platform and the platform will rotate the each plate to fill the chowmein from the chowmein dispensing machine.

The dispensing intelligent automated machine (IAM) for dispensing ready fried food (RFF)can have a com based, or card swipe based or user authentication based food dispensing. The intelligent automated machine (IAM) for dispensing ready fried food (RFF)can be instructed to deliver the quantity and taste as opted from multiple options offered to the user by the instruction box. For example the user can vary amount of vegetables and spices. Moreover the user can also opt for a lesser or more boiled food and similarly for a lesser or deep- fried food according to his choice.

The quantity of the input ingredients like noodles, vegetables and spices etc. consumed is measured and indicated automatically on a display screen so that the input ingredients can be refilled into the machine. Measurement is taken based on the weight or volume of the input material and displayed in grams or any other units. For a more complete understanding of the present research, including its features and advantages, reference is now made to the following detailed description, taken in conjugation with the accompanying drawings.

IV. INTELLIGENT AUTOMATED MACHINE (IAM) FOR PREPARATION, PROCESSING AND DISPENSING READY FRIED FOOD (RFF)

The block diagram of the intelligent automated machine (IAM) for dispensing ready fried food (RFF)is shown in figure 3. The intelligent automated machine (IAM) for dispensing ready fried food (RFF)includes three major sections: a first upper section, a second middle section and a third lower section . The upper section is includes plurality of food ingredient specific FAM-F3C sections. . The food ingredient is fed into the FAM-F3C section through an opening provided at the top surface of the FAM-F3C section. Some of these FAM-F3C sections may include a chopping means. The chopping means are also ingredient specific to ensure effective chopping of each ingredient. These FAM-F3C may further consist of a boiling structure . The FAM-F3C sections also serve to store the food ingredients when not in the chopping or boiling mode. An opening is provided at the bottom surface of each FAM-F3C section to transfer the food ingredients from the upper section to the second middle section.

The middle section mainly includes a balancing structure and a frying chamber . The food ingredients from the upper section are dispensed upon a balancing plate of the balancing structure . This dispensing can take place either in a time-based or in a mass-based manner. The balancing plate is attached with a support structure that can rotate about its vertical axis. This arrangement helps in collecting food ingredients from various FAM-F3C sections. All the food ingredients dispensed upon the balancing plate are dropped into frying chamber. The frying chamber includes an assembly of stirrers and an electric heating plate. The assembly of stirrers consists of multiple numbers of stirrers that exhibit a simultaneous rotary and oscillatory movement and thus provide a homogeneous mixing of the food ingredients. The electric heating plate is comprised of a plurality of individual plates . These plates impart an electrical heating to the food ingredients, and can converge in order to drop the prepared food further into the third lower section. The lower section , is a storing box which includes an opening at its bottom. The prepared food from the middle section is dropped into the storing box and is further dispensed into a container . The container is placed upon a balancing plate of a second balancing structure . The lower section further consists of an electronic circuit and a conveying structure . The conveying structure conveys the container to a rotary platform where the food is dropped into a take- away container.

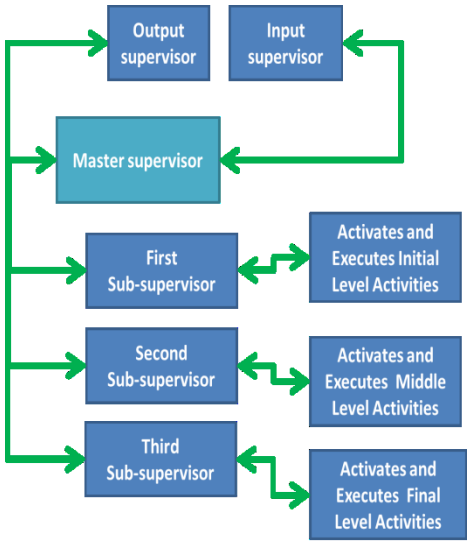


Figure 3. Block diagram of intelligent automated machine (IAM) for dispensing ready fried food (RFF)

A housing unit that houses various components of the FAM-F3C machine and a user interface panel is mounted on the outer periphery of the housing. The panel further includes a display screen , an instruction box and a payment structure . The instruction box helps user place his order by opting for the quantity and the taste of the food as desired by him. The user can vary the amount of vegetables and spices in his order and can also opt for a lesser or more boiled food and similarly for a lesser or deep- fried food. The payment structure allows for either of coin based, card swipe based or user authentication based transaction.

An alert structure is conjugated with the intelligent automated machine (IAM) for dispensing ready fried food (RFF)to give an alert when the quantity of any food ingredient in its FAM-F3C section is not sufficient to prepare the ordered food. The alert structure can give an alert by means of light indication. For example, green light when the ingredient is in sufficient quantity, orange light when it needs to be refilled soon and a red light to indicate that the ingredient is exhausted or not in a quantity required to prepare the present order. The alert structure can also be sound based that plays a particular sound to indicate the need for refilling of the food ingredients.

The intelligent automated machine (IAM) for dispensing ready fried food (RFF)includes various motors for the various sections depending upon the requirement and the motors are programmed according to provide the mechanical energy to the various sections/ modules of the machine. The motors can be synchronous. asynchronous, step or any other types of motor.

The intelligent automated machine (IAM) for dispensing ready fried food (RFF)also includes a master supervisor and a plurality of sub-supervisors to affect working of the machine as discussed below and shown in figure 4. The sub-supervisors are in communication with the master supervisor in a bi-directional manner for carrying out various functions synchronously and in a coordinated fashion. The order fed by the user through the user interface is transmitted to an input sub-supervisor. Data related to user order is than re- transmitted from the input sub-supervisor to a central master supervisor. The central master supervisor is an intelligent supervisor with database information necessary for the intelligent automated machine (IAM) for dispensing ready fried food (RFF)to prepare cooked food. The database stores information such as food name, ingredients to be used, quantity of ingredients, temperature, time for initiating certain activity, order of addition of ingredients, order of performing activities like chopping, boiling, stirring, frying, addition of ingredients, heating, mixing, cooling, dropping, dispensing and the like.

The database also stores information about odours and flavors of different types of cooked food offered by the machine. Based on the user order the central master supervisor sends out one or more instructions to the plurality of sub- supervisors which then implements the instructions received. Based on the instruction from master supervisor the plurality of sub-supervisors generates drive signals to corresponding electrical or mechanical components to execute the sequence of timed control signals corresponding to user order. The electrical or mechanical components include electrical and mechanical components of conveyor, dispensing structure , boiling structure , balancing structure , frying chamber, electric heating means, sensing structure , chopping means, motors, user interface panel, e-nose etc.

FAM-F3C contains a beep structure is incorporated within the intelligent automated machine (IAM) for dispensing ready fried food (RFF)to indicate that the ordered food has been dispensed into the takeaway container. The beep is comparatively a longer one in case of a multiple order to indicate that all the ordered numbers of containers have been filled. The rotary platform can hold different sized containers. The rotary platform rotates to position the containers of the required size so as to collect the food to be dispensed. Same sized containers are stacked together such that that the container immediately below the top container comes at the top when the user has collected his order.

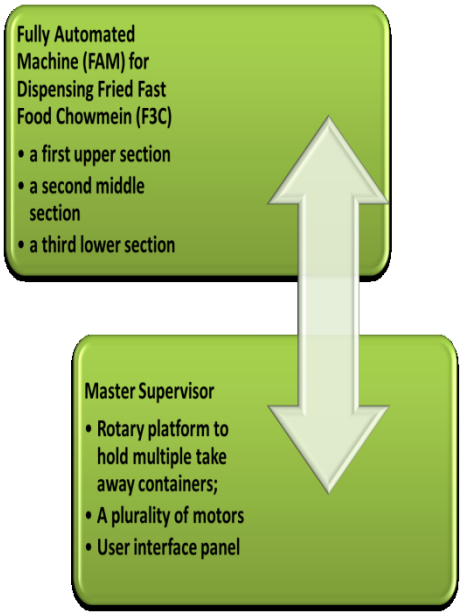


Figure 4. intelligent automated machine (IAM) for dispensing ready fried food (RFF)along with master supervisor

V. INTELLIGENT AUTOMATED MACHINE (IAM) FOR PREPARATION, PROCESSING AND DISPENSING READY FRIED FOOD (RFF) & SUPERVISION

FAM-F3C contains four sub-supervisors namely an input sub-supervisor , a first sub-supervisor, a second sub-supervisor and a third sub-supervisor. These are in communication with the central master supervisor for the execution of user order. Communication between the central master supervisor and the sub-supervisors is in a bi-directional manner. The first sub-supervisor controls, in the upper section of the machine, initial stage activities like chopping of raw food ingredients, boiling of raw food ingredients in their respective FAM-F3C sections. As soon as the user places an order with the machine, the input sub-supervisor sends data related to user order to the central master supervisor . The data includes, food type, quantity, flavour ordered by the user. Based on user order and instructions stored in database the central master supervisor sends out one or more instructions to the first sub-supervisor , for activating and executing various time controlled activities like ingredient chopping, ingredient boiling, in their respective chambers in the upper section of the machine. On completion of initial stage activities, the first sub-supervisor sends out a feedback signal to the master supervisor which also includes indication about quantity of ingredients left in FAM-F3C sections for ingredients storage.

After receiving feedback signal from the first sub-supervisor , the master supervisor activates the second sub-supervisor to execute next set of instructions together with first sub-supervisor . The second sub-supervisor controls middle stage activities, time controlled activities, like collecting food ingredients by balancing them either in a time-based or in a mass-based manner, stirring and frying of food ingredients. The second sub-supervisor performs these activities by activating the balancing structure , frying chamber, stirrers, electric heating plates and electronic nose (e-nose) structure . The-nose structure detects and recognizes odours and flavors of food in the middle section and matches this data with the odours and flavors stored in the database that corresponds to the user order. Thus e-nose also checks adequateness and accuracy of ingredients in food during food preparation process. During middle stage activities in the machine, the e-nose is in continuous communication with the master supervisor through the second sub-supervisor to report readiness of food or any inadequacy or inaccuracy of ingredients. The master supervisor commands first sub-supervisor for the dropping of needed ingredients from ingredient specific FAM-F3C sections to middle section, to even off inadequacy of ingredients reported by the e-nose. In addition, the e-nose also detects smoke level to indicate burning of food or fire in the machine. The e-nose transmits the smoke level data to the master supervisor which raises a fire alarm in an instance of a fire inside the machine. On completion of middle level activities, the master supervisor activates the third sub-supervisor through sending out further set of instructions to the third sub-supervisor. The third sub-supervisor executes and 8 activates final stage activities 108 by driving signals to execute dispensing of the food according to quantity ordered. The third

sub-supervisor performs dispensing of food by activating rotary platform, beep structure and other electrical or mechanicals components in the lower section of the machine.

Thus there has been shown and described a novel fully automated intelligent automated machine (IAM) for dispensing ready fried food (RFF)for preparation and dispensing of fried foods which fulfills all the objects and advantages sought therefore. Many changes, modifications, variations and other uses and applications of the subject research paper will, however, become apparent to those skilled in the art after considering this specification together with the accompanying drawings and claims. All such changes, modifications, variations and other uses and applications which do not depart from the spirit and scope of the research paper are deemed to be covered by the research paper which is limited only by the claims which follow.

VI. CONCLUSION

In view of the foregoing, the main objective of the present research paper is to discuss a fully automated intelligent automated machine (IAM) for dispensing ready fried food (RFF)for preparation and dispensing of cooked food. Fully automated machine (FAM) for dispensing ready fried food (RFF)includes the e- nose sensor for controlled heating of the frying pan. Another objective of the present research paper is to provide a fully automated intelligent automated machine (IAM) for dispensing ready fried food (RFF)which integrates the process for chopping, boiling and frying of food constituents to accomplish the preparation of cooked food. Further, it discusses a fully automatic intelligent automated machine (IAM) for dispensing ready fried food (RFF)for preparation and dispensing of cooked food that can dispense a desired quantity upon acceptance of coin or a card or by authentication of the user.

VII. REFERENCES

[1]. FauziahZainuddin, NorlinMohd Ali, RoslinaMohdSidek, AwanisRomli, NooryatiTalib&Mohd.Izham Ibrahim (2009) "Conceptual Modeling for Simulation: Steaming frozen Food Processing in Vending Machine" International Conference on Computer Science and Information Technology, University Malaysia Pahang, pp.145-149.

[2]. A. Monga1, B. Singh, "Finite State Machine based Vending Machine Controller with Auto-Billing Features", International Journal of VLSI design & Communication Systems (VLSICS) Vol.3, No.2, April 2012.

[3]. M. Zhou, Q. Zhang & Z. Chen (2006), "What Can Be Done to Automate Conceptual Simulation Modelling?" Proceedings of the 2006 Winter Simulation Conference, pp. 809 – 814.

[4]. P. Smith "Automatic Hot-food Vending Machine," Trends in Food Science & Technology, October 1997, Vol. 81, and pp. 349.

[5]. Peter Minns & Ian Elliott, "FSM-based Digital Design using Verilog HDL", John Wiley & Sons Ltd 2008.

[6]. M. Zhou, Q. Zhang & Z. Chen, "What Can Be Done to Automate Conceptual Simulation Modelling?" Proceedings of the 2006 Winter Simulation Conference, pp. 809 – 814.

[7]. C. J Clement Singh, K Senthil Kumar, Jayanto Gope, Suman Basu & Subir Kumar Sarkar "Single Electron Device based Automatic Tea Vending Machine", Proceedings of International Conference on Information and Communication Technology in Electrical Sciences ICTES 2007 , pp891-896.

[8]. P. Smith "Automatic Hot-food Vending Machine," Trends in Food Science & Technology October 1997, Vol. 81, and pp. 349.

[9]. M. Zhou, Y. J. Son, & Z. Chen, (2004), "Knowledge Representation for Conceptual Simulation Modeling" Proceedings of the 2004 Winter Simulation Conference, pp. 450 – 458.

[10]. Seyed Bahram Zahir Azami & Mohammad Tanabian "Automatic Mobile Payment on a nonConnected Vending Machine" proceedings of Canadian Conference on Electrical and Computer Engineering, 2004, pp- 731-734.

[11]. A. Bhatega, K. Sharma, "Secure Cancelable Fingerprint Key Generation", Power India

International Conference (PIICON) IEEE, Dec. 2014, pp-1-3
[12]. S. Dhall Sakshi, K. P. Saibal, K. Sharma, "Cryptographic Primitives for Multimedia Security", INROADS- An International Journal of Jaipur National University, 2014, Volume : 3, pp- 335- 339
[13]. J.Komer , "Digital logic and state intelligent automated machine (IAM) for dispensing ready fried food (RFF)design", 2004, 2nd ed., Oxford.
[14]. Muhammad Ali Qureshi, Abdul Aziz & Hafiz Faiz Rasool "Design and Implementation of Automatic Ticket Structure using Verilog HDL" proceedings of tnternational conference on Information Technology, pp- 707-712.

Indian J Phys
https://doi.org/10.1007/s12648-018-1167-7

ORIGINAL PAPER

Laser-pulse shape effects on magnetic field generation in underdense plasmas

K Gopal[1,2], Md A Raja[3], D N Gupta[2]*, K Avinash[2] and S C Sharma[3]

[1]Department of Physics and Electronics, Rajdhani College, University of Delhi, Delhi 110015, India

[2]Department of Physics and Astrophysics, University of Delhi, Delhi 110007, India

[3]Department of Applied Physics, Delhi Technological University, Delhi 111042, India

Received: 16 June 2017 / Accepted: 30 October 2017

Abstract: Laser pulse shape effect has been considered to estimate the self-generated magnetic field in laser-plasma interaction. A ponderomotive force based physical mechanism has been proposed to investigate the self-generated magnetic field for different spatial profiles of the laser pulse in inhomogeneous plasmas. The spatially inhomogeneous electric field of a laser pulse imparts a stronger ponderomotive force on plasma electrons. Thus, the stronger ponderomotive force associated with the asymmetric laser pulse generates a stronger magnetic field in comparison to the case of a symmetric laser pulse. Scaling laws for magnetic field strength with the laser and plasma parameters for different shape of the pulse have been suggested. Present study might be helpful to understand the plasma dynamics relevant to the particle trapping and injection in laser-plasma accelerators.

Keywords: Self-generated magnetic field; Ponderomotive force; Laser-plasma interaction

PACS No.: 52.38.-r

1. Introduction

The generation of magnetic field has been a crucial issue in the area of laser-plasma physics. Magnetic field affects the plasma dynamics and, therefore, it plays a key role in particle trapping and beam quality control in plasma-based particle accelerators [1–6]. The high magnitude magnetic fields are also of great interest in laser fusion experiments as it affects the energy flow from the light absorption to ablation region [7, 8]. In general, a plasma (magnetic-field free) can give rise to non-zero self-generated magnetic field by various mechanisms. Magnetic field can be generated in plasmas by several mechanism such as due to non-parallel electron density and temperature gradients (known as the Biermann battery [9]), by the electron temperature anisotropy (known as the Weibel instability [10]), by the counter streaming charge particle beam (known as the current filamentation instability [11]), by the inverse Faraday effect [12, 13], by the ponderomotive force of intense laser beams [14–16] and due to the dynamo mechanism [17, 18]. In laser produced plasmas, the scaling laws suggest that the self-generated magnetic field depends on the laser intensity, background plasma density and the length of inhomogeneous plasma density region.

In present work, we invoke the ponderomotive force based mechanism to study the self-generated magnetic field in an inhomogeneous plasma. The ponderomotive force is generated due to a spatially inhomogeneous laser pulse. It constitutes an important mechanism for generation of an azimuthal magnetic field in inhomogeneous plasmas. The origin of this strong magnetic field observed in numerical codes was explained on the basis of the temporal variation in pondermotive force and spatial density gradient in plasmas [19]. Previously, a non-relativistic model has been proposed for self-generated magnetic field in an inhomogeneous plasma for a transversely filamented laser pulse. In that model, the ponderomotive force perpendicular to the density gradient generates a rotational current, which further produces a magnetic field of quasistatic nature [20]. The self-generated magnetic field based on the relativistic ponderomotive force has also been explored earlier [21].

*Corresponding author, E-mail: dngupta@physics.du.ac.in

Published online: 30 January 2018

© 2018 IACS

When a circularly-polarized laser pulse is propagated through an underdense plasma, the self-generated magnetic field can be observed by the inverse Faraday effect (IFE) [22]. The strong axial current due to the flow of relativistic electrons may also generate a strong magnetic field [23]. In case of an overdense plasma, the hot electrons produced due to the resonance absorption can be accelerated in the direction of the density gradient. These accelerated electrons produce an inward flow of cold electron current (return current) and concomitant toroidal magnetic field [24]. The generation of azimuthal nonlinear-currents and the corresponding axial magnetic field depends on the transverse inhomogeneities of the plasma electron density and laser intensity [25]. The self-generated magnetic field in an inhomogeneous by an asymmetric temporal laser pulse has also been explored by using two-dimensional particle-in-cell simulations (2D PIC) [26]. A strong ponderomotive force due steeped front of the propagating laser pulse in an inhomogeneous plasma drives out the local electrons, imparting on them a stronger drift velocity. Thus, a large nonlinear current will be generated due to combined effect of the pulse asymmetry (steeped front edge of the laser pulse) and plasma inhomogeneity (in the form of density ramp). Hence, a significant enhancement in magnetic field strength was observed.

Generally, for a linearly polarized laser pulse, the magnetic field is produced due to the inhomogeneity of both the plasma density as well as the intensity of the laser beam. If there are no such in inhomogeneities, the linearly polarized laser pulse cannot produce any magnetic field in plasmas. Thus, the possibility of strong magnetic field can only be expected if the laser pulse of spatially asymmetric shape is used. A propagating symmetric laser pulse can become asymmetric due to a variety of reasons including the steepening of pulse front due to externally induced nonlinearity (say due to a strong plasma inhomogeneity), backscattering of the laser light, or nonlinear self-modulation and compression of the pulse front. Additionally, any large variation in the refractive index of the plasma can also generate asymmetries in the shape of laser pulse while propagating through it [27]. Simulation study [28] of radius tailored laser pulse propagation in underdense plasmas suggests that such pulses can remain focused over distances greater than $10\,Z_R$, where Z_R is the Rayleigh length. Radius tailored laser pulse can be constructed from a series of overlapping ultrashort Gaussian pulses. Theoretically, it has been shown that the cutoff of either front or back parts of the pulse has an essential effect on the amplitude of the plasma wakefield in context of the plasma accelerators. The cutoff of the front part of the laser pulse has stronger effect than the cutoff of the back part [29].

In this work, we propose a theoretical analysis to investigate the pulse shape effect on the yield of self-generated magnetic field in an inhomogeneous plasma. We have applied the ponderomotive force based mechanism to estimate the self-generated magnetic field in plasmas. Different shape of the pulse has been applied to estimate the strength of the magnetic field. A mathematical formulation in non-relativistic regime with a generalized spatial envelope of laser pulse has been derived. The scaling laws have also been suggested to validate the results with the previous investigations.

2. Theoretical model

We consider the propagation of a laser pulse of different envelope functions $f(\xi)$ with electric field ($\mathbf{E_L}$), $E_L = E_0^2 f(\xi)$. In our calculations we have used a density gradient given by $n_0(y) = n_0^0(1 + y/r_l)$, where r_l is the density ramp length and n_0^0 is the background plasma density. When a laser pulse envelope propagates perpendicular to the density gradient ($\nabla n_0 || \hat{y}$) (where the intensity of the laser has a variation along $\hat{z}$), the plasma electrons start to oscillate at the fundamental frequency of the laser with velocity $\boldsymbol{\upsilon} = e\mathbf{E}/mi\omega$ (where e and m is electron charge and mass, respectively). Laser pulse exerts a ponderomotive force on plasma electrons due to the inhomogeneous nature of electric field profile of the laser pulse.

Laser intensity varies in both radial and axial directions of the propagation direction of the laser beam; therefore, the electrons experience a radial ponderomotive force as well as a longitudinal ponderomotive force. Response of electrons to the electromagnetic field can be governed by the equation of motion having the inertia term in one side and the Lorentz force on other side. Electron oscillates in the direction of electric field E_L, but the magnetic field of the laser pulse distort their orbits. That is the Lorentz force, $-e\,(\boldsymbol{\upsilon} \times \mathbf{B}_L)$, which pushes the electrons in the laser pulse propagation direction. The phase of $\boldsymbol{\upsilon}$ and B_L are such that the motion does not average out to zero over an oscillation, but there is a secular drift along the laser propagation direction. If the pulse wave has uniform amplitude, no force is needed to maintain this drift. The ponderomotive force produces a drift velocity component at twice of the fundamental frequency in perpendicular direction of the laser electric field (or in x-direction). This ponderomotive force is nonparallel to the density gradient. The fast oscillations (at fundamental frequency) parallel to z-direction are neglected as they do not contribute for a net current in one complete oscillation. The ponderomotive force perpendicular to the density gradient, i.e.,$\mathbf{F}_p(\hat{x}) \perp \nabla n(\hat{y})$, generates a nonlinear current $\mathbf{J}^{NL} = -n_0(y)e\boldsymbol{\upsilon}_a = n_0(y)e^3E_L^2\mathbf{k}_1/4m^2\omega^3$, where $\boldsymbol{\upsilon}_a = -\hat{x}(e^2E_L^2\mathbf{k}_1^2/4m^2\omega^3)$ is the drift velocity associated with the

ponderomotive force. The nonlinear current driven by the ponderomotive force produces the electric and magnetic fields E_G and B_G, respectively. The relevant Maxwell's equations are

$$\nabla \times E_G = -\frac{1}{c}\frac{\partial B_G}{\partial t}, \tag{1}$$

$$\nabla \times B_G = \frac{4\pi}{c}(\mathbf{J}^{NL} + \mathbf{J}^{L}) - \frac{1}{c}\frac{\partial E_G}{\partial t}, \tag{2}$$

where $\mathbf{J}^L = -n_0(y)e^2\mathbf{E}_G/mi\omega$ is the linear-current density due to the self-consistent field $\mathbf{E}_G$. Equations (1) and (2) are combined and the expression for nonlinear current to give the equation for B_g as:

$$\nabla^2 B_G + \frac{4\omega^2}{c^2}B_G = \frac{4\pi}{c}\nabla \times \left[\frac{n_0(y)e^3E_L^2\mathbf{k}_1}{4m^2\omega^3} - \frac{n_0(y)e^3\mathbf{E}_G}{2mi\omega}\right] \tag{3}$$

$$\nabla^2 B_G + \frac{4\omega^2}{c^2}B_G = \frac{4\pi}{c}\frac{n_0^0}{d_l}\frac{e^3E_L^2\mathbf{k}}{4m^2\omega^3}. \tag{4}$$

Self-generated magnetic field can be examined by assuming that the driver beam is non-evolving, i.e. the drive laser pulse is a function of only the coordinate $\xi = x - v_g t$. Hence, all quantities will depends only on $\xi = x - v_g t$, where v_g is the group velocity of the laser pulse in a plasma. By rearranging the mathematical terms, we write the resultant differential equation as

$$\nabla^2 B_G + \frac{4\omega^2}{c^2}B_G = \frac{\omega_{pe}^2}{\omega^2}\frac{e^2E_L^2}{4m^2\omega^2}\frac{k}{d_l}\frac{m\omega}{e}, \tag{5}$$

where $\omega_p = (4\pi n_0^0 e^2/m)^{1/2}$ is the plasma electron frequency.

Here we write $E_L^2 = E_0^2 f(\xi)$, where E_0 is the peak amplitude of the sinusoidal laser pulse and $f(\xi)$ describes a particular spatial envelope of the laser pulse. By rearranging the mathematical terms, we obtain the equation for the self-generated magnetic field as

$$\frac{\partial^2 B_G}{\partial \xi^2} + \frac{4\omega^2}{c^2}B_G = \frac{\omega_{pe}^2}{\omega^2}a_0^2\frac{k}{d_l}\frac{m\omega}{e}f(\xi)\hat{z} \tag{6}$$

Equation (6) is a linear inhomogeneous second-order differential equation, which can be solved for self-generated magnetic field (B_G) corresponding to the given $f(\xi)$. Here, the normalized vector potential is defined as $a_0 = eE_L/m\omega c$, where E_L is the laser electric field, ω is the laser frequency, and e and m is electron charge and mass, respectively. In this study, different spatial profiles of the laser pulse such as sinusoidal, triangular, sawtooth-decreasing, sawtooth-increasing and rectangular-triangular (shown in Fig. 1) have been considered.

In case of sinusoidal laser pulse profile, the spatial envelope function $f(\xi)$ is given by $f(\xi) = \sin(\pi\xi/L)$, for $0 \le \xi \le L$. For this case, the analytic solution of Eq. (6) can be given by

$$B_G(\xi) = 18.8558\ \sin(\pi\xi/L) + 0.3144\ \sin(U\xi)\quad if\ 0 \le \xi \le L, \tag{7}$$

where $u = 2\omega/c$ and L is the laser pulse length.

In case of triangular laser pulse profile, the spatial envelope function $f(\xi)$ is given by $f(\xi) = 1 - \cos(\pi\xi/L)$ $for\ 0 \le \xi \le L/2$ or $1 + \cos(\pi\xi/L)\ for\ L/2 \le \xi \le L$ and the corresponding analytic solution is given by:

$$B_G(\xi) = \begin{cases} -18.861\ \cos(\pi\xi/L) + 18.8558 & if\ 0 \le \xi \le L/2 \\ 18.861\ \cos(\pi\xi/L) + 18.8558 & if\ L/2 \le \xi \le L \end{cases}. \tag{8}$$

In case of sawtooth-decreasing laser pulse profile, the spatial envelope function $f(\xi)$ is given by

$$f(\xi) = (1 - \cos(29\pi\xi/L)/2)\ for\ 0 \le \xi \le L/30;\quad or\ (1 + \cos(\pi\xi/L)/2)\ for\ L/30 \le \xi \le L.$$

The corresponding analytic solution for self-generated magnetic field is given by:

$$B_G(\xi) = \begin{cases} 2.876\cos(u\xi) - 12.3056\cos(29\pi\xi/L) + 9.427 & if\ 0 \le \xi \le L/30 \\ 5.7968\cos(u\xi) + 0.6023\sin(u\xi) + 9.4300\cos(\pi\xi/L) + 9.427 & if\ L/30 \le \xi \le L \end{cases}. \tag{9}$$

In case of sawtooth-increasing laser pulse profile, the spatial envelope function $f(\xi)$ is given by $f(\xi) = 1 - \cos(30\pi\xi/58L)$, $for\ 0 \le \xi \le 29L/30$; $or\ 1 + \cos(15\pi\xi/L)$, $for\ 29L/30 \le \xi \le 30$ and the corresponding solution for self-generated magnetic field is given by

$$B_G(\xi) = \begin{cases} -18.858\ \cos(15\pi\xi/L) + 18.858 & if\ 0 \le \xi \le 29L/30; \\ 0.473\ \cos(u\xi) + 5.203\sin(u\xi) + 20.114\,\mathrm{Cos}(15\pi\xi/L) + 18.858 & if\ 29L/30 \le \xi \le L \end{cases}. \quad (10)$$

Finally, for the rectangular triangular laser pulse profile, the the spatial envelope function is given by

$f(\xi) = \sqrt{2}\ \sin(\pi\xi/L)\ for\ 0 \le \xi \le L/4\ ;\ \ or\ 1\ for\ L/4 \le \xi \le 2L/3\ ;$
$or\ -\cos\ (3\pi\xi/2L)\ for\ 2L/3 \le \xi \le L$

while the corresponding self generated magnetic field is given by

3. Numerical results

In this section, we examine the effect of pulse intensity, background plasma density and density ramp length on magnetic field generation during laser-plasma interaction. Figure 2 shows the comparative study of self-generated magnetic field for different spatial laser pulse calculated

$$B_G(\xi) = \begin{cases} 26.6696\ \sin(\pi\xi/L) - 0.4447\sin(u\,\xi),\ for\, 0 \le \xi \le L/4;\ or\ -0.0095\ \cos(u\,\xi) - 0.766\ \sin(u\,\xi) + \\ 18.8558\,,\ \ if\ \ L/4 \le\ \xi \le 2L/3\ . \\ -0.0213\ \cos\ (u\,\xi) - 0.772\ \sin(u\,\xi) - 18.867\ \cos\ (3\pi\xi/2L),\ \ if\ \ \ 2L \le \xi \le L \end{cases} \quad (11)$$

from Eqs. (7)–(10). We take the laser strength parameter, density ramp length (d_l) and background plasma density (n_0^0) as $0.3,\ 50 \times 10^{-4}\,cm,\ and\ 10^{19}\,cm^{-3}$, respectively. Figure 2 shows that the strength of self-generated magnetic field is maximum for the sawtooth-decreasing laser pulse

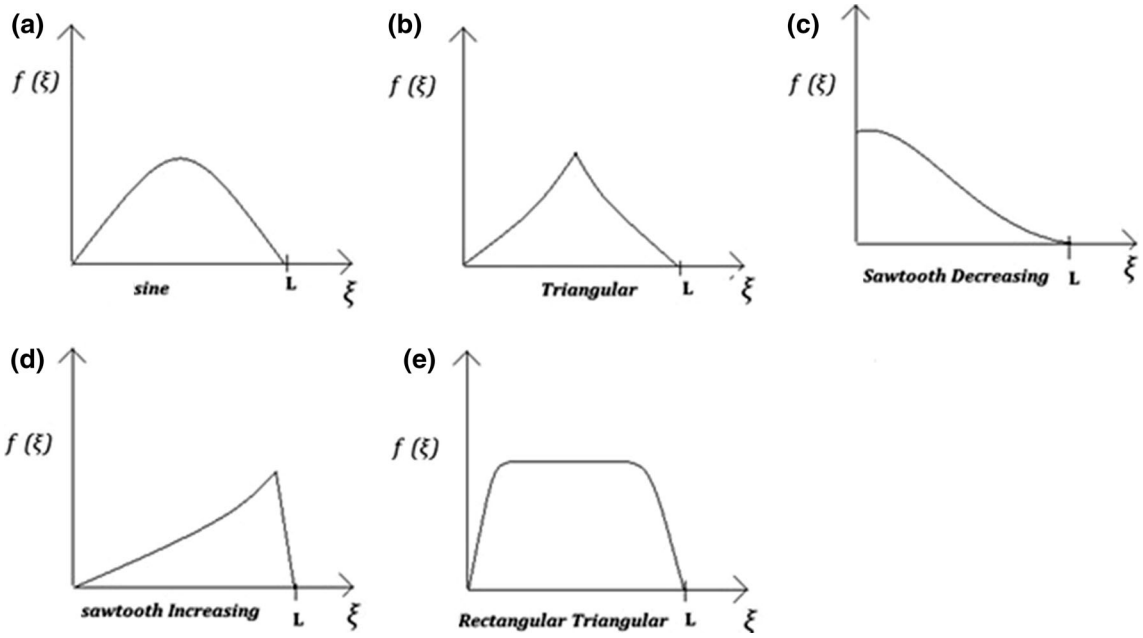


Fig. 1 Shape of spatial laser pulse (**a**) sinusoidal, (**b**) triangular, (**c**) sawtooth-decreasing, (**d**) sawtooth-increasing, and (**e**) rectangular-triangular

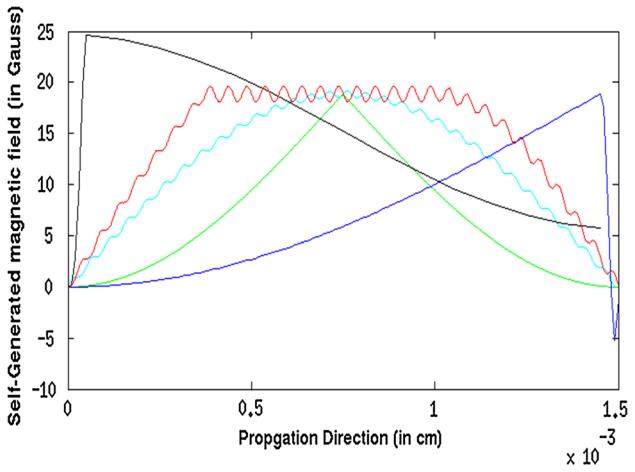


Fig. 2 Self-generated magnetic field for sinusoidal (cyan curve), triangular (green curve), sawtooth-decreasing (black curve), sawtooth-increasing (blue curve) and rectangular-triangular (red curve). The value of laser strength parameter (a_0), density ramp length (d_l) and background plasma density (n_0^0) was considered as 0.3, 50×10^{-4} cm and 10^{19} cm^{-3}, respectively

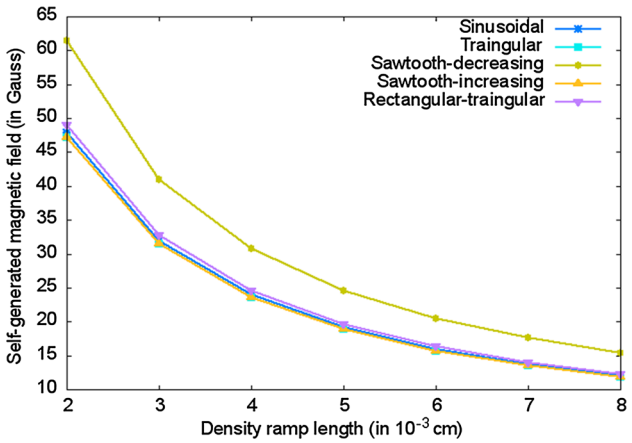


Fig. 3 Self-generated magnetic field with density ramp length (d_l) for sinusoidal, triangular, sawtooth-decreasing, sawtooth-increasing and rectangular-triangular laser pulses. The value of laser strength parameter (a_0) and background plasma density (n_0^0) was considered as 0.3, $50 \times 10^{-4}\ cm$, *and* $10^{19}\ cm^{-3}$, respectively

while the maximum magnetic field for other shapes of the laser pulses was found almost similar. Observed magnetic field contour is within the pulse (not in the back of the pulse); therefore, it is regular within the pulse. No sign of magnetic field observed in the back of laser pulse, which proves that there is no contribution of wakefield in self-generated magnetic field. The wakefield density perturbation is quite important in the back of the laser pulse, but in present research problem the observed magnetic field is within the laser pulse body not in the back of the laser pulse; therefore, the wakefield perturbation is neglected for these particular calculations.

The increased gain for sawtooth decreasing pulse is attributed to the stronger nonlinear rotational currents for longer trailing edge of the pulse, which further enhances the self-generated magnetic field. Steeped laser pulse imparts stronger ponderomotive force, which improves the rotational currents inside the laser pulse and, hence the self-generated magnetic field. Direct forward and backward scattering in plasmas plays a key role in the evolution of the pulse. The forward scattering develops in the whole body of the pulse, which affects the trailing part of the pulse.

In opposite of this, the backward scattering can be expected to become saturate already in leading part of the pulse, which affects mainly the evolution of the leading pulse edge [30]. Thus, by considering the spatially asymmetric laser pulse, the strength of the self-generated magnetic field can be enhanced reasonably in some cases in comparison to spatially symmetric laser pulse.

Figure 3 shows the variation of self-generated magnetic field with density gradient length. Our results show that a

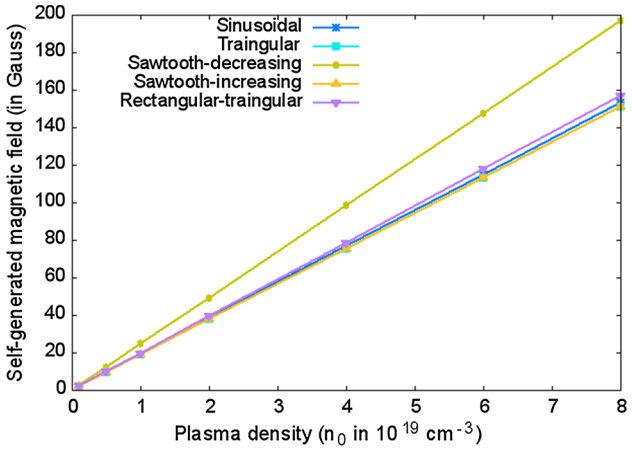


Fig. 4 Variation of self-generated magnetic field with background plasma density (n_0^0) for sinusoidal, triangular, sawtooth-decreasing, sawtooth-increasing and rectangular-triangular laser pulses. The value of laser strength parameter (a_0) and background plasma density (n_0^0) was considered as 0.3 and 50×10^{-4} cm, respectively

stronger magnetic field can be generated by lowering the density gradient length. The reason behind this is the reduction of net nonlinear current at large density gradient length. The physics behind this fact can be implied as: the net nonlinear current reduces for bigger density-gradient length due to the balance between the forward and return current within the pulse body, which further reduces the self-generated magnetic field.

The plasma density also plays a crucial role in magnetic field generation during laser-plasma interactions. In Fig. 4, we show the variation self-generated magnetic field with the equilibrium plasma density for different shapes of the pulse. The strength of the magnetic-field increases with the

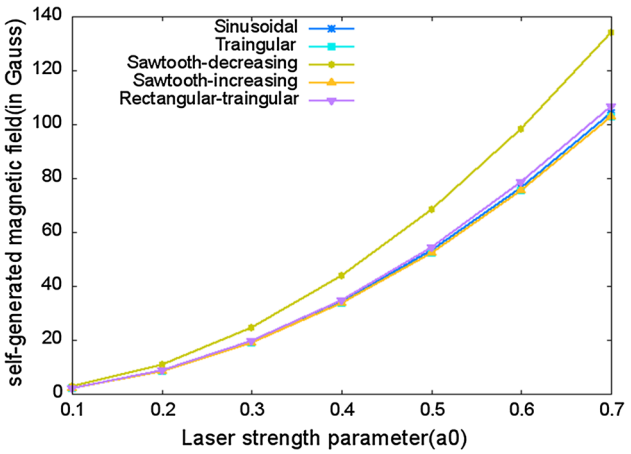


Fig. 5 Variation of self-generated magnetic field with laser strength parameter (a_0) for sinusoidal, triangular, sawtooth-decreasing, sawtooth-increasing and rectangular-triangular laser pulses. The value background plasma density (n_0^0) and density ramp length was considered as 0.3 and 50 $\times$ 10^{-4} cm, respectively

plasma density as the ponderomotive force will evacuate more electrons and large nonlinear current can be produced. Thus a large magnetic field could be in result from this analytical study.

Our study shows that the self-generated magnetic field is also sensitive with the laser intensity parameter. To confirm this, we show, in Fig. 5, the self-generated magnetic field $(\mathbf{B}_a)$ with the normalized laser intensity parameter for different spatial laser pulses.

It can be seen that the self-generated magnetic field increases with the intensity of the laser beam. From these results, one can estimate the self-generated magnetic field at a certain laser intensity for a given plasma density. The reason to increase the magnetic field with the intensity of the fundamental laser beam is basically the enhancement in nonlinear current density.

4. Conclusion

In present work, the ponderomotive force based non-relativistic model has been proposed to investigate the self-generated magnetic field for different spatial envelopes of a laser pulse in plasmas. It is concluded from this model that the peak value of self-generated magnetic field enhances for asymmetric spatial envelopes of a laser pulse in some cases such as sawtooth-decreasing. It remains almost identical for other spatial envelopes of the laser pulse such as sinusoidal, triangular, sawtooth-increasing and rectangular–triangular. The increased gain for sawtooth-decreasing pulse is attributed to the stronger nonlinear rotational currents for longer trailing edge of the pulse. The stronger nonlinear rotational currents further enhance the self-generated magnetic field. The scaling laws are concluded as the peak value of magnetic field increases quadratically with the laser intensity and linearly the plasma density. Magnetic field also decreases with increasing the density ramp length. Present study is valid for low-intensity regime (non-relativistic case), where the laser pulse intensity is too low to attain the relativistic electron velocity. Therefore, the effect of wakefield on self-generated magnetic field would be trivial in this low-intensity regime. In high-intensity regime, the nonlinearity based wakefield effects may be important and one needs to measure the magnetic field at the back of laser pulse. It is quite reasonable to predict that the self-generated magnetic field may affect the excitation of plasma waves that influence the process of charged particle acceleration. Magnetic injection scheme in laser wakefield acceleration has been proposed earlier, which states that the use of longitudinal [6] and transverse magnetic field [3] can trigger and control the electron self-injection in laser wakefield accelerators. Different spatial shapes of a laser pulse might also produce different results in the laser acceleration of plasmas shown by particle-in-cell (PIC) computations [31]. The unusual properties of non-ideal plasmas have fundamental effect on the dynamics of plasma flow in channels and the stability of the non-ideal plasmas [32, 33]. Therefore, present study can also be extended for non-ideal plasmas. The non-LTE (local thermal equilibrium) state of plasmas is also significant for explaining the avalanche processes in fusion plasmas [34] that have been applied to the new schemes of fusion reactor [35].

Acknowledgements K. Gopal thanks to Council of Science and Industrial Research (CSIR) for the financial support to carry out his thesis work. This work is financially supported by the DST-DAAD joint program 2014.

References

[1] E Esarey, C B Schroeder, W P Leemans *Rev. Mod. Phys.* **81** 1229 (2009)
[2] A Flacco, J Vieira, A Lifschitz, F Sylla, S Kahaly, M Veltcheva, L O Silva and V Malka *Nature* **11** 409 (2015)
[3] J Vieira, S F Martins,V B Pathak, R A Fonseca, B Mori and L O Silva *Phys. Rev. Lett.* **106** 225001 (2011)
[4] T Katsouleas and J M Dawson *Phys. Rev. Lett.* **51** 392 (1983)
[5] DN Gupta, K Gopal, I H Nam, V V Kulagin, H Suk *Laser Part. Beams* **32** 449 (2014)
[6] M S Hur, D N Gupta and H Suk *Phys. Lett. A* **372** 2684 (2007)
[7] J D Lindl, P Amendt, R L Berger, S G Glendinning, S H Glenzer, S H Haan, R L Kauffman, O L Landen, and L J Sutter *Phys. Plasmas* **11** 339 (2004)
[8] H Hora, B Malekynia, M Ghoranneviss, G H Miley and X He *Appl. Phys. Lett.* **93** 011101 (2008)
[9] L Biermann *Zeitschrift Naturforschung Teil A*, **5A** 65 (1950)
[10] E S Weibel Phys. Rev. Lett. **2** 83 (1959)
[11] M E Diekmann *Plasma Phys. Control. Fusion* **51** 065015 (2009)

[12] J Deschamps, M Fitaire and M Lagoutte *Phys. Rev. Lett* **25** 1330 (1970)
[13] Z Najmudin, M Tatarakis, A Pukhov, E L Clark, R J Clarke, A E Dangor, J Faure, V Malka, D Neely, M I K Santala, and K Krushelnick *Phys. Rev. Lett.* **87** 215004 (2001)
[14] I V Karpman and H Washimi *J. Plasma Phys.* **18** 173 (1977)
[15] B J Green, P *Mulser Phys. Lett.* A **37** 319 (2002)
[16] O M Gradov and L Stenflow *Phys. Lett. A* **95** 233 (1983)
[17] A Brandenburg, D Sokoloff, and K Subramanian *Space Sci. Rev.* **169** 123 (2012)
[18] S W Kulsrud, M Russell and S W Anderson *Astrophys. J.* **396** 606 (1992)
[19] S C Wilks, W L Kruer, M Tabak and A B Longdon *Phys. Rev. Lett.* **69** 1383 (1992)
[20] V K Tripathi and C S Liu *Phys. Plasmas* **1** 990 (1994)
[21] T Lehner *Phys. Scr.* **49** 704 (1994)
[22] V Y Bychenkov and V T *Laser Part. Beams* **14** 55 (1996)
[23] A Pukhov and J Meyer-ter-Vehn *Phys. Rev. Lett.* **76** 3975 (1996)
[24] P Kolodner and E Yablonovitch *Phys. Rev. Lett.* **43** 1402 (1979)
[25] Y Horovitz, S Eliezer, A Ludmirsky, Z Henis, E Moshe, R Shpitalnik, and B Arad *Phys. Rev. Lett.* **78** 1707 (1997)
[26] K Gopal, D N Gupta, Y K Kim, M S Hur and H Suk J. Appl. Phys. **119** 123101 (2016)
[27] D N Gupta, J Kim, V V Kulagin, H Suk *Laser Phys. Lett.* **11** 056003 (2014)
[28] J Krall, E Esarey, P Sprangle and G Joyce *Phys. Plasmas* **1** 1738 (1994)
[29] V I Berezhiani and I G Murusidze *Phys. Scr.* **45** 87 (1992)
[30] A S Sakharov and V I Kirsanov *Phys. Rev. E* **49** 3274 (1994)
[31] E Yazdani, R Sadighi-Bonabi, H Afarideh, J Yazdanpanah and H Hora *Laser Part. Beams* **32** 509 (2014)
[32] H Hora, P Lalousis and S Eliezer *Phys. Rev. Lett.* **53** 1650 (1984)
[33] V E Fortov and I T Jakubov *The Physics of Non-ideal Plasmas* (Singapore: World Scientific) (2002)
[34] S Eliezer, H Hora, G Korn, N Nissim and J M M Val *Phys. Plasmas* **23** 050704 (2016)
[35] H Hora et al. *Laser Part. Beams* **33** 607 (2015)

Available online at www.sciencedirect.com

ScienceDirect

Materials Today: Proceedings 5 (2018) 819–822

materialstoday: PROCEEDINGS

www.materialstoday.com/proceedings

PMME 2016

Mechanical Properties and Micrstructure of Al-5083 by TIG

Shailesh KumarSingh[a]*, Rasik Mohan Tiwari[a], Anil kumar[a],Satyajeet Kumar [a] ,QasimMurtaza[b], Sanjeev Kumar[c]

Assistant Professor, Department of Mechanical Engineering Krishna Engineering College Ghaziabad -201007 India
Associate Professor, Department of Mechanical Engineering Delhi.Technological University Delhi-110042India
Professor and Head, Department of Mechanical Engineering Krishna Engineering College Ghaziabad -201007 India
Corresponding Author-shailehsonu10@gmail.com

Abstract

The current study deals with the parametric and micro-structural analysis and of Al5083 welded specimen with an automated TIG set up. TIG provides one of the most precise and quality welding fastest welding speed can be used in marine, aerospace and ship industries. Welding speed, current, gas flow rate are the important parameters which are directly affecting the tensile strength of welded specimen and plays an important role in metallurgical changes. Wire EDM cutting is used to cut the welded specimen as per ASTM standard. Tensile strength increases by increasing welding speed till an optimum value and further decreases by increasing the welding speed. Micro-Structural changes are investigated by X-ray diffraction (XRD) and Scanning electron microscopy (SEM) and Energy dispersive spectroscopy (EDS).

© 2017 Published by Elsevier Ltd.
Selection and Peer-review under responsibility of International Conference on Processing of Materials, Minerals and Energy (July 29th – 30th) 2016, Ongole, Andhra Pradesh, India.

*Keywords:*TIG welding, Al-5083,Tensile Strength,Micro-Structure

1. Introduction

Many welding processes like Tungsten inert gas welding (TIG), Gas metal arc welding (GMAW), and Gas Tungsten arc welding (GTAW) are used for various applications in industry to weld light weight materials, aluminum, magnesium and its alloy. TIG welding process uses non consumable electrode to produce weld and welded area is shielded by Helium (He) and Argon (Ar) gases [1]. This investigation focuses to make a crystal clear understanding

*This is an open-access article distributed under the terms of the Creative Commons Attribution-Non Commercial-Share A like License, which permits non-commercial use, distribution, and reproduction in any medium, provided the original author and source are credited.

2214-7853© 2017 Published by Elsevier Ltd.
Selection and Peer-review under responsibility of International Conference on Processing of Materials, Minerals and Energy (July 29th – 30th) 2016, Ongole, Andhra Pradesh, India.

Nomenclature

He, Ar	Helium, Argon
A	Ampere

of changes in mechanical properties by the change in microstructures. A well controlled experiment of three sets and each set contains three sample shows a pattern of tensile strength with the three parameters gas flow rate, current, welding speed effect. It is suggested that caution should be exercised when using TIG method for Al5083 in HSTs where such welding technique is adopted [2]

2. Experimental Set up

Welding of Al 5083 series plate (100x20x3) mm has been done at various parameters like welding speed and welding current and gas flow rate in the set up by TIG welding as shown by block diagram in below figure-1.whereas figure-2 is actual set-up of TIG welding. Chemical compositions of Al-5083 Physical and mechanical properties are listed below in Table-1. The welding parameter ranges taken into account for welding are welding current of 118– 134 amps, gas flow rate of 6 –7 Lt/min and welding speed of 90– 105 mm/min. Welded specimen is cut by wire EDM as per ASTM standard and performed tensile test on UTM machine First point.

Table 1. Mechanical Properties of Al-5083

Density	Brinell Hardness	Tensile Strength	Yield Strength	Elasticity modulas
2.66 g/cc	85 HB	317 MPa	228 MPa	71 Pa

3. Result and Discussion

After an Exhaustive analysis of welded sample the investigation in able to represent the influence of input parameters at Tensile strength of Al-5083.

I-After cutting the sample by wire EDM as per ASTM standard tensile test carried on at UTM machine for nine successive specimens. Minimum tensile strength of specimen C is observed and maximum is observed in specimen H of welded joint. We can see a clear picture of highest tensile strength is achieved at welding current of 134 amp followed by gas flow rate 7 liter/minute and corresponding welding speed is 100 mm/minute.

A-Influence of welding current at Tensile strength

Effect of current as a input parameters reveals that among the three stages of current such as 118 amp, 124 amp and 134 amp is recorded and their mechanical properties is analyzed. Figure-3A shows the effect of current at tensile strength of welded joint. Conclusion drawn by the figure-3A tensile strength increases as the current increases at a constant gas flow rate till an optimum value of 134 amp current that shows the maximum tensile strength of 127MPa of the joint.

B-Effect of Gas Flow Rate on Tensile Strength

Effect of shielding gas flow rate as input parameters shows three different levels effect at tensile strength of welded joint is described at 6 liter/minute, 6.5 liter/minute, and 7 liter/minute. Figure-3B shows the effect of shielding gases at a constant current of three samples. Tensile strength increases by change of shielding gas to an optimum value of 7litre/minute and corresponding tensile strength is 127MPa of sample.

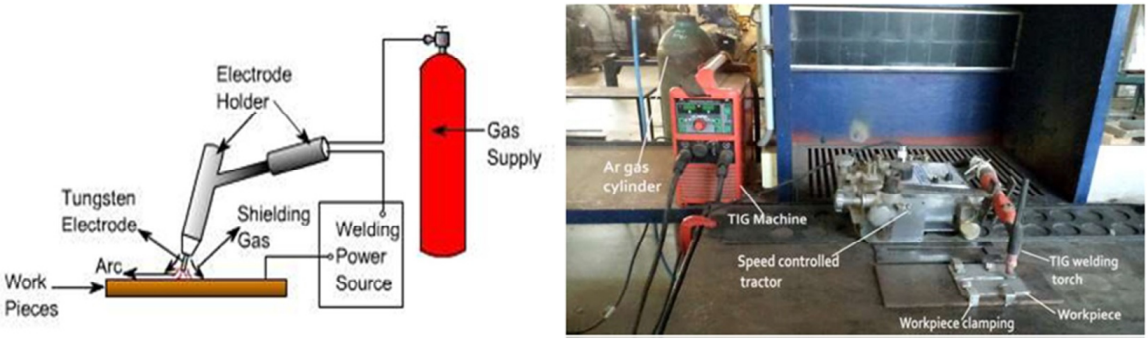
C-Effect of Welding Speed on Tensile Strength

Effect of welding speed as input parameters shows the effect on mechanical properties of weld joint such as tensile strength. Effect of welding speed can be observed in Figure-3C.At a constant current three sample has been analyzed and reveals that tensile strength increases by increasing the welding speed till optimum value of 100 mm/min at current of 134 amps that shows the maximum tensile strength of 127 MPa of weld joint. After that tensile strength starts to decrease by further increment of welding speed.

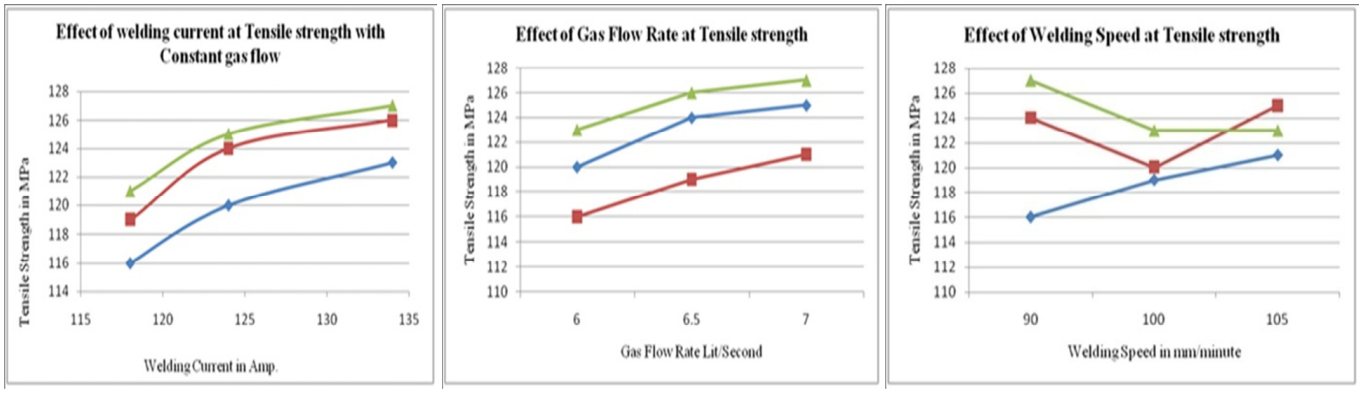
II-Micro-structural Analysis-

To characterize the fracture of welded specimen and mechanical properties with the above discussed parameters, micro-structural characteristics were analyzed. In order to better explanation weld characteristics along with change welding speed, welding current, gas flow rate were investigated in detail. From micro-structural observations, we see that grains in TIG weldments are finer but not showing uniform melting of materials and grain boundaries which can increase the strength of welded area of Al 5083; there is not proper fusion between both the plates of aluminum that might be due to low value of current.

We observed in figure-4(b) that there is not complete transition in the eqiaxed grain from columnar, In addition there is some amount of porosity in the weldment.grains are showing better bonding comparatively microstructure shown in figure-4(a) at low current of 118 Amp and this better distribution is helping to increase the tensile strength with increase in current. As we can see in figure-4(c) that there is minimum porosity because welding speed is comparatively high that is 134 Amp. It was also reported by Yao Liu et.al.(2012) that porosity is decreasing with increase in welding speed[2].figure-4(c) is showing the microstructure of refined grain because the pulses in welding process causes to rapid solidification of the weld pool, and welding seams are fused well and the structure is tight so we are getting highest tensile strength of 127 MPa.



[Figure-1& 2 Schematic Diagram of TIG welding and Experimental Set-up of TIG welding]



[Figure-3 (A)-Tensile strength Vs Welding current, Figure-3 (B)-Tensile strength Vs Gas flow rate, Figure-3 (C)-Tensile strength Vs welding speed]

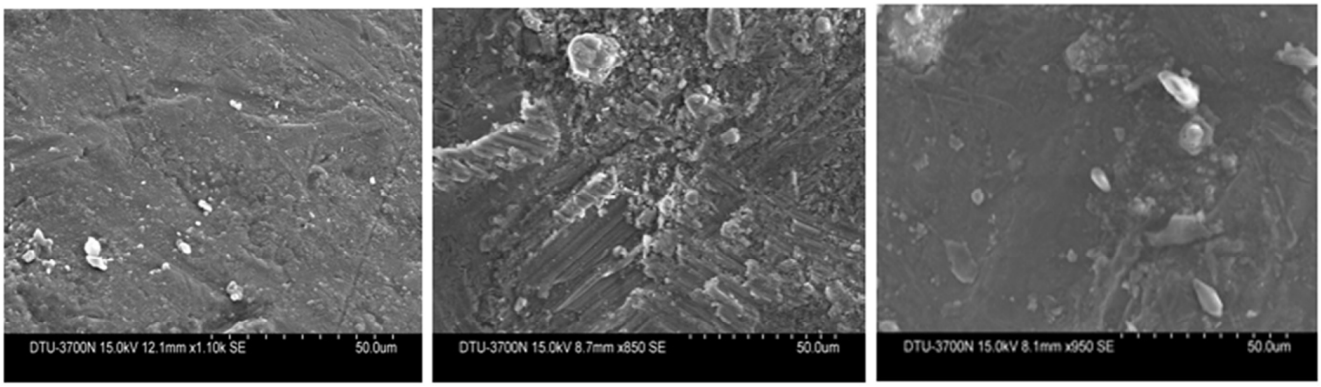


Figure-4 (a),(b) Microstructure of fracture sample at 118A and 124A current,Figure-4 (c) Microstructure of fracture sample at 134 A current

Conclusions

After Exhaustive trials of welding strength at various parameters we are able to conclude some points.

(I) Tensile strength of AL plate increases with the increase in welding speed and showing some optimization value of current 134 Amp and further tensile strength decreases b y increasing welding current.

(II) Maximum welding tensile strength is obtained at 134 Amp with flow rate of 7 lt/min and welding speed of 98 mm/minute.

(III) Evaluated optimum parameters range as134 Amp and welding current, 7 lt/min of flow rate of gas and 98 mm/min of welding speed by which efficient weld can be produced and better tensile strength can be achieved.

(IV) Microstructure of weld pool is showing in shape refined grain because the pulses in welding process causes torapid solidification of the weld pool, and welding seams are fused well and the structure is tight so we are getting highest tensile strength of 127 MPa.

Acknowledgements

We would like to express our sincere gratefulness to our department of Mechanical Engineering, KEC Ghaziabad, for giving me the opportunity to work in lab and also providing excellent guidance, encouragement, moral support and continuous assistance.

References

[1] Behnam LOTFI, Mehdi ROSTAMI, Zohreh SADEGHIAN, Effect of silicon content on microstructure of Al-Si/SiCp composite layer cladded on A380 Al alloy by TIG welding process, Transactions of Nonferrous Metals Society of China, Volume 24, Issue 9, September 2014, Pages 2824-2830, ISSN 1003-6326, http://dx.doi.org/10.1016/S1003-6326(14)63414-2. (http://www.sciencedirect.com/science/article/pii/S1003632614634142)

[2] Yao Liu, Wenjing Wang, Jijia Xie, Shouguang Sun, Liang Wang, Ye Qian, Yuan Meng, Yujie Wei, Microstructure and mechanical properties of aluminum 5083 weldments by gas tungsten arc and gas metal arc welding, Materials Science and Engineering: A, Volume 549, 15 July 2012, Pages 7-13, ISSN 0921-5093, http://dx.doi.org/10.1016/j.msea.2012.03.108.(http://www.sciencedirect.com/science/article/pii/S0921509312005175)

[3] Lio Xu-he,GU Shi-hai,WU Rui-zhi,LENG Xue-song,YAN Jiu-chun,ZHANG Mi-lin, Microstructure and mechanical properties of Mg-Li alloy after TIG welding ,Transaction of Nonferrous Metals society of China: China 21 (2011) 477-481.

ResearchGate

See discussions, stats, and author profiles for this publication at: https://www.researchgate.net/publication/322574064

Object Tracking and Suspicious Activity Identification during Occlusion

Article *in* International Journal of Computer Applications · January 2018

DOI: 10.5120/ijca2018916117

CITATIONS
0

READS
14

3 authors, including:



Raunaq Nayar
Nanyang Technological University
2 PUBLICATIONS **6** CITATIONS
SEE PROFILE



Indu Sreedevi
Delhi Technological University
42 PUBLICATIONS **88** CITATIONS
SEE PROFILE

Some of the authors of this publication are also working on these related projects:



HistExtract View project

All content following this page was uploaded by Indu Sreedevi on 23 January 2018.

The user has requested enhancement of the downloaded file.

Object Tracking and Suspicious Activity Identification during Occlusion

Ravi Teja Yakkali
NXP Semiconductors
Noida
India

Raunaq Nayar
Nanyang Technological University
Singapore

S. Indu
Professor
Delhi Technological University
Delhi, India

ABSTRACT
Rising criminal activities and demand of robust security solutions, detection and tracking of every minute detail of suspicious activity or object has become a topic of interest for researchers all around the world. In this paper, we propose an approach based on Digital Image and Video processing to detect and track the motion of multiple objects during the phenomenon of occlusion and activate an alert if an object is dropped for a long period of time in the region of concentration of camera. The proposed method can be utilized in video surveillance system and the method has been verified through extensive experimentation for multiple video.

General Terms
Image Processing, Video Processing, Computer Vision

Keywords
Occlusion, Digital Image Processing, Suspicious Object, Object Detection, Object Tracking, Video Processing

1. INTRODUCTION
Digital Image and Video Processing has been a hot research topic for the past few years due to increased processing and reduced hardware requirement particularly for security surveillance in the crowded areas where the chances of terrorist attacks and other criminal activities are growing day by day. This involves the concept of framing of a video into a sequence of images and then performing image processing as well as establishing relationship between all image frames to detect motion of multiple objects in the video. In this method of motion detection using background subtraction, a reference image is taken from the still video camera without including any objects which act as the background image. The background image is subtracted from the subsequent image frames in the video to detect objects in motion. For multiple object detection and tracking, difference in object features based on the area and grayscale level is usually taken into account. The main objective of the paper is to develop an algorithm which is used to identify a suspicious activity and track the multiple objects as well as retaining their identity which does not get affected during occlusion of multiple objects. The remainder of this paper is organized in the following manner. Section 2 describes related work in the corresponding field. Section 3 presents the problem statement. Section 4 presents the proposed algorithm of multiple object detection and tracking during occlusion. Suspicious activity identification method is proposed in Section 5. The corresponding algorithm of suspicious activity identification is explained in Section 6. The simulation results are illustrated in Section 7. Finally, we conclude with Section 8.

2. RELATED WORK
There have been many motion detection algorithms which have been in use like temporal difference technique [1], optical flow [2], [3] and background subtraction [4]. Motion detection is followed by median filter smoothening [5]. Identification of moving objects using pixel wise difference between consecutive image frames followed by application of classification matrix to identify objects as human, vehicle or background clutter [10] has also been carried out. Various other techniques of object tracking in video sequences through different phases using image processing [15] have also been discussed in detail. However, the detection methods do not take the effect of occlusion into account. Occlusion is the phenomenon in which, when multiple objects cross each other, at the point when one object overlaps other or when they touch each other on screen they behave like single object and after the occlusion, usually it is very difficult to determine the exact identity of each object. A method for detection of occlusion areas [8] and motion discontinuities using a stochastic approach to the estimation of 2D motion vector fields from time-varying images [9] is used to check whether the occlusion has occurred and to determine portion of the images where occlusion has occurred. This was further improved to accommodate [12] different methods to determine occlusion areas in high resolution images. Occlusion detection has also been carried out by judging the geometric relation between the projection of virtual points and projection of real points according to the theory of stereoscopic geometry in recent past [7]. Some more methods which have also been used are disparity maps [11], random forest method [14] to detect occlusion. Later, a method to detect and track multiple objects which do not get affected by occlusion was formulated based on difference in the area and the threshold level of the various frames in a video taken from a still camera. This was experimentally carried out on detecting and tracking multiple fish swimming in shallow water. [6]. Theoretical model of real fish occlusion tracking, imaginary fish occlusion tracking, and real and imaginary fish concurrent occlusion tracing aiming to achieve 3D fish tracking without occlusion, fulfilling the requirements beforehand for fish target behavior analysis [13] was also proposed recently.

3. PROBLEM STATEMENT
However, the existing algorithms do not detect any suspicious activity happening in the scenario and there is a need to extend the existing algorithms for detecting any suspicious activity in the scenario. So, an area as well as a grayscale level based multiple object detection technique for tracking of multiple suspicious objects along with the concept of raising a red alert if a person drops an apparently suspicious object or if theft occurs in the area under surveillance is proposed in the existing paper. Apart from the identification of suspicious

activity and raising red alert, the proposed method also identifies the exact location in the scenario where the suspicious activity has occurred. The proposed algorithm ensures stringent security check in the area under video surveillance**.**

4. PROPOSED ALGORITHM

Initially a reference image is taken from the still video camera which is assumed as default scenario. While taking the reference, the image must include all those objects whose position is expected to remain still throughout the video. It may happen that in some cases useful objects are there in the scenario which remain for long time after initial reference frame was taken, in that case background image needs to be taken again for proper operation. For detection of multiple objects, first the video is captured for a fixed amount of time and then for another fixed interval which is called processing time, the video is sampled into image-frames to ensure that the proposed DIP algorithm can be implemented. The acquired color image is converted to grayscale image format for further processing. An intermediate frame is created by subtracting the sampled frame from the initial reference frame and taking its absolute value

$$Inter\ Frame = mod(Sampled\ Frame - Reference\ Frame) \quad (1)$$

A Binary Image is then created using threshold operation to form the difference image frame and to eliminate low intensity objects and noise [4]. Finally, all the difference Image Frames are passed through a median filter [5] to remove background noise during image acquisition. An area filter is then applied to the image which removes all the objects below a certain area threshold value called clutters which are of low significance. Parameters for the area filter can be adjusted. In the final difference image, all the white pixels indicate motion and presence of objects. Thus, each group of white pixels separated by black pixels throughout in all the directions is considered as a single object. In this manner, the algorithm is used to detect multiple objects. The positions of all the objects are indicated by the locations of their corresponding centroids calculated based on the mean values of their x and y coordinates. Each object is identified by its mean grayscale value taken over the entire pixel range corresponding to that object. After detection of multiple objects, tracking of the detected multiple objects is performed. Multiple object tracking involves tracing the path followed by each object separately in a video. Tracking of multiple objects while considering the effect of occlusion between multiple objects is done by considering the various parameters such as difference in the mean grayscale levels of various objects being traced (when areas of objects under consideration is comparable).Therefore the object with maximum area (or grayscale value) is tracked by highlighting its centroid with one color, while the one with second largest area (or grayscale value)is tracked with highlighting its centroid with other color and so on. [6] Such peculiar characteristics of people are being tracked for every person even after occlusion.

5. PROPOSED SUSPICIOUS ACTIVITY IDENTIFICATION ALGORITHM

For identification of a suspicious activity and raising a corresponding alert the processing on centroid of each object is performed. If the centroid corresponding to each object in the scenario in different images does not change for a long number of consecutive frames, it implies that either an additional object has been added during the video surveillance which was not initially present in reference frame (indicating the possibility of a suspicious object being dropped which has not changes its position for a long time) or an object initially present in reference frame is missing (indicating the possibility of a theft).The time for which the object remains still with respect to the reference frame before raising the alarm can be adjusted. Once the time limit is exceeded an alarm is raised (in the form of red mark at the position corresponding to the centroid and its neighboring pixels) indicating an emergency.

6. STEPWISE EXPLANATION OF SUSPICIOUS ACTIVITY IDENTIFICATION

Step 1 - Initialize a 'Warning' matrix of the same size as that of the reference image with all elements set to zero

Step 2 - Frame=1

Step 3 - Calculate the difference image of the current image with respect to reference image.

Step 4 - Detect the position corresponding to the centroids of multiple objects in the difference image.

Step 5 - For the centroid positions corresponding to the current frame, increment the corresponding Warning pixel by one. For a non - centroid position in the current frame, Warning pixel makes zero.

Step 6 - If Value of any Warning pixel>Max Count for which object should remain, Mark the position corresponding to the warning pixel and neighbouring pixels 'red' indicating an alert.

Step 7 - Frame= Frame+1

Step 8 - If Frame < = total number of frames, Go to step 3 else exit

Algorithm carried out during suspicious activity identification (Algorithm 1) is explained in this section-

Algorithm.1- Proposed suspicious activity identification system during video surveillance.

The flowchart of the proposed algorithm is shown in Figure 6.

7. SIMULATION RESULTS

The simulation results corresponding to the proposed algorithm are shown in this section. A Real time video is taken from a Webcam and processed using MATLAB. Initially we have simulated the detection of the location of two people before (fig.1), during (fig.2) and after (fig.3) the occurrence of occlusion. From the simulation results, it is clearly evident that the mean grayscale level for two persons is different because of different feature which is colour of objects. Fig. 1(a) shows the actual video frame of the movement of both the people before the occurrence of occlusion. Fig.1(b) displays the difference video frame with respect to the reference background frame. The pixels which are white are the corresponding difference pixels. Figure 1 (c) shows the position of the two objects indicated by their

centroid (mean grayscale level). The blue mark indicates the position of the person with white shirt along with green stripes and blue jeans while the green marker indicates the person with white shirt and black jeans. Fig.1(d) checks if any activity could be termed as suspicious and since the objects have been there for short period of time less than max permissible value for scenario so there is no suspicious activity. Fig.2(a) shows the occurrence of occlusion between both the people. Fig.2(b) shows the difference image. Fig.2(c) shows the position where the occlusion has occurred. Since both the people have been passing each other during occlusion they appear as a single object, the position of which is shown by a white mark. Fig.2(d) ensures that no suspicious activity has occurred.Fig.3(a) shows the frame of the video after the occurrence of occlusion. Fig.3(b) shows the difference image.Fig.3(c) shows the position of the two objects indicated by their mean grayscale level. The position of the two objects can still be predicted accurately even after the occurrence of occlusion. The blue mark still indicates the position of the person with white shirt along with green stripes and blue jeans while the green mark continues to indicate the person with white shirt and black jeans. This shows that our object tracking works even after the occurrence of occlusion. Fig.3 (d) ensures that no suspicious activity has occurred. (Since there is no suspicious activity there are no red marks in the figure). For performing the simulation of suspicious object detection in our video we drop a chair assuming it to be an introduction of a new object into the range of view which could be a suspicious if kept still for a certain number of frames. Fig.4(a) shows the video frame where the suspicious object has been introduced into the scenario and has not been detected. Fig.4(b) shows the difference image Fig.4 (c) shows the person dropping the suspicious object with green mark and the dropped suspicious object (for demonstration purpose, we used a blue coloured chair) has been indicated with blue mark. In Fig.4(d), the suspicious activity has not been indicated yet (No red mark). However, after some time the dropped object remains still for a certain threshold number of frames. Fig.5 (b) shows the difference image. Fig.5 (c) shows the person who had dropped the suspicious object with green mark and the dropped suspicious object has been indicated with blue mark. Fig. 5 (d), after the suspicious object remains still for a threshold number of frames, the suspicious activity is indicated with a red mark (alert signal). (This algorithm even works well for theft detection where red mark appears after a certain threshold number of frames indicating the missing object). All the figures (Fig.1 to Fig.5) demonstrate the proposed video surveillance algorithm is robust which is capable of detecting and tracking the motion of multiple objects undergoing multiple occlusions while raising a RED alert when anything apparently suspicious activity occurs in the scenario under video surveillance.

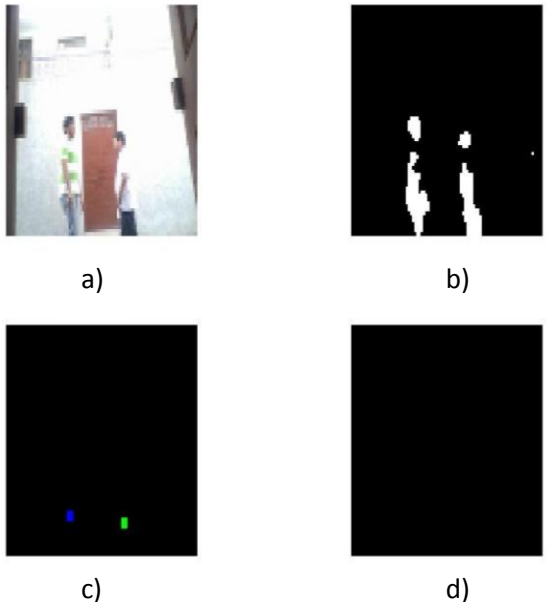


Fig.1-Two moving people before undergoing occlusion –
(a) Original Frame (top left)
(b) Difference Image corresponding to the frame (top right)
(c) Multiple Object Tracking (bottom left) based on difference in mean grayscale level (mean grayscale level corresponding to person with shirt with green and white stripes and blue jeans (indicated with blue mark) is different from the mean grayscale level of the person with white shirt and black jeans (indicated with green mark).
(d) Suspicious Object detection (No red spot implies no suspicious or missing object detected)

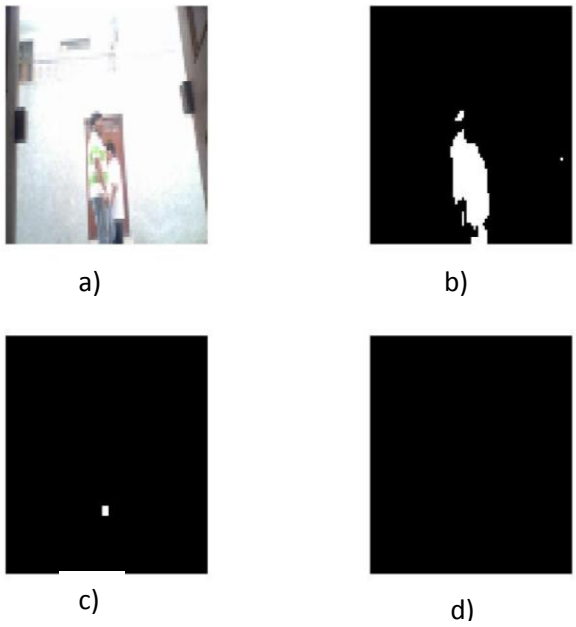


Fig.2-Two moving people during occlusion-(a)Original Frame(top left)
(b)Difference Image corresponding to the frame(top right)
(c)Multiple Object Tracking(bottom left)based on difference in mean greyscale level(During occlusion the two objects merge and appear to be in form of a single object)
(d)Suspicious Object Detection

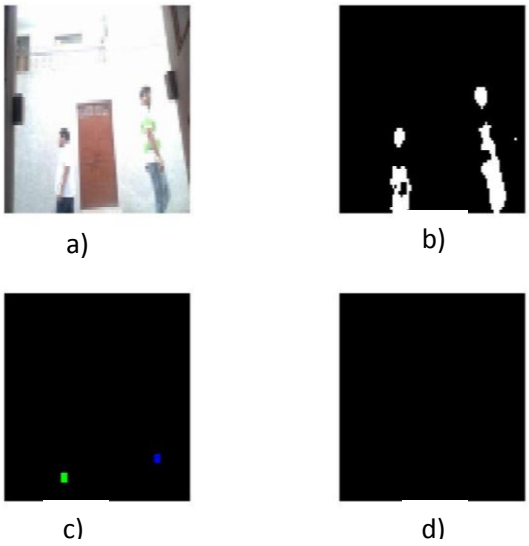


Fig.3 Two moving people after occlusion-(a)Original Frame(topleft)
(b)Difference Image corresponding to the frame(top right)
(c)Multiple Object Tracking(bottom left) based on difference in mean grayscale level(The track of two objects is not lost after occlusion)
(d)Suspicious Object Detection.(No Red spot implies no suspicious or missing object detected)

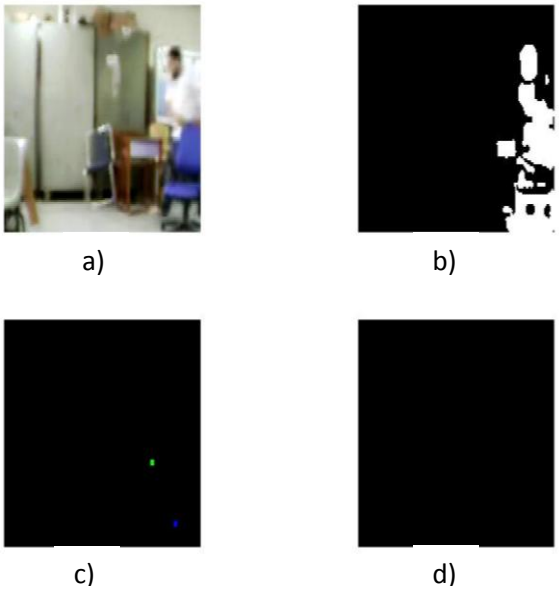


Fig.4-Before suspicious object detection(a)Original Frame(topleft)
(b)Difference Image Corresponding to the frame(top right)
(c)Multiple Object Tracking(bottom left) based on difference in mean greyscale level(Person dropping the object(green) and the object(blue)
(d)Suspicious Object Detection

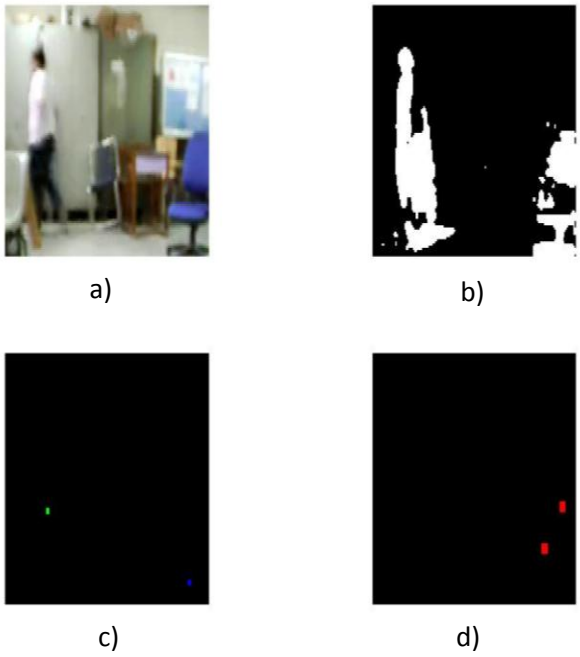


Fig.5-After suspicious object detection-
(a) Original Frame(top left).
(b)Difference Image corresponding to the frame(top left).
(c)Multiple Object Tracking (bottom left)based on difference in mean greyscale level(Person who dropped the object(green)and the object(blue))
(d)Suspicious Object Detection(Occurrence of Red spot implies detection of suspicious or missing Object).

8. CONCLUSION

In this paper, multiple object tracking during occlusion and suspicious activity detection has been described using proposed DIP Algorithm. We have used Real Time Data and it has been shown through results that multiple occlusions of objects do not affect the behaviour of the suspicious object/activity identification. The whole scenario was implemented on MATLAB 2012b. Extensive experiments were carried out to check the correctness of the proposed algorithm. The proposed algorithm can be employed for video surveillance, especially in the crowded areas like railway and bus station and can be used on CCTV footage for detecting suspicious objects on FLY as computation can be performed in very less time if multiple short videos are processed instead of a long video which consumes processing as well as capturing time.

In future, we would like to use optimization algorithms which use Machine Learning and Data Mining techniques to extract important features from the Video and Compressing it for faster processing with less overall size while not losing significant information.

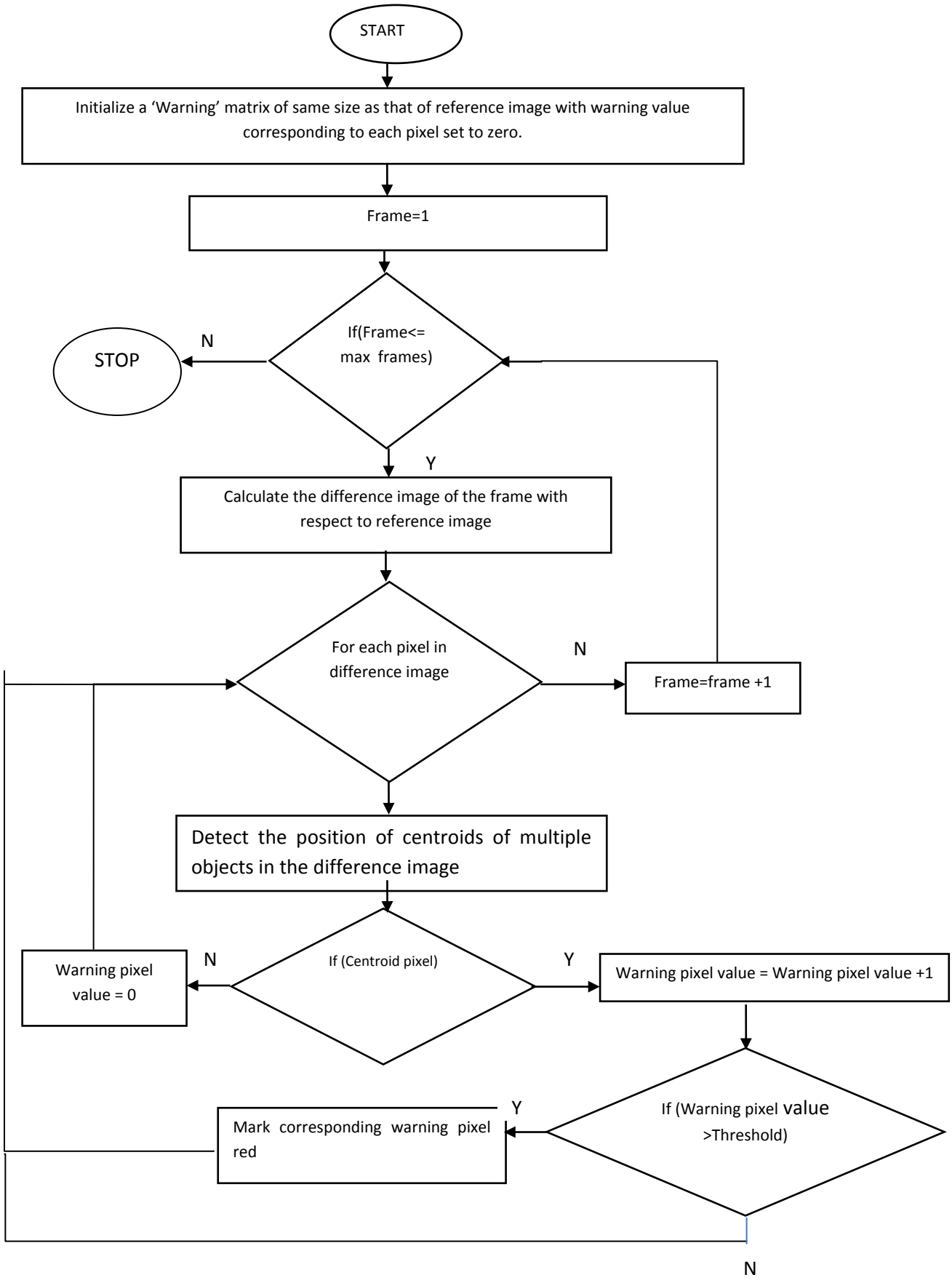


Fig: 6- Flowchart of the proposed algorithm

9. REFERENCES

[1] M. Kalpana Chowdary , S. SuparshyaBabu, S. Susrutha Babu, Dr. Habibulla Khan. "FPGA Implementation of Moving Object Detection in Frames by Using Background Subtraction Algorithm", International conference on Communication and Signal Processing, April 3-5, 2013, pp 1032-1036.

[2] K.Kinoshita, M.Enokidani, M. Izumida and K.Murakami. "Tracking of a Moving Object Using One-Dimensional Optical Flow with a Rotating Observer," 9th International Conference on Control, Automation, Robotics and Vision, 2006. ICARCV'06. 5-8 Dec. 2006, pp.1 – 6.

[3] J. L. Barron, D. J. Fleet and S. S. Beauchemin. "Performance of optical flow technique" IJCV 12:1, 1994, pp 43-77.

[4] Lijing Zhang and Yingli Liang. "Motion human detection based on background Subtraction", 2010 Second International Workshop on Education Technology and Computer Science, pp.284-287.

[5] Massimo Piccardi. "Background subtraction techniques: a review" 2004 IEEE International Conference on Systems, Man and Cybernetics, pp.3099-3104

[6] Mr.Zhi Ming Qian, Xi En Cheng, YanQiu Chen.(2014)"Automatically Detect and Track Multiple Fish Swimming in shallow Water with Frequent Occlusion",Plos ONE 9(9):e106506,doi:10.1371/journal.pone.0106506.

[7] Zhang Ruling, Sun Hanxu, JiaQingxuan, Yao Fusheng. "Research on fast and accurate occlusion detection technology of augmented reality system", Industrial Informatics, 2008. INDIN 2008. 6th IEEE International Conference on 13-16 July 2008, pp.111-116.

[8] R. Depommier and E. Dubois. "Motion Estimation with Detection of Occlusion Areas", 1992 IEEE, pp.269-272.

[9] J. Konrad and E. Dubois, "Bayesian estimation of discontinuous motion in images using simulated annealing", INRS-Telecommunications, 3 Place du Commerce,Verdum, Quebec, Canada, H3E 1H6,pp.51-60.

[10] Alan J. Lipton, Hironobu Fujiyoshi, Raju S. Patil, "Moving Target Classification and Tracking from Real-time Video", Fourth IEEE Workshop on Applications of Computer Vision,1998, WACV'98 Proceedings, pp.8-14.

[11] C. Lawrence Zitnick and Takeo Kanade, "A Cooperative Algorithm for Stereo Matching and Occlusion Detection", IEEE Transactions on Pattern Analysis and Machine Intelligence, Vol. 22, No. 7, July 2000, pp.675-684.

[12] Karlheinz Gutjahr, HannesRaggam. "Determination of Occlusion Areas in HighResolution Remote Sensing Data", 2nd GRSS/ISPRS Joint Workshop on "Data Fusion and Remote Sensing Over Urban Areas", pp.191-194.

[13] Mao Jia-Fa, Xiao Gang, Sheng Wei-Guo, Xiaohui Liu. "A 3D occlusion tracking Model of the underwater fish", 2015 IEEE International Conference on Electro/Information Technology (EIT), 21-23 May 2015, pp.82-86.

[14] Yingkun Xu, Lei Qin, Guorong Li, Qingming Huang. "An efficient occlusion detection method to improve object trackers", 2013 20th IEEE International Conference on Image Processing (ICIP), 15-18 Sept. 2013, pp.2445-2449.

[15] S. V. Kothiya, K. B. Mistree. "A review on real time object tracking in video sequences", 2015 International Conference on Electrical, Electronics, Signals, Communication and Optimization (EESCO), 24-25 Jan. 2015.

View publication stats

Wireless Pers Commun
https://doi.org/10.1007/s11277-018-5341-1

Optimal Node Clustering and Scheduling in Wireless Sensor Networks

Palvinder Singh Mann[1] · **Satvir Singh**[2]

© Springer Science+Business Media, LLC, part of Springer Nature 2018

Abstract Selection and rotation of cluster head (CH) is a well known optimization problem in hierarchical Wireless sensor networks (WSNs), which affects its overall network performance. Population-based metaheuristic particularly Artificial bee colony (ABC) has shown to be competitive over other metaheuristics for solving optimization problems in WSNs. However, its search equation contributes to its insufficiency due to poor exploitation phase and low convergence rate. This paper, presents an improved artificial bee colony (iABC) metaheuristic with an improved search equation, which will be able to search an optimal solution to improve its exploitation capabilities moreover, in order to increase the global convergence of the proposed metaheuristic, an improved approach for population sampling is introduced through *Student's-t* distribution. The proposed metaheuristic maintain a balance between exploration and exploitation search abilities with least memory requirements, with the use of first of its kind compact *Student's-t* distribution, which is particularly suitable for WSNs limited hardware environment. Further utilising the capabilities of the proposed metaheuristic, an improved artificial bee colony based clustering and scheduling (iABC-CS) scheme is introduced, to obtain optimal cluster heads (CHs) along with optimal CH scheduling in WSNs. Simulation results manifest that *iABC-CS* outperform over other well known clustering algorithms on the basis of packet delivery ratio, energy consumption, network lifetime and end to end delay.

Keywords Wireless sensor networks · Clustering and scheduling algorithm · Improved artificial bee colony (iABC) metaheuristic

✉ Palvinder Singh Mann
psmaan@hotmail.com

[1] DAV Institute of Engineering and Technology, Jalandhar, Punjab 144008, India

[2] I. K. Gujral Punjab Technical University, Kapurthala, Punjab 144001, India

Published online: 27 January 2018

1 Introduction

Wireless sensors networks (WSNs) witness tremendous growth over the last few years, due to low-cost and multi-functional capabilities which make them suitable even in diverse and complex environments such as habitant monitoring, enemy surveillance, remote sensing to name a few. WSNs contain self-configured, distributed and autonomous sensor nodes (SNs) that monitor physical or environmental activities like humidity, temperature or sound in a specific area of deployment [1]. SNs can have more than one sensor to capture data from the physical environment, wherever deployed. A sensor with limited storage and computation capabilities receive the sensed data through analogue to digital converter (ADC) and process it further for transmission to a main location, known as *Sink* or *Base Station* (BS), where the data can be analysed for decision making in variety of applications [2]. Every node also acts as a repeater for passing information of other sensor nodes to the sink. The most important part of the sensor node is its power supply, which caters to the energy requirements of sensors, processors and transceiver, however, its limited battery life can lead to premature exhaust of the network due to excessive usage [3]. As manual recharging of batteries is not possible in complex deployments, efficient use of the energy becomes a tough challenge in applications where a prolonged life of the network is required [4]. Researchers are heavily involved in designing of energy efficient solutions, however, on the other hand network life can also be extended by planning energy efficient approaches. It is well accepted that cluster based hierarchical approach is an efficient way to save energy for distributed WSNs [5, 6], which increase network life by effectively utilize the node energy and support dynamic WSNs environment. In a cluster based WSNs, SNs are divided into several groups known as clusters with a group leader known as *Cluster Head* (CH). All the SNs sense data and send it to their corresponding CHs, which finally send it to the BS for further processing. A typical cluster based WSN scenario is shown in Fig. 1. Clustering has various significant advantages over conventional schemes [5]. First, data aggregation is applied on data, received from various SNs within a cluster, to reduce the amount of data to be transmitted to BS thus energy requirements decrease sharply. Secondly, rotation of CHs helps to ensure a balanced energy consumption within the network, which prevent getting specific nodes starved due to lack of energy [7]. However, selection of appropriate CH with optimal capabilities while balancing energy-

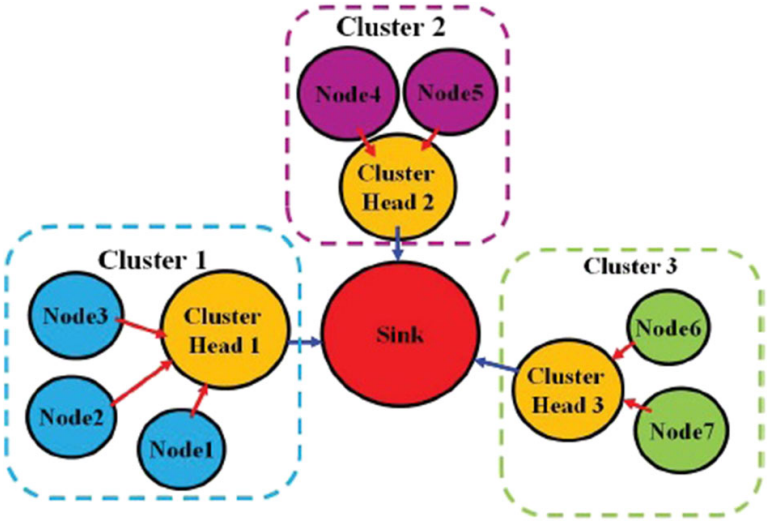


Fig. 1 A typical cluster based WSN scenario

efficiency ratio of the network is a well defined multi-modal optimization problem in WSNs [8]. Thus, metaheuristic based approaches including Evolutionary algorithms (EAs), Particle swarm optimization (PSO), Genetic algorithm (GA) and recently, Artificial bee colony (ABC), have been used extensively as population based optimization methods by different researchers for energy-efficient clustering schemes in WSNs [9]. Results shows that the performance of the ABC metaheuristic is competitive to other population-based algorithms with the advantage of employing fewer control parameters along with simplicity of use and ease of implementation [10]. However, similar to other population-based algorithms, the standard ABC metaheuristic also face some challenges, as it is considered to have poor exploitation phase, moreover convergence rate is typically slower, specially while handling multi-modal optimization problems [11]. Therefore, we propose an improved artificial bee colony (iABC) metaheuristic, with an improved search equation, which will be able to search an optimal solution to improve its exploitation capabilities and an improved approach for population sampling through the use of first of its kind compact *Student's-t* distribution to enhance the global convergence of the proposed metaheuristic. Further, utilizing the capabilities of the proposed metaheuristic, an improved artificial bee colony based clustering and scheduling (iABC-CS) scheme is introduced, which selects optimal cluster heads (CHs) along with optimal CH scheduling in WSNs.

2 Related Work

A large number of clustering schemes have been developed so far for WSNs. Here we present only the vital contributions of the researchers based on conventional as well as metaheuristic approaches; however we underline the significance of metaheuristic, as our proposed scheme is part of this approach. Low-energy adaptive clustering hierarchy (LEACH) [12], is a conventional clustering protocol which combines energy-efficient cluster-based routing to application oriented data aggregation and achieve better lifetime for a WSN. LEACH introduces algorithm for adapting clusters and rotating CHs positions to evenly distribute the energy load among all the SNs, thus enables self-organization in WSNs. LEACH remain a paradigm architect for designing clustering protocols for WSNs till date. Hybrid Energy-Efficient Distributed clustering (HEED) [13], is another conventional clustering protocol that selects CHs based on hybridisation of node residual energy and node proximity to its neighbours or node degree thus achieves uniform CH distribution across the network. HEED approach can be useful to design WSNs protocols that require scalability, prolonged network lifetime, fault tolerance, and load balancing but it only provided algorithms for building a two-level hierarchy and no idea is presented for designing protocol to multilevel hierarchies. Power-efficient and adaptive clustering hierarchy (PEACH) [14], selects CHs without additional overhead of wireless communication and supports adaptive multi-level clustering for both location-unaware and location-aware WSNs but with high latency and low scalability thus make it suitable only for small networks. T-ANT [15], a swarm-inspired clustering protocol which exploit two swarm principles, namely separation and alignment, through pheromone control to obtain a stable and near uniform distribution for selection of CHs. Energy-Efficient Multi-level Clustering (EEMC) [16], achieve less energy consumption and minimum latency in WSNs by forming multi-level clustering with minimum algorithm overhead. However, the authors ignored the issue of channel collision which happens frequently in wireless networks. Energy efficient heterogeneous clustered scheme (EEHC) [17], selects CHs based on weighted election probabilities of each node, which is a function of their

residual energy and further support node heterogeneity in WSNs. Multi-path Routing Protocol (MRP) [18], is based on dynamic clustering with Ant colony optimization (ACO) metaheuristic. A CH is selected based on residual energy of nodes and an improved ACO algorithm is applied to search multiple paths that exist between the CH and BS. MRP prolonged the network lifetime and reduces the average energy consumption effectively using proposed metaheuristic. Energy Efficient Cluster Formation protocol (EECF) [7], presents a distributed clustering algorithm where CHs are selected based on a three-way message exchange between each sensor and its neighbours while possessing maximum residual energy and degree. However the protocol donot support multi-level clustering and consider small transmission ranges. Mobility-based clustering (MBC) protocol [19] support node mobility, hence CHs will be selected based on nodes residual energy and mobility, whereas a non-CH node maintains link stability with its CH during set-up phase. UCFIA [20], is a novel energy efficient unequal clustering algorithm for large scale WSNs, which use fuzzy logic to determine node's chance to become CH based on local information such as residual energy, distance to BS and local density of nodes. In addition, an adaptive max-min ACO metaheuristic is used to construct energy-aware inter-cluster routing between CHs and BS, thus balances the energy consumption of CHs. Distributed Energy-Efficient Clustering with Improved Coverage (DEECIC) [21], selects minimum number of CHs to cover the whole network based on nodes local information and periodically updates CHs according to nodes residual energy and distribution. By reducing overheads of time synchronization and geographic location information, it prolong network lifetime and improve network coverage. Energy-Aware Evolutionary Routing Protocol (ERP) [22], is based on Evolutionary algorithms (EAs) and ensures better trade-off between lifetime and node stability period of a network with efficient energy utilization in complex WSNs environment. Harmony search algorithm based clustering protocol (HSACP) [23], is a centralized clustering protocols based on harmony search algorithm (HSA), a music-inspired metaheuristic, which is designed and implemented in real time for WSNs. It is designed to minimize the intra-cluster distances between the cluster members and their CHs thus optimize the energy distribution for WSNs. Kuila and Jana [24] presents a Linear/ Nonlinear Programming (LP/NLP) formulations of energy efficient clustering and routing problems in WSNs, followed by two algorithms for the same based on a Particle swarm optimization (PSO). Their proposed algorithms demonstrate their proficiency in terms of network life, energy consumption, and delivery of data packets to the BS. Below in Table 1, we presents a relative comparison of these clustering schemes, highlighting their features and limitations for a better insight:

It is very much clear from the comparison that conventional as well as metaheuristic approaches has their own features as well as limitations. Conventional approaches are better in self-organization, load balancing with minimum overhead but average in energy-efficiency whereas metaheuristic shown to be good in energy-efficiency which prolong network life. Therefore, metaheuristic based approaches need to be further explored and improved for energy-efficient solutions in WSNs.

3 Standard Artificial Bee Colony (ABC) Metaheuristic

Original artificial bee colony (ABC) metaheuristic is proposed by Karaboga and Akay [11] for optimizing multi-variable and multi-modal continuous functions, which has aroused much interest in research community due to less computational complexity and use of less number of control parameters. Moreover, optimization performance of ABC is competitive

Table 1 Relative comparison of clustering protocols in WSNs

Protocol	Classification	Energy-efficiency	Features	Limitations
LEACH [12]	Conventional	Average	Self-organization	High communication cost
HEED [13]	Conventional	Average	Low communication cost	High latency
PEACH [14]	Conventional	Average	Load balancing	High latency, Low scalability
T-ANT [15]	Metaheuristic	Good	Fast convergence, low overhead	Low coverage
EEMC [16]	Conventional	Average	Minimum overhead, low latency	Uniform node distribution
EEHC [17]	Conventional	Good	Support node heterogeneity	Low scalability
MRP [18]	Metaheuristic	Good	Prolong network lifetime	Need parameters adjustment
EECF [7]	Conventional	Average	Prolong network lifetime	Low transmission range
MBC [19]	Conventional	Average	High node mobility, low packet loss	High communication cost
UCFIA [20]	Metaheuristic	Good	Prolong network lifetime	Need parameters adjustment
DEECIC [21]	Conventional	Average	Better network coverage	Low scalability
ERP [22]	Metaheuristic	Average	Better network lifetime	Low scalability
HSACP [23]	Metaheuristic	Good	Fast convergence	No load balancing
PSO [24]	Metaheuristic	Good	Better packet delivery	Network overhead

to well known state-of-the-art meta-heuristics [25]. In ABC, there are three type of bees: employed bees, onlookers and scout bees. The employed bee carries *exploitation* of a food source and share information like direction and richness of food source with the onlooker bee, through a *waggle* dance, there after onlooker bee will select a food source based on a probability function related to the richness of that food source, whereas scout bee *explore* new food sources randomly around the hive. When a scout or onlooker bee finds a new food source, they become employed again, on the other hand, when a food source has been fully exploited, all the employed bees will abandon the site, and may become scouts again. In ABC metaheuristic, a food source corresponds to a possible solution to the optimization problem and the number of employed bees are equal to the number of food sources.

Below we present, the detail procedure of ABC metaheuristic in different phases [26]:

3.1 Initialization Phase

ABC metaheuristic starts with initial population number (PN), randomly-generated through D-dimensional real set of vectors. Let $x_{ij} = \{ x_{i1}, x_{i2}, \ldots x_{iD} \}$ is the i-th food source, where $j = 1, 2, \ldots D$, is obtained by:

$$x_{ij} = x_{min_j} + rand(0, 1)(x_{max_j} - x_{min_j}) \tag{1}$$

where x_{min_j} and x_{max_j} denotes lower and upper limits respectively.

3.2 Employed Bee Phase

In this phase, each employed bee obtain a new solution v_{ij} from x_{ij} using expression:

$$v_{ij} = x_{ij} + \phi_{ij}(x_{ij} - x_{kj}) \tag{2}$$

where k is randomly obtained from { 1,2,...SN } and ϕ_{ij} is a uniform random number between [− 1, 1]. The value of v_{ij} is obtained and compared to x_{ij}, further if fitness of v_{ij} comes out better than x_{ij}, then bee will forget the old solution and remember the new one. Otherwise, it will keep exploiting x_{ij}.

3.3 Onlooker Bee Phase

All employed bees share the nectar information of their food source with the onlookers, through a *waggle* dance performed at their hive, after which they select a food source depending on a probability p_i as:

$$p_i = \frac{f_i}{\sum_{n=1}^{SN} f_i} \tag{3}$$

where f_i is the fitness of x_{ij}. Onlooker bee choose a food sources with higher fitness and search x_{ij} according to Eq. (2), now if the new solution has a better fitness, it will replace x_{ij}.

3.4 Scout Bee Phase

After a number of trials, called Maximum cycle number (MCN), if a solution cannot be improved further then food source is abandoned, and the corresponding employed bee becomes a scout again. The scout will then produce a new food source randomly by using Eq. (1) again.

4 ABC Metaheuristic Variants

Various modifications has been proposed in the past to inculcate efficiency in the existing original version of the ABC metaheuristic. One of the factors, which affect the outcome of the metaheuristic is influenced by its solution search equations and thus require many modifications. Advising an improved solution search equation trying to set a balance between the exploitation and exploration capabilities of the metaheuristic. Gao and Liu [27] introduced search equations which are based on differential evolution (DE) [28] algorithms, to solve numerous real-world optimization problems.

$$v_{ij} = x_{bj} + \phi_{ij}(x_{ij} - x_{rj}) \tag{4}$$

$$v_{ij} = x_{r1j} + \phi_{ij}(x_{ij} - x_{r2j}) \tag{5}$$

where $\phi_{i,j}$ is a uniform random number and $x_{r,j}$ is the jth component of a random solution. In addition, Gao [29] introduced another variant later as

$$v_{ij} = x_{bj} + \phi_{ij}(x_{r1j} - x_{r1j}) \tag{6}$$

Other search equations are proposed by Abro [30] and Gao [31]

$$v_{ij} = x_{r1j} + \phi_{ij}(x_{r2j} - x_{r3j}) \tag{7}$$

$$v_{ij} = x_{bj} + \phi_{ij}(x_{r1j} - x_{r2j}) + \psi_{ij}(x_{r3j} - x_{r4j}) \tag{8}$$

$$v_{ij} = x_{bj} + \phi_{ij}(x_{r1j} - x_{r2j}) + \psi_{ij}(x_{sbj} - x_{ij}) \tag{9}$$

where x_{sbj} is the j coefficient of the second best solution. However, the effectiveness of these DE based equations will critically depends on the appropriate setting of population size and strategy parameters. Therefore, to obtain optimal solution, the parameters setting must be required.

These equations are further modified by Li [32] into Eq. (10), where w_{ij} is the relative weight and θ_1, θ_2 are parameters to control step size.

$$v_{ij} = w_{ij}x_{bj} + \phi_{ij}\theta_1(x_{ij} - x_{rj}) + \psi_{ij}\theta_2(x_{bj} - x_{ij}) \tag{10}$$

Although, the above mentioned solution search equation may refine the exploitation process but using two different control parameters sometimes leads to oscillation.

The search equations introduced above can be utilised in onlooker bee phase as well, however in that case neighbourhood search will be performed on most anticipating solutions with best fitness.

Scout bee phase also witnessed some improvements Guo [33] in form of new solution search Eqs. (11) and (12) as:

$$v_{ij} = x_{ij} + \phi_{ij}(x_{bj} - x_{ij}) \tag{11}$$

$$v_{ij} = x_{ij} + \phi_{ij}(x_{sbj} - x_{ij}) \tag{12}$$

In addition, some improved versions of the ABC metaheuristic [34] include some parameters, like Modification Rate (MR) and Scale Factor (SF), MR controls the neighbourhood search whereas SF controls the length of the search.

However, most of the above mentioned works do not control the adaptation of the population and does not specify any means to improve sampling space, which is a significant measure to improve the effectiveness of ABC metaheuristic.

5 Author's Contribution

The main contributions of this paper are listed as follows:

1. *Improved artificial bee colony (iABC) metaheuristic* In an attempt to further improve the convergence rate and attain a perfect balance between exploitation and exploration capabilities of existing ABC metaheuristic, we proposes an improved artificial bee colony $(iABC)$ metaheuristic with better sampling technique using **Students-t** distribution; a compact probability density function (cPDF), which requires only one control parameter to be stored on memory. *Students-t* distribution is being introduced first time from the widely acclaimed family of Estimation of Distribution Algorithms (EDAs) framework. Further, an improved search equation named **ABC/**

rand-to-opt/1 is proposed, motivated by existing Differential evolution (DE) family framework, and obtain a optimal solution from the current best solutions thus improve convergence rate of the proposed metaheuristic.

2. *Improved artificial bee colony based clustering and scheduling (iABC-CS) scheme* Utilizing capabilities of the proposed metaheuristic, we introduce improved artificial bee colony based clustering and scheduling **iABC-CS** scheme for optimal cluster head (CH) selection and optimal CH scheduling, which efficiently selects and schedule the rotation of CHs thus balances energy levels of the nodes thereby extend network life of WSNs.

6 Improved Artificial Bee Colony *(iABC)* Metaheuristic

Like standard ABC metaheuristic, its variants too faces some challenges, like the convergence rate is typically slow since they find difficulty in choosing the most promising search solution, while solving complex multi-modal optimization problems. To overcame these limitations we proposes an improved artificial bee colony $(iABC)$ metaheuristic with an improved initialization phase for better sampling and improved search equation, named ABC/rand-to-opt/1 with optimal search abilities. The details of the proposed metaheuristic are as follows:

6.1 Improved Initialization Phase

Population initialization is an important step in evolutionary algorithms as it can affect the convergence rate and quality of the final solution. Moreover, a large amount of the memory is needed either to store the trial solutions or control parameters of the problem. To reduce the memory requirements, the concept of virtual population has been introduced [35] through family of Estimation of Distribution Algorithms (EDA) [36] framework by considering compact probability density functions (cPDFs). Therefore, we propose *Student's-t* distribution [37]; a cPDF, which needs only one vector to be stored on memory thus reduces storage and step-up convergence rate. The proposed distribution can be described by Eq. (13) where $f(x_{ij})$ is the value of the cPDF corresponding to variable x_{ij}, the $(-\infty, \infty)$ domain of the proposed cPDF is truncated to $[-1, 1]$ and B represents a Beta function. By applying this cPDF, only vector κ needed to be stored on memory. This cPDF is being introduced first time in population-based metaheuristic due to its compact nature.

$$f(x_{ij}) = \frac{\left(1 + \frac{x_{ij}^2}{\kappa}\right)^{-(\kappa+1)/2}}{\sqrt{\kappa} B\left(\frac{1}{2}, \frac{\kappa}{2}\right)} \tag{13}$$

Further, we suggested a new alternative with Cumulative distribution function (CDF) of the proposed *Student's-t* distribution, where a pair of cPDFs that share the same parameters are derived through *Student's-t* CDF by taking integral from $-x$ to x with respect to dx for function $f(x)$ as mentioned below:

$$
\begin{aligned}
\int_{-x}^{x} f(x)dx &= \frac{1}{\sqrt{\kappa}B\left(\frac{1}{2},\frac{\kappa}{2}\right)} \int_{-x}^{x} \left(1+\frac{x^2}{\kappa}\right)^{-(\kappa+1)/2} dx \\
&= \frac{2}{\sqrt{\kappa}B\left(\frac{1}{2},\frac{\kappa}{2}\right)} \int_{0}^{x} \left(1+\frac{x^2}{\kappa}\right)^{-(\kappa+1)/2} dx \\
&= \frac{-2}{\sqrt{\kappa}B\left(\frac{1}{2},\frac{\kappa}{2}\right)} \int_{1}^{\kappa/\kappa+x^2} \frac{x^{\kappa+1/2}\kappa\sqrt{x}}{2x^2\sqrt{\kappa}\sqrt{(1-x)}} dx \\
&= \frac{1}{B\left(\frac{1}{2},\frac{\kappa}{2}\right)} \int_{\kappa/\kappa+x^2}^{1} (1-x)^{-1/2} x^{\kappa/2-1} dx \\
&= \frac{1}{B\left(\frac{1}{2},\frac{\kappa}{2}\right)} \left(B\left(\frac{\kappa}{2},\frac{1}{2}\right) - B_{\frac{\kappa}{\kappa+x^2}}\left(\frac{\kappa}{2},\frac{1}{2}\right)\right) \\
&= 1 - I_{\frac{\kappa}{\kappa+x^2}}\left(\frac{\kappa}{2},\frac{1}{2}\right) = I_{\frac{x^2}{\kappa+x^2}}\left(\frac{1}{2},\frac{\kappa}{2}\right)
\end{aligned}
\tag{14}
$$

where I corresponds to incomplete Beta function. Therefore, the search space corresponding to variable x_{ij} , is now divided into [− 1, 0] and [0, 1] and instead of applying one cPDF, a pair of cPDFs $P_j(x)$ (15) and $Q_j(x)$ (16) are employed for better sampling based on a parameter ξ that controls the probability of sampling.

$$
P_j(x) = \frac{1}{2} - \frac{1}{2} I_{\frac{x_{ij}^2}{\kappa+x_{ij}^2}}\left(\frac{1}{2},\frac{\kappa}{2}\right) \quad for \ -1 < x < 0 \tag{15}
$$

$$
Q_j(x) = \frac{1}{2} + \frac{1}{2} I_{\frac{x_{ij}^2}{\kappa+x_{ij}^2}}\left(\frac{1}{2},\frac{\kappa}{2}\right) \quad for \ 0 \le x < 1 \tag{16}
$$

These equations are employed to refine the sampling process which ultimately enhance the convergence rate of the proposed metaheuristic globally.

6.2 Improved Solution Search Equation

Differential evolution (DE) [38] employs most powerful stochastic real-parameter algorithms to solve multi-modal optimization problems with the optimal combination of population size, and their associated control parameters. In other words, a well-contrive parameter adaptation approach can effectively solve various optimization problems and convergence rate can improve further if the control parameters are adjusted to appropriate

values with improved search equations at different evolution stages of a specific problem. There are various DE variants which are different in their mutation strategies but **DE/rand-to-best/1** [39, 40] is one of its kind which explore *best* solutions to direct the movement of the current population and can effectively maintain population diversity as well.

$$DE/rand\text{-}to\text{-}best/1: \quad v_t = x_t + SF_1(x_{bes} - x_t) + SF_2(x_r - x_s) \tag{17}$$

where SF_1 and SF_2 are scaling factors for neighborhood search. Inspired by this DE variant (17) and inculcating properties of the ABC metaheuristic, we propose a new solution search equations **ABC/rand-to-opt/1** as follows:

$$ABC/rand\text{-}to\text{-}opt/1: \quad v_{ij} = x_{ij} + \phi_{ij}(x_{opt,j} - x_{ij}) + \psi_{ij}(x_{r_1 j} - x_{r_2 j}) \tag{18}$$

where r_1, r_2 are random variables from $1, 2, \ldots, SN$, x_{opt} is the optimal individual solution with optimal fitness in the current population with ϕ_{ij} and ψ_{ij} are scaling factors respectively.

The proposed search equation *ABC/rand-to-opt/1*, which utilizes the information of only optimal solutions in the current population can improve the convergence rate of the proposed metaheuristic.

To increase the multifariousness of the population further, a crossover operation is performed as:

$$u_{ij} = \begin{cases} v_{ij} & if\ r[0,1] \leq CR, \\ x_{opt,j} & otherwise \end{cases} \tag{19}$$

Then a selection operation will be performed as:

$$x_{i,j} = \begin{cases} u_{ij} & if\ f(u_{ij}) \leq f(x_{ij}), \\ x_{opt,j} & otherwise \end{cases} \tag{20}$$

where $f(x_{ij})$ is the fitness function, if the new solution seems to have high fitness value, then it replaces the corresponding old solution ; otherwise the old solution is retained in the memory. Therefore, with the proposed improved solution search equation, optimal solution is obtained with optimal exploration and exploitation ability thus contribute to a better convergence rate.

7 Improved Artificial Bee Colony Based Clustering and Scheduling (iABC-CS) Scheme

We inherit the capabilities of our proposed metaheuristic to solve well known multi-modal optimization problem of energy efficient clustering and scheduling in WSNs by proposing an improved artificial bee colony based clustering and scheduling *(iABC-CS)* scheme with an optimal CH selection ability along with optimal CH rotation policy.

7.1 Network Model with Notations

We use following network model of WSN with notations in our proposed work:

1. S is set of sensor nodes $S = \{ s_1, s_2, \ldots s_n\}$, which are randomly distributed over a geographical area of defined dimensions $m \times m$, whereas s_{n+1} denotes the BS. Each sensor node has a communication radius r.
2. Set of Cluster Heads (CH's) are denoted by $S_{ch} = \{ ch_1, ch_2, \ldots ch_k\}$ where $S_{ch} \epsilon$ S.
3. $D_{s_i}^{s_j}(\max)$ denotes the maximum distance between a senor node s_i and s_j , is calculated by squared euclidean distance between them as

$$\begin{aligned} D_{s_i}^{s_j}(max) &= Max\{\ dis(s_i, s_j) \quad | \quad \forall\, s_i, s_j \epsilon S \\ &= \left\| s_i - s_j \right\|^2 = \sum (s_i - s_j)^2 \quad | \quad \forall\, s_i, s_j \epsilon S \end{aligned} \tag{21}$$

4. $D_{s_i}^{s_{n+1}}(\max)$ denotes the maximum distance between a senor node s_i and BS, is calculated by squared euclidean distance between them as

$$\begin{aligned} D_{s_i}^{s_{n+1}}(max) &= Max\{\ dis(s_i, s_{n+1}) \quad | \quad \forall\, s_i \epsilon S \\ &= \left\| s_i - s_{n+1} \right\|^2 = \sum (s_i - s_{n+1})^2 \quad | \quad \forall\, s_i \epsilon S \end{aligned} \tag{22}$$

5. $D_{s_i}^{ch_j}(\max)$ denotes the maximum distance between a senor node s_i and cluster head ch_j, is calculated by squared euclidean distance between them as

$$\begin{aligned} D_{s_i}^{ch_j}(max) &= Max\{\ dis(s_i, ch_j) \quad | \quad \forall\, s_i,\ ch_j \epsilon S \\ &= \left\| s_i - ch_j \right\|^2 = \sum (s_i - ch_j)^2 \quad | \quad \forall\, s_i,\ ch_j \epsilon S \end{aligned} \tag{23}$$

6. $D_{ch_j}^{s_{n+1}}(\max)$ represents the maximum distance between a cluster head ch_j and BS, is calculated by squared euclidean distance between them as

$$\begin{aligned} D_{ch_j}^{s_{n+1}}(max) &= Max\{\ dis(ch_j, s_{n+1}) \quad | \quad \forall\, j \epsilon S_{ch} \\ &= \left\| ch_j - s_{n+1} \right\|^2 = \sum (ch_j - s_{n+1})^2 \quad | \quad \forall\, j \epsilon S_{ch} \end{aligned} \tag{24}$$

7. Transmission power of a sensor node s_i is calculated as:

$$P_{tran_i} = \frac{1}{k} \left(\frac{\gamma \cdot T_{delay}}{dc} \right)^{\alpha} \tag{25}$$

where T_{delay} is the sum of three delay components as

$$T_{delay} = T_{que} + T_{tran} + T_{ack} \tag{26}$$

The first component; T_{que} is the queuing delay, second component; T_{tran}, is the transmission delay and third one T_{ack}, is delay due to acknowledgement packet. γ , α, dc are signal to noise ratio, path loss exponent and delay constraint respectively whereas k is a power constant.

7.2 Energy Analysis

The radio model for energy analysis is assumed to be same which has been used in earlier work [12], in which CHs receive data packets from SNs for aggregation but include an additional acknowledgment packet (ACK) in return to the source node after receiving a correct packet. This is first time, we incorporate the significance of energy consumption by

the exchange of a ACK in WSNs. Therefore, the energy consumption for transmission of l bits of data is composed of three parts: the energy consumed by the transmitter E_{trans}, by the receiver E_{rec} and by the ACK packet exchange E_{ack}.

$$E_{total}(l,d) = E_{trans}(l,d) + E_{rec}(l,d) + E_{ack} \tag{27}$$

now, energy consumed for transmitting l bits of data is given by:

$$E_{trans}(l,d) = l.E_{elec} + E_{amp}(l,d) \tag{28}$$

further, if the distance between transmitter, and receiver is d, then

$$E_{trans}(l,d) = \begin{cases} lE_{elec} + l\epsilon_{fs}d^2 & if\ d < d_0, \\ lE_{elec} + l\epsilon_{mp}d^4 & if\ d \geq d_0, \end{cases} \tag{29}$$

where d_0 is the threshold distance, and to receive l bit message, the radio spends $E_{rec}(l,d)$ as

$$E_{rec}(l,d) = l.E_{elec} \tag{30}$$

energy consumed for ACK packet exchange is given by

$$E_{ack} = \tau_{ack}(E_{trans} + E_{rec}) \tag{31}$$

where $\tau_{ack} = \frac{l_{ack}}{l}$, is the ratio between length of acknowledgement packet to data packet.

Therefore, residual energy of each senor node is calculated as:

$$E_{res} = E_{total} - (E_{trans} + E_{rec} + E_{ack}) \tag{32}$$

If there will be n nodes uniformly distributed in an $m * m$ field with k clusters, then there will be $\frac{n}{k}$ nodes per cluster. Out of these, there will be one CH node and remaining $\frac{n}{k} - 1$ non-CH nodes.

Now energy consumed by a non-CH node is given by:

$$E_{non-ch}(l,d) = E_{trans}(l,d) \tag{33}$$

$$= l.E_{elec} + E_{amp}(l,d) \tag{34}$$

and energy consumed by a CH node is given by:

$$E_{ch}(l,d) = E_{trans}(l,d) + \left(\frac{n}{k} - 1\right) \cdot l.E_{elec} + \frac{n}{k} l.E_{da} + \left(\frac{n}{k} - 1\right) E_{ack} \tag{35}$$

where E_{da} is the energy consumed by CH for data aggregation at its end.

Now the total energy consumed in a cluster is given by:

$$E_{cluster} = E_{ch}(l,d) + \left(\frac{n}{k} - 1\right) E_{non-ch}. \tag{36}$$

7.3 Optimal CH Selection Algorithm

CH selection is one of the crucial task for cluster formation in WSNs as it effect the overall performance of the network. CH will be responsible for collection of data coming from

various SNs and transmission of aggregated data to the BS. Selection of appropriate node as a CH will remain a challenging multi-modal optimization problem. Therefore, we propose an optimal CH selection algorithm based on our proposed *iABC* metaheuristic for our proposed iABC-CS scheme. The working of proposed algorithm is as follows:

7.3.1 Initialization Phase

The population number (PN), corresponding food sources (SN) are initialised along with control parameters Maximum cycle number (MCN), control parameter ξ and Crossover rate (CR).

We employ the proposed improved sampling technique of *iABC* metaheuristic to generate i-th food source x_{ij}, for which we generate $r\epsilon$ [0, 1] according to uniform distribution and obtain x_{ij} as:

$$x_{ij} = \begin{cases} \frac{1}{2} - \frac{1}{2} I_{\frac{x_{ij}^2}{\kappa + x_{ij}^2}}\left(\frac{1}{2}, \frac{\kappa}{2}\right) & if\ r \leq \xi, \\ \frac{1}{2} + \frac{1}{2} I_{\frac{x_{ij}^2}{\kappa + x_{ij}^2}}\left(\frac{1}{2}, \frac{\kappa}{2}\right) & r > \xi, \end{cases} \tag{37}$$

7.3.2 Fitness Function Derivation

Now, we construct a fitness function to evaluate the fitness of individual food source of the population. There are three objectives in our proposed CH selection algorithm, firstly the node elected as CH, will have maximum residual energy i.e

$$f_i \propto Max(E_{res}) \tag{38}$$

secondly, we ensure to minimize the maximum distance between elected node as CH and BS with minimum transmission power to transmit aggregated data from CH to BS:

$$f_i \propto \frac{1}{Min(D_{ch_j}^{s_{n+1}}(max) + P_{tran_i})} \tag{39}$$

aggregating Eqs. (38) and (39) as

$$f_i \propto \frac{Max(E_{res})}{Min(D_{ch_j}^{s_{n+1}}(max) + P_{tran_i})} \tag{40}$$

$$f_i = K\frac{Max(E_{res})}{Min(D_{ch_j}^{s_{n+1}}(max) + P_{tran_i})} \tag{41}$$

where K is constant of proportionality, assuming K = 1,

$$f_i = \frac{Max(E_{res})}{Min(D_{ch_j}^{s_{n+1}}(max) + P_{tran_i})} \tag{42}$$

Therefore, Eq. (42) will determine the fitness value of each solution of population.

7.3.3 Employed Bee Phase

Now each employed bee select a new solution v_{ij} using proposed improved search Eq. (19) of proposed *iABC* metaheuristic as:

$$v_{ij} = x_{ij} + \phi_{ij}(x_{opt,j} - x_{ij}) + \psi_{ij}(x_{r1j} - x_{r2j}) \tag{43}$$

The obtained value of v_{ij} is compared to x_{ij} and if the fitness of v_{ij} comes out better than x_{ij}, the bee will forget the previous old solution and retain the new optimal solution $x_{opt,j}$ found so far , otherwise, it will keep working on x_{ij}.

7.3.4 Onlooker Bee Phase

Now, employee bee will share the information of their food source with the onlooker bee, through a *waggle* dance performed at their hive, each of whom will then generate a food source u_{ij} according to distribution as:

$$u_{ij} = \begin{cases} v_{ij} & if\ r[0,1] \leq CR, \\ x_{opt,j} & otherwise \end{cases} \tag{44}$$

where CR is crossover rate, further fitness of generated food source $f(u_{ij})$ is calculated and compared with previous food source as:

$$x_{i,j} = \begin{cases} u_{ij} & if\ f(u_{ij}) \leq f(x_{ij}), \\ x_{opt,j} & otherwise \end{cases} \tag{45}$$

where $f(x_{ij})$ is the fitness value of x_{ij}. Onlooker bee will then choose a food source with higher fitness and conduct a local search on x_{ij}, if the new solution has a better fitness, then it will replace x_{ij} with optimal solution $x_{opt,j}$ and assigned as a CH, otherwise the old solution will be retained.

7.3.5 Scout Bee Phase

Now, If the fitness cannot improve further, after a number of trials then the corresponding employed bee becomes a scout to produce a new food source randomly by using Eq. (37) again.

The detail Cluster Head(CH) Selection Algorithm is discussed as below:

Optimal Cluster Head(CH) Selection Algorithm

Input:

$PN \leftarrow Population\ number$,
$MCN \leftarrow Maximum\ cycle\ number$,
$D \leftarrow Dimension\ of\ vector\ to\ be\ optimized$,
$SN \leftarrow Food\ sources$,
$x_{min} \leftarrow Lower\ bound\ of\ each\ element$,
$x_{max} \leftarrow Upper\ bound\ of\ each\ element$,
$\xi \leftarrow Control\ parameter$,
$CR \leftarrow Crossover\ rate$.

Output:

$Ch_j \leftarrow x_{opt,j}$

begin
$round \leftarrow 0$
for $i = 1 \rightarrow SN$ **do**
  $Generate\ r\epsilon\ [0,1]\ according\ to\ uniform\ distribution.$
  if $r \leq \xi$ **then**
    $Generate\ x_{ij}\epsilon\ [-1,0]\ according\ to\ PDF\ P_j(x).$
  else
    $Generate\ x_{ij}\epsilon\ [0,1]\ according\ to\ PDF\ Q_j(x).$
    $Evaluate\ fitness\ f_i(x_{ij})$
    $trial(s) \leftarrow 0$
    $round++$
  end if
end for
repeat
until
for $i = 1 \rightarrow SN$ **do**
  $Generate\ v_{ij}\ according\ to\ Eq.$
  $Evaluate\ fitness\ f_i(v_{ij})$
  $round++$
  if $f_i(x_{ij}) < f_i(v_{ij})$ **then**
    $x_{ij} \leftarrow v_{ij}$
  $f_i(x_{ij}) \leftarrow f_i(v_{ij})$
  $trial(s) \leftarrow 0$
else
  $trial(s) \leftarrow trial(s) + 1$
end if
end for
if $round == MCN$ **then**
  $Memorize\ the\ optimal\ soloution,\ x_{opt,j}\ achieved\ so\ far\ and\ exit\ repeat.$
  $Ch_j \leftarrow x_{opt,j}$
end if
repeat
until
for $i = 1 \rightarrow SN$ **do**
  $r \leftarrow rand[0,1]$
  if $r \leq CR$ **then**
    $u_{ij} \leftarrow v_{ij}$
  else
    $u_{ij} \leftarrow x_{opt,j}$
  end if
  $Evaluate\ fitness\ f_i(u_{ij})\ and\ f_i(x_{opt,j})$
  if $f_i(u_{ij}) \leq f_i(x_{opt,j})$ **then**
    $x_{i,j} \leftarrow u_{ij}$
    if $f_i(u_{ij}) > f_i(x_{opt,j})$ **then**
      $x_{opt,j} \leftarrow u_{ij}$
      $f_i(x_{opt,j}) \leftarrow f_i(u_{ij})$
      $trial(s) \leftarrow trial(s) + 1$
    end if
  end if
  $if\ solution\ need\ to\ be\ abandoned$
  $replace\ with\ a\ new\ solution,\ produced\ using\ Eq.(37)$
  $round++$
end for
if $round == MCN$ **then**
  $Memorize\ the\ optimal\ soloution,\ x_{opt,j}\ achieved.$
  $Ch_j \leftarrow x_{opt,j}$
end if
end

7.4 Optimal CH Scheduling Algorithm

Objective of optimal CH scheduling is to have uniform energy availability at all the nodes at a given time which ultimately increases the substantially level of the whole network thus extend network life. In *iABC-CS*, we divide each node's residual energy into levels which is computed as:

$$E_{level_j} = L \times \left(\frac{E_{res}}{E_{total}} \right) \tag{46}$$

where E_{level_j} is the energy level corresponds to node j, E_{res} is residual energy and E_{total} is total energy of the node, whereas L is proposed number of energy levels. Moreover, a node is not allowed to become a CH if its energy level is lower than network energy level E_{net}. A node can keep its role as CH as long as its energy level is higher than E_{net}, otherwise, it quit its role as CH and attain the initial state with its residual energy level. The detail optimal CH scheduling algorithm is given as follows:

Optimal CH scheduling Algorithm
Input:
$msg \leftarrow message\ packet$
$E_{level_j} \leftarrow energy\ level\ of\ node\ j$
$E_{net} \leftarrow network\ energy\ level$
$quit \leftarrow Ch\ that\ will\ quit\ its\ role$
$state \leftarrow state\ of\ node$

begin
$state \leftarrow initial$
$quit \leftarrow false$
if $msg.E_{net} < E_{net}$ **then**
  $E_{net} \leftarrow msg.E_{net}$
end if
if $msg.quit \leftarrow true$ **then**
  $delete\ node\ from\ list\ and\ update\ state$
end if
if $msg.state == Ch_j$ **then**
  if $state == CH$ **then**
    if $E_{level_j} < msg.level$ **then**
      $quit \leftarrow true$
      $remove\ Ch_j\ from\ S_{ch}$
    end if
  end if
else
  $add\ Ch_j\ to\ S_{ch}\ list\ update\ state$
end if
if $state == initial\ and\ msg.state \neq\ CH$ **then**
  $state \leftarrow CH$
end if
if $quit == true$ **then**
  $quit \leftarrow false$
end if
if $state == CH$ **then**
  if $E_{level_j} > E_{net}$ **then**
    $state \leftarrow Ch_j$
  end if
end if
if $state == CH$ **then**
  if $E_{level_j} > E_{net}$ **then**
    $quit \leftarrow true$
    $state \leftarrow initial$
  end if
end if
update msg and send msg again
end

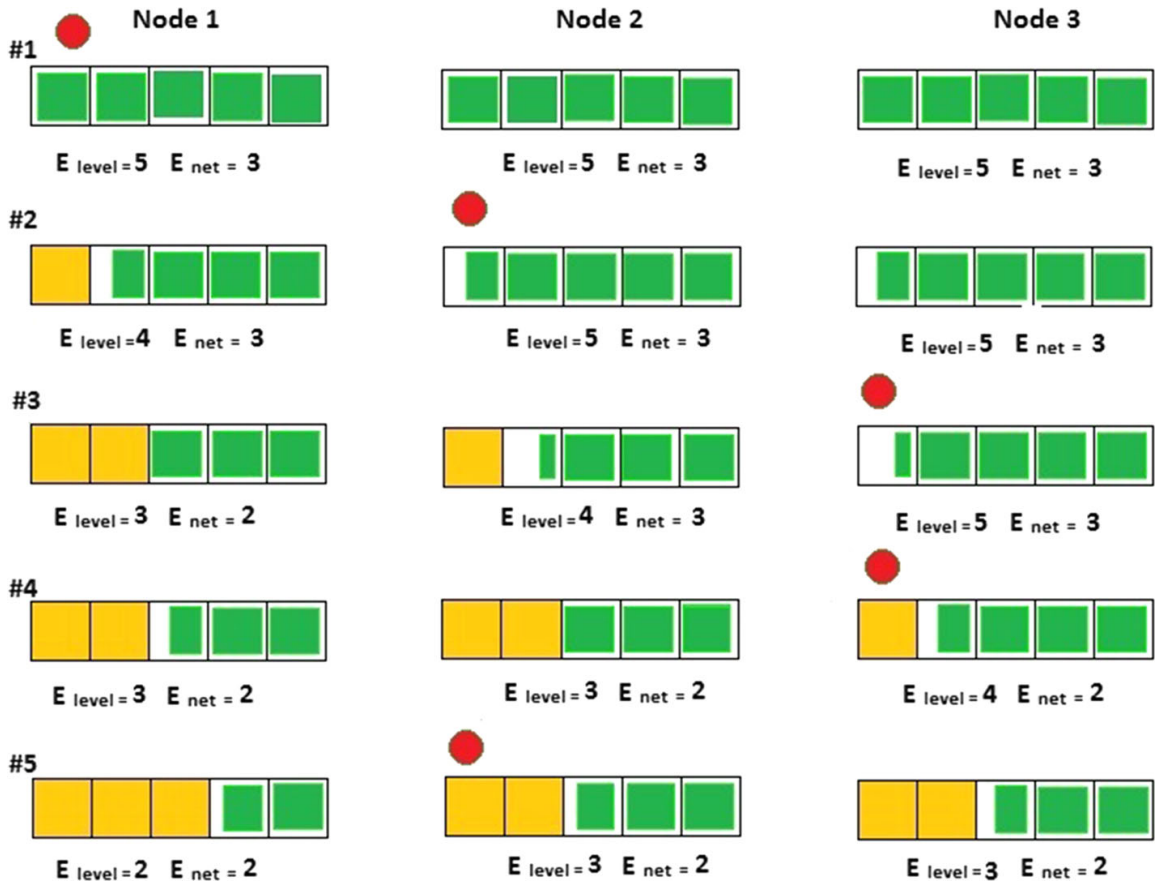


Fig. 2 Optimal CH scheduling

Figure 2 shows optimal CH scheduling of three nodes having initial energy level $E_{level} = 5$ with network energy level $E_{net} = 3$. At stage # 1, node 1 will be chosen as CH by proposed optimal CH selection algorithm, whereas in stage # 2, node 2 become CH based on its residual energy level. At stage # 3, node 3 attain the position of CH based on optimal fitness and node 2 quit the role as CH. At stage # 4, E_{net} reduces to level 2, though node 3, able to maintain its position as CH based upon its fitness again. At stage # 5, node 2 will be chosen as new optimal CH based on proposed optimal CH selection algorithm as node 3 quits, therefore maintaining a uniform energy balance in all nodes of the network, which extend network lifetime.

The proposed optimal CH scheduling algorithm helps to improve the performance of the overall network and enhance robustness. To evaluate and compare the performance of our proposed clustering and scheduling scheme based on *iABC* with standard ABC meta-heuristic, we performed simulation for 10,000 rounds and obtained number of CHs per round through both metaheuristic.

Figures 3 and 4 shows that the proposed scheme iABC-CS clearly supports more number of CHs per round compared to its peer, which in terns is contributed to its optimal search ability and better convergence rate. The proposed improved metaheuristic also supported network for more number of rounds, compared to standard metaheuristic, which is attributed to *Student's-t* distribution's compact nature that saved energy to support network for longer duration. Figure 5 shows the average percentage energy saving through proposed *iABC-CS* algorithm against standard metaheuristic, over number of nodes in a proposed WSN scenario.

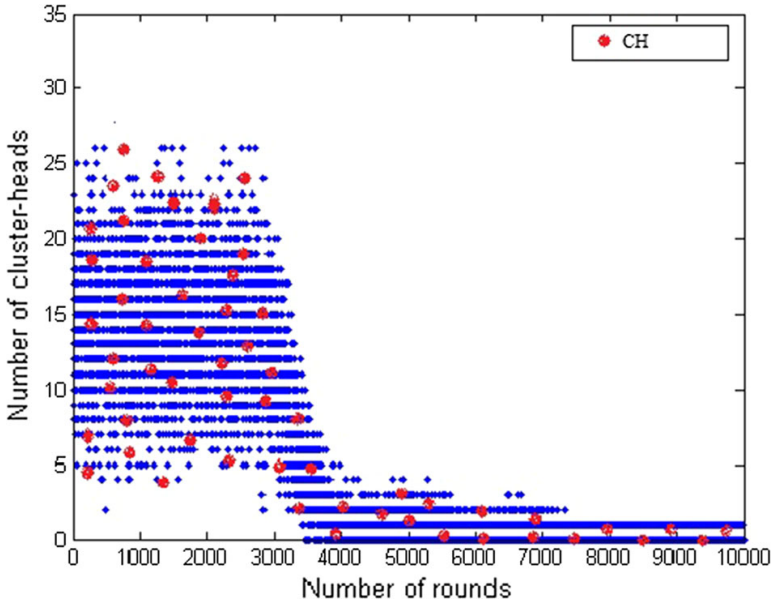


Fig. 3 CHs selected per round through iABC-CS

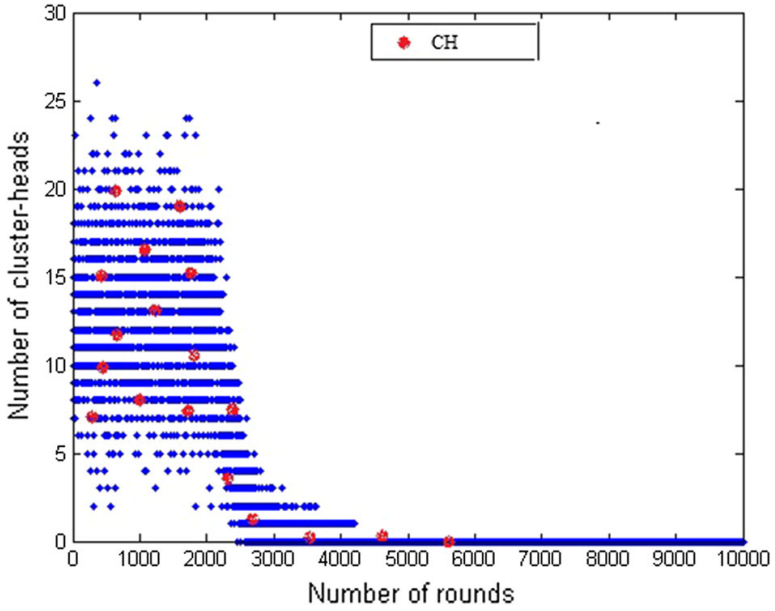


Fig. 4 CHs selected per round through ABC

7.5 Cluster Formation

After selection of CHs, each CH will advertise a Join-Request (J-REQ) message to all its neighbour nodes for cluster formation. Then each non-CH node will join the nearest CH node based on squared euclidean distance between them (24), through a Join-Acknowledgment (J-ACK) short message which will be transmitted using a CSMA/CA MAC protocol, to became member of the cluster. During this communication, all CH nodes must keep their receivers on and listen to the channel. If a particular node receive multiple J-REQ message from same CH then it discard the message to eliminate duplicate frames. After receiving J-ACK messages from all the surrounding nodes each CH must maintain a cluster member table and create a TDMA schedule for each member node of the cluster for

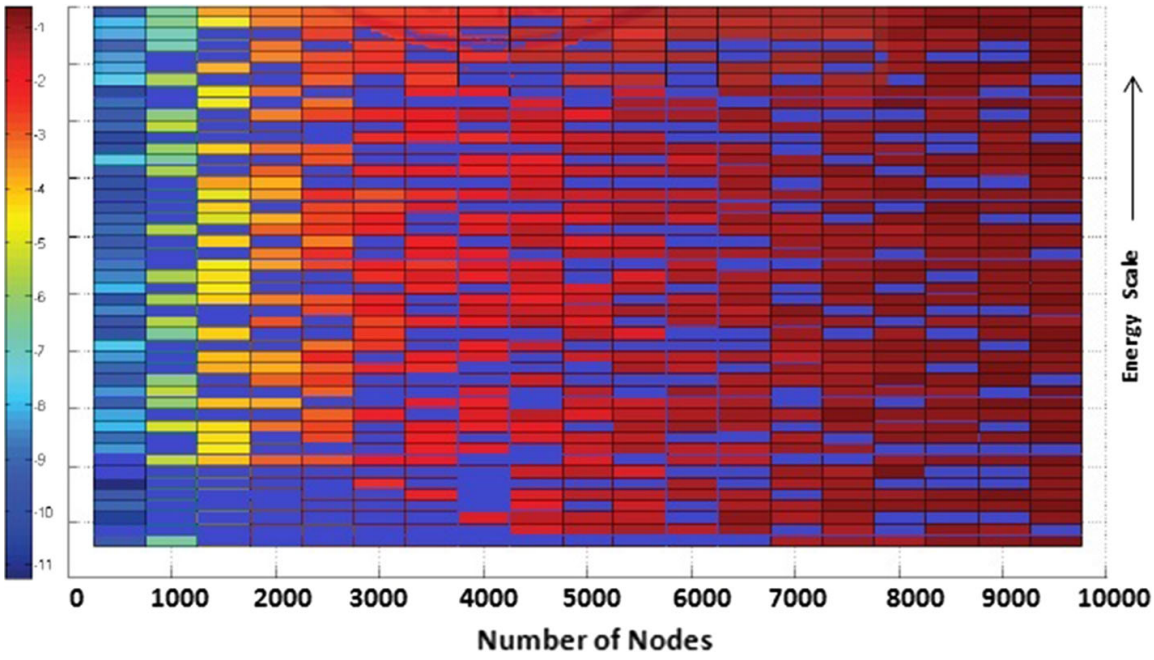


Fig. 5 Average % energy saving using iABC-CS

data transmission. During cluster formation it is ensured that each non-CH node must join a cluster under a CH to avoid node isolation.

7.6 Data Transmission

After cluster formation, when TDMA schedule is communicated to each member node for data transmission, SNs collect data and transmit it to their CH during their allocated TDMA schedule. The non-CH nodes can turn their radio transmitter off during other members transmission turn to save energy consumption. After receiving all the data, CH nodes aggregate it at its end using data aggregation algorithms and route the aggregated data packets to the BS.

8 Simulation Results and Discussion

Now we evaluate the performance of iABC-CS with existing DEECIC [21] and PSO [24] using ns-2 simulator. All are simulated over two different BS position scenarios to assess their behaviour towards packet delivery ratio, energy consumption, network lifetime and end-to-end delay. The simulation will be performed over standard MAC protocol with Free Space radio propagation and CBR traffic type, considering other parameters as shown in Table 2 below:

In the first scenario WSN # 1, a network of sensor nodes ranging from 100 to 700 are deployed randomly over an area of size $250 * 250m^2$ with a BS, located at position (50, 100 m) inside the network field whereas in second scenario WSN # 2, a BS will be placed at position (100, 300 m) outside the network field. First, we execute the protocols to compare packet delivery ratio (PDR) in the network for both the scenarios.

Table 2 Simulation parameters

Parameter	Value
Terrain size	250 * 250 m^2
MAC protocol	802.11
Radio propagation	Free space
Traffic type	CBR
ϵ_{fs}	6 pJ/bit/m
ϵ_{mp}	0.0011 pJ/bit/m4
Propagation limit	− 111 dBm
Receiver sensitivity	− 89
Data rate	2 Mbps
Packet size	3000 bits
Message size	400 bits

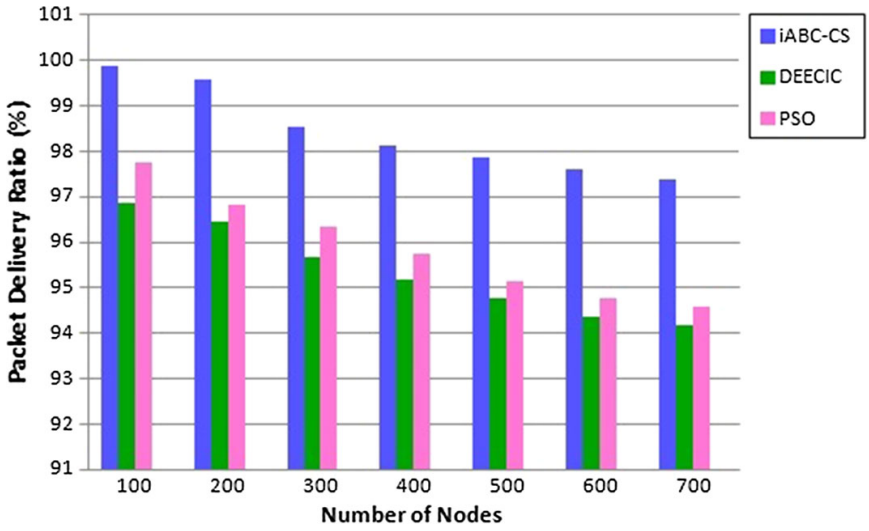


Fig. 6 Packet delivery ratio in WSN # 1

In scenario WSN # 1, Fig. 6 shows that iABC-CS deliver highest number of packets among its all peers, even at highest density of nodes. iABC-CS deliver approximately 100% packets at 100 nodes in WSN # 1 scenario. Even in WSN # 2 scenario, Fig. 7 shows that iABC-CS has highest PDR as compared to DEECIC and PSO at nodes ranging from 100 to 700. It is further analysed from above Figs. 6 and 7 that for iABC-CS, PDR remain highest even in WSN # 2 scenario where BS is placed far outside the network field.

Figure 8 shows that in scenario WSN # 1, energy consumption of iABC-CS is approximately 22 and 58% less then PSO and DEECIC respectively, which is attributed to the use of compact student's-t distribution and improved solution search equation to selects optimal CHs, thus minimise energy consumption in the network. Even in scenario WSN #2 Fig. 9, iABC-CS consumes 28% less energy as compared to its contender PSO, which clearly shows the effectiveness of the proposed metaheuristic *iABC*. In iABC-CS, Optimal CHs are selected not only based on their proximity to BS but with the condition of minimum power consumption in data transmission, moreover the CHs are rotated based on proposed scheduling algorithm, thus consume less energy and as a result the overall energy consumption of the network becomes less as compare to DEECIC and PSO. In PSO, all

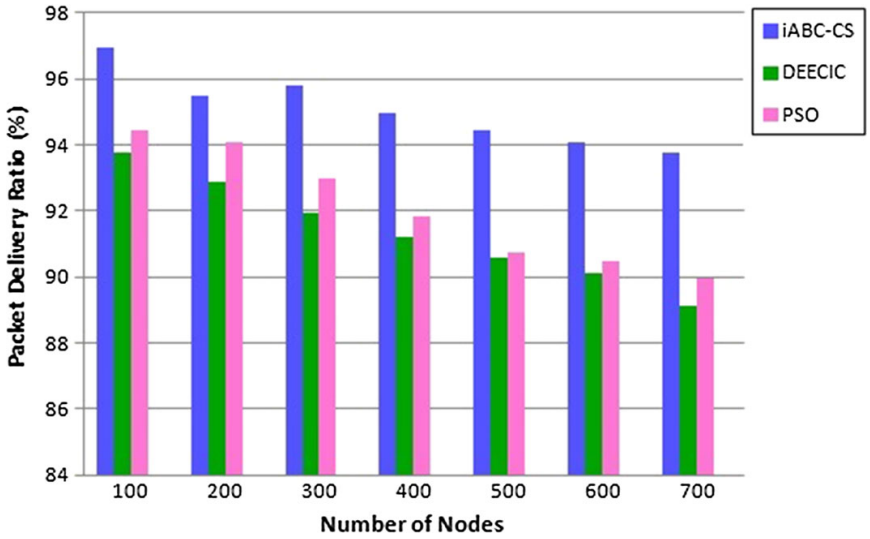


Fig. 7 Packet delivery ratio in WSN # 2

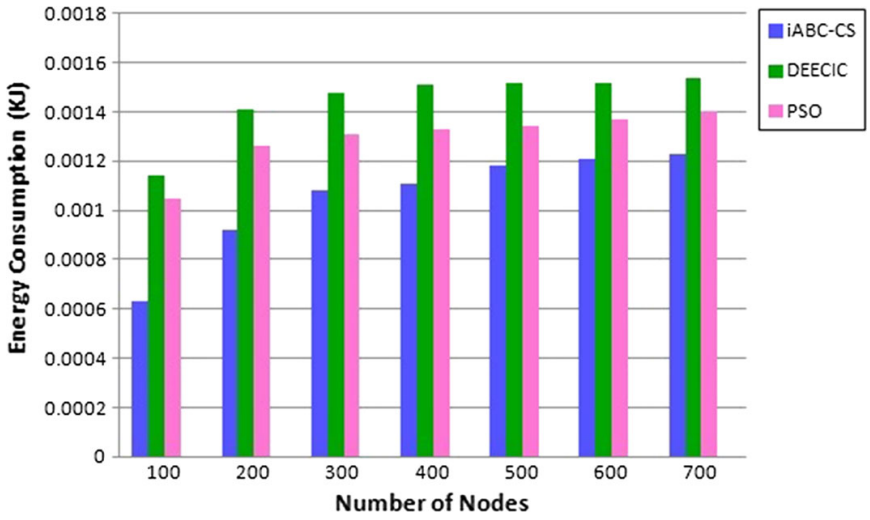


Fig. 8 Energy consumption in WSN # 1

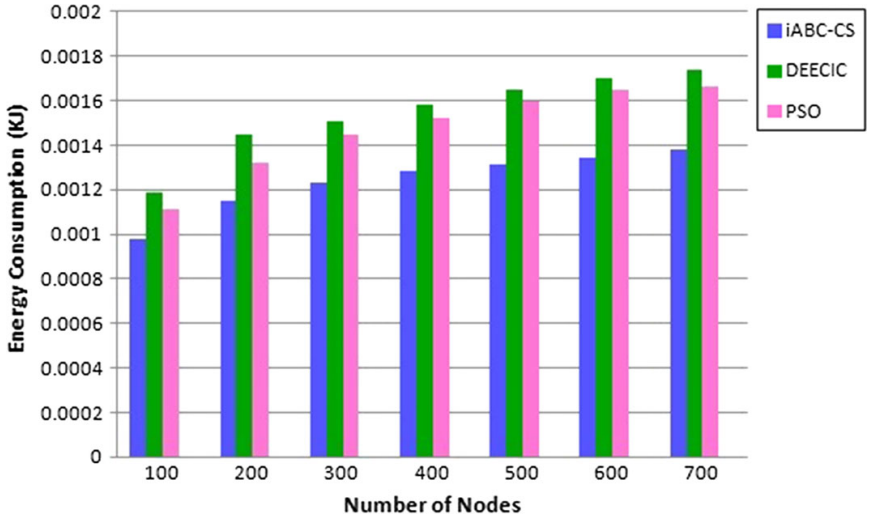


Fig. 9 Energy consumption in WSN # 2

CHs are inevitably used as a relay node to forward the data packets to the BS, therefore consume more energy whereas DEECIC selects CHs based on a pre-defined selective probability of sensor nodes which will not optimise the energy usage in complex WSNs.

Further, Figs. 10 and 11 shows that iABC-CS extend the average network lifetime by approximately 16 and 12% in WSN # 1 and WSN # 2 respectively compared to its peers, which is attributed to nodes surplus energy availability due to less computation and better convergence with an optimal selection of CHs. The energy thus saved will prolong the network lifetime and the nodes will be able to transmit data for a longer duration. In PSO, due to un-symmetric data forwarding effects on the CHs, those near to the BS will die quickly thus reduces network lifetime. DEECIC is having the least network lifetime among all its peers, due to absence of a clear data aggregation and communication framework, specially for WSN # 2 like scenarios. It is further analysed that every 1% increase in network lifetime of the proposed protocol, will increase the data delivery by 2.4% thus increase networks robustness.

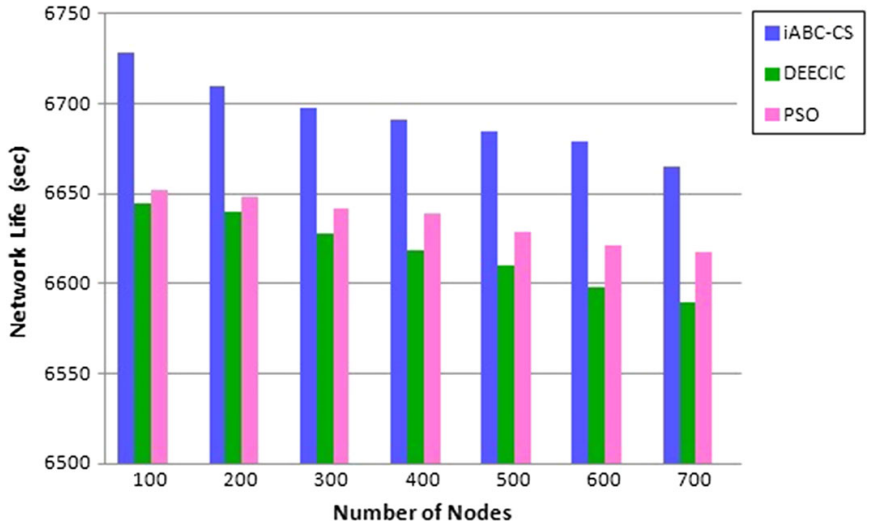


Fig. 10 Network lifetime in WSN # 1

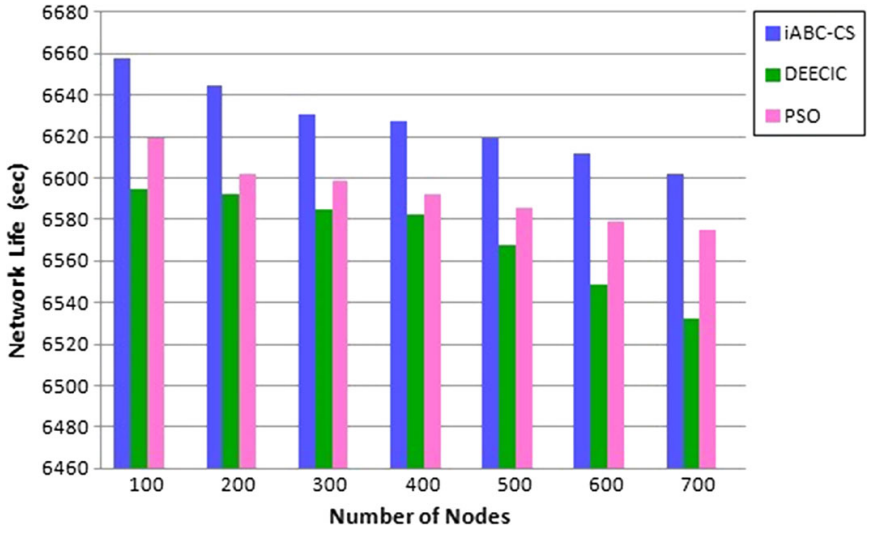


Fig. 11 Network lifetime in WSN # 2

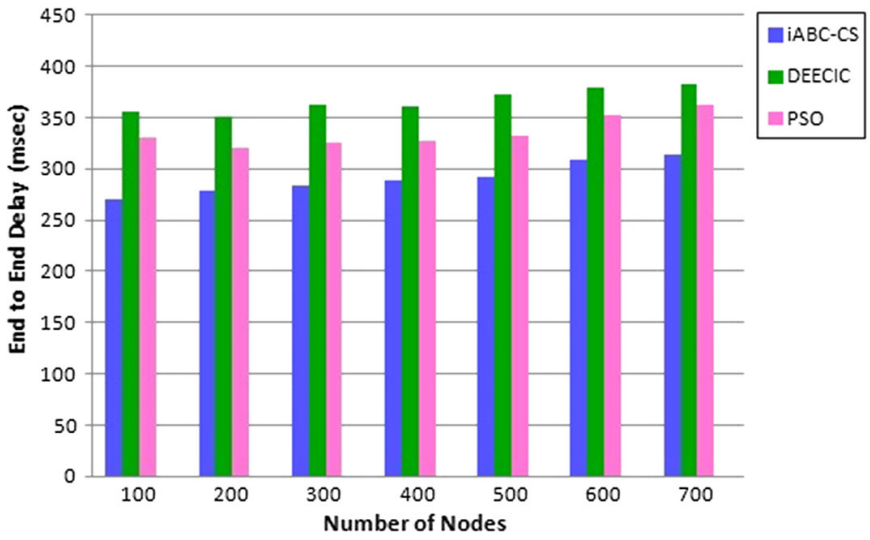


Fig. 12 End-to-end delay in WSN # 1

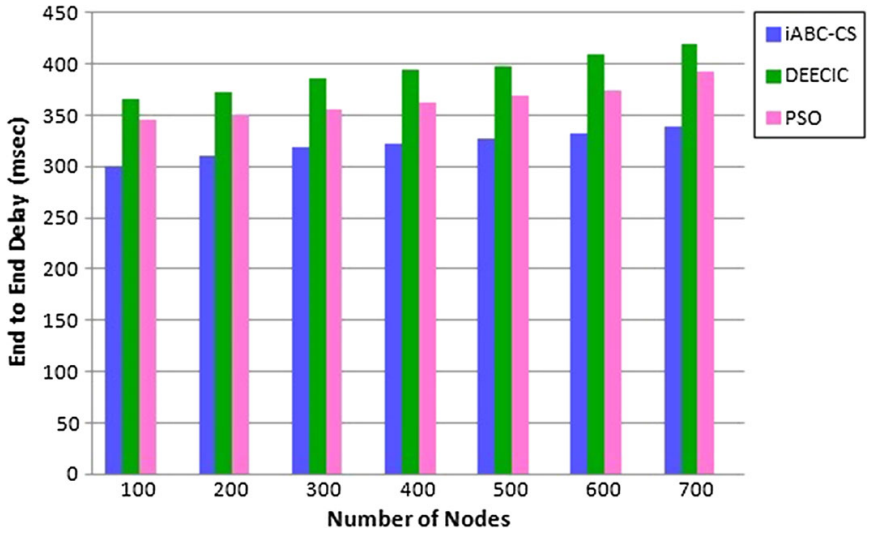


Fig. 13 End-to-end delay in WSN # 2

Figures 12 and 13 compares the end-to-end delay in both scenarios, which clearly show that iABC-CS deliver data packets with minimum end-to-end delay in both the scenarios among other which ultimately increase reliability of the network. Also in WSN #2, when the BS is located at a far distance from sensor nodes, iABC-CS will be able to delivery the highest data packets successfully with minimum delay. In PSO and DEECIC, data will be transmitted to BS using maximum number of hop-count ultimately exhaust the network with unnecessary end-to-end delay.

9 Conclusion

This paper presents an *iABC* metaheuristic, based on first of its kind *student's-t* cPDF and DE inspired improved search equation *ABC/rand-to-opt/1*, to improve exploitation capabilities a well as convergence rate of existing ABC metaheuristic. To demonstrate its improvement, we evaluated the proposed metaheuristic on scalable uni-modal and multi-

modal benchmark functions with standard metaheuristic. Further, we proposed *iABC-CS*, an artificial bee colony based clustering and scheduling scheme based on the proposed metaheuristic for WSNs, which selects optimal CHs based on an improved search equation and an efficient fitness function. In addition to this , we introduce optimal CH scheduling algorithm, which helps in balancing the energy level of the nodes thus enhance network life. At last we compare the performance of the proposed scheme with other clustering schemes to prove its validness over various performance metrics. Simulation results show that iABC-CS delivered highest PDR, consumes much less energy, extend network lifetime with minimum end-to-end delay as compared to its peers.

Acknowledgements The authors of the study acknowledge the contribution of I. K. Gujral Punjab Technical University, Kapurthala, Punjab, India.

References

1. Yick, J., Mukherjee, B., & Ghosal, D. (2008). Wireless sensor network survey. *Computer Networks*, *52*(12), 2292–2330.
2. Al-Karaki, J. N., & Kamal, A. E. (2004). Routing techniques in wireless sensor networks: A survey. *IEEE Wireless Communications*, *11*(6), 6–28.
3. Akkaya, K., & Younis, M. (2005). A survey on routing protocols for wireless sensor networks. *Ad hoc Networks*, *3*(3), 325–349.
4. Gaura, E. (2010). *Wireless sensor networks: Deployments and design frameworks*. Berlin: Springer.
5. Abbasi, A. A., & Younis, M. (2007). A survey on clustering algorithms for wireless sensor networks. *Computer Communications*, *30*(14), 2826–2841.
6. Tyagi, S., & Kumar, N. (2012). A systematic review on clustering and routing techniques based upon leach protocol for wireless sensor networks. *Journal of Network and Computer Applications*, *36*, 623–645.
7. Chamam, A., & Pierre, S. (2010). A distributed energy-efficient clustering protocol for wireless sensor networks. *Computers & Electrical Engineering*, *36*(2), 303–312.
8. Kulkarni, R. V., Forster, A., & Venayagamoorthy, G. K. (2011). Computational intelligence in wireless sensor networks: A survey. *IEEE Communications Surveys & Tutorials*, *13*(1), 68–96.
9. Das, S., Abraham, A., & Konar, A. (2009). Metaheuristic clustering. In *Studies in computational intelligence* (1st ed., Vol. 178). Berlin: Springer.
10. Samrat, L., & Udgata, A. A. S. (2010). Artificial bee colony algorithm for small signal model parameter extraction of MESFET. *Engineering Applications of Artificial Intelligence*, *11*, 1573–1592.
11. Karaboga, D., & Akay, B. (2009). A comparative study of artificial bee colony algorithm. *Applied Mathematics and Computation*, *214*(1), 108–132.
12. Heinzelman, W. B., Chandrakasan, A. P., Balakrishnan, H., et al. (2002). An application-specific protocol architecture for wireless microsensor networks. *IEEE Transactions on Wireless Communications*, *1*(4), 660–670.
13. Younis, O., & Fahmy, S. (2004). HEED: A hybrid, energy-efficient, distributed clustering approach for ad hoc sensor networks. *IEEE Transactions on Mobile Computing*, *3*(4), 366–379.
14. Yi, S., Heo, J., Cho, Y., & Hong, J. (2007). PEACH: Power-efficient and adaptive clustering hierarchy protocol for wireless sensor networks. *Computer Communications*, *30*(14), 2842–2852.
15. Selvakennedy, S., Sinnappan, S., & Shang, Y. (2007). A biologically-inspired clustering protocol for wireless sensor networks. *Computer Communications*, *30*(14), 2786–2801.
16. Jin, Y., Wang, L., Kim, Y., & Yang, X. (2008). EEMC: An energy-efficient multi-level clustering algorithm for large-scale wireless sensor networks. *Computer Networks*, *52*(3), 542–562.
17. Kumar, D., Aseri, T. C., & Patel, R. (2009). EEHC: Energy efficient heterogeneous clustered scheme for wireless sensor networks. *Computer Communications*, *32*(4), 662–667.
18. Yang, J., Xu, M., Zhao, W., & Xu, B. (2009). A multipath routing protocol based on clustering and ant colony optimization for wireless sensor networks. *Sensors*, *10*(5), 4521–4540.
19. Deng, S., Li, J., & Shen, L. (2011). Mobility-based clustering protocol for wireless sensor networks with mobile nodes. *IET Wireless Sensor Systems*, *1*(1), 39–47.
20. Song, M. A. O., & Zhao, C. (2011). Unequal clustering algorithm for WSN based on fuzzy logic and improved ACO. *The Journal of China Universities of Posts and Telecommunications*, *18*(6), 89–97.

21. Liu, Z., Zheng, Q., Xue, L., & Guan, X. (2012). A distributed energy-efficient clustering algorithm with improved coverage in wireless sensor networks. *Future Generation Computer Systems*, *28*(5), 780–790.
22. Attea, B. A., & Khalil, E. A. (2012). A new evolutionary based routing protocol for clustered heterogeneous wireless sensor networks. *Applied Soft Computing*, *12*, 1950–1957.
23. Hoang, D., Yadav, P., Kumar, R., & Panda, S. (2014). Real-time implementation of a harmony search algorithm-based clustering protocol for energy efficient wireless sensor networks. *IEEE Transactions on Industrial Informatics*, *10*, 774–783.
24. Kuila, P., & Jana, P. K. (2014). Energy efficient clustering and routing algorithms for wireless sensor networks: Particle swarm optimization approach. *Engineering Applications of Artificial Intelligence*, *33*, 127–140.
25. Karaboga, D., & Basturk, B. (2008). On the performance of artificial bee colony (ABC) algorithm. *Applied Soft Computing*, *8*(1), 687–697.
26. Zhang, R., & Wu, C. (2011). An artificial bee colony algorithm for the job shop scheduling problem with random processing times. *Entropy*, *13*(9), 1708–1729.
27. Gao, W., & L, S. (2011). Improved artificial bee colony algorithm for global optimization. *Information Processing Letters*, *111*(17), 871–882.
28. Neri, F., Iacca, G., & Mininno, E. (2013). Compact Optimization. In I. Zelinka, V. Snášel, & A. Abraham (Eds.), *Handbook of Optimization*. Intelligent Systems Reference Library (Vol. 38). Berlin: Springer
29. Gao, W., Liu, S., & Huang, L. (2012). A global best artificial bee colony algorithm for global optimization. *Journal of Computational and Applied Mathematics*, *236*(11), 2741–2753.
30. Abro, A. G., & Mohamad-Saleh, J. (2012). Enhanced global-best artificial bee colony optimization algorithm. In *Sixth UKSim-AMSS European symposium on computer modeling and simulation* (pp. 95–100).
31. Gao, W., Liu, S. Y., & Huang, L. L. (2013). A novel artificial bee colony algorithm based on modified search equation and orthogonal learning. *IEEE Transactions on Cybernetics*, *43*(3), 1011–1024.
32. Li, G., Niu, P., & Xiao, X. (2013). Development and investigation of efficient artificial bee colony algorithm for numerical function optimization. *Applied Soft Computing*, *12*(1), 320–332.
33. Guo, P., Cheng, W., & Liang, J. (2011). Global artificial bee colony search algorithm for numerical function optimization. *Seventh International Conference on Natural Computation*, *3*, 1280–1283.
34. Akay, B., & Karaboga, D. (2012). A modified artificial bee colony algorithm for real-parameter optimization. *Information Science*, *192*, 120–142.
35. Mininno, E., Cupertino, F., & Naso, D. (2008). Real-valued compact genetic algorithms for embedded microcontroller optimization. *IEEE Transactions on Evolutionary Computation*, *12*(2), 203–219.
36. Larranaga, P., & Lozano, J. A. (2001). *Estimation of distribution algorithms: A new tool for evolutionary computation*. Alphen aan den Rijn: Kluwer.
37. Walck, C. (2007). Statistical Distributions for experimentalists. Particle Physics Group.
38. Storn, R., & Price, K. (2010). Differential evolution—A simple and efficient heuristic for global optimization over continuous spaces. *Journal of Global Optimization*, *23*, 689–694.
39. Das, S., & Suganthan, P. N. (2011). Differential evolution: A survey of the state-of-the-art. *IEEE Transactions on Evolutionary Computation*, *15*, 4–31.
40. Gonuguntla, V., Mallipeddi. R., & Veluvolu, K. C. (2015). Differential evolution with population and strategy parameter adaptation. *Mathematical Problems in Engineering*.



Palvinder Singh Mann received his Bachelor's degree (B.Tech.) with Honours (Institute Gold Medal) in Information Technology from Kurukshetra University, Kurukshetra, Haryana, India in the year 2005, Master's degree (M.Tech.) in Computer Science and Engineering from Punjab Technical University, Jalandhar, Punjab, India in the year 2010 and Doctoral degree (Ph.D.) from IKG Punjab Technical University, Jalandhar, Punjab, India in the year 2017. He has published more than 50 research papers in various International Journals, International Conferences and National Conferences. His research interest includes Wireless Sensor Networks, Computational Intelligence and Digital Image Processing.



Satvir Singh received his Bachelor's degree (B.Tech.) from Dr. B. R. Ambedkar National Institute of Technology, Jalandhar, Punjab (India) with specialization in Electronics and Communication Engineering in year 1998, Master's degree (M.E.) from Delhi Technological University (Formerly, Delhi College of Engineering), Delhi (India) with distinction in Electronics and Communication Engineering in year 2000 and Doctoral degree (Ph.D.) from Maharshi Dayanand University, Rohtak, Haryana (India) in year 2011. He is Life Member of ISTE and Corporate Member of IETE. His fields of interest include Evolutionary Algorithms, High Performance Computing, Type-1 and Type-2 Fuzzy Logic Systems, Wireless Sensor Networks and Artificial Neural Networks for solving engineering problems. He has also published nearly 50 research papers in International Journals and Conferences.

PARAMETER ESTIMATION OF RC CIRCUITS USING EXTENDED KALMAN FILTER

Amit Kr Gautam[1]* and Sudipta Majumdar[2]

Electronics & Communication Engineering Department, Delhi Technological University, ShahbadDaulatpur, Delhi, 110042, India

[1*]amitgautam.cicdu@gmail.com, [2]korsudipta@rediffmail.com

Abstract

In this paper, the output voltage estimation of RC low pass filter (LPF) and RC high pass filter (HPF) has been proposed using extended Kalman filter (EKF). The proposed method demonstrates the high signal to noise ratio (SNR) as compared to least mean squares (LMS)method. Also, it has the advantage of easy design and implementation.

Keywords: **Extended Kalman filter, parameter estimation, state space representation.**

1. INTRODUCTION

Parameter estimation is an important area in the field of science and technology. Various estimation techniques have been used by researcher. There are two basic parameter estimation methods: - 1) methods based on optimization approaches and 2) methods based on stability theory. Differential evolution, particle swarm optimization are examples of optimization based methods and Lyapunov stability method, synchronization approach based on Lasalle's principle are stability based estimation methods. The parameter estimation methods based on the deterministic minimizes error function between model output and measurement data.

Various methods have been used for parameter estimation of systems. In [1], the effects of white noise perturbation on the parameters of electrical network have been analyzed and least square estimation has been used after transferring the deterministic model into stochastic models. [2] presented the total least square estimation of signal parameter via rotation invariance method. [3] proposed anextended stochastic gradient (ESG) filtering and multi innovative filtering for parameter estimation. [4] proposed a parameter estimation of permanent magnet synchronous machine using a dynamic particle swarm optimization method. We used extended Kalman filter for parameter estimation of resistor capacitor (RC) low pass filter (LPF) and high pass filter (HPF). EKF have been used in various applications such as signal processing, communication and navigation control [5]- [9].

RC low pass filter has many applications. It is used as a discrete time repetitive controller for a fly back inverter in continuous conduction mode. The RC low pass filter has been also used for tracking and rejection of periodic signals in a typical frequency range. In [10], RC circuit has application in microelectromechanical systems (MEMS) sensorthat includes a ring oscillator, an RC controlled pulse generator together with a self-tuned inverter converter. The RC high pass filter reduces the bandwidth of noise source. [11] proposed RC low pass filter with good asymptotic behavior in the pass band. In [12],

the RC LPF is also used in a flexible continuous time delta sigma modulator. [13] presents RC filter implementation in chopper stabilized thin film transistor low noise amplifier, which is used for EEG signal acquisition and biomarker extraction system. In [14], it is used in linear periodically time varying filter circuit which is used in spectrum scanner.

We proposed the output voltage estimation of RC LPF and HPF using EKF and compared the estimation performance with LMS algorithm. MATLAB simulations show that EKF gives higher SNR as compared to LMS method.

2. STATE SPACE MODELLING OF RC CIRCUITS

A second order dynamic low pass filter (LPF) with R and C components shown in Fig. 1 (a). Let $u_1(t)$ be the input sinusoidal signal. $V_{C_1}(t)$ and $V_{C_2}(t)$ are the capacitor voltages across C_1 and C_2 respectively. The state space model for the circuit shown in Fig.1(a) are obtained by using Kirchhoff current law (KCL). The equations are as follows:

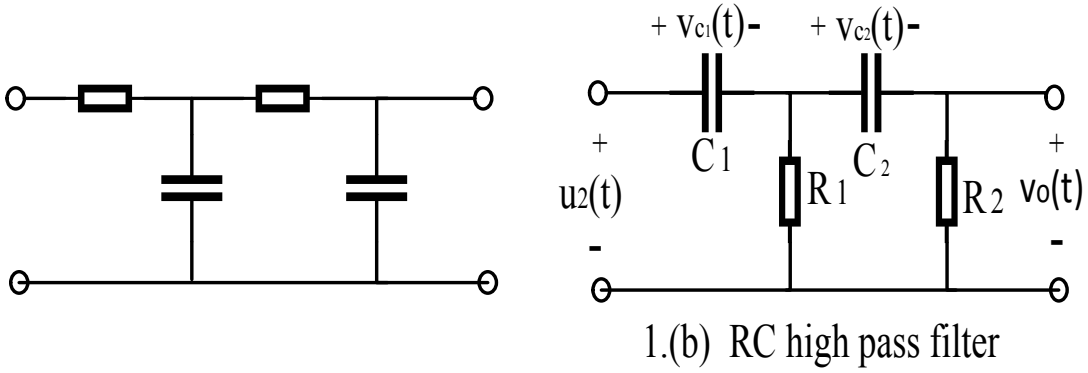


Figure 1. RC Low Pass Filter and High Pass Filter Circuit.

$$\frac{v_{c_1}(t)-u_1(t)}{R_1}+\frac{v_{c_1}(t)-v_{c_2}(t)}{R_2}+C_1\frac{dv_{c_1}}{dt}=0 \tag{1}$$

$$\frac{v_{c_2}(t)-v_{c_1}(t)}{R_2}+C_2\frac{dv_{c_2}}{dt}=0 \tag{2}$$

Representing equations (1) and (2) as state space model, we have

$$\begin{bmatrix}\frac{dv_{c_1}}{dt}\\ \frac{dv_{c_2}}{dt}\end{bmatrix}=\begin{bmatrix}\left(-\frac{1}{R_1C_1}-\frac{1}{R_2C_1}\right) & \frac{1}{R_1C_1}\\ \frac{1}{R_2C_2} & -\frac{1}{R_2C_2}\end{bmatrix}\begin{bmatrix}v_{c_1}(t)\\ v_{c_2}(t)\end{bmatrix}+\begin{bmatrix}\frac{1}{R_1C_1}\\ 0\end{bmatrix}u_1(t) \tag{3}$$

The output voltage of RCLPF can be written as:

$$y = v_{c_2}(t) \tag{4}$$

Or representing (3) and (4) in state space model, we have

$$\frac{dx}{dt} = Ax + Bu \tag{5}$$

$$y = Cx + Du \tag{6}$$

x represents the state vector and u is input vector at the time k. A, B and C are:

$$A = \begin{bmatrix} \left(-\frac{1}{R_1C_1} - \frac{1}{R_2C_1}\right) & \frac{1}{R_1C_1} \\ \frac{1}{R_2C_2} & -\frac{1}{R_2C_2} \end{bmatrix},\ B = \begin{bmatrix} \frac{1}{R_1C_1} & 0 \end{bmatrix}^T,\ C = \begin{bmatrix} 0 & 1 \end{bmatrix}$$

The state model in (5) and (6) can be discretized using first order exponential method. The transformed equations are expressed as

$$x_{k+1} = A_k x_k + B_k u_k + w_k \tag{7}$$

$$y_k = C_k x_k + D_k u_k + v_k \tag{8}$$

(7) and (8) are discrete representation of equations (5) and (6) respectively obtained using $t = k\Delta T$, where $k = 1, 2, 3...$ and ΔT is the sampling time. The matrices A_k, B_k, C_k and D_k are obtained by discretizing A, B, C and D matrices respectively. They are

$$A_k = e^{\Delta T} = I + A\Delta T = \begin{bmatrix} 1 - \left(\frac{\Delta T}{R_1C_1} + \frac{\Delta T}{R_2C_1}\right) & \frac{\Delta T}{R_1C_1} \\ \frac{\Delta T}{R_2C_2} & 1 - \frac{\Delta T}{R_2C_2} \end{bmatrix} \quad B_k = B\Delta T = \begin{bmatrix} \frac{\Delta T}{R_1C_1} & 0 \end{bmatrix}^T,$$

$$C_k = C = \begin{bmatrix} 0 & 1 \end{bmatrix} \text{ and } D_k = \begin{bmatrix} 0 \end{bmatrix}.$$

Similarly, state space model for HPF shown in Fig 1(b) can be expressed as

$$\begin{bmatrix} \frac{dv_{c_1}}{dt} \\ \frac{dv_{c_2}}{dt} \end{bmatrix} = \begin{bmatrix} \left(-\frac{1}{R_1C_1} - \frac{1}{R_2C_1}\right) & -\frac{1}{R_2C_1} \\ -\frac{1}{R_2C_2} & -\frac{1}{R_2C_2} \end{bmatrix} \begin{bmatrix} v_{c_1}(t) \\ v_{c_2}(t) \end{bmatrix} + \begin{bmatrix} \frac{1}{R_1C_1} + \frac{1}{R_2C_1} \\ \frac{1}{R_2C_2} \end{bmatrix} u_2(t) \tag{9}$$

$$y = [-1 \quad -1]\begin{bmatrix} v_{c_1}(t) \\ v_{c_2}(t) \end{bmatrix} + u_2(t) \tag{10}$$

where the matrices A_k , B_k , C_k and D_k for RC HPF can be obtained by discretizing equations (9)-(10) i.e. by substituting $t = k\Delta T$. For HPF circuit, they are:

$$A_k = \begin{bmatrix} 1-\left(\frac{\Delta T}{R_1C_1}+\frac{\Delta T}{R_2C_1}\right) & -\frac{\Delta T}{R_2C_1} \\ -\frac{\Delta T}{R_2C_2} & 1-\frac{\Delta T}{R_2C_2} \end{bmatrix}, B_k = \begin{bmatrix} \left(\frac{\Delta T}{R_1C_1}+\frac{\Delta T}{R_2C_1}\right) & \frac{\Delta T}{R_2C_2} \end{bmatrix}^T,$$

$$C_k = [-1 \quad -1] \text{ and } D_k = [1].$$

3. EXTENDED KALMAN FILTER ALGORITHM

EKF is broadly used as state estimation method. It consists of nonlinear state model and observation model. EKF is the best linear estimator with respect to minimum-mean-squared error. The EKF repeatedly computes set of recursive equations as the system operates. In general, a nonlinear system can be mathematically represented as

$$x_k = f(x_{k-1}, u_k) + w_{k-1} \tag{11}$$

$$y_k = g(x_k) + v_k \tag{12}$$

f and g are the nonlinear functions of process and observation model x_k and y_k respectively. u_k is the input vector at the time k . w_k and v_k are the white Gaussian noise with zero mean and variance $Q_k = E[w_k w_k^T]$ and $R_k = E[v_k v_k^T]$ respectively. Expanding (11) and (12) using Taylor's series, we have

$$x_k \equiv f(\hat{x}_{k-1|k-1}) + J_k(x_{k-1} - \hat{x}_{k-1|k-1}) + higher\ order\ terms \tag{13}$$

$$y_k \equiv g(\hat{x}_{k-1|k-1}) + H_k(x_{k-1} - \hat{x}_{k-1|k-1}) + higher\ order\ terms \tag{14}$$

J_k and H_k are Jacobian matrices that give partial derivates of f and g with respect to x .Therefore, we have

$$J_k = \frac{d}{dx_{k-1}} f(\hat{x}_{k-1|k-1}) \text{ and } H_k = \frac{d}{dx_k} g(x_k) \tag{15}$$

The higher order terms can be eliminated for simplify (13) and (14). The EKF steps are as follows:

3.1 Initialization of state

This step sets previous state $\hat{x}_{k-1|k-1}$ with covariance $P_{k-1|k-1}$. This step also initializes Q_k and R_k .

3.2 Prediction of state

After obtaining J_k using (15), predicted state is computed using A_k and B_k as follows:

$$\hat{x}_{k|k-1} = f(\hat{x}_{k-1|k-1})$$

or

$$\hat{x}_{k|k-1} = A_k \hat{x}_{k-1|k-1} + B_k u_k \quad (16)$$

Predicted covariance

$$P_{k|k-1} = A_k P_{k-1|k-1} A_k{}^T + Q_k \quad (17)$$

3.3 State update

This step obtains matrices C_k .

Kalman gain: This step computes the Kalman gain (K_K) using the following equation

$$K_K = P_{k|k-1} \mathrm{C_k}^T (\mathrm{C_k} P_{k|k-1} \mathrm{C_k}^T + R_k)^{-1} \quad (18)$$

Estimation of state and error covariance: This step update estimation with measurements as

$$\hat{x}_{k|k} = \hat{x}_{k|k-1} + K_k (Y_K - \mathrm{C_k}(\hat{x}_{k|k-1}) \quad (19)$$

And updates error covariance as

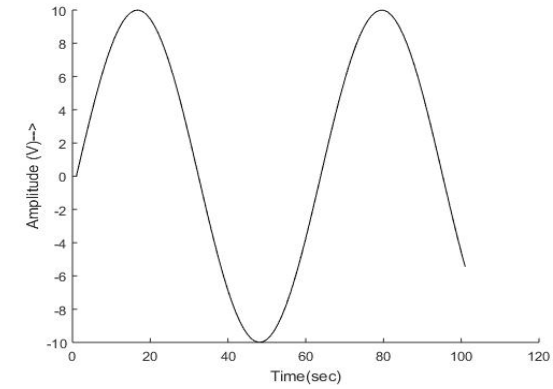
$$P_{k|k} = P_{k|k-1} (\mathrm{I} - K_k \mathrm{C_k}) \quad (21)$$

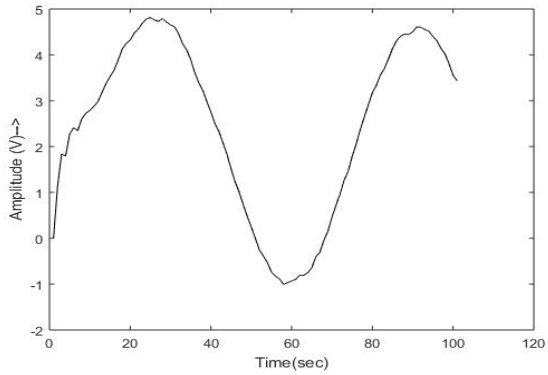
Repeat step 3.2.

After initialization, EKF uses time update and measurement updates.

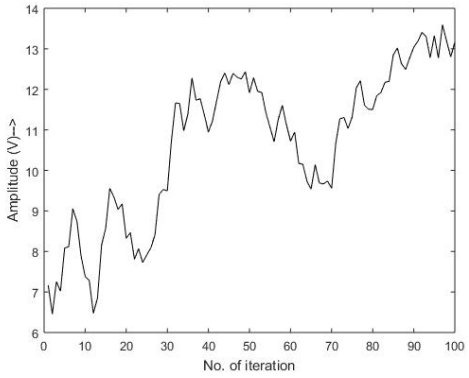
4. SIMULATION RESULTS

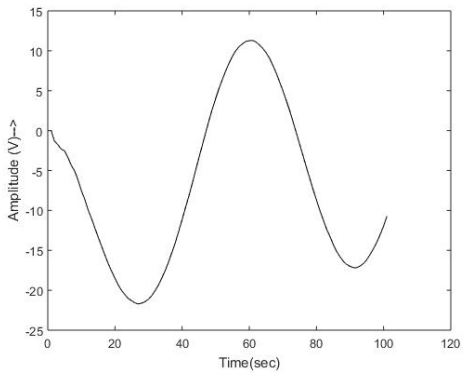
We estimated the output voltage of RC LPF and RC HPF for two different inputs. Fig. 2(a) shows the applied sinusoidal input with maximum amplitude of 10 V and frequency 0.01 Hz. The white Gaussian noise of zero mean and 0.5 variance has been used for estimation purpose. The output response of LPF circuit using EKF and LMS is shown in Fig 2 (b) and Fig 2 (c) respectively. Fig 2 (d) and Fig. 2 (e) show output voltage estimation of HPF using EKF and LMS respectively for sinusoidal noisy input. Fig. 2(f) and (g) shows the LPF estimated output voltage for noisy square wave input signal. Similarly, Fig. 2(h) and (i) shows output voltage estimation of HPF for noisy square wave input signal using EKF and LMS respectively. Table I shows the SNR in each case.


Amplitude (V)-->
Time(sec)


Amplitude (V)-->
Time(sec)

(a) (b)


Amplitude (V)-->
No. of iteration


Amplitude (V)-->
Time(sec)

(c) (d)

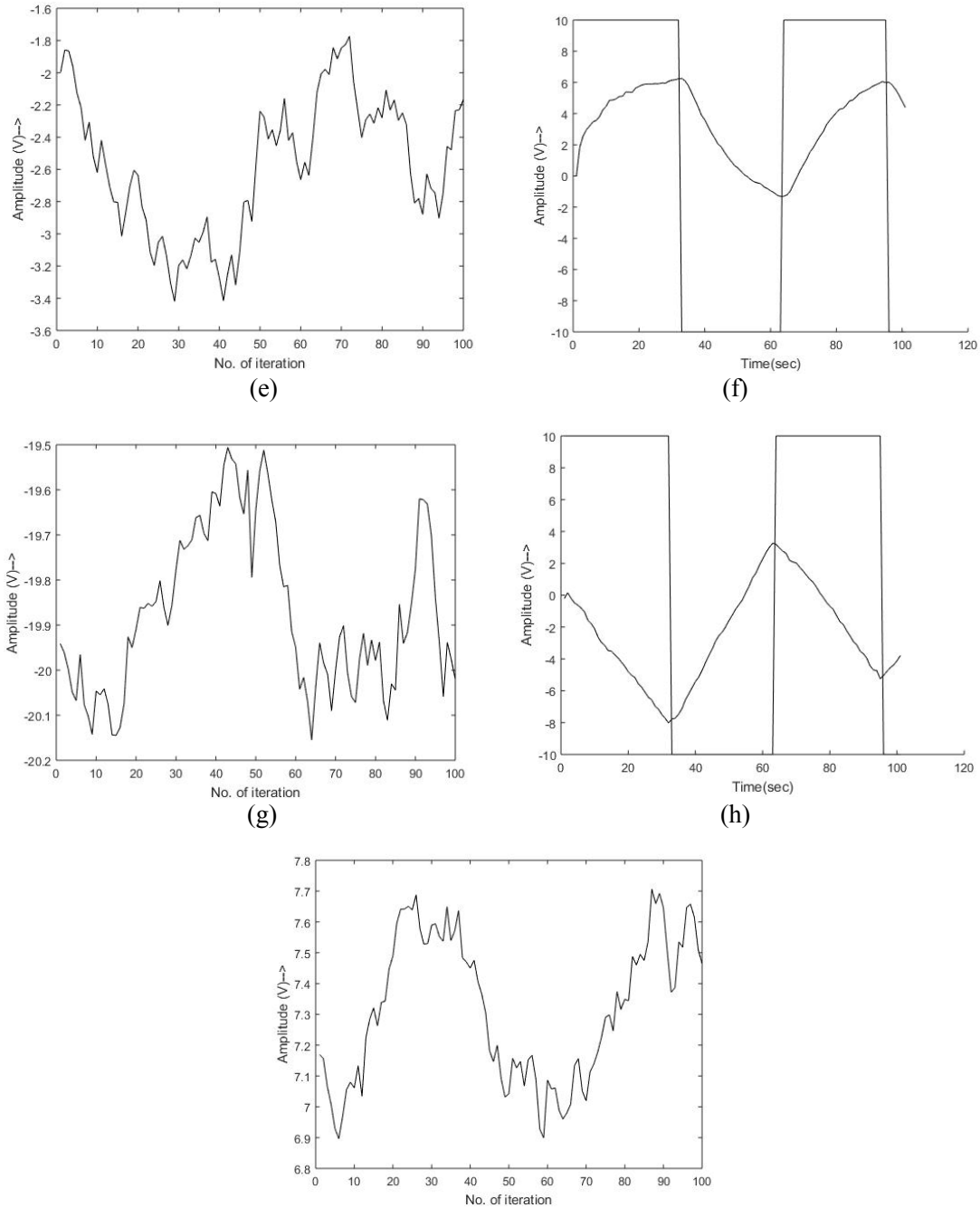


Figure 2. a) Input sinusoidal signal, b) Estimated output voltage of LPF using EKF, c) Estimated output voltage of LPF using LMS method, d) Estimated output voltage of HPF using EKF, e) Estimated output voltage of HPF using LMS method, f) Estimated output voltage of LPF using EKF with square wave input, g) Estimated output voltage of LPF using LMS method with square wave input, h) Estimated output voltage of HPF using EKF with square wave input. i) Estimated output voltage of HPF using LMS with square wave input.

Table 1. Comparison of SNR value for different method

Input signal	SNR by Proposed method (dB)	SNR by recursive LMS method (dB)
Sinusoidal signal in LPF	43.7696	32.7374
Square wave in LPF	55.994	34.314
Sinusoidal signal in HPF	58.144	26.866
Square wave in HPF	62.650	60.48

5. CONCLUSIONS

The simulations show the output voltage estimation of RC LPF and HPF using EKF. The Table I shows that EKF provide better estimation as compared to LMS method as EKF takes system noise and measurement noise into account. Also, it has the advantage of easy design and implementation.

Acknowledgment

The first author would like to thank UGC for fellowship assistance.

References:

[1] P. Nabati, R. Farnoosh, "Stochastic perspective and parameter estimation for RC and RLC electrical circuits", Int. J. Nonlinear Anal. Appl., vol. 6, no.1,**(2015)**, pp. 153-161.

[2] Y. Trachi, E. Elbouchikhi, V. Choqueuse, M.E. Benbouzid, T. Wang, "A Novel Induction Machine Fault Detector Based on Hypothesis Testing", IEEE Transactions on Industry Applications, vol. 53, no.3, **(2017)**, pp. 3039-48.

[3] Pan J, Jiang X, Wan X, Ding W,"A filtering based multi-innovation extended stochastic gradient algorithm for multivariable control systems", International Journal of Control, Automation and Systems, vol. 15, no.3, **(2017)**, pp. 1189-1197.

[4] Liu ZH, Wei HL, Zhong QC, Liu K, Xiao XS, Wu LH,"Parameter estimation for VSI-Fed PMSM based on a dynamic PSO with learning strategies", IEEE Transactions on Power Electronics,vol. 32, no. 4, **(2017)**, pp. 3154-65.

[5] Sun Y, Wu X, Cao J, Wei Z, Sun G,"Fractional extended Kalman filtering for non-linear fractional system with Lévy noises", IET Control Theory & Applications,Vol. 11, no. 3, **(2016)**, pp. 349-358.

[6] Karimipour H, Dinavahi V,"Extended Kalman filter-based parallel dynamic state estimation",IEEE transactions on smart grid,Vol. 6, no. 3, **(2015)**, pp. 1539-49.

[7] Singleton RK, Strangas EG, Aviyente S,"Extended Kalman filtering for remaining-useful-life estimation of bearings", IEEE Transactions on Industrial Electronics,Vol. 62, no. 3, **(2015)**, pp. 1781-90.

[8] Yin, Zhonggang, Guoyin Li, Yanqing Zhang, Jing Liu, Xiangdong Sun, and Yanru Zhong. "A Speed and Flux Observer of Induction Motor Based on Extended Kalman Filter and Markov Chain", vol. 32, no. 9,**(2016)**, pp.7096-7117 .

[9] Chowdhary G, Jategaonkar R,"Aerodynamic parameter estimation from flight data applying extended and unscented Kalman filter", Aerospace science and technology,vol.14, no. 2, **(2010)**, pp. 106-17.

[10] Arefin MS, Redouté JM, Yuce MR,"A Low-Power and Wide-Range MEMS Capacitive Sensors Interface IC Using Pulse-Width Modulation for Biomedical Applications", IEEE Sensors Journal,Vol. 16, no. 17, **(2016)**, pp. 6745-54.

[11] Mitros P,"Filters with decreased passband error", IEEE Transactions on Circuits and Systems II: Express Briefs,Vol. 63, no. 2, **(2016)**, pp.131-5.

[12] Yang Xu, Xinwang Zhang, Zhihua Wang, and Baoyong Chi,"A Flexible Continuous-Time ΔΣ ADC With Programmable Bandwidth Supporting Low-Pass and Complex Bandpass Architectures", IEEE transactions on very large scale integration (vlsi) systems, vol. 25, no. 3, **(2017)**,pp. 872-880.

[13] Moy T, Huang L, Rieutort-Louis W, Wu C, Cuff P, Wagner S, Sturm JC, Verma N,"An EEG acquisition and biomarker-extraction system using low-noise-amplifier and compressive-sensing circuits based on flexible, thin-film electronics", IEEE Journal of Solid-State Circuits,Vol. 52, no. 1, **(2017)**, pp. 309-21.

[14] Li J, Zheng WX, Gu J, Hua L,"Parameter estimation algorithms for Hammerstein output error systems using Levenberg–Marquardt optimization method with varying interval measurements", Journal of the Franklin Institute,Vol. 354, no. 1, **(2017)**, pp. 316-31.

International Journal of Research in Engineering and Innovation (IJREI)
journal home page: http://www.ijrei.com
ISSN (Online): 2456-6934

Performance improvement in integrated refrigeration system

R.S. Mishra

Department of Mechanical Engineering, Delhi Technological University, Delhi, India

Abstract

The integrated refrigeration system (IRS) is proposed for waste heat recovery from superheat horn of vapour compression refrigeration cycle. The waste heat rejected by the vapour compression system is recovered through heat exchanger is utilized to run the generator of absorption refrigeration system. The heat rejected by the condenser is recovered to heat the water because recovery of waste heat is contributing in conservation of energy which would help in the reduction of global warming. In this system, the waste heat is being utilized to run vapour absorption system (VARS) therefore there will be increase in overall cooling capacity of the system and increase in coefficient of performance (COP).
© 2018 ijrei.com. All rights reserved
Key words: Refrigeration systems, integrated refrigeration system, Thermodynamic Analysis systems

1. Introduction

Refrigeration and air conditioning systems have a major impact on energy demand with roughly 30% of total energy consumption in the world. A rough estimate of waste heat available from refrigeration and air conditioning system indicates that about 3-5 kW of waste energy is rejected to the environment for every kilowatt of energy expended by the compressor. The use of heat operated refrigeration systems help to reduce problems related to global environmental, such as the so called greenhouse effect from CO2 emission from the combustion of fossil fuels in utility power plants. The objective of this paper is to perform first law analysis of Integrated Refrigeration System (IRS). It shall include the computation of the following

- Selection of proper refrigerant for VCR system.
- Cooling capacity enhancement of IRS.
- Increase in overall COP.

Effect of variation in parameters such as absorber temperature, generator temperature, condenser temperature, evaporator temperature, effectiveness and efficiency of compressor etc. This paper mainly deals with the collection of waste heat from refrigeration and air conditioning plants and to utilization of that waste heat as the heat source in the generator of vapour absorption refrigeration system considering the requirement of Cooling.

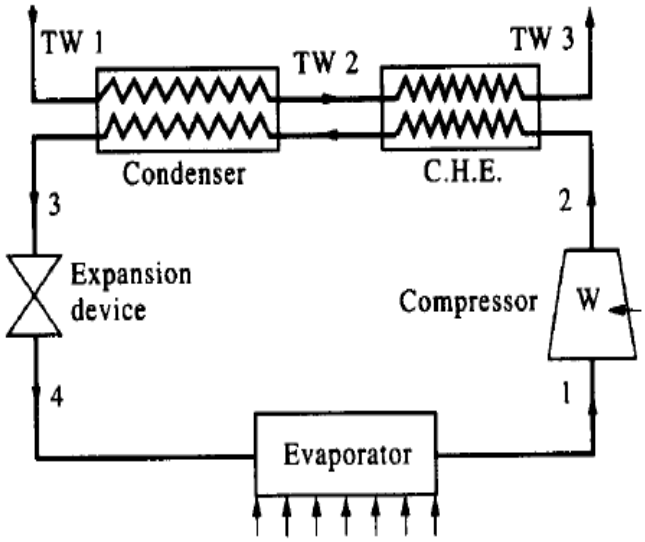


Figure 1: Vapour Compression refrigeration system

2. Literature Review

Hwang [1] presented and analyzed the performance potential of a refrigeration system that was integrated with a micro-

Corresponding author: R.S. Mishra
Email Id: hod.mechanical.rsm@dtu.ac.in

turbine and an absorption chiller (RMA). The waste heat from the micro-turbine operates the absorption chiller, which provides additional cooling. This additional cooling capacity can be utilized either to subcool the liquid exiting the condenser of the refrigeration system or to precool the air entering the condenser in the refrigeration system. Sarah Kim,[2] carried out the theoretical performance of ionic-liquid based working fluids in an absorption refrigeration system The IL 1-butyl-3-methylimidazolium hexa-fluoro-phosphate and five hydrofluorocarbons (HFCs) were selected as the absorbent and refrigerant, respectively. Using Redlich–Kwong equation of state and two-phase pressure-drop model were used for computing the thermodynamic conditions and performance of the working-fluid pairs. The effects of the disorder and absorber temperatures, solution heat exchanger, and accessibility of waste heat on the system performance were evaluated. R152a found the highest coefficient of performance, 57.3, when the disrober operated on waste heat only and the disrober and absorber were operated at 373.15 and 300.65 K, respectively. The friction-loss component of the total pumping work was observed below 2.5% of the pumping work for all refrigerants Upendra Kumar [3] analyzed configuration of combined refrigeration system consisting of a compression chiller and an absorption chiller that is driven by a micro turbine to generate cooling at low temperatures. The compression chiller is operated directly by the micro turbine at the low temperature stage and the waste heat from the micro turbine is used to drive the absorption chiller that operates at the high temperature stage and helps to the compression chiller performance and concluded that the use of this configuration of integrated refrigeration system is more efficient and less energy consuming than the system without absorption chiller. Aphornratana & Sriveerakul [4] presented an experimental investigation of a single-effect absorption using aqueous lithium–bromide as working fluid. A 2 kW cooling capacity experimental refrigerator was tested with various operating temperatures. It was found that the solution circulation ratio (SCR) has a strong effect on the system performance. The measured SCR was 2–5 times greater than the theoretical prediction and found that the low performance of the absorber. The use of solution heat exchanger could increase the COP by up to 60%. Hong guangJin [5] analyzed. the performance of a vapour compression-absorption cascaded refrigeration system (CRS) under fouled conditions by considering main effect of fouling is to decrease the effectiveness of the heat exchanger and found that the overall conductance (UA) of the heat exchanger is decreased due to fouling is to reduce the effective size of the heat exchanger and observed that the percentage decrease in the overall conductance value (UA) of evaporator and condenser due to their fouling is varied from 0 to 50% and its consequences on various aspects of CRS are generated to ascertain any possible patterns. From first law analysis for a clean evaporator and condenser, the electricity consumption is 67.5% less than vapour compression system (VCS) for the same cooling capacity. CRS is able to save only 61.3% of electrical energy when evaporator and condenser conductance is reduced by 50% due to fouling. Evaporator and condenser fouling decreased the COP and rational efficiency of the system by 4.7% and 10.5% respectively and also found that irreversibility in the evaporator and condenser is increased by 42.4% and 62.1% respectively, when their individual performance is degraded by 50% due to fouling. Kaushik and Singh [6] presented an investigation of the feasibility of heat recovery from the condenser of a vapour compression refrigeration (VCR) system through a Canopus heat exchanger (CHE) between the compressor and condenser components as shown in figure. The parametric results obtained for different working fluids, such as R-22, R-12, R-717 and R-500, had been presented. Kaynakli et.al [7] presented a detailed thermodynamic analysis of the water/lithium bromide absorption refrigeration cycle. The influences of operating temperature and effectiveness of heat exchanger on the thermal loads of components, coefficients of performance and efficiency ratio were investigated. Aprea and Renno [8] presented the experimental studies of performances of a vapour compression refrigeration plant using as working fluids R22 and its substitute R417A (R125/R134a/R600, 46.6/50/3.4% in mass). This type of plant is applied to a commercially available cold store, generally adopted for preservation of foodstuff. An integrated refrigeration system (IRS) with a gas engine, a vapour-compression chiller and an absorption chiller was set up and tested by Sun [9]. The vapour-compression refrigeration cycle was operated directly by the gas engine. The waste heat from the gas engine operates the absorption refrigeration cycle, which provides additional cooling. Riffat and Shankland [10] presented the integration of different types of absorption systems with vapour-compression systems. The performances of such systems have been analyzed thermodynamically using various refrigerant/absorbent pairs. The paper concerned with the intermittent absorption system, the intermittent absorption/vapour recompression system and the combined intermittent absorption/vapour compression system. Saskaki et al. [11] have proposed a Cascaded System comprising of Vapor-Compression and Absorption refrigeration cycle. The vapor-compression equipment cools the building space, and the absorption equipment “pumps” the heat rejected from the vapour compression system up to the temperature needed to reject it to the ambient air. In this case, the vapor-compression condenser and the absorption system evaporator are in thermal communication. The temperature lift for both refrigeration systems is reduced. Rinnai Corporation [12] has patented such a concept (2004) of Cascaded System comprising of Absorption and Vapor-Compression refrigeration cycle. The absorption equipment cools the building space, and the vapor-compression equipment “pumps” the rejected heat up to the temperature needed to reject it to the ambient air. In this case, the absorber from the absorption system is in thermal communication with the evaporator of the vapor-compression system.

3. Thermodynamic Analysis of Integrated Refrigeration System

The Thermodynamic Analysis of integrated refrigeration system (IRS) is done for vapour compression refrigeration (VCR) system with CHE and vapour absorption refrigeration system (VARS)

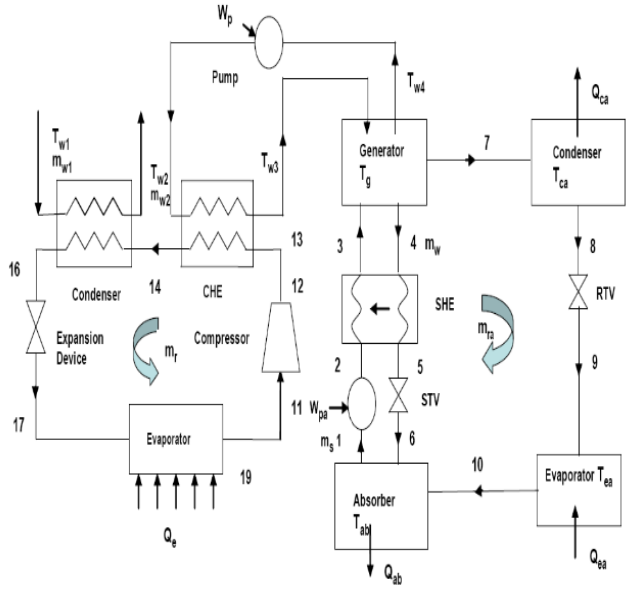


Figure .2.a Schematic diagram of an Integrated Refrigeration System (IRS)

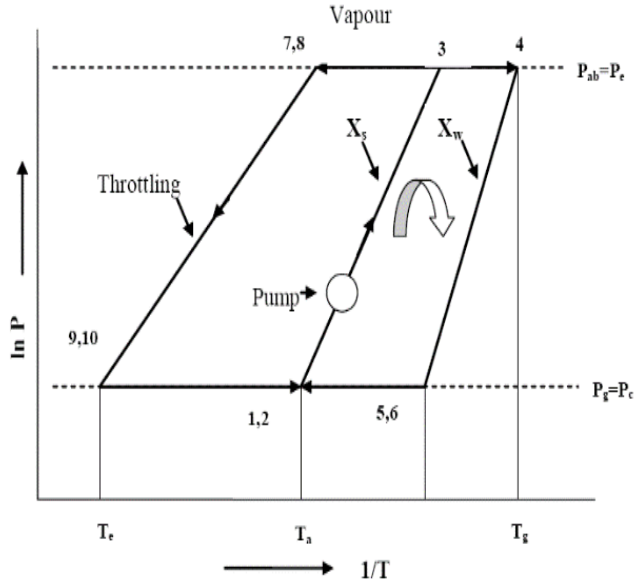


Figure 2.b: Single effect vapour absorption Réfrigération cycle on log p-1/T coordinates.

The following equations are based on mass, energy and concentration balance used in the performance analysis.

$m_s*X_s=m_w*X_w$
$m_s=m_{ra}+m_w$
Pump work $W_{pa}=m_s*V_g*(P_g-P_{ab})/1000$
$E=(Tg-T5)/(Tg-Tab)$
$W_{pa}=m_s*(h_2-h_1)$
$E1=Qg/DODS$
$m_s*(h_3-h_2)=m_w*(h_4-h_5)$
Energy balance in generator
$m_s*h_3+Q_g=m_w*h_4+m_{ra}*h_7$

3.1 Heat added to Generator

$Q_g=m_{w2}*C_{pw2}*(T_{w3}-T_{w2})+m_{w2}*h_{fg}_T_{w3}$
Heat transffer Condenser
$Q_{ca}=m_{ra}*(h_7-h_8)$
Energy balance in absorber
$Q_{ab}+m_s*h_1=m_{ra}*h_{10}+m_w*h_6$
Energy balance in Canopus Heat Exchanger
$m_{w2}*C_{pw}*(T_{w3}-T_{w2})+m_{w2}*h_{fg}_T_{w3}=m_r*(h_{13}-h_{14})$
Compressor work $W_c=m_r*(h_{12}-h_{11})$

3.2 Mass flow rate of refrigerant

$COP=h_{19}-h_{17}/(h_{12}-h_{11})$
$m_r=TR*3.5168/(h_{19}-h_{17})$
$scr=m_s/m_{ra}$

3.3 Degree of de-superheating

$DODS=m_r*(h_{13}-h_{14})$
Heat rejected by condenser+CHE
$Q_c=m_r*(h_{13}-h_{16})$

3.4 Heat Recovered By Canopus Heat Exchanger

$Qe=TR*3.5168$
$CAN=m_{w2}*C_{pw}*(T_{w3}-T_{w2})+m_{w2}*h_{fg}_T_{w3}$
$QE\%=Q_{ea}*100/Q_e$
$DODS\%=(DODS*100)/Q_c$
$COPa=Q_{ea}/(W_{pa}+Q_g)$
$COP\%=(COPc-COP)*100/COP$
$COPc=(Q_{ea}+Q_e)/(W_{pa}+W_c)$

To evaluate the integrated Refrigeration system with the following assumptions were made.

- The flow through all the components is under steady state.
- The pressure drop due to friction within the absorption refrigeration system can be neglected, except through the expansion valve.
- The fluid streams in the piping between the components and the heat exchangers are adiabatic.
- The strong solution at the outlet of the absorbers and the weak solution at the outlet of the generators are saturated.
- Refrigerant vapour alone leaves the generators, that is, it does not contain any traces of the absorbent.

- The temperature and concentration of LiBr aqueous are in equilibrium at the saturated pressure of LiBr aqueous.
- The LiBr fraction pressure is neglected: i.e. the pressure in the vapour phase is equal to the saturated pressure of water.

4. Results and Discussions

The following input data have been used to validate the proposed thermal model.
Chilling of water: -2°C, Storage of milk: -5°C, Ice silo: -10°C, Ice cream: -20°C,
Fishery item: -25°C, Cold storage & deep freezer: 30°C and simulated results from validates the proposed model table- 1.

Table-1: Simulated Results from developed Program.

Parameters	From program
COP_{VARS}	0.7659
P_{ca} KPa	7.38
P_{ea} KPa	1.2135
P_{g} KPa	7.38
Q_{ab} KW	4.34
Q_{ca} KW	3.77
Q_{ea} KW	3.517
Q_{g} KW	4.59
m_{ra} Kg/s	0.0015
Xs %	57.7
Xw %	65.4

Selection criterion for input parameters and their values are depending upon the different applications of the system the evaporator temperature has been varied in the range of -1 to -35°C in step of 1°C and the normal ambient conditions were the deciding factor for the temperature range of condenser and absorber, which is 30°C to 50°C in step of 1°C. The evaporator temperature for the vapour absorption refrigeration system is taken on the basis of various air conditioning applications and it ranges from 2-14°C. The thermodynamic and transport property functions for many fluids including water, dry and moist air. Included in the property database are thermodynamic properties for H_2O-LiBr and NH_3-H_2O mixtures used. Fig-3 shows the variation of heat added with evaporator of vapour absorption system by varying evaporator temperature of vapour compression refrigeration system VCRS for different refrigerants i.e. (R717 and R22) for 30ºC absorber temperature and 35ºC of condenser temperature, with 85ºC of water temperature along with evaporator temperature of T_{eva}=7ºC, by considering 0.80 of heat exchanger effectiveness with compressor efficiency of 0.85 and it was observed that the heat added to absorber increases when evaporator temperature is decreased in both refrigerants. The better thermodynamic performances is observed by using R717 as compared to R22 which produces global warming and depleting ozone layer. Similarly Fig-4 shows the variation of % increase in coefficient of performance with varying evaporator temperature of vapour compression refrigeration system VCRS for different refrigerants i.e. (R717 and R22) for 30ºC absorber temperature and 35ºC of condenser temperature, with 85ºC of water temperature along with evaporator temperature of T_{eva}=7ºC, by considering 0.80 of heat exchanger effectiveness with compressor efficiency of 0.85 and it was observed that the percentage coefficient of performance (% COP)of the system is increases when evaporator temperature is decreased in both refrigerants. The better thermodynamic performances is observed by using R717 as compared to R22 which produces global warming and depleting ozone layer . Fig-5 shows the variation of thermal load on Generator with varying cooling water inlet temperature for CHE for different refrigerants i.e. (R717 and R22) for 30ºC absorber temperature and 35ºC of condenser temperature, with 85ºC of water temperature along with evaporator temperature of T_{eva}=7ºC, by considering 0.80 of heat exchanger effectiveness with compressor efficiency of 0.85 and it was observed that the thermal load variation on Generator with varying cooling water inlet temperature for heat exchanger is slightly increases for different refrigerants when cooling water inlet temperature for heat exchanger is increased in both refrigerants. The better thermodynamic performances is observed by using R717 as compared to R22 which produces global warming and depleting ozone layer. Fig-6 shows the variation in coefficient of performance with varying absorber temperature for different refrigerants i.e. (R717 and R22) for -30ºC 0f evaporator temperature and 35ºC of condenser temperature, with 85ºC of water temperature along with evaporator temperature at T_{eva}=7ºC, by considering 0.80 of heat exchanger effectiveness with compressor efficiency of 0.85 and it was observed that the variation in coefficient of performance with varying absorber temperature for different refrigerants i.e. (R717 and R22) rapidly decreases for different refrigerants when absorber temperature is increases in both refrigerants. The better thermodynamic performances is observed by using R717 as compared to R22 which produces global warming and depleting ozone layer. Fig-7 shows the variation in heat added to evaporator of vapour absorption refrigeration system (VARS) with varying absorber temperature for different refrigerants i.e. (R717 and R22) for -30ºC 0f evaporator temperature and 35ºC of condenser temperature, with 85ºC of water temperature along with evaporator temperature at T_{eva}=7ºC, by considering 0.80 of heat exchanger effectiveness with compressor efficiency of 0.85 and it was observed that the heat added to evaporator of vapour absorption refrigeration system (VARS)is decreases with varying absorber temperature for different refrigerants. The better thermodynamic performances is observed by using R717 as compared to R22 which produces global warming and depleting ozone layer

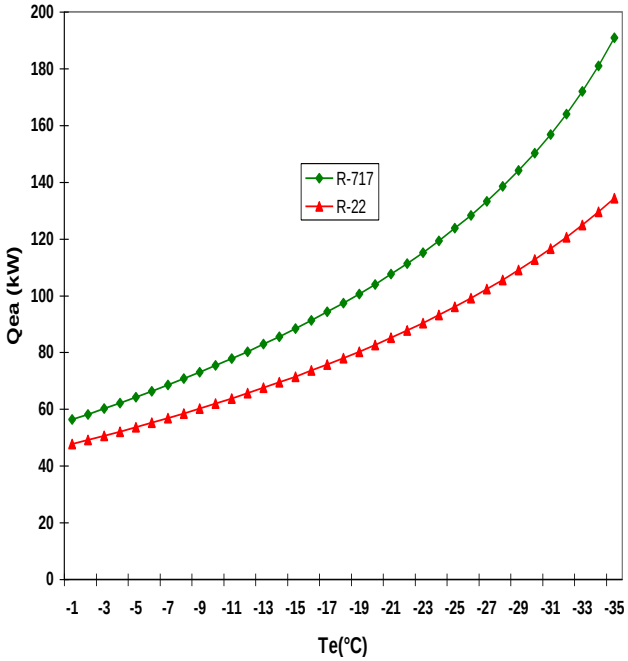


Figure 3: Heat added variations with evaporator of vapour absorption system by varying evaporator temperature of VCR for different refrigerants $T_{absorber}$=30°C, $T_{condenser}$=35°C, T_{eva}=7°C, T_{w2}=85°C, Effectiveness_$_{HE}$ =0.8, η_c=0.85

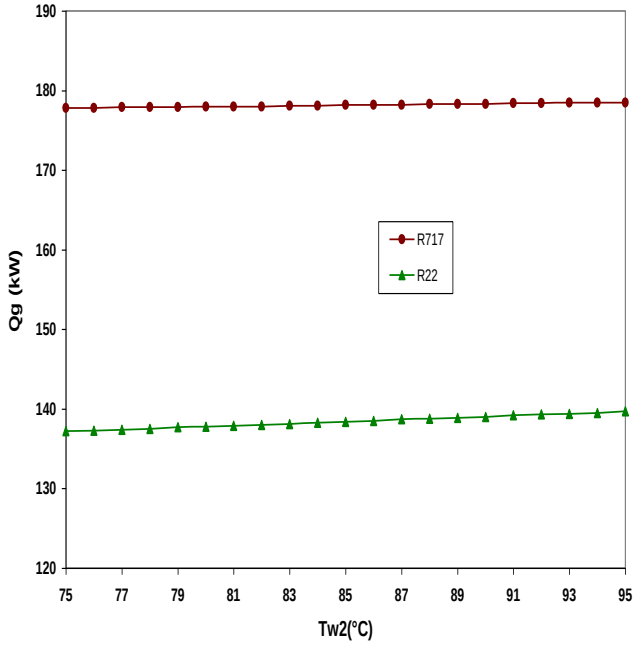


Figure 5: Variation of thermal load on Generator with varying cooling water inlet temperature for CHE for different refrigerants at T_e=30°C, T_{ab}=30°C, T_c=35°C, T_{eva}=7°C, Effectiveness_$_{HE}$ =0.8, η_c=0.85.

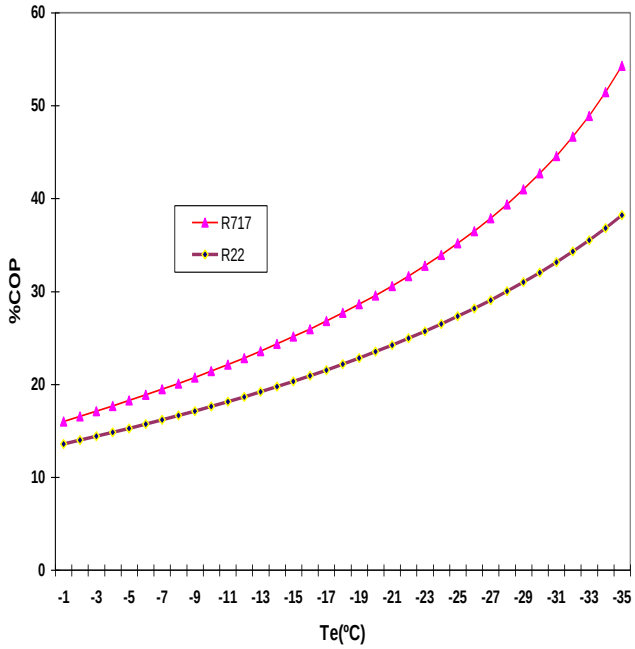


Figure 4: Variation in % increase in coefficient of performance with varying evaporator temperature For different refrigerants at $T_{absorber}$=30°C, T_{cond}=35°C, T_{eva}=7°C,T_{w2}=85°C, Effectiveness_$_{HE}$ =0.8, η_c=0.85.

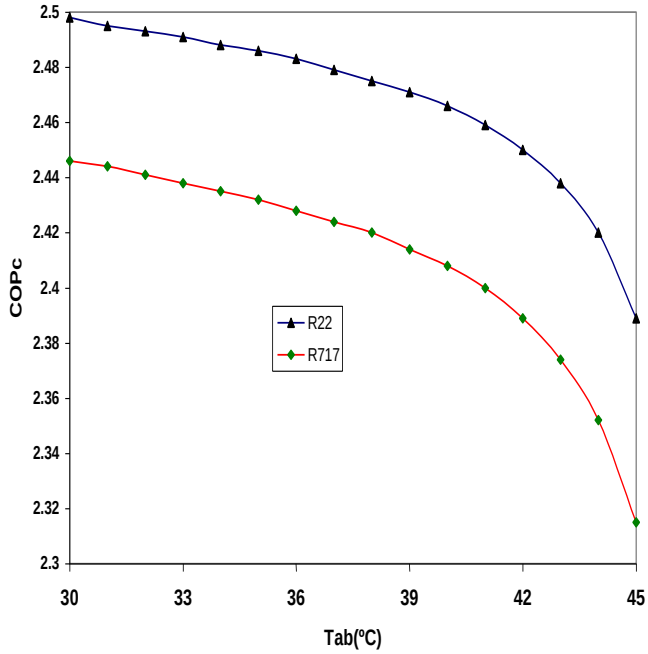


Figure 6: Variation in coefficient of performance with varying absorber temperature for different refrigerants at T_e=- 30°C, T_{w2}=85°C, T_c=35°C, T_{ea}=7°C, Effectiveness_$_{HE}$ =0.8, η_c=0.85

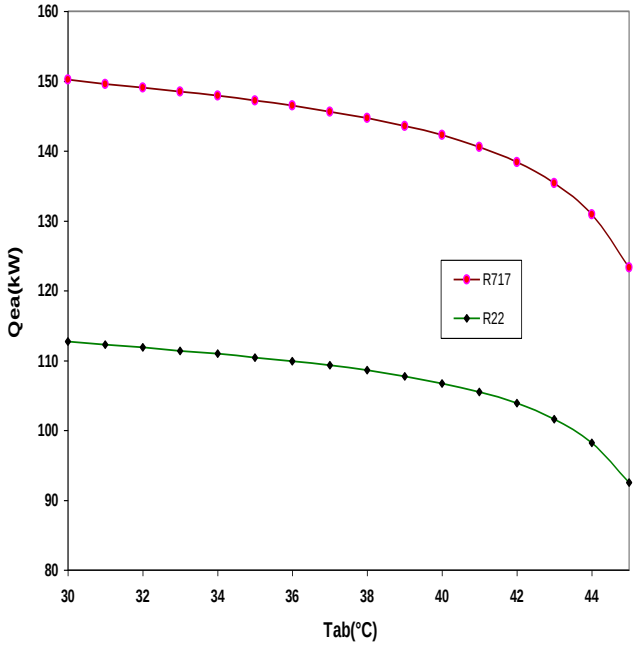


Figure 7: Variation in heat added to evaporator of VAR with varying absorber temperature for different refrigerants at T_{eva} =- 30°C, T_{w2}=85°C, T_{cond}=35°C, T_{ea}=7°C, Effectiveness_HE =0.8, η_c=0.85.

5. Conclusion

A computer program has been developed and following conclusions were made

(i) Degree of de-superheating (DODS) for different refrigerants like R-717, R-32, R-22, R-600, R-500, R-134A, R-502, R-290, R-114, R-124, R-125 and R-507A, have been computed and the value of first law efficiency in terms of COP of this system is found to be about 2–6

(ii) This increase in COP is about 40% as compared to the vapour compression refrigeration system (VCRS). The cooling capacity (Q_{ea}) is obtained in VARS system is about 150 KW by using the waste heat from superheating horn of a vapour compression refrigeration system (VCRS) system. As inlet water temperature (T_{W2}) to heat exchanger increases, its efficiency also increases slightly. Computed Results from model are better for R-717 (ammonia) as refrigerant as compared to R22.

References

[1] Y. Hwang,[2004] Potential energy benefits of integrated refrigeration system with microturbine and absorption chiller, International Journal of Refrigeration 27 (8)

[2] Sarah Kim, Nishith Patel, and Paul A. Kohl (2013), Performance Simulation of Ionic Liquid and Hydrofluorocarbon Working Fluids for an Absorption Refrigeration System Ind. Eng. Chem. Res., , 52 (19), pp 6329–6335.

[3] Upendra Kumar1 and Amit Kumar[2013] performance analysis of micro gasturbine driven through compression absorptionrefrigeration systems Int. J. Mech. Eng. & Rob. Res. 2013.

[4] Aphornratana and Sriveerakul (2007) Experimental studies of a single-effect absorption refrigerator using aqueous lithium–bromide: Effect of operating condition to system performance 2007.

[5] Hong guangJin [2014] Thermodynamic performance optimization of the absorption-generation process J. energy South. Afr. ISSN 2413-3051, vol.25 no.4.

[6] S C Kaushik, M Singh [1995] Feasibility and design studies for heat recovery from a refrigeration system with a canopus heat exchanger, Heat Recovery systems and CHP 15 (7), page.665-673.

[7] Omer Kaynakli (2014) Thermodynamic Analysis of Vapor Absorption Refrigeration Cycle with Three Heat Exchangers: User-friendly Software 2nd International Conference on Research in Science, Engineering and Technology (ICRSET'2014), March 21-22, 2014 Dubai (UAE)

[8] Ciro Aprea Carlo Renno[2004] An experimental analysis of a thermodynamic model of a vapour compression refrigeration plant on varying the compressor speed , International Journal of Energy Research 28(6):537 - 549 · May

[9] Sun [2007]. A combined heat and cold system driven by a gas industrial engine Energy Conversion and Management 48(2):366-369 · 2007.

[10] S. B. Riffat & N. Shankland.[1993] Integration of different types of absorption systems with vapour-compression systems

Available online at www.sciencedirect.com

ScienceDirect

Journal of Electrical Systems and Information Technology xxx (2017) xxx–xxx

www.elsevier.com/locate/jesit

Performance investigations of APSO tuned linear and nonlinear PID controllers for a nonlinear dynamical system

Sudarshan K. Valluru *, Madhusudan Singh

Department of Electrical Engineering, Delhi Technological University, Bawana Road, Delhi 110042, India

Received 24 September 2016; received in revised form 15 November 2017; accepted 4 February 2018

Abstract

This paper investigates the performance of adaptive particle swarm optimization (APSO) algorithm to find the best optimal gain parameters (K_p, K_i, K_d) in linear PID (L-PID) and nonlinear PID (NL-PID) controllers for the trajectory control of a nonlinear dynamical system (NLDS). Mathematical modeling, stability and performance analysis of a NLDS are being carried out with L-PID and NL-PID controllers. It is found that the APSO based tuning of NL-PID controller provides better tracking of NLDS than L-PID controller in respect of its search domain, premature convergence, and computational efficiency. Simulation analysis of various variables of controllers and system response such as error, cost function, and response of NLDS and their comparison to that of APSO tuned L-PID controller is described.

© 2018 Electronics Research Institute (ERI). Production and hosting by Elsevier B.V. This is an open access article under the CC BY-NC-ND license (http://creativecommons.org/licenses/by-nc-nd/4.0/).

Keywords: Linear PID; Non-linear PID; PID tuning; Swarm intelligence; Nonlinear dynamical system

1. Introduction

In the real world, the majority of the physical systems are nonlinear and dynamical and may exhibit unpredictable behavior due to the random external influences. Analysis of these systems is usually complicated when compared to the linear systems. The substantial characteristic of their performance is probably flouted if these nonlinear systems are investigated and designed by using linearization techniques. A nonlinear system is stable for one kind of input and may exhibit instability for another kind of input. There is no general technique for resolving nonlinear systems. Though a nonlinear dynamical system can be linearizable to some extent, discontinuity does not permit linear approximation specifically for hard nonlinearities such as Coulomb friction, dead band, plant saturation, backlash, hysteresis and

* Corresponding author.
E-mail addresses: sudarshan_valluru@dce.ac.in (S.K. Valluru), madhusudan@dce.ac.in (M. Singh).
Peer review under the responsibility of Electronics Research Institute (ERI).

Production and hosting by Elsevier

https://doi.org/10.1016/j.jesit.2018.02.001
2314-7172/© 2018 Electronics Research Institute (ERI). Production and hosting by Elsevier B.V. This is an open access article under the CC BY-NC-ND license (http://creativecommons.org/licenses/by-nc-nd/4.0/).

Please cite this article in press as: Valluru, S.K., Singh, M., Performance investigations of APSO tuned linear and nonlinear PID controllers for a nonlinear dynamical system. J. Electr. Syst. Inform. Technol. (2017), https://dx.doi.org/10.1016/j.jesit.2018.02.001

UNCORRECTED PROOF

time delays (Vidyasagar, 1993; Sastry, 1999). Therefore, development of nonlinear analysis techniques is essential to predict the dynamic system performance and also to alter the unpredictable behavior of the dynamic system to meet a desired level of performance as required by a controller.

Proportional-integral-derivative (PID) controllers were widely accepted for automatic control of physical systems since Ziegler and Nichols proposed their empirical tuning rules in 1942. The major strengths of PID control are simple construction, lucid significance, good robustness and ease of implementation. Moreover, the principle of PID controller is easier to understand than other advanced controllers (Astrom and Hagglund, 2001). Many tuning approaches are proposed for PID and PI control for systems with monotonic transient responses (Daley and Liu, 1999; Dey and Mudi, 2009; Huang et al., 2001; Padula and Visioli, 2012; Piazzi and Visioli, 2006). In recent past several artificial intelligence based Meta algorithms such as Genetic Algorithm (GA), Ant Colony Optimization (ACO), Particle Swarm Optimization (PSO), etc. have been proposed to estimate the optimized tuning gains of the PID controllers. However, particle swarm optimization has numerous benefits over other Meta algorithms regarding convergence speed, robustness, and cost function. In control of nonlinear dynamical systems, uncertainties are inevitably encountered, and change in process dynamics causes instabilities of model parameters which deteriorate the performance of PID controller. Therefore the controller needs to be regularly retuned. In this circumstances, the controller still suffers a shortage of optimized tuning rules. This has been the inspiration for some new tuning techniques that aim to compute PID gains according to the obtained model, such that optimization of classical tuning techniques is diminished. In this paper, the optimum gain parameters are derived from the novel parameter robust tuning algorithm based on the principle of swarm intelligence. A particle swarm optimization algorithm inspired by the social behavior of bird flocking and fish schooling is combined with local and global search (Banks et al., 2008, 2007). The PSO algorithm is one such direct search optimization technique and does not need gradient information and therefore can operate to minimize naturally defined cost function without complex mathematical operations. To enhance the performance ability of PSO, different variants like adaptive PSO (APSO) (Zhan et al., 2009; Hu et al., 2013; Chen et al., 2015), canonical PSO (CPSO) (Tsujimoto et al., 2011; Jin'no et al., 2014), and fully informed PSO (FPSO) (Mendes et al., 2004) had been proposed by researchers to achieve accelerating convergence speed and avoiding drawback of local optima stuck.

A simple PSO algorithm for PID controlled linear plant proposed by Akihiro et al. (2008) and obtained system identification on PID tuning tool. For a class of nonlinear PID control systems, an improved PSO algorithm has presented by Chang and Shih (2010). A simplified PSO algorithm used to determine the linear PID controller parameters for an automatic voltage regulator by Panda et al. (2012). An improved PSO algorithm tuned linear PID controller for a nonlinear gantry crane system is developed by Jaafar et al. (2012). A comparative study has made by Valluru et al. (2015) for untuned linear PID, NARMA L-2 and standard PSO tuned linear PID controllers and analyzed effects on the nonlinear dynamical system. Unlike existing literature, the work in this paper analyzes a nonlinear dynamical system with Adaptive PSO algorithm tuned linear and nonlinear PID controllers. The primary objective of this paper is to investigate and compare the performance of the nonlinear dynamical system using Adaptive PSO algorithm to find gains of L-PID, NL-PID controllers.

The paper is organized into five sections: Section 2 analyzes the modeling and stability of reference nonlinear dynamical system. Section 3 discusses the adaptive PSO algorithm for tuning L-PID and NL-PID controllers to find the best K_p, K_i, K_d gains. Section 4 explains the design of linear and nonlinear PID controllers for a nonlinear dynamical system followed by a comparative study of performance in which L-PID and NL-PID controllers are implemented in the reference nonlinear dynamical system. Section 5 presents the conclusions.

2. System modeling and stability analysis

The nonlinear dynamical system (NLDS) is represented using state equations, differential equations or difference equations. The reference nonlinear dynamical system(Kajan, 2008) considered in this paper is represented by Eq. (1), where $y(t)$ is output, and $u(t)$ is the input to the system. This system is a nonlinear, non-homogeneous and it does not produce a bounded solution which can imitate the exact solution. If some initial solution to the dependent variables is known then only the solution could be determined, otherwise, if the equilibrium point is calculated and the phase plane analysis of the system is performed with zero input, $u(t)$ to graphically analyze the system behavior. Q2

$$\frac{d^2y}{dt^2} + 0.7\frac{dy}{dt} + 0.2y + 0.3y^3 = u(t) \tag{1}$$

Please cite this article in press as: Valluru, S.K., Singh, M., Performance investigations of APSO tuned linear and nonlinear PID controllers for a nonlinear dynamical system. J. Electr. Syst. Inform. Technol. (2017), https://dx.doi.org/10.1016/j.jesit.2018.02.001

UNCORRECTED PROOF

It is not possible to find the analytical solution for NLDS, and the system equation can be solved numerically with the help of classical fourth-order Runge–Kutta method, which achieves the accuracy of Taylor's series expansion without requiring the calculations of the higher derivative. Eq. (1) rewritten as

$$y'' + 0.7y' + 0.2y + 0.3y^3 - u(t) = 0 \tag{2}$$

The initial conditions assumed as $y(0) = 0.1$, $y'(0) = 1$ and $u(t) = t$ then $y(0.2)$ are to be determined by Runge–Kutta method up to four decimal places which can be solved as $y = 0.2872$ and $y' = 0.8773$. The specific state can be described in state-space representation by two state variables y and $\dot{y}$ such that $\dot{x}_1 = x_2$ and $\dot{x}_2 = -0.7x_2 - 0.2x_1 - 0.3x_1^3 - u(t)$. The Lyapunov stability analysis is performed for NLDS through generalized Krasovskii theorem (Slotine and Li, 1991) by assuming continuous control law $u = -ky$. Therefore, the system condition when $k = 1$ is determined and rewritten as Eqs. (3) and (4)

$$\dot{x}_1 = f_1(x) = x_2 \tag{3}$$

$$\dot{x}_2 = f_2(x) = -0.7x_2 - 0.2x_1 - 0.3x_1^3 \tag{4}$$

Let us choose a positive Lyapunov function $V(x)$, such as $V(x) = x^T P x$, where P is a positive definite real symmetric matrix. Since the Lyapunov function $V(x)$ is chosen positive definite, for asymptotic stability the $\dot{V}(x)$ be negative definite.

$$\dot{V} = x^T(A^T P + PA)x \tag{5}$$

$$\dot{V}(x) = -x^T Q x \tag{6}$$

where $Q = -(A^T P + PA)$ P and Q are symmetric positive definite matrices and A is Jacobian matrix of the system. Here

$$A = \begin{bmatrix} \frac{\partial f_1}{\partial x_1} & \frac{\partial f_1}{\partial x_2} \\ \frac{\partial f_1}{\partial x_1} & \frac{\partial f_2}{\partial x_2} \end{bmatrix} \text{ also } P = \begin{bmatrix} 1 & 0 \\ 0 & 1 \end{bmatrix}$$

$$A = \begin{bmatrix} 0 & 1 \\ -0.2 - 0.9x_1^2 & -0.7 \end{bmatrix} \tag{7}$$

$$Q = -\begin{bmatrix} 0 & -0.2 - 0.9x_1^2 \\ -0.2 - 0.9x_1^2 & -1.4 \end{bmatrix} \tag{8}$$

By applying Sylvester's criterion to check positive-definiteness of Q

$$\det|Q| = -(0.2 + 0.9x_1^2)^2 \tag{9}$$

Since Q is negative definite then $\dot{V}$ must be negative

$$\dot{V}(x) = -0.33x_1^2 - 0.42x_2^2 - 0.58x_1^4 - 0.06x_1^6 + 1.10x_1x_2 + 1.26x_1^2x_2^2 + 1.54x_1^3x_2 + 0.54x_1^5x_2 \tag{10}$$

If P and Q are the two symmetric positive definite matrices, such that $\forall x \neq 0$ the matrix is negative semi-definite in some neighborhood region of the origin. If the region is whole state space and if in addition $V \to \infty$ as $\|x\| \to \infty$ then the nonlinear dynamical system is asymptotically stable at equilibrium points $(-0.816, 0)$ and $(0.816, 0)$. While its linear approximation is only marginally stable, therefor without control signal $u(t)$ the NLDS is uncontrollable.

The transient and steady-state responses of an NLDS are shown in Fig. 1 which states that the system is underdamped. The actual response is compared with a reference trajectory that represents the actual desired response of the controlled variable. This approach shows the tracking performance of the underdamped system and also finds the value of the adaptive parameters which are not the same as that of the desired parameters, the tracking is achieved as time progressive tuning of the controller.

3. Adaptive PSO for tuning of L-PID and NL-PID controllers

Particle swarm optimization is a population-based metaheuristic technique motivated by social behavior and group intelligence of animals and insects such as fish schooling, bird flocking and animal herding in nature. The investigation

Please cite this article in press as: Valluru, S.K., Singh, M., Performance investigations of APSO tuned linear and nonlinear PID controllers for a nonlinear dynamical system. J. Electr. Syst. Inform. Technol. (2017), https://dx.doi.org/10.1016/j.jesit.2018.02.001

UNCORRECTED PROOF

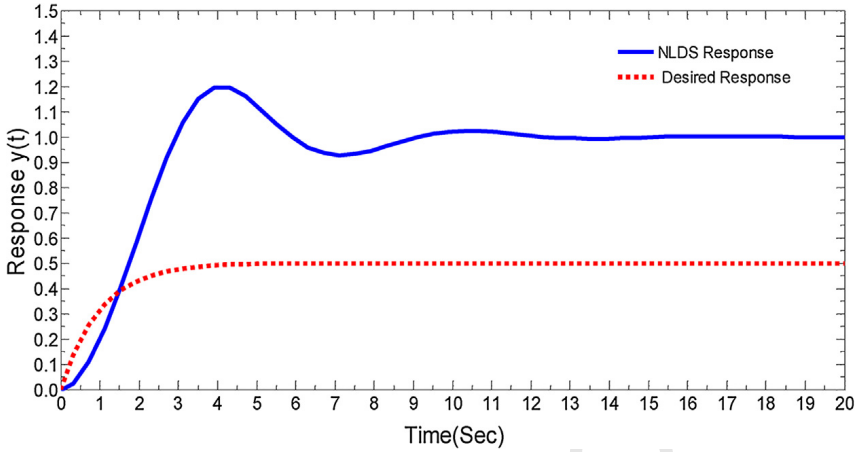


Fig. 1. Nonlinear dynamical system response.

of the search space starting from some initial guess is achieved by multiple agents known as particles, and the population is called a swarm. The APSO algorithm (Christian Blum, 2008; Zhan et al., 2009) is initialized with a group of arbitrary particles in a search space, and then the search for optima begins by updating generations. With each iteration, the particles in the search space adjust their position by using two best values. The first best comes from the greatest fitness it has achieved so far (self-experience) which is stored as *pBest* and the other best is tracked by any particle in the population (social experience) which is called the neighborhood best or *nBest*. When the algorithm finds these two best values, it updates its velocity and position. A swarm size comprises of N particles where each particle $i \in 1, 2, \ldots, N$ has D-dimensional solution space with velocity and position vectors, such as $\boldsymbol{V_i} = [v_i^1, v_i^2, \ldots, v_i^D]$ and $\boldsymbol{X_i} = [x_i^1, x_i^2, \ldots, x_i^D]$ respectively. The velocity and the position of each particle are initializes random vectors with current updated solution space of dimension d of particle 'i' respectively (Zhan et al., 2009). The innovative velocity and position vectors are determined from (11) and (12)

$$v_i^d = \omega v_i^d + \boldsymbol{c_1}\, rand_1^d(pBest_i^d - x_i^d) + \boldsymbol{c_2}\, rand_2^d(nBest^d - x_i^d) \tag{11}$$

$$x_i^d = x_i^d + v_i^d \tag{12}$$

Here ω is inertia weighted factor, '$\boldsymbol{c_1}$' and '$\boldsymbol{c_2}$' be acceleration coefficients and $rand_1^d$ and $rand_2^d$ are arbitrary distributed random numbers generated between 0 and 1. The inertia weight gradually declining with iterative generations as

$$\omega = \omega_{\max} - (\omega_{\max} - \omega_{\min})\frac{g}{G} \tag{13}$$

where g and G are generation index and pre-defined number of maximum generations respectively. In Eq. (11) $pBest_i$ is the best fitness position for the ith particle and *nBest* is neighborhood best position. Here *gBest* used in global PSO and *lBest* used in local PSO instead of *nBest*. For investigating convergence speed and avoiding local optima, the inertia weight has been replaced with constriction coefficient and the velocity update in (11) can be modified as (14) and (15)

$$v_i^d = \chi[v_i^d + \boldsymbol{c_1}\, rand_1^d(pBest_i^d - x_i^d) + \boldsymbol{c_2}\, rand_2^d(nBest^d - x_i^d)] \tag{14}$$

$$\chi = \frac{2}{\left|2 - (\boldsymbol{c_1} + \boldsymbol{c_2}) - \sqrt{(\boldsymbol{c_1} + \boldsymbol{c_2})^2 - 4(\boldsymbol{c_1} + \boldsymbol{c_2})}\right|} \tag{15}$$

The pseudo code of APSO algorithm for searching of the best parameter gains of L-PID and NL-PID controllers can be summarized as follows

Please cite this article in press as: Valluru, S.K., Singh, M., Performance investigations of APSO tuned linear and nonlinear PID controllers for a nonlinear dynamical system. J. Electr. Syst. Inform. Technol. (2017), https://dx.doi.org/10.1016/j.jesit.2018.02.001

UNCORRECTED PRC

i. Set the range of L-PID/NL-PID controller parameters as objective function contains particle parameters $J(i)$, $i = (K_P, K_I, K_D)^T$
ii. Initialize the locations of position $\boldsymbol{X_i}$ and velocity $\boldsymbol{V_i}$ for acceleration factors $c_1 = c_2 = 2.0$, $g = 0$, $\omega = 0.9$ to the controller parameters K_P, K_I, K_D each representing dimensions of particle position vector in real parameter space. Estimate the evolutionary states of the algorithm and adaptively control the parameters. Perform elitist learning operation in convergence state through Gaussian perturbation.
iii. **for** each particle ***i*** **do** is tested for fitness by evaluating the objective function $J(i)$
iv. Set the initial local best *lBest* and global best *gBest*
v. **While** stopping criteria is not reached **do**
for every particle ***i*** **do**
Generate innovative velocity and position of particle ***i***
Evaluate the objective function of new positions
Renew the current best of each particle
end for
Find the current global best
end while
vi. Output the final results of optimized global best

4. Design of APSO tuned linear and nonlinear PID controllers for NLDS

The controllers for nonlinear dynamical systems are designed and tuned by either conventional or intelligent technique. The conventional PID controller is tuned by obeying the heuristic intuitive Ziegler–Nichols rules to attain the stable control in the neighborhood operating point. In conventional automatic control systems, the self-tuning controllers are not yet sufficiently advanced to cater to the effect of parametric changes in long-term performance of dynamical systems. In these situations, system identification and intelligent techniques for development of dynamical models based on some advanced bio-inspired tuning algorithms to achieve the best overall performance for the entire operating envelope. Currently, the particle swarm optimized adaptive critic design for PID controllers is inviting much-renewed interest among the researchers to automate the design and tuning process to a useful degree.

4.1. APSO tuned linear PID controller

A general APSO tuned linear PID configuration with NLDS is shown in Fig. 2 which feeds the desired output signal to the NLDS, the error between the actual output and the desired output signal along with a controller proportional gain (K_p) integral gain (K_i) and differential gains (K_d) generate the output control signal $u(t)$ as given by Eqs. (16) and (17)

$$e(t) = y_d(t) - y(t) \tag{16}$$

$$u(t) = K_p e(t) + K_i \int e(t)\,dt + K_d \dot{e}(t) \tag{17}$$

where $u(t)$ is L-PID control output feed to the NLDS, $e(t)$ is an error or set point, $y(t)$ is NLDS output, $y_d(t)$ is desired output. The internal systematic structure design of L-PID and output control signal is shown in Figs. 3 and 4 respectively.

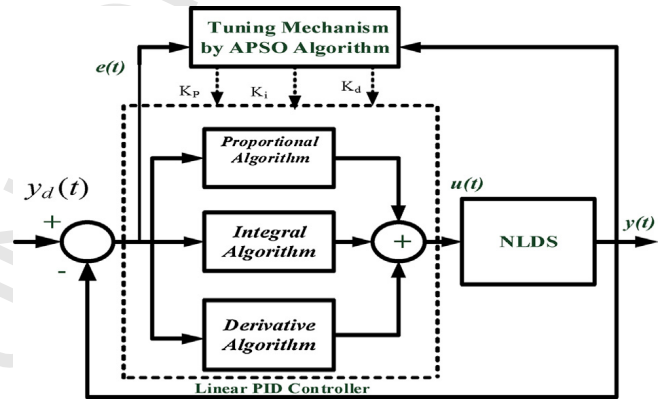


Fig. 2. APSO tuned linear PID controller with NLDS.

Please cite this article in press as: Valluru, S.K., Singh, M., Performance investigations of APSO tuned linear and nonlinear PID controllers for a nonlinear dynamical system. J. Electr. Syst. Inform. Technol. (2017), https://dx.doi.org/10.1016/j.jesit.2018.02.001

UNCORRECTED PROOF

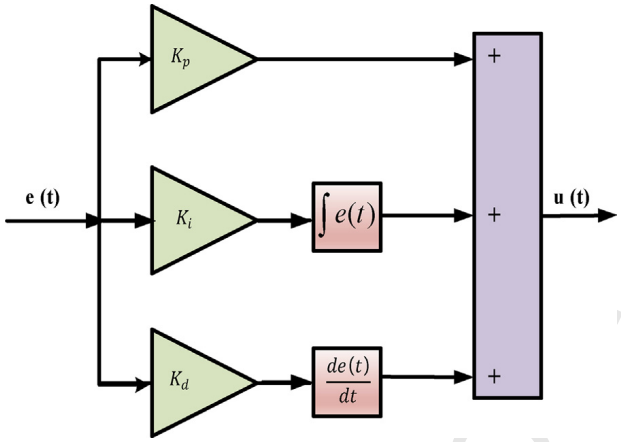


Fig. 3. Structure design of L-PID controller.

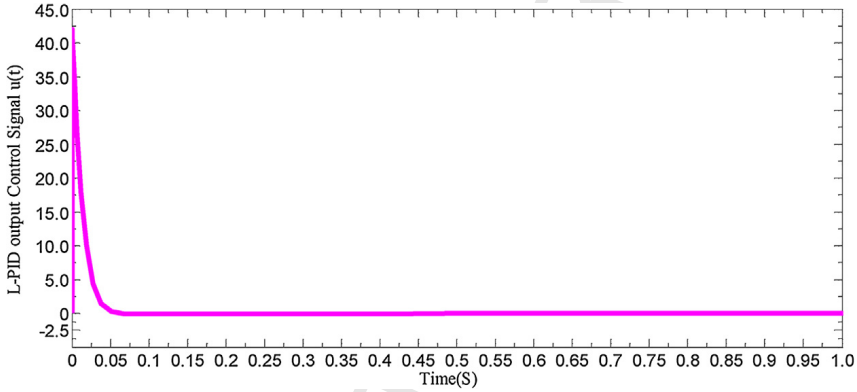


Fig. 4. L-PID output control signal.

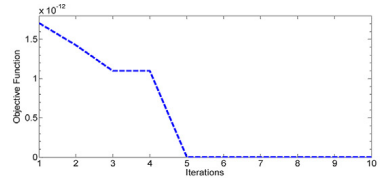
The PID control is based on linear control theory and hence is effective when used for practical linear systems. However, when the system under consideration has nonlinearity or the system parameters vary over a wide range, the performance of linear PID deteriorates considerably. This happens because the reference inputs given to the system are usually not continuous or smooth as they are subjected to the disturbance or noise signal, while the output of the system is required to be smooth and continuous. Since the smooth continuous output is taken as the direct objective of the output, the inertia influence of the system is neglected which causes unanticipated oscillations when used practically. Also, the reference signals are usually non-differentiable signals which makes it problematic to achieve the differential signal of the error. The linear combination of conventional PID causes the conflict between the overshoot variable and the reference. Initially, a high value of K_p would intensify the system response. However as the error starts reducing, the K_p value must also change automatically so that there is less overshoot. Also when the error is decreasing, and the rate of change of error is increasing, K_p must decrease gradually to reduce the overshoot, and when the change of error is decreasing, K_p must gradually decrease to avoid the overshoot. However, due to the linear combination of the PID, this is not possible. Hence we need to control such nonlinear dynamical system by an auto-tuning of the PID controller with APSO algorithm to satisfy the objective performance function. The objective is to optimize the K_p, K_i and K_d parameters to control NLDS, which minimizes the error. Hence the performance objective function $J(\theta)$ can be considered as an integral square error given in Eq. (18)

$$J(\theta) = \int i[e(\theta, i)]^2 \, di \tag{18}$$

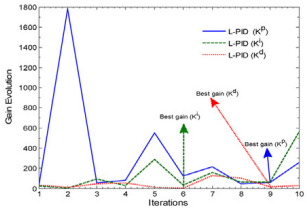
where $\theta = [K_p, K_i, K_d]$.

The APSO algorithm implemented to tune L-PID of NLDS, and the L-PID can transmit the current best values with quicker convergence during optimal tracking of model reference desired signal. Here the swarm size (N) is 10,

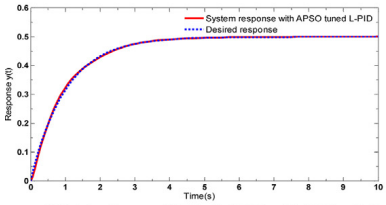
Please cite this article in press as: Valluru, S.K., Singh, M., Performance investigations of APSO tuned linear and nonlinear PID controllers for a nonlinear dynamical system. J. Electr. Syst. Inform. Technol. (2017), https://dx.doi.org/10.1016/j.jesit.2018.02.001



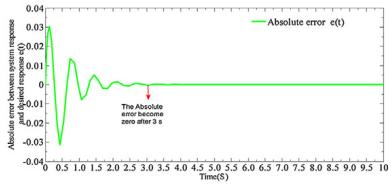
(a) Convergence behavior of APSO algorithm



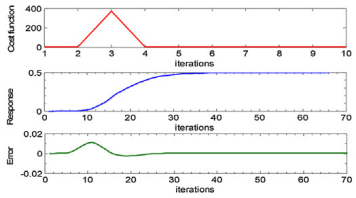
(b) Best gains evolution by APSO for L-PID controlled NLDS



(c) Trajectory Response of NLDS with APSO tuned the L-PID controller



(d) Absolute Error between APSO tuned L-PID controlled NLDS response and desired a response



(e) Minimum cost function, response, and error concerning iterations

Fig. 5. (a) Convergence behavior of APSO algorithm. (b) Best gains evolution by APSO for L-PID controlled NLDS. (c) Trajectory response of NLDS with APSO tuned the L-PID controller. (d) Absolute error between APSO tuned L-PID controlled NLDS response and desired a response. (e) Minimum cost function, response, and error concerning iterations.

dimension of the problem (D) is 3, the maximum number of iterations (i) is 10, cognitive learning factor (c_1) is 2.0, social learning acceleration factor as(c_2) is 2.0, generation index (g) which represents current number of evolutionary generation initially taken as zero and inertia weight (ω) is 0.9 are considered respectively. The convergence and fitness behavior of the APSO algorithm on objective function during 10 iterations are shown in Fig. 5(a). From Fig. 5(a) it can be understood that the PSO algorithm is recurrently avoiding local optima and reaches the optimum solution after five iterations with elapsed time of 5.98 s. The APSO algorithm estimates the best K_p, K_i and K_d parameters based on the error signal $e(t)$ as $K_p = 56.451405$, $K_i = 61.772470$, $K_d = 14.078857$ shown in Fig. 5(b). The response of NLDS with L-PID is tuned by an APSO algorithm is shown in Fig. 5(c) and the absolute error e(t)between system response and desired is shown in Fig. 5(d). The minimum cost function, response, and error of APSO tuned L-PID controlled NLDS with reference to iterations are shown in Fig. 5(e).

Please cite this article in press as: Valluru, S.K., Singh, M., Performance investigations of APSO tuned linear and nonlinear PID controllers for a nonlinear dynamical system. J. Electr. Syst. Inform. Technol. (2017), https://dx.doi.org/10.1016/j.jesit.2018.02.001

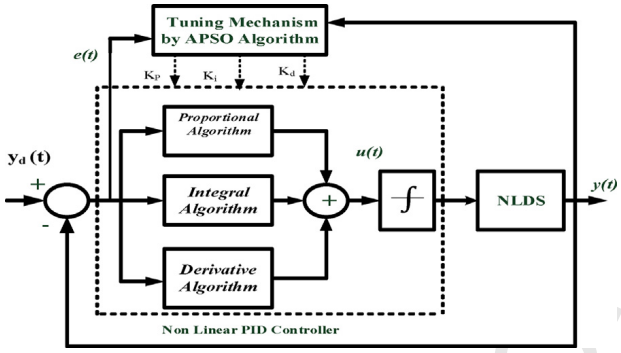


Fig. 6. NLDS with APSO tuned NL-PID controller.

4.2. APSO tuned non-linear PID controller

The PID controllers are the best-utilized controllers for control of dynamical systems. While L-PID controllers are often sufficient for controlling dynamical systems in pure linear operating mode, but for high-performance control, the capability and robustness of L-PID controllers are insufficient. This motivates the authors to propose a Non-Linear PID controller which behaves better with system variations. The general APSO tuned NL-PID configuration with NLDS is shown in Fig. 6.

The general NL-PID control structure can be represented by Eq. (19)

$$f(e,\alpha,\delta) = \begin{cases} |e|^{\alpha}\, sign(e) & |\gamma| \geq \delta \\ \dfrac{e}{\delta^{1-\alpha}} & |\gamma| < \delta \end{cases} \tag{19}$$

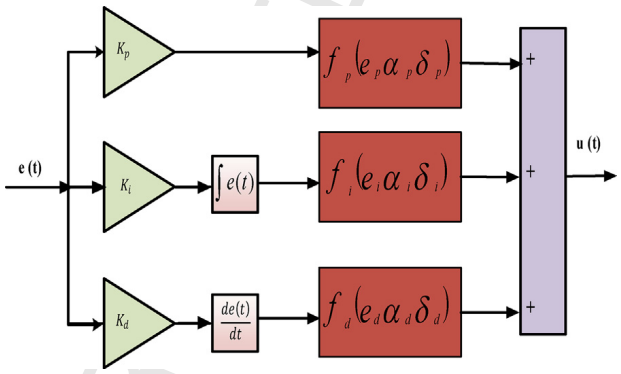


Fig. 7. Structure design of NL-PID.

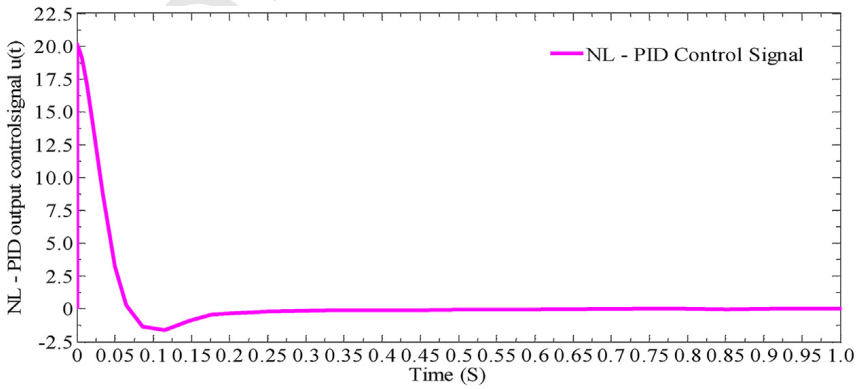
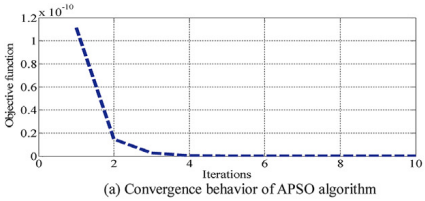
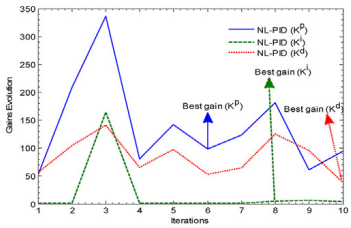


Fig. 8. NL-PID output control signal.

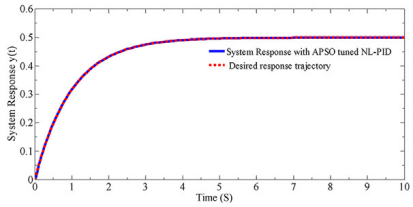
Please cite this article in press as: Valluru, S.K., Singh, M., Performance investigations of APSO tuned linear and nonlinear PID controllers for a nonlinear dynamical system. J. Electr. Syst. Inform. Technol. (2017), https://dx.doi.org/10.1016/j.jesit.2018.02.001



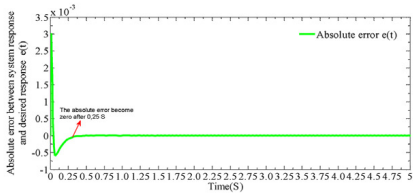
(a) Convergence behavior of APSO algorithm



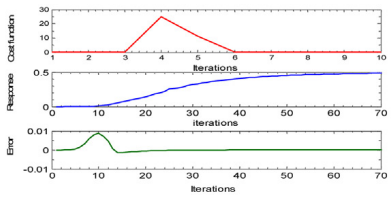
(b) Best gains evolution by APSO for NL-PID controlled NLDS



(c) Response of NLDS with APSO tuned the NL-PID controller



(d) Absolute Error between APSO tuned NL-PID controlled NLDS response and desired response



(e) Minimum cost function, response, and error with reference to iterations

Fig. 9. (a) Convergence behavior of APSO algorithm. (b) Best gains evolution by APSO for NL-PID controlled NLDS. (c) Response of NLDS with APSO tuned the NL-PID controller. (d) Absolute Error between APSO tuned NL-PID controlled NLDS response and desired response. (e) Minimum cost function, response, and error with reference to iterations.

$$sign(e) = \begin{cases} 1, & e \geq 0 \\ -1, & e < 0 \end{cases}$$

where e is the error signal, δ describes the linear range of the function f, here function f can accommodate a greater range of nonlinear characteristics which is determined by α. Hence now control signal being generated by the NL-PID is given in Eq. (20)

$$u(t) = K_p e f_p(e_p, \alpha_p, \delta_p) + K_i f_i(e_i, \alpha_i, \delta_i) \int e\,dt + K_d f_d(e_d, \alpha_d, \delta_d) \frac{de}{dt} \tag{20}$$

The function $f(\alpha, \delta, e)$ denotes the rate of error feedback, to compensate the nonlinearity of the systems considered the value of α_p is taken in the range of $\alpha_p \in [0, 1]$ since the system need to have lower gain when the error is high and vice

Please cite this article in press as: Valluru, S.K., Singh, M., Performance investigations of APSO tuned linear and nonlinear PID controllers for a nonlinear dynamical system. J. Electr. Syst. Inform. Technol. (2017), https://dx.doi.org/10.1016/j.jesit.2018.02.001

Table 1
Performance parameters of NLDS without controller, with APSO, tuned L-PID and NL-PID controllers.

Controllers	Rise time (t_r), s	Settling time (t_s), s	Peak over shoot (M_p)%	Steady state error (e_{ss})%
NLDS without controller	1.75	∞	140	0.5
APSO tuned L-PID	2.17	0.2749	0.0002	0.43
APSO tuned NL-PID	2.16	0.0479	–	0.068

versa. The integral saturation problem of the integral term can be rectified by using α_i in the range of $\alpha_i \in [-1, 0]$. The value of differential term is chosen as $\alpha_d > 1$ so that when the steady state is reached the effect of the differential term is reduced. The systematic structure design and control signal of NL-PID are shown in Figs. 7 and 8 respectively. The magnitude of NL-PID control signal is almost half of the L-PID control signal.

The APSO algorithm with the same settings was implemented for tuning of NL-PID configured with NLDS in the presence of desired model reference trajectory. The convergence and fitness behavior of an APSO algorithm on objective function for 10 iterations are shown in Fig. 9(a). From Fig. 9(a) it can be observed that the APSO algorithm is regularly avoiding local optima and reaches the optimum solution after only three iterations with an elapsed time of 22.9 s.

The APSO algorithm estimates the best K_p, K_i, K_d gain parameters based on the error signal $e(t)$ as $K_p = 94.994981$, $K_i = 3.878118$, $K_d = 38.292221$ shown in Fig. 9(b) The response of NLDS with APSO algorithm tuned NL-PID is shown in Fig. 9(c) and the absolute error $e(t)$ between system response and desired trajectory response be shown in Fig. 9(d). The minimum cost function, response, error of APSO tuned NL-PID controlled NLDS concerning iterations are shown in Fig. 9(e).

4.3. Comparative study of APSO tuned linear and nonlinear PID controllers

Comparison of the NLDS response using an adaptive particle swarm optimization tuned L-PID and NL-PID controllers are presented through a simulation study of NLDS. The reference trajectory considered is a model reference for NLDS, together with the error elimination and the transient behavior of the system has been taken into account. The system is originally unstable due to the existence of disturbances, unmodelled dynamics, and parametric variations. Figs. 5(c) and 9(c) show the system trajectory tracking responses with APSO tuned L-PID, APSO tuned NL-PID controllers in respect of various performance criteria like rise time, settling time, peak overshoot, and steady-state error, have been determined through the dynamic response analysis of NLDS and summarized in Table 1.

5. Conclusion

The adaptive particle swarm optimized L-PID and NL-PID controllers have been successfully developed and tested for their performance regarding settling time, peak overshoot and steady-state error on an NLDS. The simulation results show the efficacy of controllers with NLDS in light of widely varying operating conditions. In comparison with APSO tuned L-PID controller, the APSO tuned NL-PID controller has the advantage of almost zero settling time results in faster stabilization of response without any overshoot. The performance investigations of APSO tuned NL-PID controller, which makes up the deficiency over the APSO tuned L-PID has better adaptability for parameter variations. These investigations also reveal that the APSO algorithm tuning strategy for NL-PID controller offers better searchability, faster convergence, and computational efficiency.

References

Akihiro, O., Nakazawa, C., Matsui, T., 2008. Development of PSO-based PID tuning method. In: IEEE International Conference on Control, Automation Systems, Seoul, Korea, pp. 1917–1920.
Astrom, K.J., Hagglund, T., 2001. The future of PID control. Control Eng. Pract. 9, 1163–1175.
Banks, A., Vincent, J., Anyakoha, C., 2008. A review of particle swarm optimization. Part II: Background and development. Nat. Comput. 7, 109–124.
Banks, A., Vincent, J., Anyakoha, C., 2007. A review of particle swarm optimization. Part I: Background and development. Nat. Comput. 6, 467–484.

Please cite this article in press as: Valluru, S.K., Singh, M., Performance investigations of APSO tuned linear and nonlinear PID controllers for a nonlinear dynamical system. J. Electr. Syst. Inform. Technol. (2017), https://dx.doi.org/10.1016/j.jesit.2018.02.001

UNCORRECTED PROOF

Chang, W., Shih, S., 2010. PID controller design of nonlinear systems using an improved particle swarm optimization approach. Commun. Nonlinear Sci. Numer. Simul. 15, 3632–3639.
Chen, S., Xu, Z., Tang, Y., 2015. An improvement of fuzzy *c*-means clustering using adaptive particle swarm optimization. In: IEEE 12th Web Information System and Application Conference, pp. 275–280.
Christian Blum, X.L., 2008. Swarm intelligence in optimization. In: Christian Blum, D.M. (Ed.), Swarm Intelligence Introduction and Applications. Springer-Verlag Berlin Heidelberg, pp. 43–86.
Daley, S., Liu, G., 1999. Optimal PID tuning using direct search algorithms. Comput. Control Eng. J. 10, 51–56.
Dey, C., Mudi, R.K., 2009. An improved auto-tuning scheme for PID controllers. ISA Trans. 48, 396–409.
Hu, M., Wu, T., Weir, J.D., 2013. An adaptive particle swarm optimization with multiple adaptive methods. IEEE Trans. Evol. Comput. 17, 705–720.
Huang, S.N., Tan, K.K., Lee, T.H., 2001. A combined PID/adaptive controller for a class of nonlinear systems. Automatica 37, 611–618.
Q4 Jaafar, H.I., Mohamed, Z., Abidin, A.F.Z., Ab Ghani, Z., 2012. PSO-tuned PID controller for a nonlinear gantry crane system. In: IEEE International Conference on Control System, Computing and Engineering, Penang, Malaysia, pp. 23–25.
Jin'no, K., Shindo, T., Kurihara, T., Hiraguri, T., Yoshino, H., 2014. Canonical deterministic particle swarm optimization to sustain global search. In: IEEE International Conference on Systems, Man, and Cybernetics, pp. 2440–2445, http://dx.doi.org/10.1109/SMC.2014.6974292.
Kajan, S., 2008. Neural controllers for nonlinear systems in MATLAB. In: 16th Annual Conference on Technical Computing, Prague, Czech, pp. 1–10.
Mendes, R., Kennedy, J., Neves, J., 2004. The fully informed particle swarm: simpler, maybe better. IEEE Trans. Evol. Comput. 8, 204–210, http://dx.doi.org/10.1109/TEVC.2004.826074.
Padula, F., Visioli, A., 2012. Optimal tuning rules for proportional-integral-derivative and fractional-order proportional-integral-derivative controllers for integral and unstable processes. IET Control Theory Appl. 6, 776–786.
Piazzi, A., Visioli, A., 2006. A noncausal approach for PID control. J. Process Control 16, 831–843.
Panda, S., Sahu, B.K., Mohanty, P.K., 2012. Design and performance analysis of PID controller for an automatic voltage regulator system using simplified particle swarm optimization. J. Frankl. Inst. 349, 2609–2625.
Sastry, S., 1999. Nonlinear Systems Analysis Stability and Control. Springer-Verlag Inc., NewYork, USA.
Slotine, J.J.E., Li, W., 1991. Applied Nonlinear Control. Prentice-Hall Inc., Englewood Cliffs, NJ, USA.
Tsujimoto, T., Shindo, T., Jinano, K., 2011. The neighborhood of canonical deterministic PSO. In: IEEE Congress of Evolutionary Computation, pp. 1811–1817, http://dx.doi.org/10.1109/CEC.2011.5949835.
Valluru, S.K., Singh, M., Bhushan, 2015. Comparative analysis of PID, NARMA L-2 and PSO tuned PID controllers for nonlinear dynamical system. J. Autom. Syst. Eng. 9, 94–108.
Vidyasagar, M., 1993. Nonlinear System Analysis. Prentice-Hall Inc., Englewood Cliffs, NJ, USA.
Zhan, Z.-H., Zhang, J., Li, Y., Chung, H.S.-H., 2009. Adaptive particle swarm optimization. IEEE Trans. Syst. Man Cybern. 39, 1362–1381.

UNCORRECTED PROOF

Please cite this article in press as: Valluru, S.K., Singh, M., Performance investigations of APSO tuned linear and nonlinear PID controllers for a nonlinear dynamical system. J. Electr. Syst. Inform. Technol. (2017), https://dx.doi.org/10.1016/j.jesit.2018.02.001

This article has been accepted for inclusion in a future issue of this journal. Content is final as presented, with the exception of pagination.

Physical Insights on Negative Capacitance Transistors in Nonhysteresis and Hysteresis Regimes: MFMIS Versus MFIS Structures

Girish Pahwa, *Student Member, IEEE*, Tapas Dutta, *Member, IEEE*, Amit Agarwal, and Yogesh Singh Chauhan, *Senior Member, IEEE*

***Abstract*— We present a comprehensive comparison of the two different types of ferroelectric negative capacitance FET (NCFET) structures: metal-ferroelectric-metal-insulator-semiconductor (MFMIS) and metal-ferroelectric-insulator-semiconductor (MFIS). A new segmentation approach is proposed to simulate MFIS NCFET, which correctly takes care of the nonuniformity in potential and horizontal electric field at the ferroelectric–oxide interface. We show that MFMIS NCFET provides a higher ON-current than MFIS NCFET except for the ferroelectrics with very low remnant polarization (P_r) in the high operating voltage regime. We find that this behavior is caused by a reduction or enhancement of the longitudinal electric field in the channel of MFIS structure depending upon P_r of the ferroelectric and the operating voltage. Moreover, there exists an optimum P_r which provides maximum ON-current for both the devices. We also find that MFIS NCFET is more prone to hysteresis and starts showing a hysteretic behavior at a lower ferroelectric thickness compared with MFMIS NCFET.**

***Index Terms*— Ferroelectric, metal-ferroelectric-insulator-semiconductor (MFIS), metal-ferroelectric-metal-insulator-semiconductor (MFMIS), negative capacitance (NC), NCFET.**

I. Introduction

FERROELECTRIC-BASED negative capacitance (NC) transistors, which can enable sub-60-mV/dec switching [1], are being actively researched for ultralow power applications [2], [3]. The experimental demonstrations of NCFET have mainly employed two different types of NCFET structures, as shown in Fig. 1. One of the structures involves a metal layer (floating gate) between the ferroelectric and the internal gate oxide (a metal-ferroelectric-metal-insulator-semiconductor (MFMIS) FET [4]–[8]), as shown in Fig. 1(a).

Manuscript received July 17, 2017; revised November 5, 2017; accepted January 13, 2018. This work was supported in part by the Department of Science and Technology, in part by Science and Engineering Research Board, and in part by Semiconductor Research Corporation. The review of this paper was arranged by Editor D. Esseni. *(Corresponding author: Girish Pahwa.)*

G. Pahwa, T. Dutta, and Y. S. Chauhan are with the Nanolab, Department of Electrical Engineering, IIT Kanpur, Kanpur 208016, India (e-mail: girish@iitk.ac.in; chauhan@iitk.ac.in).

A. Agarwal is with the Department of Physics, IIT Kanpur, Kanpur 208016, India.

Color versions of one or more of the figures in this paper are available online at http://ieeexplore.ieee.org.

Digital Object Identifier 10.1109/TED.2018.2794499

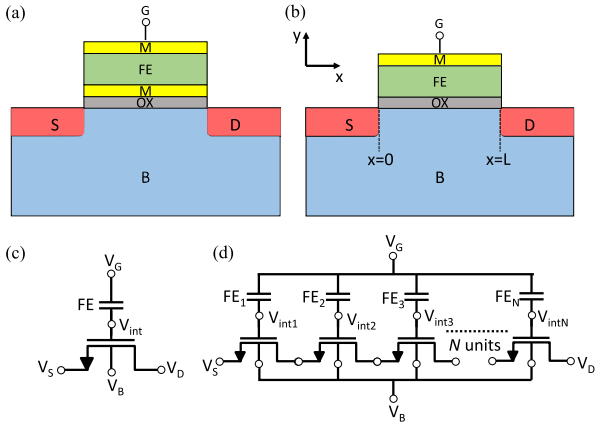


Fig. 1. Different NCFET structures. (a) MFMIS. (b) MFIS. Circuit equivalents of (c) MFMIS and (d) MFIS. Each unit in the MFIS equivalent network represents an MFMIS structure. V_{int} denotes internal voltage at the ferroelectric–oxide interface. For MFIS, V_{int} varies along the longitudinal direction when a nonzero drain bias is applied and hence, it has been modeled by the arrangement shown.

While in the other structure shown in Fig. 1(b), the ferroelectric is in a direct contact with the oxide layer (a metal-ferroelectric-insulator-semiconductor (MFIS) FET [9]–[12]). Recently, Duarte *et al.* [13] and we [14] have reported that MFIS provides a higher ON-state current compared with MFMIS, however, we find this not to be true for all the ferroelectric materials. Furthermore, a detailed physical interpretation of the behavior of the two structures and a relative performance analysis is still missing in the literature. In this paper, we perform an extensive one-to-one comparison between MFMIS and MFIS structures of NCFET using a compact modeling approach. We show that the relative value of ON-current is a strong function of remnant polarization of the ferroelectric when comparing MFMIS and MFIS structures. We also investigate and explain the hysteresis behavior of the two structures highlighting the differences in their underlying hysteresis mechanisms for the first time.

II. Simulation Methodology

We use a compact modeling approach to simulate the two types of NCFET structures. For MFMIS, due to the presence of a metal layer, the ferroelectric capacitor and the baseline MOSFET can be considered as two different circuit elements

0018-9383 © 2018 IEEE. Personal use is permitted, but republication/redistribution requires IEEE permission.
See http://www.ieee.org/publications_standards/publications/rights/index.html for more information.

This article has been accepted for inclusion in a future issue of this journal. Content is final as presented, with the exception of pagination.

simply connected by a wire, as shown in Fig. 1(c). The MFMIS structure can thus be simulated by a lumped model approach by self-consistently solving the Landau–Devonshire (L–D) model of the ferroelectric with the MOSFET physics [13], [15]–[19]. L–D equation relates the voltage drop across the ferroelectric, $V_{\rm fe}$ and the gate charge density, Q_G as $V_{\rm fe} = 2\alpha Q_G + 4\beta {Q_G}^3$, where α and β are the material-dependent parameters. α and β can also be related to the ferroelectric material properties, the remnant polarization (P_r), and the coercive field (E_c) [20]. In this paper, we solve the L–D equation with the Berkeley short-channel IGFET model bulk (BSIM-BULK) (formerly BSIM6) MOSFET model [21], [22] in Verilog-A to simulate the MFMIS NCFET.

However, for the MFIS structure, the above-mentioned approach cannot be used, as the voltage at the ferroelectric–oxide interface (internal voltage, $V_{\rm int}$) varies in the longitudinal (source to drain) direction when a nonzero drain bias is applied. This structure has been modeled either by adopting a full analytical approach [14], [23] or by a distributed modeling approach [13] to calculate the channel current. In this paper, we apply a segmentation approach to model MFIS NCFET as a series network of N identical MFMIS units, as shown in Fig. 1(d), where each unit is modeled using L–D and BSIM-BULK as explained earlier. Ideally, N should be very large, but our simulation results show that the electrical characteristics start to saturate when N becomes as large as 100 except for the hysteretic operation regimes. Thus, for simplicity and to avoid large simulation time, we have assumed $N = 100$ for the nonhysteretic cases and $N = 300$ for the hysteretic cases. All the simulations have been carried out using the commercial Cadence Spectre SPICE simulator. For the MFIS device simulation, SPICE satisfies conditions of channel potential continuity in between the subtransistors and the channel current continuity in all the subtransistors. Simulation using the above-mentioned method provides node voltages and node currents associated with each node and other electrical quantities of interest used in this paper as follows. For any nth subtransistor (an MFMIS NCFET), the local gate charge density, Q_{Gn} (=gate charge per unit area of the n th subtransistor) can be accessed from the BSIM-BULK Verilog-A code, which calculates it using an analytical expression [21], [22]. The local ferroelectric and internal gate capacitance densities can then be calculated by the expressions $C_{{\rm fe}n} = \partial Q_{Gn}/\partial V_{{\rm fe}n}$ and $C_{{\rm int}n} = \partial Q_{Gn}/\partial V_{{\rm int}n}$, respectively, where $V_{{\rm fe}n}$ and $V_{{\rm int}n}$, respectively, denote ferroelectric and internal node voltages. The inversion charge density at each node (Q_{In}) along the channel can again be accessed from the BSIM-BULK code. BSIM-BULK evaluates inversion charge densities at the source and drain of each subtransistor, which are further used to calculate the surface potential at these nodes [21], [22]. Once, surface potential is obtained as a function of position, the horizontal x-component of the electric field is calculated by taking its negative gradient along the channel.

In this paper, we have assumed a long channel internal MOSFET for both the MFMIS and MFIS NCFETs with length $L = 1$ μm, width $W = 1$ μm, body doping concentration $N_a = 5 \times 10^{17}$ cm^{-3}, interfacial oxide thickness $t_{\rm ox} = 1$ nm, and electron mobility $\mu = 500$ cm^2/V-s. We have neglected second-order effects, such as mobility degradation, short channel effects, and so on, in order to compare the two structures only on the basis of the NC effect. Recently, it has been reported that the NC state in MFMIS NCFET may become unstable in practical devices in the presence of leakage current [24] or domain formation [25], which need to be duly addressed [26]. We have assumed the devices to be leakage free in this paper. We have used the L–D equation parameters for a CMOS process compatible Gd:HfO_2 ferroelectric in the simulations [27]. P_r and E_c values calculated from the L–D parameters are found to be 12.13 μC/cm^2 and $\approx$1 MV/cm, respectively [20]. We also discuss results with other possible material parameters of HfO_2-based ferroelectrics later in Section III-C.

III. Results and Discussion

A. Drain Current

Fig. 2(a)–(d) compares the I_D–V_G and I_D–V_D characteristics and the corresponding derivatives for MFMIS and MFIS NCFETs. It is evident that the MFMIS structure shows higher ON-current, transconductance (g_m), and output conductance ($g_{\rm ds}$) compared with MFIS for $P_r = 12.13$ μC/cm^2. Note that both the structures show a lower threshold voltage and a larger OFF-current compared with the reference MOSFET ($t_{\rm fe} = 0$) due to the internal voltage amplification caused by NC effect, which is present even for $V_G = 0$ as the flat band voltage ($V_{\rm FB}$) $\neq 0$. Fig. 2(e) shows the variation of the ON-current with the thickness of the ferroelectric layer ($t_{\rm fe}$) at iso-$I_{\rm OFF}$ of 1 nA/μm. Iso-$I_{\rm OFF}$ is achieved using a $V_{\rm FB}$ tuning. As shown in the figure, ON-current of both the structures increases with $t_{\rm fe}$ with MFMIS excelling MFIS for all the $t_{\rm fe}$ values. These results are in quite contrast with previously reported results [13], [14] which use different ferroelectric materials, as explained later.

For the low values of drain voltage, both the structures show similar current values as evident in Fig. 2(b). This is expected, since, for low V_D values the internal voltage ($V_{\rm int}$ in Fig. 1) does not vary much from source to drain making the MFIS structure behavelike MFMIS.

B. Hysteresis Behavior

Fig. 3(a) compares the hysteresis characteristics of the two structures observed for large $t_{\rm fe}$ values. First, we note that the MFIS device shows a smoother hysteresis compared with the sharp jumps at transition points in the MFMIS device, consistent with [13]. In MFMIS, dipoles in the ferroelectric capacitor behave in unison due to the presence of an equipotential metal layer at the ferroelectric–oxide interface, causing a large change in the polarization and hence, the current. On the other hand, in MFIS, different dipoles require different gate voltages to reach hysteresis transition depending upon the value of the electron–hole quasifermi level difference (V_C) in the channel, as shown in Fig. 3(b). Hysteresis threshold voltages (V_G values at which hysteretic jumps occur) increase with V_C. Thus, as V_G is swept forward, first of all, the dipole at the source end ($V_C = 0$) makes a hysteretic jump followed by other dipoles one by one in continuation from the source

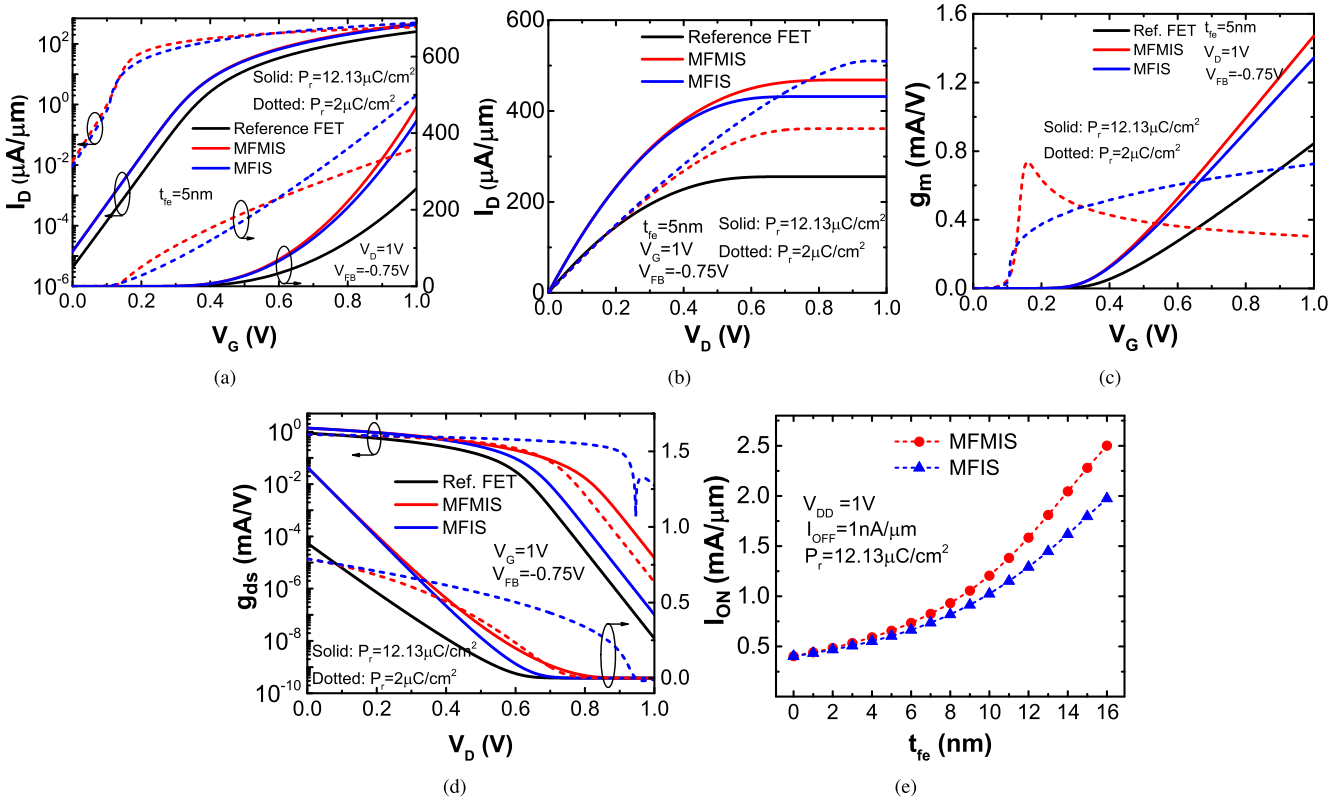


Fig. 2. Comparison of (a) I_D–V_G, (b) I_D–V_D, (c) transconductance, and (d) output conductance of MFMIS and MFIS NCFETs for different remnant polarization values. Solid lines correspond to Gd:HfO_2 ferroelectric. MFMIS structure exhibits higher I_{ON}, g_m, and g_{ds} compared with MFIS for the high P_r. On the contrary, for the low P_r case, MFIS exhibits higher I_{ON}, g_{ds}, and g_m (in the high V_G range) than MFMIS. (e) ON-current variation with ferroelectric thickness for MFMIS and MFIS NCFETs at iso-I_{OFF}. V_{FB} and t_{fe} denote the flat band voltage and the thickness of the ferroelectric layer, respectively. $E_c = 1$ MV/cm is used for all the plots.

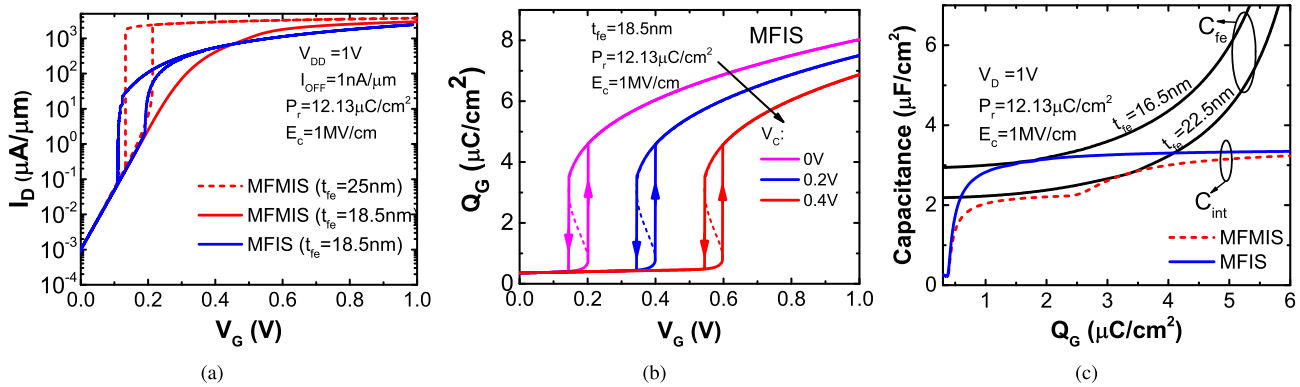


Fig. 3. (a) Hysteresis characteristics of MFMIS and MFIS devices. MFMIS exhibits hysteresis at larger ferroelectric thickness compared with MFIS. Hysteresis plots are shown for the equal maximum width of hysteresis (0.1 V) of the two structures. (b) Impact of electron–hole quasifermi level difference on hysteresis characteristics of ferroelectric dipoles in MFIS NCFET. (c) Variation of ferroelectric (C_{fe}) and internal MOS capacitances (C_{int}) as the functions of the gate charge density. In this figure, for MFIS, C_{fe}, C_{int}, and Q_G signify local densities at the source end while for MFMIS they signify the total value of the quantity/gate area.

toward the drain end. This results in a smooth hysteresis behavior in I_D–V_G characteristics of MFIS NCFET. When V_G is swept backward, dipoles again one by one return to lower polarization values but at different (lower) threshold voltages compared with those in the forward sweep, giving rise to a hysteresis behavior.

In Fig. 3(a), hysteresis characteristics of MFMIS and MFIS structures are shown for the equal maximum widths of hysteresis windows. Note that the MFMIS structure shows the same hysteresis window at a much larger ferroelectric thickness (t_{fe}) compared with the MFIS structure. Also, note that it does not exhibit hysteresis at t_{fe} =18.5 nm whereas the MFIS does, but still provides a comparable ON-current. Hysteresis in any ferroelectric–dielectric system occurs when the absolute value of negative ferroelectric capacitance becomes equal to the value of positive dielectric

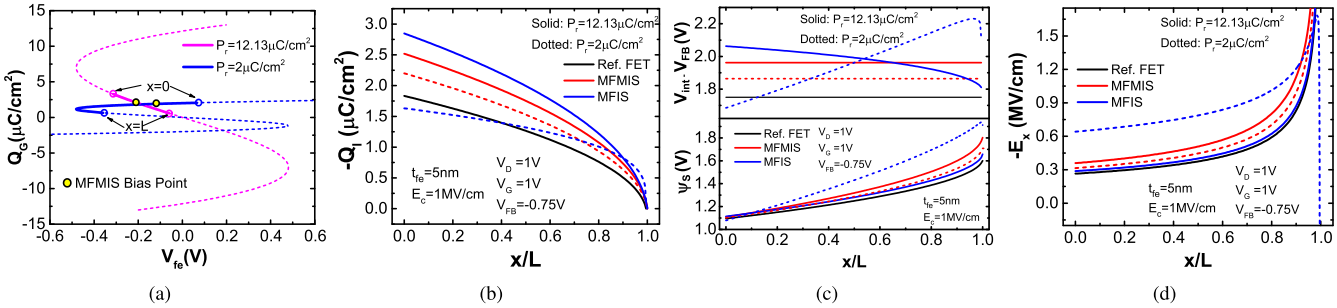


Fig. 4. (a) Gate charge density as a function of ferroelectric voltage drop for MFIS NCFET along source to drain direction for different P_r values. Gate charge density values for the corresponding MFMIS NCFETs are also shown by MFMIS bias points. (b) Inversion charge density profiles in the channel along source to drain direction. (c) Internal gate voltage (V_{int}) and surface potential (ψ_s) profiles along source to drain direction. Internal gate voltage levels for the corresponding MFMIS devices are also given (horizontal lines) for a comparison purpose. (d) Horizontal component of electric field in the channel along source to drain direction.

capacitance [1], [28]. For MFIS, the onset of hysteresis is decided by the hysteresis transition in the source end dipole, i.e., by the capacitance divider formed there by ferroelectric and internal MOS capacitances. Note that, the capacitance matching at the source side remains unaffected by the drain voltage (in a long channel MOSFET). On the other hand, due to the lumped nature of MFMIS, hysteresis is governed by the capacitance divider formed between total ferroelectric capacitance and total internal MOS capacitance, which is influenced by the drain voltage [29]. Fig. 3(c) shows these capacitances as a function of gate charge density Q_G. At $t_{\text{fe}} = 16.5$ nm, ferroelectric capacitance $|C_{\text{fe}}|$ matches exactly with internal MOS capacitance C_{int} for MFIS implying the onset of hysteresis. However, in the case of MFMIS, capacitance matching gets disturbed by reduction in C_{int} caused by a drain to channel coupling resulting in a nonhysteretic behavior at the same t_{fe}. MFMIS shows hysteresis only when t_{fe} is increased to 22.5 nm at which $|C_{\text{fe}}|$ reduces and matches with the lower C_{int}. Thus, for logic applications, where hysteresis is unwanted, MFMIS can be considered as a better choice over a rather hysteresis susceptible MFIS structure for a given t_{fe}.

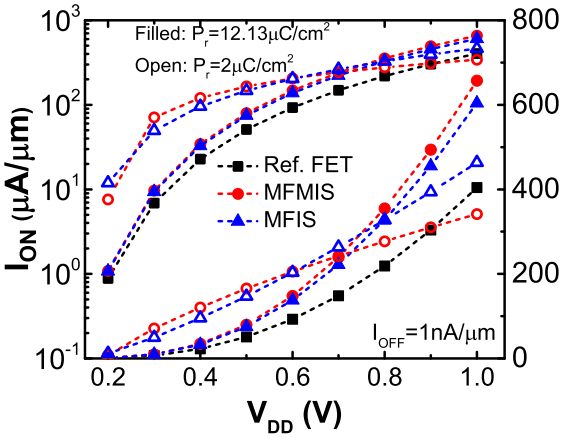
C. Impact of Ferroelectric Material Parameters

In general, P_r value of HfO_2-based ferroelectrics can lie in a range beginning from a small value of 1 to 30 μC/cm^2, while E_c remains close to 1 MV/cm [6], [27], [30]–[33]. Therefore, in this section, we explore the behavior of MFMIS and MFIS NCFETs with respect to different values of P_r.

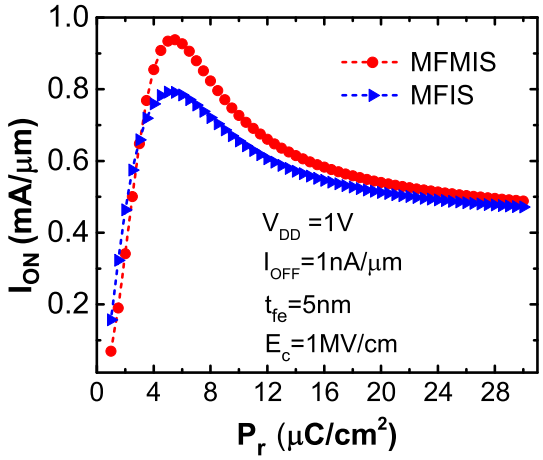
Fig. 2(a)–(d) shows electrical characteristics of MFMIS and MFIS NCFETs for two different P_r values. For a low P_r value of 2 μC/cm^2, MFIS shows a higher ON-current and output conductance (g_{ds}) compared with an MFMIS contrary to the trends at a higher $P_r = 12.13$ μC/cm^2. Moreover, MFIS shows a slightly negative g_{ds} or a negative differential resistance for high V_D values [16]. Both the MFIS and MFMIS for low P_r case show a sudden rise in transconductance (g_m) in low V_G region with MFMIS also exhibiting a peak in g_m in accordance with [13]. For MFMIS, g_m starts to decrease in high V_G region while for MFIS, it maintains a monotonically increasing trend. The channel current in the strong inversion region can be approximated by $\mu W E_x Q_I$ (drift current) calculated near the source end [29] where Q_I denotes inversion charge density and E_x denotes the horizontal component of the electric field. Therefore, we investigate the Q_I and E_x profiles in the channel for low and high values of P_r in the following to explain the above-mentioned observations.

Fig. 4(a) shows gate charge density versus ferroelectric voltage curves for MFIS NCFET for both the high and low P_r values. The corresponding MFMIS gate charge densities appear as single bias points in the figure (as all the dipoles in MFMIS have the same polarization value). Note that in MFIS, Q_G always decreases in the source to drain direction due to drain to channel coupling regardless of the value of P_r. For high P_r, all the dipoles in the ferroelectric of MFIS reside in the NC regime, as shown in Fig. 4(a). Fig. 4(b) shows the inversion charge density profiles in the channel from source toward drain for MFMIS and MFIS structures. MFMIS shows a lower Q_I in the channel compared with MFIS for the high P_r. This observation can be explained by considering a simple case of Q_I near the source which is a direct function of internal voltage V_{int}. The V_{int} at the source side [V_{int1} in Fig. 1(d)] in MFIS is decided only by the local capacitor divider built of C_{fe1} and C_{int1}, which is independent of V_D. While, for MFMIS, it is decided by the total lumped capacitances, C_{fe} and C_{int} [or the total gate charge, see Fig. 1(c)] which are the functions of V_D too in addition to the applied gate voltage. V_D disturbs the matching of the capacitances, as discussed in Section III-B, giving rise to a lower V_{int}, as shown in Fig. 4(c) and therefore, a lower Q_I in MFMIS compared with MFIS. However, V_{int} in MFIS structure decreases in the source to drain direction since, $V_{\text{int}} = V_G - V_{\text{fe}}$, and V_{fe} increases with a decrease in Q_G in NC region. Note that, the surface potential (ψ_s) shown in Fig. 4(c) still increases but rather gradually compared with MFMIS. The decreasing V_{int} profile in MFIS thus, produces a counter effect causing a reduction in the horizontal component of electric field in the channel, as shown in Fig. 4(d) compared with MFMIS for which V_{int} remains a constant throughout. This results in a lower ON-current for MFIS than MFMIS in the case of high P_r ferroelectric despite a higher inversion charge density in the channel for MFIS [Fig. 4(b)].

In case of the low P_r ferroelectric, all the dipoles in MFMIS structure and most of the dipoles in MFIS structure are able to



(a)



(b)

Fig. 5. (a) Variation of ON-current with supply voltage for MFMIS and MFIS structures. For a higher P_r, MFMIS outperforms MFIS for all the supply voltages. For lower P_r material, MFIS shows a better performance compared with MFMIS at higher supply voltages. (b) ON-current variation with remnant polarization for MFMIS and MFIS NCFETs. Both the figures are shown at iso-I_{OFF} = 1 nA/μm.

reach a positive capacitance (PC) state, as shown in Fig. 4(a). Some of the dipoles close to the drain end in an MFIS structure still reside in the NC region due to a strong drain to channel coupling there, which reduces their polarization. Interestingly, MFIS exhibits a lower Q_I compared with MFMIS for low P_r ferroelectric devices which derives from a lower V_{int} for the same, as shown in Fig. 4(c) (we again focus near the source side for simplicity). This is due to the fact that for the dipoles near the source, $V_{\text{fe}} > 0$ [Fig. 4(a)], which implies $V_{\text{int}} < V_G$. While for MFMIS, Q_G bias point is lower in value (due to drain voltage effect) with $V_{\text{fe}} < 0$ in spite of lying in the PC branch, which implies $V_{\text{int}} > V_G$. This explains a lower Q_I for the MFIS structure. Contrary to the high P_r case, V_{int} in the MFIS structure for low P_r increases from the source toward the drain because V_{fe} decreases with a decrease in Q_G in the PC region except very close to the drain end where dipoles lie in the NC state and therefore, V_{int} starts to decrease. It causes the surface potential for MFIS to increase rapidly compared with MFMIS in most of the part of the channel which significantly enhances the horizontal electric field, as shown in Fig. 4(d). This leads to a larger ON-current for MFIS than MFMIS [Fig. 2(b)] despite the former having a lower inversion charge density compared with the latter. In addition to this, the surface potential for MFIS in this case can be seen to decrease near the drain due to a rapidly falling V_{int}. This causes the electric field to reverse its direction in the channel as also been reported in a recent TCAD study [34]. In this region of the channel, the drift current also reverses its direction, which is now compensated by a larger diffusion current ($=\mu W V_t d Q_I/dx$, where V_t denotes thermal voltage [29]) in the opposite direction, to maintain a current continuity in the channel. Note that there is a large Q_I gradient near the drain side for $P_r = 2$ μC/cm^2 in Fig. 4(b).

Fig. 5(a) shows the variation of ON-current with supply voltage V_{DD} for different P_r values at iso-I_{OFF} of 1 nA/μm. For the higher P_r, MFMIS remains superior to MFIS for all supply voltages. For lower P_r, a different trend is observed with MFIS being better than MFMIS for higher V_{DD} values and vice versa for smaller V_{DD} values. For low V_{DD}, V_G is also small, and most of the dipoles now lie in NC region even for low P_r ferroelectric, and thus, I_{ON} shows trends similar to high P_r case with MFMIS excelling over MFIS.

The variation of ON-current with P_r, for a fixed V_{DD}, is shown in Fig. 5(b). I_{ON} shows a similar behavior for both the structures. In low P_r region, I_{ON} is low because the device gets biased in a PC regime and its ferroelectric dipoles saturate at low polarization values [see Fig. 4(a)]. As we increase P_r, a greater number of dipoles start to stay in NC region, which increases the value of current. However, in high P_r region, I_{ON} starts to fall with P_r due to an increase in mismatch between the ferroelectric and internal MOSFET capacitances [14], [18], [35]. The optimum remnant polarization ≈ 6 μC/cm^2 provides a maximum ON-current for both the structures. Furthermore, MFMIS in Fig. 5(b) can be seen to outperform MFIS for all the P_r except very low values (<4 μC/cm^2), as explained earlier.

IV. Conclusion

We provide the new physical insights into the operation of the MFMIS and the MFIS structures of NCFET. Our analysis shows that for high remnant polarization ferroelectric-based NCFETs, MFMIS structure excels the MFIS in terms of ON-current with respect to supply voltage and ferroelectric thickness variation. However, for very low remnant polarization materials, the MFIS shows a relatively better performance compared with the MFMIS at high supply voltages. We also show that the MFMIS incurs a hysteresis at a larger ferroelectric thickness compared with the MFIS while maintaining comparable ON-current, which makes it a more suitable choice for hysteresis-free logic applications.

References

[1] S. Salahuddin and S. Datta, "Use of negative capacitance to provide voltage amplification for low power nanoscale devices," *Nano Lett.*, vol. 8, no. 2, pp. 405–410, 2007, doi: 10.1021/nl071804g.

[2] X. Li *et al.*, "Enabling energy-efficient nonvolatile computing with negative capacitance FET," *IEEE Trans. Electron Devices*, vol. 64, no. 8, pp. 3452–3458, Aug. 2017, doi: 10.1109/TED.2017.2716338.

[3] T. Dutta, G. Pahwa, A. R. Trivedi, S. Sinha, A. Agarwal, and Y. S. Chauhan, "Performance evaluation of 7-nm node negative capacitance FinFET-based SRAM," *IEEE Electron Device Lett.*, vol. 38, no. 8, pp. 1161–1164, Aug. 2017, doi: 10.1109/LED.2017.2712365.

[4] A. Rusu, G. Salvatore, D. Jimenez, and A. Ionescu, "Metal-ferroelectric-metal-oxide-semiconductor field effect transistor with sub-60 mv/decade subthreshold swing and internal voltage amplification," in *IEDM Tech. Dig.*, Dec. 2010, pp. 16.3.1–16.3.4, doi: 10.1109/IEDM.2010.5703374.

[5] J. Jo, W. Y. Choi, J.-D. Park, J. W. Shim, H.-Y. Yu, and C. Shin, "Negative capacitance in organic/ferroelectric capacitor to implement steep switching MOS devices," *Nano Lett.*, vol. 15, no. 7, pp. 4553–4556, 2015, doi: 10.1021/acs.nanolett.5b01130.

[6] K.-S. Li *et al.*, "Sub-60 mv swing negative-capacitance FinFET without hysteresis," in *IEDM Tech. Dig.*, Dec. 2015, pp. 22.6.1–22.6.4, doi: 10.1109/IEDM.2015.7409760.

[7] A. I. Khan, K. Chatterjee, J. P. Duarte, Z. Lu, A. Sachid, S. Khandelwal, R. Ramesh, C. Hu, and S. Salahuddin, "Negative capacitance in short-channel FinFETs externally connected to an epitaxial ferroelectric capacitor," *IEEE Electron Device Lett.*, vol. 37, no. 1, pp. 111–114, Jan. 2016, doi: 10.1109/LED.2015.2501319.

[8] J. Zhou *et al.*, "Ferroelectric HfZrOx Ge and GeSn PMOSFETs with Sub-60 mV/decade subthreshold swing, negligible hysteresis, and improved Ids," in *IEDM Tech. Dig.*, Dec. 2016, pp. 12.2.1–12.2.4, doi: 10.1109/IEDM.2016.7838401.

[9] G. A. Salvatore, D. Bouvet, and A. M. Ionescu, "Demonstration of subthrehold swing smaller than 60 mV/decade in Fe-FET with P(VDF-TrFE)/SiO_2 gate stack," in *IEDM Tech. Dig.*, Dec. 2008, pp. 1–4, doi: 10.1109/IEDM.2008.4796642.

[10] S. Dasgupta, A. Rajashekhar, K. Majumdar, N. Agrawal, A. Razavieh, S. Troiier-McKinstry, and S. Datta, "Sub-kT/q switching in strong inversion in $PbZr_{0.52}Ti_{0.48}O_3$ gated negative capacitance FETs," *IEEE J. Exploratory Solid-State Comput. Device Circuits*, vol. 1, pp. 43–48, Dec. 2015, doi: 10.1109/JXCDC.2015.2448414.

[11] M. H. Lee *et al.*, "Prospects for ferroelectric HfZrOx FETs with experimentally CET=0.98 nm, SSfor=42 mV/dec, SSrev=28 mV/dec, switch-off <0.2V, and hysteresis-free strategies," in *IEDM Tech. Dig.*, Dec. 2015, pp. 22.5.1–22.5.4, doi: 10.1109/IEDM.2015.7409759.

[12] M. H. Lee *et al.*, "Physical thickness 1.x nm ferroelectric HfZrOx negative capacitance FETs," in *IEDM Tech. Dig.*, Dec. 2016, pp. 12.1.1–12.1.4, doi: 10.1109/IEDM.2016.7838400.

[13] J. Duarte *et al.*, "Compact models of negative-capacitance FinFETs: Lumped and distributed charge models," in *IEDM Tech. Dig.*, Dec. 2016, pp. 30.5.1–30.5.4, doi: 10.1109/IEDM.2016.7838514.

[14] G. Pahwa, T. Dutta, A. Agarwal, and Y. S. Chauhan, "Compact model for ferroelectric negative capacitance transistor with MFIS structure," *IEEE Trans. Electron Devices*, vol. 64, no. 3, pp. 1366–1374, Mar. 2017, doi: 10.1109/TED.2017.2654066.

[15] G. Pahwa *et al.*, "Analysis and compact modeling of negative capacitance transistor with high ON-current and negative output differential resistance—Part I: Model description," *IEEE Trans. Electron Devices*, vol. 63, no. 12, pp. 4981–4985, Dec. 2016, doi: 10.1109/TED.2016.2614432.

[16] G. Pahwa *et al.*, "Analysis and compact modeling of negative capacitance transistor with high ON-current and negative output differential resistance—Part II: Model validation," *IEEE Trans. Electron Devices*, vol. 63, no. 12, pp. 4986–4992, Dec. 2016, doi: 10.1109/TED.2016.2614436.

[17] A. Aziz, S. Ghosh, S. Datta, and S. K. Gupta, "Physics-based circuit-compatible SPICE model for ferroelectric transistors," *IEEE Electron Device Lett.*, vol. 37, no. 6, pp. 805–808, Jun. 2016, doi: 10.1109/LED.2016.2558149.

[18] G. Pahwa, T. Dutta, A. Agarwal, and Y. S. Chauhan, "Designing energy efficient and hysteresis free negative capacitance FinFET with negative DIBL and 3.5X ION using compact modeling approach," in *Proc. IEEE Eur. Solid-State Device Res. Conf. (ESSDERC)*, Sep. 2016, pp. 41–46, doi: 10.1109/ESSDERC.2016.7599584.

[19] Y. Li, Y. Lian, K. Yao, and G. S. Samudra, "Evaluation and optimization of short channel ferroelectric MOSFET for low power circuit application with BSIM4 and Landau theory," *Solid-State Electron.*, vol. 114, pp. 17–22, Dec. 2015, doi: 10.1016/j.sse.2015.07.001.

[20] D. Ricinschi, C. Harnagea, C. Papusoi, L. Mitoseriu, V. Tura, and M. Okuyama, "Analysis of ferroelectric switching in finite media as a Landau-type phase transition," *J. Phys., Condens. Matter*, vol. 10, no. 2, pp. 477–492, Apr. 1998, doi: 10.1088/0953-8984/10/2/026.

[21] Y. S. Chauhan *et al.*, "BSIM6: Analog and RF compact model for bulk MOSFET," *IEEE Trans. Electron Devices*, vol. 61, no. 2, pp. 234–244, Feb. 2014, doi: 10.1109/TED.2013.2283084.

[22] *BSIM6 Technical Manual*. Accessed: Jun. 10, 2017. [Online]. Available: http://bsim.berkeley.edu/models/bsimbulk/

[23] D. Jiménez, E. Miranda, and A. Godoy, "Analytic model for the surface potential and drain current in negative capacitance field-effect transistors," *IEEE Trans. Electron Devices*, vol. 57, no. 10, pp. 2405–2409, Oct. 2010, doi: 10.1109/TED.2010.2062188.

[24] A. I. Khan, U. Radhakrishna, K. Chatterjee, S. Salahuddin, and D. A. Antoniadis, "Negative capacitance behavior in a leaky ferroelectric," *IEEE Trans. Electron Devices*, vol. 63, no. 11, pp. 4416–4422, Oct. 2016, doi: 10.1109/TED.2016.2612656.

[25] M. Hoffmann, M. Pešić, S. Slesazeck, U. Schroeder, T. Mikolajick, and T. Mikolajick, "Modeling and design considerations for negative capacitance field-effect transistors," in *Proc. Joint Int. EUROSOI Workshop Int. Conf. Ultimate Integr. Silicon (EUROSOI-ULIS)*, Apr. 2017, pp. 1–4, doi: 10.1109/ULIS.2017.7962577.

[26] A. I. Khan, U. Radhakrishna, S. Salahuddin, and D. Antoniadis, "Work function engineering for performance improvement in leaky negative capacitance FETs," *IEEE Electron Device Lett.*, vol. 38, no. 9, pp. 1335–1338, Sep. 2017, doi: 10.1109/LED.2017.2733382.

[27] M. Hoffmann *et al.*, "Direct observation of negative capacitance in polycrystalline ferroelectric HfO_2," *Adv. Funct. Mater.*, vol. 26, no. 47, pp. 8643–8649, 2016, doi: 10.1002/adfm.201602869.

[28] A. Khan, C. Yeung, C. Hu, and S. Salahuddin, "Ferroelectric negative capacitance MOSFET: Capacitance tuning and antiferroelectric operation," in *IEDM Tech. Dig.*, Dec. 2011, pp. 11.3.1–11.3.4, doi: 10.1109/IEDM.2011.6131532.

[29] Y. Tsividis and C. McAndrew, *Operation and Modeling of the MOS Transistor*. Oxford, U.K.: Oxford Univ. Press, 2011.

[30] S. Mueller *et al.*, "Incipient ferroelectricity in Al-doped HfO_2 thin films," *Adv. Funct. Mater.*, vol. 22, no. 11, pp. 2412–2417, 2012, doi: 10.1002/adfm.201103119.

[31] J. Müller *et al.*, "Ferroelectricity in simple binary ZrO_2 and HfO_2," *Nano Lett.*, vol. 12, no. 8, pp. 4318–4323, 2012, doi: 10.1021/nl302049kPMID:22812909.

[32] H. J. Kim *et al.*, "Grain size engineering for ferroelectric $Hf_{0.5}Zr_{0.5}O_2$ films by an insertion of Al_2O_3 interlayer," *Appl. Phys. Lett.*, vol. 105, no. 19, p. 192903, 2014, doi: 10.1063/1.4902072.

[33] H. Ota, S. Migita, J. Hattori, K. Fukuda, and A. Toriumi, "Material and device engineering in fully depleted silicon-on-insulator transistors to realize a steep subthreshold swing using negative capacitance," *Jpn. J. Appl. Phys.*, vol. 55, no. 8S2, p. 08PD01, 2016, doi: 10.7567/jjap.55.08pd01.

[34] H. Ota, T. Ikegami, J. Hattori, K. Fukuda, S. Migita, and A. Toriumi, "Fully coupled 3-D device simulation of negative capacitance FinFETs for sub 10 nm integration," in *IEDM Tech. Dig.*, Dec. 2016, pp. 12.4.1–12.4.4, doi: 10.1109/IEDM.2016.7838403.

[35] C. I. Lin, A. I. Khan, S. Salahuddin, and C. Hu, "Effects of the variation of ferroelectric properties on negative capacitance FET characteristics," *IEEE Trans. Electron Devices*, vol. 63, no. 5, pp. 2197–2199, May 2016, doi: 10.1109/TED.2016.2514783.



Girish Pahwa (S'16) received the B.Tech. degree in electronics and communication engineering from Delhi Technological University, New Delhi, India in 2014. He is currently pursuing the Ph.D. degree with IIT Kanpur, Kanpur, India.

His current research interests include the physics and modeling of negative capacitance transistors.

This article has been accepted for inclusion in a future issue of this journal. Content is final as presented, with the exception of pagination.



Tapas Dutta (M'16) received the Ph.D. degree in nanoelectronics and nanotechnology from the Institut National Polytechnique de Grenoble, Grenoble, France, in 2014.

He then joined IIT Kanpur, Kanpur, India, as a Post-Doctoral Researcher, where he involved in multiscale simulations of III–V and 2-D material-based FETs, and compact modeling of negative capacitance transistors and the BSIMSOI model.



Amit Agarwal received the M.Sc. and Ph.D. degrees in theoretical physics from the Indian Institute of Science, Bengaluru, India, in 2005 and 2009, respectively.

In 2012, he joined IIT Kanpur, Kanpur, India, as an Assistant Professor. His current research interests include theoretical condensed matter theory, particularly low-dimensional systems, and nanoscale device modeling.



Yogesh Singh Chauhan (SM'12) was with ST Microelectronics, Noida, India, from 2003 to 2004, IBM, Bengaluru, from 2007 to 2010, the Tokyo Institute of Technology, Tokyo, Japan, in 2010, and the University of California at Berkeley, Berkeley, CA, USA, from 2010 to 2012. He is currently an Associate Professor at IIT Kanpur, Kanpur, India. His current research interests include the characterization, modeling, and simulation of semiconductor devices.

INTERNATIONAL JOURNAL OF BASIC AND APPLIED RESEARCH
www.pragatipublication.com

ISSN 2249-3352 (P) 2278-0505 (E)

Prediction of traffic noise descriptors using artificial neural network

Paras Kumar
Assistant professor, Mechanical Engineering Department,
Delhi Technological University, Delhi-110042, India

Abstract

Present work predicts the traffic noise descriptors using artificial neural network (ANN) model and compares its prediction capability for three different transfer functions used in the hidden layer. Gradient descent with momentum and adaptive learning rate (GDX) algorithm is used to update weights in the ANN model. The model input parameters are total vehicle volume/hour, percentage of heavy vehicles and average vehicle speed, while the output parameters are 10 percentile exceeded sound level (L_{10}) and equivalent continuous sound level (L_{eq}).

The network performance is measured in terms of individual and combined root mean square errors for both the output parameters. It is observed that the tan and log sigmoid transfer functions in the hidden layer give better performance during training and testing both, while the inverse transfer function shows worst performance. The computation time is least for log sigmoid transfer function followed by inverse and tan sigmoid transfer functions. It is concluded that the log sigmoid transfer function performs well in terms of accuracy and computation time using GDX weight updating algorithm.

Keywords: Artificial neural network (ANN), Traffic noise, Transfer function, Gradient decent with momentum and adaptive learning rate (GDX).

1. Introduction

The increasing number of vehicles on the roads increases traffic noise pollution and distresses the human life in terms of health. Out of the several vehicle categories, the number of two wheelers is more in India. Various traffic noise prediction models [1-5] were proposed in literature to predict traffic noise in different countries. Cammarata et al. [1] proposed an ANN model to predict the equivalent sound pressure level caused by urban traffic. Givargis et al. [2] presented the mathematical logarithmic, statistical linear regression and neural models to predict maximum A – weighted noise level ($L_{A,max}$) for Teran-karaj express train. Rahmani et al. [3] proposed two mathematical models to predict equivalent continuous sound level (L_{eq}) on flat road using genetic algorithm approach. Kumar et al. [4] developed an ANN model (3-8-2) to predict L_{10} and L_{eq} in India. This model predicted the traffic noise more accurately and considered the vehicle parameters/ characteristics according to Indian traffic conditions.

The accuracy and prediction capability of an ANN model is further improved by selecting an appropriate transfer function and weight updating algorithm. This paper aims to compare the prediction accuracy of an artificial neural network 3-8-2 by using three transfer functions in

Received: 5 January Revised: 13 January Accepted: 22 January
Index in Cosmos
February 2018 Volume 8 Number 2
UGC APPROVED

INTERNATIONAL JOURNAL OF BASIC AND APPLIED RESEARCH
www.pragatipublication.com
ISSN 2249-3352 (P) 2278-0505 (E)

hidden layer (tan sigmoid, log sigmoid and inverse) and gradient decent with momentum and adaptive learning rate (GDX) weight updating technique.

2. Measurement of sound pressure level

The traffic noise measurement is done on a two lane straight patch in Patiala city (Punjab, India). This site is located 4 Km away towards Sirhind road where no traffic light, speed barker and crossing are seen. The noise level is measured using Sound level meter (SLM) form morning to evening during April to May. The microphone of the sound level meter is set perpendicular at a distance of 8.5 meter from the centre of the inner /outer lane at a height of 1.2 meter. Equivalent continuous sound level (L_{eq}), 10 percentile exceed sound level (L_{10}), traffic density of heavy vehicles, vehicles counts of seven different categories (heavy trucks, medium truck, buses, tractors, cars, tempos and scooters/mopeds/motorcycles), average vehicle speed are measured simultaneously.

3. Artificial neural network (ANN)

The ANN model consists of three different layers i.e. input layer, hidden layer and output layer [5] as shown in Fig. 1. These layers are connected to each other through neurons. The neurons in each layer, except input layer, get input information and produce output depending upon their activation function.

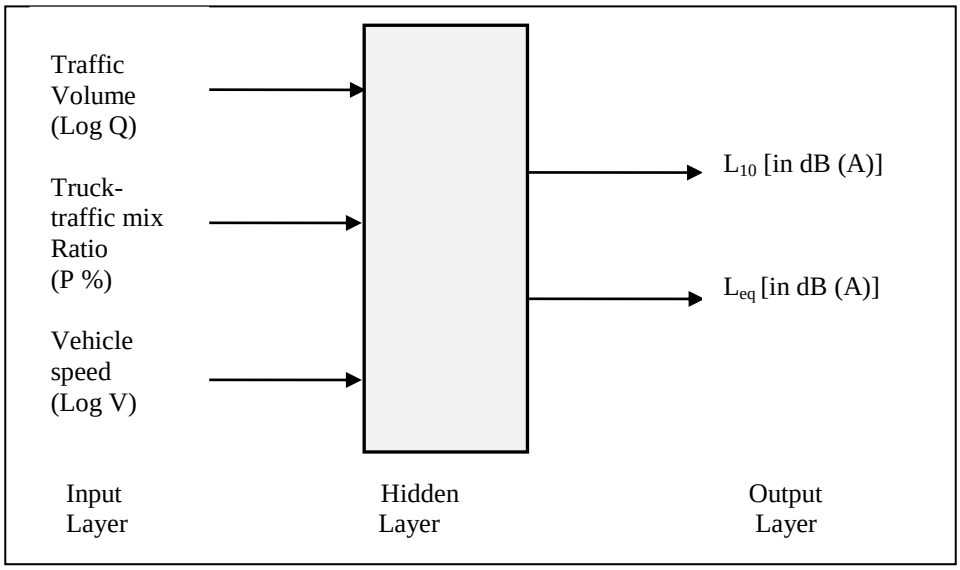


Fig. 1 Artificial neural network (3-8-2) (Kumar et al. 2014)

Received: 5 January Revised: 13 January Accepted: 22 January
Index in Cosmos
February 2018 Volume 8 Number 2
UGC APPROVED

INTERNATIONAL JOURNAL OF BASIC AND APPLIED RESEARCH
www.pragatipublication.com
ISSN 2249-3352 (P) 2278-0505 (E)

The input – output relation of the four different transfer functions used in the present work are expressed as:

$$f(x) = \begin{cases} \dfrac{(e^{x} - e^{-x})}{(e^{x} + e^{-x})}, & Tan\ sigmoid\ transfer\ function \\ \dfrac{1}{(1 + e^{-x})}, & Log\ sigmoid\ transfer\ function \\ \dfrac{1}{x}, & Inverse\ transfer\ function \\ x & Linear\ transfer\ function \end{cases} \quad (1)$$

Two important elementary processes for modeling using neural network are training and testing. During training process, the network is trained for known values of input and output parameters. The network output is tested against targeted output and the error is propagated backward to update weights during each epoch. When the training process is completed, the next step is to test the network's prediction capability against the testing data set.

Table-1 Training data set

S. No.	Input Parameters			Output Parameters	
	Log Q (Vehicles/hour)	P (%)	Log V (Km/hour)	L_{10} [dB(A)]	$L_{eq.}$ [dB(A)]
1	3.14	10.2	1.62	77.4	75.3
2	3.06	9.4	1.71	76.0	74.1
3	3.03	7.4	1.74	76.4	73.7
4	3.06	13.3	1.73	75.4	73.2
5	3.01	12.9	1.73	75.8	74.5
6	3.09	10.7	1.71	76.4	74.4
7	3.2	9.1	1.74	77.8	75.9
8	3.24	7.1	1.75	77.1	75.0
9	3.23	8.1	1.76	77.3	75.0
10	3.11	10.3	1.74	75.8	72.9
11	3.14	7.3	1.72	76.2	74.2
12	3.16	7.2	1.74	75.8	73.2
13	3.23	10.4	1.73	78.2	76.1
14	3.2	7.8	1.75	76.2	73.2
15	3.19	10.7	1.74	77.8	75.9
16	3.12	12.4	1.75	76.1	73.8
17	3.14	9.3	1.76	76.4	74.2

Received: 5 January Revised: 13 January Accepted: 22 January
Index in Cosmos
February 2018 Volume 8 Number 2
UGC APPROVED

INTERNATIONAL JOURNAL OF BASIC AND APPLIED RESEARCH
www.pragatipublication.com
ISSN 2249-3352 (P) 2278-0505 (E)

18	3.17	11.3	1.75	76.2	74.0
19	3.18	9.2	1.70	78.3	75.7
20	3.17	9.4	1.68	78.2	75.4
21	3.16	8.1	1.73	77.7	75.5
22	3.1	9.9	1.70	77.6	74.5
23	3.14	9.6	1.75	77.8	75.4
24	3.21	8.9	1.71	79.9	77.4
25	3.11	11.0	1.68	78.8	76.1
26	3.14	11.0	1.73	77.7	75.4
27	3.11	9.3	1.72	77.3	75.0
28	3.07	12.4	1.73	75.7	73.6
29	3.07	12.1	1.74	76.5	74.2
30	3.19	10.2	1.71	78.6	76.8
31	3.20	8.8	1.74	77.1	75.8
32	3.24	6.3	1.73	76.6	75.2
33	3.22	7.2	1.75	77.2	75.9
34	3.08	9.7	1.74	75.8	74.4
35	3.09	7.8	1.75	76.4	74.9
36	3.23	6.1	1.75	75.3	74.1

Table-2 Testing data set

S. No	Model input parameters			Model Output parameters	
	Log Q	P	Log V	L_{10}	L_{eq}
1	3.14	10.2	1.7	77.8	75.0
2	3.11	11.5	1.7	77.3	74.5
3	3.09	10.7	1.69	77.9	76.4
4	3.08	18.4	1.69	77.5	74.8
5	3.07	12.2	1.73	76.7	74.2
6	3.13	10.8	1.74	77.3	74.6
7	3.12	8.0	1.7	76.8	74.6
8	3.14	6.9	1.68	75.6	72.9
9	3.07	9.2	1.72	76.0	74.1
10	3.04	6.4	1.74	76.4	74.5
11	3.06	6.3	1.73	77.2	75.3
12	3.14	4.7	1.73	75.7	73.9
13	3.12	9.4	1.7	77.0	75.2
14	3.14	10.1	1.73	76.4	74.9

Received: 5 January Revised: 13 January Accepted: 22 January
Index in Cosmos
February 2018 Volume 8 Number 2
UGC APPROVED

INTERNATIONAL JOURNAL OF BASIC AND APPLIED RESEARCH
www.pragatipublication.com
ISSN 2249-3352 (P) 2278-0505 (E)

15	3.09	10.1	1.75	77.1	75.8
16	3.03	12.8	1.73	76.4	74.8
17	3.08	8.5	1.72	76.2	74.5
18	3.19	10.1	1.73	76.6	74.5

Table-3 Comparison of root mean square error (RMSE) during training and testing for ANN architecture (3-8-2)

S. No.	Training algorithm	Transfer function (Hidden Layer)	Time (Sec.)	Root mean square error (RMSE) [dB(A)]					
				Training			Testing		
				L_{10}	L_{eq}	Combined	L_{10}	L_{eq}	Combined
1.	Gradient Descent with Momentum and Adaptive Learning Rate (GDX)	Tan Sigmoid	6.7566	1.0656	1.0514	1.0585	0.6803	0.7401	0.9537
		Log Sigmoid	4.3136	1.0656	1.0514	1.0585	0.6803	0.7401	0.9537
		Inverse	4.8465	21.906	19.676	20.8216	24.8275	17.1445	28.6235

4. Results and discussion

In the present work, the ANN architecture (3-8-2) [4] is used to predict traffic noise descriptors. The ANN model consists of three, eight and two neurons in the input, hidden and output layers respectively. Table-1 shows the training data set [4] used to developed ANN architecture (3-8-2). The convergence results show that the sigmoid transfer functions (tan and log) have similar convergence trend and better performance as compared to inverse transfer function with GDX weight updating algorithm. Once the network training is completed, the prediction capability of ANN model is tested for the testing data set as shown in Table-2.

The results of RMSE (Training) and RMSE (Testing) along with computation time are shown in Table-3. During training, the least RMSE values are 1.0656 dB (A) for L_{10} and 1.0514 dB (A) for L_{eq}

Received: 5 January Revised: 13 January Accepted: 22 January
Index in Cosmos
February 2018 Volume 8 Number 2
UGC APPROVED

ISSN 2249-3352 (P) 2278-0505 (E)

with tan and log sigmoid transfer functions. During training, the least combined RMSE value is 1.0585 with tan and log sigmoid transfer functions. During testing, the least RMSE values are 0.6803 dB (A) for L_{10} and 0.7401 dB (A) for L_{eq} with tan and log sigmoid transfer functions. The least combined RMSE value during testing is 0.9537 with tan and log sigmoid transfer functions.
The inverse transfer function shows highest combined RMSE values of 20.82 dB (A) and 28.62 dB (A) during training and testing respectively. The performance of the tan and log sigmoid transfer functions is equally good for training and testing data sets using GDX weight updating algorithm. The maximum error during training and testing is observed for inverse transfer function.
But for a given network, the weight updating algorithm and transfer function should be selected in such a way that it gives better prediction capability along with least RMSE values during training /testing and computation time. The analysis shows that for the given architecture 3-8-2, the least training/testing error and the better prediction are achieved using tan and log sigmoid transfer functions in hidden layer. The network training time using GDX weight updating algorithm is least for log sigmoid transfer function.

5. Conclusions

Multilayer feed forward back propagation (BP) neural network (3-8-2) is used to predict L_{10} and L_{eq} highway noise descriptors. The ANN model performance is measured in terms of root mean square error (RMSE) value during training and testing both.
During training and testing, the individual and combined root mean square errors in predicting L_{10} and L_{eq} are least using tan and log sigmoid transfer functions in the hidden layer. The worst performance is observed for inverse transfer function using GDX algorithm during training and testing both. The GDX weight updating algorithm with tan/log sigmoid transfer functions in hidden layer and linear transfer function in output layer gives better performance for the given ANN architecture 3-8-2. The computation time is least for log sigmoid function followed by inverse and tan transfer functions.

References

[1] G. Cammarata, S. Cavalieri, A. Fichera, A neural network architecture for noise prediction, Neural Networks, 8(6) (1995), 963-973.
[2] S. Givargis, H. Karimi, Mathematical, statistical and neural models capable of predicting $L_{A,max}$ for the Tehran- Karaj express train, Applied Acoustics, 70 (2009), 1015-1020.
[3] S. Rahmani, S.M. Mousavi, M. J. Kamali, Modeling of road-traffic noise with the use of genetic algorithm, Applied Soft Computing, 11(2011), 1008-1013.
[4] P. Kumar, S. P. Nigam, N. Kumar, Vehicular traffic noise modeling using artificial neural network approach, Transportation Research Part C, 40 (2014), 111-122.
[5] M.A. Burgess, Noise prediction for urban traffic conditions-related to measurements in the Sydney metropolitan area, Applied Acoustics, 10 (1977), 1–7.
[6] L. Fausett, Fundamentals of neural networks: architectures, algorithms and applications. Prentice-Hall, NJ, (1994).

Received: 5 January Revised: 13 January Accepted: 22 January
Index in Cosmos
February 2018 Volume 8 Number 2
UGC APPROVED

This article has been accepted for inclusion in a future issue of this journal. Content is final as presented, with the exception of pagination.

Reliability Issues of In_2O_5Sn Gate Electrode Recessed Channel MOSFET: Impact of Interface Trap Charges and Temperature

Ajay Kumar, *Student Member, IEEE*, M. M. Tripathi, *Senior Member, IEEE*, and Rishu Chaujar, *Senior Member, IEEE*

***Abstract*— In this paper, reliability issues of In_2O_5Sn (indium–tin oxide: a transparent material) transparent gate recessed channel (TGRC)-MOSFET has been analyzed by considering the effect of interface trap charges (both positive and negative) present at the Si/SiO_2 interface. Following device, characteristics are studied in terms of static, linearity, and intermodulation figure of merits. It is found that with the amalgamation of the transparent gate indium tin oxide on conventional recesses channel (CRC) MOSFET, it exhibits improved immunity against interface trap charges in comparison to CRC-MOSFET. In addition, the influence of ambient temperature (150–300 K) along with trap charges on TGRC-MOSFET has also been explored with an aim to analyze at which temperature of the device is more stable in the presence of interface defects (trap charges). Results obtained reveal that TGRC shows improved device performance at low temperature with trap charges being less influenced. Thus, this paper demonstrates that TGRC MOSFET can act as a promising candidate for low-power linear analog applications, where low temperature is required.**

***Index Terms*— Conventional recesses channel (CRC)-MOSFET, interface trap charges, indium tin oxide (ITO), temperature, transparent gate recessed channel (TGRC)-MOSFET.**

I. Introduction

TODAY, most of the IC applications are based on CMOS technology and subsequently it goes to subnanometer node technology to enhance its performance in terms of density, speediness, lower power ingesting, and cost. From past few years, the high interest has been rising on device reliability as it is always a major issue. This paper discusses the reliability issues by considering the defects/impurities arise due to oxide charges. During fabrication processes, various types of charges or traps being carelessly incorporated into the oxide, and thus degrades the performance of the device [1]. Four different types of trap charges are present in the thermally grown oxide, i.e., 1) interface trapped charges; 2) field oxide charges; 3) mobile ionic charge; and 4) oxide trapped charge. Among them, the most important one to study is the interface trap charges owing to the wide-ranging and degrading effect on device characteristics. These charges are due to the electronic energy-levels situated at the interface of Si/SiO_2 with energy states in the Si band gap that can change their charge state by capturing or emitting electrons (or holes). These electrons arise owing to incomplete bonds (dangling), adsorption of extraneous impurity atoms at the silicon surface, and other defects, such as lattice mismatch at the interface, which is triggered by either radiation or bond-breaking processes [2]–[5]. These charges are also known as surface states or interface states (or traps) and the position of Fermi level decides the occupancy of interface trap charges under equilibrium state. In contrast to conduction and valence bands, the interface trap charges have energy level situated in the forbidden gap. The trap charges (both electrons and holes) are present in this gap and cannot move quickly due to large space between the interfacial trivalent silicon atoms. The energy level of an acceptor interface trap charge (or negative trap charges) lies above the valence band and below Fermi energy level, while the energy level of donor interface trap charge (or positive trap charges) lies below the conduction band and above the Fermi energy level [1]. Moreover, the trap density is very subtle to even small process variation, which subsequently leads to mobility and threshold voltage degradation, and thus results in a decrement in device transconductance. Hence, there is essential to examine the consequence of these trap charges on the analog behavior of the device.

From past few years, various innovative MOS structures and gate materials have been emerged to overcome the scaling limitations, i.e., short-channel effects (SCEs). It has been found that trench gate (recessed channel) MOSFET prominently overcome the SCEs [6] and also it is one of the promising planar structure as it is extending the scaling limit of conventional MOSFET. However, its carrier transport efficiency is limited by two potential barriers created at two corners due to which carriers need more energy to cross these high barriers, and thus limits the current driving capability. Thus, In_2Sn_5O

Manuscript received December 4, 2017; accepted January 10, 2018. This work was supported by the University Grants Commission. The work of A. Kumar was supported in part by the Delhi Technological and University Grants Commission. The review of this paper was arranged by Editor W. Tsai. *(Corresponding author: Rishu Chaujar.)*

The authors are with the Electrical Engineering Department, Delhi Technological University, New Delhi 110042, India, and also with the Applied Physics Department, Delhi Technological University, New Delhi 110042, India (e-mail: ajaykumar@dtu.ac.in; mmtripathi@dce.ac.in; chaujar.rishu@dtu.ac.in).

Color versions of one or more of the figures in this paper are available online at http://ieeexplore.ieee.org.

Digital Object Identifier 10.1109/TED.2018.2793853

0018-9383 © 2018 IEEE. Personal use is permitted, but republication/redistribution requires IEEE permission.
See http://www.ieee.org/publications_standards/publications/rights/index.html for more information.

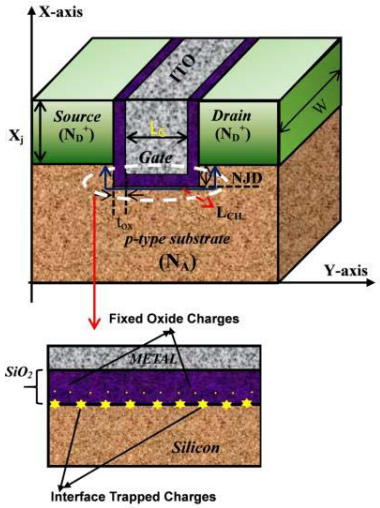


Fig. 1. Device design of TGRC-MOSFET (3-D device) with interface traps charges.

(indium–tin oxide) is used as gate material instead of conventional metal gate owing to its high conductivity, thermal stability, cost, and durability [7]–[9].

In this paper for the first time, the reliability issues of indium tin oxide (ITO) gate recessed channel MOSFET in the presence of uniform interface trap charges has been examined. In addition, the influence of low temperature (150–300 K) is also studied to find out at which temperature the device shows improved reliability in the presence of defects.

II. Device Design and It's Description

Fig. 1 shows the schematic 3-D view of transparent gate recessed channel (TGRC)-MOSFET consists of interfaced trap charges at the Si/SiO_2 interface. The gate length (L_G) is 30 nm while channel length (L_{CH}) is 54 nm [$L_G + 2t_{ox} + 2$ negative junction depth (NJD)], oxide thickness (t_{ox}) = 2 nm, NJD = 10 nm, and groove depth = 38 nm, for both devices [conventional recesses channel (CRC)- and TGRC-MOSFETs]. The source/drain region is heavily n+-doped (5×10^{20} cm^{-3}) whereas channel is p-doped (1×10^{17} cm^{-3}) for both CRC- and TGRC-MOSFETs. The gate material which plays a role in determining the current driving capability of MOSFET is taken In_2O_5Sn in the proposed device (TGRC-MOSFET) having workfunction of 4.7 eV, whereas, in CRC-MOSFET, aluminum (4.4 eV) is used as gate metal.

III. Simulation Methodology and Calibration

ATLAS is a powerful simulation tool, which is used for the extracting of reliability results and all figure of merits (FOMs) [10]. Various simulation models have been used, such as the Lombardi CVT model is used to consider all the mobilities such as scattering mechanism that is caused by the parallel and perpendicular fields applied on the device. For carrier generation-recombination, we have used Shockley–Read–Hall (SRH) recombination. Fermi–Dirac statistics is used in the case of very highly doped material. In order to consider the information about the low energy (temperature) of the carriers, we have used energy balance transport model [10]. The calibration of physical model parameters of the simulated device with the experimental results, by Appenzeller *et al.* in 2002 [11], is shown in Fig. 2. So as to validate the simulations results, the statistics have been drawn-out [11] for 36-nm groove MOSFET and then plotted as evident in Fig. 2. It is detected from Fig. 2 that simulated results almost matched with the experimental results in sub-40-nm groove MOSFET thus validating the simulation models. In this analysis, the value of trap charge density at the interface is chosen $1e^{12}$ cm^{-2} with uniform profiles according to previously published work [12], [13].

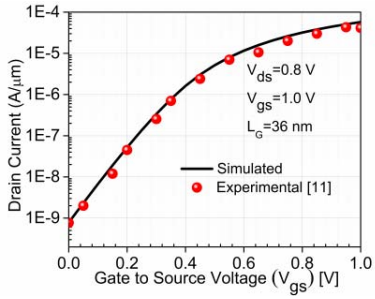


Fig. 2. Calibrated transfer characteristics of recessed channel MOSFET (36-nm gate length) with experimental and simulation data.

To explore the effect of trap charges on the subnanometer device, the total gate length is considered as the damaged region due to the high field in the channel region owing to scaling.

IV. Results and Discussion

There are many parameters which influence the performance of a MOSFET. In this section, reliability is examined and calculated in terms of analog and linearity FOMs. In addition, the effect of low temperature is explored on reliability issues of TGRC-MOSFET in the presence of trap charges (i.e., defects).

A. Impact of Interface Trap Charges on Analog Performance

Trap charges (both positive and negative) present beneath the Si/SiO_2 region are responsible for the change in flat-band voltage, and it is given by [12]

$$\Delta V_{\text{fb}} = \frac{qN_f}{C_{\text{ox}}} \tag{1}$$

where ΔV_{fb} is the change in flat-band voltage, N_f is the charge density, and C_{ox} is gate oxide capacitance. Fig. 3(a) shows the impact of interface trap charges (positive and negative) on the surface potential along the channel.

The trap charges are considered along with the entire gate length (L_G), and it is revealed from the figure that, the positive trap charges (donor type) enhances the potential while negative trap charges (acceptor type) reduces the potential in TGRC- and CRC-MOSFETs. This enhancement (reduction) in

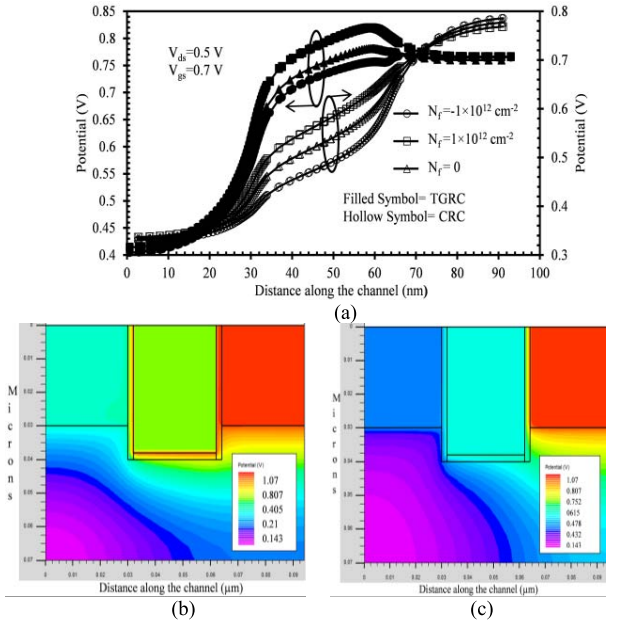


Fig. 3. (a) Potential with respect to the distance along the channel for CRC- and TGRC-MOSFETs. (b) Contour plot CRC-MOSFET with the impact of positive interface trap charge. (c) Contour plot TGRC-MOSFET with the impact of positive interface trap charge.

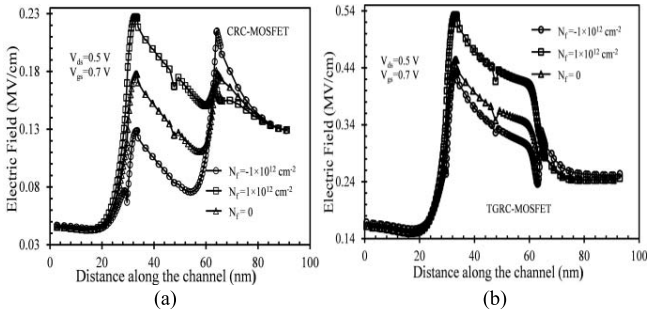


Fig. 4. Electric field distribution along the channel for (a) CRC-MOSFET and (b) TGRC-MOSFET.

potential is due to lowering (rising) of flat-band voltage which increases (decreases) the gate control over the channel and thus the surface potential. It is also found that surface potential enhances significantly in TGRC-MOSFET in comparison to CRC-MOSFET owing to the high conductivity of transparent gate as clearly reflected through 2-D contour plots shown in Fig. 3(b) and (c). It is observed from Fig. 4(a) and (b) that electric field in the channel region enhances appreciably in TGRC-MOSFET due to high surface potential in the channel region and owing to transparent gate metal having higher workfunction in comparison to the aluminum metal gate. Electric field near the drain end reduces and enhances near the source side as compared with CRC-MOSFET. The presence of positive (negative) trap charges increases (decreases) the electric field near the source end in comparison to drain end, owing to the creation of more (less) charges in the channel region, and thus leads to more (less) number of charge carriers being flow. However, from Figs. 3 and 4, it is clearly observed that the influence of trap charges is less pronounced in TGRC in comparison with CRC-MOSFET.

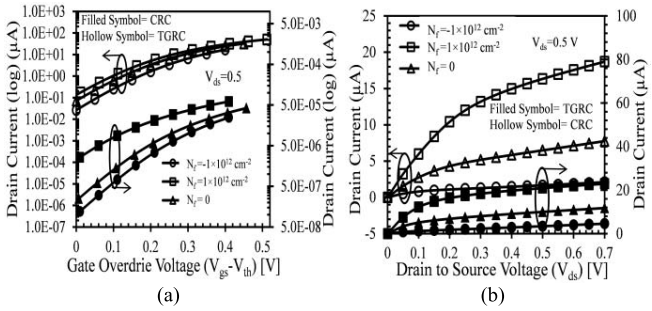


Fig. 5. (a) Transfer characteristics with respect to V_{gs} and (b) output characteristics with respect to V_{ds}, for CRC- and TGRC-MOSFETs.

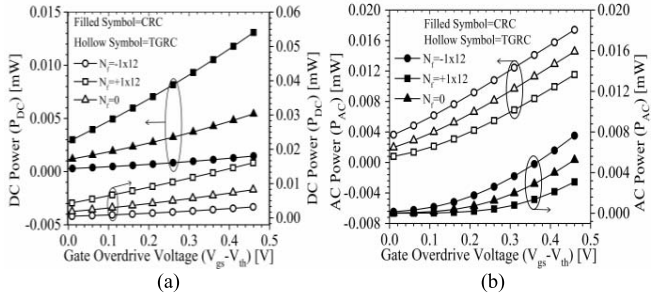


Fig. 6. (a) dc power (P_{dc}) and (b) ac power (P_{ac}) with respect to V_{gs}, for CRC- and TGRC MOSFETs.

The impact of trap charges on transfer characteristics (I_{ds}–V_{gs}) and output characteristics is also examined. Fig. 5(a) and (b) indicates that the effect of trap charges is more prominent in the subthreshold region than linear region. It is found that in the presence of positive (negative) trap charges, drain current increases (decreases) owing to high (low) field at the source end, and enhance (reduce) gate control. However, TGRC indicates nearly insignificant change in ON-current due to interface traps/damage region when it worked in inversion region.

Electrical power is the "rate" at which energy is being consumed in a circuit. The impact of interface trap charges on the low-power performance parameter, such as P_{dc} (dc power) and P_{ac} (ac power), has also been evaluated using the following:

$$P_{DC} = V_{DC} \times I_{DC} \tag{2}$$

$$P_{AC} = V_{rms} \times I_{rms}. \tag{3}$$

It is found that dc power starts increasing with increase in gate overdrive voltage and its value is numerically smaller in TGRC-MOSFET in comparison to CRC-MOSFET, as evidently shown from Fig. 6(a). Moreover, it is also observed that the effect of trap charges in TGRC-MOSFET shows lesser impact on dc power in comparison to CRC-MOSFET. This improvement is due to lower OFF-current and improved current driving capability. In addition, ac power is also studied and is found that ac power in TGRC-MOSFET is more immune to interface trap charges in comparison to CRC-MOSFET, as shown in Fig. 6(b). Thus, it can be concluded that in the presence of trap charges, TGRC-MOSFET will be suitable for low-power applications.

TABLE I
P_{AC} VARIATION WITH L_G

Gate length (L_G) (nm)	20	30	40
P_{AC} (mW)	0.01325	0.015	0.018

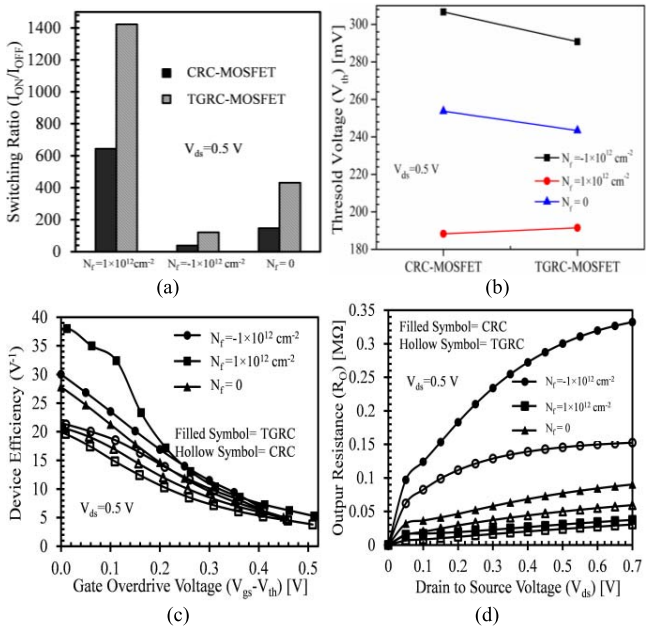


Fig. 7. Effect of interface trap charges on (a) switching ratio, (b) threshold voltage, (c) device efficiency, and (d) output resistance, for CRC- and TGRC MOSFETs.

Furthermore, it is also analyzed that with the tuning of TGRC's parameters, such as L_G(from 40 to 20 nm) and NJD (from 15 to 5 nm), its linearity performance enhances appreciably [14] while power (P_{ac}) degrades, as clearly reflected in Table I. Therefore, depending on the application, we may utilize the tradeoff between improved linearity or improved P_{ac} at a given device feature size.

Moreover, due to enhancement in drain current, switching ratio (I_{ON}/I_{OFF}) of TGRC enriches significantly as evident from Fig. 7(a) and it is calculated by the ratio of current at $V_{gs} = 0.7$ V (I_{ON}) and $V_{gs} = 0$ V (I_{OFF}). In TGRC, the ratio is enhanced by 125%, 128%, and 166% for positive, negative, and neutral trap charges, respectively, as compared with CRC device, shown in Fig. 7(a). However, CRC-MOSFET shows a more significant influence of interface traps charges for switching ratio than TGRC-MOSFET. In addition, the threshold voltage (V_{th}) which is a significant parameter for analog applications, also improves in TGRC-MOSFET in comparison to CRC-MOSFET, as shown in Fig. 7(b). This improvement is due to reduced leakage current owing to the transparent gate, which results in reduced SCEs (hot-carrier and drain induced barrier lowering) [15].

V_{th} is also affected by trap charges, as reflected in Fig. 7(b), but the effect is more in CRC in comparison to TGRC due to less change in flat-band voltage. Influence of trap charges on transconductance to the current ratio (g_m/I_d) or device efficiency and output resistance have also been analyzed for both devices, as shown in Fig. 7(c) and (d). In the design of analog circuits, device efficiency is a vital factor, which offers the measure of effectiveness to convert power into speed. It is evident from Fig. 7(c) that the device efficiency is higher (lower) in TGRC-MOSFET when positive (negative) trap charges are present in comparison to CRC-MOSFET. It is also observed in Fig. 7(c) that the impact of interface trap charges on device efficiency is less prominent in TGRC, and thus signify superior efficiency in TGRC than CRC. The output resistance (R_o) is the transposed of the output conductance in a MOSFET and for high performance; R_o should be as small as possible. When positive (negative) trap charges have been taken into consideration, R_o is very less (high) while it is less prominent for negative and neutral trap charges in TGRC-MOSFET as compared with conventional counterpart, as shown in Fig. 7(d). Thus, recessed channel MOSFET with transparent gate material (ITO) shows reliable performance in the presence of interface trap charges as compared with CRC device.

B. Impact of Interface Trap Charges on Linearity and Distortion Performance

High linearity and lower intermodulation distortions (IMDs) are essential requirements for a CMOS device when working with weak signals. Nonlinearity introduces IMD and generates an undesired distorted signal in the output of different frequency signals compared with an input signal, which results in degradation in device behavior [16]. For that reason, in this subsection, the influence of interface trap charges on linearity and IMD of TGRC device are studied and results obtained are simultaneously compared with CRC-MOSFET. The performance metrics used in this analysis are g_{m3} (higher order transconductance coefficient), third-order voltage intercept point (VIP3), third-order current intercept point (IIP3), third-order IMD (IMD3), and second- and third-order harmonic distortions (HD2 and HD3). To assure higher linearity, higher order transconductance coefficient (g_{m3}) must be minimal.

From the dc parameters, VIP3 is used to evaluate the distortion characteristics. IIP3 and VIP3 should be high, but IMD3 and HD3 should be low for lower distortion. The device linearity FOMs are evaluated, as shown in (4)–(7) [17]

$$\text{VIP3} = \sqrt{24 \times g_{m1}/g_{m3}} \tag{4}$$

where $g_{m1} = (\partial I_d/\partial V_{gs})$ and $g_{m2} = (\partial^2 I_d/\partial V_{gs}^2)$. $g_{m3} = (\partial^3 I_d/\partial V_{gs}^3)$

$$\text{IIP3} = \frac{2}{3}\frac{g_{m1}}{g_{m3} \times Rs} \tag{5}$$

where $R_S = 50\ \Omega$ for analog and RF applications

$$\text{IMD3} = \left(\frac{9}{2} \times (VIP3)^3 \times g_{m3}\right)^2 \times R_S \tag{6}$$

$$\text{HD2} = 0.5V_a\frac{\left(\frac{dg_{m1}}{dV_{GT}}\right)}{2g_{m1}} \tag{7}$$

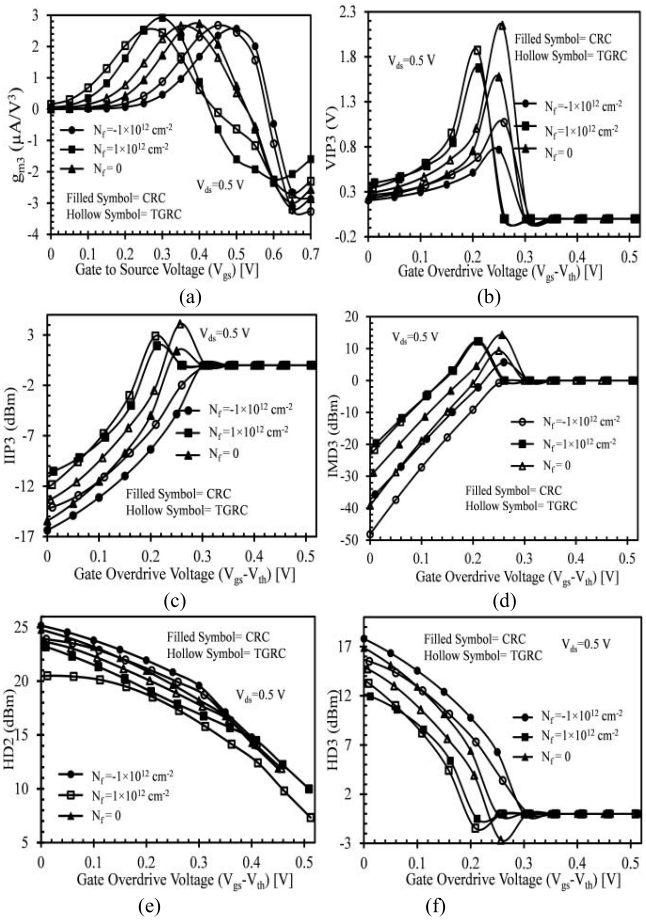


Fig. 8. Effect of interface trap charges on (a) g_{m3}, (b) VIP3, (c) IIP3, (d) IMD3, (e) HD2, and (f) HD3, for CRC- and TGRC MOSFETs.

$$\mathrm{HD3} = 0.25V_a^2 \frac{\left(\frac{d^2 g_{m1}}{dV_{GT}^2}\right)}{6g_{m1}} \tag{8}$$

where $R_S = 50\ \Omega$ for analog and RF applications. V_a is the amplitude of ac signal and considered about 50 mV (which is minuscule) for integral function method (IFM) analysis.

Ideally, g_{m3} should be as low as possible because g_{m3} decides the dc bias point for optimal device operation and determines the limits on the distortion. Fig. 8(a) illustrates the variation of g_{m3} with respect to V_{gs} for damaged (positive and negative traps) and undamaged region. g_{m3} is a higher order derivative of transfer characteristics and it is observed that g_{m3} reduces (enhances) in case of TGRC in the presence of positive (negative) trap charges although this variation is very less in comparison to CRC-MOSFET. This is due to less dependence on trap charges on transfer characteristics and transconductance, which reflects TGRC, is more reliable in the presence of interface trap charges/damage. Fig. 8(b) and (c) reflects the influence of interface trap charges on VIP3 and IIP3, respectively. For low distortion and high linearity, the peak value of IIP3 and VIP3 should be high. VIP3 signifies extrapolated input voltage at which first- and third-order harmonics of drain current are equal and expressed as in (4), while IIP3 is a theoretical point at which the third-order distortion signal amplitudes equal the input signals, and it is useful in determining the linearity condition of an amplifier [18]. The amplitude of VIP3 and IIP3 is high for TGRC-MOSFET as compared with CRC-MOSFET, and it also implies that the damaged device (in the presence of trap charges) shows less linearity in comparison with the undamaged device, but TGRC architecture shows better linearity and less distortion in comparison to CRC-MOSFET. This is due to the higher conductivity of ITO as compared with the metal gate that enhances current driving capability [19], and thus improves linearity performance in the presence of interface traps. In addition, IMD3, HD2, and HD3 are major issues in linear amplifiers that arise owing to the nonlinearity performance of the device [18] and stated in (6)–(8). IMD3 represents the intermodulation current at which the first- and third-order intermodulation harmonic currents are the same. IMD3 is analyzed considering the influence of interface trap charges on TGRC device. IFM is used for the calculation of the distortion since this approach authorizations for the extraction of distortion from dc measurements deprived of an ac characterization, dissimilar to Fourier-based methods [20], [21] as shown in (6)–(8). The output conductance of TGRC is negligible. Hence, the device gains are improved [22], [23]. Fig. 8(d) reveals that IMD3 reduces in TGRC-MOSFET owing to the reduced g_{m3} value in comparison to VIP3, which dominates the value of IMD3 [Fig. 8(a)] as compared with CRC-MOSFET. Meanwhile, it is also observed that TGRC reduces (increase) HD2 and HD3 when positive (negative) trap charges are considered and exhibit the very less effect of traps charges as compared with its conventional counterpart, as shown in Fig. 8(e) and (f). Thus, TGRC exhibits improved linearity and distortion-less performance for ultra large scale integration (ULSI) in the presence of interface trap charges.

C. Effect of Interface Trap Charges at Low Temperature on Analog, Linearity, and Intermodulation Distortion

This subsection describes the effect of temperature on the above-mentioned parameters for TGRC-MOSFET in the occurrence of interface trap charges to analyze the reliability of TGRC-MOSFET at low temperatures (150–300 K). Electrical behavior of CMOS devices changes with change in temperature. As the temperature increases, the carrier mobility [24] decreases as

$$\mu(T) = \mu(T_0)\left(\frac{T}{T_0}\right)^{-n} \tag{9}$$

where "n" is an exponent, which varies from 1.6 to 2.4 [25]. If mobility is decreased, then the output current also reduces, and hence with the increase in temperature, switching ratio decreases, as shown in Fig. 9(a). Moreover, change in ambient temperature also influences the traps charges created during the fabrication process. It is found that in the presence of positive (negative) trap charges, the number of charge carriers increased (decrease), due to which mobility reduced (enhance) and hence switching ratio and output resistance (inset) reduced (improves), as evident from Fig. 9(a). Furthermore, the threshold voltage (V_{th}) of the MOSFET is inversely proportional to the temperature [26] and it increases at low temperature due

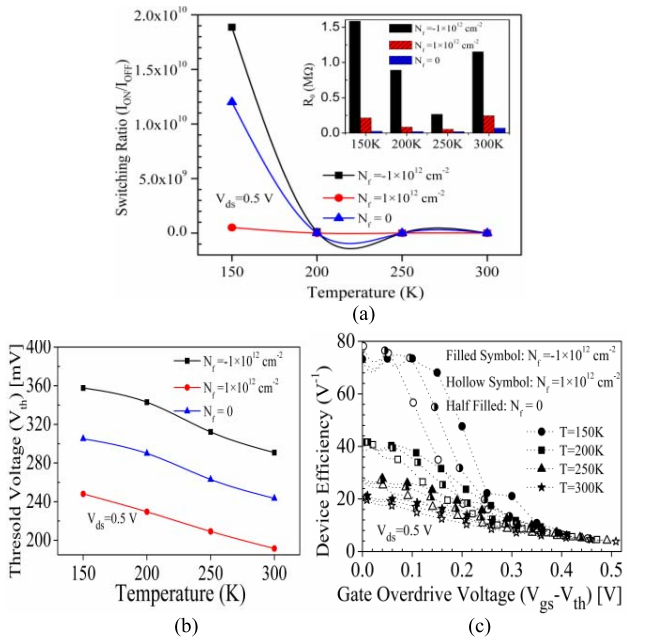


Fig. 9. Effect of temperature on (a) switching ratio, inset: output resistance, (b) threshold voltage, and (c) device efficiency, in TGRC-MOSFET with interface trap charge density.

to the rise in Fermi potential (ϕ_F) and depletion charges [27]. In the absence of trap charges V_{th} is 0.243 V at room temperature. Fig. 9(b) shows the variation of the threshold voltage, and it is observed that as the temperature rises from 150 to 300 K, V_{th} reduced and it is higher (lower) for negative (positive) trap charges due to the change in flat-band voltage and mobility. Besides, both mobility and threshold voltage also influenced the drain to source current I_{ds} [28] as

$$I_{\text{ds}}(T) \propto \mu(T)[V_{\text{gs}} - V_{\text{th}}(T)] \tag{10}$$

Fig. 9(c) illustrates the higher device efficiency at a lower temperature, and in the presence of positive (negative) trap charges, device efficiency is more (less) with respect to neutral trap charges. Hence, TGRC-MOSFET shows better performance at low temperature owing to reduced fluctuations. Fig. 10(a) shows higher order transconductance (g_{m3}) as a function of the gate to source voltage for different ambient temperatures in the presence of positive (donor), and negative (acceptor) interface trap charges. At $T = 150$ K, positive (negative) trap charges exhibit low (high) distortion owing to improved transconductance. Furthermore, at high temperature (>150 K), distortion is increased (low peaks are observed in g_{m3}). Fig. 10(b) and (c) reflects the improved performance of TGRC-MOSFET at a lower temperature (<300 K) in terms of VIP3 and IIP3, respectively, in the presence of trap charges. It is found that peak value of VIP3 and IIP3 is enhancing at a low temperature which indicates less distortion and high linearity, when the device is working at low temperature. Besides, it is also observed that impact of interface trap charges on TGRC's linearity performance at low temperature is less prominent, as clearly indicated from Fig.10(b) and (c). Thus, TGRC-MOSFET acts as a potential candidate for linear amplifiers working at low temperatures in CMOS ULSI. Harmonic distortion is an essential reliability issue which

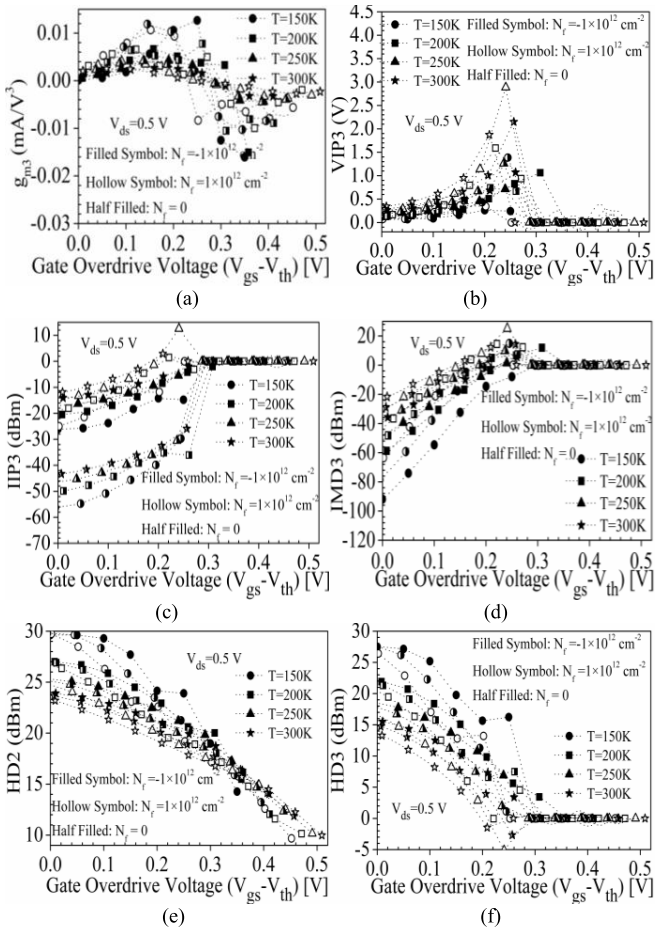


Fig. 10. Effect of temperature with interface trap charges on (a) g_{m3}, (b) VIP3, (c) IIP3, (d) IMD3, (e) HD2, and (f) HD3 in TGRC-MOSFET.

arises due to the nonlinear performance of MOSFET. Thus, HD in terms of IMD3, HD2, and HD3 are examined as a function of both temperature and interface trap charges and are illustrated in Fig. 10(d)–(f), respectively. Change in ambient temperature plays a major role in amplifiers working in communication systems and sometimes it causes an undesirable change in signals and thus causes distortion in the band of interest. This is due to the random motion of electrons which results in thermal noise within the device, and thus degrades the device performance. At low temperatures (<300 K), harmonic distortions (IMD3, HD2, and HD3) are reduced in TGRC-MOSFET, as evident from Fig. 10 (d)–(f). It is also observed that in the presence of positive (negative) trap charges, g_{m3} lowers (increase) owing to improved (reduce) current driving capability, and thus lowers (rise) the distortion. This effect is more at low temperatures in TGRC due to enhancement in transconductance and reduction in g_{m3} [see Fig. 10(a)].

V. Conclusion

This paper studies the influence of interface trap charges on the static, linearity, and distortion FOMs to explore the reliability issues of TGRC-MOSFET. The performance of this device has also been compared with CRC-MOSFET through extensive device simulation. The proposed device is

This article has been accepted for inclusion in a future issue of this journal. Content is final as presented, with the exception of pagination.

suitable for high switching applications even in the presence of trap charges. It has been shown that the TGRC-MOSFET exhibits superior current driving capability, and high linearity (VIP3 and IIP3) with low distortions. It has also been observed that TGRC-MOSFET is more immune to interface trap charges than CRC-MOSFET. Likewise, it is also found that TGRC-MOSFET at low temperature (150 K) in the presence of interface trap charges show negligible variation in device behavior in terms of I_{ds}, g_m, VIP3, IIP3, HD2, HD3, and IMD3. Thus, the TGRC-MOSFET is more reliable at low temperatures and serves as a promising candidate for analog and low-power high-linearity applications.

REFERENCES

[1] N. D. Arora, *MOSFET Models for VLSI Circuit Simulation: Theory and Practice*. New York, NY, USA: Springer, 1993.

[2] H. Jo, S. Choi, S. Rhee, and Y. J. Park, "An analytical model for the threshold voltage of intrinsic channel MOSFET having bulk trap charges," *IEEE Trans. Electron Devices*, vol. 64, no. 5, pp. 2113–2120, May 2017.

[3] Y. H. Lho and K. Y. Kim, "Radiation effects on the power MOSFET for space applications," *ETRI J.*, vol. 27, no. 4, pp. 449–452, 2005.

[4] L. Trabzon and O. O. Awadelkarim, "Damage to n-MOSFETs from electrical stress relationship to processing damage and impact on device reliability," *Microelectron. Rel.*, vol. 38, no. 4, pp. 651–657, 1998.

[5] E. H. Poindexter, "MOS interface states: Overview and physicochemical perspective," *Semicond. Sci. Technol.*, vol. 4, no. 12, p. 961, 1989.

[6] S. Veeraraghavan and J. G. Fossum, "Short-channel effects in SOI MOSFETs," *IEEE Trans. Electron Devices*, vol. 36, no. 3, pp. 522–528, Mar. 1989.

[7] R. G. Gordon, "Criteria for choosing transparent conductors," *MRS Bull.*, vol. 25, pp. 52–57, Aug. 2000.

[8] V. Singh, C. K. Suman, and S. Kumar, "Indium Tin Oxide (ITO) films on flexible substrates for organic light emitting diodes," in *Proc. ASID*, 2006, pp. 388–391.

[9] R. Murali and J. D. Meindl, "Modeling the effect of source/drain junction depth on bulk-MOSFET scaling," *Solid-State Electron.*, vol. 51, no. 6, pp. 823–827, 2007.

[10] *ATLAS User's Manual*, SILVACO, Santa Clara, CA, USA, 2011.

[11] J. Appenzeller *et al.*, "Sub-40 nm SOI V-groove n-MOSFETs," *IEEE Electron Device Lett.*, vol. 23, no. 2, pp. 100–102, Feb. 2002.

[12] T.-K. Chiang, "A compact model for threshold voltage of surrounding-gate MOSFETs with localized interface trapped charges," *IEEE Trans. Electron Devices*, vol. 58, no. 2, pp. 567–571, Feb. 2011.

[13] S. Shabde, A. Bhattacharyya, R. S. Kao, and R. S. Müller, "Analysis of MOSFET degradation due to hot-electron stress in terms of interface-state and fixed-charge generation," *Solid-State Electron.*, vol. 31, no. 11, pp. 1603–1610, 1988.

[14] A. Kumar, "Effect of trench depth and gate length shrinking assessment on the analog and linearity performance of TGRC-MOSFET," *Superlattices Microstruct.*, vol. 109, pp. 626–640, Sep. 2017.

[15] A. Kumar, N. Gupta, and R. Chaujar, "Analysis of novel transparent gate recessed channel (TGRC) MOSFET for improved analog behaviour," *Microsyst. Technol.*, vol. 22, no. 11, pp. 2665–2671, 2016.

[16] B. Razavi and R. Behzad, *RF Microelectronics*, vol. 1. Englewood Cliffs, NJ, USA: Prentice-Hall, 1998.

[17] R. Chaujar, R. Kaur, M. Saxena, M. Gupta, and R. S. Gupta, "TCAD assessment of Gate Electrode Workfunction Engineered Recessed Channel (GEWE-RC) MOSFET and its multi-layered gate architecture, Part II: Analog and large signal performance evaluation," *Superlattices Microstruct.*, vol. 46, no. 4, pp. 645–655, 2009.

[18] N. Gupta and R. Chaujar, "Optimization of high-k and gate metal workfunction for improved analog and intermodulation performance of Gate Stack (GS)-GEWE-SiNW MOSFET," *Superlattices Microstruct.*, vol. 97, pp. 630–641, Sep. 2016.

[19] A. Kumar, M. M. Tripathi, and R. Chaujar, "Investigation of parasitic capacitances of In_2O_5Sn gate electrode recessed channel MOSFET for ULSI switching applications," *Microsyst. Technol.*, vol. 23, no. 12, pp. 5867–5874, 2017.

[20] A. Cerdeira, M. A. Alemán, M. Estrada, and D. Flandre, "Integral function method for determination of nonlinear harmonic distortion," *Solid-State Electron.*, vol. 48, no. 12, pp. 2225–2234, 2004.

[21] R. T. Doria, A. Cerdeira, J.-P. Raskin, D. Flandre, and M. A. Pavanello, "Harmonic distortion analysis of double gate graded-channel MOSFETs operating in saturation," *Microelectron. J.*, vol. 39, no. 12, pp. 1663–1670, 2008.

[22] A. Kumar, N. Gupta, and R. Chaujar, "Power gain assessment of ITO based Transparent Gate Recessed Channel (TGRC) MOSFET for RF/wireless applications," *Superlattices Microstruct.*, vol. 91, pp. 290–301, Mar. 2016.

[23] R. van Langevelde and F. M. Klaassen, "Accurate drain conductance modeling for distortion analysis in MOSFETs," in *IEDM Tech. Dig.*, Dec. 1997, pp. 313–316.

[24] R. van Langevelde and F. M. Klaassen, "Effect of gate-field dependent mobility degradation on distortion analysis in MOSFETs," *IEEE Trans. Electron Devices*, vol. 44, no. 11, pp. 2044–2052, Nov. 1997.

[25] S. M. Sze and K. K. Ng, *Physics of Semiconductor Devices*. New York, NY, USA: Wiley, 2006.

[26] G. Groeseneken, J. Colinge, H. E. Maes, J. C. Alderman, and S. Holt, "Temperature dependence of threshold voltage in thin-film SOI MOSFETs," *IEEE Electron Device Lett.*, vol. 11, no. 8, pp. 329–331, Aug. 1990.

[27] T. Elewa *et al.*, "Performance and physical mechanisms in SIMOX MOS transistors operated at very low temperature," *IEEE Trans. Electron Devices*, vol. 37, no. 4, pp. 1007–1019, Apr. 1990.

[28] N. Gupta and R. Chaujar, "Investigation of temperature variations on analog/RF and linearity performance of stacked gate GEWE-SiNW MOSFET for improved device reliability," *Microelectron. Rel.*, vol. 64, pp. 235–241, Sep. 2016.



Ajay Kumar (S'15) received the B.Tech. degree in electronics and communication from Uttar Pradesh Technical University, Lucknow, India, in 2009, and the M.Tech. degree in nanoscience and technology from Delhi Technological University, New Delhi, India, in 2014, where he is currently pursuing the Ph.D. degree with Electrical Engineering Department.



M. M. Tripathi (SM'16) received the B.Tech. degree from the Madan Mohan Malaviya Engineering College, Gorakhpur, India, in 1994, and the Ph.D. degree from Gautam Buddh Technical University, Lucknow, India, in 2010.

He is currently a Professor with the Electrical Engineering Department, Delhi Technological University, New Delhi, India.



Rishu Chaujar (SM'16) received the B.Sc. (H), M.Sc., and Ph.D. degrees in electronics from the University of Delhi, New Delhi, India, in 2003, 2005, 2009 respectively.

She is currently an Assistant Professor with the Department of Applied Physics, Delhi Technological University, New Delhi.

ResearchGate

See discussions, stats, and author profiles for this publication at: https://www.researchgate.net/publication/322984841

Study of reflection losses in tuned and EBG power dividers at S, C, X and upper Ku bands

Article · December 2017

DOI: 10.26438/ijsrnsc/v5i6.2126

CITATIONS
0

READS
8

4 authors, including:



Karteek Viswanadha
Birla Institute of Technology and Science Pilani
3 PUBLICATIONS **0** CITATIONS

SEE PROFILE

Some of the authors of this publication are also working on these related projects:



high gain and bandwidth antenna View project

All content following this page was uploaded by Karteek Viswanadha on 16 February 2018.

The user has requested enhancement of the downloaded file.

www.ijsrnsc.org

Available online at www.ijsrnsc.org

IJSRNSC

Volume-5, Issue-6, December 2017
Research Paper

Int. J. Sc. Res. in Network Security and Communication

E-ISSN:2321-3256

Study of reflection losses in tuned and EBG power dividers at S, C, X and upper Ku bands

Suresh Angadi[1*], Karteek Viswanadha[2], R.Roopa Sree[3], Sowjanya Madaka[4]

[1*]Department of Electronics and Communication Engineering, VITAM, Visakhapatnam, India.
[2]Department of Electronics and Communication Engineering, Delhi Technological University, New Delhi, India.
[3]Department of Electronics and Communication Engineering, VITAM, Visakhapatnam, India.
[4]Department of Electronics and Communication Engineering, VITAM, Visakhapatnam, India.

E-mail: suresh.angadi.101@gmail.com[1], karteekviswanath@gmail.com[2], rokkamroopasree@gmail.com[3], sowjanya.devi46@gmail.com[4]

[*]*Corresponding Author: suresh.angadi.101@gmail.com, Tel.: 918919840988*

***Abstract*—**This paper presents the study of reflection losses in a tuned 8 port power divider with circular and square slotted Electromagnetic Bandgap structures (EBG) by varying the dimensions of the slots as well as the transmission lines. Further, the tuning feature makes the proposed power divider not only compact but also to work at S, C, X and the upper Ku bands by introducing periodic structures and thus enhancing the bandwidth with less reflection losses. Various parameters like reflection coefficient, insertion loss of the tuned EBG power divider are studied by varying the number of slots in the ground plane using Agilent Advanced Design System 2009 and 2016 simulators respectively.

***Keywords*—** Power divider , bandwidth, insertion loss, reflective loss, X, Ku-band,ADS.

I. INTRODUCTION

Wireless communications are shifting towards the ultra high frequencies and data rates in order to meet the technological advancements. Usually high data rates are achieved using antenna arrays which are highly directional. The gain of an antenna depends on the power it receives from the preceded device which in deed acts as power feeder to antennas. The feeding devices for the antenna arrays should have high isolation, low insertion and reflection losses. Many power dividers like 'T'-junctions, Wilkinson and Geysel are used as power feeding devices for antenna arrays [1]. Wilkinson power divider consists of quarter wavelength transformers on the output lines and a resistor connecting the two output lines which improves the isolation between the output ports [2-3]. Wilkinson power dividers are usually narrow band devices and thereby require cascading of quarter wavelength transformers in order to increase the bandwidth. Conventional power dividers have one input and '2^n' output ports. Power dividers are proposed with 6 output ports in order to achieve good insertion loss and improve reflective losses [4]. But, Wilkinson power dividers are limited to low or medium power applications. Wide bandwidth is achieved in L-band by using the power divider with 6-outputs than compared to that of a conventional 1:2 power divider [4]. Performance parameters of the power dividers can also be improved by changing the properties of the substrate. Slots etched periodically on the ground plane also enhance bandwidth along with reduction in the surface waves and these structures are called as Electromagnetic Band gap Structures (EBG). Bandwidth of power divider can further be enhanced by mounting later on the EBG structures and introducing tuning elements like capacitor and inductor by varying the dimensions of the transmission line. These structures are often used with coupled lines where the power division is achieved by varying the spacing between the lines. Coupled lines facilitate the introduction of tuning elements by varying the spacing between the microstrip lines. These power dividers have wide bandwidth due to the tuning elements present inside them [5]. Apart from the equal power dividers, unequal power dividers are proposed depending on the application. Unequal power dividers often possess wide bandwidths without utilizing the tuning

© 2017, IJSRNSC All Rights Reserved

elements [6]. For high power applications, Geysel power dividers are used [7]. These power dividers not only improve the power handling capability but also keeps track on the imbalance at the output ports. Unequal power dividers are designed by cascading the transmission line transformers which improves performance parameters [8]. Wilkinson power divider designed below the dielectric substrate using double-sided parallel strip line increases the bandwidth up to 4GHz [9]. Waveguide power divider is designed using Multi Cavity Modeling Technique (MCMT) and acts as an efficient feed for antenna arrays [10]. Waveguide power dividers also perform filtering functions in order to select the band of interest and suppress the harmonics [11-12]. The improved form of waveguide called Substrate Integrated Waveguide (SIW) is often used to design the power dividers in order to improve the compactness and ease the integration. SIW power dividers proposed can work in K, V, W bands thus improves the isolation [13-14]. Ring type SIW power dividers with 1.5λ length are proposed [15]. Moreover, the impedance of SIW power divider is independent of cut off frequency and isolation resistance [16]. Alternate method for enhancing the bandwidth is realizing power dividers with stepped-impedance transmission lines and stubs [17]. The transmission lines introduce capacitive path in order to suppress the harmonics [17]. Coplanar wave guide (CPW) is another form of planar transmission line which eases the process of integration.

II. DESIGN OF THE PROPOSED POWER DIVIDER

The proposed power divider is designed on the Rogers RT/duroid 5880 substrate of height 0.254mm and relative dielectric constant of 2.2.The whole design is carried out in ADS 2009 schematic as well as in momentum using method of moments. The characteristic impedance of the input transmission line is fixed at 50 Ω. Quarter wavelength lines of with operational frequency of 10 GHz are designed to have the characteristic impedances of $50\sqrt{2}$ Ω each. Dimensions of main lines (50 Ω lines) especially are tuned stepwise. By doing so, main lines introduce filtering feature to the power divider.

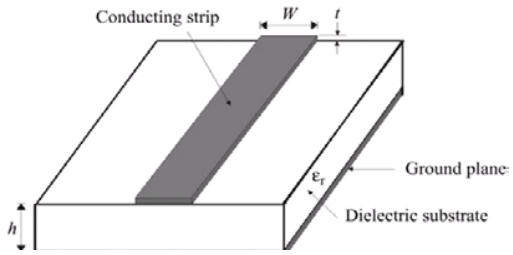


Figure 1. Microstrip Line.

From fig.1, the width and length of the input transmission line at 10GHz is calculated by using the following equations:

$$\varepsilon_{eff} = \frac{\varepsilon_r+1}{2} + \frac{\varepsilon_r-1}{2}\frac{1}{\sqrt{1+12h/W}} \quad (1)$$

Where 'ε_r' is the relative dielectric constant and 'h' is the height of the dielectric and 'W' is the width of quarter wavelength impedance transformer line. Characteristic impedance is given by:

$$Z_o = \frac{60}{\sqrt{\varepsilon_{eff}}}\ln\left(\frac{8h}{W}+\frac{W}{4h}\right), \text{ for W/h} \leq 1 \quad (2)$$

$$Z_o = \frac{120\pi}{\sqrt{\varepsilon_{eff}}\left[\frac{W}{h}+1.393+0.667+\ln\left(\frac{W}{h}+1.444\right)\right]}, \text{ for W/h} \geq 1 \quad (3)$$

$$\frac{W}{h} = \frac{8e^A}{e^{2A}-2}, \text{ for W/h} < 2 \quad (4)$$

$$\frac{W}{h} = \frac{2}{\pi}\left[B-1-\ln(2B-1)+\frac{\varepsilon_r-1}{2\varepsilon_r}\left\{\ln(B-1)+0.39-\frac{0.61}{\varepsilon_r}\right\}\right] \quad (5)$$

Where $A = \frac{Z_o}{60}\sqrt{\frac{\varepsilon_r+1}{2}} + \frac{\varepsilon_r-1}{\varepsilon_r+1}\left\{0.23+\frac{0.11}{\varepsilon_r}\right\}$

$$B = \frac{377\pi}{2Z_o\sqrt{\varepsilon_r}}$$

Using the above design equations, the width (w_o) of the input transmission line is obtained as 0.762 mm and the electrical length (l_o) is tuned to 155^0 or equivalently 9.39mm in order to introduce the shunt L-C elements on the input line. Using the below equation for calculating the length of the quarter wavelength transformer,

Line length= $\frac{c}{4f\sqrt{\varepsilon_{eff}}}$ where 'c' is the velocity of light and 'f' is the frequency of operation. The width of quarter wavelength lines (w_1) is 0.457mm each. Electrical lengths (l_1) of the quarter wavelength lines are tuned to 82° or equivalently 5.08mm in order to introduce the series L-C elements. The transmission line equivalent of the proposed power divider is designed in ADS-2009 schematic as shown in fig.2. The basic idea behind the proposed structure of power divider is to make the divider compact and providing power closest to the ideal value of 8 output power divider.

S-parameter matrix of the tuned power divider is same as that of Wilkinson power divider given by:

$$\frac{-j}{\sqrt{2}}\begin{bmatrix}0 & 1 & 1\\ 1 & 0 & 0\\ 1 & 0 & 0\end{bmatrix}$$

© 2017, IJSRNSC All Rights Reserved

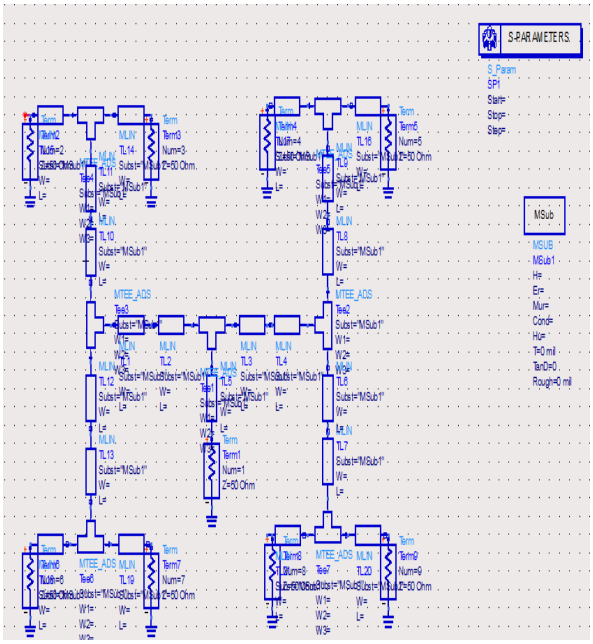


Figure 2. Schematic of the proposed power divider

Fig. 3(a) & 3(b) shows the proposed tuned power divider and its layout in ADS-momentum. As quarter wavelength line is not an impedance matcher and therefore, it introduces tuning elements like inductor and capacitor at each junction of the power divider. These tuning elements form a fourth order band pass filter with wide band pass response and divides power over a large range of frequencies.

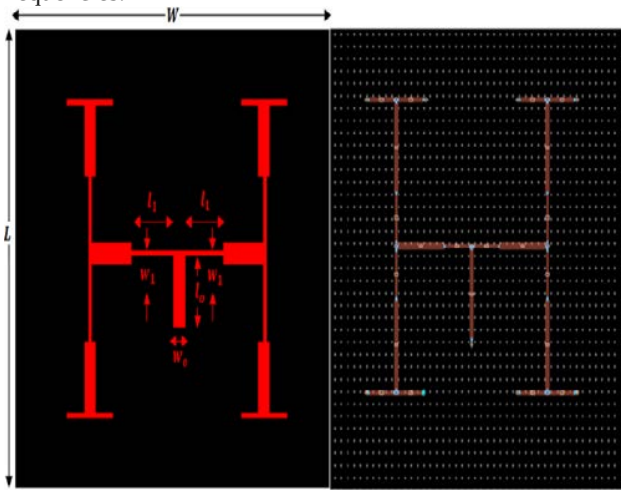


Figure 3(a). Proposed tuned power divider
Figure 3(b). Layout of the proposed tuned power divider

III. DESIGN OF THE PROPOSED POWER DIVIDER WITH SQUARE AND CIRCULAR EBG STRUCTURES

The proposed power divider is implemented using Electronic Band gap Structures (EBG) with width (W) 30.54mm and length (L) of 25.4mm with square and circular etched. Fig. 4(a) & 4(b) shows the proposed 15 slotted EBG tuned power divider and its layout. For the 15 slotted EBG shown in fig. 4(a), the dimensions of square slot (a) are 2.54mm by 2.54mm and the radius (r) of circular slot is 1.25mm. Horizontal (s) and vertical (s_o) spacing is chosen to be 9mm and 3mm respectively..

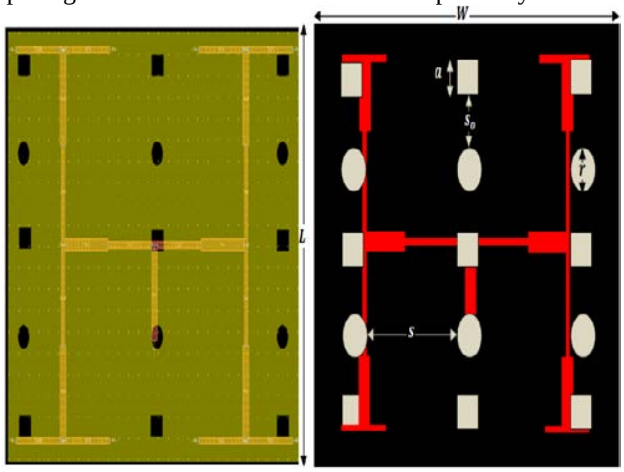


Figure 4(a). Proposed tuned power divider with 15 slotted EBG structure
Figure 4(b). Layout of the tuned power divider with 15 slotted EBG structure

Fig. 5(a) & 5(b) shows the proposed 42 slotted EBG tuned power divider and its layout. For the 42 slotted EBG structure shown in fig. 5, the dimensions of square slot (a') are taken as 1mm by 1mm and the radius (r_o) of circular slot is 0.5mm. Horizontal spacing (s') between the slots is chosen to be 3.2 mm and vertical spacing (s_o') is chosen to be 4.1mm.

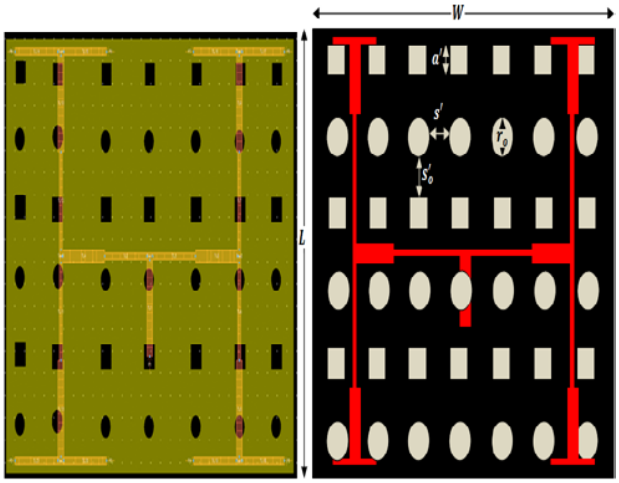


Figure 5(a). Layout of the proposed power divider with 42 slotted EBG
Figure 5(b). Proposed power divider with 42 slotted EBG

IV. RESULTS AND DISCUSSIONS

All the simulated results are observed at 3.152 GHz, 5 GHz, 11.32 GHz, 12 GHz and 12.11 GHz respectively

© 2017, IJSRNSC All Rights Reserved

using ADS-2009 simulator using method of moments. The schematic of the proposed power divider is simulated using

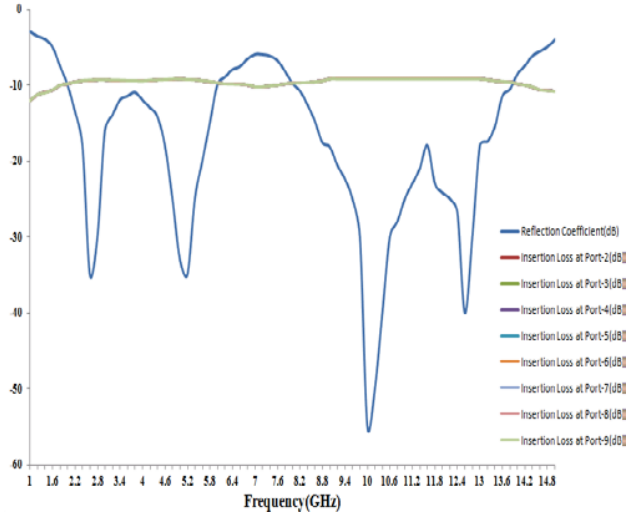


Figure 6. Consolidated plot of reflection coefficient and insertion loss of the tuned power divider

Fig. 6 shows the consolidated plot of reflection coefficient and insertion loss of the schematic layout of proposed tuned power divider shown in fig.2.

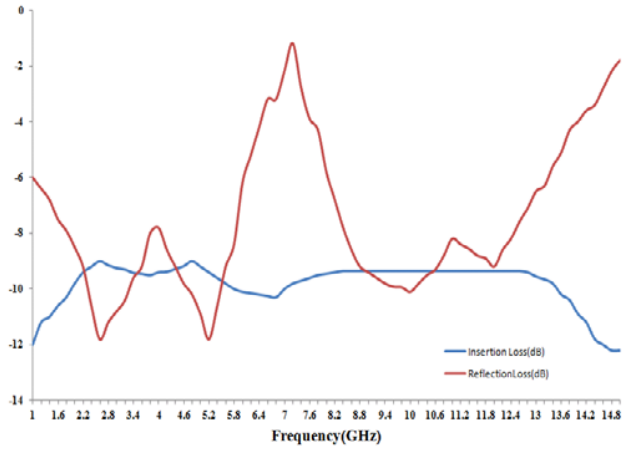


Figure 7. Consolidated plot of reflection co-efficient and insertion loss of the proposed power divider in momentum

A flat band with low ripples is observed between 8.2 GHz to 13.4 GHz. Theoretical insertion loss is given by:

$$S_{21(\text{Theoritical})} = 10\log\left[\frac{\text{Power}_{\text{received}}}{\text{Power}_{\text{inputted}}}\right]$$

Theoretically the insertion loss for an 8:1 power divider has to be -9.03dB. Consolidated plot of insertion loss and reflection coefficient for the layout in momentum are shown in fig. 7.

$$S_{21(\text{Practical})} = 10\log\left[\frac{\text{Power}_{\text{received}} - \text{Power}_{\text{losses}}}{\text{Power}_{\text{inputted}}}\right]$$

Losses considered are conductor, dielectric and insertion type.

Fig. 8(a) shows the plot of reflection coefficient (blue graph) and insertion loss (red graph) of a 15 slotted EBG power divider as shown in fig. 4(a) and fig. 8(b) shows the plot of reflection co-efficient for the 42 slotted EBG power shown in fig. 5(a).

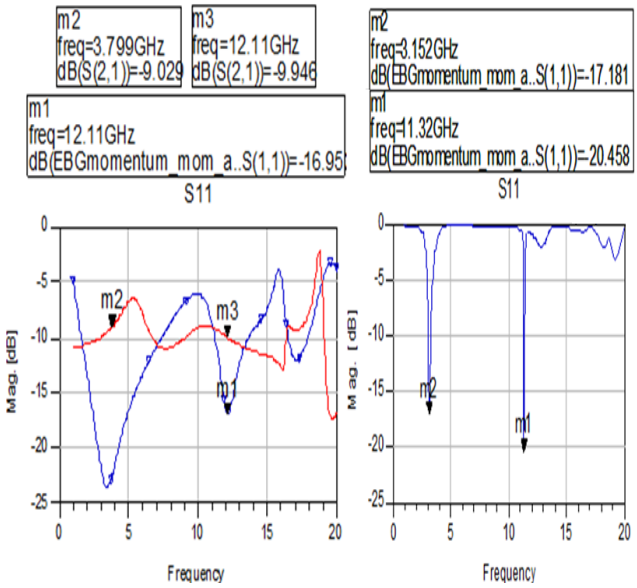


Figure 8(a).Reflection coefficient and insertion loss plot of 15 slotted EBG power divider.

Figure 8(b). Reflection coefficient plot of a 42 slotted EBG power divider

A 0.01mm change in the side of a square slot shifts the dips to K and K_a bands and the insertion loss of less than -15.12dB is obtained. A 0.01mm change in the radius of the circular slot shifts the frequencies to lower gigahertz range with high insertion loss. Therefore, a trade-off has been chosen to obtain proper return and insertion loss values. Table.1. shows the tabular data of reflection losses of normal power divider, 15 slotted and 42 slotted EBG power dividers in the S and Ku bands. Reflective losses are highly reduced at S, C, X and Ku bands. 15 slotted EBG power divider works at multiple bands than that of a 42 slotted EBG power divider.

TABLE I COMPARISON BETWEEN EBG POWER DIVIDERS AND TUNED POWER DIVIDER.

Frequency (GHz)	S_{11} of tuned power divider(dB) [Fig.7]	S_{11} of 15 slotted EBG power divider(dB) [Fig.8(a)]	S_{11} of 42 slotted EBG power divider(dB) [Fig.8(b)]
3.152	-10	-23.8	-17.181
5	-11.6	-17	-0.1
11.32	-8.1	-14	-20.458
12	-9	-16	-0.8
12.11	-9.1	-16.95	-1

© 2017, IJSRNSC All Rights Reserved

V. CONCLUSIONS

Reflective losses of EBG and tuned power dividers are studied and compared. The designer can choose these power dividers depending on the type of application. High degree of compactness is achieved by using the proposed power dividers. Subsequently, the antenna array size gets reduced with increased gain and directivity when fed with the proposed power divider. EBG power dividers have low reflective losses with square, circular slots but frequency range of operation is limited. Further, EBG power dividers have insertion loss closest to the ideal value. These power dividers can be used in the TDRS (Tracking Data Relay Satellites) in order to feed the phased array antennas in the satellites.

VI. REFERENCES

[1] A.Nassiri, "*Power dividers and couplers*", Massachusetts Institute of Technology, U.S.Particle Accelerator School, pp.**1-66**, **2010**.

[2] Mohsen Hayati, Ashkan Abdipour, Arash Abdipour, "*A Wilkinson Power Divider with Harmonic Suppression and Size Reduction using High-low Impedance Resonator Cells*", Radio Engineering, Vol.**24**, Issue.**1**, **2015**.

[3] Sandeep kumar, Mithilesh kumar, "*Modified Wilkinson Compact Wide Band (2-12GHz) Equal Power Divider*", American Journal of Engineering Research (AJER), Vol.**03**,Issue.**10**, pp. **90–98**, **2014**.

[4] S. S Chorage, Shilpa. V. Joshi, Harshada. S. Ahiwale, Archana. M. Gaikwad, ,"*Design And Performance Analysis Of 1:6 Power Divider For L Band Frequency*", International Journal of Wireless Networks and Communications., Vol.**8**, Issue.**1**, pp. **15–21**,**2016**.

[5] Gurrachman, T., Object, Arisesa, H., Putu Hernida. I.D, Permana, D. "*Design and implementation of coupled-line Wilkinson power Dividers using alumina substrate*", International Journal of Engineering Trends and Technology, Vol.**9**,Issue.**7**, pp. **363–365**, **2014**.

[6] T. R. Subramanian , "*Dual Band Wilkinson Power divider without Reactive Components*", Department of Electronics System Engineering,Indian Institute of Science, pp.**1-6**,**2012**.

[7] S. Banu, A. Vishwapriya, R. Yogamathi, A. V. Meenakshi, S. P. K Babu, "*Comparison of Wilkinson Power Divider And Gysel Power Divider Using Ads For The Frequency Range of 3 Ghz*", Fourth International Workshop on Computer Networks & Communications,pp.**1-8**, **2012**.

[8] Qaroot, A.M., Dib, N.I.,Gheethan, A.A., "*Design methodology of multi-frequency unequal spilt Wilkinson power dividers using transmission line transformers*", Progress In Electromagnetics Research B, Vol.**22**, pp. **1–21**, **2010**.

[9] Nor, M.Z.B.M., Rahim, S.K.A., Sabran, M.I. bin, Rani, M.S.B.A., "*Wideband planar Wilkinson power divider using double-sided parallel-strip line technique*" Progress In Electromagnetics Research C, Vol.**36**, pp. **181–193**,**2013**.

[10]. Debendra Kumar Panda, Ajay Chakraborty, "*Analysis of a 1:2 Rectangular Waveguide Power Divider for Phased Array Application Using Multiple Cavity Modeling Technique*", IEEE Progress In Electromagnetics Research Symposium, Cambridge, USA,pp.**361-368**, **2006**.

[11] Ali Musa Mohammed, Yi Wang, "*Four-way Waveguide Power Dividers with Integrated Filtering Function*", IEEE- European Microwave Conference (EuMC), Europe, pp.**486-489**, **2015**.

[12] Song, K., Fan, Y. ,Zhang, B., "*Ku-band multiway rectangular waveguide power divider*", Microwave and Optical Technology Letters, Vol.**52**, Issue.**11**, pp. **2560–2563**, **2015**.

[13] Rahali, B., "*Design of K-band substrate integrated Waveguide coupler, Circulator and power divider*", International Journal of Information and Electronics Engineering, Vol.**4**, Issue.**1**, pp.**47-53, 2015**.

[14] Bouchra Rahali, Mohammed Feham, Junwu Tao, "*Design of K-band substrate integrated waveguide coupler,circulator and power divider*", International Journal of Information and Electronics, Vol.**4**,Issue.**1**, pp.**1-6**, **2014**.

[15] Djerafi, T., Hammou, D., Wu, K. , Tatu, S.O. , "*Ring-shaped substrate integrated Waveguide Wilkinson power Dividers/Combiners*", IEEE Transactions on Components, Packaging and Manufacturing Technology, Vol.**4**,Issue.**9**, pp. **1461–1469**, **2014**.

[16] Deslandes, D., Boone, F., Wu, K., "*Composite corporate traveling-wave power dividers for slot array waveguide antennas*", International Journal of RF and Microwave Computer-Aided Engineering, Vol.**19**, Issue.**2**, pp. **177–186**,**2009**.

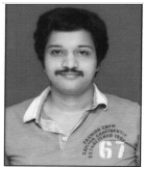
[17] Deng, P.-H., Guo, J.-H. ,Kuo, W.-C., "*New Wilkinson power dividers based on compact stepped-impedance transmission lines and shunt open stubs*", Progress In Electromagnetics Research, Vol.**123**, pp. **407–426**,**2012**.

[18] Arpit Nagar, Khem Singh Solanki, "*Design and analysis of microstrip patch antenna*", International Journal of Scientific Research in Network Security and Communications, Vol.**1**, Issue.**1**, pp.**1-5**, **2013**.

Authors Profile



Mr. Suresh Angadi pursued his B.Tech in electronics and communication engineering from G.V.P College of Engineering (Autonomous), Visakhapatnam in 2007 and M.Tech in digital communication from Maulana Azad National Institute of Technology (NIT-Bhopal) in 2009. He is presently working as assistant professor in the department of electronics and communication engineering at VITAM College of engineering, Visakhapatnam. He has published twenty six journals of repute.



Mr. Karteek Viswanadha pursued his B.Tech in electronics and communication from G.V.P College of Engineering (Autonomous), Visakhapatnam in 2007 and M.Tech in communication systems from Birla Institute of Technology and Sciences, Pilani (B.I.T.S, Pilani) in 2009. He is presently pursuing Ph.D in the area of millimeter wave devices and antennas from Delhi Technological University (Formerly Delhi College of Engineering), New Delhi.



Ms. Rokkam Roopa Sree pursued her B.Tech degree in electronics and communication engineering from Aditya College of Engineering, Tekkali in 2014 and M.Tech from Gayatri College of Engineering for Women, Visakhapatnam in 2017. She is presently working as assistant professor in department of electronics and communication engineering at VITAM College of Engineering, Visakhapatnam.

© 2017, IJSRNSC All Rights Reserved



Ms. Sowjanya Madaka pursued her B.Tech in electronics and communication engineering from Nightingale College of Engineering, Visakhapatnam in 2013 and M.Tech from Gayatri College of Engineering for Women in 2015. She is presently working as assistant professor in the department of electronics and communication engineering at VITAM College of engineering, Visakhapatnam.

© 2017, IJSRNSC All Rights Reserved

View publication stats

emeraldinsight

World Journal of Science, Technology and Sustainable Development

Sustainability enhancement of corporate governance regime in India
Ruchi Kansil, Archana Singh,

Article information:

To cite this document:
Ruchi Kansil, Archana Singh, "Sustainability enhancement of corporate governance regime in India", World Journal of Science, Technology and Sustainable Development, https://doi.org/10.1108/WJSTSD-08-2017-0026
Permanent link to this document:
https://doi.org/10.1108/WJSTSD-08-2017-0026

Downloaded on: 21 February 2018, At: 20:13 (PT)
References: this document contains references to 0 other documents.
To copy this document: permissions@emeraldinsight.com
The fulltext of this document has been downloaded 1 times since 2018*
Access to this document was granted through an Emerald subscription provided by emerald-srm:544911 []

For Authors

If you would like to write for this, or any other Emerald publication, then please use our Emerald for Authors service information about how to choose which publication to write for and submission guidelines are available for all. Please visit www.emeraldinsight.com/authors for more information.

About Emerald www.emeraldinsight.com

Emerald is a global publisher linking research and practice to the benefit of society. The company manages a portfolio of more than 290 journals and over 2,350 books and book series volumes, as well as providing an extensive range of online products and additional customer resources and services.

Emerald is both COUNTER 4 and TRANSFER compliant. The organization is a partner of the Committee on Publication Ethics (COPE) and also works with Portico and the LOCKSS initiative for digital archive preservation.

*Related content and download information correct at time of download.

Downloaded by Delhi Technological University At 20:13 21 February 2018 (PT)

Sustainability Enhancement of Corporate Governance Regime in India

I am a Research Scholar at Delhi School of Management, Delhi Technological University, New Delhi-110042, India and working as Assistant Professor at School of Business Studies, Vivekananda Institute of Professional Studies, Pitam Pura, Delhi-110034, India.

Downloaded by Delhi Technological University At 20:13 21 February 2018 (PT)

Abstract

Purpose – There is lack of research on key governance issues to expedite the sustainability of corporate governance reforms in the Indian context. The aim of this paper is to formulate a list of key governance issues (KGIs) that would help in sustainability enhancement of corporate governance regime in India vis a vis other global counterparts.

Design/methodology/approach – First, governance issues have been identified after thorough literature review and after taking opinion and suggestions of experts. Second, data has been collected through the questionnaire survey. Lastly, a model based on fuzzy set theory has been designed to identify KGIs for the sustainability enhancement of corporate governance regime in the Indian context.

Findings – Five KGIs have been identified in this study based on fuzzy set theory namely, Ownership structure of the companies, Code of best practices of corporate governance, Regulatory framework including monitoring institutions of the country, Untrue independence of independent directors in decision-making and Judiciary system of the country.

Practical implications – The KGIs identified for the Indian economy in this study can be a useful reference for the regulators and policymakers to fill the present quality gap and devise

© Emerald Publishing Limited
This is a pre-print of a paper and is subject to change before publication. This pre-print is made available with the understanding that it will not be reproduced or stored in a retrieval system without the permission of Emerald Publishing Limited.

measures to curb noncompliance and/or implementation of laws on the ground level.

Originality/value – The novelty of this study stems from the fact that very few studies have assessed the perception of stakeholder's about the current corporate regime in India. No study has identified KGIs.

Keywords: Corporate Governance Regime, Sustainability, Fuzzy set theory, Key governance issues, emerging economy, India

Paper type: Research paper

Downloaded by Delhi Technological University At 20:13 21 February 2018 (PT)

Introduction

Corporate governance problems in corporations boil down to the practice and implementation of best of the best class codes, norms and rules. At the same time, it is believed that mere practice and implementation of existing codes, norms and rules would not suffice. Rather, corporations are to be run in an ethical manner that serves and protects the interests of all its stakeholders. Freeman (1994) originated the stakeholder theory realising the fact that an organisation is an integration of various diverse systems, each requiring equal attention and strategic thinking. The diverse systems represent the various interest groups namely, shareholders, employees, creditors, lenders, customers, suppliers, public interest groups, government agencies and bodies etc. having a stake in the growth and well-being of the organisation (Ansoff, 1987). The organisation owes a responsibility towards all of them. Hence, it has to strive for the fulfilment of economic interests of all the interest groups. In such a scenario, the interaction between the interest groups creates and enhances the value of the organisation which is called "the shared sense of the value".

© Emerald Publishing Limited
This is a pre-print of a paper and is subject to change before publication. This pre-print is made available with the understanding that it will not be reproduced or stored in a retrieval system without the permission of Emerald Publishing Limited.

Henceforth, the theory of shareholder wealth maximization has been replaced by the stakeholder theory.

In the year 2004, Freeman et al advanced the stakeholder theory which rested on the identification of the purpose of the firm which would drive all its actions and decisions. In this continuum, the concept of responsibility of the firm changed and broadened. As per the stakeholder view, the firm is responsible towards all its stakeholders and hence the managers need to first identify their relationships with all stakeholders and try to act in the best interests of all. Practically, it is found that most of the times the economic interests of various stakeholder groups would not align and in such a scenario the mechanism of natural selection "survival of the fittest" would prevail. The managers would decide how they want to do business and the kind of relationships they would create with their stakeholders. They would aim at balancing the interests of various stakeholders and their satisfaction. However, Ansoff (1987) did not agree with the broader stakeholder view and argued that the shareholders have their entire investment at risk and therefore should be the primary, if not sole, recipients of superior firm performance. The other stakeholders enjoy added protection due to the presence of shareholders and thus should be the secondary recipients of benefits of firm performance.

Based on the foregoing, it is established that stakeholders are the centre of corporate governance reforms. Various measures which are undertaken to implement and mandate the best of corporate governance codes, norms or rules focus on fulfilment of interests of all stakeholders. It appears that there is a need to assess the stakeholder's perception of current corporate governance regime and identify key governance issues in the Indian context. The present study would unfold the present quality gap, if any, and uncover the key governance issues for sustainability enhancement of corporate governance regime in India.

Downloaded by Delhi Technological University At 20:13 21 February 2018 (PT)

© Emerald Publishing Limited
This is a pre-print of a paper and is subject to change before publication. This pre-print is made available with the understanding that it will not be reproduced or stored in a retrieval system without the permission of Emerald Publishing Limited.

The rest of the paper is organized as follows: Section 2 presents the literature review on existing studies related to the stakeholder's perception of governance issues. Section 3 discusses the research methodology. Section 4 presents the data analysis which is followed by a discussion of the results in section 5. The last section 6 documents the conclusions and policy implications.

Literature Review

The contemporary literature on corporate governance has put considerable emphasis on stakeholder theory. Kay and Silberston (1995) claim no justification to the fact that the interests of shareholders do or should enjoy precedence over the interests of other stakeholders. Cook and Deakin (1999) compare the stakeholder and shareholder approaches to corporate governance. While the shareholder model considers only the financial performance as the sole measure of firm's long term success, the stakeholder model encompasses both quantitative (financial and market share) and qualitative (trust and commitment) aspects of performance. Practically, the interests of shareholders and stakeholders are closely connected (Charkham and Simpson, 1999). Shareholders are one of the stakeholder groups. Further, stakeholders other than shareholders, namely employees, lenders, customers etc may become shareholders. This can be understood from the fact that institutional investors, namely pension funds, insurance companies, mutual funds and others are a large group of shareholders whose assets are drawn from the savings of the individuals, working class, pension plans etc. These groups are representatives as well as a part of society at large. The role that these groups play or could play in the corporate governance of firms they invest in can be instrumental in sustainability enhancement of corporate governance regime. Institutional investors shareholding, when taken as a proxy for corporate governance

Downloaded by Delhi Technological University At 20:13 21 February 2018 (PT)

© Emerald Publishing Limited
This is a pre-print of a paper and is subject to change before publication. This pre-print is made available with the understanding that it will not be reproduced or stored in a retrieval system without the permission of Emerald Publishing Limited.

improves firm value was found by Singh and Kansil (2016).

Bhasa (2003) studied the shareholder theory and found that companies focus only on shareholder wealth maximization and all other stakeholders are ignored. On the contrary, companies should strive for maximizing stakeholders wealth instead of only focusing on shareholders wealth because all the stakeholders who are either directly or indirectly related to the company must be compensated either in monetary or non-monetary terms. Panchali and Baid (2002) in a study found evidence of companies doing well by optimizing the interest of stakeholders which is the result of pursuing the objective of maximizing the wealth of shareholders. Thus, the acceptance of the principle of shareholder wealth leads to optimize the interests of all stakeholders. At the same time, the majority believed that priority of shareholders interests over other stakeholders would damage the long-term survival and success of the business. Practically, the interests of various groups of stakeholders need to be optimized by striking a balance between the interests of all of them.

There are various factors that influence the quality of governance, namely, the integrity of the management, ability and commitment level of the board, adequacy of the process, quality of corporate reporting and of stakeholders' participation in the management (Arora and Singh, 2003). Amongst them the integrity, ability and commitment of the board is most important because the boards manage and run the businesses. A study by Sonnenfeld (2002) found that most of the performing companies have debatable boards that disagree and treat all subjects as discussable. Further, it reiterated the fact that over a period of time, the boards should build up to a robust group in fulfiling its mission of protecting the interests of entire stakeholders. To conclude, a company is a social institution that is accountable to the members of the society. Its legitimacy comes from its ability and desire to fulfil the needs of

Downloaded by Delhi Technological University At 20:13 21 February 2018 (PT)

© Emerald Publishing Limited
This is a pre-print of a paper and is subject to change before publication. This pre-print is made available with the understanding that it will not be reproduced or stored in a retrieval system without the permission of Emerald Publishing Limited.

the society (Mahajan, 2003). In this context, Indian regulators namely, Securities and Exchange Board of India (SEBI) and Stock Exchanges have put a major emphasis on ethical behavior, transparency and voluntary disclosures of the company.

Research methodology

In order to assess the key governance issues for enhancing sustainability leading to the global competitiveness of corporate governance regime, firstly, an in-depth literature review has been conducted to find out the governance issues in various emerging economies. Opinion and suggestions of experts have been taken and sixteen governance issues are identified in the Indian context. Second, a questionnaire survey has been conducted to collect data from various groups of stakeholders to analyse the significance of selected governance issues. Stakeholders are asked to indicate the significance of selected governance issues as per their own perception by using the five-point Likert scale. Then, data analysis has been conducted with both reliability and validity of the data being checked by the statistical tool Statistical Package for the Social Sciences (SPSS). Scale ranking for overall and each group has been established based on the mean values of the significance of indicators. Finally, a model based on fuzzy set theory has been designed to identify KGIs for enhancing sustainability and competitiveness of Indian corporate governance regime.

Questionnaire Survey

From the literature review based on Indian and international studies, items of different countries have been borrowed with slight modifications to fit the specific context of corporate governance regime in India. The questionnaire is an adapted version of the scale used by

Downloaded by Delhi Technological University At 20:13 21 February 2018 (PT)

© Emerald Publishing Limited
This is a pre-print of a paper and is subject to change before publication. This pre-print is made available with the understanding that it will not be reproduced or stored in a retrieval system without the permission of Emerald Publishing Limited.

Nam and Nam (2004) in order to determine the issues constituting corporate governance regime. Some modifications, adaptations and eliminations have been done to adapt the content for the Indian capital markets and economy. A corporate governance assessment instrument consisting of 21 items has been formulated and the opinion and suggestions of experts have been sought. Overlapping, complicated and irrelevant items have been eliminated. The original instrument has been modified and the final questionnaire consists of 16 items on a five-point Likert scale. Suitable measures have been taken while designing the same which would result in less of discrepancies arising from missing frequencies and outliers in data. Table 1 lists the 16 selected governance issues for which data has been collected through the questionnaire survey. In responding the questionnaire, respondents have been asked to indicate the level of significance of each governance issue. The level of importance is measured on a five-point Likert scale, where Extremely Unimportant '1', Unimportant '2', Neutral '3', Important '4' and extremely Important '5'. Similarly, strongly disagree '1', strongly agree '5'; extremely bad '1', extremely good '5'; extremely unlikely '1', extremely likely '5'; extremely low '1', extremely high '5'; very infrequently '1', very frequently '5'.

INSERT TABLE 1 HERE

In addition to the above, the respondents provided information related to their demographic profiles for the purpose of classification, such as their designation, age, experience. An extensive section of respondents have been covered through an online source. Some respondents who did not respond to the questionnaire through electronic mode where contacted in person and/or through telephonic calls to increase the responses and sample representation. The respondents have been chosen from all over India falling in any of the

Downloaded by Delhi Technological University At 20:13 21 February 2018 (PT)

© Emerald Publishing Limited
This is a pre-print of a paper and is subject to change before publication. This pre-print is made available with the understanding that it will not be reproduced or stored in a retrieval system without the permission of Emerald Publishing Limited.

stakeholder group using convenience sampling. Special care has been taken as to in which capacity the respondent is answering. The responses of the respondents who could fall in more than one group were cross checked and analysed. While collecting the data through the questionnaire, it has been personally monitored and administered that no field is left unanswered by the respondent. Moreover, special care is taken to ensure that each of the research subjects who responded to the questionnaire had basic understanding and knowledge relating to various aspects of current corporate governance regime and thus could strengthen the representativeness of perceptions received from these respondents.

Nearly 450 respondents have been contacted and only 235 responses have been received after a repeated follow-up and reminders on a weekly basis. After a thorough data cleaning exercise, only 215 responses have been finally taken for data analysis giving a response rate of 47 percent. The overall response rate is favourable as to previous studies (Balasubramanian, Black and Khanna, 2008; Ho, 2005; Nam and Nam, 2004) due to a combination of methods used for collecting responses.

INSERT TABLE 2 HERE

Table 2 presents the summary of the survey respondent groups. Out of the total responses received 62 (28 percent) were received from **employees**, 85 (39 percent) were from **independent** analysts, auditors, accountants, representatives of regulatory authorities, capital markets, centres of governance and **others** 68 (31 percent) were researchers, professors, bankers and investors. Most of the respondents were male (84.65 percent) as compared to 15.35 percent of females. With regard to age, the data shows that most of the respondents were 50 years of age and over with a nearly equal number of respondents were of age 30-39 and 40-49. With respect to qualification, nearly half (48 percent) of the respondents had a

Downloaded by Delhi Technological University At 20:13 21 February 2018 (PT)

© Emerald Publishing Limited
This is a pre-print of a paper and is subject to change before publication. This pre-print is made available with the understanding that it will not be reproduced or stored in a retrieval system without the permission of Emerald Publishing Limited.

professional degree while 32 percent had done post-graduation and rest 20 percent were graduates.

Data analysis

Internal consistency and reliability of the five-point scale have been tested using Cronbach's Alpha. The value of Cronbach Alpha is 0.684 and therefore, the data does not suffer from sampling bias. Three statistical analyses, namely, scale ranking, ANOVA, and Fuzzy set theory have been undertaken on the data. The detailed analysis and findings of the study are presented in the following sections.

Ranking of governance issues

Ranking of selected governance issues has been obtained by calculating the means for the overall sample as well as for separate groups of respondents. If two or more issues have the same mean then the one with lower standard deviation has been assigned a higher rank. The ranking results are shown in Table 3. The results indicate that independents and others consider ownership structure of companies (GI 4 Rank 1) as the most important governance issue in India. However, employees consider the independence of directors (GI 16 Rank 1) as the most important one and rank ownership structure of companies (GI 4) as rank 2. Further, code of best practices (GI 5) is ranked second by independents whereas others rank judiciary system of the country (GI 2) as the second major issue in corporate governance.

INSERT TABLE 3 HERE

Furthermore, there exist some noticeable differences between the rankings of governance issues across various respondent groups. Lack of integrity and ethics among top management

Downloaded by Delhi Technological University At 20:13 21 February 2018 (PT)

© Emerald Publishing Limited
This is a pre-print of a paper and is subject to change before publication. This pre-print is made available with the understanding that it will not be reproduced or stored in a retrieval system without the permission of Emerald Publishing Limited.

is ranked high by employees whereas others rank inadequate protection of minority shareholders rights as more important. Independents consider regulatory framework including monitoring institutions of the country as the third important key issue in corporate governance regime.

Analysis of variance (ANOVA)

The one-way ANOVA has been conducted to explore the presence of divergence in perception among various stakeholder groups. The p values of one-way ANOVA comparing the mean scores of selected governance issues of corporate governance regime have been obtained. From the results, it can be inferred that significant difference of opinion exists for four governance issues, namely, ownership structure of the companies, regulatory framework including monitoring institutions of the country, code of best practices of corporate governance and companies internal management structure and the board. The three groups of respondents agree on rest of the governance issues.

Analysis of KGIs based on fuzzy set theory

Zadeh (1965) introduced fuzzy set theory which has been widely applied in management and social sciences. In this paper, survey data has been gathered from three groups of respondents, namely, employees, independents and others. The three groups will result in different means, standard deviation (SD), Z values (standard normal variable), which are presented in respective columns of Table 4 as, $Z = \frac{Mean-4}{SD}$. The fuzzy sets of the three groups are represented by $A_E, A_I, and\ A_O$ respectively. Accordingly, the degree of membership for each indicator (CUM) has been calculated as using NORM.S.DIST function in excel which gives *the standard normal cumulative probability of the distribution*. The final integrated fuzzy set for performance indicators as calculated from the union of 3 fuzzy sets resulted

Downloaded by Delhi Technological University At 20:13 21 February 2018 (PT)

© Emerald Publishing Limited
This is a pre-print of a paper and is subject to change before publication. This pre-print is made available with the understanding that it will not be reproduced or stored in a retrieval system without the permission of Emerald Publishing Limited.

from three groups of data, is described as follows (Xu, Chan and Qian, 2012):

$$A = A_E \cup A_I \cup A_O = \{x, m_{A_E \cup A_I \cup A_O}(x)/x \in X\}$$

Where,

$$m_{A_E \cup A_I \cup A_O}(x) = Integrated\ m(xi) = \min\left\{1, \left(m_{A_E}(x)^n + m_{A_I}(x)^n + m_{A_O}(x)^n\right)^{\frac{1}{n}}\right\}$$

N is the number of indicators, i.e. n=16 (Li and Moosa, 2015). In order to identify the KGIs, λ cut set method is adopted where λ is set at 0.7. So, considering the indicator x_i, if $Integrated\ m(xi)$ is equal or greater than 0.7 (Xu, Chan and Qian, 2012), x_i is selected as KGI. In this study 5 KGIs for enhancement of sustainability of current corporate governance regime are identified and ranked by their degree of membership (Table 4). The identified KGI's are: *Ownership structure of the companies* (KGI 1), *Code of best practices of corporate governance* (KGI 2), *Regulatory framework including monitoring institutions of the country* (KGI 3), *Untrue independence of independent directors in decision making* (KGI 4) and *Judiciary system of the country* (KGI 5).

INSERT TABLE 4 HERE

Discussion on findings

KGI 1 - Ownership structure of the companies

The ownership structure of companies has been ranked first by independents and others while employees have ranked ownership structure as second. Thus, there emerges a strong consensus on the role and importance of ownership structure in the corporate governance of Indian firms. It is important to note that all stakeholders together perceive ownership structure as the key governance issue. The findings are consonant with the findings of several previous studies which have examined the role and importance of different types of owners in corporate governance of the firms they have invested in. It is well established that firms differ across ownership structures as to the type of owners (insiders, foreign, institutional)

Downloaded by Delhi Technological University At 20:13 21 February 2018 (PT)

© Emerald Publishing Limited
This is a pre-print of a paper and is subject to change before publication. This pre-print is made available with the understanding that it will not be reproduced or stored in a retrieval system without the permission of Emerald Publishing Limited.

and the type of ownership (whether concentrated or not). Studies by Imam and Malik (2007) and Mishra and Kapil (2016) examined how corporate governance is practiced through ownership structure and how firm's performance as well as its dividend payout policy is influenced by different ownership pattern. It was found that foreign holding is positively and significantly related to the firm performance. Further, Singh and Kansil (2017) suggest that better governance can be achieved by strengthening both the internal and external corporate governance mechanisms wherein ownership structure is the most important internal governance mechanism.

Foreign investors lay considerable amount of emphasis on appointment of independent directors thus leading to improved corporate governance was found by Bowman and Min (2012). Kansil and Singh (2016c) presented important evidence and vision on the activism of institutional investors in corporate governance of companies they invest in. It is suggested that institutional investors must actively exercise their voting rights and must demonstrate their fiduciary duties towards the investors. Further, it was found that institutional investors when act as activists lead to improved corporate governance and restrain boards expropriation behavior (Gillan and Starks, 2003).

Previous studies have also studied the relationship between large shareholders and corporate monitoring and governance wherein mixed results have been advocated. Sarkar and Sarkar (2000) revealed the role of large block shareholders in monitoring company value for India. Singh and Kansil (2017) found evidence that non-controlling stake of foreign shareholders impacts corporate governance. On the contrary, Ananchotikul (2006) found that large stakes of foreign industrial companies do not improve corporate governance because they can exploit minority due to their large stakes. Thus, the type of owner and the type of ownership

Downloaded by Delhi Technological University At 20:13 21 February 2018 (PT)

© Emerald Publishing Limited
This is a pre-print of a paper and is subject to change before publication. This pre-print is made available with the understanding that it will not be reproduced or stored in a retrieval system without the permission of Emerald Publishing Limited.

matters. .

KGI 2- Code of best practices of corporate governance

The presence of best practices of corporate governance through codes and rules has been ranked second by independents and eighth by other two categories of respondents. The survey results reveal that independents who are the lawmakers and/or regulators of codes and rules place them at second rank whereas employees and others do not agree to the importance of codes and rules amongst top five governance issues. This may be due to the fact that employees might not wish to have stringent and mandatory codes and rules to comply with. Consequently, it can be expressed that Indian employees and others recognize high importance of some other issues in corporate governance. This is an interesting finding because it is believed that voluntary commitments and business practices would ensure an efficient corporate governance regime.

The development of adequate norms, guidelines, codes is the first most important step towards improving corporate governance has been iterated by Chakrabati (2005). Once these are at place then their proper implementation becomes the bigger challenge. At present, India has best of the best corporate governance laws but their poor implementation has affected the desired outcome. Anyhow, whatever codes and rules may be framed and mandated today, they would certainly require adjustments in future due to changes in business circumstances and new experiences accruing to firms and economies (OECD, 2004). Thus, high level of commitment amongst employees and practitioners would only facilitate enhancement of sustainability of current corporate governance regime.

KGI 3 - Regulatory framework including monitoring institutions of the country

The regulatory framework including monitoring institutions of the country has been ranked

Downloaded by Delhi Technological University At 20:13 21 February 2018 (PT)

© Emerald Publishing Limited
This is a pre-print of a paper and is subject to change before publication. This pre-print is made available with the understanding that it will not be reproduced or stored in a retrieval system without the permission of Emerald Publishing Limited.

third by independents, fifth by others while employees have ranked regulatory framework as sixth. The respondents are not in consensus on the importance of regulatory framework including monitoring institutions of the country in enhancing the sustainability of present corporate governance regime. Regulation pertains to the overall regulatory setup of the economy (Li and Moosa, 2015). Also, regulation has a significant influence on economy's institutional structure and further investments by institutional investors would depend upon regulatory setup and investor protection (Mayer, 2000). At the same time, the regulation would decrease the importance of managerial function as well as the costs of observing managerial performance in a firm (Kole and Lehn, 1997). However, it would provide protection to minority shareholders and reduce wealth misappropriations. Thus, the present literature expressed out the benefits as well as costs of regulation. Regulators enjoy the powers of the legislature, executive as well as the judiciary. In their functioning, they need to strike a balance between the interests of the public and businesses because they cannot outrightly favour one (Agarwal, 2013). This in itself is quite challenging and debatable.

KGI 4 - Untrue independence of independent directors in decision making

The independence of directors has been ranked first by employees, and third by both independents and others. There exists a consensus on the need for the existence of an independent board of directors amongst all respondent groups. Many previous studies have emphasised on the idea of independent boards. Demirbas and Yukhanaev (2011) concluded that the independence of the board through the presence of outside directors on the board can be a useful tool for good corporate governance within the organisations. However, there is little evidence of the real independence of boards in practice. As a result, the boards are not discharging their functions properly. The reason for this in the Indian context is that most of the boards comprise of controlling insiders, who enjoy considerable opportunities to exploit minority shareholders (Sarkar, 2010). In such a scenario, the board and its independence is

Downloaded by Delhi Technological University At 20:13 21 February 2018 (PT)

© Emerald Publishing Limited
This is a pre-print of a paper and is subject to change before publication. This pre-print is made available with the understanding that it will not be reproduced or stored in a retrieval system without the permission of Emerald Publishing Limited.

just a statutory addition (Okpara, 2011). The firms are practically managed and governed by as well as in best interests of controlling insiders.

The effectiveness of the board is considerably affected when management and decisionmaking are in the hands of concentrated owners (Fama and Jensen, 1983).In such a scenario, boards play a passive role in corporate affairs. Okpara (2011) opined it as managerial hegemony theory and Xue (2001) called it as window dressing. Here, the governing board of the organisation plays no role in management and decision-making. Also, Zhang (1999) called independent directors as symbolic with no ability to give useful suggestions and exert substantial influence on owners or the board. At present, it is important to increase the effectiveness of independent directors in monitoring the board, especially to strengthen their independence.

KGI 5 - Judiciary system of the country

Judiciary system has been ranked second by both independents and others while employees have ranked judiciary system as seventh. It seems as if employees do not want litigation and courts to enter the corporate governance regime. But, independents and others feel that judiciary would play an extremely important role in corporate governance regime. The result is in line with recent literature that has documented mixed responses towards the role of the judiciary in corporate governance. Since, corporate governance framework of a country would depend upon local laws, customs and cultures (Anderson, 2010), they together make legal systems.

A recent study by Madhani (2016) with respect to Indian listed companies reiterated the fact that legal and regulatory environment influence firm level governance practices. The effective legal systems would bring benefits to all the stakeholders. Strong legal protection of

Downloaded by Delhi Technological University At 20:13 21 February 2018 (PT)

© Emerald Publishing Limited
This is a pre-print of a paper and is subject to change before publication. This pre-print is made available with the understanding that it will not be reproduced or stored in a retrieval system without the permission of Emerald Publishing Limited.

shareholders makes ownership concentration inconsequential and thus redundant (Kansil and Singh, 2017). La Porta et al. (1998) has emphasised that effective legal systems would ensure the protection of minority shareholders' interests. Further, protection of minority shareholders would improve firm's performance and value (Shleifer and Vishny, 1997) and hence better corporate governance. Thus, one can assert that effective and strong legal systems would enhance sustainability of current corporate governance regime.

The legal systems and levels of corruption are relevant in establishing corporate governance systems (Floyd and Summan, 2008). In this context, firms need to adapt to the limitations of the existing legal system, if any, and operate within those limitations. Weak legal system and high level of corruption due to poor regulation is a major threat to sustainability enhancement of corporate governance regime. One of the possible solution could be legal regulatory mergerLazarides and Drimpetas (2010) expressed that legal regulatory merger in case of distinct institutional and governance systems may cause problems and not a solution to the real issue of corporate governance. Hence, legal and regulatory systems are to be dealt carefully in a holistic manner.

Conclusions and Policy Implications

The international capital inflows in an economy are dependent upon political, economic as well as legal factors. The capital providers constantly review the governance regime of the economy's they invest in. Corporate governance plays a major role in augmenting the external capital inflows leading to an economy's growth and development. In this context, corporate governance regime should deserve the utmost attention in emerging economies like India who need external capital inflows for their growth and development. The present study

Downloaded by Delhi Technological University At 20:13 21 February 2018 (PT)

© Emerald Publishing Limited
This is a pre-print of a paper and is subject to change before publication. This pre-print is made available with the understanding that it will not be reproduced or stored in a retrieval system without the permission of Emerald Publishing Limited.

identified and ranked five KGI as per fuzzy set theory according to their importance based on the perception of stakeholders regarding the current corporate governance regime. The stakeholders include employees, practitioners, policymakers, regulators, researchers and investors. The key issues identified in this study that can hinder the sustainability enhancement of corporate governance regime in India include: Ownership structure of the companies, Code of best practices of corporate governance, Regulatory framework including monitoring institutions of the country, Untrue independence of independent directors in decision making and Judiciary system of the country. It can be concluded that India has codes and laws that are designed to ensure good corporate governance regime but the implementation of existing laws, as well as voluntary commitments and business practices constitute a major challenge in corporate governance regime.

The previous literature unfolds two distinct schools of thought about the most appropriate approach to corporate governance namely, regulatory approach and free market approach (Farrar, 1999). The regulatory approach also called prescriptive approach relates to prescription of specific corporate governance rules and practices by regulations. The free market approach also called nonprescriptive approach leaves the development of corporate governance regime to market forces allowing companies to incorporate practices that would help them to sustain in the competitive business environment. It is debatable as to which approach would be the best. It is the stakeholders at large who would have to set the tone for the quality of corporate governance systems through any approach that they seem fit. However, a mixed approach wherein only the basic framework and regulations of corporate governance would be prescribed and companies would be allowed to develop more detailed practices by their own could also be a possible solution.

Downloaded by Delhi Technological University At 20:13 21 February 2018 (PT)

© Emerald Publishing Limited
This is a pre-print of a paper and is subject to change before publication. This pre-print is made available with the understanding that it will not be reproduced or stored in a retrieval system without the permission of Emerald Publishing Limited.

Furthermore, the path dependence theory suggested by Bebchuk and Roe (1999) highlighted two sources of path dependence, namely, structure driven and rule driven. On one hand, Indian corporate governance regime has adopted and mandated the best of the best international practices (Sarkar, 2010). But, the structure of corporates in India remains as high leveraged firms with significant control of owners, despite having lesser equity. This highlights the fact that there exists suitable corporate governance regime while controlling owners control their firms. These controlling owners should act in the best interests of all stakeholders and if not, the non-controlling owners would bear the costs. Two parallel lines of action emerge: first, controlling owners, top management and board of directors should not be allowed to exploit or abuse the non-controlling owners. Secondly, the non-controlling owners must exercise their rights and entitlements as owners. In this context, the policymakers and regulators need to restrict hands of controlling shareholders and work towards aligning the interests of all the stakeholders.

Based on the above, it is expected that in times to come, the corporate governance regime within the framework of present codes, laws and model of corporate governance would be strengthened. The present quality gap which emerges from the implementation of the present framework and structural setup is likely to be narrowed down. The policymakers and regulators will have to devise measures to curb noncompliance and/or implementation of laws at the ground level, and take all possible actions that would enhance and support investor confidence. The more the investor confidence, the more would be the foreign capital inflows.

References

Agarwal, A.K. (2013) 'Corporate Governance: Financial Regulators and Courts Need To Be On the

Downloaded by Delhi Technological University At 20:13 21 February 2018 (PT)

© Emerald Publishing Limited
This is a pre-print of a paper and is subject to change before publication. This pre-print is made available with the understanding that it will not be reproduced or stored in a retrieval system without the permission of Emerald Publishing Limited.

Same Page', *Vikalpa*, vol. 38, no. 1, pp. 1-12.
Ananchotikul, S. (2006) 'Does foreign investment really improve corporate governance? Evidence from Thailand', November, Available: http://eml.berkeley.edu/~webfac/gourinchas/e281_f06/Bo.pdf [07 June 2013].
Anderson, R. (2010) 'Risk management and corporate governance', Available: http://www.oecd.org/corporate/ca/corporategovernanceprinciples/42670210.pdf [10 August 2017].
Ansoff, I.H. (1987) *Corporate Strategy*, London: Penguin.
Arora, A. and Singh, M.M. (2003) *Corporate Governance: Concept, Structure and Process*.
Balasubramanian, B.N., Black, B.S. and Khanna, V.S. (2008) 'Firm-level corporate governance in emerging markets: A case study of India', *ECGI-Law Working Paper*, vol. 119, no. 2009, pp. 08-011.
Bebchuk, L.A. and Roe, M.J. (1999) 'A theory of path dependence in corporate ownership and governance', *Stanford Law Review*, vol. 52, pp. 127-170.
Bhasa, M.P. (2003) 'From Property Rights to Shareholder-Stakeholder Debate: A Brief Look Into The Emergence of the Notion of Corporate Governance', *ICFAI Journal of Corporate Governance*, vol. II, no. 2, pp. 88-99.
Bowman, G. and Min, B. (2012) 'The Positive Impact of Corporate Governance on Foreign Equity Ownership: Evidence from Korea', Financial Markets & Corporate Governance Conference.
Chakrabarti, R. (2005) 'Corporate Governance in India - Evolution and Challenges', January, Available: Chakrabarti, Rajesh, Corporate Governance in India - Evolution and Challenges (Januaryhttp://ssrn.com/abstract=649857 [29 July 2013].
Charkham, J. and Simpson, A. (1999) *Fair Shares: The Future of Shareholder Power and Responsibility: The Future of Shareholder Power and Responsibility*, Oxford: OUP.
Cook, J. and Deakin, (1999) 'Stakeholding and corporate governance: theory and evidence on economic performance', *Cook, Jennifer, and Simon Deakin. "Stakeholding and corporate governance: theory and evidence on economic performance." Centre for Business Research, Cambridge (1999).*, Available: http://www.cbr.cam.ac.uk/publications/index.htm [9 June 2013].
Demirbas, D. and Yukhanaev, A. (2011) 'Independence of board of directors, employee relation and harmonisation of corporate governance: Empirical evidence from Russian listed companies', *Employee Relations*, vol. 33, no. 4, pp. 444-471.
Fama, E.F. and Jensen, M.C. (1983) 'Separation of ownership and control', *The Journal of Law and Economics*, vol. 26, no. 2, pp. 301-325.
Farrar, J., (1999) 'The New Financial Architecture and Effective Corporate Governance', *The International Lawyer*, pp. 927-954.
Floyd, and Summan, S. (2008) 'Understanding the main motives for foreign direct investment, an East-West country contrast: is the host country legislation an important factor?', *Corporate Governance: The international journal of business in society*, vol. 8, no. 5, pp. 661-668.
Freeman, E.R. (1994) 'The politics of stakeholder theory: Some future directions', *Business ethics quarterly*, vol. 4, no. 4, pp. 409-421.
Freeman, E.R., Wicks, C. and Parmar, B. (2004) 'Stakeholder theory and "the corporate objective revisited"', *Organization Science*, vol. 15, no. 3, pp. 364-369.
Gillan, S.L. and Starks, L.T. (2003) 'Corporate Governance, Corporate Ownership and the Role of Institutional Investors: A Global Perspective', *Journal Of Applied Finance*, vol. 13, no. 2, pp. 4 -22.
Ho, C.K. (2005) 'Corporate governance and corporate competitiveness: an international analysis', *Corporate Governance: An International Review*, vol. 13, no. 2, pp. 211-253.
Imam, M.O. and Malik, (2007) 'Firm performance and corporate governance through ownership structure: Evidence from Bangladesh stock market', *International Review of Business Research Papers*, vol. 3, no. 4, pp. 88-110.
Kansil, R. and Singh, A. (2016a) 'Foreign Shareholdings On Bombay Stock Exchange –An Empirical Assessment', *Global Journal for Research Analysis*, vol. 5, no. 5, pp. 32-33.
Kansil, R. and Singh, A. (2016b) 'Internal Stakeholders' Perception of Current Corporate Governance Regime', *International Journal of Scientific Research*, vol. 5, no. 11, pp. 1-4.
Kansil, R. and Singh, A. (2016c) 'Shareholders activism as a Corrective Mechanism: A Case Study Of Indian Mutual Funds AMC', *Journal of Global Economics, Management and Business Research*, vol. 7, no. 4, pp. 306-312.
Kansil, R. and Singh, A. (2017) 'Firm Characteristics and Foreign Institutional Ownership: Evidence

Downloaded by Delhi Technological University At 20:13 21 February 2018 (PT)

© Emerald Publishing Limited
This is a pre-print of a paper and is subject to change before publication. This pre-print is made available with the understanding that it will not be reproduced or stored in a retrieval system without the permission of Emerald Publishing Limited.

from India', *Institutions and Economies*, vol. 9, no. 2, pp. 35-53.
Kay, J. and Silberston, A. (1995) 'Corporate Governance', *National Institute Economic Review*, vol. 153, no. 1, pp. 84-107.
Kole, S. and Lehn, K. (1997) 'Deregulation, the evolution of corporate governance structure, and survival', *The American Economic Review*, vol. 87, no. 2, pp. 421-425.
La Porta, Lopez□de□Silanes, Shleifer, A. and Vishny, R.W. (1998) 'Law and Finance', *Journal of Political Economy*, vol. 106, no. 6, pp. 1113-1155.
Lazarides, T. and Drimpetas, (2010) 'Corporate governance regulatory convergence: a remedy for the wrong problem', *International Journal of Law and Management*, vol. 52, no. 3, pp. 182-192.
Li, L. and Moosa, I. (2015) 'Operational risk, the legal system and governance indicators: a country-level analysis', *Applied Economics*, vol. 47, no. 20, pp. 2053-2072.
Madhani, P.M. (2016) 'The Impact of Legal and Regulatory Environment: A Study of Corporate Governance and Disclosure Practices of Firms Listed on Bombay Stock Exchange', *The IUP Journal of Corporate Governance*, vol. XV, no. 2, pp. 7-36.
Mahajan, V. (2003) 'Improving the Efficiency of Corporate Governance', in Arya, P.P., Tandon, B.B. and Vashisht, A.K. *Corporate Governance*, New Delhi: Deep and Deep publications (P) Limited.
Mayer, C. (2000) 'Investment and Growth: The Role of Corporate Governance'.
Mishra, K. and Kapil, S. (2016) 'Study on corporate governance mechanisms', *International Journal of Indian Culture and Business Management*, vol. 12, no. 2, pp. 179-203.
Nam, S.-W. and Nam, I.C. (2004) 'Corporate Governance in Asia- Recent Evidence from Indonesia, Republic of Korea, Malaysia and Thailand', Available: http://adbi.adb.org/files/2005.01.book.corporate.governance.asia.pdf.
OECD (2004) 'The OECD principles of corporate governance'.
Okpara, J.O. (2011) 'Corporate governance in a developing economy: barriers, issues, and implications for firms', *Corporate Governance: The international journal of business in society*, vol. 11, no. 2, pp. 184-199.
Panchali, J.N. and Baid, (2002) 'Corporate Governance: An Alternate Approach', *Vision: The Journal of Business Perspective*, vol. 6, no. 1, pp. 41-44.
Rediker, K.J. and Seth, A. (1995) 'Boards of Directors and Substitution Effects of Alternative Governance Mechanisms', *Strategic Management Journal*, vol. 16, no. 2, pp. 85-99.
Sarkar, J. (2010) 'Ownership and corporate governance in Indian firms', *Corporate governance: An emerging scenario, National Stock Exchange of India Ltd.*, pp. 217-267.
Sarkar, J. and Sarkar, S. (2000) 'Large Shareholder Activism in Corporate Governance in Developing Countries: Evidence from India', *International Review of Finance*, vol. 1, no. 3, pp. 161-194, Available: http://onlinelibrary.wiley.com/doi/10.1111/1468-2443.00010/full.
Shleifer, A. and Vishny, (1997) 'A survey of corporate governance', *The Journal of Finance*, vol. 52, no. 2, pp. 737-783.
Singh, A. and Kansil, R. (2016) 'Institutional Ownership and Firm value: A Case Study of Listed Firms in Indian Stock Exchanges', *Journal of Research: THE BEDE ATHENAEUM*, vol. 7, no. 1, pp. 98-106.
Singh, A. and Kansil, R. (2017) 'Impact of Foreign Shareholdings on Corporate Governance Score: Evidence from Bombay Stock Exchange, India', *International Journal of Business and Globalisation*, vol. 19, no. 1, pp. 93-110.
Sonnenfeld, J.A. (2002) 'What Makes Great Board Great', Available: https://hbr.org/2002/09/what-makes-great-boards-great [7 November 2012].
Varma, J.R. (1997) 'Corporate governance in India: disciplining the dominant shareholder', *IIM-B Management Review*, vol. 9, no. 4, pp. 5-18.
Xu, P.P., Chan, E.H.W. and Qian, Q.K. (2012) 'Key performance indicators (KPI) for the sustainability of building energy efficiency retrofit (BEER) in hotel buildings in China', *Facilities*, vol. 30, no. 9/10, pp. 432-448.
Xue, J.F. (2001) *Ownership structure, corporate governance and corporate performance.*
Zadeh, L.A. (1965) 'Fuzzy sets', *Information and control*, vol. 8, no. 3, pp. 338-353.
Zhang, W.Y. (1999) 'The Non-compensation of Loss in Control Right and Ownership Transfer Barrier during the SOE's Takeover', *Economic Research Journal*, vol. 7, no. 1, pp. 3-11.

Downloaded by Delhi Technological University At 20:13 21 February 2018 (PT)

© Emerald Publishing Limited
This is a pre-print of a paper and is subject to change before publication. This pre-print is made available with the understanding that it will not be reproduced or stored in a retrieval system without the permission of Emerald Publishing Limited.

Table 1 : Selected Governance Issues

Code	Indicator
GI 1	Companies internal management structure and the board
GI 2	Judiciary system of the country
GI 3	Regulatory framework including monitoring institutions of the country
GI 4	Ownership structure of the companies
GI 5	Code of best practices of corporate governance
GI 6	Culture and value system of the society
GI 7	The standard of CG in India is comparable to that of Asian countries
GI 8	The existing CG regulations are effectively implemented by most India firms
GI 9	Regulatory monitoring of CG compliance is adequate
GI 10	Most listed companies have already taken measures to strengthen their CG
GI 11	Lack of integrity and ethics among top management
GI 12	Insider trading
GI 13	Inadequate protection of minority shareholders' rights
GI 14	Conflicts of interest of directors
GI 15	Drain off of funds through associate or subsidiary companies
GI 16	Independent directors do not exercise true independence in decision making

Table 2 : Summary of respondent groups

Respondent group	Number	Percentage (%)
Employees	62	28.84
Independents	85	39.53
Others	68	31.63
Total	215	100

Downloaded by Delhi Technological University At 20:13 21 February 2018 (PT)

© Emerald Publishing Limited
This is a pre-print of a paper and is subject to change before publication. This pre-print is made available with the understanding that it will not be reproduced or stored in a retrieval system without the permission of Emerald Publishing Limited.

Downloaded by Delhi Technological University At 20:13 21 February 2018 (PT)

© Emerald Publishing Limited
This is a pre-print of a paper and is subject to change before publication. This pre-print is made available with the understanding that it will not be reproduced or stored in a retrieval system without the permission of Emerald Publishing Limited.

Table 3 : Ranks and ANOVA for different groups of respondents

		Employees (n= 62)			Independents (n= 85)			Others (n= 68)			Total (n= 215)			ANOVA	
SGI		Mean	SD	Rank	Mean	SD	Rank	Mean	SD	Rank	Mean	SD	Rank	F	Sig.
Independent directors do not exercise true independence in decision making	GI 16	3.984	.922	1	3.871	.870	6	3.853	1.123	3	3.897	.968	3	.344	.709
Ownership structure of the companies	GI 4	3.887	.851	2	4.282	.983	1	4.088	.805	1	4.107	.903	1	3.537	0.031*
Insider trading	GI 12	3.823	1.079	3	3.635	1.163	10	3.824	1.064	5	3.749	1.107	8	.737	.480
Lack of integrity and ethics among top management	GI 11	3.806	1.199	4	4.047	1.101	5	3.779	1.244	6	3.893	1.177	4	1.215	.299
Inadequate protection of minority shareholders' rights	GI 13	3.790	1.073	5	3.812	.970	9	3.853	1.149	4	3.819	1.054	6	.060	.942
Regulatory framework including monitoring institutions of the country	GI 3	3.774	.965	6	4.071	.923	3	3.706	.882	7	3.870	.933	5	3.418	0.035*
Judiciary system of the country	GI 2	3.774	.948	7	4.047	.962	4	4.029	1.007	2	3.963	.976	2	1.644	.196
Code of best practices of corporate governance	GI 5	3.694	.898	8	4.071	.768	2	3.603	.900	8	3.814	.872	7	6.597	0.002**
Most listed companies have already taken measures to strenghthen their CG	GI 10	3.677	.988	9	3.859	.966	7	3.544	1.085	10	3.707	1.015	9	1.867	.157
Regulatory monitoring of CG compliance is adequate	GI 9	3.661	1.101	10	3.812	.880	8	3.603	1.024	9	3.702	.993	10	.909	.404
The standard of CG in India is comparable to that of Asian countries	GI 7	3.629	1.028	11	3.376	1.123	12	3.412	.981	13	3.460	1.053	11	1.138	.322
The existing CG regulations are effectively implemented by most India firms	GI 8	3.452	.970	12	3.471	1.097	11	3.441	1.164	12	3.456	1.079	12	.015	.986

Downloaded by Delhi Technological University At 20:13 21 February 2018 (PT)

© Emerald Publishing Limited
This is a pre-print of a paper and is subject to change before publication. This pre-print is made available with the understanding that it will not be reproduced or stored in a retrieval system without the permission of Emerald Publishing Limited.

Companies internal management structure and the board	GI 1	3.032	1.159	13	3.035	1.219	13	3.515	1.178	11	3.186	1.205	13	3.798	0.024*
Drain off of funds through associate or subsidiary companies	GI 15	2.145	1.053	14	2.318	1.026	15	2.059	1.006	15	2.186	1.029	14	1.267	.284
Conflicts of interest of directors	GI 14	2.939	1.067	15	3.022	1.064	13	2.970	1.069	14	2.982	1.073	14	2.100	.709
Culture and value system of the society	GI 6	2.854	1.074	16	2.933	1.072	13	2.887	1.072	15	2.896	1.079	15	2.128	0.031*

* 5 percent level of significance, ** 1 percent level of significance

Downloaded by Delhi Technological University At 20:13 21 February 2018 (PT)

© Emerald Publishing Limited
This is a pre-print of a paper and is subject to change before publication. This pre-print is made available with the understanding that it will not be reproduced or stored in a retrieval system without the permission of Emerald Publishing Limited.

Table 4 : The degree of membership of indicators of KGI

Governance Issues		Employees				Independents				Others				Integrated m(xi)	
		MEAN	STD DEV	Z	CUM	MEAN	STD DEV	Z	CUM	MEAN	STD DEV	Z	CUM		
Ownership structure of the companies	GI 4	3.887	0.851	0.465	0.679	4.282	0.983	0.389	0.651	4.088	0.805	0.492	0.689	**0.726**	**KGI 1**
Code of best practices of corporate governance	GI 5	3.694	0.898	0.419	0.662	4.071	0.768	0.517	0.697	3.603	0.900	0.402	0.656	**0.724**	**KGI 2**
Regulatory framework including monitoring institutions of the country	GI 3	3.774	0.965	0.402	0.656	4.071	0.923	0.431	0.667	3.706	0.882	0.428	0.666	**0.710**	**KGI 3**
Independent directors do not exercise true independence in decision making	GI 16	4.000	0.923	0.432	0.667	3.871	0.870	0.454	0.675	3.853	1.123	0.352	0.638	**0.710**	**KGI 4**
Judiciary system of the country	GI 2	3.774	0.948	0.409	0.659	4.047	0.962	0.414	0.661	4.029	1.007	0.396	0.654	**0.705**	**KGI 5**
Regulatory monitoring of CG compliance is adequate	GI 9	3.661	1.101	0.346	0.635	3.812	0.880	0.443	0.671	3.603	1.024	0.361	0.641	0.699	
Most listed companies have already taken measures to strenghthen their CG	GI 10	3.677	0.988	0.383	0.649	3.859	0.966	0.409	0.659	3.544	1.085	0.337	0.632	0.694	
Inadequate protection of minority shareholders' rights	GI 13	3.790	1.073	0.365	0.642	3.812	0.970	0.404	0.657	3.853	1.149	0.344	0.635	0.691	
Insider trading	GI 12	3.823	1.079	0.365	0.642	3.635	1.163	0.326	0.628	3.824	1.064	0.370	0.644	0.684	
The standard of CG in India is comparable to that of Asian countries	GI 7	3.629	1.028	0.364	0.642	3.376	1.123	0.304	0.620	3.412	0.981	0.340	0.633	0.677	
Lack of integrity and ethics among top management	GI 11	3.806	1.199	0.328	0.629	4.047	1.101	0.362	0.641	3.779	1.244	0.316	0.624	0.677	
The existing CG regulations are effectively implemented by most India firms	GI 8	3.452	0.970	0.351	0.637	3.471	1.097	0.324	0.627	3.441	1.164	0.305	0.620	0.673	
Companies internal management structure and the board	GI 1	3.032	1.159	0.243	0.596	3.035	1.219	0.239	0.595	3.515	1.178	0.311	0.622	0.649	
Conflicts of interest of directors	GI 14	2.097	1.051	0.074	0.529	2.329	1.117	0.117	0.546	2.059	1.006	0.062	0.525	0.573	
Drain off of funds through associate or subsidiary companies	GI 15	2.145	1.053	0.080	0.532	2.318	1.026	0.101	0.540	2.059	1.006	0.062	0.525	0.571	

Downloaded by Delhi Technological University At 20:13 21 February 2018 (PT)

Culture and value system of the society	GI 6	2.065	0.866	0.038	0.515	1.953	0.898	0.033	0.513	2.029	0.846	0.031	0.512	0.550		

© Emerald Publishing Limited
This is a pre-print of a paper and is subject to change before publication. This pre-print is made available with the understanding that it will not be reproduced or stored in a retrieval system without the permission of Emerald Publishing Limited.

International Journal of Research in Engineering and Innovation (IJREI)
journal home page: http://www.ijrei.com
ISSN (Online): 2456-6934



Thermodynamic model analysis of vapour compression refrigeration systems by using ecofriendly refrigerant (R1234yf) in primary circuit and R718 in the secondary circuit by mixing Nano particles (Al_2O_3) for improving thermal efficiencies

R.S. Mishra

Department of Mechanical Engineering, Delhi Technological University, Delhi, India

Abstract

Simple thermal model was developed for predicting first law thermal performance in term of coefficient of performance (COP) which is the ratio of refrigeration effect to the network input given to the system of refrigeration system is evaluated. Therefore the coefficient of performance (COP) of vapour compression refrigeration system can be improved either by increasing evaporator load (i.e. Refrigeration effect) or by reducing high grade energy in terms of exergy of fuel (i.e. work input) given to the system.

The constant enthalpy process is also known as throttling process in VCR is an irreversible expansion process causing internal irreversibility computed using entropy changes multiplied by ambient temperature (i.e. reference temperature of 298 K) . In the expansion process, the factors responsible for exergy loss in thermos-syphonic cycle performances. Normally in the throttling process, because of entering the portion of the refrigerant flashing to vapour in evaporator which will not only reduce the cooling capacity but also increases the size of evaporator. This problem can be eliminated by adopting multi-stage expansion where the flash vapors is removed after each stage of expansion as a consequence there will be increase in cooling capacity or reduce the size of the evaporator by using nano refrigerants . This thermal model predicts condenser refrigerant temperature along with evaporator temperature, which is a function of brine mass flow rate and condenser water flow rate & pressure, inlet water temperature and inlet brine temperature & pressure.

© 2018 ijrei.com. All rights reserved

Key words: Simple thermal model, Coefficient of Performance, First and second law performances, Nano refrigerants

1. Introduction

The refrigeration is a technology which absorbs heat at low ambient temperature and provides temperature below the surrounding by rejecting heat energy to the surroundings at higher temperature. Simple vapour compression refrigeration system which consists of four major components compressor, expansion valve, condenser and evaporator in which total cooling load is carried at one temperature by single evaporator but in many applications like large hotels, food storage and food processing plants, food items are stored in different compartment and at different temperatures. Therefore there is need of multi evaporator vapour compression refrigeration
It is well known that throttling process in VCR is an irreversible expansion process. Expansion process is one of the main factors responsible for exergy loss in cycle performance system. The systems under vapour compression technology consume huge amount of electricity, this problem can be solved by improving performance of system. The thermal performance of systems based on vapour compression refrigeration technology can be improved by following:
The first law thermal performance of refrigeration system is evaluated in term of coefficient of performance (COP) which is the ratio of refrigeration effect to the net work input given to the system. Therefore the coefficient of performance (COP) of vapour compression refrigeration system can be improved either by increasing evaporator load (i.e. Refrigeration effect) or by reducing high grade energy in terms of exergy of fuel (i.e. work input) given to the system.
because of entering the portion of the refrigerant flashing to vapour in evaporator which will not only reduce the cooling capacity but also increase the size of evaporator. This problem

Corresponding author: R.S. Mishra
Email Id: hod.mechanical.rsm@dtu.ac.in

can be eliminated by adopting multi-stage expansion where the flash vapours is removed after each stage of expansion as a consequence there will be increase in cooling capacity and reduce the size of the evaporator.

2. Literature Review

Kumar et al. (1989) carried out energy and exergy analysis of vapour compression refrigeration system by the use of exergy-enthalpy diagram. They did first law analysis or energy analysis for calculating the coefficient of performance and exergy analysis for evaluation of various losses occurred in different components of vapour compression cycle using R11 and R12 as refrigerants [1]. Nikolaidis and Probert (1998) studied analytically that change in evaporator and condenser temperatures of two stage vapour compression refrigeration plant using R22 add considerable effect on plant irreversibility. They suggested that there is need for optimizing the conditions imposed upon the condenser and evaporator [2]. Yumrutas et al. (2002) carried out exergy analysis based investigation of effect of condensing and evaporating temperature on vapour compression refrigeration cycle in terms of pressure losses, COP, second law efficiency and exergy losses. Variation in temperature of condenser as well as have negligible effect on exergy losses of compressor and expansion valve, also first law efficiency and exergy efficiency increase but total exergy losses of system decrease with increase in evaporator and condenser temperature [3].

Halimic et al. (2003) is also compared thermal performance of R401A, R290 and R134A with R12 by using in vapour compression refrigeration system, which is originally designed for R12.Due to similar performance of R134a in comparison with R12,R134A can be replaced in the same system without any medication in the system components. But in reference to greenhouse impact R290 presented best results [4]. Cabello et al. (2007) observed the effect of operating parameters on COP, work input and cooling capacity of single-stage vapour compression refrigeration system. There is great influence on energetic parameters due change in suction pressure, condensing and evaporating temperatures [5]

Cabello et al. (2004) effect of condensing pressure, evaporating pressure and degree of superheating was experimentally investigated on single stage vapour compression refrigeration system using R22, R134a and R407C. It was observed that mass flow rate is greatly affected by change in suction conditions of compressor in results on refrigeration capacity because refrigeration capacity depended on mass flow rate through evaporator. It was also found that for higher compression ratio R22 gives lower COP than R407C [6]. Ahamed et al. (2011) suggested the use of hydrocarbons and mixture of hydrocarbons and R134a in vapour compression refrigeration system and found that compressor shows much higher exergy destruction as compared to rest of components of vapour compression refrigeration system and this exergy destruction can be minimized by using of nanofluid and nano lubricants in compressor [7]. Ahamed et al. (2012) carried out the experimental investigation of domestic refrigerator with hydrocarbons (isobutene and butane) by energy and exergy analysis. They reached to the results that energy efficiency ratio of hydrocarbons comparable with R134a but exergy efficiency and sustainability index of hydrocarbons much higher than that of R134a at considered evaporator temperature and found that compressors shows highest system defect (69%) among components of considered system [8]. Spatz and Motta (2004) suggested the replacement of R12 with R410a through experimental investigation of medium temperature vapour compression refrigeration cycles. In terms of thermodynamic analysis, comparison of heat transfer and pressure drop characteristics, R410a gives best performance among R12, R404a and R290a [9].

Han et al. (2007) conducted the experiment under different working conditions and found that there could be replacement of R407C in vapour compression refrigeration system having rotor compressor with mixture of R32/R125/R161 showing higher COP, less pressure ratio and slightly high discharge compressor temperature without any modification in the same system [10].

Getu and Bansal (2008) also optimized the design and operating parameters of like condensing temperature, sub-cooling temperature, evaporating temperature, superheating temperature and temperature difference in cascade heat exchanger R744-R717 cascade refrigeration system. A regression analysis was also done to obtain optimum thermodynamic parameters of same system [11].

Padilla et al. (2010) carried out the exergy analysis of domestic vapour compression refrigeration system with R12 and R413A was done. They concluded that performance in terms of power consumption, irreversibility and exergy efficiency of R413A is better than R12, so R12 can be replaced with R413A in domestic vapour compression refrigeration system [12].

Mohanraj et al. (2009) carried out the experimental investigation of domestic refrigerator they arrived on conclusions that under different environmental temperatures COP of system using mixture of R290 and R600a in the ratio of 45.2: 54.8 by weight showing up to 3.6% greater than same system using R134a, also discharge temperature of compressor with mixture of R290 and R600a is lower in the range of 8.5-13.4 K than same compressor with R134a [13].Bolaji et al. (2011) carried out the experimentally comparative analysis of R32, R152a and R134a refrigerants in vapour compression refrigerator. They reached to the conclusions that R32 shows lowest performance whereas R134a and R152a showing nearly same performance but best performance was obtained of system using R152a [14].

Stanciu et al. (2011) carried out numerical and graphical investigation on one stage vapour compression refrigeration system for studied refrigerants (R22, R134a, R717, R507a, R404a) in terms of COP, compressor work, exergy efficiency and refrigeration effect. Effect of sub-cooling, superheating and compression ratio was also studied on the same system using considered refrigerants and present system optimization when working with specific refrigerant [15].

Eastman et al. (1996) found the pool boiling heat transfer characteristics of R11 refrigerant with TiO2 nanoparticles and showed that the heat transfer enhancement reached 20% at a particle loading of 0.01 g/L [16].

Kang et al. (2006) is found 75% thermal conductivity enhancement for ethylene glycol with 1.2% (v/v) diamond nanoparticles between 30 and 50 nm in diameter. Despite these remarkable results, some researchers have measured the thermal conductivity of nanofluids and have found no anomalous results [17].

Liu et al. (2006) found the effects of carbon nanotubes (CNTs) on the nucleate boiling heat transfer of R123 and HFC134a refrigerants. Authors reported that CNTs increase the nucleate boiling heat transfer coefficients for these refrigerants. Authors noticed large enhancements of up to 36.6% at low heat fluxes of less than 30 kW/m2. Thus, the use of nanoparticles in refrigeration systems is a new, innovative way to enhance the efficiency and reliability in the refrigeration system [18].

Elcock (2007) observed that TiO2 nanoparticles can be used as additives to enhance the solubility of the mineral oil with the hydrofluorocarbon (HFC) refrigerant. Authors also reported that refrigeration systems using a mixture of HFC-134a and mineral oil with TiO2 nanoparticles appear to give better performance by returning more lubricant oil to the compressor with similar performance to systems using HFC-134a and POE oil [19].

Hindawi (2009) carried out an experimental study on the boiling heat transfer characteristics of R22 refrigerant with Al2O3 nanoparticles and found that the nanoparticles enhanced the refrigerant heat transfer characteristics with reduced bubble sizes [20].

Reddy et al. (2012) carried out numerical analysis of vapour compression refrigeration system using R134a, R143a, R152a, R404A, R410A, R502 and R507A and discussed the effect of evaporator temperature, degree of sub-cooling at condenser outlet, superheating of evaporator outlet, vapour liquid heat exchanger effectiveness and degree of condenser temperature on COP and exergetic efficiency. They reported that evaporator and condenser temperature have significant effect on both COP and exergetic efficiency and also found that R134a has the better performance while R407C has poor performance in all respect [21].

Mahbubul et al. (2013) carried out the thermos-physical properties, pressure drop and heat transfer performance of Al2O3 nanoparticles suspended in R-134a was investigated .To determine the thermal conductivity and viscosity of the nano-refrigerants for the nanoparticle concentrations of 1 to 5 vol.% existing model was studied . The thermal conductivity of Al2O3/R-134a nano-refrigerant increased with the augmentation of particle concentration and temperature however, decreased with particle size intensification. In addition, the results of viscosity, pressure drop, and heat transfer coefficients of the nano-refrigerant show a significant increment with the increase of volume fractions. The frictional pressure drop shows rapid increment of more than 3 vol.% with particle volume fraction, and the pumping power increases with particle concentration similar to pressure drop increment. The pumping power is proportional to the pressure drop of nano-refrigerant. Based on the literature it was observed that researchers have gone through detailed first law analysis in terms of coefficient of performance and second law analysis in term of exergetic efficiency of simple vapour compression refrigeration system with single evaporator. Authors also analyzed the effect of Nano fluids on simple vapour compression cycle in the term of pool boiling, COP, Thermal conductivity etc [22]..

Selladurai and Saravanakumar (2013) compared thermal performance between R134a and R290/R600a mixture on a domestic refrigerator which is originally designed to work with R134a and found that R290/R600a hydrocarbon mixture showed higher COP and exergetic efficiency than R134a. In their analysis highest irreversibility obtained in the compressor compare to condenser, expansion valve and evaporator [23].

Hao et al. (2009) studied the heat transfer characteristics of refrigerant-based Nano fluids flow boiling inside a smooth tube at different nanoparticles concentration, mass fluxes, heat fluxes, and inlet vapor qualities to analyze the influence of nanoparticles on the heat transfer characteristics of refrigerant-based Nano fluid flow boiling inside the smooth tube and presented a correlation for predicting the heat transfer coefficient of refrigerant-based Nano fluid and the predicted heat transfer coefficients agree with 93% of the experimental data and found the heat transfer coefficient of refrigerant-based nanofluid in flow boiling is larger than that of pure refrigerant and the maximum enhancement is about 29.7% when observed with a mass fraction of nanoparticles 0–0.5 wt%. it was observed that the reduction of the boundary layer height due to the disturbance of nanoparticles enhances the heat transfer [24].

Hao et al. (2010) investigated experimentally the nucleate pool boiling heat transfer characteristics of refrigerant/oil mixture with diamond nanoparticles. The refrigerant was R113 and the oil was VG68. The results indicate that the nucleate pool boiling heat transfer coefficient of R113/oil mixture with diamond nanoparticles is larger than that of R113/oil mixture by maximum of 63.4% and the enhancement increases with the increase of nanoparticles concentration in the nanoparticles/oil suspension and decreases with the increase of lubricating oil concentration. Authors developed a correlation for predicting the nucleate pool boiling heat transfer coefficient of refrigerant/oil mixture with nanoparticles and it agrees well with the experimental data of refrigerant/oil mixture with nanoparticles [25].

Hwang et al. (2006) observed that the thermal conductivity enhancement of nanofluids is greatly influenced by thermal conductivity of nanoparticles and base fluid. For instance, thermal conductivity of water based nanofluid with multiwall carbon nano tube has noticeably higher thermal conductivity compared to SiO2 nanoparticles in the same base fluid [26].

Lee et al. (2008) observed Nano fluids thermal conductivity effect by pH level and addition of surfactant during Nano fluids preparation stage. Better dispersion of nanoparticles is

achieved with addition of surfactant such as sodium dodecylbenzene sulfonate and found the optimum combination of pH and surfactant leads to 10.7% thermal conductivity enhancement of 0.1% Cu/H2O Nano fluids [27].

Wang et al. (2006) did an experimental study of the boiling heat transfer characteristics of R22 refrigerant with Al2O3 nanoparticles and found that the nanoparticles enhanced the refrigerant heat transfer characteristics with reduced bubble sizes that moved quickly near the heat transfer surface [28].

Li et al. (2006) observed the pool boiling heat transfer characteristics of R11 refrigerant with TiO2 nanoparticles and showed that the heat transfer enhancement reached 20% at a particle loading of 0.01 g/L [29].

Peng et al. (2009) find out the influence of nanoparticles on the heat transfer characteristics of refrigerant-based Nano fluids flow boiling inside a horizontal smooth tube, and presented a correlation for predicting heat transfer performance of refrigerant based Nano fluids. For the convenience of preparing refrigerant based Nano fluids, R113 refrigerant and CuO nanoparticles were used by the authors. Authors reported that the heat transfer coefficient of refrigerant-based Nano fluids is higher than that of pure refrigerant, and the maximum enhancement of heat transfer coefficient found to be about 29.7% [30].

Kumar and Elansezhian (2014) experimentally analyzed the effect of concentration of Nano Zno ranges in the order of 0.1%, 0.3% and 0.5% v with particle size of 50 nm on various parameters like COP, suction temperature, input power and pressure ratio with 152a as working fluid. In simple vapour compression refrigeration system. They found that maximum COP of 3.56 and 21% reduction of power input was obtained with 0.5% v of ZnO. Pressure ratio decreases with increase in Nano Zno concentration [31]. Xuan and Chen (2004) presented in this manuscript about the replacement of R502 by mixture of HFC-161.Through experimental study it was found that mixture of HFC-161 gives same and higher performance than R404A at lower and higher evaporative temperature respectively on the vapor compression refrigeration system designed for R404A [32]

Jiang et al. (2009) also found the effect of added that thermal conductivity of Nano fluids which depends on the nanoparticles size and temperature [33].

Jiang et al. (2009) found experimentally the thermal conductivities of carbon nanotube (CNT) Nano refrigerants are much higher than those of CNT–water Nano fluids or spherical nanoparticle–R113 Nano refrigerants. Authors reported that the smaller the diameter of CNT larger the thermal conductivity enhancement of CNT Nano refrigerant [34].

Yoo et al. (2007) also found that surface to volume ratio of nanoparticles is a dominant factor that influences the Nano fluids thermal conductivity rather than nanoparticles thermal conductivity. Surface to volume ratio is increased with smaller sizes of nanoparticles [35].

Choi et al. (2001) observed 150% thermal conductivity enhancement of poly (a-olefin) oil with the addition of multiwall carbon nanotubes (MWCNT) at 1% volume fraction [36]. Yang (2006) found a 200% thermal conductivity enhancement for poly (a-olefin) oil containing 0.35% (v/v) MWCNT. It is important to note that this thermal conductivity enhancement was accompanied by a three order of magnitude increase in viscosity [37].

Trisaksri and Wongwises (2009) studied the nano particles TiO_2 mixed in HCFC 1416 in a cylindrical copper tube and found that the nucleate pool boiling heat transfer deteriorated with increasing nanoparticle concentrations especially at higher heat fluxes [38].

Eastman et al. (2001) found a 40% thermal conductivity enhancement for ethylene glycol with 0.3% (v/v) copper nanoparticles (10 nm diameter), although the authors added about 1% (v/v) thioglycolic acid to aid in the dispersion of the nanoparticles. The addition of this dispersant yielded a greater thermal conductivity than the same concentration of nanoparticles in the ethylene glycol without the dispersant [39]. Mastani Joybari et al. (2013) performed experimental investigation on a domestic refrigerator originally manufactured to use of 145g of R134a and concluded the exergetic defect occurred in compressor was highest as compare to other components and through their analysis it has been found that instead of 145g of R134a if 60g of R600a is used in the considered system gave same performance which ultimately result into economic advantages and reduce the risk of flammability of hydrocarbon refrigerants [40].

Wu et al. (2008) found the pool boiling heat transfer was enhancement at low nanoparticles concentration of TiO2 in R11 but deteriorated under the condition of high nanoparticles concentration [41].

Anand and Tyagi (2012) carried out detailed exergy analysis of two ton of refrigeration window air conditioning test rig with R22 as working fluid and reached to the conclusions that irreversibility in system components will be highest when the system is 100% charged and lowest when 25% charged and irreversibility in compressor is highest among system components [42].

Arora and Kaushik (2008) developed numerical model of actual vapour compression refrigeration system with liquid vapour heat exchanger and did energy and exergy analysis on the same in the specific temperature range of evaporator and condenser and concluded that R502 is the best refrigerant compare to R404A and R507A, compressor is the worst and liquid vapour heat exchanger is best component of the system.

Jana et al. (2006) computed thermal conductivity of a similar copper containing Nano fluid, except the base fluid was water and laurate salt was used as a dispersant and observed a 70% thermal conductivity enhancement for 0.3% (v/v) cu nanoparticles in water. Researchers did not go through the computation of irreversibility in terms of exergy destruction ratio (EDR) using second law analysis of multiple evaporators systems with multi-stage expansion in vapour compression refrigeration systems. Researchers did not go through computing irreversibility's occurred in the each component in terms of exergy destruction using entropy generation and second law analysis of single and multi-stage vapour

compression refrigeration systems by using of Nano fluid in the secondary circuit of evaporator or by using of Nano fluid in the secondary circuit of condenser [43].

To improve thermal performance of vapour compression refrigeration systems (both single and multiple evaporator system) by improving:

According to first law of thermodynamic energetic efficiency /COP is defined as the ratio of net refrigeration effect to the per unit power consumed. First law analysis restricted to calculate only coefficient of performance of the systems and second law efficiency. The concept of exergy was given by second law of thermodynamics. Second law efficiency is the exergy of the heat abstracted in to the evaporators from the space to be cooled and exergy of fuel is actual compressor work input and reduction of system defect by using of nanoparticles in vapour compression refrigeration systems which results into reduction of work input.

Table-1(a) Effect of compressor speed on Performance of Vapour compression Refrigeration System by using HFO-1234yf in the primary circuit and Nano Particle (Al_2O_3) mixed with R-718, m_{brine} (kg/sec)=0.007, m_{water} (kg/sec)=0.008, $L_{_eva}$=0.72m, $L_{_Cond}$=1.2m, P_brine=P_water=2.0 Bar

Speed of Compressor (R P M)	First law Efficiency (COP)	Exergy Destruction Ratio(EDR)	Exergetic Efficiency	Evaporator Temperature (^oC)	Condenser Temperature (^oC)	Evaporator overall heat transfer coefficient (W/m^2K)	Condenser overall heat transfer coefficient (W/m^2K)	Evaporator Pressure (bar)
2500	3.631	3.249	0.2353	6.861	325.6	1314.24	708.26	3.731
2600	3.583	3.234	0.2362	6.574	326.0	1312.60	709.11	3.695
2700	3.542	3.219	0.2370	6.310	326.4	1313.30	710.38	3.661
2800	3.507	3.203	0.2379	6.066	326.8	1315.94	712.02	3.631
2900	3.477	3.186	0.2389	5.841	327.1	1320.21	714.01	3.602
3000	3.451	3.169	0.2399	5.631	327.1	1325.84	716.29	3.576

Table-1(b) Effect of compressor speed on Performance of Vapour compression Refrigeration System by using HFO-1234yf in the primary circuit and Nano Particle (Al_2O_3) mixed with R-718, m_{brine} (kg/sec)=0.007, m_{water} (kg/sec)=0.008, $L_{_eva}$=0.72m, $L_{_Cond}$=1.2m, P_brine=P_water=2.0 Bar

Speed of Compressor (R P M)	First law Efficiency (COP)	Condenser Pressure (bar)	Isentropic Efficiency of Compressor	Volumetric Efficiency of Compressor	Condenser Liquid_ LMTD	Condenser Vapour_ LMTD	Evap-LMTD	Q_Cond_Liquid (W)	Q_Cond_vapour (W)
2500	3.631	14.02	0.7860	0.6537	32.82	16.67	12.91	427.9	34.31
2600	3.583	14.16	0.7924	0.642	33.14	16.83	13.1	434.9	39.85
2700	3.542	14.29	0.7991	0.6409	33.42	16.96	13.27	441.9	35.29
2800	3.507	14.42	0.8060	0.6348	33.67	17.07	13.41	448.8	35.65
2900	3.477	14.55	0.8131	0.6289	33.89	17.17	13.54	455.7	35.93
3000	3.451	14.67	0.8203	0.6232	34.07	17.24	13.65	462.5	36.13

Table-1(c) Effect of compressor speed on Performance of Vapour compression Refrigeration System by using HFO-1234yf in the primary circuit and Nano Particle (Al_2O_3) mixed with R-718, m_{brine} (kg/sec)=0.007, m_{water} (kg/sec)=0.008, $L_{_eva}$=0.72m, $L_{_Cond}$=1.2m, P_brine=P_water=2.0 Bar

Speed of Compressor (R P M)	First law Efficiency (COP)	Exergy Destruction Ratio(EDR)	Exergetic Efficiency	Evaporator Load (W)	Condenser Heat rejected (W)	Compressor Work (W)
2500	3.631	3.249	0.2353	365.40	462.2	100.6
2600	3.583	3.234	0.2362	370.3	469.8	103.3
2700	3.542	3.219	0.2370	375.2	477.2	105.9
2800	3.507	3.203	0.2379	380.1	484..5	108.4
2900	3.477	3.186	0.2389	384.9	491.6	110.7
3000	3.451	3.169	0.2399	389.7	498.6	112.9

Table-1(d) Effect of evaporator Mass flow rate of brine on Performance of Vapour compression Refrigeration System by using HFO-1234yf in the primary circuit and Nano Particle (Al_2O_3) mixed with R-718, m_{brine} (kg/sec)=0.007, m_{water} (kg/sec)=0.008, $L_{_eva}$=0.72m, $L_{_Cond}$=1.2m, P_brine=P_water=2.0 Bar

Speed of Compressor (R P M)	First law Efficiency (COP)	Exergy Destruction Ratio(EDR)	Exergetic Efficiency	Reynold Number_Brine	Re_23	Re_Cap	Rem
2500	3.631	3.249	0.2353	104.3	180907	25045	$1.407X10^6$
2600	3.583	3.234	0.2362	104.3	187581	25451	$1.407X10^6$
2700	3.542	3.219	0.2370	104.3	194088	25858	$1.407X10^6$
2800	3.507	3.203	0.2379	104.3	200428	26265	$1.407X10^6$
2900	3.477	3.186	0.2389	104.3	206601	26671	$1.407X10^6$
3000	3.451	3.169	0.2399	104.3	212608	27074	$1.407X10^6$

Table-2(a) Effect of evaporator Mass flow rate of brine on Performance of Vapour compression Refrigeration System with Nano Particle (Al_2O_3) mixed with R-718, compressor speed (rpm)=2900, m_{water} (kg/sec)=0.008, $L_{_eva}$=0.72m, $L_{_Cond}$=1.2m, P_brine=P_water=2.0 Bar

Evaporator Mass flow rate of brine (Kg/sec)	First law Efficiency (COP)	System Exergy Destruction Ratio (EDR)	System Exergetic Efficiency	Condenser Temperature (K)	Evaporator Temperature (°C)	Outlet water Condenser Temperature (°C)	Outlet brine Evaporator Temperature (°C)	System Exergy Destruction Ratio based on input
0.007	3.477	3.186	0.2389	327.1	5.841	41.69	13.86	0.7611
0.008	3.549	3.277	0.2338	327.5	6.583	42.02	15.19	0.7662
0.009	3.609	3.357	0.2295	327.9	7.179	42.29	16.27	0.7705
0.010	3.658	3.427	0.2259	328.2	7.669	42.52	17.18	0.7741

Table-2(b) Effect of evaporator Mass flow rate of brine on thermal Performance of Vapour compression Refrigeration System by using HFO-1234yf in the primary circuit and Nano Particle (Al_2O_3) mixed with R-718, compressor speed(rpm)=2900, m_{water} (kg/sec)=0.008, $L_{_eva}$=0.72m, $L_{_Cond}$=1.2m, $P_{_brine}$=$P_{_water}$=2.0 Bar

Evaporator Mass flow rate of brine (Kg/sec)	First law Efficiency (COP)	Second Law Efficiency/ Exergetic Efficiency	Exergy of product (W)	Exergy of fuel (W)	Isentropic Efficiency of Compressor	Volumetric Efficiency of Compressor
0.007	3.477	0.2389	26.45	110.7	0.8131	0.6289
0.008	3.549	0.2338	26.04	111.4	0.8222	0.6313
0.009	3.609	0.2295	25.68	111.9	0.8297	0.6332
0.010	3.658	0.2259	25,36	108.3	0.8360	0.6349

Table-2(c) Effect of evaporator Mass flow rate of brine on Performance of Vapour compression Refrigeration System by using HFO-1234yf in the primary circuit and Nano Particle (Al_2O_3) mixed with R-718, compressor speed (rpm)=2900, m_{water} (kg/sec)=0.008, $L_{_eva}$=0.72m, $L_{_Cond}$=1.2m, P_brine=P_water=2.0 Bar

Evaporator Mass flow rate of brine (Kg/sec)	First law Efficiency (COP)	Evaporator overall heat transfer coefficient (W/m^2K)	Condenser overall heat transfer coefficient (W/m^2K)	Evaporator Pressure (bar)	Condenser Pressure (bar)	Evaporator Load (W)	Condenser Heat rejected (W)	Compressor Work (W)	Exergetic Efficiency
0.007	3.477	1320.21	714.01	3.602	14.55	384.9	491.6	110.7	0.2389
0.008	3.549	1342.87	722.63	3.696	14.70	395.3	502.7	111.4	0.2338
0.009	3.609	1361.93	729.54	3.772	14.83	403.8	511.7	111.9	0.2295
0.010	3.658	1378.26	735.19	3.835	14.93	410.9	516.2	108.3	0.2259

Table-2(d) Effect of evaporator Mass flow rate of brine on thermal performances of Vapour compression Refrigeration System by using HFO-1234yf in the primary circuit and Nano Particle (Al_2O_3) mixed with R-718, compressor speed (rpm)=2900, m_{water} (kg/sec)=0.008, $L_{_eva}$=0.72m, $L_{_Cond}$=1.2m, $P_{_brine}$=$P_{_water}$=2.0 Bar

Evaporator Mass flow rate of brine (Kg/sec)	First law Efficiency (COP)	Exergy Destruction Ratio(EDR)	Exergetic Efficiency	Reynold Number_Brine	Re_23	Re_Cap	Re_m
0.007	3.477	3.186	0.2389	104.3	206601	26671	$1.407X10^6$
0.008	3.549	3.277	0.2338	119.2	207155	27703	$1.407X10^6$
0.009	3.609	3.357	0.2295	134.10	207682	28558	$1.407X10^6$
0.010	3.658	3.427	0.2259	149.0	208170	29281	$1.407X10^6$

Table-3(a) Performance of Vapour compression Refrigeration System by using HFO-1234yf in the primary circuit and Nano Particle (Al_2O_3) mixed with R-718, compressor speed (rpm)=2900, m_{brine} (kg/sec)=0.007, $L_{_eva}$=0.72m, $L_{_Cond}$=1.2m, P_brine=P_water=2.0 Bar

Condenser Mass flow rate of water (Kg/sec)	First law Efficiency (COP)	System Exergy Destruction Ratio based on input	Second Law Efficiency/ Exergetic Efficiency	Exergy of product (W)	Exergy of fuel (W)	Evaporator Temperature (K)	Condenser Temperature (^oC)	Outlet water Condenser Temperature (^oC)	Outlet brine Evaporator Temperature (^oC)
0.007	3.379	0.7726	0.2274	25.53	112.3	6.212	328.7	43.65	14.04
0.008	3.477	0.7611	0.2389	26.45	110.7	5.841	327.1	41.69	13.86
0.009	3.557	0.7517	0.2483	27.16	109.4	5.581	325.9	40.14	13.71
0.010	3.625	0.7440	0.2560	27.73	108.3	5.344	324.9	38.89	13.59

Table-3(b) Performance of Vapour compression Refrigeration System by using HFO-1234yf in the primary circuit and Nano Particle (Al_2O_3) mixed with R-718, compressor speed (rpm)=2900, m_{brine} (kg/sec)=0.007, $L_{_eva}$=0.72m, $L_{_Cond}$=1.2m, P_brine=P_water=2.0 Bar

Condenser Mass flow rate of water (Kg/sec)	First law Efficiency (COP)	System Exergy Destruction Ratio (EDR)	System Exergetic Efficiency	Evaporator overall heat transfer coefficient (W/m^2K)	Condenser overall heat transfer coefficient (W/m^2K)	Evaporator Pressure (bar)	Condenser Pressure (bar)	Isentropic Efficiency of Compressor	Volumetric Efficiency of Compressor
0.007	3.379	3.398	0.2274	1327.54	692.96	3.649	15.13	0.8198	0.6239
0.008	3.477	3.186	0.2389	1320.21	714.01	3.682	14.55	0.8131	0.6289
0.009	3.557	3.028	0.2483	1315.88	731.28	3.568	14.11	0.808	0.6328
0.010	3.625	2.906	0.2560	1313.34	745.71	3.541	13.76	0.8041	0.6359

Table-3(c) Performance of Vapour compression Refrigeration System by using HFO-1234yf in the primary circuit and Nano Particle (Al_2O_3) mixed with R-718, compressor speed (rpm)=2900, m_{brine} (kg/sec)=0.007, $L_{_eva}$=0.72m, $L_{_Cond}$=1.2m, P_brine=P_water=2.0 Bar

Condenser Mass flow rate of water (Kg/sec)	First law Efficiency (COP)	Exergy Destruction Ratio(EDR)	Exergetic Efficiency	Evaporator Load (W)	Condenser Heat rejected (W)	Compressor Work (W)
0.007	3.379	3.398	0.2274	379.4	487.5	112.3
0.008	3.477	3.186	0.2389	384.9	491.6	110.7
0.009	3.557	3.028	0.2483	389.3	494.8	109.4
0.010	3.625	2.906	0.2560	392.7	497.4	108.3

Table-3(d) Performance of Vapour compression Refrigeration System by using HFO-1234yf in the primary circuit and Nano Particle (Al_2O_3) mixed with R-718, compressor speed (rpm)=2900, m_{brine} (kg/sec)=0.007, $L_{_eva}$=0.72m, $L_{_Cond}$=1.2m, P_brine=P_water=2.0 Bar

Condenser Mass flow rate of water (Kg/sec)	First law Efficiency (COP)	Condenser Liquid portion LMTD (K)	Condenser Vapour portion LMTD (K)	Evaporator LMTD (K)	$Q_{_Cond_Liquid}$ (W)	$Q_{_Cond_Vapour}$ (W)
0.007	3.379	35.15	16.82	13.27	451.4	36.02
0.008	3.477	33.89	17.17	13.54	455.7	35.93
0.009	3.557	32.73	17.45	13.74	459.0	35.84
0.010	3.625	31.8	17.68	13.89	461.6	35.75

3. Results and Discussion

Tables-1(a)-(1(d) showing the variation of compressor speed with first and second law Performances of Vapour compression Refrigeration System with Nano Particle (Al_2O_3) mixed with R-718 in the secondary circuit of evaporator and it was observed that when compressor speed is increasing, first law efficiency in terms of COP along with system exergy destruction ratio (EDR), volumetric efficiency of compressor, Evaporator Pressure, Evaporator overall heat transfer coefficient (W/m^2K) Condenser overall heat transfer coefficient (W/m^2K) are decreasing and second law efficiency (i.e exergetic efficiency), compressor isentropic Efficiency, Condenser Pressure , L.M.T.D. of condenser Liquid , L.M.T.D. of condenser Vapour and L.M.T.D. of Evaporator is increasing. The developed model is also predicting unknown the condenser temperature , which is increasing and decreasing evaporator refrigerant temperature. Similarly increasing compressor speed is the increasing condenser liquid and vapour heat and condenser Reynold and Capillary Reynold numbers for constant Reynold number of evaporator refrigerant and brine Reynold numbers. Similarly Table-2(a)-2(d) shows the variation of Evaporator Mass flowrate of brine (Kg/sec) with first and second law Performances of Vapour compression Refrigeration System with Nano Particle (Al_2O_3) mixed with R-718 in the secondary circuit of evaporator and it was observed that when Evaporator Mass flow rate of brine (Kg/sec) is increasing, first law efficiency in terms of COP, compressor isentropic Efficiency along with system exergy destruction ratio (EDR), volumetric efficiency of compressor, Evaporator Pressure, Evaporator overall heat transfer coefficient (W/m^2K) Condenser overall heat transfer coefficient (W/m^2K) are increasing and second law efficiency (i.e. exergetic

efficiency), exergy of Product , exergy of fuel, Condenser Pressure , L.M.T.D. of condenser Liquid , L.M.T.D. of condenser Vapour and L.M.T.D. of Evaporator is increasing. The developed model is also predicting unknown the condenser temperature , which is increasing and decreasing evaporator refrigerant temperature. Similarly increasing Evaporator Mass flow rate of brine is the increasing condenser liquid and vapour heat and condenser Reynold and Capillary Reynold number Reynold number of evaporator refrigerant and brine Reynold numbers are also increasing. Tables-3(a)-3(d) shows the variation of Condenser Mass flowrate of brine (Kg/sec) with first and second law Performances of Vapour compression Refrigeration System with Nano Particle (Al_2O_3) mixed with R-718 in the secondary circuit of evaporator and it was observed that when Condenser Mass flow rate of brine (Kg/sec) is increasing, first law efficiency in terms of COP, compressor isentropic Efficiency along with volumetric efficiency of compressor, Evaporator Pressure, Condenser overall heat transfer coefficient (W/m^2K) are increasing and second law efficiency (i.e exergetic efficiency), exergy of Product , exergy of fuel, Condenser Pressure , L.M.T.D. of condenser Vapour and L.M.T.D. of Evaporator is increasing while decreasing system exergy destruction ratio (EDR) and Evaporator overall heat transfer coefficient (W/m^2K), Condenser evaporator Temperatures, outlet water condenser temperature, outlet brine evaporator temperature L.M.T.D. of condenser Liquid . The developed model is also predicting unknown the condenser temperature , which is increasing and decreasing evaporator refrigerant temperature. Similarly increasing Condenser Mass flow rate of condenser water , the decreasing condenser liquid and vapour heat and condenser Reynold and Capillary Reynold number Reynold number of evaporator refrigerant and brine Reynold numbers are also increasing.

4. Conclusion

Following conclusions were drawn

(i) The first law performance in terms of COP is decreased and increased second law efficiency by increasing compressor speed.

(ii) The first law performance in terms of COP and system exergy destruction ratio (EDR) based on output increased and decreased second law efficiency by increasing evaporator mass flow rate of brine,

(iii) The first law performance in terms of COP and second law efficiency is increased and decreased system exergy destruction ratio (EDR) based on output by increasing condenser mass flow rate of water.

References

[1] S.Kumar, M.Prevost, R.Bugarel- Exergy analysis of a vapour compression refrigeration system. Heat Recovery Systems & CHP.1989;9:151-157.

[2] C. Nikolaidis, D. Probert-Exergy method analysis of a two-stage vapour-compression refrigeration-plants performance. Int J Applied Thermal Engineering.1998; 60:241-256.

[3] RecepYumrutas, Mehmet Kunduz, Mehmet Kanoglu-Exergy analysis of vapor compression refrigeration systems. Exergy, An International Journal.2002; 2:266-272.

[4] E. Halimic, D. Ross, B. Agnew, A. Anderson, I. Potts. A comparison of the operating performance of alternative refrigerants. Int J Applied Thermal Engineering.2003; 23:1441-1451.

[5] R. Cabello, J. Navarro-Esbrı, R. Llopis, E. Torrella. Analysis of the variation mechanism in the main energetic parameters in a single-stage vapour compression plant. Int J Applied Thermal Engineering.2007; 27:167-176.

[6] R.Cabello a, E.Torrella b, J.Navarro-Esbr. Experimental evaluation of a vapour compression plant performance using R134a, R407C and R22 as working fluids. Int J Applied Thermal Engineering.2004; 24:1905-1917.

[7] J.U. Ahamed, R.Saidur, H.H.Masjuki. A review on exergy analysis of vapor compression refrigeration system. Int J Renewable and sustainable energy reviews.2011; 15:1593-1600.

[8] J.U. Ahamed, R.Saidur, H.H.Masjuki. A review on exergy analysis of vapor compression refrigeration system. Int J Renewable and sustainable energy reviews.2011; 15:1593-1600.

[9] Mark W Spatz, Samuel F. Yana Motta. An evaluation of options for replacing HCFC-22 in medium temperature refrigeration systems. Int J Refrigeration.2004; 27:475-483.

[10] X.H. Han, Q. Wang, Z.W. Zhu, G.M. Chen. Cycle performance study on R32/R125/R161 as an alternative refrigerant to R407C. Int J Applied Thermal Engineering.2007; 27:2559-2565

[11] H.M Getu, P.K Bansal. Thermodynamic analysis of an R744-R717 cascade refrigeration system. Int J Refrigeration.2008; 31:45-54.

[12] M. Padilla, R. Revellin, J. Bonjour. Exergy analysis of R413A as replacement of R12 in a domestic refrigeration system. Int J Energy Conversion and Management.2010; 51:2195-2201.

[13] M. Mohanraj, S. Jayaraj, C. Muraleedharan, P. Chandrasekar.Experimental investigation of R290/R600a mixture as an alternative to R134a in a domestic refrigerator. Int J Thermal Sciences.2009; 48:1036-1042.

[14] B.O. Bolaji, M.A. Akintunde, T.O. Falade. Comparative analysis of performance of three ozone-friends HFC refrigerants in a vapor compression refrigerator. Int J Sustainable Energy & Environment.2011; 2:61-64.

[15] Camelia Stanciu, Adina Gheorghian, Dorin Stanciu, Alexandru Dobrovicescu- Exergy analysis and refrigerant effect on the operation and performance lomits of a one stage vapour compression refrigeration system.Termotehnica.2011;1:36-42.

[16] Eastman JA, Choi US, Thompson LJ, Lee S. Enhanced thermal conductivity through the development of nanofluids. Mater Res Soc Symp Proc 1996;457:3–11

[17] Kang HU, Kim SH, Oh JM. Estimation of thermal conductivity of nanofluid using experimental effective particle. Experimental Heat Transfer 2006;19(3):181–91

[18] Liu MS, Lin MCC, Huang IT, Wang CC. Enhancement of thermal conductivity with CuO for Nanofluids. Chemical Engineering and Technology 2006;29(1):72–7.

[19] Elcock D. Potential impacts of nanotechnology on energy transmission applications and needs. Environmental Science Division, Argonne National Laboratory;2007.

[20] Hindawi, Special issue on heat transfer in nanofluids; 2009

[21] V. Siva Reddy, N.L Panwar, S.C Kaushik-Exergy analysis of a vapour compression refrigeration system with R134a,R143a,R152a, R404A, R407C, R410A, R502 and R507A.Clean Techn Environ Policy.2012;14:47-53.

[22] I.M. Mahbubul,S.A. Fadhilah, R. Saidur, K.Y. Leong, M.A. Amalina .Thermophysical properties and heat transfer performance of Al2O3/R-134a nanorefrigerants.International Journal of Heat and Mass Transfer ;2013;57:100–108s.

[23] R.Saravana kumar, V.Selladurai-Exergy analysis of a domestic refrigerator using eco-friendly R290/R600a refrigerant mixture as an alternative to R134a.Int J Therm Anal Calorim.2013;

[24] Hao P, Guoliang D, Weiting J, Haitao H, Yifeng G. Heat transfer characteristics of refrigerant-based nanofluid flow boiling inside a horizontal smooth tube. International Journal of Refrigeration 2009;32:1259–70.

[25] Hao P, Guoliang D, Haitao H, Weiting J, Dawei Z, Kaijiang W. Nucleate pool boiling heat transfer characteristics of refrigerant/oil mixture with diamond nanoparticles. International Journal of refrigeration 2010;33:347–58.

[26] Hwang YJ, Ahn YC, Shin HS, Lee CG, Kim GT, Park HS, et al. Investigation on characteristics of thermal conductivity enhancement of nanofluids. Current Applied Physics 2006;6(6):1068–71.

[27] Lee J-H, Hwang KS, Jang SP, Lee BH, Kim JH, Choi SUS, et al. Effective viscosities and thermal conductivities of aqueous nanofluids containing low volume concentrations of Al2O3 nanoparticles. International Journal of Heat and Mass Transfer 2008;51(11–12):2651–6.

[28] Wang KJ, Ding GL, Jiang WT. Nano-scale thermal transporting and its use in engineering. In: Proceedings of the 4th symposium on refrigeration and air condition; 2006. p. 66–75.

[29] Li P, Wu XM, Li H. Pool boiling heat transfer experiments of refrigerants with nanoparticle TiO2. In: Proceedings of the 12th symposium on engineering thermophysics; 2006. p. 325–8.

[30] Peng H, Ding G, Jiang W, Hu H, Gao Y. Heat transfer characteristics of refrigerant-based nanofluid flow boiling inside a horizontal smooth tube.International Journal of Refrigeration ;2009;32:1259–70.

[31] D.Sendil Kumar, R. Elansezhian.Zno nanorefrigerant in R152a refrigeration system for energy conservation and green environment.J Front Mech Engg ; 2014;1-6

[32] Yongmei Xuan, Guangming Chen. Experimental study on HFC-161 mixture as an alternative refrigerant to R502. Int J Refrigeration. Article in Press.

[33] Jiang W, Ding G, Peng H. Measurement and model on thermal conductivities of carbon nanotube nanorefrigerants. International Journal of Thermal Sciences 2009;48:1108–15

[34] Jiang W, Ding G, Peng H. Measurement and model on thermal conductivities of carbon nanotube nanorefrigerants. International Journal of Thermal Sciences 2009;48:1108–15.

[35] Yoo D-H, Hong KS, Yang H-S. Study of thermal conductivity of nanofluids for the application of heat transfer fluids. Thermochimica Acta 2007;455(1–2):66–9.

[36] Choi SUS, Zhang ZG, Yu W, Lockwood FE, Grulke EA. Anomalous thermal conductivity enhancement in nanotube suspensions. Applied Physics Letters 2001;79(14):2252–4.

[37] Yang Y. Carbon nanofluids for lubricant application. University of Kentucky;2006.

[38] Trisaksri V, Wongwises S. Nucleate pool boiling heat transfer of TiO2–R141b nanofluids. International Journal of Heat and Mass Transfer 2009;52(5–6):1582–8.

[39] Eastman JA, Choi SUS, Li S, Yu W, Thompson LJ. Anomalously increased effective thermal conductivities of ethylene glycol-based nanofluids containing copper nanoparticles. Applied Physics Letters 2001;78(6):718–20.

[40] Mastani Joybari Mahmood, Mohammad Sadegh Hatamipour, Amir Rahimi, Fatemeh Ghadiri Modarres- Exergy analysis and optimization of R600a as a replacement of R134a in a domestic refrigerator system. International Journal of refrigeration.2013; 36:1233-1242.

[41] Wu XM, Li P, Li H, Wang WC. Investigation of pool boiling heat transfer of R11 with TiO2 nano-particles. Journal of Engineering Thermophysics 2008;29(1):124–6.

[42] S.Anand ,S.KTyagi-Exergy analysis and experimental study of a vapour compression refrigeration cycle.Int J Therm Anal Calorim.2012; 110:961-971.

[43] AkhileshArora, S.C. Kaushik. Theoretical analysis of a vapour compression refrigeration system with R502, R404A and R507A. Int J Refrigeration.2008; 31:998-1005.